



Quantum Electrodynamic Corrections in Quantum Chemistry

Maen Salman

► To cite this version:

Maen Salman. Quantum Electrodynamic Corrections in Quantum Chemistry. Theoretical and/or physical chemistry. Université Paul Sabatier - Toulouse III, 2022. English. NNT : 2022TOU30032 . tel-03715663

HAL Id: tel-03715663

<https://theses.hal.science/tel-03715663v1>

Submitted on 6 Jul 2022

HAL is a multi-disciplinary open access archive for the deposit and dissemination of scientific research documents, whether they are published or not. The documents may come from teaching and research institutions in France or abroad, or from public or private research centers.

L'archive ouverte pluridisciplinaire **HAL**, est destinée au dépôt et à la diffusion de documents scientifiques de niveau recherche, publiés ou non, émanant des établissements d'enseignement et de recherche français ou étrangers, des laboratoires publics ou privés.



THÈSE

**En vue de l'obtention du
DOCTORAT DE L'UNIVERSITÉ DE TOULOUSE
Délivré par l'Université Toulouse 3 - Paul Sabatier**

**Présentée et soutenue par
Maen SALMAN**

Le 28 janvier 2022

Corrections électrodynamiques quantiques en chimie quantique

Ecole doctorale : **SDM - SCIENCES DE LA MATIERE - Toulouse**

Spécialité : **Physico-Chimie Théorique**

Unité de recherche :

LCPQ-IRSAMC - Laboratoire de Chimie et Physique Quantiques

Thèse dirigée par
Trond SAUE

Jury

M. Peter SCHWERDTFEGER, Rapporteur
Mme Eva LINDROTH, Rapporteur
M. Jean-Philippe KARR, Examineur
Mme Pina ROMANIELLO, Examinatrice
M. Julien TOULOUSE, Examineur
M. Mathieu LEWIN, Examineur
M. Trond SAUE, Directeur de thèse

Quantum Electrodynamic Corrections in Quantum Chemistry

Maen Salman

Laboratoire de Chimie et Physique Quantiques
Université Toulouse-III Paul-Sabatier

27-04-2022

وَكُنْتُ تُنْصِرُ فِي الْهَيْجَا بِكَفِّ حَصَى
إِذَا رَمَيْتَ بِهِ جَمْعَ الْعِدَى هَمْدًا
لَكِنَّ رَبِّي أَرَادَ الْحَرْبَ مُجْهِدَةً
وَالنَّفْسُ تَظْهَرُ إِنْ عَوَّدَتْهَا الْجُهِدَا

تميم البرغوثي - البردة

Acknowledgments

First of all, I would like to sincerely thank my parents, Elias and Raghdad, for providing an endless amount of unconditional love both sentimentally and intellectually. To a large extent, this thesis is written because of them, and it is therefore dedicated to them. Second, I would like to express my honest gratitude to Trond Saue, for being an extraordinary supervisor, in the scientific sense, and a wonderfully friendly and welcoming person on a social/personal level. The discussions I had with him enriched my knowledge of many scientific and cultural aspects enormously. Thirdly, I must thank the excellent colleagues and friends I met in the beautiful pink city (Toulouse) for the good times I had with them, making my stay at this distant country (geographically and mentally) very enjoyable. Finally, a special thanks go to Mathieu Lewin and Eric Séré for the excellent discussions I had with them, both physically (in Paris) and virtually, about the Dirac equation, the QED corrections, and many other mathematical and physical topics.

Contents

1	Introduction	1
1.1	Quantum electrodynamic corrections to the Dirac theory	1
1.2	Thesis structure	6
1.3	Numerical details	7
2	The Dirac equation	8
2.1	The Klein-Gordon equation:	
	A first relativistic quantum theory	9
2.2	Problems with the Klein-Gordon theory	10
2.3	Towards the Dirac equation	12
2.4	The Dirac equation	13
2.5	A few words on Dirac's negative-energy states	16
2.6	Time-dependent Dirac equation	17
	2.6.1 The free-particle problem: Dirac plane waves	18
	2.6.2 Dirac particle in an external electromagnetic potential	20
	2.6.3 Dirac particle in a time-independent external electromagnetic potential	21
2.7	Radial Dirac equation	21
	2.7.1 The $\boldsymbol{\alpha} \cdot \hat{\mathbf{p}}$ operator	22
	2.7.2 The radial Dirac equation	24
	2.7.3 Free Dirac equation in spherical coordinates	24
2.8	Discrete symmetries of the Dirac equation	28
	2.8.1 Charge conjugation	28
	2.8.1.1 \mathcal{C} -symmetry in the time-independent regime	29
	2.8.1.2 \mathcal{C} -symmetry in the spherical problem	30
	2.8.2 Time-reversal	32
	2.8.2.1 \mathcal{T} -symmetry in the time-independent problem	34
	2.8.2.2 \mathcal{T} -symmetry in the spherical problem	34
	2.8.3 Parity	34
	2.8.3.1 \mathcal{P} -symmetry in the radial problem	36
	2.8.4 Discrete symmetries summary	36
2.9	Finite basis approximation of the Dirac equation	36
	2.9.1 The general problem	37
	2.9.2 Gaussian basis set	38
2.10	Problems with relativistic basis sets	39
	2.10.1 Kinetic balance	41
	2.10.2 Numerical tests on restricted kinetic balance	43
	2.10.3 Inverse kinetic balance	45

2.10.4	Dual kinetic balance	46
2.10.5	Atomic balance	47
2.10.6	A short summary on relativistic basis functions	49
2.11	\mathcal{C} -symmetry in the finite basis set	50
2.11.1	An unexpected symmetry in the free-particle problem of RKB	51
2.11.2	Can we make RKB symmetric by \mathcal{C} -conjugation?	54
2.11.3	A new basis for confined systems	56
2.11.4	The basis of free solutions	57
2.11.5	A Solution to the normalizability problem of the free basis	60
2.11.6	\mathcal{C} - symmetry in DKB	61
3	Quantum electrodynamics	64
3.1	Quantum mechanical pictures	65
3.1.1	Schrödinger picture	65
3.1.2	Heisenberg picture	65
3.1.3	Interaction (intermediate) picture	66
3.2	Time-evolution operator	67
3.2.1	Time-evolution operator for the Schrödinger picture	67
3.2.2	Time-evolution operator for the Interaction picture	68
3.3	The scattering matrix	71
3.4	Solving the perturbed problem	72
3.4.1	Corrected wavefunctions	74
3.4.2	Corrected energies	74
3.5	The electron-photon field interaction: QED theory	75
3.5.1	Photon field operator	75
3.5.2	Electron field operator	76
3.5.3	Adding the QED interaction to the non-interacting problem	77
3.6	Time-independent Wick's theorem	78
3.6.1	Creation and annihilation operators	78
3.6.2	Normal ordering	78
3.6.3	Contraction	79
3.6.4	Products of n -operators	79
3.7	Wick's theorem	81
3.8	Photon propagator	82
3.8.1	Time-ordered photon propagator	84
3.8.2	Different gauges for the photon propagator	86
3.8.3	Feynman photon propagator as a time-ordered vacuum expectation value	87
3.9	Electron propagator	89
3.9.1	Free Dirac propagator	89
3.9.2	Time-ordered free Dirac propagator	90
3.9.3	Propagator for time-dependent external potential	91
3.9.4	Propagator for time-independent external potential	92
3.9.5	Feynman electron propagator as a time-ordered vacuum expectation value	92
3.9.6	Electron propagator and Green's function	94
3.10	\mathcal{S} -matrix expansion and Feynman diagrams	96
3.10.1	Wick's theorem for the \mathcal{S} -matrix in QED	96
3.10.2	\mathcal{S} -matrix expansion for the no-photon BSQED	97
3.10.3	Physical and vacuum diagrams	101

3.10.4	The BSQED corrections of the second-order e^2	104
3.10.5	Single-photon exchange	105
3.10.6	Vacuum polarization	107
3.10.7	Self-energy	109
3.11	Furry's theorem	110
3.12	Effective QED potentials	112
3.12.1	Vacuum polarization effective potentials	112
3.12.2	Self-energy effective potentials	114
3.12.2.1	Pyykkö and Zhao potentials	114
3.12.2.2	Flambaum and Ginges potentials	115
3.12.2.3	Shabaev, Tupitsyn, and Yerokhin potentials	116
3.13	Hartree-Fock with QED	117
3.13.1	A Hartree-Fock warm-up	117
3.13.2	Hartree-Fock with QED: The approach of Saue	118
3.13.3	Hartree-Fock with QED: The new approach	119
4	Vacuum polarization	122
4.1	Introduction	122
4.2	Vacuum polarization current in the time-reversible problem	124
4.3	Vacuum polarization density in the free-problem	125
4.4	Vacuum polarization density in the atomic problem	126
4.4.1	The free spherical vacuum polarization density	127
4.4.2	Expansion of the vacuum polarization density	127
4.4.3	Radial Green's function	128
4.4.4	Radial vacuum polarization density and Green's function expansion	130
4.5	Vacuum polarization in a finite basis set	132
4.5.1	VP density in restricted kinetic balance	133
4.5.2	VP density in dual kinetic balance	135
4.5.3	\mathcal{C} -symmetric Dual Kinetic Balance	136
4.5.4	Extra calculations: same exponents	140
4.5.5	A closer look on numerical solutions of \mathcal{C} -DKB	140
4.5.6	Comparison between RKB and \mathcal{C} -DKB	142
4.5.7	Non-vanishing vacuum polarization density in RKB	144
4.5.8	Conclusions	144
4.6	Vacuum polarization expansion in the finite basis set	145
4.6.1	The zero-potential vacuum polarization density	146
4.6.2	The one-potential vacuum polarization density	146
4.6.3	The n -potential vacuum polarization density	147
4.6.4	Furry's theorem in the finite basis set	148
5	Conclusions and perspectives	151
5.1	Conclusions	151
5.1.1	Charge conjugation symmetry in a finite basis	151
5.1.2	Vacuum polarization density derivations and calculations	152
5.2	Perspectives	153
5.2.1	Regularization and renormalization	153
5.2.2	Regularization and renormalization in a finite basis	154
5.2.3	Hartree-Fock with QED	154

6	French résumé	156
A	Notations and definitions	178
B	Identities	180
B.1	Gamma matrices	180
B.1.1	Products	180
B.1.2	Traces of gamma matrices	181
B.1.2.1	$\text{Tr} [\gamma^\mu] = 0$	181
B.1.2.2	$\text{Tr} [\gamma^\mu \gamma^\nu] = 4g^{\mu\nu}$	181
B.1.2.3	$\text{Tr} [\gamma^{\mu_1} \dots \gamma^{\mu_n}] = 0$ for odd n	182
B.1.2.4	$\text{Tr} [\gamma^\mu \gamma^\nu \gamma^\rho \gamma^\sigma]$	182
B.1.2.5	$\text{Tr} [\gamma^{\mu_1} \dots \gamma^{\mu_n}]$ for even n	183
C	Spherical Bessel functions	185
C.1	The Bessel equation and its solutions	185
C.2	Spherical Bessel equation and solutions	185
C.3	Limiting forms	186
C.4	Normalization to Dirac-delta	187
C.5	Derivatives	188
C.6	Orthogonality within a spherical box	189
D	Identities	191
D.1	Dirac relation	191
D.2	Spin angular momentum	191
D.3	Spherical Harmonics	192
D.3.1	Complex conjugation	193
D.3.2	Parity	193
D.4	Spherical spinors	193
D.4.1	Clebsch-Gordan coefficients: Angular momenta coupling	193
D.4.1.1	Spin-orbit coupling	195
D.4.2	Spherical spinors	196
D.4.3	Orthonormalization	197
D.4.4	Parity	198
D.4.5	Complex conjugation	198
D.4.6	$\sigma_r \Omega_{\kappa, m_j}$	199
D.4.7	$\sum_{m_j} \Omega_{\kappa, m_j}(\hat{\mathbf{x}}) \Omega_{\kappa, m_j}^\dagger(\hat{\mathbf{y}})$	201
D.4.8	$\sum_{m_j} \Omega_{-\kappa, m_j}(\hat{\mathbf{x}}) \Omega_{\kappa, m_j}^\dagger(\hat{\mathbf{y}})$	202
E	Matrix equations and integrals for kinetic balances	203
E.1	Restricted and Inverse Kinetic Balances (RKB and IKB)	203
E.1.1	RKB matrices	204
E.1.2	IKB matrices	205
E.1.3	Integrals	205
E.2	Dual Kinetic Balance (DKB)	206
E.3	Exponents for Gaussian function	207
E.3.1	Even-tempered Gaussians	208
F	Complex integrations	211

F.1	Cauchy's integral theorem	211
F.2	Cauchy's integral formula	212
F.3	Cauchy's differential formula	212
F.4	Jordan's lemma	212
F.4.1	Upper half-plane	213
F.4.2	Lower half-plane	214
F.5	Conclusion	215
F.6	$\alpha(Z\alpha)^n$: n -potential interactions complex integral	216
F.6.1	Zero-potential integral: One pole	217
F.6.2	One-potential integral: Two poles	219
F.6.3	n -potential integral: $n + 1$ poles	221
G	Time-ordered products	224
G.1	Electronic field currents	224
G.1.1	First-order	224
G.1.2	Second-order	225
G.1.3	Third-order	226
G.2	Photon field products	229
G.2.1	First-order	229
G.2.2	Second-order	229
G.2.3	Third-order	229
G.2.4	Fourth-order	229
G.2.5	Fifth-order	230
H	Fourier transforms	232
H.1	Definitions	232
H.2	Dirac δ distribution	233
H.3	Derivative transformation	233
H.4	Product transformation	233
H.5	Locality in real- and momentum-space	234
H.6	Dirac equation in Fourier-space	234
I	Integrals	235
I.1	Time-integral and $\Delta_\epsilon(a)$	235
I.2	Angular Fourier integral	236
I.3	Radial photon function	237
J	Quantum mechanical equations and currents	239
J.1	Free and interacting equations	239
J.2	Probability currents	241

Chapter 1

Introduction

1.1 Quantum electrodynamic corrections to the Dirac theory

The main goal of this thesis is to translate the Quantum ElectroDynamic (QED) corrections to the language of relativistic quantum chemistry: to the framework of the finite basis approximation of the Dirac equation. Unconsciously, our brains are used to assigning large speeds with large distances, which makes it difficult for us to understand, at first glance, why the atomic theory of electrons might need to account for special relativity. It can be shown, however, that the average speed of an electron occupying the ground-state of a hydrogen-like atom is given by:

$$v = (\alpha Z) c, \quad (1.1.1)$$

where $\alpha = e^2 / (4\pi\epsilon_0\hbar c) \approx 1/137$ is the fundamental dimensionless fine structure constant, Z is the atomic number, and c is the speed of light. This simple expression indicates that the relativistic effects can be neglected for light elements, but should be generally taken into account, especially for the heavy elements. Example: the ground-state electron of the hydrogen-like radon atom ($Z = 86$) has an average velocity of $v = 0.62 c$. In 1928 the British physicist Paul Dirac proposed a relativistic quantum theory which despite its simple (compact) form, was able to account for a large part of physics that was missing in the previous quantum theory of Schrödinger. Despite its superiority (generality) over Schrödinger's equation, Dirac's equation failed to predict various quantum phenomena, and especially the following two:

1. The electron spin magnetic moment, which is experimentally found to be around $g_{\text{exp.}} \approx 2.0023193$ [1], while predicted by the Dirac theory to be $g_{\text{Dirac}} = 2$.
2. The Lamb shift [2]: the splitting between $2s_{\frac{1}{2}}$ and $2p_{\frac{1}{2}}$ states of the hydrogen atom (See fig. 1.1.1), predicted to be degenerate by the Dirac theory.

It turned out that a large part of the reason behind this discrepancy problem lies in the theory of quantum electrodynamics (QED), which gave numerical results that were marvelously able to fill an enormous percentage of the gap between the relativistic Dirac theory and the experiment. QED is the theory that couples the quantized electronic field with the quantized photonic field, through the QED interaction Hamiltonian density:

$$\mathcal{H}^{\text{QED}}(x) = -ec\bar{\Psi}(x)\gamma^\mu\Psi(x)A_\mu(x), \quad (1.1.2)$$

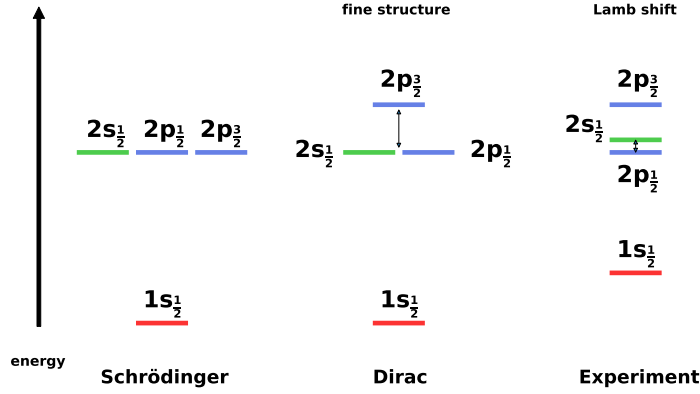


Figure 1.1.1: Pictorial comparison of different spectra.

where Ψ (and $\bar{\Psi}$) and A_μ are the quantized electron and photon field operators, respectively. Their job is to annihilate electrons and photons at spacetime point x . The unbold symbol x denotes spacetime coordinates (ct_x, \mathbf{x}) (see appendix A for notations). In this context, the non-interacting Hamiltonian contains the free electronic one (non-interacting bound electrons) in addition to the free photonic one. In the \mathcal{S} -matrix formalism, the above interaction coupling between the two fields is treated perturbatively (in powers of this interaction), as we shall see in chapter 3. We finally note that the electron-electron interaction will rise from this last interaction term, where the photon field operator creates and annihilates virtual photons that are exchanged by electrons: Electrons sense each other's existence through the exchange of photons. To give a general idea about the problem, we shall talk about the lowest-order QED corrections. In its lowest-order (e^2 or α), and with no real-photons, the scattering matrix gives rise to three QED corrections presented in fig. 1.1.2:

1. The single-photon exchange: fig. 1.1.2a
2. The vacuum-polarization: fig. 1.1.2b
3. The self-energy: fig. 1.1.2c

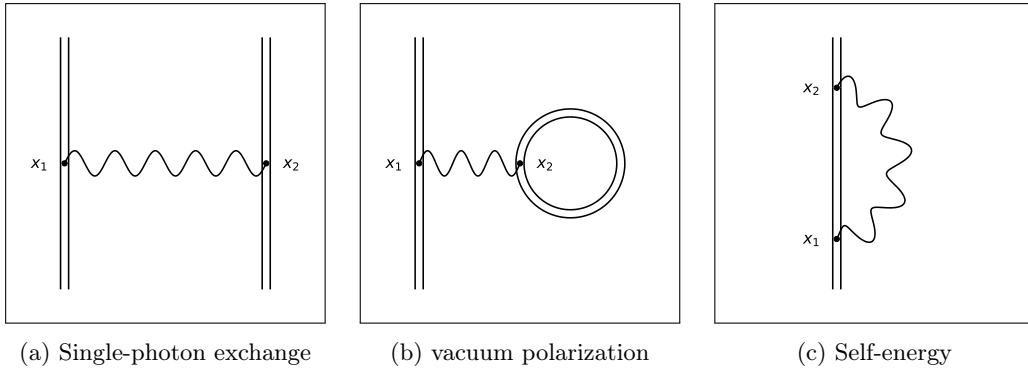


Figure 1.1.2: The lowest-order BSQED corrections

A few points to note about these diagrams:

1. x_1 and x_2 are spacetime points.
2. The external double (straight) lines represent electrons whose wavefunctions are solutions of the Dirac equation in the presence of the time-independent classical external potential (the Furry representation [3] [4, section 15g]): the Coulomb field for example.
3. The double internal electron line (as in figs. 1.1.2b and 1.1.2c) represents the electron propagator (the Dirac Green's function) which includes the effect of the time-independent external potential (the Furry representation).
4. The wiggly line represents the propagation of a virtual photon, between two spacetime points: x_1 and x_2 in our case.

The first correction concerns the interaction between two-electrons, to its lowest-order, where an electron feels the existence of (interacts with) the other electron through the exchange of a virtual photon. This correction only exists if the number of electrons in the studied system is $n \geq 2$, and can be shown to contain two contributions similar to the two-electron terms in the Hartree-Fock theory, where one is local: as the Hartree (direct) term, and the other is non-local as the Fock (exchange) term.

The second and third corrections only contain a single (straight) electron line, these corrections are to be taken into account for all systems, ranging from a simple hydrogen-like (1-electron) atom, to the complicated many-electron system.

We shall now concentrate on the simple 1-electron atoms, where the last two corrections are to be taken into account. The second diagram represents the vacuum polarization effect, which describes the interaction of an electron at x_1 with a vacuum bubble at x_2 . This bubble represents the vacuum polarization current, generated in space when an inducer (such as an atom) exists, see [5] and [6]. We shall see that this current reduces to the vacuum polarization density in the case where the inducing potential is a purely scalar one, i.e. in the case where the time-reversal symmetry is preserved. Furthermore, in the absence of an inducer, this correction will vanish, and this can be shown using Furry's theorem (charge conjugation symmetry) which will be discussed in section 3.11. The vacuum polarization effect is highly localized, and lives at very small distances close to the nucleus, strongly within the Compton wavelength: $r < \frac{\hbar}{mc}$. More precisely, the potential associated with the lowest-order (larger contribution) vacuum polarization, i.e. the Uehling potential: of order $\alpha(\alpha Z)$, decays exponentially when r becomes larger than the Compton wavelength, this is mentioned in the work of Mohr *et al.* [7, Page 268] in addition to Greiner and Reinhardt [8, Page 283]. The potential associated with the higher-order vacuum polarization: The Wichmann-Kroll term of $\alpha(\alpha Z)^3$, decays slower than the Uehling potential, and as a consequence, this correction dominates the Uehling one for atomic states with large quantum numbers n and j (getting far from the nucleus) as shown by Soff and Mohr [9, Table I], in addition to Huang [10, eqs.(23-25), eqs.(30,33)]. Generally speaking, lower bound-states will be more affected by the total $\alpha(\alpha Z)^{n \geq 1}$ vacuum polarization effects, than the higher ones. It should be noted that a process associated with an $\alpha^m(\alpha Z)^n$ -order is represented by a Feynman diagram containing m virtual photons (internal photon lines), while n in $(\alpha Z)^n$ represents the number of interactions with the external potential. The effective QED potential associated with such process is usually (in literature) written as V_{mn} . This notation was used by Huang [10], Blomqvist [11], and many others.

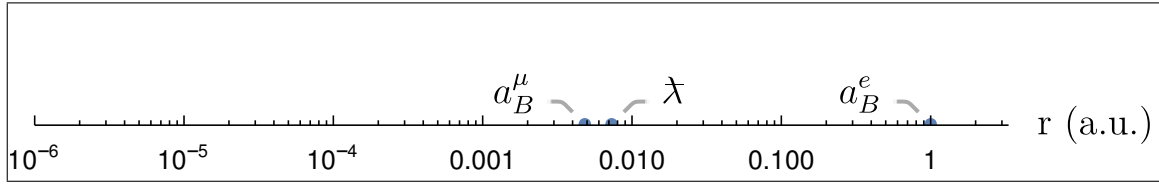
Contrary to vacuum polarization, the self-energy is a non-local effect, and it is thus (generally speaking) more complicated to evaluate, in both senses: mathematically (analytically), and numerically. As the diagram of fig. 1.1.2c shows, this effect describes a virtual photon emission and absorption by an electron. In electronic atoms, the self-energy is the dominant QED correction,

and this fact can be observed in the work of Soff *et al.* [12, Figure. 10] where they show different contributions to the Lamb shift (in hydrogen-like atoms): The Lamb shift is the splitting between the $2s_{\frac{1}{2}}$ and $2p_{\frac{1}{2}}$ states of the hydrogen-like atoms, which the Dirac equation fails to predict, and is largely described by these two QED corrections.

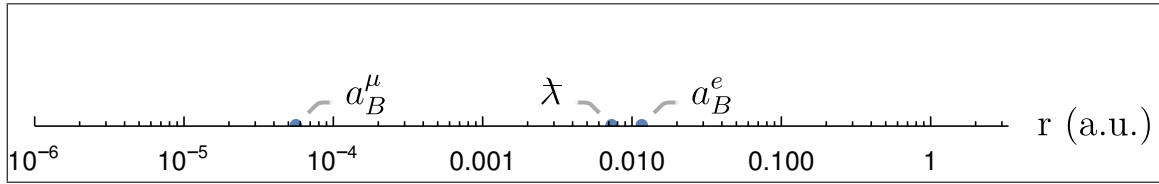
This fact of dominance of the self-energy correction in the electronic atoms is reversed once the muonic atom, instead of the electronic one, is considered. The reason behind this claim, is the very large muon mass. With a mass of around $m_\mu \approx 200m_e$, the muon thus orbits two hundred times closer to the nucleus (than an electron do), and this fact is seen by the change of the Bohr radius:

$$a_B^\mu \approx \frac{a_B^e}{200}, \quad (1.1.3)$$

as shown in figs. 1.1.3a and 1.1.3b, for the hydrogen $Z = 1$, and the radon $Z = 86$ atoms, respectively. See also [13, Fig. 1]. At these very small distances the vacuum polarization effect lives, and thus dominates the self-energy, as mentioned by Mohr *et al.* [7, Page 266] Greiner and Reinhardt [8, Pages 288-290] (see also the work of Dubler *et al.* [14]).



(a) The hydrogen atom case.



(b) The radon atom case.

Figure 1.1.3: The reduced Compton wavelenght $\lambda = \frac{\hbar}{mc}$, with electronic a_B^e and muonic a_B^μ Bohr radii in hydrogen and radon atoms.

Once the perturbation (correction) expansion of the energy (or wavefunction) is performed, one obtains two kinds of contributions:

- Radiative corrections: in which the representing Feynman diagrams contain electron loops or electron-photon loops, as the ones shown in figs. 1.1.2b and 1.1.2c.
- Non-radiative corrections: in which electrons only exchange virtual photons. In its lowest-order, two electrons can exchange a single-photon, giving rise to the electron-electron interaction (including the effect of retardation), which is presented in fig. 1.1.2a. The higher-order diagrams account for higher-orders of photon exchanges (correlation corrections).

For discussions about this distinction, the reader may consult the book of Lindgren [15], in addition to the chapter of Indelicato and Mohr [16].

So far, in quantum chemistry, as well as in molecular physics, electron correlation effects are very well studied and understood, while radiative corrections are not to the same extent. The inclusion of these QED corrections in numerical computations is a very challenging task, due to the enormous complication which arises when a system consists of a relatively big number of electrons orbiting a molecular (generally non-radial) nuclear potential. The main attempts to take these radiative corrections into account were made by including some of the low-order corrections in the form of effective potentials (Hamiltonians), describing the vacuum polarization and the self-energy processes. These potentials are going to be discussed in section 3.12. The reader should note that the two main limitations, associated with the inclusion of the QED corrections in numerical calculations are:

1. Although the effective self-energy potentials (discussed in section 3.12.2) have demonstrated their ability to obtain accurate energy corrections -compared to more sophisticated calculations- (remember that these potentials are made to do so), their validity for other quantities such as the wavefunction or the molecular properties is undoubtedly questionable.
2. One can, in principle, proceed in the hard way, using much more accurate methods, without the need for any kind of energy fitting (as for the effective self-energy potentials), as done in: [6, 7, 17, 18, 19, 20] and many other related references, to get very good results. Unfortunately, this track is not very well suited for practical calculations and can only be taken for "simple" systems, such as one- to few-electron atoms, but not for the many-electron molecules, which is the obvious reason why we use the effective potentials instead.

Due to these two limitations, we decide to proceed on a completely different path: Computing these corrections in a quantum-chemistry fashion: in a fast numerical way. In this procedure, the QED quantities are constructed from the numerical solutions (energies and wavefunctions) of the Dirac equation. The main advantages of this choice of path are:

1. The obtained quantities are free of energy parametrization (fitting) and as a consequence, the obtained quantities, such as the wavefunctions and the molecular properties are more valid, at least in principle.
2. It is not very computer time expensive (numerically speaking), as we expect so far.

Due to the complexity of the non-local self-energy correction, this thesis will focus on the vacuum polarization correction, since it is relatively easier to handle, both analytically and numerically. The reader should note that this massaging of the relativistic quantum chemistry to test its capability to compute the vacuum polarization density, leads to a better understanding of how we can extend our acquired skills/manipulations to solve the:

1. Self-energy problem in the finite basis set.
2. The Hartree-Fock problem which includes the QED corrections.
3. Extend the QED-effects inclusion to high-level quantum chemistry methods.

Unfortunately, the work for this thesis is limited in time, and these three points will be beyond this Ph.D. project. Nevertheless, we are going to give our vision on how one can proceed to attack these problems in section 3.13, and the final section of this thesis will concern our perspectives about the future steps to be taken.

1.2 Thesis structure

In chapter 2, we shall discuss the Dirac equation and its associated discrete symmetries, both in the abstract mathematical form and once this equation is approximated by a finite number of basis functions, typically by Gaussian functions. The charge conjugation symmetry (\mathcal{C} -symmetry) will be of central importance in this thesis, and the study associated with it has gave birth to our article titled "Charge Conjugation Symmetry in the Finite Basis Approximation of the Dirac Equation" [21] where we carefully point out the conditions which make the finite basis set \mathcal{C} -symmetric. In the basis set approximation, a set of basis functions must be carefully designed to avoid the numerical instabilities and the occurrence of unphysical (spurious) solutions. This chapter shall discuss different choices of basis set schemes and present their associated pros and cons. At the end of the chapter, we shall present the results of a few calculations done on the one-electron Dirac problem in the presence of a Coulombic $-\frac{Ze^2}{4\pi\epsilon_0 r}$ potential, and discuss the practical realization of the charge conjugation symmetry, in the finite basis approximation.

In chapter 3, we will derive the \mathcal{S} -matrix (scattering matrix) and present the mathematical machinery associated with it. In addition, we will compute the second-order $\mathcal{S}^{(2)}$ -matrices associated with the three physical QED processes discussed in the previous section. Furthermore, the three corresponding energy-shifts are going to be derived. Usually, these derivations are very briefly presented in literature, with missing important derivation steps. We have therefore decided to provide a detailed derivation that suits (up to some extent) a new learner of Bound State Quantum Electrodynamics (BSQED), in the context of the \mathcal{S} -matrix theory. Furthermore, we will briefly discuss the effective QED potentials in the last part of this chapter. Finally, this chapter will end with a general discussion that concerns the foundations for including QED corrections in the simplest many-electron approximation, i.e., the Hartree-Fock theory, without the need to use effective potentials. Once this machinery is made working, this will pave the way for the more sophisticated quantum chemical methods such as coupled-cluster or configuration-interaction methods. It should be also noted that including these corrections in a self-consistent manner will allow the inclusion of some higher-order corrections, that can be represented by reducible diagrams. The main challenge is still to handle divergences that exist, not only on paper but also in numerical computations. These divergences can be seen in our case by inspecting the non-converging numerical QED quantities once the basis set size (number of basis functions) is increased.

Chapter 4 will be dedicated to the vacuum polarization problem, already encountered in chapter 3. We shall first concentrate on deriving the mathematical quantities, and then attack the numerical evaluation problem. Several vacuum polarization density calculations associated with different choices of basis sets will be performed, presented, and discussed in detail. On top of that, we shall use what we have learned in the first chapter about the \mathcal{C} -symmetry to design better basis functions. In addition, the time-reversal symmetry (\mathcal{T} -symmetry) is going to be used simplify the vacuum polarization density expression in the cases where the external vector potential vanishes.

All the equations of this thesis are written in SI units, in order to make it easier for the reader to convert to his desired system of units. The general notations and definitions of several elementary quantities are given in appendix A. Finally, the extra information, derivations, and results are placed in the remaining appendices B to J and referred to from our four chapters.

1.3 Numerical details

In all our numerical calculations using Mathematica [22], we are going to set the fine structure constant parameter to be the latest experimental result [23, table XXX]:

$$\alpha = 7.2973525693(11) \times 10^{-3}. \quad (1.3.1)$$

This information is needed in case one wants to reproduce our results. In addition, we note that the performed calculations are of very high precision. The general mathematical expressions are taken in their exact form, which means that there is no loss of precision at this level. On the other hand, the evaluation of the eigenvalue problems is (surely) done numerically, with a precision of up to a hundred significant decimal digits. In our approximations of the radial Dirac equation, we are going to use the Gaussian basis functions, of the following form:

$$\pi_{\ell,i}(r) = r^{\ell+1} e^{\zeta_{\ell,i} r^2}, \quad \text{for } i = 1, n_\ell \quad (1.3.2)$$

with n_ℓ the number of basis functions associated with the orbital quantum number ℓ . For each quantum number ℓ , a basis set is constructed with respect to a list of exponents:

$$\zeta_\ell = \{\zeta_{\ell,1}, \dots, \zeta_{\ell,n_\ell}\}. \quad (1.3.3)$$

Kenneth Dyall has optimized these exponents for the two-electron noble gases, such that they lead to the lowest possible energy for the two-electron system in their ground-state [24] (See section E.3). We are going to use these exponents in our one-electron calculations, which is perfectly safe, as we shall see in chapter 2. Our calculations will all be on the radon atom ($Z = 86$), and the motivations to do so were 1) we have the exponents of Dyall exponents, and 2) this is a heavy element, which indicates that its QED corrections will be more pronounced. The exponents associated with this element are presented in tables E.3 to E.5 of the appendix.

Chapter 2

The Dirac equation

It seems that if one is working from the point of view of getting beauty in one's equations, and if one has really a sound insight, one is on a sure line of progress.

Paul Adrien Maurice Dirac [25]

In this chapter, we shall discuss the historical roots of the Dirac equation, as well as many of its interesting features, including its associated discrete symmetries, its radial form (the atomic problem), and its approximation with a finite number of basis functions (the finite basis approximation). We shall also discuss how these relativistic basis sets must be carefully designed by taking into account some "proper" requirements in order to maintain numerical stability: prevent numerical failures such as 1) appearance of spurious solutions 2) converging to an energy that is lower than the exact one 3) violation of quantum mechanical (discrete) symmetries. An additional significant problem concerns the consideration of the negative-energy solutions. When solving the time-independent Dirac equation, one obtains a set of positive and negative-energy solutions. Conventionally, in (relativistic) atomic physics and quantum chemistry, we are interested in the (experimentally observed) bound-states. This interest bias has led us to pay less attention to (and eventually discard) the negative-energy solutions, and this is clearly justified. This disregard of the negative-energy solutions can (and will) be problematic when these solutions are needed to construct some specific physical quantities, as the quantum electrodynamic ones, for example: vacuum polarization and self-energy quantities, as we shall see in the following two chapters. We will thus consider some specific basis functions prescriptions that guarantee 1) a fair description for both positive and negative-energy solutions and 2) the obedience of the physical symmetry between them: the charge conjugation symmetry (\mathcal{C} -symmetry). Consequently, we shall see in chapter 4 how these two considerations are going to considerably improve the validity of the numerically calculated quantum electrodynamic quantities.

2.1 The Klein-Gordon equation: A first relativistic quantum theory

In his article [26], Gordon proposed replacing the momentum and energy values by their corresponding operator form [26, eq.(1)]:

$$\mathbf{p} \rightarrow -i\hbar \nabla \quad (2.1.1)$$

$$E \rightarrow +i\hbar \frac{\partial}{\partial t}, \quad (2.1.2)$$

in the relativistic energy-momentum relation:

$$E^2 = m^2 c^4 + c^2 \mathbf{p}^2. \quad (2.1.3)$$

His attempt was inspired by the (non-relativistic) Schrödinger equation, which can be obtained from the classical energy expression of a particle of mass m freely traveling with a momentum \mathbf{p} :

$$E = \frac{\mathbf{p}^2}{2m}. \quad (2.1.4)$$

After substituting energy and momentum as given in eqs.(2.1.1,2.1.2), one obtains the Schrödinger equation:

$$i\hbar \frac{\partial}{\partial t} \psi(x) = -\frac{\hbar^2}{2m} \nabla^2 \psi(x) \quad (2.1.5)$$

that acts on the wavefunction $\psi(x)$. This simple approach leads to the first relativistic (Lorentz-invariant) quantum mechanical equation of motion:

$$\left[\square + \left(\frac{mc}{\hbar} \right)^2 \right] \psi(x) = 0; \quad \square = \frac{1}{c^2} \frac{\partial^2}{\partial t^2} - \nabla^2, \quad (2.1.6)$$

known as the Klein-Gordon equation. For details about the historical development of this equation, the reader can consult [27]. The obvious good thing about the Klein-Gordon equation is that it is a relativistic equation, and as a consequence, it treats time and space derivatives equally and thus is Lorentz invariant, unlike the Schrödinger equation, where the time- and space-derivatives are not of the same order. In addition, it can be shown that this equation recovers, in the non-relativistic limit, the Schrödinger equation. See, for instance, [28, section 1.3]. Dirac was not satisfied by the Klein-Gordon equation, for the reasons discussed in the next section. He has thus decided to give the problem another try. Here are the words of Dirac about an incident that happened during the 1927 fifth Solvay Conference [29, page 1047]:

During the period before the lecture started on one occasion, Bohr came up to me and asked me: “What are you working on now?” I said: “I’m trying to get a relativistic theory of the electron.” Then Bohr said: “But Klein has already solved this problem.” I was a bit taken aback by this.

Paul Adrien Maurice Dirac

In the next section, we will present the downsides of the Klein-Gordon equation once used to predict the electron behavior. These downsides induced Paul Dirac to come up with a new elegant quantum equation, later known as the Dirac equation, that has generalized the Schrödinger equation to the relativistic domain and predicted various behaviors of the electron (spin 1/2 particles).

2.2 Problems with the Klein-Gordon theory

The first point that does not fit with our knowledge of the non-relativistic theory, is the existence of the negative-energy solutions, which cannot be simply discarded, since quantum mechanics (in contrary to classical mechanics) tells us that a particle can perform transitions from a positive-energy state to a negative-ones, and emit an amount of energy (as mentioned by Dirac [30, page 612]), which in our considered case is enormous (at least equal to $2mc^2$). The second trouble comes from the probability density that enters the continuity equation (probability conservation) associated with the Klein-Gordon equation. To see how, we shall start by the Schrödinger equation. After multiplying the Schrödinger equation with the conjugate of the wave function, one obtains:

$$i\hbar\psi^*\frac{\partial}{\partial t}\psi = -\frac{\hbar^2}{2m}\psi^*\nabla^2\psi, \quad (2.2.1)$$

and by complex conjugating this equation, one would get:

$$i\hbar\psi\frac{\partial}{\partial t}\psi^* = \frac{\hbar^2}{2m}\psi\nabla^2\psi^*. \quad (2.2.2)$$

Summing up these two equations leads to the continuity equation associated with the conservation of the probability:

$$\frac{\partial}{\partial t}(\psi\psi^*) = -\frac{\hbar}{2mi}[\psi^*\nabla^2\psi - \psi\nabla^2\psi^*] = -\nabla \cdot \frac{\hbar}{2mi}[\psi^*\nabla\psi - \psi\nabla(\psi)^*], \quad (2.2.3)$$

where one sees that the time-derivative of the modulus square of the wavefunction:

$$\rho(x) = \psi(x)\psi^*(x), \quad (2.2.4)$$

which is interpreted as a probability density, equals the negative divergence of \mathbf{j} :

$$\mathbf{j}(x) = \frac{\hbar}{2mi}[\psi^*(x)\nabla\psi(x) - \psi(x)\nabla\psi^*(x)], \quad (2.2.5)$$

which is interpreted as a probability current. The extension of this approach to the Klein-Gordon equation leads to conceptual problems. This form of continuity equation (2.2.3) already appears in different fields of physics and math, such as: fluid dynamics, classical electrodynamics, probability distributions, and finally, quantum mechanics. We shall briefly present the main concepts of a general continuity equation. The general continuity equation has the following form:

$$\frac{\partial}{\partial t}\rho(x) + \nabla \cdot \mathbf{j}(x) = s(x), \quad (2.2.6)$$

where one sees:

1. The density ρ of some physical quantity, we shall call q .
2. The current density \mathbf{j} of this quantity, related to the density by $\mathbf{j} = \rho\mathbf{v}$, where \mathbf{v} is the velocity field vector.
3. The source term s which is generally a function of spacetime x . This term can be:
 - (a) of a positive value: The amount of q increases in the system (source case).
 - (b) of a negative value: The amount of q decreases in the system (sink case).

(c) vanishing: The amount of q is conserved.

An important point to note, is that the continuity equation (current expression) tells us that the wavefunction must be complex, and that the increase/decrease of the density of q with the time-flow, competes with the divergence of the current density (flow of ρ). The divergence of some vector-field measures the outward flux of this vector field throughout the surface that encloses an infinitesimal volume at the point in question. In the case where the studied quantity is conserved, the decrease/increase of the density ρ when time passes, is exactly balanced by the positive/negative flux of the q flow. This concept is extended to quantum mechanics, where the general quantity q becomes the probability that flows dynamically in space and time, as a fluid.

Following the (almost) identical steps used to obtain the probability current associated with the Schrödinger equation, one obtains the compact relativistic probability current conservation (continuity) equation:

$$\partial_\mu j^\mu(x) = 0; \quad j^\mu(x) = \frac{i\hbar}{2m} [\psi^*(x) \partial^\mu \psi(x) - \psi(x) \partial^\mu \psi^*(x)], \quad (2.2.7)$$

associated with the Klein-Gordon solution. One main problem that arise here, is the probability density:

$$\rho(x) = j^0(x)/c = \frac{i\hbar}{2mc^2} [\psi^*(x) \partial_t \psi(x) - \psi(x) \partial_t \psi^*(x)]. \quad (2.2.8)$$

These expressions for probability density and current have first appeared in the work of Gordon [26, eq.(21.a)] and Klein [31, eq.(18)]. The problem with the last expression of probability is that it is not positive definite, and this can be seen by the replacement of $i\hbar\partial_t$ by the energy E (factorization of the wavefunction), leading to [32, eq.(2.4.9)] [4, page 55 eq.(7)]:

$$\rho(x) = \frac{E}{mc^2} \psi^*(x) \psi(x), \quad (2.2.9)$$

which for negative-energy solutions –allowed by the Klein-Gordon (Energy momentum relation)– gives a negative probability density, and this is not physically accepted. In addition, in his discussion, Grant [32, section 2.4] shows that this probability density can be negative also for positive-energy solutions (see eq.(2.4.16) of the citation), when the electron is allowed to interact with a (time-independent) scalar external potential. This shows another problematic aspect of the Klein-Gordon equation, which is also pointed out by Ohlsson in [33, section 2.4], Schweber [4, page 63 eq.(49)] and Greiner [28, eq.(1.130)]. The interacting Klein-Gordon's four-current that satisfies the continuity equation is found to be (see eq.(J.2.2)):

$$j^\mu = \frac{i\hbar}{2m} (\psi^* \partial^\mu \psi - \psi \partial^\mu \psi^*) + \frac{e}{m} A^\mu \psi^* \psi, \quad (2.2.10)$$

where A^μ is the external electromagnetic potential, and $\psi(x)$ is now a solution of the interacting Klein-Gordon equation:

$$\left[\left(\partial^\mu + \frac{e}{i\hbar} A^\mu \right) \left(\partial_\mu + \frac{e}{i\hbar} A_\mu \right) + \frac{m^2 c^2}{\hbar^2} \right] \psi(x) = 0. \quad (2.2.11)$$

The Klein-Gordon's probability density is the zeroth component of eq.(2.2.10):

$$\rho = j^0/c = \frac{E + e\varphi}{mc^2} \psi^* \psi, \quad (2.2.12)$$

which for a point nuclear charge, and a positive-energy state, is negative for a radius smaller than:

$$r < \frac{Ze^2}{4\pi\epsilon_0 E}. \quad (2.2.13)$$

The third problem, is that the Klein-Gordon equation is of second-derivative in time instead first- (as in the Schrödinger equation case), which means that one needs to know the wavefunction that one needs to know the wavefunction $\psi(t_0)$ and its derivative $\frac{\partial\psi}{\partial t}|_{t=t_0}$ at some initial time $t = t_0$, in order to determine the wavefunction at a later time $\psi(t)$, with $t > t_0$, which added an extra degree of freedom which was not present in the Schrödinger theory. In addition, this second derivative in time did not fit with the “transformation theory” developed by Paul Dirac in [34], on which he commented in 1977 [35, page 89]:

“I think that is the piece of work which has most pleased me of all the works that I’ve done in my life ... The transformation theory (became) my darling I just couldn’t face giving up the transformation theory.”

This theory which was based on an equation of motion of the form of:

$$H\psi = i\hbar \frac{\partial}{\partial t} \psi, \quad (2.2.14)$$

(as mentioned by Dirac in [30, page 612]) which is sometimes called a Schrödinger-type equation, and which is clearly not the case of the Klein-Gordon equation. All these arguments motivated Paul Dirac to seek for an alternative relativistic equation, which should be consistent with the Klein-Gordon equation, i.e. obey the Einstein energy-momentum relation, but in which the time derivative is of first-order instead of second.

2.3 Towards the Dirac equation

As pointed out by Schweber in [36, p.57-58], having a Hamiltonian equation with the form of the last equation will always lead to a positive probability density. We thus consider a Hamiltonian operator H which can, in general, be a matrix containing linear differential, and multiplicative (as the potential) operators. This Hamiltonian acts on the wavefunction ψ that satisfies the eq.(2.2.14) of motion. Notice that this is consistent with the Schrödinger and Pauli equations (as well as the Dirac one, as we shall shortly see). After the multiplication of this equation by the conjugate transpose solution from the left side, one obtains:

$$\psi^\dagger H \psi = +i\hbar \psi^\dagger \frac{\partial}{\partial t} (\psi). \quad (2.3.1)$$

The corresponding conjugate transpose equation is thus:

$$\psi^\dagger \overleftarrow{H} \psi = -i\hbar \frac{\partial}{\partial t} (\psi^\dagger) \psi, \quad (2.3.2)$$

where the arrow on the top of the Hamiltonian indicates that it differential operator(s) acts on the left-side instead of the right one. After taking the difference between these two equations, one gets:

$$\frac{1}{i\hbar} \left\{ \psi^\dagger H \psi - \psi^\dagger \overleftarrow{H} \psi \right\} = \frac{\partial}{\partial t} (\psi^\dagger \psi), \quad (2.3.3)$$

where one directly notices the term that is time-differentiated:

$$\psi^\dagger \psi = \rho. \quad (2.3.4)$$

This term is never negative, and can be interpreted as a probability density. The reader can notice that the equation of motion we have started with solves two problems that appeared with the Klein-Gordon theory:

1. The need of the $\partial\psi/\partial t|_{t=t_0}$ value to determine the wavefunction at a future time $t > t_0$.
2. The probability density that can be negative.

Finally, the remaining term of the l.h.s. of eq.(2.3.3) which we assume can be written as:

$$\frac{1}{i\hbar} \left\{ \psi^\dagger H \psi - \psi^\dagger \overleftarrow{H} \psi \right\} = -\nabla \cdot \mathbf{j}, \quad (2.3.5)$$

where \mathbf{j} is the probability current, completes the continuity equation. At this point, Dirac sets the goal to seek for a new relativistic equation which can be thought as a “square-root” of the Klein-Gordon one, an equation consistent with the latter one, but this time with a first-order time-derivative, and therefore, with first-order space derivatives, since relativity, by its essence is a theory that treats space and time equally, as mentioned by Dirac in [30, page 613].

2.4 The Dirac equation

In his great book [37], Dirac explains in a pedagogical way how he one can proceed to reach the celebrated final Dirac equation. As a first proposal of what might this equation be, he suggests:

$$\left[\hat{p}_0 - \sqrt{\hat{\mathbf{p}}^2 + m^2 c^2} \right] \psi(x) = 0; \quad \text{where} \quad \begin{cases} \hat{p}_0 &= +\frac{i\hbar}{c} \frac{\partial}{\partial t} \\ \hat{\mathbf{p}} &= -i\hbar \nabla \end{cases}, \quad (2.4.1)$$

which after the application of the operator $\left[\hat{p}_0 + \sqrt{\hat{\mathbf{p}}^2 + m^2 c^2} \right]$ from the right, leads to the Klein-Gordon eq.(2.1.6), and thus, such equation describes a particle obeying the energy-momentum relation. Dirac then states that the problem with this proposal is that it does not treat space- and time-derivatives equitably, and proposes the following equation:

$$[\hat{p}_0 - \alpha_1 \hat{p}_1 - \alpha_2 \hat{p}_2 - \alpha_3 \hat{p}_3 - mc\beta] \psi(x) = 0, \quad (2.4.2)$$

where the three quantities α_i and β are constants of unknown nature. After the application of the operator $[\hat{p}_0 + \alpha_1 \hat{p}_1 + \alpha_2 \hat{p}_2 + \alpha_3 \hat{p}_3 + mc\beta]$ on the left side of the last equation gives:

$$\begin{aligned} & \left[\hat{p}_0^2 - m^2 c^2 \beta^2 - \hat{p}_1^2 \alpha_1 \alpha_1 - \hat{p}_2^2 \alpha_2 \alpha_2 - \hat{p}_3^2 \alpha_3 \alpha_3 \right. \\ & - \hat{p}_2 \hat{p}_1 \alpha_2 \alpha_1 - \hat{p}_1 \hat{p}_2 \alpha_1 \alpha_2 - \hat{p}_3 \hat{p}_2 \alpha_3 \alpha_2 - \hat{p}_2 \hat{p}_3 \alpha_2 \alpha_3 - \hat{p}_1 \hat{p}_3 \alpha_1 \alpha_3 - \hat{p}_3 \hat{p}_1 \alpha_3 \alpha_1 \\ & \left. - mc\hat{p}_1 \alpha_1 \beta - mc\hat{p}_1 \beta \alpha_1 - mc\hat{p}_2 \alpha_2 \beta - mc\hat{p}_2 \beta \alpha_2 - mc\hat{p}_3 \alpha_3 \beta - mc\hat{p}_3 \beta \alpha_3 \right] \psi(x) = 0. \end{aligned} \quad (2.4.3)$$

In order for this equation to reduce to the Klein-Gordon equation the quantities α_i 's and β should obey the following relations [30, eq.(6)] [28, eq.(2.8)]:

$$\beta^2 = \mathbb{1}_4 \quad (2.4.4)$$

$$\alpha_i \alpha_j + \alpha_j \alpha_i = 2\delta_{ij} \mathbb{1}_4 \quad (2.4.5)$$

$$\alpha_i \beta + \beta \alpha_i = \mathbb{0}_4, \quad (2.4.6)$$

for all $i = 1, 2, 3$. This means that these quantities cannot be scalar ones, and should be matrices. In addition, for physical purposes, these matrices should be hermitian. Dirac first tried with the three Pauli matrices and later commented [29, page 1052]:

“It took me quite a while, studying over this dilemma, before I suddenly realized that there was no need to stick to the quantities σ , which can be represented by matrices with just two rows and columns”

In [38, exercise 13.1] of Greiner’s book we see that any 2×2 matrix can be written in the basis of the three Pauli matrices and the unit operator $\mathbb{1}_2$, which means that it is only possible to have three commutation relations associated with the basis elements of a 2×2 matrix. In addition, in his book on relativistic quantum mechanics [28, chapter 2] it is shown that the dimensions of these matrices should be even, and since the 2×2 case is discarded, the smallest possible dimensions for the Dirac matrices are 4×4 (see also Gross [39, section 5.1], Bjorken and Drell [40, section 1.3]) and all higher dimensional cases can be reduced to four dimensions. The Dirac equation can be written in a compact covariant form as:

$$\left[i\hbar\gamma^\mu \frac{\partial}{\partial x^\mu} - mc\mathbb{1}_4 \right] \psi(x) = 0, \quad (2.4.7)$$

where the summation runs over $\mu = 0, 1, 2, 3$, and the gamma matrices are related to the previous matrices by:

$$\gamma^\mu = \begin{cases} \beta & \text{for } \mu = 0 \\ \beta\alpha^\mu & \text{for } \mu = 1, 2, 3. \end{cases} \quad (2.4.8)$$

and as a consequence, the anticommutation relations that these gamma matrices should obey are compactified in:

$$\{\gamma^\mu, \gamma^\nu\} = \gamma^\mu\gamma^\nu + \gamma^\nu\gamma^\mu = 2g^{\mu\nu}\mathbb{1}_4, \quad (2.4.9)$$

where $g^{\mu\nu} = \text{diag}(+1, -1, -1, -1)$ is the flat-space Minkowski metric tensor. Any choice of gamma (related to alpha and beta) matrices that respects the anticommutation relations of eq.(2.4.9) is a valid choice, and is called a representation of the Dirac matrices. Here are the main representations:

1. The Dirac (standard) representation:

$$\gamma_D^0 = \begin{bmatrix} +\mathbb{1}_2 & 0 \\ 0 & -\mathbb{1}_2 \end{bmatrix}, \quad \text{and} \quad \gamma_D^i = \begin{bmatrix} 0 & +\sigma_i \\ -\sigma_i & 0 \end{bmatrix}, \quad (2.4.10)$$

where subscript “D” stands for Dirac. This is the most popular representation, in which the Dirac equation spinor is written as:

$$\psi_D = \begin{bmatrix} \psi_D^L \\ \psi_D^S \end{bmatrix}, \quad (2.4.11)$$

where ψ_D^L and ψ_D^S are the large and small two-component wavefunctions, respectively. The reason behind this naming is that for positive-energy solutions (in which physicists and chemists are interested) the upper component wavefunction is (on average) larger than the lower one. To show why this is right, we consider the case of an electron interacting with an external scalar potential φ . The lower component can be written as:

$$\psi_D^S = \frac{c\boldsymbol{\sigma} \cdot \mathbf{p}}{mc^2 + E + e\varphi} \psi_D^L, \quad (2.4.12)$$

which “very roughly speaking” behaves as $\psi_D^S \approx \frac{v}{2c} \psi_D^L$ for the minimal positive-energy $E = mc^2$. It is important to note that this choice of matrices is not unique. Following Pauli [41, Théorème fondamental], Feynman [42, Equivalence Transformation p.44] and Ohlsson [33, s.Theorem 3.1], one can consider any invertible constant (variable-independent) 4×4 matrix, let us call it S , and act with it on the Dirac equation (2.4.7), in addition, insert the unit matrix $S^{-1}S$, to obtain:

$$\left[i\hbar S \gamma_D^\mu S^{-1} \frac{\partial}{\partial x^\mu} - mc \mathbb{1}_4 \right] S \psi_D(x) = 0. \quad (2.4.13)$$

If we now call $S \psi_D(x) = \psi_X(x)$ our new (matrix-transformed) wavefunction in the X representation, and $S \gamma_D^\mu S^{-1} = \gamma_X^\mu$ the new gamma matrices, one can show that the new γ_X^μ matrices do obey the defining anticommutation relations of eq.(2.4.9), and thus correspond to a valid choice of matrices. Next, we present some of the other choices of gamma matrices.

2. The Weyl representation:

$$\gamma_W^0 = \begin{bmatrix} 0 & +\mathbb{1}_2 \\ +\mathbb{1}_2 & 0 \end{bmatrix}, \quad \text{and} \quad \gamma_W^i = \begin{bmatrix} 0 & +\sigma_i \\ -\sigma_i & 0 \end{bmatrix}, \quad (2.4.14)$$

which can be generated from the Dirac representation matrices:

$$\gamma_W^\mu = S \gamma_D^\mu S^{-1}; \quad \text{with} \quad S = \frac{1}{\sqrt{2}} (\mathbb{1}_4 - \gamma_D^5 \gamma_D^0), \quad (2.4.15)$$

where γ_D^5 is the fifth gamma matrix given in eq.(A.0.11).

3. The Majorana representation:

$$\begin{aligned} \gamma^0 &= \begin{bmatrix} 0 & +\sigma_2 \\ +\sigma_2 & 0 \end{bmatrix}, & \gamma^1 &= \begin{bmatrix} +i\sigma_3 & 0 \\ 0 & +i\sigma_3 \end{bmatrix} \\ \gamma^2 &= \begin{bmatrix} 0 & -\sigma_2 \\ +\sigma_2 & 0 \end{bmatrix}, & \gamma^3 &= \begin{bmatrix} -i\sigma_1 & 0 \\ 0 & -i\sigma_1 \end{bmatrix}, \end{aligned} \quad (2.4.16)$$

where all matrices are imaginary ones. This representation has the advantage of making the Dirac equation real, since $i\hbar \partial_\mu \gamma^\mu$ is, as pointed out by [43, footnote page 49]. These matrices are generated from the Dirac ones by:

$$\gamma_M^\mu = S \gamma_D^\mu S^{-1}; \quad \text{with} \quad S = \frac{1}{\sqrt{2}} \gamma_D^0 (\mathbb{1}_4 + \gamma_D^2). \quad (2.4.17)$$

For the rest of this thesis, we are only going to consider working with the Dirac-representation choice of gamma matrices and we shall thus drop the D subscript. In addition, when a matrix quantity is summed with a scalar one, the reader has to remember that this scalar quantity is always multiplied by the unit matrix $\mathbb{1}_4$.

The great success of the Dirac equation comes from the fact that despite its compact form, it encodes an enormous amount of physics, which is one way of defining poetry, that (unfortunately) Dirac did not admire (see [44, page 8]). The Dirac equation was able to account, in a natural way, for:

- The electron spin. This result was consistent with that of the Pauli equation, which was invented to describe the spin angular momentum theory (or what Pauli called: “two-valuedness not describable classically” in his great noble prize lecture [45]), and which was missing in the Schrödinger theory.

- The fine structure splitting: the splitting between $2p_{\frac{1}{2}}$ and $2p_{\frac{3}{2}}$ states, which was predicted to vanish (degeneracy) by the Schrödinger theory, see fig. 1.1.1. This splitting comes after adding the relativistic corrections to the Schrödinger theory, with the spin-orbit coupling term, which is thus related to the previous point.

If one performs an expansion of the Dirac equation in the limit of small velocities (non-relativistic limit), as described for example by Gross [39, section 5.7], Schwabl [46, section 9.1.3 eq.9.1.22] and Greiner [28, section 11.1], one can see that the Dirac equation contains the following terms:

- The relativistic mass correction to the non-relativistic kinetic energy operator.
- Electron spin magnetic moment g-factor.
- The Zeeman term: the interaction between the external magnetic field, and the total angular momentum (spin and orbital).
- The spin-orbit interaction.
- The Darwin term, which represents the *Zitterbewegung* effect: a jittery motion of the electron around its region. For a point nucleus, the Darwin term only affects wavefunctions that does not vanish at the origin ($\ell \geq 1$).
- The prediction of antimatter, which manifested by the charge conjugation symmetry of the Dirac equation.

2.5 A few words on Dirac's negative-energy states

Despite the greatness of his equation (1928) in predicting the hydrogen spectrum (the positive-energy eigenvalues), Dirac struggled with giving a physical meaning of the negative-energy solutions, and this was expressed in Dirac's words during a conversation with Jagdish Mehra in Miami, Florida, 28 March 1969 [29, page 693]:

“I felt that writing this paper on the electron was not so difficult as writing the paper on the physical interpretation.”

Two years after publishing his equation, Dirac published an article titled “A theory of electrons and protons ” in 1930 [47] in which he proposed:

“The most stable states for an electron (the states of lowest energy) are those with negative energy and very high velocity. All the electrons in the world will tend to fall into these states with emission of radiation. The Pauli exclusion principle, however, will come into play and prevent more than one electron going into any one state”

which was later known as the Dirac sea of occupied negative-energy electron states. As the last article's title tells, Dirac investigated what might this negative-energy particle be, and pointed out to what paradoxes arise if one declares this particle to be a proton (see page 362 of the last citation). Later, in 1931, Dirac said [48, page 61]:

“Subsequent investigations, however, have shown that this particle necessarily has the same mass as an electron and also that, if it collides with an electron, the two will have a chance of annihilating one another much too great to be consistent with the known stability of matter.”

and cited Weyl's book, which was hopefully translated to English by Robertson [49, page 225]:

“ ... But this can be done by retaining the same external field with potentials f and replacing e by $-e$. We denote such a particle, whose mass is the same as that of the electron but whose charge is e instead of $-e$, as a "positive electron"; it is not observed in Nature !”

Two years after, Anderson [50] detected this positive electron, which was later called positron. See also [51]. On the other hand, electron and positron wavefunctions are related by the following formulas:

$$\psi_e(x) = \psi_e(\mathbf{x}) e^{-iE_e t} \quad (2.5.1)$$

$$\begin{aligned} \psi_p(x) &= \psi_p(\mathbf{x}) e^{-iE_p t} \\ &= \mathcal{C} \{ \psi_e(\mathbf{x}) e^{-iE_e t} \} = \{ \mathcal{C} \psi_e(\mathbf{x}) \} e^{+iE_e t} = \{ \mathcal{C} \psi_e(\mathbf{x}) \} e^{-iE_e(-t)}, \end{aligned} \quad (2.5.2)$$

through the charge conjugation operation (\mathcal{C}), which will be soon discussed. This fact motivated Stückelberg (supported by Feynman) to propose that positrons are electrons, propagating backwards in time. See Feynman [52]. Finally, we should note that these vague metaphoric phrases need to be understood in a more abstract (poetic) way rather than a religious (strict) one, since the latter way can lead to problematic conceptual confusions. We thus quote Zee [53, page 113]:

In closing this chapter let me ask you some rhetorical questions. Did I speak of an electron going backward in time? Did I mumble something about a sea of negative energy electrons? This metaphorical language, when used by brilliant minds, the likes of Dirac and Feynman, was evocative and inspirational, but unfortunately confused generations of physics students and physicists.

For interesting discussions on the history of the relativistic quantum mechanics, the reader may consult Weinberg [54, section 1.1], Mehra in [35] and [29].

2.6 Time-dependent Dirac equation

The time-dependent Dirac equation is given by:

$$[i\hbar\gamma^\mu\partial_\mu - mc]\psi(x) = 0, \quad (2.6.1)$$

where the elementary terms are:

1. The four-gradient $\partial_\mu = \frac{\partial}{\partial x^\mu} = (\frac{1}{c}\frac{\partial}{\partial t}, \nabla)$.
2. The four-gamma matrix $\gamma^\mu = (\gamma^0, \boldsymbol{\gamma})$. We shall stick with the Dirac representation.
3. The four-component wavefunction (spinor): $\psi(x) = [\psi_1(x), \psi_2(x), \psi_3(x), \psi_4(x)]^t$.

The Minkowski metric tensor we choose to use during our manipulations is going to be:

$$g^{\mu\nu} = \text{diag}(+1, -1, -1, -1), \quad (2.6.2)$$

which has different names:

- The east-coast metric.
- The timelike metric.
- The Landau–Lifshitz sign convention.

For extra details about notations and definitions, the reader can check the appendix A.

2.6.1 The free-particle problem: Dirac plane waves

We start with the following ansatz for the free solutions:

$$\psi(x) = u(p) e^{-\frac{i}{\hbar} p \cdot x} = \psi(x) e^{-\frac{i}{\hbar} Et}; \quad p \cdot x = Et - \mathbf{p} \cdot \mathbf{x}, \quad (2.6.3)$$

where $u(p)$ is a function that can only depend on p (energy and momentum) and the spatial dependence is contained in the plane wave exponential. After inserting this ansatz in the free Dirac equation of eq.(2.6.1), it can be easily seen that:

1. $\psi(x)$ and E satisfy the time-independent Dirac equation:

$$[c\boldsymbol{\alpha} \cdot [-i\hbar\nabla] + \beta mc^2] \psi(x) = E\psi(x), \quad (2.6.4)$$

where E represents the eigenvalue of the Hamiltonian operator: the energy level, while $\psi(x) = u(p) e^{+\frac{i}{\hbar} p \cdot x}$ represents the stationary-state wavefunction associated with E .

2. \mathbf{p} represents the momentum-vector eigenvalue, satisfying the following eigenvalue equation:

$$-i\hbar\nabla\psi(x) = \mathbf{p}\psi(x). \quad (2.6.5)$$

It is worth noting that \mathbf{p} is sometimes used to represent momentum variable and in other cases, the quantized momentum (differential) operator $\hat{\mathbf{p}} = -i\hbar\nabla$, which can sometimes leads to confusions. We thus make a clear distinction in our appendix A, between eq.(A.0.3) and eq.(A.0.4), and in the case where the quantity is a differential operator, we shall write it as $\hat{\mathbf{p}}$ (wearing a hat), or in its explicit form as done here.

3. Finally, the $u(p)$ function should satisfy the following eigenvalue equation:

$$[c\boldsymbol{\alpha} \cdot \mathbf{p} + \beta mc^2] u(p) = Eu(p), \quad (2.6.6)$$

which is simply the momentum space Dirac equation:

$$[\gamma^\mu p_\mu - mc] u(p) = 0; \quad \text{with } p_0 = \frac{E}{c}, \quad (2.6.7)$$

and $u(p)$ is the Fourier transform of the coordinate space solution:

$$u(p) = \int d^4x e^{+ip \cdot x} \psi(x). \quad (2.6.8)$$

Because of the $\boldsymbol{\alpha}$ matrices structure, it is useful to write our equation in a two two-component form:

$$\begin{bmatrix} mc^2 & c\boldsymbol{\sigma} \cdot \mathbf{p} \\ c\boldsymbol{\sigma} \cdot \mathbf{p} & -mc^2 \end{bmatrix} u(p) = Eu(p). \quad (2.6.9)$$

We now use what is sometimes called “the Dirac relation” that first appeared in his own work [30, eq.(16)] (see appendix D.1):

$$(\boldsymbol{\sigma} \cdot \mathbf{a})(\boldsymbol{\sigma} \cdot \mathbf{b}) = \mathbf{a} \cdot \mathbf{b} + i\boldsymbol{\sigma} \cdot (\mathbf{a} \times \mathbf{b}), \quad (2.6.10)$$

to obtain the eigenvalue equation, which leads to:

$$E^2 = c^2 \mathbf{p}^2 + m^2 c^4, \quad (2.6.11)$$

which is the famous relativistic energy-momentum relation. We shall thus replace our dependence of u on p by \mathbf{p} . We end up with two twice-degenerated eigenvalues:

$$\begin{aligned} E_+ &= +|E| = +\sqrt{c^2\mathbf{p}^2 + m^2c^4} \quad \text{twice} \\ E_- &= -|E| = -\sqrt{c^2\mathbf{p}^2 + m^2c^4} \quad \text{twice} \end{aligned} \quad (2.6.12)$$

We decompose the $u(\mathbf{p})$ solution into two two-component functions:

$$u(\mathbf{p}) = \begin{bmatrix} v(\mathbf{p}) \\ w(\mathbf{p}) \end{bmatrix}. \quad (2.6.13)$$

For $E = E_+$ (positive-energy)

one gets the following solution form:

$$u^+(\mathbf{p}) = \begin{bmatrix} v(\mathbf{p}) \\ \frac{c\boldsymbol{\sigma}\cdot\mathbf{p}}{E_+ + mc^2} v(\mathbf{p}) \end{bmatrix}, \quad (2.6.14)$$

meaning that two linearly independent solutions can be formed (labeled by 1 and 2):

$$u_{1,2}^+(\mathbf{p}) = \begin{bmatrix} \chi_{1,2} \\ \frac{c\boldsymbol{\sigma}\cdot\mathbf{p}}{E_+ + mc^2} \chi_{1,2} \end{bmatrix}, \quad (2.6.15)$$

where we choose $v(\mathbf{p}) = \chi_{1,2}$, with these vectors given by:

$$\chi_1 = \begin{bmatrix} 1 \\ 0 \end{bmatrix}; \quad \chi_2 = \begin{bmatrix} 0 \\ 1 \end{bmatrix}, \quad (2.6.16)$$

which represent the eigenvectors (basis) of the spin operator s_z . The + superscript indicates that these spinors are associated with positive-energy solutions. We then do the same for the two other negative-energy states.

For $E = E_-$ (negative-energy)

The solution can be written as:

$$u^-(\mathbf{p}) = \begin{bmatrix} \frac{c\boldsymbol{\sigma}\cdot\mathbf{p}}{E_- - mc^2} w(\mathbf{p}) \\ w(\mathbf{p}) \end{bmatrix}, \quad (2.6.17)$$

and we can construct two linearly independent solutions formed with respect to $w(\mathbf{p}) = \chi_{1,2}$ that was given in eq.(2.6.16):

$$u_{1,2}^-(\mathbf{p}) = \begin{bmatrix} \frac{c\boldsymbol{\sigma}\cdot\mathbf{p}}{E_- - mc^2} \chi_{1,2} \\ \chi_{1,2} \end{bmatrix}. \quad (2.6.18)$$

Again the minus superscript indicates that our solutions are negative-energy solutions.

Results

Finally we collect the findings, and write the four solutions of the Dirac equation as:

$$\begin{aligned} \psi_1^+(x, \mathbf{p}) &= u_1^+(\mathbf{p}) e^{-\frac{i}{\hbar}[E_+ t - \mathbf{p}\cdot\mathbf{x}]} & \bullet \\ \psi_2^+(x, \mathbf{p}) &= u_2^+(\mathbf{p}) e^{-\frac{i}{\hbar}[E_+ t - \mathbf{p}\cdot\mathbf{x}]} & \bullet \\ \psi_1^-(x, \mathbf{p}) &= u_1^-(\mathbf{p}) e^{-\frac{i}{\hbar}[E_- t - \mathbf{p}\cdot\mathbf{x}]} & \bullet \\ \psi_2^-(x, \mathbf{p}) &= u_2^-(\mathbf{p}) e^{-\frac{i}{\hbar}[E_- t - \mathbf{p}\cdot\mathbf{x}]} & \bullet \end{aligned} \quad (2.6.19)$$

Two things to observe from these results:

1. Same energy solutions are associated with opposite spin projection, and this can be seen by observing that in the rest frame of the electron ($\mathbf{p} = 0$), we have:

$$\begin{aligned} S_z \psi_1^+ (x, 0) &= +\frac{\hbar}{2} \psi_1^+ (x, 0) \quad \uparrow \\ S_z \psi_2^+ (x, 0) &= -\frac{\hbar}{2} \psi_2^+ (x, 0) \quad \downarrow \\ S_z \psi_1^- (x, 0) &= +\frac{\hbar}{2} \psi_1^- (x, 0) \quad \uparrow \\ S_z \psi_2^- (x, 0) &= -\frac{\hbar}{2} \psi_2^- (x, 0) \quad \downarrow \end{aligned} \tag{2.6.20}$$

where S_z is the generalized (to four-components) Pauli spin operator, given by:

$$S_z := \frac{\hbar}{2} [1_2 \otimes \sigma_z] = \frac{\hbar}{2} \begin{bmatrix} \sigma_z & 0 \\ 0 & \sigma_z \end{bmatrix}. \tag{2.6.21}$$

2. Opposite energy solutions (same dot color) are related by the charge conjugation symmetry by:

$$\begin{aligned} \mathcal{C} \psi_1^+ (x, \mathbf{p}) &= +\psi_2^- (x, -\mathbf{p}) \\ \mathcal{C} \psi_2^+ (x, \mathbf{p}) &= -\psi_1^- (x, -\mathbf{p}) \end{aligned} \tag{2.6.22}$$

where $\mathcal{C} = i\gamma^2 \mathcal{K}_0$ is the charge conjugation operator, which describes the symmetry between a particle and its anti-particle partner, and between positive and negative-energy solutions in the free particle case. This symmetry is discussed in section 2.8.1, and will be a very important tool in our design of numerical basis sets which approximate the Dirac equation.

2.6.2 Dirac particle in an external electromagnetic potential

Once the electron is allowed to interact with an external electromagnetic potential $A_\mu (x)$, the four-momentum operator of the free Dirac equation should be modified with respect to minimal coupling [55, eq.(3.2)] [30, section 4]:

$$i\hbar\partial_\mu \rightarrow i\hbar\partial_\mu - qA_\mu (x), \quad \text{with } q = -e \quad : \text{The electron charge} \tag{2.6.23}$$

which replaces the canonical momentum operator by the (total) kinetic momentum operator, leading to the interacting Dirac equation [30, eq.14]:

$$[\gamma^\mu (i\hbar\partial_\mu + eA_\mu (x)) - mc] \psi (x) = 0, \tag{2.6.24}$$

where the external EM potential contains the scalar potential in its time component, and the vector potential in its remaining spatial components:

$$A^\mu (x) = \left(\frac{1}{c} \varphi (x), \mathbf{A} (x) \right). \tag{2.6.25}$$

2.6.3 Dirac particle in a time-independent external electromagnetic potential

In the case of a static electromagnetic potential, i.e. $A_\mu(x) = A_\mu(\mathbf{x})$, the Dirac equation allows for the decoupling of the time and space components of the wavefunction, in a given inertial frame, and eventually to write the wave function as:

$$\psi(x) = \psi(\mathbf{x}) e^{-\frac{iE}{\hbar}t}, \quad (2.6.26)$$

where the space E and $\psi(\mathbf{x})$ form an eigensolution of the time-independent Dirac equation:

$$[c\boldsymbol{\alpha} \cdot (\hat{\mathbf{p}} + e\mathbf{A}(\mathbf{x})) - e\varphi(\mathbf{x}) + \beta mc^2] \psi(\mathbf{x}) = E\psi(\mathbf{x}), \quad (2.6.27)$$

where the time-independent four-potential was simply expanded with respect to eq.(2.6.25).

2.7 Radial Dirac equation

In this section, we shall derive the radial Dirac equation where one takes advantage of the spherical symmetry of the scalar potential that traps the electron, to simplify the general equation. The equation we are going to study is of the following form:

$$H_D \psi(\mathbf{x}) = E\psi(\mathbf{x}); \quad \text{with } H_D = -i\hbar c\boldsymbol{\alpha} \cdot \boldsymbol{\nabla} + V(r) + \beta mc^2. \quad (2.7.1)$$

Here $V(r) = -e\varphi(r)$ is the radial electric potential energy, $\varphi(r)$ is the electric potential. It can be easily shown that the orbital angular momentum does not commute with this Dirac equation. After calculating the commutator of the Dirac Hamiltonian with the i -th component angular momentum operator one obtains:

$$[L_i, H_D] = +c\hbar^2 \epsilon_{jki} \alpha_j \nabla_k + i\hbar e \epsilon_{jki} x_j \nabla_k \varphi(r), \quad (2.7.2)$$

where ϵ_{ijk} is the cyclic Levi-Civita symbol. Since the scalar potential is radial, the last term vanishes, because it can be written as L_i (purely angular operator) acting on a radial function:

$$-eL_i \varphi(|\mathbf{x}|) = 0. \quad (2.7.3)$$

As a conclusion, we find that the orbital angular momentum cannot be taken as a good quantum number. In addition, the commutator between the i -th 4×4 spin operator:

$$\Sigma_i = \frac{\hbar}{2} 1_2 \otimes \sigma_i = \frac{\hbar}{2} \begin{bmatrix} \sigma_i & 0 \\ 0 & \sigma_i \end{bmatrix}, \quad (2.7.4)$$

and our Hamiltonian gives:

$$[\Sigma_i, H_D] = -c\hbar^2 \epsilon_{jki} \alpha_j \nabla_k, \quad (2.7.5)$$

Again, the spin is also not a good quantum number, but if we sum the two commutators of eqs.(2.7.2 and 2.7.5), we obtain:

$$[J_i, H_D] = 0. \quad (2.7.6)$$

This means that j is a good quantum number, as discussed by Gross in [39, section 6.1]. This result tells us that the Dirac equation conserves the total angular momentum (it is thus called a “constant of motion”), and that the angular eigenfunctions of the Hamiltonian can be constructed from those of the total angular momentum squared (The Casimir invariant) \mathbf{J}^2 and the projection J_z . In the

appendix, we present the eigenfunctions of these operators by the following two-component functions eq.(D.4.42):

$$\Omega_{\kappa, m_j}(\hat{\mathbf{x}}) = \begin{bmatrix} \text{sgn}(-\kappa) \sqrt{\frac{\kappa + \frac{1}{2} - m_j}{2\kappa + 1}} Y_{\ell, m_j - \frac{1}{2}}(\hat{\mathbf{x}}) \\ \sqrt{\frac{\kappa + \frac{1}{2} + m_j}{2\kappa + 1}} Y_{\ell, m_j + \frac{1}{2}}(\hat{\mathbf{x}}) \end{bmatrix}, \quad (2.7.7)$$

the origin of κ , will be soon clear. On the other hand, it is useful to write the Dirac equation in its two two-component form:

$$\begin{bmatrix} mc^2 - e\varphi(r) & c\boldsymbol{\sigma} \cdot \hat{\mathbf{p}} \\ c\boldsymbol{\sigma} \cdot \hat{\mathbf{p}} & -mc^2 - e\varphi(r) \end{bmatrix} \begin{bmatrix} \psi^L \\ \psi^S \end{bmatrix} = E \begin{bmatrix} \psi^L \\ \psi^S \end{bmatrix}, \quad (2.7.8)$$

where ψ^L and ψ^S are the large and small component functions, and the reason behind this naming, will be clarified in the future. We shall now write the kinetic operator $\boldsymbol{\alpha} \cdot \hat{\mathbf{p}}$ operator in a form where its radial and angular parts are separated, to understand how it is going to transform the angular parts of ψ^L and ψ^S .

2.7.1 The $\boldsymbol{\alpha} \cdot \hat{\mathbf{p}}$ operator

We first would like to write the two-component $\boldsymbol{\sigma} \cdot \hat{\mathbf{p}}$ operator which appears in the last equation in a form where the radial and angular parts of the momentum operator are decoupled as done in [32, section 3.2.3]. To do so, we first multiply our operator by the unit operator $(\boldsymbol{\sigma} \cdot \mathbf{e}_r)(\boldsymbol{\sigma} \cdot \mathbf{e}_r)$, so we can write it as:

$$\boldsymbol{\sigma} \cdot \hat{\mathbf{p}} = \sigma_r \frac{1}{r} (\boldsymbol{\sigma} \cdot \mathbf{x}) (\boldsymbol{\sigma} \cdot \hat{\mathbf{p}}). \quad (2.7.9)$$

Recall that the three-coordinate vector can be written as $\mathbf{x} = r\mathbf{e}_r$. Using Dirac's relation of eq.(D.1.1) this operator can be written as [56, page 158]:

$$\boldsymbol{\sigma} \cdot \hat{\mathbf{p}} = i\sigma_r \left[-\hbar\partial_r + \frac{1}{r} \boldsymbol{\sigma} \cdot \hat{\mathbf{L}} \right], \quad (2.7.10)$$

where we used the radial Pauli matrix, which is given by:

$$\sigma_r = \mathbf{e}_r \cdot \boldsymbol{\sigma} = \begin{pmatrix} \cos(\theta) & e^{-i\varphi} \sin(\theta) \\ e^{i\varphi} \sin(\theta) & -\cos(\theta) \end{pmatrix}. \quad (2.7.11)$$

We shall now introduce a new angular momentum operator that we shall call $\hat{\kappa}$, defined by:

$$\hat{\kappa} = -(\boldsymbol{\sigma} \cdot \hat{\mathbf{L}}) - \hbar \quad (2.7.12)$$

which will allow us to write our $\boldsymbol{\sigma} \cdot \hat{\mathbf{p}}$ operator as [32, eq.(3.2.14)]:

$$\boldsymbol{\sigma} \cdot \hat{\mathbf{p}} = -i\sigma_r \left[\hbar \frac{\partial}{\partial r} + \frac{1}{r} (\hat{\kappa} + \hbar) \right]. \quad (2.7.13)$$

We now would like to guess how this $\hat{\kappa}$ operator will act on our spherical spinors. We first note that the operator $\boldsymbol{\sigma} \cdot \mathbf{L}$ can be written as:

$$\boldsymbol{\sigma} \cdot \mathbf{L} = \frac{1}{\hbar} [\mathbf{J}^2 - \mathbf{L}^2 - \mathbf{S}^2], \quad (2.7.14)$$

which will allow us to write our $\hat{\kappa}$ as:

$$\hat{\kappa} = -\frac{1}{\hbar} [\mathbf{J}^2 - \mathbf{L}^2 - \mathbf{S}^2] - \hbar. \quad (2.7.15)$$

After acting with this operator on the spherical spinors, we get:

$$\hat{\kappa} \Omega_{\kappa, m_j}(\hat{\mathbf{x}}) = \left\{ -\frac{1}{\hbar} [\mathbf{J}^2 - \mathbf{L}^2 - \mathbf{S}^2] - \hbar \right\} \Omega_{\kappa, m_j}(\hat{\mathbf{x}}) \quad (2.7.16)$$

$$= \hbar \left\{ -j(j+1) + \ell(\ell+1) - \frac{1}{4} \right\} \Omega_{\kappa, m_j}(\hat{\mathbf{x}}), \quad (2.7.17)$$

which shows that Ω_{κ, m_j} is an eigenfunction of the $\hat{\kappa}$ operator, associated with the $\hbar\kappa$ eigenvalue, with:

$$\kappa = -j(j+1) + \ell(\ell+1) - \frac{1}{4}. \quad (2.7.18)$$

Since for a well defined ℓ , j can be a half-integer number with:

$$\left| \ell - \frac{1}{2} \right| \leq j \leq \left| \ell + \frac{1}{2} \right|, \quad (2.7.19)$$

our quantum number κ , will be related to ℓ by:

$$\kappa = \begin{cases} +\ell & \text{for } j = \ell - \frac{1}{2} \\ -\ell - 1 & \text{for } j = \ell + \frac{1}{2} \end{cases}. \quad (2.7.20)$$

The reader should notice, at this point, that our choice of κ values we have done in the appendix eq.(D.4.41) is now justified. On the other hand, following the same steps, one can write the four-component operator $\boldsymbol{\alpha} \cdot \hat{\mathbf{p}}$ as ([57, eq.(8.8)] and [58, eq.(2.9)]):

$$\boldsymbol{\alpha} \cdot \hat{\mathbf{p}} = -i\alpha_r \left[\hbar \frac{\partial}{\partial r} + \frac{1}{r} (-\beta \hat{K} + \hbar) \right], \quad (2.7.21)$$

where the corresponding angular momentum operator \hat{K} , is given by:

$$\hat{K} = \beta (\boldsymbol{\Sigma} \cdot \mathbf{L} + \hbar) = \begin{bmatrix} \boldsymbol{\sigma} \cdot \mathbf{L} + \hbar & 0 \\ 0 & -\boldsymbol{\sigma} \cdot \mathbf{L} - \hbar \end{bmatrix} = \begin{bmatrix} -\hat{\kappa} & 0 \\ 0 & +\hat{\kappa} \end{bmatrix}. \quad (2.7.22)$$

This \hat{K} operator commutes with our radial Dirac Hamiltonian, and has an eigenvalue of $-\hbar\kappa$, as stated in the last cited references. Since our spherical spinors are eigenfunctions of the $\hat{\kappa}$ operator:

$$\hat{\kappa} \Omega_{\kappa, m_j} = \hbar\kappa \Omega_{\kappa, m_j}, \quad (2.7.23)$$

which will be used to construct the spherical Dirac spinor, the last matrix in equation.(2.7.22) shows that the angular parts of the large and small component functions have opposite κ signs, and thus motivates the following form of the spherical Dirac solution:

$$\psi_{\kappa, m_j}(r, \theta, \varphi) = \begin{bmatrix} R_{\kappa}^L(r) \Omega_{\kappa, m_j}(\theta, \varphi) \\ i R_{\kappa}^S(r) \Omega_{-\kappa, m_j}(\theta, \varphi) \end{bmatrix}, \quad (2.7.24)$$

where $R_{\kappa}^L(r)$ and $R_{\kappa}^S(r)$ are purely radial functions. In the lower component an imaginary number is added in order to make these radial functions real. We shall next derive the radial Dirac equation that couples these radial functions.

2.7.2 The radial Dirac equation

From the discussion of the last section, we allow ourselves to write the Dirac equation as:

$$\left[-i\alpha_r \left[\hbar \frac{\partial}{\partial r} + \frac{1}{r} \left(-\beta \hat{K} + \hbar \right) \right] + \beta mc^2 - e\varphi(r) \right] \psi_{\kappa, m_j}(r, \theta, \varphi) = E \psi_{\kappa, m_j}(r, \theta, \varphi). \quad (2.7.25)$$

We then let the \hat{K} operator given in eq.(2.7.22) act on the spherical Dirac spinor of eq.(2.7.24), and obtain:

$$\begin{bmatrix} mc^2 - e\varphi(r) & -i\hbar \left[\frac{\partial}{\partial r} + \frac{(\kappa+1)}{r} \right] \sigma_r \\ -i\hbar \left[\frac{\partial}{\partial r} + \frac{(\kappa+1)}{r} \right] \sigma_r & -mc^2 - e\varphi(r) \end{bmatrix} \psi_{\kappa, m_j}(r, \theta, \varphi) = E \psi_{\kappa, m_j}(r, \theta, \varphi). \quad (2.7.26)$$

The operator σ_r , acts on the angular functions through the following relation:

$$\sigma_r \Omega_{\kappa, m_j} = -\Omega_{-\kappa, m_j}, \quad (2.7.27)$$

derived in section D.4.6. Using this relation, the angular parts of our Dirac equation will cancel out, and we will be left with the well-known radial Dirac equation:

$$\begin{bmatrix} mc^2 - e\varphi(r) & -\hbar \left[\frac{d}{dr} + \frac{1-\kappa}{r} \right] \\ \hbar \left[\frac{d}{dr} + \frac{1+\kappa}{r} \right] & -mc^2 - e\varphi(r) \end{bmatrix} \begin{bmatrix} R_{\kappa}^L(r) \\ R_{\kappa}^S(r) \end{bmatrix} = E \begin{bmatrix} R_{\kappa}^L(r) \\ R_{\kappa}^S(r) \end{bmatrix}. \quad (2.7.28)$$

It will be now convenient to define new radial functions P_{κ} and Q_{κ} , related to the previous ones by:

$$P_{\kappa} = r R_{\kappa}^L(r) \quad (2.7.29)$$

$$Q_{\kappa} = r R_{\kappa}^S(r). \quad (2.7.30)$$

This new choice will lead to the following form of the radial Dirac equation [32, eq.(3.2.16)]:

$$\begin{aligned} [mc^2 - e\varphi - E] P_{\kappa} - \hbar \left[\frac{d}{dr} - \frac{\kappa}{r} \right] Q_{\kappa} &= 0 \\ \hbar \left[\frac{d}{dr} + \frac{\kappa}{r} \right] P_{\kappa} - [mc^2 + e\varphi + E] Q_{\kappa} &= 0 \end{aligned} \quad (2.7.31)$$

Next, we shall discuss the free-particle problem: $\varphi = 0$ and obtain the analytical solutions of the last coupled first-order differential equations. Finally, after discussing the discrete symmetries associated with the Dirac equation, we shall show how to approximate the radial Dirac Hamiltonian by a matrix representation in a finite set of basis functions. In other words, how large and small component functions (P_{κ} and Q_{κ}) are going to be approximated by this set of functions.

2.7.3 Free Dirac equation in spherical coordinates

The free Dirac solution is usually presented as a plane wave, as we have previously done in section 2.6.1. In the current section we are going to solve this problem in spherical coordinates instead. The reason why we are doing so, is the following. When one would like to solve the Dirac equation on a computer (numerically discretize it), as we shall see in section 2.9, one sets the origin to be at the atomic position, and choose between generating: 1) a radial grid on which the wavefunction is discretized, or 2) a set of basis functions in which the wavefunction is expanded. For atomic calculations, the first choice is a better one because of the spherical symmetry of the problem. In

contrast, for molecular calculations (complicated non-radial potentials), one must go for the second choice, which will be carefully consider in this thesis.

In the current section, we shall provide the derivation of the analytical free particle solutions in spherical coordinates, and the results are going to help us to 1) understand the charge conjugation symmetry in the framework of the spherical problem, and will 2) guide us on how to design our numerical basis functions. Finally, we note that the plane wave solutions and the spherical waves can be related by the plane wave expansion (see, for instance, [57, section 2.13] and [59, page 29 eq.(1.70) and page 163 eq.(5.15)]).

In the absence of external scalar potential, the radial Dirac eq.(2.7.31) reduces to:

$$[mc^2 - E] P_\kappa - c\hbar \left[\frac{d}{dr} - \frac{\kappa}{r} \right] Q_\kappa = 0 \quad (2.7.32)$$

$$c\hbar \left[\frac{d}{dr} + \frac{\kappa}{r} \right] P_\kappa - [mc^2 + E] Q_\kappa = 0. \quad (2.7.33)$$

From the second line equation, we can write Q_κ as a function of P_κ , we plug this result in the first equation and obtain the following second-order differential equation:

$$\left[\frac{d^2}{dr^2} - \frac{\kappa(1+\kappa)}{r^2} + \mathbf{k}^2 \right] P_\kappa = 0, \quad (2.7.34)$$

where \mathbf{k}^2 is the wave vector squared, related to the energy level by:

$$\mathbf{k}^2 = \frac{E^2 - m^2 c^4}{c^2 \hbar^2}. \quad (2.7.35)$$

Notice that $\mathbf{k}^2 \geq 0$, and the energy is a real number in: $E \in (-\infty, -mc^2] \cup [mc^2, +\infty)$. We now perform a change of variables to $x = rk$, and get:

$$\left[\frac{d^2}{dx^2} - \frac{\kappa(1+\kappa)}{x^2} + 1 \right] P_\kappa(x) = 0. \quad (2.7.36)$$

This equation is the spherical Bessel equation given in eq.(C.2.3), and has two linearly-independent solutions:

$$P_\kappa(r) = c_1 r j_\kappa(kr) + c_2 r y_\kappa(kr) \quad (2.7.37)$$

known as the spherical Bessel functions of the first- and second-kind, $j_\kappa(kr)$ and $y_\kappa(kr)$ respectively. With c_1 and c_2 some arbitrary constants that will be fixed with respect to the physical boundary conditions of the wavefunction: they must not diverge at the origin, and should vanish at infinity:

$$\lim_{r \rightarrow \infty} P_\kappa(r) = \lim_{r \rightarrow +\infty} Q_\kappa(r) = 0. \quad (2.7.38)$$

Recall that our wavefunction should behave properly in order to be physical. This means that the encountered cases where the wavefunction diverges at the origin or at infinity are simply discarded (unnormalizable wavefunctions). At small distances, the spherical Bessel functions can be problematic, since they behave as (see eq.(C.3.1) and eq.(C.3.2)):

$$j_\kappa(kr) \approx \alpha_1 (kr)^\kappa \quad (2.7.39)$$

$$y_\kappa(kr) \approx \alpha_2 (kr)^{-\kappa-1}, \quad (2.7.40)$$

where α_1 and α_2 are some constants given previously. We will divide our problem into two parts, first for positive-integer κ , then for negative-ones.

Positive integer κ case For positive integer κ , the second kind functions $y_\kappa(kr)$ diverge at the origin and are therefore omitted, meaning that the large component radial function of eq.(2.7.39), reduces to:

$$P_\kappa = c_1 r j_\kappa(kr). \quad (2.7.41)$$

We now generate the small component function using eq.(2.7.33):

$$Q_\kappa = \frac{c\hbar}{mc^2 + E} \left[\frac{d}{dr} + \frac{\kappa}{r} \right] P_\kappa. \quad (2.7.42)$$

The first derivative of the j_κ function is given in eq.(C.5.2). With $f_\kappa = j_\kappa$, $m = 1$, and $z = kr$, the mentioned equation reduces to:

$$\frac{d}{dr} j_\kappa(kr) = k j_{\kappa-1}(kr) - \frac{1+\kappa}{r} j_\kappa(kr), \quad (2.7.43)$$

leading to a simplification of the small component radial wavefunction expression of eq.(2.7.42):

$$Q_\kappa = \frac{c_1 c \hbar k}{mc^2 + E} r j_{\kappa-1}(kr). \quad (2.7.44)$$

Negative integer κ case In this case, the $j_\kappa(kr)$ function is not accepted as a physical solution because of the divergent behavior when $r \rightarrow 0$, as seen in eq.(2.7.39), and thus, the general solution of eq.(2.7.37) reduces to:

$$P_\kappa = c_2 r y_\kappa(kr). \quad (2.7.45)$$

The small component radial function is then generated by means of eq.(2.7.33):

$$Q_\kappa = \frac{c_2 c \hbar}{mc^2 + E} \left[\frac{d}{dr} + \frac{\kappa}{r} \right] y_\kappa(kr). \quad (2.7.46)$$

We again use eq.(C.5.2), which gives:

$$\frac{d}{dr} y_\kappa(kr) = k y_{\kappa-1}(kr) - \frac{\kappa+1}{r} y_\kappa(kr), \quad (2.7.47)$$

to get rid of the derivative of $y_\kappa(kr)$, and obtain:

$$Q_\kappa = \frac{c_2 c \hbar k}{mc^2 + E} r y_{\kappa-1}(kr). \quad (2.7.48)$$

Now, we would like to express all our spherical Bessel functions in terms of the first-kind function, using [60, eq.(10.1.15)]:

$$y_\kappa(kr) = (-1)^{\kappa+1} j_{-\kappa-1}(kr); \quad n = 0, \pm 1, \pm 2, \dots \quad (2.7.49)$$

leading to the following expressions:

$$P_\kappa = (-1)^{\kappa+1} c_2 r j_{-\kappa-1}(kr) \quad (2.7.50)$$

$$Q_\kappa = (-1)^\kappa \frac{c_2 c \hbar k}{mc^2 + E} r j_{-\kappa}(kr). \quad (2.7.51)$$

Results For both signs of κ , wavefunctions were chosen such that they do not diverge at the origin ($r = 0$). For large radius r , all our radial functions vanish, and the reason is that the argument of the spherical Bessel function kr is real, thus the exponential term in eq.(C.3.4) vanishes, forcing the Bessel functions to behave as damped sinusoidal functions. To summarize and compactify our results, we use ℓ instead of κ , and obtain one expression valid for both κ signs:

$$\psi_{\kappa, m_j}(\mathbf{x}, E) = \left[i \frac{ch\kappa \operatorname{sgn}(\kappa)}{mc^2 + E} j_{\ell - \operatorname{sgn}(\kappa)}(kr) \Omega_{-\kappa, m_j}(\theta, \varphi) \right]; \quad \operatorname{sgn}(\kappa) = \frac{\kappa}{|\kappa|}. \quad (2.7.52)$$

These solutions will now be normalized to an energy delta function (energy is not quantized for continuum states) using spherical Bessel functions normalization formula of eq.(C.4.8). The angular parts are already normalized to angular quantum numbers Kronecker-deltas. These two points indicate that we are looking for a radial normalization such that:

$$\int d^3\mathbf{x} \psi_{\kappa, m_j}^\dagger(\mathbf{x}, E) \psi_{\kappa', m_j'}(\mathbf{x}, E') = \delta_{\kappa, \kappa'} \delta_{m_j, m_j'} \delta(E - E'). \quad (2.7.53)$$

This relation leads to the following normalized free-particle spherical solution of the Dirac equation:

$$\psi_{\kappa, m_j}(\mathbf{x}, E) = \sqrt{\frac{1}{c^3 \hbar^3 \pi}} \begin{bmatrix} R_\kappa^L(r, E) \Omega_{\kappa, m_j}(\theta, \varphi) \\ i R_\kappa^S(r, E) \Omega_{-\kappa, m_j}(\theta, \varphi) \end{bmatrix}, \quad (2.7.54)$$

where large and small component wavefunctions are found to be [21, eq.(10,11)]:

$$R_\kappa^L(r, E) = |E - mc^2|^{\frac{1}{4}} |E + mc^2|^{\frac{3}{4}} j_{|\kappa + \frac{1}{2}| - \frac{1}{2}}(kr) \quad (2.7.55)$$

$$R_\kappa^S(r, E) = \operatorname{sgn}(\kappa) \operatorname{sgn}(E) |E + mc^2|^{\frac{1}{4}} |E - mc^2|^{\frac{3}{4}} j_{|\kappa - \frac{1}{2}| - \frac{1}{2}}(kr), \quad (2.7.56)$$

where we used the fact that the large and small component Bessel function orders (indices) can be written as a function of κ :

$$\ell = \left| \kappa + \frac{1}{2} \right| - \frac{1}{2} \quad (2.7.57)$$

$$\ell - \operatorname{sgn}(\kappa) = \left| \kappa - \frac{1}{2} \right| - \frac{1}{2}. \quad (2.7.58)$$

References that discuss the free particle problem in spherical coordinates are:

1. Grant [32, section 3.2.6]. In his derivation, the corresponding author misses the $\operatorname{sgn}(E)$ sign factor in his eq.([32, eqs.(3.2.26,28)]), which we have in our small component radial function.
2. Rose [56, eq.(5.12)] and Strange's [57, section 8.2] (as well as Messiah [61, section 26]) results coincide with our result (up to a normalization factor), and this is seen after writing the denominators of their small component wavefunction as:

$$\frac{1}{E + mc^2} = \frac{\operatorname{sgn}(E + mc^2)}{|E + mc^2|} = \frac{\operatorname{sgn}(E)}{|E + mc^2|}. \quad (2.7.59)$$

In figure 2.7.1, we plot the large and small components of the normalized free particle spinor, that are given in eqs.(2.7.55 and 2.7.56), in addition to their probability densities:

$$\rho_\kappa(r, E) = 4\pi r^2 \left([R_\kappa^L(r, E)]^2 + [R_\kappa^S(r, E)]^2 \right). \quad (2.7.60)$$

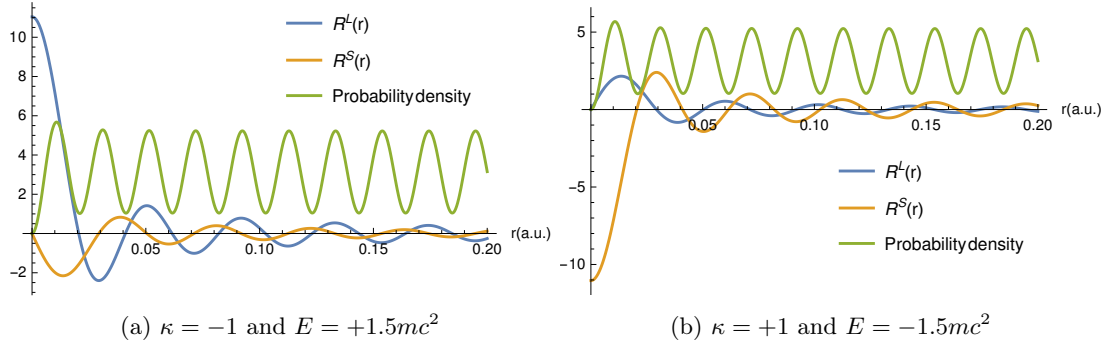


Figure 2.7.1: Radial wavefunctions with corresponding scaled radial probability densities $\rho_\kappa(r, E)/200$.

Notice that the large component function is called large, since in the case where the state in question is a positive-energy state, the large component wavefunction is “larger” than the small component, as seen in figure 2.7.1a. For negative-energy solutions, the story gets reversed, since the large component wavefunction becomes “smaller” than the small one, as seen in figure 2.7.1b. It is worth noting that upon flipping the sign of 1) the κ -quantum number, and 2) the energy, one goes from one figure to another (up to a minus sign), and as seen, as a result, the radial functions are swapped:

$$R^L \rightleftharpoons -R^S. \quad (2.7.61)$$

This symmetry is known as the charge conjugation symmetry, it is going to be discussed in detail, and will be a central concept in our design of our relativistic basis functions (for numerical calculations).

2.8 Discrete symmetries of the Dirac equation

In this section, we shall derive the operators associated with the symmetries of the Dirac equation: the charge conjugation (\mathcal{C}), the time-reversal (\mathcal{T}), and the Parity (\mathcal{P}) symmetry. These symmetries will be used as a guiding torch in simplifying the encountered mathematical expressions and pointing out for physical meaning. As a result, some restrictions will be imposed on the external four-potential, so the symmetries get obeyed.

2.8.1 Charge conjugation

The charge conjugation symmetry, or the \mathcal{C} -symmetry, relates a particle to its corresponding antiparticle: which has the same physical characteristics as the particle, except an opposite charge sign. To derive the charge conjugation operator, we start with the Dirac equation of an electron in an arbitrary four-potential $A_\mu(x)$ given in eq.(2.6.24):

$$[\gamma^\mu (i\hbar\partial_\mu + eA_\mu(x)) - mc] \psi(x) = 0. \quad (2.8.1)$$

The goal is to figure out what operations should act on the wavefunction, such that the modified one satisfies the positronic equation (opposite electron charge sign):

$$[\gamma^\mu (i\hbar\partial_\mu - eA_\mu(x)) - mc] \mathcal{C}\psi(x) = 0. \quad (2.8.2)$$

We start by complex conjugating the first equation, so the imaginary number gets a minus sign:

$$[(\gamma^\mu)^* (-i\hbar\partial_\mu + eA_\mu(x)) - mc] \psi^*(x) = 0. \quad (2.8.3)$$

It is seen at this point that in order obtain the Dirac equation describing the positron (eq.(2.8.2)), it is sufficient to apply a matrix operation, which we shall call it U_c , that flips the sign of the complex conjugated gamma matrices in the last equation, i.e. respecting the following conditions:

$$U_c (\gamma^\mu)^* U_c^{-1} = -\gamma^\mu, \quad (2.8.4)$$

and thus, leading to the following charge conjugated equation:

$$[U_c (\gamma^\mu)^* U_c^{-1} (-i\hbar\partial_\mu + eA_\mu(x)) - mc] U_c \psi^*(x) = 0 \quad (2.8.5)$$

$$[\gamma^\mu (i\hbar\partial_\mu - eA_\mu(x)) - mc] \mathcal{C}\psi(x) = 0, \quad (2.8.6)$$

where the charge conjugation operator contains both operations $\mathcal{C} = U_c \mathcal{K}_0$ of matrix the matrix operator U_c and the complex conjugation \mathcal{K}_0 . In the Dirac representation of the gamma matrices (eq.(2.4.10)), the matrix U_c respecting the four conditions of eq.(2.8.4) is found to be (up to a phase factor):

$$U_c = \gamma^2. \quad (2.8.7)$$

To summarize, we started by an electron, whose wavefunction $\psi(x)$ satisfies the electron Dirac equation.(2.8.1) and ended up with a positron, whose wavefunction $\mathcal{C}\psi(x)$ satisfies the corresponding antiparticle equation.(2.8.2). The final form of the \mathcal{C} -operation is found to be:

$$\mathcal{C} = \gamma^2 \mathcal{K}_0; \quad \mathcal{K}_0: \text{Complex conjugation} \quad (2.8.8)$$

The term “charge-conjugation” was coined by Kramers [62]. This symmetry has lead Dirac to predict the existence of the anti-electron, i.e. the positron. An interesting chapter on antiparticles was written by Feynman in [63].

2.8.1.1 \mathcal{C} -symmetry in the time-independent regime

The time-independent Dirac equation, is of the following form:

$$[c\boldsymbol{\alpha} \cdot [-i\hbar\nabla + e\mathbf{A}(\mathbf{x})] + \beta mc^2 - e\varphi(\mathbf{x})] \psi(\mathbf{x}) = +E\psi(\mathbf{x}), \quad (2.8.9)$$

as given in eq.(2.6.27). The charge-conjugated solution $\mathcal{C}\psi(\mathbf{x})$, obeys the same equation but with an opposite energy and charge signs:

$$[c\boldsymbol{\alpha} \cdot [-i\hbar\nabla - e\mathbf{A}(\mathbf{x})] + \beta mc^2 + e\varphi(\mathbf{x})] \mathcal{C}\psi(\mathbf{x}) = -E\mathcal{C}\psi(\mathbf{x}). \quad (2.8.10)$$

This additional negative-energy sign can (in addition) be traced to the fact that the \mathcal{C} operator has a complex conjugation operator in it, and therefore, it flips the energy-time wavefunction part of eq.(2.6.26):

$$\mathcal{C}\psi(x) = \mathcal{C}\psi(\mathbf{x}) e^{-\frac{iE}{\hbar}t} = \gamma^2 \psi^*(\mathbf{x}) e^{+\frac{iE}{\hbar}t}. \quad (2.8.11)$$

In figure 2.8.1, we present the pictorial spectra of the following systems:

1. An electron placed in an attractive Coulomb field (Example: the hydrogen atom). This is exactly equivalent to having a positron placed in a repulsive field, since the electric potential energy will depend on the sign of the product of both charges: $(+Ze)(-e) = (-Ze)(+e)$.
2. A free-electron placed in an empty space. It is worth noting that this could be a positron instead, since, in the absence of the external potential, the particle's charge does not enter in the Dirac equation.
3. A positron placed in an attractive Coulomb field. This case is equivalent to the placing an electron in a repulsive Coulomb field, since $(+Ze)(+e) = (-Ze)(-e)$.

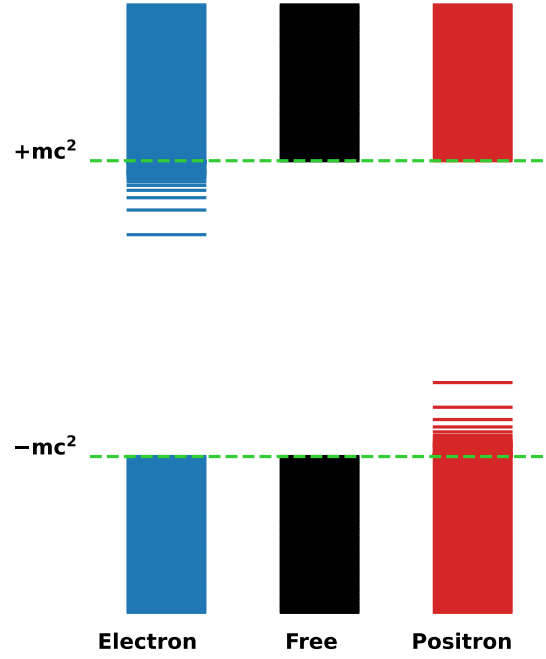


Figure 2.8.1: Dirac spectra for:

- 1) Electron in an attractive Coulomb field
- 2) Free electron/positron
- 3) Positron in an attractive Coulomb field

In the time-independent regime, the charge conjugation symmetry allows the linking between the wavefunctions of opposite energy and charge particles, as predicted by eqs.(2.8.9 and 2.8.10) and presented in the first and last spectra of figure 2.8.1 (notice the energy-sign flip between these spectra).

In addition, the reader should note that in the free-particle case (middle spectrum of figure 2.8.1), which is a special case of the time-independent problem, eqs.(2.8.9 and 2.8.10) reduce to:

$$[c\boldsymbol{\alpha} \cdot [-i\hbar\nabla] + \beta mc^2] \psi(\mathbf{x}) = +E\psi(\mathbf{x}) \quad (2.8.12)$$

$$[c\boldsymbol{\alpha} \cdot [-i\hbar\nabla] + \beta mc^2] \mathcal{C}\psi(\mathbf{x}) = -E\mathcal{C}\psi(\mathbf{x}), \quad (2.8.13)$$

and the charge sign and magnitude are meaningless. These equations show that the charge conjugated partners belong to the same problem: they solve the same equation but with an opposite energy sign, concluding that the charge conjugation symmetry links between free solutions of opposite energy signs.

2.8.1.2 \mathcal{C} -symmetry in the spherical problem

As discussed before, in section 2.7, the spherical spinor can be written in the following form:

$$\psi_{n,\kappa,m_j}(\mathbf{x}) = \begin{bmatrix} R_{n,\kappa}^L(r) \Omega_{\kappa,m_j}(\hat{\mathbf{x}}) \\ iR_{n,\kappa}^S(r) \Omega_{-\kappa,m_j}(\hat{\mathbf{x}}) \end{bmatrix}, \quad \text{with } r = |\mathbf{x}|. \quad (2.8.14)$$

The charge conjugated spherical solution reads:

$$\mathcal{C}\psi_{n,\kappa,m_j}(\mathbf{x}) = \gamma^2 \psi_{n,\kappa,m_j}^*(\mathbf{x}) = - \begin{bmatrix} iR_{n,\kappa}^S \sigma_2 \Omega_{-\kappa,m_j}^* \\ R_{n,\kappa}^L \sigma_2 \Omega_{\kappa,m_j}^* \end{bmatrix}, \quad (2.8.15)$$

Using the following relation:

$$\sigma_2 \Omega_{\kappa,m_j}^* = i \operatorname{sgn}(-\kappa) (-1)^{m_j - \frac{1}{2}} \Omega_{\kappa,-m_j}, \quad (2.8.16)$$

which can be easily verified, one can write the charge conjugated solution as ([32, 5.8.5] and [56, 5.6]):

$$\mathcal{C}\psi_{n,\kappa,m_j}(\mathbf{x}) = \operatorname{sgn}(\kappa) (-1)^{m_j - \frac{1}{2}} \begin{bmatrix} R_{n,\kappa}^S \Omega_{-\kappa,-m_j} \\ iR_{n,\kappa}^L \Omega_{\kappa,-m_j} \end{bmatrix}. \quad (2.8.17)$$

Notice that upon the switch of particle's charge sign, the radial functions are interchanged, and the angular quantum numbers flip their signs. This is summarized in table 2.1.

	Particle	Antiparticle
Charge	$-e$	$+e$
Large component	$R_{n,\kappa}^L$	$R_{n,\kappa}^S$
Small component	$R_{n,\kappa}^S$	$R_{n,\kappa}^L$
Angular quantum num. κ	κ	$-\kappa$
Angular quantum num. m_j	m_j	$-m_j$

Table 2.1: What an antiparticle is for a particle, in spherical symmetry?

Using the result we have just derived, we shall show how our free spherical solutions, presented in eqs.(2.7.54, 2.7.55 and 2.7.56), transform under charge conjugation operation, and hope to link opposite energy solutions as done with the trivial plane wave solutions of eq.(2.6.22). Using eq.(2.8.17) we can write these free spherical solutions as:

$$\mathcal{C}\psi_{\kappa,m_j}(\mathbf{x}, E) = \operatorname{sgn}(\kappa) (-1)^{m_j - \frac{1}{2}} \sqrt{\frac{1}{c^3 \hbar^3 \pi}} \begin{bmatrix} R_{\kappa}^S(r, E) \Omega_{-\kappa,-m_j} \\ iR_{\kappa}^L(r, E) \Omega_{\kappa,-m_j} \end{bmatrix}. \quad (2.8.18)$$

After observing the following relations between large and small component (radial) functions:

$$\begin{aligned} R_{\kappa}^S(r, E) &= \operatorname{sgn}(\kappa) \operatorname{sgn}(E) R_{-\kappa}^L(r, -E) \\ R_{\kappa}^L(r, E) &= \operatorname{sgn}(\kappa) \operatorname{sgn}(E) R_{-\kappa}^S(r, -E), \end{aligned} \quad (2.8.19)$$

we can write the charge conjugated solution as we have found in our paper [21, eq.(14)]:

$$\mathcal{C}\psi_{\kappa,m_j}(\mathbf{x}, E) = \operatorname{sgn}(E) (-1)^{m_j - \frac{1}{2}} \sqrt{\frac{1}{c^3 \hbar^3 \pi}} \begin{bmatrix} R_{-\kappa}^L(r, -E) \Omega_{-\kappa,-m_j} \\ iR_{-\kappa}^S(r, -E) \Omega_{\kappa,-m_j} \end{bmatrix} \quad (2.8.20)$$

$$= \operatorname{sgn}(E) (-1)^{m_j - \frac{1}{2}} \psi_{-\kappa,-m_j}(\mathbf{x}, -E), \quad (2.8.21)$$

which clearly shows that opposite energy (and quantum numbers signs) solutions are related by charge conjugation symmetry.

2.8.2 Time-reversal

Now, we would like to discuss the time-reversal (\mathcal{T}) symmetry, where we will derive the equation that describes an electron that perceives an opposite flow of time. We write the Dirac equation in a form that is convenient with our derivation:

$$\left[\gamma^0 \left(\frac{i\hbar}{c} \frac{\partial}{\partial t} + eA_0(\mathbf{x}, t) \right) + \boldsymbol{\gamma} \cdot (i\hbar \boldsymbol{\nabla} - e\mathbf{A}(\mathbf{x}, t)) - mc \right] \psi(\mathbf{x}, t) = 0. \quad (2.8.22)$$

After complex conjugating it, and acting on it with a matrix operation U_t , we get:

$$\begin{aligned} & \left[U_t \gamma^0 U_t^{-1} \left(-\frac{i\hbar}{c} \frac{\partial}{\partial t} + eA_0(\mathbf{x}, t) \right) + U_t (\boldsymbol{\gamma})^* U_t^{-1} \cdot (-i\hbar \boldsymbol{\nabla} - e\mathbf{A}(\mathbf{x}, t)) - mc \right] \\ & \times U_t \psi^*(\mathbf{x}, t) = 0 \end{aligned} \quad (2.8.23)$$

Recall that the current goal is to recover the first equation eq.(2.8.22), but with an opposite time sign, after the application of some operator which will be absorbed by the wavefunction. To do the job, we would like that the U_t operation:

- keeps the sign of γ^0 , since it already has a negative time sign (thanks to complex conjugation),
- flips the sign of the gamma matrices vector $\boldsymbol{\gamma}$

This means that our matrix operation should respect the following conditions:

$$U_t \gamma^0 U_t^{-1} = \gamma^0 \quad (2.8.24)$$

$$U_t (\boldsymbol{\gamma})^* U_t^{-1} = -\boldsymbol{\gamma} \quad (2.8.25)$$

Following the conditions of eqs.(2.8.24 and 2.8.25), the matrix is found to be [28, eq.(12.60)] (up to a phase):

$$U_t = \gamma^1 \gamma^3, \quad (2.8.26)$$

which leaves us with the following equation:

$$\left[\gamma^0 \left(\frac{i\hbar}{c} \frac{\partial}{\partial t} + eA_0(\mathbf{x}, t) \right) + \boldsymbol{\gamma} \cdot (i\hbar \boldsymbol{\nabla} + e\mathbf{A}(\mathbf{x}, t)) - mc \right] U_t \psi^*(\mathbf{x}, t) = 0. \quad (2.8.27)$$

Clearly, we would not recover the opposite time sign of eq.(2.8.22), unless we put more restrictions on the potentials, particularly:

$$A_0(\mathbf{x}, -t) = A_0(\mathbf{x}, t) \quad (2.8.28)$$

$$\mathbf{A}(\mathbf{x}, -t) = -\mathbf{A}(\mathbf{x}, t), \quad (2.8.29)$$

otherwise, the time-reversal symmetry will be violated. In this case, the time-reversal operator that combines complex conjugation and the matrix operation is found to be:

$$\mathcal{T}_1 = U_t \mathcal{K}_0 = \gamma^1 \gamma^3 \mathcal{K}_0. \quad (2.8.30)$$

A similar derivation is provided by Sakurai [64, pages 504-505] where he deals with the free Hamiltonian instead of the general interacting one (what we have done here). We have recently found these

potential restrictions in Greiner [28, eqs.(12.52-53)]. Notice that in the time-independent regime, our restrictions reduce to:

$$A_0(\mathbf{x}) = A_0(\mathbf{x}) \quad (2.8.31)$$

$$\mathbf{A}(\mathbf{x}) = -\mathbf{A}(\mathbf{x}), \quad (2.8.32)$$

meaning that the vector potential $\mathbf{A}(\mathbf{x})$ should vanish so the symmetry can get conserved. There exist another way to derive the time-reversal operator, leading to a different operator form than the one just discussed, and where slightly different potential restrictions are found, this will be discussed in the next paragraph.

Another Time-reversal operator (without complex conjugation)

This time, the derivation is done without complex conjugation. The action of the matrix operation U_t reads:

$$\left[U_t \gamma^0 U_t^{-1} \left(\frac{i\hbar}{c} \frac{\partial}{\partial t} + eA_0(\mathbf{x}, t) \right) \right. \quad (2.8.33)$$

$$\left. + U_t \boldsymbol{\gamma} U_t^{-1} \cdot (i\hbar \boldsymbol{\nabla} - e\mathbf{A}(\mathbf{x}, t)) - mc \right] U_t \psi(\mathbf{x}, t) = 0. \quad (2.8.34)$$

Notice that we only need to add a minus sign in front of the time derivative, i.e. to flip the γ^0 matrix sign. The conditions are thus:

$$U_t \gamma^0 U_t^{-1} = -\gamma^0 \quad (2.8.35)$$

$$U_t \boldsymbol{\gamma} U_t^{-1} = \boldsymbol{\gamma}, \quad (2.8.36)$$

leading to the following equation:

$$\left[\gamma^0 \left(\frac{i\hbar}{c} \frac{\partial}{\partial t} - eA_0(\mathbf{x}, t) \right) + \boldsymbol{\gamma} \cdot (i\hbar \boldsymbol{\nabla} - e\mathbf{A}(\mathbf{x}, t)) - mc \right] U_t \psi(\mathbf{x}, t) = 0. \quad (2.8.37)$$

Again, new restrictions are to be put on the potentials in order to make the last equation time-reversed (with respect to the main equation.(2.8.22)), in particular, one should have:

$$A_0(\mathbf{x}, -t) = -A_0(\mathbf{x}, t) \quad (2.8.38)$$

$$\mathbf{A}(\mathbf{x}, -t) = \mathbf{A}(\mathbf{x}, t). \quad (2.8.39)$$

If these conditions are respected, then there exists a time-reversal symmetry relating between two particles that experience opposite time-direction flows, represented by the following operator:

$$\mathcal{T}_2 = U_t = \gamma^1 \gamma^2 \gamma^3, \quad (2.8.40)$$

where this matrix is derived with respect to the conditions eqs.(2.8.35 and 2.8.36). Contrary to the previous time-reversal symmetry, in a time-independent framework, this symmetry is conserved when the scalar potential is set to zero, $A_0(\mathbf{x}) = 0$. The problem with this symmetry is that it does not commute with the free Hamiltonian:

$$[\mathcal{T}_2, H] \neq 0, \quad (2.8.41)$$

which means that for a specific wavefunction/energy of the Hamiltonian, this symmetry cannot be conserved. We shall thus discard it, and call the time-reversal symmetry:

$$\mathcal{T} = \mathcal{T}_1, \quad (2.8.42)$$

which was discussed in the previous subsection.

2.8.2.1 \mathcal{T} -symmetry in the time-independent problem

The time-independent Dirac equation reads:

$$[c\boldsymbol{\alpha} \cdot [-i\hbar\nabla + e\mathbf{A}(\mathbf{x})] + \beta mc^2 - e\varphi(\mathbf{x})] \psi(\mathbf{x}) = E\psi(\mathbf{x}). \quad (2.8.43)$$

We have learned in the last section that in order for the time-reversal symmetry (given in eq.(2.8.30)) to be conserved, we should set $\mathbf{A}(\mathbf{x}) = 0$. We thus do so, and get the following equation:

$$[c\boldsymbol{\alpha} \cdot [-i\hbar\nabla] + \beta mc^2 - e\varphi(\mathbf{x})] \psi(\mathbf{x}) = E\psi(\mathbf{x}). \quad (2.8.44)$$

After applying the time-reversal operator, we obtain the following equation:

$$[c\boldsymbol{\alpha} \cdot [-i\hbar\nabla] + \beta mc^2 - e\varphi(\mathbf{x})] \mathcal{T}\psi(\mathbf{x}) = E\mathcal{T}\psi(\mathbf{x}). \quad (2.8.45)$$

After comparing these two equations, we see that both $\psi(\mathbf{x})$ and $\mathcal{T}\psi(\mathbf{x})$ satisfy the same equation, and have the same energy level E .

2.8.2.2 \mathcal{T} -symmetry in the spherical problem

After applying the time-reversal operator to the spherical solutions, one gets:

$$\mathcal{T}\psi_{n,\kappa,m_j}(\mathbf{x}) = \gamma^1 \gamma^3 \mathcal{K}_0 \begin{bmatrix} R_{n,\kappa}^L \Omega_{\kappa,m_j} \\ iR_{n,\kappa}^S \Omega_{-\kappa,m_j} \end{bmatrix} = \begin{bmatrix} iR_{n,\kappa}^L \sigma_2 \Omega_{\kappa,m_j}^* \\ R_{n,\kappa}^S \sigma_2 \Omega_{-\kappa,m_j}^* \end{bmatrix}, \quad (2.8.46)$$

using the identity of eq.(2.8.16), one finds:

$$\mathcal{T}\psi_{n,\kappa,m_j}(\mathbf{x}) = \text{sgn}(+\kappa) (-1)^{m_j - \frac{1}{2}} \begin{bmatrix} R_{n,\kappa}^L \Omega_{\kappa,-m_j} \\ iR_{n,\kappa}^S \Omega_{-\kappa,-m_j} \end{bmatrix}, \quad (2.8.47)$$

meaning that the time-reversal symmetry simply switches the sign of the secondary total angular momentum quantum number m_j . This result was not found in literature.

2.8.3 Parity

In order to derive the parity operator that describes the space inversion symmetry, we start by the Dirac equation:

$$[\gamma^0 [i\hbar\partial_0 + eA_0(\mathbf{x},t)] + \boldsymbol{\gamma} \cdot [i\hbar\nabla_{\mathbf{x}} - e\mathbf{A}(\mathbf{x},t)] - mc] \psi(\mathbf{x},t) = 0. \quad (2.8.48)$$

We now apply the matrix operation U_p associated with the parity operator \mathcal{P} , and get the following equation:

$$[U_p \gamma^0 U_p^{-1} [i\hbar\partial_0 + eA_0(\mathbf{x},t)] + U_p \boldsymbol{\gamma} U_p^{-1} \cdot [i\hbar\nabla_{\mathbf{x}} - e\mathbf{A}(\mathbf{x},t)] - mc] U_p \psi(\mathbf{x},t) = 0, \quad (2.8.49)$$

and set the following conditions to be respected:

$$U_p \gamma^0 U_p^{-1} = \gamma^0 \quad (2.8.50)$$

$$U_p \boldsymbol{\gamma} U_p^{-1} = -\boldsymbol{\gamma}, \quad (2.8.51)$$

that simply adds a minus factor to the gradient operator $\nabla_{\mathbf{x}}$, leading to:

$$[\gamma^0 [i\hbar\partial_0 + eA_0(\mathbf{x},t)] + \boldsymbol{\gamma} \cdot [-i\hbar\nabla_{\mathbf{x}} + e\mathbf{A}(\mathbf{x},t)] - mc] U_p \psi(\mathbf{x},t) = 0. \quad (2.8.52)$$

One has to keep in mind that the goal is to obtain the following equation:

$$[\gamma^0 [i\hbar\partial_0 + eA_0(-\mathbf{x}, t)] + \boldsymbol{\gamma} \cdot [i\hbar\nabla_{-\mathbf{x}} - e\mathbf{A}(-\mathbf{x}, t)] - mc] U_p \psi(\mathbf{x}, t) = 0, \quad (2.8.53)$$

which has the same form as the main equation, but with a minus sign in front of the space vector \mathbf{x} . Clearly, new restrictions has to be put on the electromagnetic potentials:

$$A_0(-\mathbf{x}, t) = A_0(\mathbf{x}, t) \quad (2.8.54)$$

$$\mathbf{A}(-\mathbf{x}, t) = -\mathbf{A}(\mathbf{x}, t). \quad (2.8.55)$$

This result was found in the work of Greiner [28, page 313]. Finally, the matrix operation that respects both conditions 2.8.50 and 2.8.51 leads to the following form of the Parity operator:

$$\mathcal{P}_1 = \gamma^0 P, \quad (2.8.56)$$

where P is the operator that flips the coordinate vector sign $\mathbf{x} \rightarrow -\mathbf{x}$. Similarly to the time-reversal operator, another parity operator can be derived, where one has slightly modified potential assumptions. This point will be discussed below.

Another Parity operator (with complex conjugation)

Letting a U_p matrix operation act on the complex conjugated Dirac equation will lead to:

$$[U_p \gamma^0 U_p^{-1} [-i\hbar\partial_0 + eA_0(\mathbf{x}, t)] + U_p (\boldsymbol{\gamma})^* \cdot U_p^{-1} [-i\hbar\nabla_{\mathbf{x}} - e\mathbf{A}(\mathbf{x}, t)] - mc] U_p \psi^*(\mathbf{x}, t) = 0. \quad (2.8.57)$$

After forcing the matrix U_p to respect the following conditions:

$$U_p \gamma^0 U_p^{-1} = -\gamma^0 \quad (2.8.58)$$

$$U_p (\boldsymbol{\gamma})^* \cdot U_p^{-1} = \boldsymbol{\gamma}, \quad (2.8.59)$$

we can directly see that if, on the other hand, our potentials respect the following potential:

$$A_0(-\mathbf{x}, t) = -A_0(\mathbf{x}, t) \quad (2.8.60)$$

$$\mathbf{A}(-\mathbf{x}, t) = \mathbf{A}(\mathbf{x}, t), \quad (2.8.61)$$

then parity symmetry can be obeyed. The second condition simply implies that the vector potential (instead of the scalar one) should be spherically symmetric. Finally, the corresponding parity operator is found to be:

$$\mathcal{P}_2 = \gamma^0 \gamma^2 \mathcal{K}_0. \quad (2.8.62)$$

As in the time-reversal symmetry, this operator does not commute with the Dirac Hamiltonian, and should thus be discarded, since \mathcal{P}_2 and H cannot be simultaneously measured, and thus, the expectation value of \mathcal{P}_2 cannot be considered a constant of motion, even if this operator is time-independent (Ehrenfest Theorem). We shall thus call \mathcal{P} as:

$$\mathcal{P} = \mathcal{P}_1, \quad (2.8.63)$$

given in the previous section.

2.8.3.1 \mathcal{P} -symmetry in the radial problem

In the radial problem, the parity simply adds a minus sign to the small component function:

$$\mathcal{P}\psi_{n,\kappa,m_j}(\mathbf{x}) = \gamma^0\psi_{n,\kappa,m_j}(-\mathbf{x}) = \begin{bmatrix} R_{n,\kappa}^L(r) \Omega_{\kappa,m_j}(-\hat{\mathbf{x}}) \\ -iR_{n,\kappa}^S(r) \Omega_{-\kappa,m_j}(-\hat{\mathbf{x}}) \end{bmatrix}. \quad (2.8.64)$$

We now use the parity relation associated with the spherical spinor $\Omega_{\kappa,m_j}(-\hat{\mathbf{x}})$, of eq.(D.4.53), in addition to the relation between ℓ and κ quantum numbers, of eq.(2.7.20), one directly gets:

$$\mathcal{P}\psi_{n,\kappa,m_j}(\mathbf{x}) = (-1)^\ell \begin{bmatrix} R_{n,\kappa}^L(r) \Omega_{\kappa,m_j}(\hat{\mathbf{x}}) \\ iR_{n,\kappa}^S(r) \Omega_{-\kappa,m_j}(\hat{\mathbf{x}}) \end{bmatrix}. \quad (2.8.65)$$

Notice that this operator gives an overall plus sign for *Gerade* (even) spinors and a minus sign for *Ungerade* (odd) ones.

2.8.4 Discrete symmetries summary

Results of the previous sections about the discrete symmetries of the Dirac equation with their corresponding operator form, and the associated restrictions that has to be set on the external potential are given compactly in the following table 2.2.

Symmetry	Operator	Potential restrictions
Charge-conjugation	$\mathcal{C} = \gamma^2\mathcal{K}_0$	None
Time-reversal	$\mathcal{T} = \gamma^1\gamma^3\mathcal{K}_0$	$A_0(\mathbf{x}, -t) = A_0(\mathbf{x}, t)$ $\mathbf{A}(\mathbf{x}, -t) = -\mathbf{A}(\mathbf{x}, t)$
Parity	$\mathcal{P} = \gamma^0$	$A_0(-\mathbf{x}, t) = A_0(\mathbf{x}, t)$ $\mathbf{A}(-\mathbf{x}, t) = -\mathbf{A}(\mathbf{x}, t)$

Table 2.2: The discrete symmetries of the Dirac equation.

2.9 Finite basis approximation of the Dirac equation

In quantum chemistry, as well as in molecular physics, one uses a set of one-particle basis functions (a basis set), in general, centered at nuclei positions, to construct (strictly speaking: to approximate) the molecular/atomic many-electron wavefunctions. The use of such a scheme allows the transformation of the differential equation (the Dirac equation in our case) into a matrix eigenvalue equation that can be solved on a computer in a very efficient manner.

We shall put dots on our i's: we are going to approximate the radial Dirac equation (in the presence of a radial potential) by a matrix, whose elements are integrals of the Dirac operator. If one solves the exact problem analytically, one obtains an infinite set of discrete

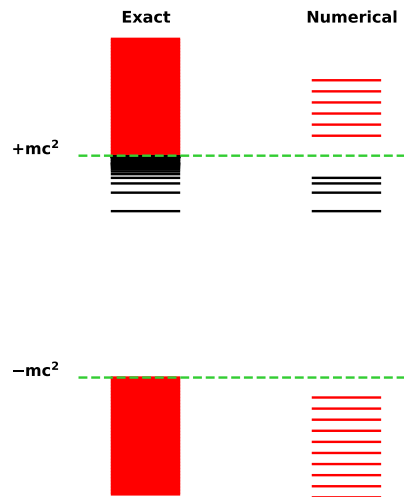


Figure 2.9.1: Pictorial comparison between exact and numerical spectra

bound-states with $0 < E < +mc^2$ shown in black in the left spectrum of figure 2.9.1, and two continua of energy states with $|E| > mc^2$ that are presented in red. Numerically, when using the finite basis set approximation, one obtains a number of solutions that is equal to the number of basis functions. In addition, if the basis is carefully constructed: balanced (obeying certain necessary conditions, that we shall soon discuss), we will have an even number of basis functions n , and the numerical spectrum will split between $\frac{n}{2}$ positive and $\frac{n}{2}$ negative-energy solutions, as presented in the right spectrum of figure 2.9.1.

2.9.1 The general problem

In the atomic case, one specifies a basis set for each component of the Dirac solution, associated with one quantum number κ , and thus one approximates the exact radial functions $P_\kappa(r)$ and $Q_\kappa(r)$ by expansions over the basis sets elements $\mathcal{P}_\kappa(r)$, $\mathcal{Q}_\kappa(r)$ as:

$$\begin{aligned} P_\kappa(r) &\approx \mathcal{P}_\kappa(r) = \sum_{i=1}^{n_\kappa^L} c_{\kappa,i}^L \pi_{\kappa,i}^L(r) \\ Q_\kappa(r) &\approx \mathcal{Q}_\kappa(r) = \sum_{i=1}^{n_\kappa^S} c_{\kappa,i}^S \pi_{\kappa,i}^S(r) \end{aligned} \quad (2.9.1)$$

The functions $\pi_{\kappa,i}^{L/S}(r)$ are large and small radial basis functions, associated with the expansion coefficients $c_{\kappa,i}^{L/S}$, $n_\kappa^{L/S}$ simply represent the number of basis elements for each of the sets. Strictly speaking, the α -th (radial) numerical solution of the Dirac equation is given by:

$$\varphi_{\alpha,\kappa}(r) = \begin{bmatrix} \mathcal{P}_{\alpha,\kappa}(r) \\ \mathcal{Q}_{\alpha,\kappa}(r) \end{bmatrix} = \sum_{i=1}^{n_\kappa^L} c_{\alpha,\kappa,i}^L \begin{bmatrix} \pi_{\kappa,i}^L(r) \\ 0 \end{bmatrix} + \sum_{i=1}^{n_\kappa^S} c_{\alpha,\kappa,i}^S \begin{bmatrix} 0 \\ \pi_{\kappa,i}^S(r) \end{bmatrix}, \quad (2.9.2)$$

which leads to the following matrix representation of the Dirac eigenvalue problem:

$$H_\kappa \mathbf{c}_{\alpha,\kappa} = \epsilon_{\alpha,\kappa} S_\kappa \mathbf{c}_{\alpha,\kappa}, \quad (2.9.3)$$

where the elements of this equation are the $(n_\kappa^L + n_\kappa^S) \times (n_\kappa^L + n_\kappa^S)$ Hamiltonian matrix H_κ , the overlap matrix S_κ (same dimensions) and the eigensolutions $\mathbf{c}_{\alpha,\kappa}$ of dimensions $(n_\kappa^L + n_\kappa^S) \times 1$ associated with the energy eigenvalue $\epsilon_{\alpha,\kappa}$ and the numerical solution $\varphi_{\alpha,\kappa}(r)$. These terms are respectively given by:

$$H_\kappa = \begin{bmatrix} mc^2 S_\kappa^{LL} - e\varphi_\kappa^{LL} & c\hbar \Pi_\kappa \\ c\hbar \Pi_\kappa^t & -mc^2 S_\kappa^{SS} - e\varphi_\kappa^{SS} \end{bmatrix} \quad (2.9.4)$$

$$S_\kappa = \begin{bmatrix} S_\kappa^{LL} & 0 \\ 0 & S_\kappa^{SS} \end{bmatrix}; \quad \{\epsilon_{\alpha,\kappa}, \mathbf{c}_{\alpha,\kappa}\} = \left\{ \epsilon_{\alpha,\kappa}, \begin{bmatrix} \mathbf{c}_{\alpha,\kappa}^L \\ \mathbf{c}_{\alpha,\kappa}^S \end{bmatrix} \right\}. \quad (2.9.5)$$

The elements of matrices are given by the following radial integrals:

$$[S_\kappa^{XX}]_{ij} = \int_0^\infty \pi_{\kappa,i}^X \pi_{\kappa,j}^X dr \quad (2.9.6)$$

$$[\varphi_\kappa^{XX}]_{ij} = \int_0^\infty \pi_{\kappa,i}^X \varphi_{\kappa,j}^X dr \quad (2.9.7)$$

$$[\Pi_\kappa]_{ij} = - \int_0^\infty \pi_{\kappa,i}^L \left[\frac{d}{dr} - \frac{\kappa}{r} \right] \pi_{\kappa,j}^S dr, \quad (2.9.8)$$

where X can be one of the two letters $X = L, S$ (for large and small components). One sees that the off-diagonal matrices of the Hamiltonian matrix of eq.(2.9.4) are related by a transpose operation, and this is a consequence of the fact that our wavefunction respects the physical boundary conditions:

$$\pi_{\kappa,i}^X(0) = \pi_{\kappa,i}^X(+\infty) = 0. \quad (2.9.9)$$

More precisely, these functions should respect the following conditions:

$$\pi_{\kappa,i}^S \frac{d}{dr} \pi_{\kappa,j}^L \Big|_0^{+\infty} = \pi_{\kappa,j}^L \frac{d}{dr} \pi_{\kappa,i}^S \Big|_0^{+\infty} = 0, \quad \forall i, j \quad (2.9.10)$$

so that the two off-diagonal matrices can be related by the transpose operation. Finally, we present the radial probability density associated with a numerical solution α (eq.(2.9.2)):

$$\rho_{\alpha,\kappa}(r) = \varphi_{\alpha,\kappa}^\dagger(r) \varphi_{\alpha,\kappa}(r) = \sum_{i,j=1}^{n_\kappa^L} (c_{\alpha,\kappa,i}^L)^* c_{\alpha,\kappa,j}^L \pi_{\kappa,i}^L \pi_{\kappa,j}^L + \sum_{i,j=1}^{n_\kappa^S} (c_{\alpha,\kappa,i}^S)^* c_{\alpha,\kappa,j}^S \pi_{\kappa,i}^S \pi_{\kappa,j}^S, \quad (2.9.11)$$

which integrates to 1 once the state $\varphi_{\alpha,\kappa}(r)$ is normalized.

2.9.2 Gaussian basis set

We shall concentrate on the Gaussian-type basis functions, since they play a central role in the relativistic quantum chemistry calculations, and the reason they do so comes from the fact that we have analytical formulas for the radial integrals that build the Hamiltonian, for both non-relativistic and relativistic cases. These functions are given by:

$$\pi_{\kappa,i}^L = \mathcal{N}_{\kappa,i}^L r^{\gamma_L(\kappa)} e^{-\zeta_{\kappa,i}^L r^2} \quad (2.9.12)$$

$$\pi_{\kappa,i}^S = \mathcal{N}_{\kappa,i}^S r^{\gamma_S(\kappa)} e^{-\zeta_{\kappa,i}^S r^2}, \quad (2.9.13)$$

For each radial problem of a quantum number κ , we have a set of functions labeled $i = 1, \dots, n_\kappa$, where basis elements have different constant Gaussian exponents $\zeta_{\kappa,i}^{L/S}$. For a many-electron atom (as well as a single-electron one), these exponents are chosen to minimize the ground-state energy (more precisely: to make it stationary). $\mathcal{N}_{\kappa,i}^{L/S}$ are some normalization constants, and the powers of r ($\gamma_L(\kappa)$ and $\gamma_S(\kappa)$) are chosen such that the basis functions recover the right behavior of the exact radial wavefunction at small distances (where the exponential term reduces to 1) as given by [32, eq.(5.4.8,9)]:

$$\lim_{r \rightarrow 0} P_\kappa(r) \propto r^{\gamma_L} \quad \text{with} \quad \gamma_L = \left| \kappa + \frac{1}{2} \right| + \frac{1}{2} \quad (2.9.14)$$

$$\lim_{r \rightarrow 0} Q_\kappa(r) \propto r^{\gamma_S} \quad \text{with} \quad \gamma_S = \left| \kappa - \frac{1}{2} \right| + \frac{1}{2}, \quad (2.9.15)$$

for finite nuclear size models, which does not include the Coulomb point charge nuclear model. Using the limiting form of the spherical Bessel function at small distances eq.(C.3.1), one can see that this also corresponds to the behavior of the free-particle wavefunctions of eqs.(2.7.56 and 2.7.55) at the origin.

2.10 Problems with relativistic basis sets

Early numerical computations of the one-electron radial Dirac equation in the framework of finite basis sets of the form of eq.(2.9.2) (as well as the many-electron 4-component relativistic Hartree-Fock method), which were based on our knowledge of non-relativistic calculations, failed badly. These failures were manifested by three cause-related indications:

1. The obtention of unphysical numerical solutions: known as “spurious” solutions:

These solutions are highly oscillating ones, and their eigenvalues pop up in a region where they should not:

- (a) Energy levels between $-mc^2$ and the ground state (in the Hydrogen problem), as seen in Goldman’s work [65, Page 3542].
- (b) Unphysical energy levels that degenerate with the physical ones:
An energy level of $1p_{\frac{1}{2}}$ (unphysical) degenerated with the real ground-state $1s_{\frac{1}{2}}$ energy. See, for instance, Tupitsyn and Shabaev [66, Tables 1-3].

2. In one-electron problems:

The fall of a positive bound eigenvalue into the negative-energy continuum, as the basis set increases or as the basis set parameters are.

3. In many-electron SCF problems:

The convergence to an energy level that is lower than the “correct” one. This point is related to the previous one.

What is common between all the indication is that they persist even after the increase of the basis set size. The main reasons behind the encountered failures can be summarized in the following two causes:

1. The fact that (unlike the Schrödinger case), the Dirac Hamiltonian is unbounded from below.
2. The naive choice of independent large and small radial basis functions: missing the right coupling between exact components, or at least the approximation of the exact coupling.

We are mainly going to be concerned with the second cause, because it turned out that once the second problem is solved, the first one is automatically solved. In 1982, Schwarz and Wallmeier [67] (see also Grant [68] of the same year) pointed out that if large and small component functions (of some finite basis set), did not respect the right coupling predicted by the radial Dirac equation of eq.(2.7.31), then numerical instabilities and failures will occur. The argument goes as follows: The relativistic energy can be written as:

$$E = \int d^3x \psi^\dagger \{H_D - mc^2\} \psi, \quad \text{with } \psi = \begin{bmatrix} \psi^L \\ \psi^S \end{bmatrix}, \quad (2.10.1)$$

where H_D is the Dirac Hamiltonian including the radial scalar potential $-e\varphi(r)$. We (on intention) have shifted this Hamiltonian with $-mc^2$ so we can bring our expression closer to the non-relativistic

Schrödinger energy expression (removing the rest energy). This energy is then written as:

$$\begin{aligned}
 E = & -e \int d^3x \psi^{L\dagger} \varphi(r) \psi^L \\
 & + c \int d^3x \psi^{L\dagger} \boldsymbol{\sigma} \cdot \hat{\mathbf{p}} \psi^S + c \int d^3x \psi^{S\dagger} \boldsymbol{\sigma} \cdot \hat{\mathbf{p}} \psi^L \\
 & - \int d^3x \psi^{S\dagger} \{2mc^2 + e\varphi(r)\} \psi^S
 \end{aligned} \tag{2.10.2}$$

After playing around with the equation $\{H_D - mc^2\} \psi = E\psi$, ψ^S can be written in terms of the large one as:

$$\psi^S = \frac{c}{E + 2mc^2 + e\varphi(r)} \boldsymbol{\sigma} \cdot \hat{\mathbf{p}} \psi^L, \tag{2.10.3}$$

which shows the explicit coupling between the spinor components. Since this relation includes the energy, which is a sought unknown, one can overcome this problem by realizing that in the non-relativistic limit (of very large c), we are allowed to write:

$$\psi^S \approx \frac{1}{2mc} \boldsymbol{\sigma} \cdot \hat{\mathbf{p}} \psi^L. \tag{2.10.4}$$

This approximation assumes that the potential is bounded. If we then plug this last expression of ψ^S , in our energy expression of eq.(2.10.2), and use the Dirac relation of eq.(D.1.1), we directly get the following expression:

$$\begin{aligned}
 E \approx & -e \int d^3x \psi^{L\dagger} \varphi(r) \psi^L + \int d^3x \psi^{L\dagger} \frac{\hat{\mathbf{p}}^2}{2m} \psi^L \\
 & - \frac{e}{4m^2c^2} \int d^3x \psi^{L\dagger} \boldsymbol{\sigma} \cdot \hat{\mathbf{p}} \varphi(r) \boldsymbol{\sigma} \cdot \hat{\mathbf{p}} \psi^L.
 \end{aligned} \tag{2.10.5}$$

Since the last term is of order $\mathcal{O}(c^{-2})$, it can be neglected, in the non-relativistic limit, and we thus get:

$$E \approx -e \int d^3x \psi^{L\dagger} \varphi(r) \psi^L + \int d^3x \psi^{L\dagger} \frac{\hat{\mathbf{p}}^2}{2m} \psi^L, \tag{2.10.6}$$

This is the energy expression of a non-relativistic (Schrödinger or Pauli-Schrödinger) particle in the presence of a scalar potential $\varphi(r)$. We realize at this moment that to smoothly go from the relativistic energy expression of eq.(2.10.2) to the non-relativistic one of eq.(2.10.6), one must respect the right coupling between the large and the small components of eq.(2.10.3), and more precisely its non-relativistic approximation of eq.(2.10.4).

As discussed in section 2.9.1, one generally introduces two radial basis sets (one for each of the components), and solves the numerical radial eigenproblem. In the language of finite basis set, the above discussion translates to the following statement:

If the small component basis functions are not dependent on the large ones by means of eq.(2.10.4), then the non-relativistic kinetic energy operator is poorly represented, and numerical problems will/can occur: appearance of spurious solutions, and occurrence of “variational collapse”, and this comes from the fact that the kinetic energy is defectively represented in such bases. See Kutzelnigg [69]. On the other hand, if one introduces a set of basis functions that do respect the relation given in eq.(2.10.4), then one is on the safe track.

Nice explanations of this problem were provided by Stanton and Havriliak in [70] (who termed this scheme as “kinetic balance”), Kutzelnig [71] and Dyll *et al.* [72]. We finally would like to note that the problem of spurious solutions also occurs in other numerical methods such as Finite difference, finite element, and other methods. See, for instance, the PhD thesis of Almanasreh [73, chapter 3]. In the next sections we are going to expand, and make use of, the above discussion, in the construction of numerical basis sets for the radial Dirac equation.

2.10.1 Kinetic balance

The radial Dirac equation given in eq.(2.7.31) can be written in a slightly different form:

$$Q_\kappa = \frac{\hbar}{mc} \frac{1}{1 + \frac{e\varphi + E}{mc^2}} \left[\frac{d}{dr} + \frac{\kappa}{r} \right] P_\kappa \quad (2.10.7)$$

$$P_\kappa = \frac{\hbar}{mc} \frac{1}{1 - \frac{e\varphi + E}{mc^2}} \left[\frac{d}{dr} - \frac{\kappa}{r} \right] Q_\kappa. \quad (2.10.8)$$

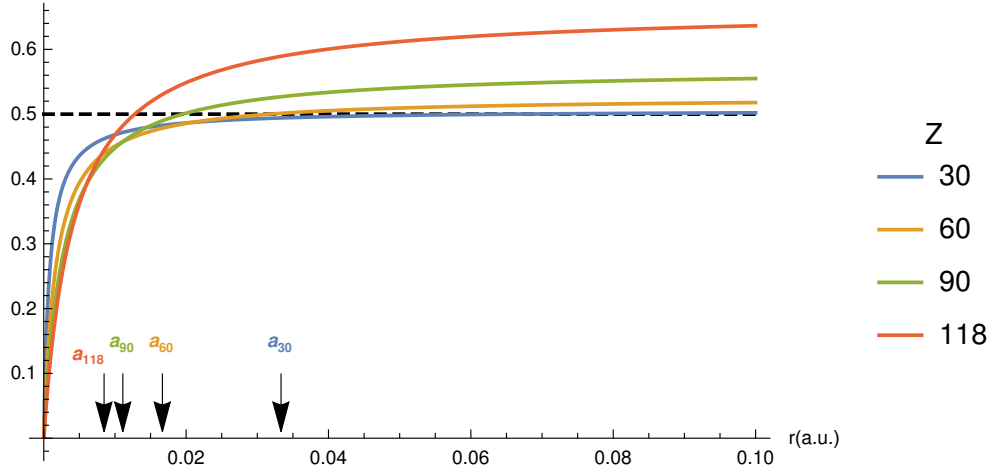
For the positive part of the spectrum, the solutions we are interested in (bound ones) live around $E \approx mc^2$ (just below it). After assuming that $e\varphi$ (the electric potential) is negligible in front of mc^2 , and thus, in front of mc^2 , the coupling between small and large components of eq.(2.10.7) can be approximated by:

$$Q_\kappa \approx \frac{\hbar}{2mc} \left[\frac{d}{dr} + \frac{\kappa}{r} \right] P_\kappa, \quad (2.10.9)$$

in the non-relativistic limit, since $\lim_{c \rightarrow \infty} cQ_\kappa = \frac{\hbar}{2m} \left[\frac{d}{dr} + \frac{\kappa}{r} \right] P_\kappa$. This is, at the level of individual basis functions, known as the (restricted) kinetic balance condition (RKB) [70] (see also [74]). Notice that this condition approximates the following function:

$$f(r, Z) = \left[1 + \frac{e\varphi(r, Z) + E(Z)}{mc^2} \right]^{-1}, \quad (2.10.10)$$

which appears in eq.(2.10.7), by 1/2. This function is plotted in the following figure 2.10.1 for different nuclear charges, where we use point nuclear model potential: $\varphi(r, Z) = \frac{Ze}{4\pi\epsilon_0 r}$, and the corresponding ground state energy level $E(Z) = mc^2\sqrt{1 - \alpha^2 Z^2}$. In addition, we add the locations of the Bohr radii, where the ground-state electron is most probably found, associated with each nuclear charge: $a_Z = \frac{1}{Z}$ (a.u.).

Figure 2.10.1: $f(r, Z)$ for a bound state electron in different Coulomb field strengths

Clearly, in the region of very small distances $r < 0.01$ a.u. and for large nuclear charges, the approximation does not work well: we deviate from the approximation (dashed) line, since the potential term can no longer be neglected (as assumed). Nevertheless, one should not be worried, since numerically, our calculation is “flexibility” thanks to the fact that large and small component functions vary freely, i.e. the coupling is not totally fixed. Numerically, one introduces a large component basis set for each κ , that we shall call $\{\pi_{\kappa,i}^L\}_{i=1}^{n_\kappa}$, where n_κ is the number of basis elements, and generate the small component functions using the previous prescription, i.e. :

$$\pi_{\kappa,i}^S = \frac{\hbar}{2mc} \left[\frac{d}{dr} + \frac{\kappa}{r} \right] \pi_{\kappa,i}^L. \quad (2.10.11)$$

The radial Dirac function is then constructed with respect to eq.(2.9.2) by:

$$\varphi_{\alpha,\kappa}(r) = \begin{bmatrix} \mathcal{P}_{\alpha,\kappa}(r) \\ \mathcal{Q}_{\alpha,\kappa}(r) \end{bmatrix} = \sum_{i=1}^{n_\kappa} c_{\alpha,\kappa,i}^L \begin{bmatrix} \pi_{\kappa,i}^L(r) \\ 0 \end{bmatrix} + \sum_{i=1}^{n_\kappa} c_{\alpha,\kappa,i}^S \begin{bmatrix} 0 \\ \frac{\hbar}{2mc} \left[\frac{d}{dr} + \frac{\kappa}{r} \right] \pi_{\kappa,i}^L(r) \end{bmatrix}, \quad (2.10.12)$$

leading to an eigenvalue problem, whose elements are given in an appendix section E.1.1. Stanton and Havriliak (in [70]) termed this procedure as “kinetic balance” for the following reasons:

1. “Kinetic” to indicate that the kinetic energy is recovered in the non-relativistic limit.
2. “Balance” to remind us that each large component function $\pi_{\kappa,i}^L(r)$ should be balanced by small component function generated by: $\frac{\hbar}{2mc} \left[\frac{d}{dr} + \frac{\kappa}{r} \right] \pi_{\kappa,i}^L(r)$, as seen in this section.

After this discussion, we should note that the RKB method is not perfectly safe, since in cases where a contracted basis set is used, this method can fail (in extreme cases), as shown by Visscher *et al.* [75] and references therein. In addition, Lewin and Séré [76, Theorem 3 and Pages 11-12], considered the problem of the spectral pollution (apparition of spurious modes) in the Dirac spectrum, once the RKB scheme is considered. Their conclusion is that in the case of a (negative) bounded potential, the RKB prescription for the Dirac problem is safe from spurious solutions (see also [77, Theorem 3.3 (i)]), while for the unbound (singular) Coulomb potential, this is not guaranteed, and a spurious solution can appear anywhere in the gap $(-mc^2, mc^2)$. They supported their discussion by a simple

Coulombic calculation of the $s_{\frac{1}{2}}$ states of the Zn^{+29} atom, using an $s_{\frac{1}{2}}$ Gaussian basis set (6-31G basis) appended with an additional basis element (last term in the curly brackets):

$$\pi^L = r \left(e^{-\zeta_1 r^2}, \dots, e^{-\zeta_n r^2}, \left\{ e^{-br^2} + \delta^{\frac{1}{4}} e^{-b\delta r^2} \right\} \right). \quad (2.10.13)$$

This additional basis function is constructed with two very localized Gaussians, associated with the parameters $(b, \delta) = (10^6 \alpha^2, \sim 10^4)$, which can feel (capture) the singular behavior of the Coulomb potential at very small distances (in the vicinity of the nucleus). They then generate the small component basis functions using the kinetic balance condition of eq.(2.10.11) and build the matrix eigenproblem then diagonalize it. They finally find a spurious solution which appears in the forbidden region of the $(-mc^2, mc^2)$ gap: below the exact ground state energy level. In addition, what is more critical about the appearance of these solutions, is that they also contaminate the other solutions (see Page 7 of the same reference).

Before ending this section, we would like to mention a final point, which concerns the coupling function of eq.(2.10.10) for continuum states in the same Coulomb field. In figures 2.10.2a and 2.10.2b, we plot $f(r, Z)$ for $E = mc^2$ and $1.5mc^2$. As predicted, the results show that as long as we are close to $E = mc^2$, our approximation of $f(r, Z)$ is valid (up to some extent), and the more we go up in energy, the more we will overestimate this function.

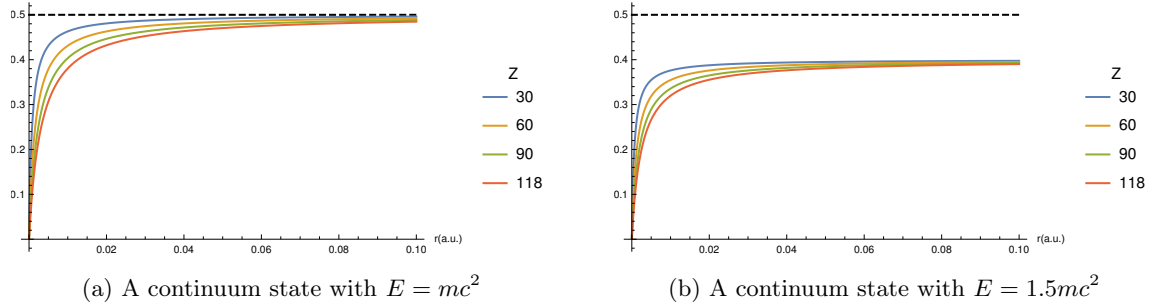


Figure 2.10.2: $f(r, Z)$ of eq.(2.10.10) for continuum states.

Finally, we should note that the kinetic balance method works (in principle) safely, in the presence of a Coulomb potential (point charge nucleus), if one does not go for extreme applications of heavy contractions or over-localized contracted basis sets. In the next section, we shall present a few real numerical calculations on a 1e atom to show what one gets (in practice) when using the RKB prescription to approximate the Dirac problem.

2.10.2 Numerical tests on restricted kinetic balance

To give the reader a flavor of this method, we performed seven calculations with the RKB scheme, each one corresponds to a different set of exponents. These exponents are discussed in section E.3 and tabulated in tables E.3-E.5. In tables 2.3 and 2.4, we present the first five eigenvalues (bound-states) of the 1e radon atom ($Z = 86$) obtained with different (sizes of) basis sets for $\kappa = \pm 1$ ($s_{\frac{1}{2}}$ and $p_{\frac{1}{2}}$ solutions), and finally, we compare these numerical results with the ones of the exact energy

State	Exact energy	7z	6z	5z	4z	3z	2z
$1s_{\frac{1}{2}}$	14620.4407	14620.8223	14620.8301	14620.8454	14620.8758	14621.0332	14625.9554
$2s_{\frac{1}{2}}$	17708.7697	•17734.6284	17774.2051	17804.1892	17843.9843	17971.0908	18685.3956
$3s_{\frac{1}{2}}$	18317.4540	19038.1400	19533.7230	19845.4006	20222.1960	21294.9092	26528.6243
$4s_{\frac{1}{2}}$	18525.0944	21471.4203	23096.6926	24112.1801	25341.2250	28887.9678	48016.0298
$5s_{\frac{1}{2}}$	18618.9832	25727.2000	29562.9802	32008.3565	35024.9668	44078.4829	104896.7087

Table 2.3: First five $s_{\frac{1}{2}}$ energy solutions of the 1e radon atom, in atomic units of energy (a.u.).

State	Exact energy	7z	6z	5z	4z	3z	2z
$2p_{\frac{1}{2}}$	17708.7697	•18202.8689	18320.3769	18517.5072	18862.1277	19601.2646	21459.3704
$3p_{\frac{1}{2}}$	18317.4540	22507.3672	23260.5908	24451.5497	26697.4458	31214.6471	
$4p_{\frac{1}{2}}$	18525.0944	31321.1154	33638.0115	37852.5808	45834.3427		
$5p_{\frac{1}{2}}$	18618.9832	47035.1760	53733.7750	66399.4588			
$6p_{\frac{1}{2}}$	18669.0892	75045.9625	94535.0943				

Table 2.4: First five $p_{\frac{1}{2}}$ energy solutions of the 1e radon atom (a.u.).

expression of the bound Dirac-solutions [28, Page 230 eq.(34)]:

$$E_{n,\kappa} = \frac{mc^2}{\sqrt{1 + \left(\frac{\alpha Z}{n - |\kappa| + \sqrt{\kappa^2 - (\alpha Z)^2}} \right)^2}}. \quad (2.10.14)$$

This above energy expression (with its associated wavefunction) solves the 1e radial Dirac equation in the presence of the Coulombic point nucleus, that generates the electric Coulomb-potential: $\phi(r) = \frac{Ze}{4\pi\epsilon_0 r}$, and thus, this potential is chosen for these numerical calculations, and enters in the matrix elements given in eqs.(E.1.16 and E.1.18). The eigenvalues colored in red correspond to solutions with $E > mc^2$ (positive continuum), and empty boxes simply indicate that the number of eigenvalues (dimensions of the Hamiltonian matrix) is less then 5. As the tables show, the exponents associated with each basis set are optimized to describe the ground-state energy, and not the excited ones.

In addition, we can see that the larger the basis set is, the lower the energies get, and thus, the closer we come to the exact energy values. We must also note that the wavefunctions of the ground state highly overlap with the exact hydrogenic wavefunctions, which can, for instance, be found in Greiner [28, Exercice 9.6]. To show this, we evaluate the integral following integral:

$$I = \int_0^\infty |\rho^{\text{num}}(r) - \rho^{\text{exact}}(r)| dr, \quad (2.10.15)$$

which measures the deviation of the numerical probability density given in eq.(E.1.6) from the exact probability density computed “exactly” with Mathematica [22], using the formulas of last citation. This Mathematica program can be found in our Gitlab directory [78]. The results of this integral for different basis sets are tabulated in table 2.5.

The reader might ask himself the following question:

The energy expression of eq.(2.10.14) shows that the energy only depends on n and κ quantum numbers, why are the numerical $2s_{\frac{1}{2}}$ and $2p_{\frac{1}{2}}$ energy values of tables 2.3 and 2.4, different? (See, for instance, the energies with a small dot •)

Bases	I
Exact	0.0000000
7z	0.0001568
6z	0.0001509
5z	0.0001711
4z	0.0002229
3z	0.0006561
2z	0.0077331

Table 2.5: Values of the I integral of eq.(2.10.15) for different bases.

The answer is given by the following argument: Unfortunately, this difference is not due to the QED corrections, since we did not include them in our calculations. The reason behind this discrepancy is simply due to the poverty of the basis sets we are using. In general, if we use an infinite basis, and a computer with an infinite numerical precision (to avoid linear dependencies) the numerical energy and wavefunctions must coincide with what the exact Dirac solutions provide. Since infinity is not naturally reachable (see Hilbert's chapter [79]), we go for a very large basis sets. We specifically used the following set of exponents:

$$\zeta_i = (1.93)^{i-1} \times 0.02, \quad \text{for } i = 1, \dots, 50 \quad (2.10.16)$$

which was made by hand, to construct both Hamiltonians associated with $\kappa = \pm 1$. After diagonalization, we got the following results for the first excited states:

$$E_{2s_{\frac{1}{2}}}^{\text{num.}} = 17708.7698\textcolor{red}{28} \quad (2.10.17)$$

$$E_{2p_{\frac{1}{2}}}^{\text{num.}} = 17708.7698\textcolor{red}{09}, \quad (2.10.18)$$

where we color in red the non-matching digits (with the exact energy). This result shows that, generally speaking, the larger the basis set is, the closer we get to degeneracy. In addition, for this large basis set we find I of eq.(2.10.15) to be $I = 2 \times 10^{-6}$. So far this analysis covered the case of positive-energy solutions and uses the coupling of eq.(2.10.7), but what about the negative-energy ones? The answer will be given in the next section by focusing on the second equation.(2.10.8) instead of the first one.

2.10.3 Inverse kinetic balance

Since the Dirac equation is symmetric between positive and negative-energy solutions (\mathcal{C} -symmetry in the time-independent problem), one would directly guess that in order to have a balanced picture, we should also consider negative-energy solutions. Alternatively to what we have discussed in the previous section, we can approximate the coupling of eq.(2.10.8) in the non-relativistic limit as:

$$P_\kappa \approx \frac{\hbar}{2mc} \left[\frac{d}{dr} - \frac{\kappa}{r} \right] Q_\kappa, \quad (2.10.19)$$

since $\lim_{c \rightarrow \infty} cP_\kappa = \frac{\hbar}{2m} \left[\frac{d}{dr} - \frac{\kappa}{r} \right] Q_\kappa$. We again assume that $e\varphi(r, Z)$ can be neglected in front of the energy which is around $E \approx -mc^2$ in eq.(2.10.8). Again, at the level of basis functions, this condition translates to:

$$\pi_{\kappa,i}^L = \frac{\hbar}{2mc} \left[\frac{d}{dr} - \frac{\kappa}{r} \right] \pi_{\kappa,i}^S, \quad (2.10.20)$$

where a set of small radial functions is first introduced, and the large set is then generated with respect to this relation. This choice of basis functions leads to a matrix representation of the Dirac problem that is presented in eqs.(E.0.1, E.1.13 and E.1.14) of appendix E. This prescription was introduced by Sun *et al.* [80], where they have presented an expanded discussion on the comparison between different prescriptions for constructing a basis set for the Dirac equation. In addition, they have performed several calculations (using Gaussian basis sets), one of them was presented in table 3 (of the cited reference) and showed that the IKB prescription did not perform as well as the RKB prescription, especially for the smallest considered basis. This is mainly due to the fact that the IKB condition approximates the right coupling between the two components for a negative-energy solution. We started this section by saying that we should be more balanced between both energy signs solutions, and to do so, we shall consider the Dual Kinetic Balance prescription.

2.10.4 Dual kinetic balance

The dual kinetic balance (DKB) scheme ensures the proper approximates coupling between large and small component functions for both positive- and negative-energy solutions at the same time. This method uses four-component basis functions instead of two-component ones (as in RKB and IKB), and expands the Dirac solution in the following manner:

$$\varphi_{\alpha,\kappa}(r) = \sum_{i=1}^{n_{\kappa}^{[+]}} c_{\alpha,\kappa,i}^{[+]} \varphi_{\kappa,i}^{[+]}(r) + \sum_{i=1}^{n_{\kappa}^{[-]}} c_{\alpha,\kappa,i}^{[-]} \varphi_{\kappa,i}^{[-]}(r); \quad (2.10.21)$$

$$\varphi_{\kappa,i}^{[+]}(r) = \left[\frac{\hbar}{2mc} \left[\frac{d}{dr} + \frac{\kappa}{r} \right] \pi_{\kappa,i}^{+}(r) \right] \quad (2.10.22)$$

$$\varphi_{\kappa,i}^{[-]}(r) = \left[\frac{\hbar}{2mc} \left[\frac{d}{dr} - \frac{\kappa}{r} \right] \pi_{\kappa,i}^{-}(r) \right], \quad (2.10.23)$$

where the positive superscript indicates that the basis elements approximate the right coupling between large and small components for positive-energy solutions, and the negative-one does the same for negative-energy solutions. This shows that the DKB scheme “combines” both RKB and IKB schemes. The Dual Kinetic Balance (DKB) scheme was first introduced by Shabaev *et. al* [81], where they used B-spline functions to compute the first-order (single-loop) self-energy correction for one-electron atoms. The advantage of this scheme is that it is democratic between positive and negative-energy solutions, i.e. it does not favor one on the other. In addition, as we shall soon see, this prescription allows the realization of the charge conjugation symmetry without adding a restriction on the type of functions one must use (unlike in the RKB scheme, as we shall see in section 2.11.2). The associated eigenvalue equation associated with the DKB scheme, is presented with its matrices and matrix elements in appendix section E.2. We have constructed this eigenvalue problem with the exponents of the 7z basis set (used in for the RKB calculations: section 2.10.1) in Mathematica [22]. In table 2.6, we present the first five eigenvalues of the numerical Dirac Hamiltonian of $\kappa = -1$, built with respect to the DKB scheme, and compare these results with:

1. The previous results we have obtained with RKB 2.3 (using the same basis: 7z).
2. The exact Dirac energies from eq.(2.10.14).

From the first glance, the reader might think that this is not an improvement, but the reader should also know that the used exponents were originally optimized for RKB. This means that DKB is performing well.

State	Exact	DKB - 7z	RKB - 7z
$1s_{\frac{1}{2}}$	14620.4407	14620.7605	14620.8223
$2s_{\frac{1}{2}}$	17708.7697	17734.9031	17734.6284
$3s_{\frac{1}{2}}$	18317.4540	19045.5995	19038.1400
$4s_{\frac{1}{2}}$	18525.0944	21516.09305	21471.4203
$5s_{\frac{1}{2}}$	18618.9832	25906.58707	25727.2000

Table 2.6: First five $s_{\frac{1}{2}}$ energy solutions of the 1e radon atom, in atomic units of energy (a.u.).

2.10.5 Atomic balance

In section 2.10.1, we mentioned the fact that the Kinetic Balance method can fail under extreme conditions. A solution to this failure is the use the Atomic Balance (AB) prescription (see [77]). In this new prescription, the coupling between large and small component functions is approximated, by setting $E = mc^2$ (as in the RKB case), but without neglecting the scalar potential (as done in the RKB). Contrary to RKB, AB can capture the possible singular behavior of the external scalar potential as mentioned by Lewin and Séré in the cited reference. To show how this is true, we define the following three small component radial function as:

$$Q_{n,\kappa}^{\text{exact}} = \frac{\hbar}{mc} \frac{1}{1 + \frac{e\varphi + E_{n,\kappa}}{mc^2}} \left[\frac{d}{dr} + \frac{\kappa}{r} \right] P_{n,\kappa}^{\text{exact}} \quad (2.10.24)$$

$$Q_{n,\kappa}^{\text{AB}} = \frac{c\hbar}{2mc^2 + e\varphi} \left[\frac{d}{dr} + \frac{\kappa}{r} \right] P_{n,\kappa}^{\text{exact}} \quad (2.10.25)$$

$$Q_{n,\kappa}^{\text{RKB}} = \frac{\hbar}{2mc} \left[\frac{d}{dr} + \frac{\kappa}{r} \right] P_{n,\kappa}^{\text{exact}}, \quad (2.10.26)$$

where the first one is simply the exact small component function, generated from the exact large component radial function (using the exact coupling), the second function is the Atomic Balance small component, which is constructed from the approximated coupling (by setting $E = mc^2$), and finally, the third one is the RKB approximation, which we have already discussed in a previous section.

In the next figure 2.10.3 we plot these three functions associated with the ground-state: $(n, \kappa) = (1, -1)$ of the one-electron radon atom ($Z = 86$), and observe together. The graph shows the RKB coupling fails to correctly describe the small component wavefunction at very small distances, while the atomic balance coupling successes in capturing this behavior. At large distances, both prescriptions provide a fair description of the small radial function.

We should, in addition, note that we have observed this divergent behavior of the RKB approximation only for states associated with $\kappa = \pm 1$, and not for other values of κ (see, for instance, figure 2.10.4), which is probably related to the fact that Visscher *et al.* [75] observed failures of the RKB prescription for heavily contracted $s_{\frac{1}{2}}$ - and $p_{\frac{1}{2}}$ -type basis functions. This point is to be further investigated.

We must also note that the “atomic balance” discussed here, as in the work of Lewin and Séré is not to be confused with the “atomic balance” usually discussed in quantum chemistry literature, that simply designates the exact coupling between radial components, seen for instance in eq.(2.10.24), and which comes from the work of Visscher *et al.* [75].

The atomic balance prescription tells us that at the level of basis functions, the numerical wave-

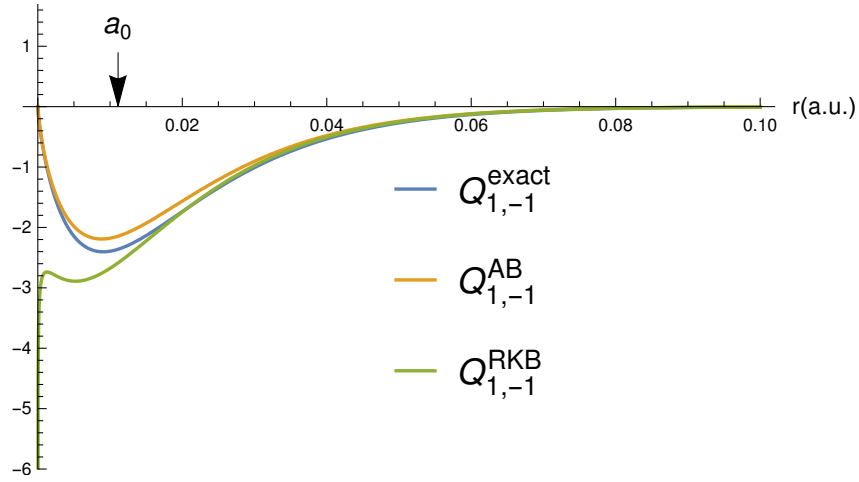
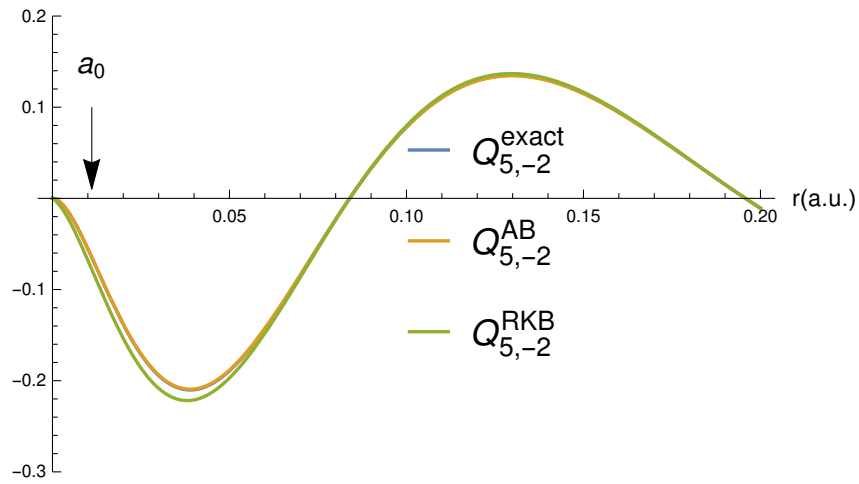


Figure 2.10.3: Approximations of the small component function of the radon atom ground state.

Figure 2.10.4: Approximations of the small component function $Q_{n,\kappa}(r)$, with $(n, \kappa) = (5, -2)$.

function should be expanded as:

$$\varphi_{\alpha,\kappa}(r) = \begin{bmatrix} \mathcal{P}_{\alpha,\kappa}(r) \\ \mathcal{Q}_{\alpha,\kappa}(r) \end{bmatrix} = \sum_{i=1}^{n_\kappa} c_{\alpha,\kappa,i}^L \begin{bmatrix} \pi_{\kappa,i}^L(r) \\ 0 \end{bmatrix} + \frac{\hbar c}{2mc^2 + e\varphi(r)} \sum_{i=1}^{n_\kappa} c_{\alpha,\kappa,i}^S \begin{bmatrix} 0 \\ \left[\frac{d}{dr} + \frac{\kappa}{r}\right] \pi_{\kappa,i}^L(r) \end{bmatrix}. \quad (2.10.27)$$

The main disadvantage of this prescription is its advantage, i.e., the existence of the $e\varphi(r)$ term in the denominator. Although this term provides a better description of the small component function, it complicates the integrals associated with the matrix representation of the Dirac problem. As far as we know, this method has never been employed in practical calculations.

Finally, we would like to note that, as in the Kinetic Balance context, we had IKB and DKB, one can imagine two alternative basis set prescriptions associated with the Atomic Balance, which we shall call:

1. The Inverse Atomic Balance (IAB) where the numerical functions are expanded as:

$$\varphi_{\alpha,\kappa}(r) = \frac{\hbar c}{2mc^2 - e\varphi(r)} \sum_{i=1}^{n_\kappa} c_{\alpha,\kappa,i}^L \begin{bmatrix} \left[\frac{d}{dr} - \frac{\kappa}{r}\right] \pi_{\kappa,i}^S(r) \\ 0 \end{bmatrix} + \sum_{i=1}^{n_\kappa} c_{\alpha,\kappa,i}^S \begin{bmatrix} 0 \\ \pi_{\kappa,i}^S(r) \end{bmatrix}. \quad (2.10.28)$$

2. The Dual Atomic Balance (DAB), where this expansion becomes:

$$\varphi_{\alpha,\kappa}(r) = \sum_{i=1}^{n_\kappa^L} c_{\alpha,\kappa,i}^{[+]} \varphi_{\kappa,i}^{[+]}(r) + \sum_{i=1}^{n_\kappa^S} c_{\alpha,\kappa,i}^{[-]} \varphi_{\kappa,i}^{[-]}(r); \quad (2.10.29)$$

$$\varphi_{\kappa,i}^{[+]}(r) = \frac{1}{r} \begin{bmatrix} \pi_{\kappa,i}^L(r) \\ \frac{i\hbar c}{2mc^2 + e\varphi} \left[\frac{d}{dr} + \frac{\kappa}{r}\right] \pi_{\kappa,i}^L(r) \end{bmatrix} \quad (2.10.30)$$

$$\varphi_{\kappa,i}^{[-]}(r) = \frac{1}{r} \begin{bmatrix} \frac{\hbar c}{2mc^2 - e\varphi} \left[\frac{d}{dr} - \frac{\kappa}{r}\right] \pi_{\kappa,i}^S(r) \\ i\pi_{\kappa,i}^S(r) \end{bmatrix}. \quad (2.10.31)$$

These two prescriptions were never discussed in the literature and need to be further examined. The second scheme is of importance since:

1. It can sense the Coulomb potential singularity (point nucleus), which is an excellent property, especially for calculating extremely localized quantities (example: The vacuum polarization density).
2. It is balanced between positive and negative-energy solutions, as the dual kinetic balance prescription.
3. It can be made symmetric under charge conjugation.

2.10.6 A short summary on relativistic basis functions

So far, the most widespread prescription is the restricted kinetic balance. This method has proved its efficiency since its early proposition and showed that it only fails in very specific (extreme) regions. Although the atomic balance can feel the singularity of the Coulomb potential, the computational cost that this method demand does not make it a viable option. The inverse kinetic balance method, which is the negative-energy version of the restricted kinetic balance, does not give better results for the positive-energy solutions (mainly: bound-states), as we expect (by pure intuition), and as Sun *et al.* have shown. Finally, the Dual kinetic balance method provides a more symmetric description of

the Dirac equation, since it treats both positive and negative-energy solutions democratically. This last prescription shares with restricted kinetic balance the difficulty of feeling/catching the Coulomb singularity (as mentioned by Lewin and Séré in the next references). For a rigorous investigation on the possibility of spurious states occurrence, in the finite basis Dirac equation, the reader may consult the works of Lewin and Séré [76, 77].

We are next going to investigate the obedience of the \mathcal{C} -symmetry in the framework of relativistic finite basis sets. This investigation will fructify additional new results and will guide us in constructing basis sets that can be used in computing QED quantities, as we shall see in the next chapter.

2.11 \mathcal{C} -symmetry in the finite basis set

We say that a basis set is symmetric under \mathcal{C} -symmetry if the charge conjugation of any element of the basis set is an element of the basis set itself:

$$\mathcal{C}\varphi_i \in \{\varphi_i\}_{i=1}^n, \quad \forall i. \quad (2.11.1)$$

More specifically, in two-component basis sets, the numerical solutions are expanded in large and small component spherical basis functions as:

$$\varphi_{\kappa, m_j}(\mathbf{x}) = \sum_{i=1}^{n_{\kappa}^L} c_{\kappa, i}^L \varphi_{\kappa, i, m_j}^L(\mathbf{x}) + \sum_{i=1}^{n_{\kappa}^S} c_{\kappa, i}^S \varphi_{\kappa, i, m_j}^S(\mathbf{x}); \quad (2.11.2)$$

$$\text{with } \varphi_{\kappa, i, m_j}^L = \begin{bmatrix} \pi_{\kappa, i}^L \Omega_{\kappa, m_j} \\ 0 \end{bmatrix}; \quad \varphi_{\kappa, i, m_j}^S = \begin{bmatrix} 0 \\ i\pi_{\kappa, i}^S \Omega_{-\kappa, m_j} \end{bmatrix}. \quad (2.11.3)$$

After the application of the \mathcal{C} -operation of eq.(2.8.17) on the large and small basis elements, one gets:

$$\mathcal{C}\varphi_{\kappa, i, m_j}^L = \text{sgn}(\kappa) (-1)^{m_j - \frac{1}{2}} \begin{bmatrix} 0 \\ i\pi_{\kappa, i}^L \Omega_{\kappa, -m_j} \end{bmatrix} \quad (2.11.4)$$

$$\mathcal{C}\varphi_{\kappa, i, m_j}^S = \text{sgn}(\kappa) (-1)^{m_j - \frac{1}{2}} \begin{bmatrix} \pi_{i, \kappa}^S \Omega_{-\kappa, -m_j} \\ 0 \end{bmatrix}. \quad (2.11.5)$$

The phase constants can be neglected. Large and small basis elements associated with opposite sign quantum numbers $-\kappa, -m_j$ are given by:

$$\varphi_{-\kappa, i, -m_j}^L = \begin{bmatrix} \pi_{-\kappa, i}^L \Omega_{-\kappa, -m_j} \\ 0 \end{bmatrix} \quad (2.11.6)$$

$$\varphi_{-\kappa, i, -m_j}^S = \begin{bmatrix} 0 \\ i\pi_{-\kappa, i}^S \Omega_{\kappa, -m_j} \end{bmatrix}. \quad (2.11.7)$$

By comparison of the charge conjugated basis elements of eqs.(2.11.4 and 2.11.5) with the negative sign quantum numbers basis elements of eqs.(2.11.6 and 2.11.7), one directly notices that in order to force the charge conjugated basis elements to be (themselves) basis elements (as stated in eq.(2.11.1)), restrictions has to be added on the basis functions, that is:

$$\pi_{-\kappa, i}^L = \pi_{\kappa, i}^S \quad \text{and} \quad \pi_{-\kappa, i}^S = \pi_{\kappa, i}^L, \quad (2.11.8)$$

κ	α	Eigenvalues	Coefficients			
			$c_{\alpha,\kappa,1}^L$	$c_{\alpha,\kappa,2}^L$	$c_{\alpha,\kappa,1}^S$	$c_{\alpha,\kappa,2}^S$
-1	1	+18784.7467	4.9279	-10.2191	4.9272	-10.2175
	2	+18780.0698	3.8892	-2.6523	3.8890	-2.6522
	3	-18780.0698	0.0220	-0.0150	-686.6667	468.2902
	4	-18784.7467	0.0616	-0.1279	-393.7591	816.5381
+1	1	+18786.6788	-4.0603	13.2692	-4.0594	13.2665
	2	+18780.9834	-4.1081	3.5555	-4.1079	3.5553
	3	-18780.9834	0.0309	-0.0267	-546.9943	473.4147
	4	-18786.6788	0.0586	-0.1914	-281.4727	919.8613

Table 2.7: Results of the free particle RKB calculation.

Note: Energy eigenvalues are in Hartree atomic units.

which are equivalent. Notice that this is trivially consistent with what we got when considering the charge conjugation symmetry in the spherical problem (see section 2.8.1.2).

We note that if the chosen basis functions are spherical Gaussian functions, which were given in eqs.(2.9.12 and 2.9.13), then the last restriction translates into a restriction on the Gaussian exponents, given by:

$$\zeta_{\pm\kappa,i}^S = \zeta_{\mp\kappa,i}^L. \quad (2.11.9)$$

Even though this basis is now \mathcal{C} -symmetric, we should warn the reader that this is not a good choice of basis functions. The reason for this claim is that this basis does not respect the proper coupling between its large and small components, and it will thus lead to numerical instabilities (as previously discussed in section 2.10). It is, therefore, necessary to note that the reasoning made in this paragraph is made, not to be used literally, but rather to go further in the analysis (next section).

2.11.1 An unexpected symmetry in the free-particle problem of RKB

In our earlier attempts to understand how the \mathcal{C} -symmetry is manifested in the RKB scheme, which is the main scheme used in relativistic calculations, we performed a free calculation, i.e. by simply setting the nuclear charge parameter Z to zero. The reason we did so, is because we know that in the free particle problem, the \mathcal{C} -symmetry exists between opposite energy solutions, as seen in the plane wave problem of section 2.6.1, the general time-independent problem of section 2.8.1.1 and the specific spherical problem of section 2.8.1.2. Being inspired our previous results, we set the same exponent list for both $\kappa = \pm 1$:

$$\zeta_{\kappa=\pm 1}^L = \{1, 2\}, \quad (2.11.10)$$

for the large component Gaussian basis functions of eq.(2.9.12), since we expect the \mathcal{C} -symmetry to exist between opposite κ -sign problems. We then construct the two RKB matrix problems (each associated with a κ), and diagonalize them. The obtained results of eigenvalues and normalized coefficients (of the corresponding eigenvectors) are presented in table 2.7. At the first glance, we saw that the eigenvalues were exactly symmetric but within each of the κ problems separately (which is not expected), and by “exactly”, we note that the matching digits are up to a hundred (our numerical precision). Unfortunately, after comparing the coefficients we see no apparent symmetry: matching coefficients between opposite energy solutions.

We then take a pencil and a paper, and write the free RKB equation (E.0.1) using eqs. (E.1.9 and E.1.10):

$$\begin{bmatrix} mc^2 S & T \\ T & -\frac{1}{2}T \end{bmatrix} \begin{bmatrix} \mathbf{c}^L \\ \mathbf{c}^S \end{bmatrix}_\alpha = \epsilon_\alpha \begin{bmatrix} S & 0 \\ 0 & \frac{1}{2mc^2}T \end{bmatrix} \begin{bmatrix} \mathbf{c}^L \\ \mathbf{c}^S \end{bmatrix}_\alpha, \quad (2.11.11)$$

where we have dropped all indices on matrices. This matrix equation can be expanded into two coupled matrix equations:

$$T\mathbf{c}_\alpha^S = [\epsilon_\alpha - mc^2] S\mathbf{c}_\alpha^L \quad (2.11.12)$$

$$T\mathbf{c}_\alpha^L = \left[\frac{\epsilon_\alpha + mc^2}{2mc^2} \right] T\mathbf{c}_\alpha^S. \quad (2.11.13)$$

We then replace $T\mathbf{c}_\alpha^S$ in the second equation by its value from the first one to get:

$$T\mathbf{c}_\alpha^L = \lambda_\alpha S\mathbf{c}_\alpha^L, \quad \text{with} \quad \lambda_\alpha = \frac{\epsilon_\alpha^2 - m^2 c^4}{2mc^2}. \quad (2.11.14)$$

This is the eigenvalue equation of the kinetic energy operator, of a free particle (notice the relativistic energy-momentum relation), which again indicates that once the RKB is used, one recovers the non-relativistic kinetic energy operator. Notice that the existence of ϵ_α^2 term, in the last formula, indicates that a single value of λ_α , corresponds to two values of ϵ_α :

$$\epsilon_\alpha = \pm \sqrt{2mc^2 \lambda_\alpha + m^2 c^4}, \quad (2.11.15)$$

which is consistent with what we got in our numerical calculation, and leads to the following opposite energy eigenvector pair:

$$N_\alpha^+ \begin{bmatrix} \mathbf{c}_\alpha^L \\ \frac{2mc^2}{|\epsilon_\alpha| + mc^2} \mathbf{c}_\alpha^L \end{bmatrix}, \quad \text{and} \quad N_\alpha^- \begin{bmatrix} \mathbf{c}_\alpha^L \\ -\frac{2mc^2}{|\epsilon_\alpha| + mc^2} \mathbf{c}_\alpha^L \end{bmatrix}, \quad (2.11.16)$$

where N_α^+ and N_α^- are normalization constants. The numerical evaluation of these expressions gave matching results with what we have encountered in our calculation presented in the previous table. We should also note that we have recently found this analysis in Quiney's chapter [82, Section 2.4].

The free RKB problem displays a symmetric energy spectrum, which we, at first, naively associated with the \mathcal{C} -symmetry. After further study, we have found a different algebraic symmetry, which cannot, in any way, be related to the \mathcal{C} -symmetry. In our publication [21] we have discussed this point, and pointed out that the RKB and IKB schemes are related by charge conjugation symmetry. To show how, we write the matrix equations of RKB and IKB as:

$$H_{-e,\kappa}^{\text{RKB}} \mathbf{c}_{-e,\alpha,\kappa}^{\text{RKB}} = \epsilon_{-e,\alpha,\kappa}^{\text{RKB}} S_{\kappa}^{\text{RKB}} \mathbf{c}_{-e,\alpha,\kappa}^{\text{RKB}} \quad (2.11.17)$$

$$H_{-e,\kappa}^{\text{IKB}} \mathbf{c}_{-e,\alpha,\kappa}^{\text{IKB}} = \epsilon_{-e,\alpha,\kappa}^{\text{IKB}} S_{\kappa}^{\text{IKB}} \mathbf{c}_{-e,\alpha,\kappa}^{\text{IKB}}, \quad (2.11.18)$$

where we added a subscript of $-e$ to indicate that this is an electronic problem. The positronic one will thus have a $+e$ subscript instead. Recall that the RKB problem is written in terms of $\pi_{i,\kappa}^L$ while the IKB problem is written in terms of $\pi_{i,\kappa}^S$. Being inspired by the results on the charge conjugation symmetry in the spherical problem (see table 2.1), we write IKB problem associated with $-\kappa$ and $+e$ as:

$$H_{+e,-\kappa}^{\text{IKB}} \mathbf{c}_{+e,\alpha,-\kappa}^{\text{IKB}} = \epsilon_{+e,\alpha,-\kappa}^{\text{IKB}} S_{-\kappa}^{\text{IKB}} \mathbf{c}_{+e,\alpha,-\kappa}^{\text{IKB}}, \quad (2.11.19)$$

for a postironic problem, and set its (small) basis functions equal to the large basis functions of the RKB problem of $+\kappa$, i.e. : $\pi_{i,-\kappa}^S = \pi_{i,+\kappa}^L$. After setting this restriction on basis functions, it can be then shown that the Hamiltonians, and the overlap matrices of these two problems:

					Coefficients			
	κ	q	α	Eigenvalue	$c_{\alpha,\kappa,1}^L$	$c_{\alpha,\kappa,2}^L$	$c_{\alpha,\kappa,1}^S$	$c_{\alpha,\kappa,2}^S$
RKB	-1	-e	1	+18771.6260	5.8812	-7.5685	5.8807	-7.5672
			2	+18757.5795	2.1957	-7.3609	2.1956	-7.3615
			3	-18787.9710	-0.0249	0.0210	704.5024	-506.3431
			*4	-18801.4342	0.0606	-0.1270	-360.8792	+793.5029
IKB	+1	+e	*1	+18801.4342	-360.8792	793.5029	0.0606	-0.1270
			2	+18787.9710	704.5024	-506.3431	-0.0249	0.0210
			3	-18757.5795	2.1956	-7.3615	2.1957	-7.3609
			4	-18771.6260	5.8807	-7.5672	5.8812	-7.5685

Table 2.8: The \mathcal{C} -symmetry between RKB and IKB problems.

1. Electronic RKB problem with $+\kappa, -e$.
2. Positronic IKB problem with $-\kappa, +e$.

are connected by the following relations:

$$\sigma_1 S_{\kappa}^{\text{RKB}} \sigma_1 = S_{-\kappa}^{\text{IKB}} \quad (2.11.20)$$

$$\sigma_1 H_{-e,\kappa}^{\text{RKB}} \sigma_1 = -H_{+e,-\kappa}^{\text{IKB}}, \quad (2.11.21)$$

where σ_1 is the first Pauli matrix. These two relations lead to the following eigen-equation:

$$H_{+e,-\kappa}^{\text{IKB}} \{ \sigma_1 \mathbf{c}_{-e,\alpha,\kappa}^{\text{RKB}} \} = -\epsilon_{-e,\alpha,\kappa}^{\text{RKB}} S_{-\kappa}^{\text{IKB}} \{ \sigma_1 \mathbf{c}_{-e,\alpha,\kappa}^{\text{RKB}} \}. \quad (2.11.22)$$

This obtained equation clearly indicates a symmetry between eigensolutions:

$$\begin{aligned} \mathbf{c}_{+e,\alpha,-\kappa}^{\text{IKB}} &= \sigma_1 \mathbf{c}_{-e,\alpha,\kappa}^{\text{RKB}} \\ \epsilon_{+e,\alpha,-\kappa}^{\text{IKB}} &= -\epsilon_{-e,\alpha,\kappa}^{\text{RKB}}, \end{aligned} \quad (2.11.23)$$

which shows that opposite energy-, charge- and κ -sign equations of both problems are related by the \mathcal{C} -symmetry. This result is consistent with what was mentioned by Sun *et al.* [80, Section 2.2]. To show how this symmetry manifests itself in practice, we perform two small calculations:

1. RKB with $\kappa = -1$, and an electron: charge $q = -e$.
2. IKB with $\kappa = +1$, and a positron: charge $q = +e$.

We in addition set the exponent list $\zeta = (1, 2)$ for both large and small component functions, that enters in RKB and IKB, respectively. The results are then presented in table 2.8, and one must keep in mind that α is simply a labeling of the obtained eigen-solutions. These numerical results clearly show that our analytical result of eq.(2.11.23) is a correct one. Take for instance the fourth and the first solutions of the RKB and IKB problems, respectively (asterisked solutions): these two solutions correspond to opposite energy-, charge- and κ -signs. In addition, we see that the large component coefficients of one solution are the small ones of the other, as predicted by the first line of eq.(2.11.23).

At this point, a question directly popped up in our mind:

Can we make RKB (by itself) symmetric by \mathcal{C} -conjugation?

This question will be answered in the next section.

2.11.2 Can we make RKB symmetric by \mathcal{C} -conjugation?

The RKB small radial function generator is given by eq.(2.10.11):

$$\pi_{\kappa,i}^S = \eta \left[\frac{d}{dr} + \frac{\kappa}{r} \right] \pi_{\kappa,i}^L \quad \text{with } \eta = \frac{2mc}{\hbar}. \quad (2.11.24)$$

After the imposition of the radial functions restrictions of eq.(2.11.8), one obtains the following large component function equation:

$$\left(\frac{d^2}{dr^2} - \frac{\kappa(1+\kappa)}{r^2} - \eta^2 \right) \pi_{\kappa,i}^L = 0. \quad (2.11.25)$$

This equation looks very similar to eq.(C.2.3), and, using the following change of variable: $x = i\eta r$, our equation becomes:

$$\left(\frac{d^2}{dx^2} - \frac{\kappa(1+\kappa)}{x^2} + 1 \right) \pi_{\kappa,i}^L = 0. \quad (2.11.26)$$

Following what we have done in the case of the free radial Dirac equation, of section 2.7.3, the solution of the last equation can be written as a linear combination of the spherical Bessel functions:

$$\pi_{\kappa,i}^L(r) = c_1 r j_\kappa(i\eta r) + c_2 r y_\kappa(i\eta r). \quad (2.11.27)$$

We then discard solutions that diverge at the origin ($r = 0$), and obtain the following radial solutions:

$$\text{For positive } \kappa : \begin{cases} \pi_{\kappa,i}^L &= c_1 r j_\kappa(i\eta r) \\ \pi_{\kappa,i}^S &= \frac{ic_1 \hbar \eta}{2mc} r j_{\kappa-1}(i\eta r) \end{cases} \quad (2.11.28)$$

$$\text{For negative } \kappa : \begin{cases} \pi_{\kappa,i}^L &= c_2 (-1)^{\kappa+1} r j_{-\kappa-1}(i\eta r) \\ \pi_{\kappa,i}^S &= \frac{ic_2 \hbar \eta}{2mc} (-1)^\kappa r j_{-\kappa}(i\eta r) \end{cases}, \quad (2.11.29)$$

where the wave vector k (in the cited section) is replaced by $i\eta$, and the free-electron energy E is replaced by mc^2 . These two cases can be combined into one:

$$\begin{aligned} \pi_{\kappa,i}^L &= r j_\ell(i\eta r) \\ \pi_{\kappa,i}^S &= \frac{\hbar i \eta \text{sgn}(\kappa)}{2mc} r j_{\ell-\text{sgn}(\kappa)}(i\eta r) \end{aligned} \quad (2.11.30)$$

One has to notice that the constant η in $\pi_{\kappa,i}^S = \eta \left[\frac{d}{dr} + \frac{\kappa}{r} \right] \pi_{\kappa,i}^L$, can be anything, since at the end, the expansion of eq.(2.9.2) can absorb any multiplicative constant (for large and small radial functions). We further examine what should the constant η be, in order for the radial functions to behave well at large distances. We start by writing η as a general complex number:

$$\eta = a + ib, \quad \text{with } a, b \in \mathbb{R}. \quad (2.11.31)$$

We know that at large distances, the spherical Bessel functions j_n behave as:

$$j_n(i\eta r) \sim + (i\eta r)^{-1} \sin\left(i\eta r - \frac{n\pi}{2}\right) + e^{|\Im(i\eta r)|} \mathcal{O}\left((i\eta r)^{-2}\right), \quad (2.11.32)$$

as given in eq.(C.3.4). The first term is clearly safe since the inverse term $(i\eta r)^{-1}$ will damp the sinusoidal function, while the second one can cause problems due to the existence of the exponential

factor that can grow faster than $(z)^{-2}$ and can thus lead to a divergent behavior of the function in the limit $r \rightarrow +\infty$. This apparent problem can only be solved by setting η to be purely imaginary, and this sets this problematic exponential to $e^{|\Im(i\eta r)|} = 1$. For simplicity reasons, we set:

$$\eta = -ib, \quad (2.11.33)$$

which will reduce our radial functions of eq.(2.11.30) to:

$$\begin{aligned} \pi_{\kappa,i}^L &= r j_\ell(br) \\ \pi_{\kappa,i}^S &= \frac{\hbar b \operatorname{sgn}(\kappa)}{2mc} r j_{\ell-\operatorname{sgn}(\kappa)}(br). \end{aligned} \quad (2.11.34)$$

Numerically speaking, one can consider specifying a vector of scaling constants $\{b_{\kappa,i}\}_{i=1}^{n_\kappa}$, and expand the α (label) wavefunction in the following basis:

$$\varphi_{\alpha,\kappa,m_j}(\mathbf{x}) = \sum_{i=1}^{n_\kappa} c_{\alpha,\kappa,i}^L \begin{bmatrix} r j_\ell(b_{\kappa,i}r) \Omega_{\kappa,m_j} \\ 0 \end{bmatrix} + \sum_{i=1}^{n_\kappa} c_{\alpha,\kappa,i}^S \begin{bmatrix} 0 \\ i r j_{\ell-\operatorname{sgn}(\kappa)}(b_{\kappa,i}r) \Omega_{-\kappa,m_j} \end{bmatrix}. \quad (2.11.35)$$

In figures 2.11.1a and 2.11.1b we plot the large and small basis functions $\pi_{\kappa,i}^L/r$ and $\pi_{\kappa,i}^S/r$ for the $s_{\frac{1}{2}}$ -type functions ($\kappa = -1$), and we randomly choose the $b_{\kappa,i}$ vector to be:

$$b_{\kappa,i} = i, \quad \text{for } i = 1, \dots, 5. \quad (2.11.36)$$

and normalize our functions over the radial region, extending from the origin to $r = 10$. In figures 2.11.1c and 2.11.1d we do the same for the $p_{\frac{3}{2}}$ -type functions ($\kappa = -2$).

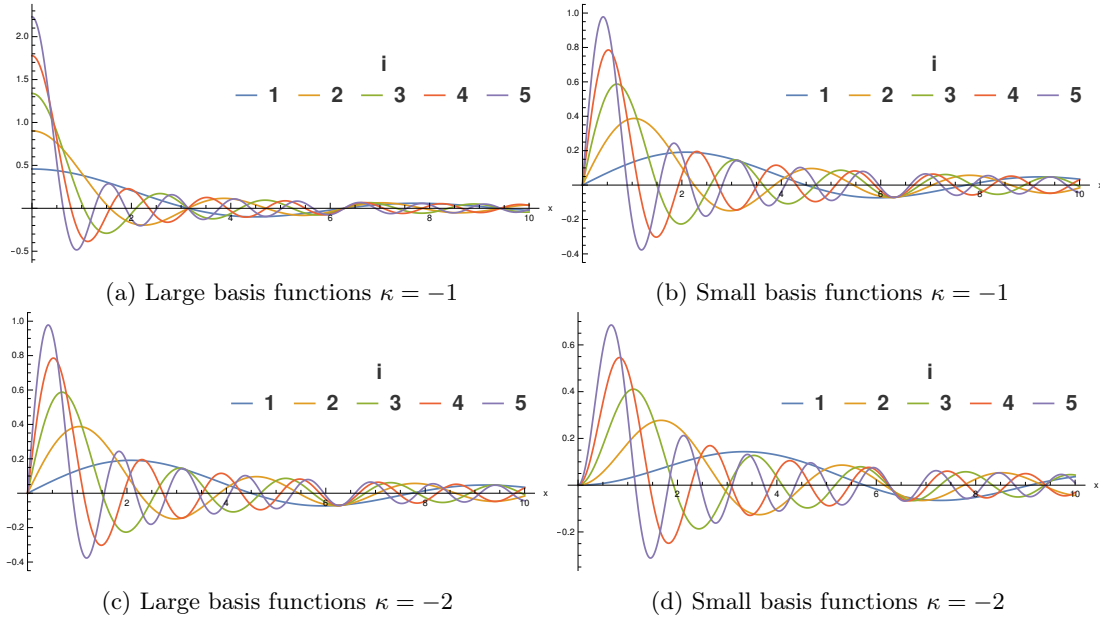


Figure 2.11.1: Normalized Bessel basis functions built out of the $b_{\kappa,i}$ vector of eq.(2.11.36).

2.11.3 A new basis for confined systems

The problem with the previous functions is that they cannot be normalized to 1 (over the infinite space), but inside a spherical box (of finite radius) one can surely do so. In addition, an important feature of this basis can be exposed when special scaling factors $b_{\kappa,i}$ are chosen. This feature concerns the problem of the relativistic-electron confined within a sphere of some large radius R , where if one chooses the scaling factors $b_{\kappa,i}$ to be:

$$b_{\kappa,i} = \frac{\gamma_{\kappa,i}}{R}, \quad (2.11.37)$$

where $\gamma_{\kappa,i}$ is the i -th zero of the first-kind spherical Bessel function of order κ , $j_\kappa(r)$, then one guaranties that all basis functions will vanish at $r = R$, and can verify that all these basis elements are automatically orthogonal, within the confinement radius. A set of the $\gamma_{\kappa,i}$ coefficients for the first eight values of κ were computed using Mathematica [22] and are presented in the appendix table C.1. Coefficients $\gamma_{\kappa,i}$ with positive κ can be collected from Abramowitz and Stegun [60, Table 10.6]. Choosing the coefficients $b_{\kappa,i}$ with respect to eq.(2.11.37), forces the radial functions to vanish at $r = R$, and insures the orthogonality of these functions within the sphere:

$$\int_0^R dr r^2 j_\kappa \left(\gamma_{\kappa,i} \frac{r}{R} \right) j_\kappa \left(\gamma_{\kappa,j} \frac{r}{R} \right) = \frac{R^3}{2} (j_{\kappa+1}(\gamma_{\kappa,i}))^2 \delta_{ij}. \quad (2.11.38)$$

See the appendix equation.(C.6.1). This last relation diverges for $R \rightarrow +\infty$, as expected with respect to eq.(C.4.8). Clearly one can normalize these functions, and get eq.(C.6.2):

$$\tilde{j}_\kappa \left(\gamma_{\kappa,i} \frac{r}{R} \right) = \frac{1}{|j_{\kappa+1}(\gamma_{\kappa,i})|} \sqrt{\frac{2}{R^3}} j_\kappa \left(\gamma_{\kappa,i} \frac{r}{R} \right) \quad (2.11.39)$$

We shall call these functions: the confined Bessel basis functions. In figure 2.11.2 we plot the four confined basis elements corresponding to the first four zeros of the spherical Bessel functions $b_{\kappa,i}$ of eq.(2.11.37) (taken from table C.1).

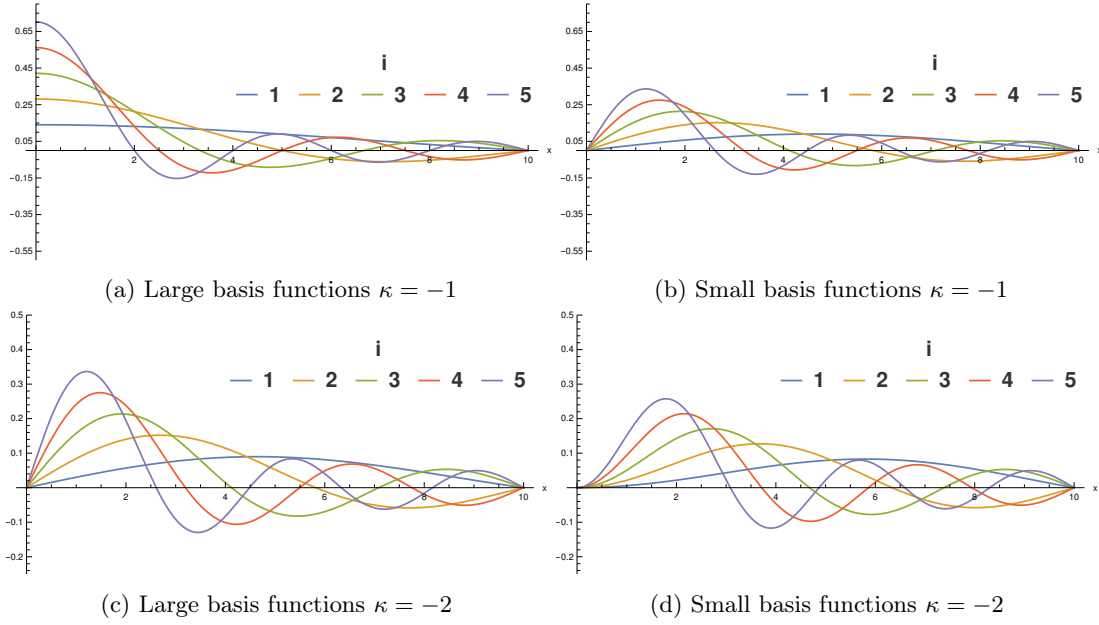


Figure 2.11.2: Orthonormalized confined Bessel basis functions of eq.(2.11.39): using $b_{\kappa,i} = \frac{\gamma_{\kappa,i}}{R}$.

Conclusion

We conclude that the RKB prescription can be made symmetric under charge conjugation if one uses the spherical Bessel basis functions as in eq.(2.11.30). In addition, in order to ensure vanishing functions at large radii, one must set the constant η of eq.(2.11.30) to be a purely imaginary one, as done in eq.(2.11.33). Furthermore, if one chooses the scaling constants $b_{\kappa,i}$ to be: $b_{\kappa,i} = \frac{\gamma_{\kappa,i}}{R}$ where $\gamma_{\kappa,i}$ is the i -th zero location of the spherical Bessel function of order κ , one can construct an orthogonal (and normalizable) set of basis functions, in the region that extends from $r = 0$ to $r = R$, and let both components vanish at $r = R$ (confining radius). As far as we know, this choice of basis was not used nor discussed in literature.

2.11.4 The basis of free solutions

These basis functions we have just proposed are (almost) identical to the free-particle solutions, which lets the reader ask the following question:

Why do we not construct a basis set out of the free-particle solutions?

One can imagine having a four-component basis set whose element are given by eq.(2.7.52):

$$\begin{aligned} \psi_{\kappa,m_j}^{\text{Free}}(\mathbf{x}, E_{\kappa,i}) &= \begin{bmatrix} j_{|\kappa+\frac{1}{2}|-\frac{1}{2}}(k_{\kappa,i}r) \Omega_{\kappa,m_j} \\ i \frac{ch k_{\kappa,i} \text{sgn}(\kappa)}{mc^2 + E_{\kappa,i}} j_{|\kappa-\frac{1}{2}|-\frac{1}{2}}(k_{\kappa,i}r) \Omega_{-\kappa,m_j} \end{bmatrix} \\ \text{or } \psi_{\kappa}^{\text{Free}}(r, E_{\kappa,i}) &= \begin{bmatrix} j_{|\kappa+\frac{1}{2}|-\frac{1}{2}}(k_{\kappa,i}r) \\ \frac{ch k_{\kappa,i} \text{sgn}(\kappa)}{mc^2 + E_{\kappa,i}} j_{|\kappa-\frac{1}{2}|-\frac{1}{2}}(k_{\kappa,i}r) \end{bmatrix}, \end{aligned} \quad (2.11.40)$$

where each basis element is associated with a special $k_{\kappa,i}$ (or $E_{\kappa,i}$) value: a re-scaling of the Bessel functions. The radial wavefunction which solves the numerical Dirac equation:

$$\begin{bmatrix} mc^2 - e\varphi(r) & -c\hbar \left[\frac{d}{dr} - \frac{\kappa}{r} \right] \\ c\hbar \left[\frac{d}{dr} + \frac{\kappa}{r} \right] P_\kappa & -mc^2 - e\varphi(r) \end{bmatrix} \psi_\kappa^{\text{num}}(r) = \mathcal{E} \psi_\kappa^{\text{num}}(r), \quad (2.11.41)$$

is expanded in the radial basis set of the free particle solutions given eq.(2.11.40):

$$\psi_\kappa^{\text{num}}(r) = \sum_{i=1}^n c_i^\kappa \psi_\kappa^{\text{Free}}(r, E_{\kappa,i}). \quad (2.11.42)$$

The matrix problem will thus become $H_{ij}^\kappa c_j^\kappa = \mathcal{E}_j S_{ij}^\kappa c_j^\kappa$, where the Hamiltonian and the overlap matrices are respectively given by:

$$H_{ij}^\kappa = \int_0^\infty dr \psi_\kappa^{\text{Free}\dagger}(r, E_{\kappa,i}) \begin{bmatrix} mc^2 - e\varphi(r) & -c\hbar \left[\frac{d}{dr} - \frac{\kappa}{r} \right] \\ c\hbar \left[\frac{d}{dr} + \frac{\kappa}{r} \right] P_\kappa & -mc^2 - e\varphi(r) \end{bmatrix} \psi_\kappa^{\text{Free}}(r, E_{\kappa,j}) \quad (2.11.43)$$

$$S_{ij}^\kappa = \int_0^\infty dr \psi_{\kappa,m_j}^{\text{Free}\dagger}(r, E_{\kappa,i}) \psi_{\kappa,m_j}^{\text{Free}}(r, E_{\kappa,j}). \quad (2.11.44)$$

From a mathematical point of view, we note that this choice of scheme has a very nice property: it does not allow for the emergence of spurious solutions within the $(-mc^2, +mc^2)$ energy gap, when using any kind of potentials: positive or negative bounded potentials, in addition to the singular (problematic) Coulomb potential, which makes it the best choice when comparing the following options of basis functions:

1. Uncoupled large and small component function
2. Restricted kinetic balance
3. Atomic balance
4. Dual kinetic balance
5. Free-particle solution basis

This was pointed out by Lewin and Séré in [76, Pages 14-15] and [77, Theorems 2.10-11]. See, in particular, table 2 of the latter reference. On the other hand, what can problematic about these four-component functions is that they cannot be normalized over the whole space, which is consistent with what we know about the nature of the plane-waves (continuum). To see more, we hold the torch and proceed. The scalar product of two basis elements associated with (E_i, κ, m_j) and (E_j, κ', m'_j) is:

$$\int d^3\mathbf{x} \psi_{\kappa,m_j}^{\text{Free}\dagger}(\mathbf{x}, E_{\kappa,i}) \psi_{\kappa',m'_j}^{\text{Free}}(\mathbf{x}, E_{\kappa,j}) \quad (2.11.45)$$

$$\begin{aligned} &= \delta_{\kappa,\kappa'} \delta_{m_j,m'_j} \int_0^\infty r^2 dr \left[j_{|\kappa+\frac{1}{2}|-\frac{1}{2}}(k_{\kappa,i}r) j_{|\kappa+\frac{1}{2}|-\frac{1}{2}}(k_{\kappa,j}r) \right] \\ &+ \frac{\delta_{\kappa,\kappa'} \delta_{m_j,m'_j} c^2 \hbar^2 k_{\kappa,i} k_{\kappa,j}}{(mc^2 + E_{\kappa,i})(mc^2 + E_{\kappa,j})} \int_0^\infty r^2 dr \left[j_{|\kappa-\frac{1}{2}|-\frac{1}{2}}(k_{\kappa,i}r) j_{|\kappa'-\frac{1}{2}|-\frac{1}{2}}(k_{\kappa,j}r) \right]. \end{aligned} \quad (2.11.46)$$

After making use of eq.(C.4.1), this expression reduces to:

$$\begin{aligned} & \int d^3\mathbf{x} \psi_{\kappa, m_j}^{\text{Free}\dagger}(\mathbf{x}, E_{\kappa, i}) \psi_{\kappa', m'_j}^{\text{Free}}(\mathbf{x}, E_{\kappa, j}) \\ &= \delta_{\kappa, \kappa'} \delta_{m_j, m'_j} \frac{\pi}{2k_{\kappa, i}^2} \delta(k_{\kappa, i} - k_{\kappa, j}) \left[1 + \frac{c^2 \hbar^2 k_{\kappa, i}^2}{(mc^2 + E_{\kappa, i})^2} \right], \end{aligned} \quad (2.11.47)$$

which diverges once we try to normalize it by setting $(E_{\kappa, j}, \kappa', m'_j) = (E_{\kappa, i}, \kappa, m_j)$, and vanishes if at least one of these parameters of the left state is different from the one associated with the right state (orthogonality). But, one can always normalize these oscillating basis functions on some finite radial region, as we usually do in such cases. In addition, it is impossible to orthogonalize these functions within the region $r \in (0, R)$ and let both large and small component functions vanish simultaneously at the walls of the sphere of radius R (as we have done for the confined basis of section 2.11.3). The reason behind this claim is the following: if one sets the scaling functions $k_{\kappa, i}$ and $k_{\kappa, j}$ to be:

$$k_{\kappa, i/j} = \frac{\gamma_{|\kappa + \frac{1}{2}| - \frac{1}{2}, i/j}}{R}, \quad (2.11.48)$$

then the first line of eq.(2.11.46) gets an orthogonalization relation, while the second does not, since it needs:

$$k_{\kappa, i/j} = \frac{\gamma_{|\kappa - \frac{1}{2}| - \frac{1}{2}, i/j}}{R}, \quad (2.11.49)$$

instead of the previous relation, and since the $k_{\kappa, i/j}$ factors should be unique, orthogonalization of the free basis is not possible, and as a conclusion:

1. Large and small basis functions cannot be made vanishing at the wall of the sphere, where $r = R$, simultaneously.
2. These basis functions cannot be normalized (over the whole radial region $r \in (0, +\infty)$).

We can therefore choose:

$$k_{\kappa, i/j}^L = \frac{\gamma_{|\kappa + \frac{1}{2}| - \frac{1}{2}, i/j}}{R}, \quad k_{\kappa, i/j}^S = \frac{\gamma_{|\kappa - \frac{1}{2}| - \frac{1}{2}, i/j}}{R}, \quad (2.11.50)$$

for large and small component basis functions, but this would no longer be the basis of the free solutions. The second point means that this choice of basis functions is not the best one for computing bound-solutions, which should be represented by a normalized state, but as mentioned before, one can consider a system confined in a radius R , and normalize his free basis functions with respect to his region (not integrate over whole space). Two questions directly rose:

How to let both component vanish at the walls?

How to have a normalizable basis?

The answer to both questions is the following:

By decoupling large and small components of the free-basis, as what we have done for RKB (and IKB), and pick up the right scaling factors of the spherical Bessel functions.

In the next section, we expand this answer.

2.11.5 A Solution to the normalizability problem of the free basis

Recall that in the RKB problem we did not fix the coupling between large and small basis functions (see 2.10.12), and by doing so with these free particle solutions, the radial wavefunction shall be expanded in two sets of basis functions:

$$\psi_{n,\kappa}(r) = \sum_{i=1}^n a_i^\kappa \psi_\kappa^{\text{Free-L}}(r, E_{\kappa,i}^L) + \sum_{i=1}^n b_i^\kappa \psi_\kappa^{\text{Free-S}}(r, E_{\kappa,i}^S), \quad (2.11.51)$$

where $\psi_\kappa^{\text{Free-L}}(r, E_i)$ and $\psi_\kappa^{\text{Free-S}}(r, E_i)$ are the large and small basis elements, given by:

$$\psi_\kappa^{\text{Free-L}}(r, E_{\kappa,i}) = \begin{bmatrix} j_{|\kappa+\frac{1}{2}|-\frac{1}{2}}(k_{\kappa,i}^L r) \\ 0 \end{bmatrix}; \quad \psi_\kappa^{\text{Free-S}}(r, E_i) = \begin{bmatrix} 0 \\ j_{|\kappa-\frac{1}{2}|-\frac{1}{2}}(k_{\kappa,i}^S r) \end{bmatrix}. \quad (2.11.52)$$

There are three important points to note here:

1. The factor in front of the small component function was removed, since it will be absorbed by the final orthonormalization of the numerical solutions.
2. This basis is the same as the one obtained when trying to make RKB symmetric by charge conjugation.
3. This basis (or two bases) are now orthogonalizable.

Concerning the third point, using the box orthogonality relation of eq.(C.6.1), the large component overlap integral can be made equal to:

$$\int_0^R r^2 dr \psi_\kappa^{\text{Free-L}\dagger}(r, E_{\kappa,i}^L) \psi_\kappa^{\text{Free-L}}(r, E_{\kappa,j}^L) = \frac{R^3}{2} \left(j_{|\kappa+\frac{1}{2}|+\frac{1}{2}} \left(\gamma_{|\kappa+\frac{1}{2}|-\frac{1}{2},i} \right) \right)^2 \delta_{ij}, \quad (2.11.53)$$

after setting the large component scaling factors $k_{\kappa,i/j}^L$ to:

$$k_{\kappa,i/j}^L = \frac{\gamma_{|\kappa+\frac{1}{2}|-\frac{1}{2},i/j}}{R}. \quad (2.11.54)$$

Similarly for the small component basis functions, we have:

$$\int_0^R r^2 dr \psi_\kappa^{\text{Free-S}\dagger}(r, E_i) \psi_\kappa^{\text{Free-S}}(r, E_j) = \frac{R^3}{2} \left(j_{|\kappa-\frac{1}{2}|+\frac{1}{2}} \left(\gamma_{|\kappa-\frac{1}{2}|-\frac{1}{2},i} \right) \right)^2 \delta_{ij}, \quad (2.11.55)$$

after setting the small component scaling factors $k_{\kappa,i/j}^S$ to be:

$$k_{\kappa,i/j}^S = \frac{\gamma_{|\kappa-\frac{1}{2}|-\frac{1}{2},i/j}}{R}. \quad (2.11.56)$$

As a conclusion, we say that to make the RKB method symmetric by charge conjugation, one has to use decoupled free-particle solutions as basis functions for one's calculations. In addition, if the scaling constants $k_{\kappa,i}$'s (or the previous ones: $b_{\kappa,i}$'s) are chosen with respect to eqs.(2.11.54 and 2.11.56), one will get:

1. Othonormalizable basis functions.
2. Vanishing large and small components at the spherical wall of the cavity (at $r = R$).

In the next section, we are going to see that the realization of the C -symmetry can be nicely realized in the dual kinetic balance scheme, under certain general conditions, without being forced to use special kind of functions.

2.11.6 \mathcal{C} - symmetry in DKB

We now seek to find the circumstances under which the DKB method can be \mathcal{C} -symmetric, i.e., its basis elements satisfy the condition of eq.(2.11.1). We first proceed by applying the spherical \mathcal{C} -operation of eq.(2.8.17) on the $[+]$ and $[-]$ basis elements of the DKB method, given in eqs.(2.10.22 and 2.10.23), to get:

$$\mathcal{C}\varphi_{i,\kappa,m_j}^{[+]}(\mathbf{x}) = \text{sgn}(\kappa) (-1)^{m_j - \frac{1}{2}} \frac{1}{r} \left[\frac{\hbar}{2mc} \left[\frac{d}{dr} + \frac{\kappa}{r} \right] \pi_{\kappa,i}^+(r) \Omega_{-\kappa,-m_j} \right. \\ \left. i\pi_{\kappa,i}^+(r) \Omega_{+\kappa,-m_j} \right] \quad (2.11.57)$$

$$\mathcal{C}\varphi_{i,\kappa,m_j}^{[-]}(\mathbf{x}) = \text{sgn}(\kappa) (-1)^{m_j - \frac{1}{2}} \frac{1}{r} \left[i\frac{\hbar}{2mc} \left[\frac{d}{dr} - \frac{\kappa}{r} \right] \pi_{\kappa,i}^-(r) \Omega_{-\kappa,-m_j} \right. \\ \left. \pi_{\kappa,i}^-(r) \Omega_{+\kappa,-m_j} \right]. \quad (2.11.58)$$

After looking at the basis functions associated with opposite κ and m_j signs (see also table 2.1):

$$\varphi_{i,-\kappa,-m_j}^{[+]}(\mathbf{x}) = \frac{1}{r} \left[i\frac{\hbar}{2mc} \left[\frac{d}{dr} - \frac{\kappa}{r} \right] \pi_{-\kappa,i}^+(r) \Omega_{-\kappa,-m_j} \right. \\ \left. \pi_{-\kappa,i}^+(r) \Omega_{+\kappa,-m_j} \right] \quad (2.11.59)$$

$$\varphi_{i,-\kappa,-m_j}^{[-]}(\mathbf{x}) = \frac{1}{r} \left[\frac{\hbar}{2mc} \left[\frac{d}{dr} + \frac{\kappa}{r} \right] \pi_{-\kappa,i}^-(r) \Omega_{-\kappa,-m_j} \right. \\ \left. i\pi_{-\kappa,i}^-(r) \Omega_{+\kappa,-m_j} \right], \quad (2.11.60)$$

we clearly see that the charge conjugated basis elements $\mathcal{C}\varphi_{i,\kappa,m_j}^{[+]}$ and $\mathcal{C}\varphi_{i,\kappa,m_j}^{[-]}$ become proportional –up to an insignificant phase factor of $\text{sgn}(\kappa) (-1)^{m_j - \frac{1}{2}}$ – to $\varphi_{i,\kappa,m_j}^{[-]}$ and $\varphi_{i,\kappa,m_j}^{[+]}$ respectively, if one sets:

$$\pi_{-\kappa,i}^-(r) = \pi_{\kappa,i}^+(r) \\ \pi_{-\kappa,i}^+(r) = \pi_{\kappa,i}^-(r), \quad (2.11.61)$$

which are the same conditions obtained when we tried to make two-component basis functions \mathcal{C} -symmetric (see eq.(2.11.8)). We thus conclude that in order to make the DKB basis, \mathcal{C} -symmetric, for each κ basis set one must introduce a $-\kappa$ basis, where the basis functions of the latter set should be related to the one associated with the former one by the last relations. For spherical Gaussian-type functions of eqs.(2.9.12 and 2.9.13), these last conditions lead to the following restriction on the Gaussian exponents:

$$\zeta_{\pm\kappa,i}^L = \zeta_{\mp\kappa,i}^S. \quad (2.11.62)$$

This relation means that one has to provide the same set of basis functions for opposite κ , opposite L/S functions, as presented in table 2.9, where the set of exponents for table boxes containing same color bullets are equal. This shows that the large and small component exponents for the same κ do not have to be the same, and this gives a numerical flexibility by approximating different components with different sets of exponents.

κ	ζ_{κ}^L	ζ_{κ}^S
-1	●	●
+1	●	●
-2	●	●
+2	●	●

Table 2.9: Exponents of the \mathcal{C} -symmetric DKB problem. Same color dots exponents indicates same sets of exponents.

In addition, less generally, if the Gaussian exponents are set to be the same for large and small component functions, the last restriction reduces to:

$$\zeta_{\pm\kappa,i} = \zeta_{\mp\kappa,i}, \quad (2.11.63)$$

meaning that the same exponent list should be set for opposite κ -sign problems (large and small), as presented in table 2.10. This second restriction leads to what is known as the j -basis, which we

κ	ζ_{κ}^L	ζ_{κ}^S
-1	•	•
+1	•	•
-2	•	•
+2	•	•

Table 2.10: The j -basis DKB exponents.

Notice that this is a special case of the previous table.
Same color dots exponents indicates same sets of exponents.

mention in our appendix section E.3. It was in addition mentioned by Dyll [83, Page 38] that this choice of exponents conserves the charge conjugation symmetry in the DKB scheme.

In order to see how the charge conjugation partners can be related within the DKB scheme, we consider the two following DKB matrix equations:

$$\begin{aligned} H_{-e,\kappa} \mathbf{c}_{-e,\alpha,+ \kappa} &= \epsilon_{-e,\alpha,+ \kappa} S_{+\kappa} \mathbf{c}_{-e,\alpha,+ \kappa} \\ H_{+e,-\kappa} \mathbf{c}_{+e,\alpha,- \kappa} &= \epsilon_{+e,\alpha,- \kappa} S_{-\kappa} \mathbf{c}_{+e,\alpha,- \kappa}, \end{aligned} \quad (2.11.64)$$

associated with $(-e, +\kappa)$ (electronic problem) and $(+e, -\kappa)$ (positronic problem), respectively. After playing around with these Hamiltonians and overlap matrices, given in eqs.(E.2.4 and E.2.5), one can show that the following relations:

$$\begin{aligned} \sigma_1 H_{-e,+ \kappa} \sigma_1 &= -H_{+e,- \kappa} \\ \sigma_1 S_{+\kappa} \sigma_1 &= +S_{-\kappa}, \end{aligned} \quad (2.11.65)$$

hold, and this translates into the charge conjugation symmetry between between eigensolutions of these equations:

$$\epsilon_{+e,\alpha,- \kappa} = -\epsilon_{-e,\alpha,+ \kappa} \quad (2.11.66)$$

$$\mathbf{c}_{-e,\alpha,- \kappa} = \sigma_1 \mathbf{c}_{-e,\alpha,+ \kappa}. \quad (2.11.67)$$

To underline this result, we have performed two simple DKB calculations:

- Electronic calculation ($q = -e$) with $\kappa = -1$.
- Positronic calculation ($q = +e$) with $\kappa = +1$.

in the presence of a Coulomb potential with $Z = 50$, and using $\zeta_{\pm 1} = \{10, 20\}$. The results of these two calculations are presented in table 2.11. The results show a clear symmetry between eigenvalues of both problems, as predicted by eq.(2.11.66), in addition to the symmetry between components of these opposite energy- (κ - and charge-)solutions, as predicted by eq.(2.11.67), and seen in table 2.1. See, for instance, the two solutions whose eigenvalues are marked with a small red dot, and notice the swapping between larger and small component functions coefficients.

κ	q	α	Eigenvalue (a.u.)	Coefficients			
				$c_{\alpha,\kappa,1}^{[+]}$	$c_{\alpha,-1,2}^{[+]}$	$c_{\alpha,-1,1}^{[-]}$	$c_{\alpha,-1,2}^{[-]}$
-1	-e	1	+18650.67234	-32.38429	40.36185	-0.00043	0.00699
		2	+18414.94674	-14.01065	43.48589	0.00939	-0.03560
		3	-18929.12245	-0.00085	0.00132	-87.93880	116.82878
		4	- 19117.00120	0.00081	-0.00519	52.95793	-214.29435
+1	+e	1	+ 19117.00120	-52.95793	214.29435	-0.00081	0.00519
		2	+18929.12245	-87.93880	116.82878	-0.00085	0.00132
		3	-18414.94674	-0.00939	0.03560	14.01065	-43.48589
		4	-18650.67234	-0.00043	0.00699	-32.38429	40.36185

Table 2.11: Two small DKB calculations using a \mathcal{C} -symmetric basis set.

It should be finally noted that in the case where the radial basis functions are κ -independent (example: B-splines bases), then the charge conjugation symmetry is automatically conserved within the DKB scheme. As a conclusion, we find that, in contrary to the RKB problem, the charge conjugation symmetry can be obeyed in the DKB scheme, “without” restriction on the choice of basis functions. We shall come back to the results obtained in this chapter, once we attack the vacuum polarization problem in the finite basis approximation. We shall now show, step by step, how the quantum electrodynamic corrections (example: the vacuum polarization) can be derived within the \mathcal{S} -matrix formalism.

Chapter 3

Quantum electrodynamics

There is a most profound and beautiful question associated with the observed coupling constant e the amplitude for a real electron to emit or absorb a real photon. It is a simple number that has been experimentally determined to be close to 0.08542455. (My physicist friends won't recognize this number, because they like to remember it as the inverse of its square: about 137.03597 with an uncertainty of about 2 in the last decimal place). It has been a mystery ever since it was discovered more than fifty years ago, and all good theoretical physicists put this number upon their wall and worry about it. Immediately you would like to know where this number for a coupling comes from: is it related to π , or perhaps to the base of natural logarithms? Nobody knows. It's one of the greatest damn mysteries of physics: a magic number that comes to us with no understanding by man. You might say the "hand of God" wrote that number, and "we don't know how He pushed His pencil." We know what kind of a dance to do experimentally to measure this number very accurately, but we don't know what kind of a dance to do on a computer to make this number come out without putting it in secretly!

Richard P. Feynman - QED: The Strange Theory of Light and Matter [84]

Our ultimate goal in this chapter is to show how one can derive bound state QED corrections, starting from the non-interacting electron and photon field operators and propagators, passing by the \mathcal{S} -matrix formalism, and ending by the QED energy-shift expressions associated with different orders of the \mathcal{S} -matrix. We will derive in detail the second-order \mathcal{S} -matrix energy-shifts, which will be then ready (at least in principle) to get employed in practical numerical calculations. The derivation of these energy-shifts can be found, in separate parts, in the literature. We have thus decided to consider a "full" derivation in this chapter, which will be very useful for new learners of the field. Furthermore, in the last sections of this chapter we will consider the effective QED potentials, i.e. the position-space Hamiltonian representation of the some of the lowest-order QED processes, in addition to a general discussion on how one can include QED effects in the Hartree-Fock theory. It should be finally noted that the self-consistent inclusion of a low order correction, will allow the account for some of the higher-order corrections, more specifically, the ones that can be represented by reducible Feynman diagrams.

3.1 Quantum mechanical pictures

In quantum mechanics there exist three dynamical pictures, in which one can formulate the mathematics of a quantum problem. In principle, these pictures are equivalent, since the measured physical quantity (nature) should be picture-independent of human made quantities. In the next subsections we shall present these representations and discuss their important distinct features.

3.1.1 Schrödinger picture

The Schrödinger picture considers the case where observables that are represented by Hermitian operators are fixed (time-independent) while the quantum states evolve in time, and do solve an equation of motion. The Schrödinger state $|\psi_S(t)\rangle$, satisfies the Schrödinger equation:

$$i\hbar \frac{d}{dt} |\psi_S(t)\rangle = \hat{H}_S |\psi_S(t)\rangle, \quad (3.1.1)$$

where \hat{H}_S is some time-independent Hamiltonian. In this picture, the state evolves from t_0 to some time t , with the help of the time-evolution operator:

$$|\psi_S(t)\rangle = U(t, t_0) |\psi_S(t_0)\rangle. \quad (3.1.2)$$

Since \hat{H}_S is time-independent, the time-evolution operator is found to be:

$$U(t, t_0) = e^{-i\hat{H}_S(t-t_0)/\hbar}, \quad (3.1.3)$$

as will be seen in section 3.2.1. The expectation value of some observable associated with the operator $\hat{O}_S(t)$, is given by:

$$\langle \hat{O} \rangle = \langle \psi_S(t) | \hat{O}_S(t) | \psi_S(t) \rangle. \quad (3.1.4)$$

3.1.2 Heisenberg picture

In this picture, operators evolve in time, while wavefunctions do not. The Heisenberg state is obtained from the Schrödinger one by:

$$|\psi_H\rangle = e^{i\hat{H}_S(t-t_0)/\hbar} |\psi_S(t)\rangle = |\psi_S(t_0)\rangle, \quad (3.1.5)$$

where one sees that this state is defined to be the Schrödinger state at $t = t_0$ (fixed in time), while the time evolution is manifested by the observable operator. Again, one has to keep in mind that the Hamiltonian is time-independent. Using this last equation, we can write our expectation value of eq.(3.1.4) as:

$$\langle \hat{O} \rangle = \langle \psi_H | e^{i\hat{H}_S(t-t_0)/\hbar} \hat{O}_S(t) e^{-i\hat{H}_S(t-t_0)/\hbar} | \psi_H \rangle, \quad (3.1.6)$$

where the operator sandwiched between Heisenberg states, defines the Heisenberg operator:

$$\hat{O}_H(t) = e^{i\hat{H}_S(t-t_0)/\hbar} \hat{O}_S(t) e^{-i\hat{H}_S(t-t_0)/\hbar}. \quad (3.1.7)$$

Notice that even if $\hat{O}_S(t)$ is time-independent, in the Heisenberg picture this operator gains (in general) a time-dependence. After differentiation the Heisenberg observable operator with respect

to time, one obtains the Heisenberg equation of motion associated with the operator (instead of the wavefunction as in Schrödinger's picture):

$$i\hbar \frac{d}{dt} \hat{O}_H(t) = [\hat{O}_H(t), \hat{H}_H] + i\hbar \left\{ \frac{d}{dt} \hat{O}_S(t) \right\}_H, \quad (3.1.8)$$

where $\left\{ \frac{d}{dt} \hat{O}_S \right\}_H = e^{i\hat{H}_S t/\hbar} \frac{d}{dt} \hat{O}_S e^{-i\hat{H}_S t/\hbar}$. It is worth noting that the Hamiltonian operator is unchanged:

$$\hat{H}_H(t) = e^{i\hat{H}_S(t-t_0)/\hbar} \hat{H}_S e^{-i\hat{H}_S(t-t_0)/\hbar} = \hat{H}_S = \hat{H}_H, \quad (3.1.9)$$

where we used the trivial fact that \hat{H}_S commutes with itself. In addition, we recall that observables are time-independent in the Schrödinger picture, which leads to a vanishing of the curly bracket term of eq.(3.1.3), but time-dependence is assumed for future purposes (to allow comparison between different pictures). It should be now clear why the Schrödinger's quantum mechanics was called wave-mechanics: since the equation of motion describes the evolution of the wavefunction, while Heisenberg's one is referred to as matrix-mechanics: since its associated equation of motion describes the evolution of the operator instead. Dirac proposed a third picture, called the interaction picture, which "combines" both pictures, and is more suitable for perturbation problems. This picture shall be discussed in the next section.

3.1.3 Interaction (intermediate) picture

This picture is actually a hybrid of the last two. The Hamiltonian here is written as a sum of a time-independent free Hamiltonian \hat{H}_S^0 , and an interaction Hamiltonian $\hat{H}_S^1(t)$ which might be time-dependent:

$$\hat{H}_S(t) = \hat{H}_S^0 + \hat{H}_S^1(t). \quad (3.1.10)$$

The fact that the interaction term has a time dependence might be confusing for the reader, since two section ago, we stated that the Hamiltonian in the Schrödinger picture is strictly time-independent. This should cause no problem since this term only exists to link between the two pictures, and the subscript S is there (on $\hat{H}_S^1(t)$) to remind us that when changing pictures this term should be treated as (and is) a Schrödinger operator. Notice at this point that the Schrödinger-state evolution operator can no longer be written as an exponential, as in eq.(3.1.3), since the Hamiltonian is now time-dependent. As in the Heisenberg picture, the interaction picture state vector is defined as a transformed Schrödinger state, but this time the exponential only includes the free (time-independent) Hamiltonian:

$$|\psi_I(t)\rangle = e^{i\hat{H}_S^0 t/\hbar} |\psi_S(t)\rangle. \quad (3.1.11)$$

As a result the observable operator in this picture becomes related to the Schrödinger one by:

$$\hat{O}_I(t) = e^{i\hat{H}_S^0 t/\hbar} \hat{O}_S(t) e^{-i\hat{H}_S^0 t/\hbar}. \quad (3.1.12)$$

We first plug $|\psi_S(t)\rangle$ of eq.(3.1.11) in the Schrödinger equation of eq.(3.1.1), and obtain the first equation of motion associated with the interaction state:

$$i\hbar \frac{d}{dt} |\psi_I(t)\rangle = \hat{H}_I^1(t) |\psi_I(t)\rangle; \quad \text{with} \quad \hat{H}_I^1(t) = e^{+i\hat{H}_S^0 t/\hbar} \hat{H}_S^1(t) e^{-i\hat{H}_S^0 t/\hbar}, \quad (3.1.13)$$

where only the interaction Hamiltonian $\hat{H}_I^1(t)$ (in the interaction picture) appears. After differentiating the observable operator of eq.(3.1.12) with respect to time, one obtains the second equation

	Schrödinger	Interaction	Heisenberg
State $ \psi_X(t)\rangle$	$e^{-i\hat{H}_S^0(t-t_0)/\hbar} \psi_S(t_0)\rangle$	$e^{i\hat{H}_S^0 t/\hbar} \psi_S(t)\rangle$	$e^{-\frac{1}{i\hbar} \int_{t_0}^t dt_1 \hat{H}_S(t_1)} \psi_S(t)\rangle = \psi_S(t_0)\rangle$
Observable \hat{O}_X	$\hat{O}_S(t)$	$e^{i\hat{H}_S^0 t/\hbar} \hat{O}_S(t) e^{-i\hat{H}_S^0 t/\hbar}$	$e^{-\frac{1}{i\hbar} \int_{t_0}^t dt_1 \hat{H}_S(t_1)} \hat{O}_S(t) e^{\frac{1}{i\hbar} \int_{t_0}^t dt_1 \hat{H}_S(t_1)}$

Table 3.1: Comparison between quantum mechanical pictures. $X = S, I, H$.

of motion, associated with the observable operator:

$$i\hbar \frac{d}{dt} \hat{O}_I(t) = [\hat{O}_I(t), \hat{H}_S^0] + i\hbar \left\{ \frac{d}{dt} \hat{O}_S(t) \right\}_I. \quad (3.1.14)$$

It is clearly seen at this point that this picture combines both pictures, by having a state equation of motion (EOM) as in the Schrödinger picture, and an observable EOM as in the Heisenberg picture, meaning that time evolution is manifested in both quantities. As claimed, the observable expectation value (measurement), is, as it should be, picture independent:

$$\langle \hat{O} \rangle = \langle \psi_S(t) | \hat{O}_S(t) | \psi_S(t) \rangle \quad (3.1.15)$$

$$= \langle \psi_H | \hat{O}_H(t) | \psi_H \rangle \quad (3.1.16)$$

$$= \langle \psi_I(t) | \hat{O}_I(t) | \psi_I(t) \rangle. \quad (3.1.17)$$

We present a summary of the quantum mechanical pictures in table 3.1. For detailed discussions about quantum mechanical pictures, the reader might consult [85, 86, 64].

3.2 Time-evolution operator

In this section, we shall derive the time-evolution operator that takes a state from some time t_1 to another time t_2 for both Schrödinger and Dirac (interaction) pictures of quantum mechanics.

3.2.1 Time-evolution operator for the Schrödinger picture

In the Schrödinger picture the state satisfies the state equation of motion:

$$i\hbar \frac{d}{dt} |\psi_S(t)\rangle = \hat{H}_S^0 |\psi_S(t)\rangle, \quad (3.2.1)$$

where \hat{H}_S^0 is a time-independent Hamiltonian. We first define the time-evolution operator, as the operation which evolves the state from a time t_0 to some time t , i.e. :

$$|\psi_S(t)\rangle = \hat{U}(t, t_0) |\psi_S(t_0)\rangle. \quad (3.2.2)$$

For logical consistency, this operator has to have the following properties:

$$\hat{U}(t, t) = 1 \quad (3.2.3)$$

$$\hat{U}(t_1, t_2) \hat{U}(t_2, t_1) = 1 \quad (3.2.4)$$

$$\hat{U}(t_2, t_1) \hat{U}(t_1, t_0) = \hat{U}(t_2, t_0). \quad (3.2.5)$$

These properties are explained below:

- If one does not evolve the state, it should be left unchanged, i.e. the time-evolution reduces to the identity operation.
- Evolving the state from some time t_1 to t_2 , then going back, should also leave the state unchanged, which means that the operator with exchanged times is the inverse of the original operator:

$$\hat{U}(t_2, t_1) = \left(\hat{U}(t_1, t_2) \right)^{-1}. \quad (3.2.6)$$

- Finally, two consecutive time-evolutions are equivalent to a single evolution.

In addition, to ensure state normalization at all times, this time-evolution operator must be unitary. Assuming that the initial state is normalized:

$$\langle \psi_S(t_0) | \psi_S(t_0) \rangle = 1. \quad (3.2.7)$$

If \hat{U} is a unitary operator, then the evolved state will also be normalized:

$$\langle \psi_S(t) | \psi_S(t) \rangle = \langle \psi_S(t_0) | \left(\hat{U}(t, t_0) \right)^\dagger \hat{U}(t, t_0) | \psi_S(t_0) \rangle \quad (3.2.8)$$

$$= \langle \psi_S(t_0) | \psi_S(t_0) \rangle = 1. \quad (3.2.9)$$

After plugging the evolved state of eq.(3.2.2) in the Schrödinger equation of eq.(3.2.1), one obtains the following equation for the time-evolution operator:

$$i\hbar \frac{d}{dt} \hat{U}(t, t_0) = \hat{H}_S^0 \hat{U}(t, t_0), \quad (3.2.10)$$

where its solution is easily found to be:

$$\hat{U}(t, t_0) = e^{+\frac{i}{\hbar} \hat{H}_S^0 (t-t_0)}. \quad (3.2.11)$$

3.2.2 Time-evolution operator for the Interaction picture

Again, we define the time evolution operator as the application that takes the interaction state from t_0 to t :

$$|\psi_I(t)\rangle = \hat{U}(t, t_0) |\psi_I(t_0)\rangle. \quad (3.2.12)$$

We plug this expression in the associated equation of motion of eq.(3.1.13), and obtain the equation for the time-evolution operator:

$$i\hbar \frac{d}{dt} \hat{U}(t, t_0) = \hat{H}_I^1(t) \hat{U}(t, t_0). \quad (3.2.13)$$

Notice that the interaction operator is time-dependent, unlike the previous case of eq.(3.2.10) where \hat{H}_S^0 was time-independent, and this complicates the problem. We shall next show how to untie this knot.

First attempt: After being inspired by the time-evolution operator for the Schrödinger picture states, one can imagine a solution of the following form:

$$\hat{U}(t, t_0) = e^{\frac{1}{i\hbar} \int_{t_0}^t \hat{H}_I(t') dt'}, \quad (3.2.14)$$

which clearly satisfies the time-evolution equation (3.2.13) (one may check using Leibniz integral rule). This solution is discarded because it sets a commutation restriction on the interaction Hamiltonian, which is not guaranteed. This can be seen from the third property of the \hat{U} operator given in eq. (3.2.5), which (in this case) becomes:

$$e^{\frac{1}{i\hbar} \int_{t_1}^{t_2} \hat{H}_I(t') dt'} e^{\frac{1}{i\hbar} \int_{t_0}^{t_1} \hat{H}_I(t'') dt''} = e^{\frac{1}{i\hbar} \int_{t_0}^{t_2} \hat{H}_I(t') dt'}, \quad (3.2.15)$$

and this is problematic, since we know that:

$$e^{\hat{A}} e^{\hat{B}} \neq e^{\hat{A}+\hat{B}}, \quad \text{if } [\hat{A}, \hat{B}] \neq 0, \quad (3.2.16)$$

which means that the third property is respected only in the case where the interaction Hamiltonian commutes with itself:

$$[\hat{H}_I^1(t_1), \hat{H}_I^1(t_2)] = 0, \quad (3.2.17)$$

for all times t_1 , and t_2 , which is not generally the case. Notice that when $\hat{H}_I^1(t)$ is replaced by the time-independent \hat{H}_S , this solution works and gives eq. (3.2.11), since the last commutation condition holds in that case.

Second attempt: Another way to attack the equation, is to integrate it with respect to time:

$$i\hbar \int_{t_0}^{t'} dt \frac{d}{dt} \hat{U}(t, t_0) = \int_{t_0}^{t'} dt \hat{H}_I(t) \hat{U}(t, t_0), \quad (3.2.18)$$

which after forcing the first property of eq. (3.2.3) to be obeyed (boundary-condition), leads to:

$$\hat{U}(t, t_0) = 1 + \frac{1}{i\hbar} \int_{t_0}^t dt' \hat{H}_I^1(t') \hat{U}(t', t_0). \quad (3.2.19)$$

Using Leibniz integral rule, this solution can be verified to satisfy eq. (3.2.13). Since this last equation shows the solution as an integral function of the solution itself, one gets rid of this dependence by iteratively replacing $\hat{U}(t', t_0)$ on the right side of the last equation by its value, for infinitely many times, and this leads to:

$$\hat{U}(t, t_0) = 1 + \frac{1}{i\hbar} \int_{t_0}^t dt' \hat{H}_I^1(t') \left(1 + \frac{1}{i\hbar} \int_{t_0}^{t'} dt'' \hat{H}_I^1(t'') \left(1 + \frac{1}{i\hbar} \int_{t_0}^{t''} dt''' \hat{H}_I^1(t''') (\dots) \right) \right), \quad (3.2.20)$$

which can be rearranged as a sum of integrals over powers of the interaction Hamiltonian, as follows:

$$\begin{aligned} \hat{U}(t, t_0) &= 1 & \hat{U}_0 \\ &+ \frac{1}{i\hbar} \int_{t_0}^t dt_1 \hat{H}_I^1(t_1) & \hat{U}_1 \\ &+ \frac{1}{(i\hbar)^2} \int_{t_0}^t dt_1 \int_{t_0}^{t_1} dt_2 \hat{H}_I^1(t_1) \hat{H}_I^1(t_2) & \hat{U}_2 \\ &+ \frac{1}{(i\hbar)^3} \int_{t_0}^t dt_1 \int_{t_0}^{t_1} dt_2 \int_{t_0}^{t_2} dt_3 \hat{H}_I^1(t_1) \hat{H}_I^1(t_2) \hat{H}_I^1(t_3) & \hat{U}_3 \\ &+ \dots \end{aligned} \quad (3.2.21)$$

Notice that while the lower integration limits are all t_0 , the upper ones are different from each others. This mismatch can be overcome using the time-ordering operator. To see how this is done, we focus on the two-interaction \hat{U}_2 -term, and follow what was done by Fetter in [87, section 6] and Schweber in [4, section 11f], where this integral is written as half the sum of two equivalent integrations:

$$\begin{aligned}\hat{U}_2(t, t_0) &= \int_{t_0}^t dt_1 \int_{t_0}^{t_1} dt_2 \hat{H}_I^1(t_1) \hat{H}_I^1(t_2) \\ &= \frac{1}{2} \left(\int_{t_0}^t dt_1 \int_{t_0}^{t_1} dt_2 \hat{H}_I^1(t_1) \hat{H}_I^1(t_2) + \int_{t_0}^t dt_2 \int_{t_2}^t dt_1 \hat{H}_I^1(t_1) \hat{H}_I^1(t_2) \right).\end{aligned}\quad (3.2.22)$$

To help visualize the integrations, we plot the integration regions in figure 3.2.1. The first integral in the last equation is performed along the blue region that scans the lower triangle, while the second integral scans this triangle along the red region, these integrations are thus equivalent. Notice that these integrations lie in the region where $t_1 > t_2$. We then exchange the integration variables $t_1 \leftrightarrow t_2$ in the second integral and obtain:

$$\hat{U}_2(t, t_0) = \frac{1}{2} \left(\int_{t_0}^t dt_1 \int_{t_0}^{t_1} dt_2 \hat{H}_I^1(t_1) \hat{H}_I^1(t_2) + \int_{t_0}^t dt_1 \int_{t_1}^t dt_2 \hat{H}_I^1(t_2) \hat{H}_I^1(t_1) \right), \quad (3.2.23)$$

where the second integral now scans the upper triangle region, as pictured in figure 3.2.2. We can now extend these integrations to cover both triangles, i.e. the whole square, if we multiply each integrand by a Heaviside function that vanishes in the unwanted region, we therefore write:

$$\hat{U}_2(t, t_0) = \frac{1}{2} \left(\int_{t_0}^t dt_1 \int_{t_0}^t dt_2 \hat{H}_I^1(t_1) \hat{H}_I^1(t_2) \Theta(t_1 - t_2) + \int_{t_0}^t dt_1 \int_{t_0}^t dt_2 \hat{H}_I^1(t_2) \hat{H}_I^1(t_1) \Theta(t_2 - t_1) \right). \quad (3.2.24)$$

Now, these two integrals are combined into a single one, where the integration limits more elegant, by being decoupled:

$$\hat{U}_2(t, t_0) = \frac{1}{2} \int_{t_0}^t dt_1 \int_{t_0}^t dt_2 T \left[\hat{H}_I^1(t_1) \hat{H}_I^1(t_2) \right], \quad (3.2.25)$$

where we introduced the time-ordering operator T , which orders a string of time-dependent operators with respect to their time, such that later-time operators act after early ones:

$$T \left[\hat{H}_I^1(t_1) \hat{H}_I^1(t_2) \right] = \begin{cases} \hat{H}_I^1(t_1) \hat{H}_I^1(t_2) & \text{if } t_1 > t_2 \\ \hat{H}_I^1(t_2) \hat{H}_I^1(t_1) & \text{if } t_2 > t_1 \end{cases}. \quad (3.2.26)$$

So far we have discussed the two-interaction Hamiltonian term, this approach can be generalized to an n -interaction Hamiltonian term:

$$\hat{U}_n(t, t_0) = \frac{1}{(i\hbar)^n} \int_{t_0}^t dt_1 \int_{t_0}^{t_1} dt_2 \dots \int_{t_0}^{t_{n-1}} dt_n \hat{H}_I^1(t_1) \hat{H}_I^1(t_2) \dots \hat{H}_I^1(t_n), \quad (3.2.27)$$

which, using the same previous approach, can be written as:

$$\hat{U}_n(t, t_0) = \frac{1}{n!} \frac{1}{(i\hbar)^n} \int_{t_0}^t dt_1 \int_{t_0}^t dt_2 \dots \int_{t_0}^t dt_n T \left[\hat{H}_I^1(t_1) \hat{H}_I^1(t_2) \dots \hat{H}_I^1(t_n) \right], \quad (3.2.28)$$

where the $\frac{1}{n!}$ term appears because one can permute the time string (t_1, \dots, t_n) and obtain $n!$ permutations, following the same trick discussed above for $n = 2$. Finally, since the time-ordering operator

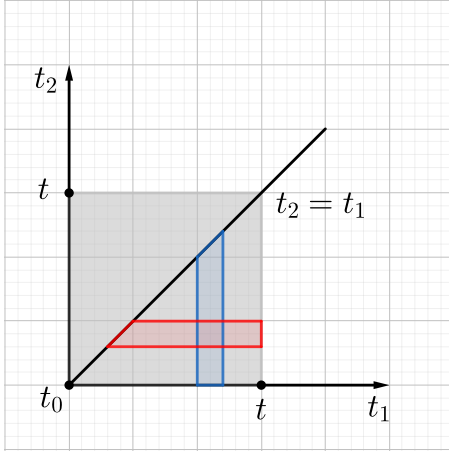


Figure 3.2.1: Integrations of eq.(3.2.22)

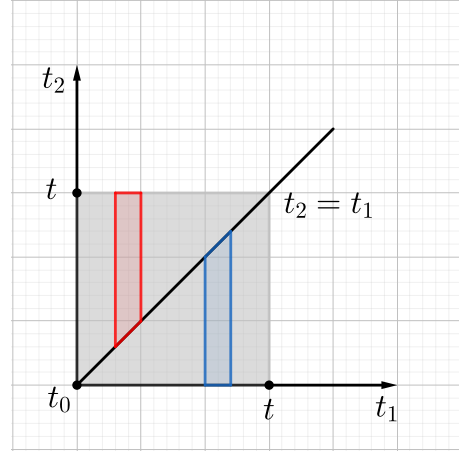


Figure 3.2.2: Integrations of eq.(3.2.23)

can be taken out of the integration sign, the full time-evolution operator can be written as:

$$\hat{U}(t, t_0) = \sum_{n=1}^{\infty} \hat{U}_n(t, t_0) = \text{T} \left[e^{\frac{1}{i\hbar} \int_{t_0}^t dt_1 \hat{H}_I^1(t_1)} \right], \quad (3.2.29)$$

which is known as the Dyson series of the time-evolution operator [88]. The exponential of the last expression is to be understood as:

$$e^{\frac{1}{i\hbar} \int_{t_0}^t dt_1 \hat{H}_I^1(t_1)} = 1 + \frac{1}{i\hbar} \int_{t_0}^t dt_1 \hat{H}_I^1(t_1) + \frac{1}{2!} \frac{1}{(i\hbar)^2} \int_{t_0}^t dt_1 \int_{t_0}^t dt_2 \hat{H}_I^1(t_1) \hat{H}_I^1(t_2) + \dots \quad (3.2.30)$$

For further discussions on the time-evolution operator of the interaction picture, the reader may consult Greiner and Reinhardt [89, section 8.3], in addition to Tannoudji *et al.* [90, chapter XX section A].

3.3 The scattering matrix

The scattering matrix is defined as the time-evolution operator that evolves the state from the very past to the very future. In other words, it relates the initial state of system (before any interaction) at $t = -\infty$, represented by $|\psi_I(-\infty)\rangle$, to the corresponding final state at $t = +\infty$, $|\psi_I(+\infty)\rangle$, after all sorts of interactions, that are manifested by the interaction Hamiltonian term $\hat{H}_I^1(t)$. In the next section we shall see that this can be made if this interaction Hamiltonian contains a damping factor of the form of $e^{-\frac{\epsilon}{\hbar}|t|}$ which turns off the interaction at large times. This exponential factor is not present in the conventional QED theory that treats free-electrons, but is needed in our case: in Bound State Quantum Electrodynamics, where electrons are represented by wavefunctions that do solve the bound Dirac equation instead of the free-one. See, for instance, Labzowsky *et al.* [91, section 1.3]. The action of the $\hat{\mathcal{S}}$ -matrix on the state vector is mathematically represented by the following equation:

$$|\psi_I(t = +\infty)\rangle = \hat{\mathcal{S}} |\psi_I(t = -\infty)\rangle; \quad \hat{\mathcal{S}} = \hat{U}(+\infty, -\infty), \quad (3.3.1)$$

where the scattering matrix operator $\hat{\mathcal{S}}$ becomes, using eq.(3.2.29):

$$\hat{\mathcal{S}} = \text{T} \left[e^{\frac{1}{i\hbar} \int_{-\infty}^{+\infty} dt \hat{H}_I(t)} \right]. \quad (3.3.2)$$

Contrary to the time-evolution operator, the scattering matrix is Lorentz invariant, if the interaction Hamiltonian is. See Weinberg [92, section 3.3] for instance. The interaction Hamiltonian can be written as a spatial integral of the interaction Hamiltonian density $\hat{\mathcal{H}}_I(x)$:

$$\hat{H}_I(t) = \int d^3\mathbf{x} \hat{\mathcal{H}}_I(x). \quad (3.3.3)$$

This form of the interaction Hamiltonian leads to an \mathcal{S} -matrix form where the integrations scans the whole spacetime:

$$\hat{\mathcal{S}} = \text{T} \left[e^{\frac{1}{i\hbar} \int d^4x \hat{\mathcal{H}}_I(x)} \right], \quad (3.3.4)$$

where the speed of light is added to keep the right dimensions, since $x^0 = ct$. This $\hat{\mathcal{S}}$ -matrix can be expanded with respect to eq.(3.2.30):

$$\hat{\mathcal{S}} = \sum_{n=0}^{\infty} \hat{\mathcal{S}}^{(n)}, \quad (3.3.5)$$

where the n -th $\hat{\mathcal{S}}$ -matrix is given by [93, (6. 23)]:

$$\hat{\mathcal{S}}^{(n)} = \frac{1}{n! (i\hbar)^n} \int d^4x_1 \dots \int d^4x_n \text{T} \left[\hat{\mathcal{H}}_I(x_1) \dots \hat{\mathcal{H}}_I(x_n) \right]. \quad (3.3.6)$$

3.4 Solving the perturbed problem

We should now focus on solving the perturbed problem, and show how one can write the perturbed states and energies, as a function of the unperturbed ones. We first consider a total Hamiltonian of the following form:

$$\hat{H}_S = \hat{H}_S^0 + \lambda \hat{H}_S^1, \quad (3.4.1)$$

which contains the following two terms:

1. A simple free Hamiltonian, which describes the mechanics of the non-interacting particles, and whose eigensolutions are assumed to be solved in an exact manner (analytically).
2. A perturbation Hamiltonian $\lambda \hat{H}_S^1$ that complicates the problem, and prevent us from treating the whole problem exactly. Here, λ represents the dimensionless perturbation parameter, that can be varied between 0 (perturbation set off), to 1 (full perturbation), this parameter will help us keep track of the perturbation order.

The free time-independent Hamiltonian equation whose solutions are in our hands, is given by:

$$\hat{H}_S^0 |\Phi_0^\alpha\rangle_S = E_0^\alpha |\Phi_0^\alpha\rangle_S; \quad |\Phi_0^\alpha(t)\rangle_S = e^{-iE_0^\alpha t/\hbar} |\Phi_0^\alpha\rangle_S, \quad (3.4.2)$$

where the α superscript labels solutions (states and associated energy levels) and 0 indicates that these eigensolutions solve the non-perturbed problem. The ultimate goal, is to find the solutions of the total problem:

$$\hat{H}_S |\Phi^\alpha\rangle_S = E^\alpha |\Phi^\alpha\rangle_S; \quad |\Phi^\alpha(t)\rangle_S = e^{-iE^\alpha t/\hbar} |\Phi^\alpha\rangle_S, \quad (3.4.3)$$

in which the perturbation is taken into account. The first step towards solving this problem starts by the following replacement of the perturbation Hamiltonian:

$$\hat{H}_S^1 \rightarrow \hat{H}_S^1(t; \epsilon) = e^{-\frac{\epsilon}{\hbar}|t|} \hat{H}_S^1, \quad (3.4.4)$$

which consists of multiplying it by an exponential factor $e^{-\frac{\epsilon}{\hbar}|t|}$ known as the adiabatic switching term. This term was invented/used by Lippmann and Schwinger in [94, page 437]. See also Lab-zowsky *et al.* [91, section 1.3]. For future purposes, the reduced Planck constant \hbar is added to the denominator of the exponent so that the variable ϵ gets the units of energy. The total Hamiltonian is now:

$$\hat{H}_S(t; \epsilon) = \hat{H}_S^0 + \lambda \hat{H}_S^1(t; \epsilon), \quad (3.4.5)$$

which clearly bridges the gap (interpolates) between the total Hamiltonian that we seek to solve, and the unperturbed one:

$$\hat{H}_S(0; \epsilon) = \hat{H}_S \quad (3.4.6)$$

$$\hat{H}_S(\pm\infty; \epsilon) = \hat{H}_S^0. \quad (3.4.7)$$

The Schrödinger equation becomes:

$$i\hbar \frac{\partial}{\partial t} |\Phi^\alpha(t; \epsilon)\rangle_S = \hat{H}_S(t; \epsilon) |\Phi^\alpha(t; \epsilon)\rangle_S. \quad (3.4.8)$$

After switching to the interaction picture, the state becomes:

$$|\Phi^\alpha(t; \epsilon)\rangle_I = e^{i\hat{H}_S^0 t/\hbar} |\Phi^\alpha(t; \epsilon)\rangle_S, \quad (3.4.9)$$

and satisfies the following equation:

$$i\hbar \frac{\partial}{\partial t} |\Phi^\alpha(t; \epsilon)\rangle_I = \lambda \hat{H}_I^1(t; \epsilon) |\Phi^\alpha(t; \epsilon)\rangle_I. \quad (3.4.10)$$

The perturbation Hamiltonian in the interaction picture is:

$$\hat{H}_I^1(t; \epsilon) = e^{+i\hat{H}_S^0 t/\hbar} \hat{H}_S^1(t; \epsilon) e^{-i\hat{H}_S^0 t/\hbar}. \quad (3.4.11)$$

Following what was done in section 3.1, the interaction picture state at time t , $|\Phi^\alpha(t; \epsilon)\rangle_I$ can be written as a time-evolution of a different state:

$$|\Phi^\alpha(t; \epsilon)\rangle_I = \hat{U}(t, t_0; \epsilon, \lambda) |\Phi^\alpha(t_0; \epsilon)\rangle_I, \quad (3.4.12)$$

where the time-evolution operator satisfies the equation:

$$i\hbar \frac{\partial}{\partial t} \hat{U}(t, t_0; \epsilon, \lambda) = \lambda \hat{H}_I^1(t; \epsilon) \hat{U}(t, t_0; \epsilon, \lambda), \quad (3.4.13)$$

and similarly to the previous discussion of section 3.2.2, the solution of this equation is written as:

$$\hat{U}(t, t_0; \epsilon, \lambda) = \mathcal{T} \left[e^{\frac{\lambda}{i\hbar} \int_{t_0}^t dt_1 e^{-\frac{\epsilon}{\hbar}|t_1|} \hat{H}_I^1(t_1)} \right]; \quad \text{with} \quad \hat{H}_I^1(t) = e^{+i\hat{H}_S^0 t/\hbar} \hat{H}_S^1 e^{-i\hat{H}_S^0 t/\hbar}. \quad (3.4.14)$$

In accordance with this expression of the time-evolution operator, the $\hat{\mathcal{S}}$ -matrix becomes:

$$\hat{\mathcal{S}}(\epsilon, \lambda) = \hat{U}(+\infty, -\infty; \epsilon, \lambda) = \mathcal{T} \left[e^{\frac{\lambda}{i\hbar c} \int d^4x_1 e^{-\frac{\epsilon}{\hbar}|t_1|} \hat{\mathcal{H}}_I(x_1)} \right], \quad (3.4.15)$$

and will thus expand as:

$$\begin{aligned}\hat{\mathcal{S}}(\epsilon, \lambda) &= \sum_{i=0}^{\infty} \hat{\mathcal{S}}^{(i)}(\epsilon, \lambda) \\ &= 1 + \frac{1}{1!} \frac{\lambda}{i\hbar c} \int d^4x_1 e^{-\frac{\epsilon}{\hbar}|t_1|} \mathbf{T} \left[\hat{\mathcal{H}}_I(x_1) \right] \\ &\quad + \frac{1}{2!} \left(\frac{\lambda}{i\hbar c} \right)^2 \int d^4x_1 \int d^4x_2 e^{-\frac{\epsilon}{\hbar}(|t_1|+|t_2|)} \mathbf{T} \left[\hat{\mathcal{H}}_I(x_1) \hat{\mathcal{H}}_I(x_2) \right] + \mathcal{O}(\lambda^3)\end{aligned}\tag{3.4.16}$$

We shall indicate what we are going to do next, so we can set the compass in the right direction. In the next sections, we shall:

1. Present the Gell-Mann and Low theorem which expresses the corrected (perturbed) states of eq.(3.4.3) in terms of the last time-evolution operator given in eq.(3.4.14), and the unperturbed states of eq.(3.4.2).
2. Show how the corrected energy levels E^α of eq.(3.4.3) are related to the corrected one, given in eq.(3.4.2), using the Sucher's formula, that corresponds to a symmetrization of the Gell-Mann and Low formula.
3. Specify the interaction density Hamiltonian $\hat{\mathcal{H}}_I(x_1)$ associated with the QED interaction: the coupling between the quantized photon and electron field operators.
4. Introduce the Wick's theorem [95] which will allow us to write the time-ordered products that appear in the last \mathcal{S} -matrix expansion of eq.(3.4.16) in terms of normal ordered products, which are ultimately represented by Feynman diagrams.

3.4.1 Corrected wavefunctions

Gell-Mann and Low first derived the relation between both states: the solutions of eqs.(3.4.2 and 3.4.3), and obtained the following result [96, eq.(10)]:

$$|\Phi^\alpha\rangle = \lim_{\substack{\epsilon \rightarrow 0 \\ \lambda \rightarrow 1}} \left[\frac{\hat{U}(0, -\infty; \epsilon, \lambda) |\Phi_0^\alpha\rangle}{\langle \Phi_0^\alpha | \hat{U}(0, -\infty; \epsilon, \lambda) | \Phi_0^\alpha \rangle} \right], \tag{3.4.17}$$

in which the perturbed state is written as a function of the unperturbed one and the time-evolution operator which includes the interactions. This was later known as the Gell-Mann and Low theorem, which claims that if the $\lim_{\epsilon \rightarrow 0}$ in the previous equation exists, then $|\Phi^\alpha\rangle$ is an eigenvector of the perturbed Hamiltonian. See Greiner and Reinhardt [89, Example 8.1].

3.4.2 Corrected energies

The associated energy-shift, experienced by the system of particles in the $|\Phi^\alpha\rangle$ state, is given by [97, eq.(6.24)]:

$$\Delta E^\alpha = E^\alpha - E_0^\alpha = \lim_{\substack{\epsilon \rightarrow 0 \\ \lambda \rightarrow 1}} \left[i\epsilon \lambda \frac{\partial}{\partial \lambda} \ln \langle \Phi_0^\alpha | \hat{U}(0, -\infty; \epsilon, \lambda) | \Phi_0^\alpha \rangle \right]. \tag{3.4.18}$$

Discussions and proofs of the Gell-Mann and Low theorem can be found in [87, pages 61-64] [89, Chapter 8] and [4, Section 11.f]. Six years later, Sucher provided a more time-symmetric formula for the energy-shift, in which the $\hat{\mathcal{S}}$ -matrix appears [98, eqs.(4,15)]:

$$\Delta E^\alpha = \lim_{\substack{\epsilon \rightarrow 0 \\ \lambda \rightarrow 1}} \left[\frac{i\epsilon\lambda}{2} \frac{\partial}{\partial \lambda} \ln \left\langle \Phi_0^\alpha \left| \hat{\mathcal{S}}(\epsilon, \lambda) \right| \Phi_0^\alpha \right\rangle \right]; \quad \text{with} \quad \hat{\mathcal{S}}(\epsilon, \lambda) = \hat{U}(+\infty, -\infty; \epsilon, \lambda). \quad (3.4.19)$$

instead of the time-evolution operator. At this point it is worth noting that the natural logarithm is dimensionless, and thus the last expressions has units of ϵ , i.e. the units of energy. See eq.(3.4.4) and the paragraph below.

3.5 The electron-photon field interaction: QED theory

In this section, we shall present the specific form of the QED interaction Hamiltonian that enters in our scattering matrix. We shall first introduce our electron and photon field operators, then discuss how these fields do interact, treat this interaction perturbatively (as done in previous sections), and finally discuss the lowest-order interaction corrections: the Quantum ElectroDynamic corrections.

3.5.1 Photon field operator

The quantized photon-field operator can be written a sum of two sub-sums:

$$A_\mu(x) = A_\mu^+(x) + A_\mu^-(x), \quad (3.5.1)$$

which runs over positive and negative-energy modes respectively. See Mandl and Shaw [93, eqs.(1.15,1.38)]. The individual sums are given by the following formulas:

$$A_\mu^+(x) = \sum_{r=0}^3 \sum_{\mathbf{k}} \sqrt{\frac{\hbar}{2\epsilon_0\omega_{\mathbf{k}}V}} \epsilon_\mu(\mathbf{k}, r) a(\mathbf{k}, r) e^{-ik \cdot x} \quad (3.5.2)$$

$$A_\mu^-(x) = \sum_{r=0}^3 \sum_{\mathbf{k}} \sqrt{\frac{\hbar}{2\epsilon_0\omega_{\mathbf{k}}V}} \epsilon_\mu(\mathbf{k}, r) a^\dagger(\mathbf{k}, r) e^{+ik \cdot x}, \quad (3.5.3)$$

where the zeroth component of the four-wavevector is simply the absolute value of the wave vector, $k_0 = |\mathbf{k}| = \omega_{\mathbf{k}}/c$. The multiplicative constant $\sqrt{\hbar/(2\epsilon_0\omega_{\mathbf{k}}V)}$ gives the quantized photon field operator the units of the classical external potential: mc/e , and leads to a normalization of the photon energy $\hbar\omega_{\mathbf{k}}$ within a box of volume V . Each electromagnetic mode is represented by a quantum harmonic oscillator, whose creation and annihilation operators obey the bosonic algebra [89, eqs.(7.32a,b)]:

$$[a(\mathbf{k}, r), a^\dagger(\mathbf{k}', s)] = \delta_{rs} \zeta_r \delta_{\mathbf{k}, \mathbf{k}'} \quad (3.5.4)$$

$$[a(\mathbf{k}, r), a(\mathbf{k}', s)] = [a^\dagger(\mathbf{k}, r), a^\dagger(\mathbf{k}', s)] = 0, \quad (3.5.5)$$

where δ_{rs} is the Kronecker delta, and ζ_r is a scalar quantity which is defined by:

$$\zeta_r = \begin{cases} +1 & r = 0 \\ -1 & r = 1, 2, 3 \end{cases}. \quad (3.5.6)$$

$a(\mathbf{k}, r)$ is the annihilation operator that destroys a photon with wave vector \mathbf{k} and polarization state r . The photonic vacuum state, denoted $|0_p\rangle$ where “p” stands for photonic, is defined through the following relation:

$$a(\mathbf{k}, r)|0_p\rangle = 0, \quad \forall \mathbf{k}, r \quad \rightarrow \quad A_\mu(x)|0_p\rangle = 0 \quad \forall \mu, x. \quad (3.5.7)$$

The final term is the polarization four-vector $\varepsilon_\mu(\mathbf{k}, r)$ that forms a basis of four linearly-independent vectors, for $r = 0, 1, 2, 3$. In the Feynman Gauge, these polarization vectors obey the following relation [93, eq.(5.39)]:

$$\sum_r \zeta_r \varepsilon^\mu(\mathbf{k}, r) \varepsilon^\nu(\mathbf{k}, r) = -g^{\mu\nu}. \quad (3.5.8)$$

3.5.2 Electron field operator

Similarly to the photon field operator, the electron field operator is expanded, in the basis of the Dirac solutions:

$$\Psi(x) = \sum_{i: \forall E_i} c_i \psi_i(x) = \sum_{i: E_i > 0} a_i \psi_i(x) + \sum_{i: E_i < 0} b_i^\dagger \psi_i(x). \quad (3.5.9)$$

Here, c_i is a general annihilator, associated with the wavefunction ψ_i that can be a positive or negative-energy solution. These annihilation (and creation) operators obey the fermionic anticommutation relations:

$$\{c_i^\dagger, c_j^\dagger\} = \{c_i, c_j\} = 0 \quad (3.5.10)$$

$$\{c_i, c_j^\dagger\} = \delta_{ij}. \quad (3.5.11)$$

On the other hand a_i annihilates a positive-energy electron, while b_i^\dagger creates a positive-energy positron because in the context of the hole theory, annihilating a negative-energy electron is equivalent to creating a positive-energy positron. These operators again obey the last relations. With these definitions, the vacuum state is defined to be:

$$c_i|0_e\rangle = a_i|0_e\rangle = b_i^\dagger|0_e\rangle = 0, \quad \forall i \quad \rightarrow \quad \Psi(x)|0_p\rangle = 0 \quad \forall x. \quad (3.5.12)$$

This state does not contain any positive-energy electron, and has no free seat for a new negative-energy electron: The Dirac sea is fully occupied. In different regions of this thesis we shall use the quantity $\Psi_\alpha(x)$, that represents the α -component of the electron field operator, which is expanded in the basis of the α -component Dirac solutions $\psi_{i,\alpha}(x)$ and the associated annihilation operators c_i as:

$$\Psi_\alpha(x) = \sum_{i: \forall E_i} c_i \psi_{i,\alpha}(x) \quad (3.5.13)$$

The reader should note that these expansions are valid only if the external potential is time-independent, and the wavefunctions are solutions of the time-independent Dirac equation, i.e. the wavefunction can be written as $\psi_i(x) = \psi_i(\mathbf{x}) e^{-\frac{i}{\hbar} E_i t}$, where the eigensolutions solve:

$$[c\boldsymbol{\alpha} \cdot (-i\hbar\nabla + e\mathbf{A}(\mathbf{x})) - e\varphi(\mathbf{x}) + \beta mc^2] \psi_i(\mathbf{x}) = E_i \psi_i(\mathbf{x}). \quad (3.5.14)$$

in the presence of a time-independent external potential $A^\mu(x) = (\varphi(\mathbf{x})/c, \mathbf{A}(\mathbf{x}))$. This approach where the field operator is expanded in the basis of wavefunctions that solve the Dirac equation in the presence of an external potential is known as the Furry picture [3], and leads to what is known as the bound state QED (BSQED). Alternatively, one can set the external four-potential to zero, so the wavefunctions describe the free-particle behavior, which will allow the study of scattering problems and their radiative corrections, as conventionally done in QED.

3.5.3 Adding the QED interaction to the non-interacting problem

Recall that the Hamiltonian we deal with has the following form of eq.(3.4.5):

$$\hat{H}_S(t; \epsilon) = \hat{H}_S^0 + \lambda \hat{H}_S^1(t; \epsilon), \quad (3.5.15)$$

where \hat{H}_S^0 is the free-Hamiltonian that is assumed to be solvable in an exact manner, and $\hat{H}_S^1(t; \epsilon)$ is the perturbation Hamiltonian that needs to be taken into account. The non-interacting Hamiltonian \hat{H}_S^0 contains both free electronic and photonic Hamiltonians, in their normal ordered form:

$$\hat{H}_S^0 = \hat{H}_{\text{electron}}^0 + \hat{H}_{\text{photon}}^0 \quad (3.5.16)$$

$$\begin{aligned} \hat{H}_{\text{electron}}^0 &= \int d^3x : \Psi^\dagger(x) H^D \Psi(x) : \\ &= \sum_{E_i > 0} E_i a_i^\dagger a_i - \sum_{E_i < 0} E_i b_i^\dagger b_i \end{aligned} \quad (3.5.17)$$

$$\begin{aligned} \hat{H}_{\text{photon}}^0 &= \int d^3x : \left[-\frac{1}{\mu_0} (\partial^0 A^\mu(x)) (\partial_0 A_\mu(x)) + \frac{1}{2\mu_0} (\partial^\nu A^\mu(x)) (\partial_\nu A_\mu(x)) \right] : \\ &= \sum_{\mathbf{k}} \sum_{r=0}^3 \hbar \omega_{\mathbf{k}} \zeta_r a^\dagger(\mathbf{k}, r) a(\mathbf{k}, r) \end{aligned} \quad (3.5.18)$$

Where the positive-energy electron annihilator a_i is not to be confused with the photon annihilator $a(\mathbf{k}, r)$. Definitions of these operators and the corresponding field operators are presented in the last two sections: 3.5.1 and 3.5.2. Details about the free photon Hamiltonian can be found in [89, chapter 7] and [93, chapter 5]. In the interaction representation, this full Hamiltonian becomes:

$$\hat{H}_I(\epsilon, t) = \hat{H}_S^0 + \lambda \hat{H}_I^1(t; \epsilon); \quad \text{with} \quad \hat{O}_I = e^{+i\hat{H}_S^0 t/\hbar} \hat{O}_S e^{-i\hat{H}_S^0 t/\hbar}. \quad (3.5.19)$$

This interaction Hamiltonian can be written as an integral over all space, of some interaction Hamiltonian density $\hat{\mathcal{H}}_I(x)$ as:

$$\hat{H}_I^1(t; \epsilon) = \int d^3x \hat{\mathcal{H}}_I(x; \epsilon), \quad (3.5.20)$$

cf. eq.(3.3.3). The QED Hamiltonian density is given by the following expression:

$$\hat{\mathcal{H}}_I(x; \epsilon) = j^\mu(x) A_\mu(x) e^{-\frac{\epsilon}{\hbar}|t|}, \quad \text{with} \quad \epsilon > 0, \quad (3.5.21)$$

which couples the quantized electronic current density operator $j^\mu(x)$, with the quantized photonic field $A_\mu(x)$. The electron current is a function of the field operators, given by:

$$j^\mu(x) = -ec\bar{\Psi}(x)\gamma^\mu\Psi(x). \quad (3.5.22)$$

This QED interaction term is obtained by performing a minimal substitution to the Dirac operator in the Dirac Lagrangian density. See, for instance, [4, chapter 10], Peskin and Schroeder [99, chapter 4] and Greiner and Reinhardt [89, section 8.6].

We are next going to discuss Wick's theorem: a strong tool that will let us write/expand a time-ordered product of operators in terms of normal ordered ones. This discussion will ultimately let us expand our \mathcal{S} -matrix, and we shall afterwards represent each of the obtained terms by a Feynman diagram.

3.6 Time-independent Wick's theorem

In order to motivate the reader, we shall start by the simple case where we consider the product (string) of time-independent creation and annihilation operators. In this case, Wick's theorem [95] simplifies to a very special case, and we shall call it: The time-independent Wick's theorem, as done in [100, section 5.3.1].

3.6.1 Creation and annihilation operators

The creation and annihilation operators in a multi-particle system do satisfy:

1. The following commutation relations for a bosonic system:

$$[a_i, a_j] = 0 \quad (3.6.1)$$

$$[a_i^\dagger, a_j^\dagger] = 0 \quad (3.6.2)$$

$$[a_i, a_j^\dagger] = \delta_{ij}, \quad (3.6.3)$$

that encode the symmetric nature of bosons.

2. And the following anticommutation relations for fermionic system:

$$\{a_i, a_j\} = 0 \quad (3.6.4)$$

$$\{a_i^\dagger, a_j^\dagger\} = 0 \quad (3.6.5)$$

$$\{a_i, a_j^\dagger\} = \delta_{ij}, \quad (3.6.6)$$

that encode the antisymmetric nature of fermions.

In addition, the vacuum state, we shall denote it by: $|0\rangle$, is defined to be state which vanishes once an annihilation operator acts on it:

$$a_i |0\rangle = 0, \quad (3.6.7)$$

we shall also define it to be normalized: $\langle 0|0\rangle = 1$.

3.6.2 Normal ordering

The normal ordering operation arranges a string of creation and annihilation operators by moving all the former to the left, and as a consequence, all the latter to the right. It should be seen, at this point, that the vacuum expectation value of any normal ordered string of operators, vanishes. Under this normal ordering, the previous commutation and anticommutation relations behave as if we had the following relations instead:

$$[a_i, a_j^\dagger] = 0 \quad (3.6.8)$$

$$\{a_i, a_j^\dagger\} = 0, \quad (3.6.9)$$

for bosons and fermions respectively. We shall use the $:xy:$ notation, which indicates that the xy product is normal ordered. For a product of two general operators a and b , where both a and b are

assumed to be either fermionic or bosonic, the four possible normal orderings are:

$$: a_i b_j : = a_i b_j \quad (3.6.10)$$

$$: a_i^\dagger b_j^\dagger : = a_i^\dagger b_j^\dagger \quad (3.6.11)$$

$$: a_i^\dagger b_j : = a_i^\dagger b_j \quad (3.6.12)$$

$$: a_i b_j^\dagger : = \mp b_j^\dagger a_i. \quad (3.6.13)$$

The first three products are unchanged, since they are already ordered, while the last one do change. The minus sign in the last ordered product is present in the case where the two operators a_i and b_j are both of fermionic nature, if not, then a plus sign should be there instead (these \pm signs come from eqs.(3.6.8 and 3.6.9)). In addition, we should note that the vacuum expectation value of any normal ordered product will always vanish, since the annihilation operator which acts on the right will destroy the right vacuum state, and the creation operators on the left (annihilations), will do the same.

3.6.3 Contraction

The contraction, denoted by a line above the product which links the two contracted operators is defined to be the difference between the product itself, and its normal ordered form:

$$\overline{xy} \equiv xy - : xy : \quad (3.6.14)$$

Using this definition, we evaluate the possible contractions of a product of two operators, and obtain the following results:

$$\overline{a_i b_j} = a_i b_j - : a_i b_j : = a_i b_j - a_i b_j = 0 \quad (3.6.15)$$

$$\overline{a_i^\dagger b_j^\dagger} = a_i^\dagger b_j^\dagger - : a_i^\dagger b_j^\dagger : = a_i^\dagger b_j^\dagger - a_i^\dagger b_j^\dagger = 0 \quad (3.6.16)$$

$$\overline{a_i^\dagger b_j} = a_i^\dagger b_j - : a_i^\dagger b_j : = a_i^\dagger b_j - a_i^\dagger b_j = 0 \quad (3.6.17)$$

$$\overline{a_i b_j^\dagger} = a_i b_j^\dagger - : a_i b_j^\dagger : = a_i b_j^\dagger \pm b_j^\dagger a_i = \delta_{ij}. \quad (3.6.18)$$

In the last relation, the plus sign exists if both operators are fermionic, and a minus sign otherwise. In both possible cases, one will get a Kronecker delta between the two indices, coming from the commutation and anticommutation relations introduced just above. If at this point we take the vacuum expectation value of the contraction in eq.(3.6.14), using the fact that the normal ordered product will always vanish under vacuum expectation value (previous section), the contraction of a product of two operators, can be written as a vacuum expectation value of this product:

$$\overline{xy} = \langle 0 | xy | 0 \rangle. \quad (3.6.19)$$

3.6.4 Products of n -operators

These previous manipulations can be generalized to a product of n -operators. This product can be written as a sum of normal ordered contractions, which runs from zero contraction (main product),

a sum over all possible single contractions, a sum over double contractions, and so on:

$$\begin{aligned}
X_1 X_2 X_3 X_4 \dots X_n &= : X_1 X_2 X_3 X_4 \dots X_n : \\
&+ \sum_{\text{single}} : \overline{X_1 X_2} X_3 X_4 \dots X_n : \\
&+ \sum_{\text{double}} : \overline{X_1 X_2 X_3 X_4} \dots X_n : \\
&+ \sum_{\text{triple}} + \dots
\end{aligned} \tag{3.6.20}$$

To give a flavor of how this machinery works, we apply the Wick's theorem on the product $c_i c_j c_k^\dagger c_l^\dagger$, and write it as:

$$\begin{aligned}
c_i c_j c_k^\dagger c_l^\dagger &= : c_i c_j c_k^\dagger c_l^\dagger : \\
&+ : \overline{c_i c_j} c_k^\dagger c_l^\dagger : + : \overline{c_i c_k^\dagger} c_j c_l^\dagger : + : \overline{c_i c_l^\dagger} c_j c_k^\dagger : + : \overline{c_j c_k^\dagger} c_i c_l^\dagger : \\
&+ : \overline{c_j c_l^\dagger} c_i c_k^\dagger : + : \overline{c_k^\dagger c_l^\dagger} c_i c_j :
\end{aligned} \tag{3.6.21}$$

$$+ : \overline{c_i c_k^\dagger} c_j c_l^\dagger : + : \overline{c_i c_l^\dagger} c_j c_k^\dagger : + : \overline{c_j c_k^\dagger} c_i c_l^\dagger : + : \overline{c_j c_l^\dagger} c_i c_k^\dagger : \tag{3.6.22}$$

where we only evaluate the non-vanishing contractions, of the form of $\overline{c_i c_j^\dagger}$, as seen in eq.(3.6.18). We then use the fact that a minus sign should appear whenever an odd number of fermionic operators exchanges are made, this allows us to obtain:

$$\begin{aligned}
c_i c_j c_k^\dagger c_l^\dagger &= : c_i c_j c_k^\dagger c_l^\dagger : \\
&\mp \overline{c_i c_k^\dagger} : c_j c_l^\dagger : + \overline{c_i c_l^\dagger} : c_j c_k^\dagger : + \overline{c_j c_k^\dagger} : c_i c_l^\dagger : \mp \overline{c_j c_l^\dagger} : c_i c_k^\dagger :
\end{aligned} \tag{3.6.23}$$

$$\mp \overline{c_i c_k^\dagger} \overline{c_j c_l^\dagger} + \overline{c_i c_l^\dagger} \overline{c_j c_k^\dagger} \tag{3.6.24}$$

Then, we use eq.(3.6.18) and the normal ordering relations, to obtain:

$$\begin{aligned}
c_i c_j c_k^\dagger c_l^\dagger &= c_k^\dagger c_l^\dagger c_i c_j \\
&+ \delta_{ik} c_l^\dagger c_j \mp \delta_{il} c_k^\dagger c_j \mp \delta_{jk} c_l^\dagger c_i + \delta_{jl} c_k^\dagger c_i
\end{aligned} \tag{3.6.25}$$

$$\mp \delta_{ik} \delta_{jl} + \delta_{il} \delta_{jk}. \tag{3.6.26}$$

Alternatively, one can obtain the result in the most primitive way, using the commutation and anticommutation relations of fermionic and bosonic systems:

$$c_i c_j c_k^\dagger c_l^\dagger = c_i \left(\delta_{kj} \mp c_k^\dagger c_j \right) c_l^\dagger \tag{3.6.27}$$

$$= \delta_{kj} c_i c_l^\dagger \mp c_i c_k^\dagger c_j c_l^\dagger \tag{3.6.28}$$

$$= \delta_{kj} \delta_{il} \mp \delta_{kj} c_l^\dagger c_i \mp \left(\delta_{ik} \mp c_k^\dagger c_i \right) c_j c_l^\dagger \tag{3.6.29}$$

$$= \delta_{kj} \delta_{il} \mp \delta_{kj} c_l^\dagger c_i \mp \delta_{ik} c_j c_l^\dagger + c_k^\dagger c_i c_j c_l^\dagger \tag{3.6.30}$$

$$= \delta_{kj} \delta_{il} \mp \delta_{kj} c_l^\dagger c_i \mp \delta_{ik} \delta_{jl} + \delta_{ik} c_l^\dagger c_j + \left(\delta_{jl} c_k^\dagger c_i \mp c_k^\dagger c_i c_l^\dagger c_j \right) \tag{3.6.31}$$

$$= \delta_{kj} \delta_{il} \mp \delta_{kj} c_l^\dagger c_i \mp \delta_{ik} \delta_{jl} + \delta_{ik} c_l^\dagger c_j + \delta_{jl} c_k^\dagger c_i \mp \delta_{il} c_k^\dagger c_j + c_k^\dagger c_l^\dagger c_i c_j \tag{3.6.32}$$

$$= \delta_{kj} \delta_{il} \mp \delta_{kj} c_l^\dagger c_i \mp \delta_{ik} \delta_{jl} + \delta_{ik} c_l^\dagger c_j + \delta_{jl} c_k^\dagger c_i \mp \delta_{il} c_k^\dagger c_j + c_k^\dagger c_l^\dagger c_i c_j. \tag{3.6.33}$$

At this point, the reader can start to see the importance of Wick's theorem, which gets more important when evaluating the vacuum expectation values of a string of creation and annihilation operators, since only the fully contracted terms will survive. So far this is an introduction, the real problem we shall attack is the expansion of the time-ordered products of time-dependent operators.

3.7 Wick's theorem

For two operators $A(x_1)$ and $B(x_2)$, depending on times t_1 and t_2 , it can be shown that their normal order product can be written as:

$$: A(x_1) B(x_2) : = T[A(x_1) B(x_2)] - \langle 0 | T[A(x_1) B(x_2)] | 0 \rangle, \quad (3.7.1)$$

the difference between the time-ordered product, and vacuum expectation of this latter. In addition, if the time-dependence is eliminated, this equation directly reduces to the analysis of the previous section. The contraction of these operators is equal (by definition) to the vacuum expectation value of the time-ordered product of these two operators:

$$\overline{A(x_1) B(x_2)} \equiv \langle 0 | T[A(x_1) B(x_2)] | 0 \rangle. \quad (3.7.2)$$

See eq.(3.6.19). Wick's theorem, which was introduced in 1950 [95], tells us that the time-ordered product of a string of n operators can be written as the normal ordering of all the terms, including the zero-contraction, all possible single-contractions, and so on:

$$\begin{aligned} & T[A_1(x_1) A_2(x_2) A_3(x_3) A_4(x_4) \dots A_n(x_n)] \\ & = : A_1(x_1) A_2(x_2) A_3(x_3) A_4(x_4) \dots A_n(x_n) : \\ & + \sum_{\text{single}} : \overline{A_1(x_1) A_2(x_2)} A_3(x_3) A_4(x_4) \dots A_n(x_n) : \\ & + \sum_{\text{double}} : \overline{A_1(x_1) A_2(x_2) A_3(x_3) A_4(x_4)} \dots A_n(x_n) : + \dots \end{aligned} \quad (3.7.3)$$

Using the contraction definition of eq.(3.7.2), the Wick's result can be written as:

$$\begin{aligned} & T[A_1(x_1) A_2(x_2) A_3(x_3) A_4(x_4) \dots A_n(x_n)] \\ & = : A_1(x_1) A_2(x_2) A_3(x_3) A_4(x_4) \dots A_n(x_n) : \\ & + \sum_{\text{single}} \langle 0 | T[A_1(x_1) A_2(x_2)] | 0 \rangle : A_3(x_3) A_4(x_4) \dots A_n(x_n) : \\ & + \sum_{\text{double}} \langle 0 | T[A_1(x_1) A_4(x_4)] | 0 \rangle \langle 0 | T[A_2(x_2) A_3(x_3)] | 0 \rangle : \dots A_n(x_n) : + \dots \end{aligned} \quad (3.7.4)$$

This theorem is going to be used when expanding the \mathcal{S} -matrix perturbatively. Recall that our \mathcal{S} -matrix contained electron and photon field operators (see eq.(3.5.21)). We shall thus now show how the vacuum expectation values of the time-ordered products of two photon/electron field operator (the contractions), can be written in terms of the Feynman photon and electron propagators that do solve the Dirac and Maxwell Green's functions equations. Interesting discussions on Wick's theorem can be found in Fetter [87], Greiner and Reinhardt [89, section 8.5], Schwartz [101, section 7.A], Drake [100, section 5.3] and Schweber [4, section 13c].

3.8 Photon propagator

The existence of a four-current J^ν in spacetime, describing a charge distribution moving through space, generates electromagnetic fields, that satisfy the (inhomogeneous) Maxwell equation:

$$\partial_\mu F^{\mu\nu} = \mu_0 J^\nu, \quad (3.8.1)$$

where μ_0 is the magnetic constant (vacuum permeability), related to the electric one by $\epsilon_0 \mu_0 = c^{-2}$. The electromagnetic field components are matrix elements of the electromagnetic tensor, given by:

$$F^{\mu\nu} = \begin{bmatrix} 0 & -\frac{\mathbf{E}}{c} \\ +\frac{\mathbf{E}}{c} & -\epsilon^{ijk} B_k \end{bmatrix} = \begin{bmatrix} 0 & -\frac{E_1}{c} & -\frac{E_2}{c} & -\frac{E_3}{c} \\ +\frac{E_1}{c} & 0 & -B_3 & +B_2 \\ +\frac{E_2}{c} & +B_3 & 0 & -B_1 \\ +\frac{E_3}{c} & -B_2 & +B_1 & 0 \end{bmatrix}, \quad (3.8.2)$$

and related to four-potential which is generated by this current by the following relation:

$$F^{\mu\nu} = \partial^\mu A^\nu - \partial^\nu A^\mu. \quad (3.8.3)$$

After inserting the last equation.(3.8.3) in the first one eq.(3.8.1), one gets the following differential equation:

$$[g_\mu^\nu \partial_\sigma \partial^\sigma - \partial_\mu \partial^\nu] A^\mu = \mu_0 J^\nu. \quad (3.8.4)$$

This homogeneous differential equation can be solved by the introduction of the Green's function of the homogeneous problem, i.e. that satisfies the following following Green's equation:

$$[g_\mu^\nu \partial_\sigma \partial^\sigma - \partial_\mu \partial^\nu] D^{\mu\theta}(x, y) = \frac{g^{\nu\theta}}{\epsilon_0 c} \delta(x - y), \quad (3.8.5)$$

The Green's function $D^{\mu\sigma}(x, y)$, known as the photon propagator, which measures the probability amplitude that a photon travels from a spacetime point y to x . The seeked solution A^μ can be thus written as:

$$A^\mu(x) = \phi^\mu(x) + \sqrt{\epsilon_0 \mu_0} \int d^4 y D^{\mu\sigma}(x, y) J_\sigma(y), \quad (3.8.6)$$

where $\phi^\mu(x)$ is simply a solution of the homogeneous equation:

$$[g_\mu^\nu \partial_\sigma \partial^\sigma - \partial_\mu \partial^\nu] \phi^\mu(x) = 0, \quad (3.8.7)$$

which represents the free potential, i.e. in the absence of an external source $J^\nu = 0$. Our next goal is to determine the photon propagator $D^{\mu\theta}(x, y)$. We first define the Fourier transformed photon propagator $D^{\mu\theta}(p)$ as:

$$D^{\mu\theta}(x, y) = \int \frac{d^4 p}{(2\pi\hbar)^4} e^{-\frac{i}{\hbar} p \cdot (x-y)} G^{\mu\theta}(p), \quad (3.8.8)$$

and plug this expression in equation.(3.8.5):

$$\int \frac{d^4 p}{(2\pi\hbar)^4} [-g_\mu^\nu p^2 + p_\mu p^\nu] G^{\mu\theta}(p) e^{-\frac{i}{\hbar} p \cdot (x-y)} = \frac{\hbar^2 g^{\nu\theta}}{\epsilon_0 c} \delta(x - y), \quad (3.8.9)$$

where we used techniques that are given in appendix appendix H. By comparing with eq.(H.2.2), one sees that the following equation must hold:

$$[-g_{\mu}^{\nu} p^2 + p_{\mu} p^{\nu}] G^{\mu\theta}(p) = \frac{\hbar^2 g^{\nu\theta}}{\epsilon_0 c}. \quad (3.8.10)$$

This equation means that the photon propagator is defined as the inverse of the 4×4 matrix M , whose matrix elements are $M_{\mu}^{\nu} = p_{\mu} p^{\nu} - p^2 g_{\mu}^{\nu}$. Unfortunately, this matrix is not invertible, as mentioned by Bogoliubov and Shirkov [102, Section 4.3] and Peskin and Schroeder [99, section 9.4], since its determinant vanishes. This can be seen by the fact that p_{ν} is an eigenvector of M_{μ}^{ν} , with a zero eigenvector:

$$p_{\nu} M_{\mu}^{\nu} = 0. \quad (3.8.11)$$

See, for instance, Schwartz [101, page 267]. One can overcome this problem by imposing the Lorentz-gauge condition, and take into account the fact that the physics (nature) is invariant under gauge transformations, as will be discussed in the next section.

Gauge transformation

One can observe that under a gauge transformation:

$$A^{\mu} \rightarrow \mathcal{A}^{\mu} = A^{\mu} + \partial^{\mu} \chi, \quad (3.8.12)$$

where the four-potential A^{μ} is replaced by \mathcal{A}^{μ} that contains an additional gradient of some arbitrary function χ , the electromagnetic fields:

$$F^{\mu\nu} \rightarrow \partial^{\mu} \mathcal{A}^{\nu} - \partial^{\nu} \mathcal{A}^{\mu} = \partial^{\mu} A^{\nu} - \partial^{\nu} A^{\mu} = F^{\mu\nu}, \quad (3.8.13)$$

as well as the four-current, are invariant. This shows that the four-potential is not an observable, and one can always perform a gauge transformation as in eq.(3.8.12), and still obtain the same electromagnetic fields, and currents. Restrictions can be thus imposed on the new four-potential \mathcal{A}^{μ} , and absorbed by the arbitrary function χ . Different gauge choices can lead to simplifications in the calculations derived for different problems. The Lorenz-gauge condition implies a divergenceless four-potential:

$$\partial^{\mu} \mathcal{A}_{\mu} = 0, \quad (3.8.14)$$

which imposes the following relation:

$$\partial^{\mu} \partial_{\mu} \chi = -\partial^{\mu} A_{\mu}, \quad (3.8.15)$$

between the old potential A_{μ} and the introduced function χ . This condition reduces the potential equation to:

$$\partial_{\sigma} \partial^{\sigma} \mathcal{A}^{\nu} = \mu_0 J^{\nu}, \quad (3.8.16)$$

where one can check that the electromagnetic current is invariant under gauge transformation. As a consequence, the photon propagator equation becomes:

$$\partial_{\sigma} \partial^{\sigma} D^{\nu\theta}(x, y) = \frac{g^{\nu\theta}}{\epsilon_0 c} \delta(x - y), \quad (3.8.17)$$

which is fortunately invertible! since the problematic second term of eq.(3.8.5), is no longer present in our new equation, and the metric tensor is invertible. We now plug the Fourier form of the photon propagator of eq.(3.8.8), in the previous equation, and obtain:

$$\int \frac{d^4 p}{(2\pi\hbar)^4} D^{\nu\theta}(p) \left[-\frac{p_\sigma p^\sigma}{\hbar^2} \right] e^{-\frac{i}{\hbar} p \cdot (x-y)} = \frac{g^{\nu\theta}}{\epsilon_0 c} \delta(x-y). \quad (3.8.18)$$

$p_\sigma p^\sigma$ is simply p^2 (a scalar quantity), thus the photon propagator is written as:

$$D^{\nu\theta}(p) = -\frac{\hbar^2}{c\epsilon_0} \frac{g^{\nu\theta}}{p^2}. \quad (3.8.19)$$

This is known as the photon propagator in the Feynman gauge. We then go back to real-space using eq.(3.8.8):

$$D^{\mu\nu}(x, y) = -\frac{\hbar^2}{c\epsilon_0} g^{\mu\nu} \int \frac{d^4 p}{(2\pi\hbar)^4} \frac{e^{-\frac{i}{\hbar} p \cdot (x-y)}}{p^2}. \quad (3.8.20)$$

After separating scalar and vector integration component, one gets:

$$D^{\mu\nu}(x, y) = -\frac{\hbar^2}{c\epsilon_0} g^{\mu\nu} \int \frac{d^3 p}{(2\pi\hbar)^3} e^{+\frac{i}{\hbar} \mathbf{p} \cdot (\mathbf{x}-\mathbf{y})} \int_{-\infty}^{+\infty} \frac{dp_0}{2\pi\hbar} \frac{e^{-\frac{i}{\hbar} p_0(x^0-y^0)}}{p_0^2 - \mathbf{p}^2}. \quad (3.8.21)$$

At this point one notices that once the p_0 integration hits the points $p_0 = \pm |\mathbf{p}|$ the integral diverges. This problem is treated by what is known as the ‘‘Feynman prescription’’, which shifts poles above/below the real axis with a small imaginary number, so the integration can be taken along the real axis, then the limit of the small number is taken to zero. Different choices of pole shifting lead to different propagators: advanced and retarded, and eventually the Feynman (time-ordered) propagator, which we shall discuss in the next section. We should also note that since the exponential inside the Fourier integral depends on the difference $x - y$, we shall allow ourselves to write:

$$D^{\mu\nu}(x, y) = D^{\mu\nu}(x - y) \quad (3.8.22)$$

Finally, our four-potential, can be written as:

$$\mathcal{A}^\nu(x) = \phi^\nu(x) - \hbar^2 \mu_0 \int d^4 y \int \frac{d^4 p}{(2\pi\hbar)^4} \frac{e^{-\frac{i}{\hbar} p \cdot (x-y)}}{p^2} J^\nu(y). \quad (3.8.23)$$

Discussions about the photon propagator can be found in [103, section 7.1] and [102, section 4].

3.8.1 Time-ordered photon propagator

The time-ordered propagator is called the Feynman propagator. The justification of the first name shall be clear in section 3.8.3, and for the second name, it is because the timelike momentum integral is to be taken along the Feynman path, which is equivalent as shifting the positive-energy pole below the real axis, and the negative-energy pole above it, as seen in fig. 3.8.1c. This photon propagator is defined by the following formula:

$$D^{\mu\nu}(x - y) = -\frac{\hbar^2}{c\epsilon_0} g^{\mu\nu} \lim_{\epsilon \rightarrow 0} \int \frac{d^4 p}{(2\pi\hbar)^4} \frac{e^{-\frac{i}{\hbar} p \cdot (x-y)}}{p_0^2 - |\mathbf{p}|^2 + i\epsilon}, \quad (3.8.24)$$

where positive and negative-energy poles are shifted below and above the real axis respectively:

$$p_0 = +\sqrt{|\mathbf{p}|^2 - i\epsilon} \quad (3.8.25)$$

$$p_0 = -\sqrt{|\mathbf{p}|^2 - i\epsilon}, \quad (3.8.26)$$

as seen in figure fig. 3.8.1c, which follows the Feynman choice of contour integration. There are two ways to evaluate this integral:

1. One can first evaluate the spatial momentum-component integral:

$$D_F^{\mu\nu}(x-y) = -\frac{\hbar^2}{c\epsilon_0} g^{\mu\nu} \lim_{\epsilon \rightarrow 0} \int \frac{dp_0}{2\pi\hbar} e^{-\frac{i}{\hbar}p_0(x^0-y^0)} \int \frac{d^3\mathbf{p}}{(2\pi\hbar)^3} \frac{e^{+\frac{i}{\hbar}\mathbf{p}\cdot(\mathbf{x}-\mathbf{y})}}{p_0^2 - |\mathbf{p}|^2 + i\epsilon}, \quad (3.8.27)$$

using eq.(I.3.5), one obtains:

$$D_F^{\mu\nu}(x-y) = \frac{1}{c\epsilon_0\hbar 8\pi^2 |\mathbf{x}-\mathbf{y}|} g^{\mu\nu} \lim_{\epsilon \rightarrow 0} \int_{-\infty}^{+\infty} dp_0 e^{-\frac{i}{\hbar}p_0(x^0-y^0)} e^{+\frac{i}{\hbar}\sqrt{p_0^2+i\epsilon}|\mathbf{x}-\mathbf{y}|}. \quad (3.8.28)$$

At $\sqrt{p_0^2+i\epsilon} = 0$, this integral has two branch points, meaning that one should specify the branch cut to avoid letting the integrand being multivalued. This form is usually used by Mohr, Soff and Indelicato [104, eqs.(29,30)] [5, eq.(4)].

2. One can first evaluate the timelike momentum integral, which we shall call:

$$I(x^0 - y^0, |\mathbf{p}|) = \frac{1}{2|\mathbf{p}|} \int_{-\infty}^{+\infty} dp_0 e^{-\frac{i}{\hbar}p_0(x^0-y^0)} \left[\frac{1}{p_0 - |\mathbf{p}| + i\epsilon} - \frac{1}{p_0 + |\mathbf{p}| - i\epsilon} \right]. \quad (3.8.29)$$

Again, using Jordan's lemma, two cases are to be considered:

- For $y^0 > x^0$, only the upper pole will contribute, and we thus have:

$$I(x^0 - y^0, |\mathbf{p}|) = -\frac{\pi i}{|\mathbf{p}|} e^{+\frac{i}{\hbar}|\mathbf{p}|(x^0-y^0)}. \quad (3.8.30)$$

- For $x^0 > y^0$, only the lower pole will contribute, and we thus have:

$$I(x^0 - y^0, |\mathbf{p}|) = -\frac{\pi i}{|\mathbf{p}|} e^{-\frac{i}{\hbar}|\mathbf{p}|(x^0-y^0)}. \quad (3.8.31)$$

These two cases allow us to write our integral as:

$$I(x^0 - y^0, |\mathbf{p}|) = -\frac{\pi i}{|\mathbf{p}|} \left[e^{+\frac{i}{\hbar}|\mathbf{p}|(x^0-y^0)} \Theta(y^0 - x^0) + e^{-\frac{i}{\hbar}|\mathbf{p}|(x^0-y^0)} \Theta(x^0 - y^0) \right]. \quad (3.8.32)$$

Now this integral is purely radial, i.e. it only depends on $|\mathbf{p}|$. We shall next evaluate the angular integration of the remaining spatial one. We first call $|\mathbf{p}| = r_p$, and use the result of eq.(I.2.5), to write the photon propagator as:

$$D_F^{\mu\nu}(x-y) = \frac{i}{4\pi^2\hbar c\epsilon_0 r_{x-y}} g^{\mu\nu} \int_0^\infty dr_p e^{-\frac{i}{\hbar}r_p|y^0-x^0|} \sin\left(\frac{r_p r_{x-y}}{\hbar}\right), \quad (3.8.33)$$

which can be related to the work of Lindgren [15, section 4.3.1].

It is worth noting that the photon propagator equation.(3.8.17) can be related to the Klein-Gordon propagator equation, by taking the mass limit $m \rightarrow 0$, in the latter equation. See Ohlsson [33, eq.(5.14)] and Ryder [103, eq.(7.7)]. As we know, the physics is unchanged under gauge transformations. This fact leads to a freedom in choosing the propagator, and we shall discuss this in the next section.

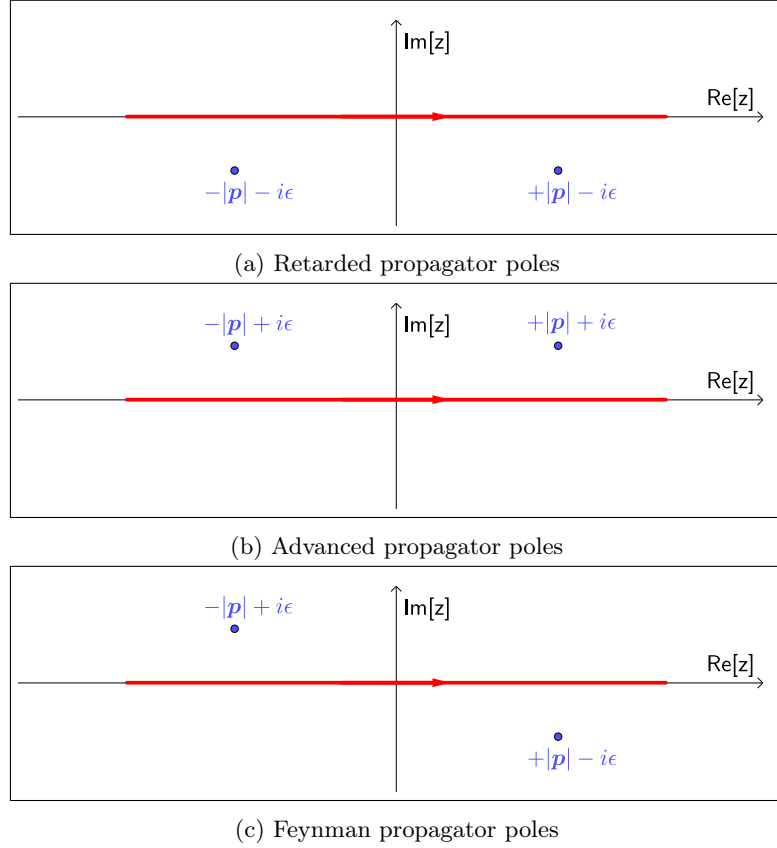


Figure 3.8.1: The possible boundary conditions (choices) of the photon propagator. The reader should keep in mind the fact that pole shifting is equivalent to placing poles at the real line and deforming the contours (red lines).

3.8.2 Different gauges for the photon propagator

So far, the momentum space photon propagator we worked with is Feynman one of eq.(3.8.19):

$$D_F^{\mu\nu}(q) = -\frac{\hbar^2 g^{\mu\nu}}{c\epsilon_0 q^2}, \quad (3.8.34)$$

where the F subscript is added to indicate that this is the Feynman propagator, where the pole at $q^2 = 0$ can be shifted in three different ways, giving three different propagators in real-space. We shall see that this momentum-space form is only one way to define this propagator. The photon propagator is always sandwiched between two electron vertices (when evaluating probability amplitudes or bound-electron level-shifts), which when combined with spinors gives two four-current densities, and one has a term of the following form:

$$\int d^4x d^4x' j_\mu(x) D^{\mu\nu}(x-x') j'_\nu(x'). \quad (3.8.35)$$

Gauge	$f_\mu(q) = g_\mu(q)$	$D_X^{\mu\nu}(q)$
Feynman	0	$D_F^{\mu\nu}(q) = -\frac{\hbar^2 g^{\mu\nu}}{c\epsilon_0 q^2}$
Landau	$\frac{1}{2c\epsilon_0} \frac{\hbar^2 q_\mu}{q^4}$	$D_L^{\mu\nu}(q) = -\frac{\hbar^2}{c\epsilon_0 q^2} \left(g^{\mu\nu} - \frac{q^\mu q^\nu}{q^2} \right)$
Coulomb	$\frac{1}{2c\epsilon_0} \frac{\hbar^2}{q^2} \frac{1}{q^2} (q_0, -q_i)$	$D_C^{\mu\nu}(q) = \frac{\hbar^2}{c\epsilon_0} \begin{bmatrix} \frac{1}{q^2} & 0 \\ 0 & \frac{\hbar^2 \delta_{ij}}{q^2} \left(1 - \frac{q^j q^i}{q^2} \right) \end{bmatrix}$

Table 3.2: Momentum space photon propagator in different gauges.

In Fourier-space, using eq.(H.5.1), the last non-local integral can be written as a local-one:

$$\int \frac{d^4 q}{(2\pi\hbar)^4} j_\mu(q) D^{\mu\nu}(q) j'_\nu(q). \quad (3.8.36)$$

The continuity equation that the four-current has to obey, in order for the charge current to stay conserved is given by:

$$\partial_\mu j^\mu(x) = \partial_0 j^0(x) + \nabla \cdot \mathbf{j}(x) = 0, \quad (3.8.37)$$

where we used eqs.(A.0.2 and A.0.6). In Fourier-space, this equation becomes:

$$\int d^4 x e^{+\frac{i}{\hbar} q \cdot x} \left\{ \frac{\partial}{\partial x^\mu} j^\mu(x) \right\} = -\frac{i}{\hbar} q_\mu j^\mu(q) = 0 \quad \rightarrow \quad q^\mu j_\mu(q) = 0. \quad (3.8.38)$$

At this point, one has to notice that if we add any term that proportional to q^μ or q^ν to the photon propagator:

$$D^{\mu\nu}(q) \rightarrow D^{\mu\nu}(q) + f^\nu(q) q^\mu + g^\mu(q) q^\nu, \quad (3.8.39)$$

where $f^\nu(q)$ and $g^\nu(q)$ are some arbitrary functions, eq.(3.8.36) and thus eq.(3.8.35) is unchanged, i.e. the physics is unchanged, as mentioned by Berestetskii *et al.* [105, page 301] and Greiner and Reinhardt [89, pages 185-187]. This freedom shows that the propagator is not uniquely defined. In table 3.2, we present three different gauges associated with three different choices of $f^\nu(q)$ and $g^\nu(q)$ functions, found in [8, pages 249-250].

3.8.3 Feynman photon propagator as a time-ordered vacuum expectation value

In this section we will show that the photon propagator can be written as a vacuum expectation value of time-ordered product of two photon-field operators:

$$D_{\mu\nu}^F(x, y) = \frac{1}{i\hbar} \langle 0_p | T[A_\mu(x) A_\nu(y)] | 0_p \rangle. \quad (3.8.40)$$

In eq.(3.5.1) of section 3.5.1, we present the photon field operator as a sum of two sum:

$$A_\mu(x) = A_\mu^+(x) + A_\mu^-(x), \quad (3.8.41)$$

given in eqs.(3.5.2 and 3.5.3). Since A_μ^+ and A_μ^- contain annihilation and creation operators respectively, one can directly see that the only non-vanishing terms under the vacuum expectation value of eq.(3.8.40) are:

$$\begin{aligned} & \langle 0_p | T[A_\mu(x) A_\nu(y)] | 0_p \rangle \\ &= \Theta(x^0 - y^0) \langle 0_p | A_\mu^+(x) A_\nu^-(y) | 0_p \rangle + \Theta(y^0 - x^0) \langle 0_p | A_\nu^+(y) A_\mu^-(x) | 0_p \rangle \end{aligned} \quad (3.8.42)$$

The other contributions simply vanish because they either contain two creation or annihilation operators, or contain a creation operator acting to the left with an annihilation operator acting to the right. These two terms are then found to be:

$$\begin{aligned}\langle 0_p | A_\mu^+(x) A_\nu^-(y) | 0_p \rangle &= \sum_{\mathbf{k}} \frac{\hbar}{2\epsilon_0 V} \frac{1}{\omega_{\mathbf{k}}} e^{-i\mathbf{k} \cdot (x-y)} (-g_{\mu\nu}) \\ \langle 0_p | A_\nu^+(y) A_\mu^-(x) | 0_p \rangle &= \sum_{\mathbf{k}} \frac{\hbar}{2\epsilon_0 V} \frac{1}{\omega_{\mathbf{k}}} e^{-i\mathbf{k} \cdot (y-x)} (-g_{\nu\mu}).\end{aligned}\quad (3.8.43)$$

We then perform the usual replacement:

$$\sum_{\mathbf{k}} f(\mathbf{k}) \rightarrow V \int \frac{d^3\mathbf{k}}{(2\pi)^3} f(\mathbf{k}), \quad (3.8.44)$$

which transforms the sum over a continuous three-variable to an integral, and write the time-ordered product as:

$$\begin{aligned}\langle 0_p | T[A_\mu(x) A_\nu(y)] | 0_p \rangle \\ = -\frac{g_{\mu\nu}\hbar}{2\epsilon_0} \int \frac{d^3\mathbf{k}}{(2\pi)^3} \frac{1}{\omega_{\mathbf{k}}} e^{+i\mathbf{k} \cdot (x-y)} \left[\Theta(x^0 - y^0) e^{-i|\mathbf{k}| \cdot (x^0 - y^0)} + \Theta(y^0 - x^0) e^{-i|\mathbf{k}| \cdot (y^0 - x^0)} \right].\end{aligned}\quad (3.8.45)$$

Using Jordan's lemma, one can show that the terms inside the square brackets, can be written as the following integral [103, pages 193,194,244] and [101, eq.(6.28)]:

$$e^{-i|\mathbf{k}|(x^0 - y^0)} \theta(x^0 - y^0) + e^{-i|\mathbf{k}|(y^0 - x^0)} \theta(y^0 - x^0) = \frac{i|\mathbf{k}|}{\pi} \int_{-\infty}^{+\infty} dk_0 \frac{e^{-ik_0 \cdot (x^0 - y^0)}}{k_0^2 - |\mathbf{k}|^2 + i\eta}, \quad (3.8.46)$$

with η a small positive real, which shifts the integrand poles above and below the real-line. Notice that this pole shifting corresponds to the Feynman choice of contour integration. This integral can be written as:

$$\frac{i|\mathbf{k}|}{\pi} \int_{-\infty}^{+\infty} dk_0 \frac{e^{-ik_0 \cdot (x^0 - y^0)}}{k_0^2 - |\mathbf{k}|^2 + i\eta} = \frac{i|\mathbf{k}|}{\pi} \int_{C_F} dk_0 \frac{e^{-ik_0 \cdot (x^0 - y^0)}}{k_0^2 - |\mathbf{k}|^2} \quad (3.8.47)$$

where C_F indicates that the chosen path is the Feynman one. This shows that vacuum expectation value of the photon operators corresponds to the propagator whose energy (zeroth component momentum) integral is taken along the Feynman path, and justifies why we put an "F" superscript on the propagator in eq.(3.8.40). Our vacuum expectation value then becomes:

$$\langle 0_p | T[A_\mu(x) A_\nu(y)] | 0_p \rangle = i\hbar \left[-\frac{g_{\mu\nu}}{c\epsilon_0} \int \frac{d^4k}{(2\pi)^4} \frac{e^{-ik \cdot (x-y)}}{k^2 + i\eta} \right], \quad (3.8.48)$$

which finally allows us to write the photon propagator as a vacuum expectation value:

$$D_{\mu\nu}^F(x, y) = \frac{1}{i\hbar} \langle 0_p | T[A_\mu(x) A_\nu(y)] | 0_p \rangle. \quad (3.8.49)$$

For discussions on the photon field operator, the reader may consult Greiner and Reinhardt [89, chapter 7], Mandl and Shaw [93, chapter 5] and Ohlsson [33, section 8.4]. Recall that the goal was to show that vacuum expectation values of the time-ordered products are related to propagators. So far we have discussed the photon propagator, and it is thus now the time for the electron one.

3.9 Electron propagator

3.9.1 Free Dirac propagator

The free Dirac propagator satisfies the following free Dirac equation:

$$\left[i\hbar\gamma^\mu \frac{\partial}{\partial y^\mu} - mc \right] S_0(y, x) = \mathbb{1}_4 \delta(y - x), \quad (3.9.1)$$

which is a Green's function type equation. The Green's function here is the Dirac propagator $S_0(y, x)$. The zero subscript is there just to remind us that the S propagator is a free (absence of any external potential). We shall now show to use Fourier transforms to derive this propagator. We start by the following expression:

$$S_0(y, x) = \int \frac{d^4 p}{(2\pi\hbar)^4} e^{-\frac{i}{\hbar} p \cdot (y-x)} S_0(p), \quad (3.9.2)$$

which assumes that our propagator can be written as an inverse Fourier transform of the Fourier-space propagator $S_0(p)$. After plugging this expression in the first equation, one gets:

$$\int \frac{d^4 p}{(2\pi\hbar)^4} e^{-\frac{i}{\hbar} p \cdot (y-x)} \{[\gamma^\mu p_\mu - mc] S_0(p)\} = \mathbb{1}_4 \delta(y - x), \quad (3.9.3)$$

meaning that the term that is inverse transformed (within the curly brackets) is just the unit matrix $\mathbb{1}_4$. This means that if we set the Fourier space propagator to be:

$$S_0(p) = \frac{1}{\gamma^\mu p_\mu - mc} = \frac{\gamma^\mu p_\mu + mc}{p^2 - m^2 c^2}. \quad (3.9.4)$$

Then the propagator of the form of eq.(3.9.2):

$$S_0(y, x) = \int \frac{d^4 p}{(2\pi\hbar)^4} \frac{e^{-\frac{i}{\hbar} p \cdot (y-x)}}{\gamma^\mu p_\mu - mc} = \int \frac{d^4 p}{(2\pi\hbar)^4} e^{-\frac{i}{\hbar} p \cdot (y-x)} \frac{\gamma^\mu p_\mu + mc}{p^2 - m^2 c^2}, \quad (3.9.5)$$

is the propagator we are looking for, i.e., that satisfies the propagator equation.(3.9.1). The denominator again diverges, this time at the massive particle energy-momentum relation $p^2 = m^2 c^2$, instead of the massless one (as the photon propagator case) $p^2 = 0$. In the last step we have just multiplied the integral by the unit matrix:

$$\mathbb{1}_4 = \frac{\gamma^\mu p_\mu + mc}{\gamma^\mu p_\mu + mc}. \quad (3.9.6)$$

Notice that this free propagator only depends on the difference of spacetime points. Greiner and Reinhardt commented on this point by saying: "This property is a manifestation of the homogeneity of space and time and in general would not be valid for the interacting propagator" [8, Page 42] (See also in Itzykson and Zuber [43, Page 90]). We shall thus allow ourselves to write $S_0(y - x)$ instead of $S_0(y, x)$. Finally, as in the photon propagator case, different choices of poles shifting can be taken, which eventually lead to different definitions of the propagator: Retarded, Advanced, or Feynman (time-ordered) propagator, which we shall discuss in the next section.

3.9.2 Time-ordered free Dirac propagator

The time-ordered free Dirac propagator is defined with respect to the eq.(3.9.5) by:

$$S_0^F(y, x) = \lim_{\epsilon \rightarrow 0} \int \frac{d^4 p}{(2\pi\hbar)^4} e^{-\frac{i}{\hbar} p \cdot (y-x)} \frac{\gamma^\mu p_\mu + mc}{p^2 - m^2 c^2 + i\epsilon}, \quad (3.9.7)$$

where ϵ is a small positive number. Note that we added the superscript F to indicate that this is the Dirac-Feynman-propagator, i.e. it corresponds to the Feynman choice of the p_0 contour integration that goes above the positive-energy pole and below the negative-energy one. It is worth noting that since the Dirac and Klein-Gordon equations are related, the propagators are too. The free Dirac equation is written as:

$$\left[i\hbar\gamma^\mu \frac{\partial}{\partial x^\mu} - mc \right] \psi_i(x) = 0. \quad (3.9.8)$$

After the application of the $[i\hbar\gamma^\nu \frac{\partial}{\partial x^\nu} + mc]$ operator on the last equation, one obtains:

$$\left[i\hbar\gamma^\nu \frac{\partial}{\partial x^\nu} + mc \right] \left[i\hbar\gamma^\mu \frac{\partial}{\partial x^\mu} - mc \right] \psi_i(x) = \left[\square + \left(\frac{mc}{\hbar} \right)^2 \right] \psi_i(x) = 0, \quad (3.9.9)$$

which shows that each of the four components of the Dirac spinor satisfy the Klein-Gordon equation, that is given at the very beginning of this thesis, in eq.(2.1.6). See, for instance, Schwartz [101, page 172]. Following the same procedure of the photon-propagator section, the time-ordered (Feynman) Klein-Gordon propagator, which we shall call $K_0^F(y, x)$, can be written as:

$$K_0^F(y, x) = \lim_{\epsilon \rightarrow 0} \int \frac{d^4 p}{(2\pi\hbar)^4} \frac{e^{-\frac{i}{\hbar} p \cdot (y-x)}}{p^2 - m^2 c^2 + i\epsilon}, \quad (3.9.10)$$

and it satisfies the following Green's function equation:

$$\left[\square_y + \left(\frac{mc}{\hbar} \right)^2 \right] K_0^F(y, x) = \delta(x - y). \quad (3.9.11)$$

This last equation can be written as:

$$\left[i\hbar\gamma^\mu \frac{\partial}{\partial y^\mu} - mc \right] \left[i\hbar\gamma^\nu \frac{\partial}{\partial y^\nu} + mc \right] K_0^F(y, x) = \delta(x - y). \quad (3.9.12)$$

If one compares this last equation with eq.(3.9.1), one can directly deduce that the Dirac propagator in the referred equation can be written as [33, eq.(7.73)]:

$$S_0^F(y, x) = \left[i\hbar\gamma^\nu \frac{\partial}{\partial y^\nu} + mc \right] K_0^F(y, x). \quad (3.9.13)$$

The reason we have done so, is that the Klein-Gordon propagator is relatively easier to evaluate since it is radial (a function of p^2) in Fourier-space, and the Dirac propagator can be obtained by means of the last expression. The Klein-Gordon propagator was discussed in [89, section 4.5], [53, pages 23-24] and many other books on relativistic quantum mechanics and quantum field theory. Finally, we should note that the closed form of our Dirac propagator was provided by Ohlsson [33, eq.(7.83)]:

$$S_0^F(y, x) = \left[\frac{1}{mc} \frac{(x^\mu - y^\mu) \gamma_\mu}{|x - y|^5} + \frac{1}{\hbar |x - y|^3} \right] J_1 \left(\frac{mc}{\hbar} |x - y| \right). \quad (3.9.14)$$

So far we have discussed the free-electron propagator associated with the Dirac equation, with the contour boundary condition set by the choice of Feynman, that corresponds to time-ordered products of field operators, as we shall soon see why. In the next section we will discuss the propagator of an electron in the presence of an arbitrary external electromagnetic potential $A_\mu(x)$.

3.9.3 Propagator for time-dependent external potential

The Dirac equation of an electron that interacts with a time-dependent electromagnetic potential is given by:

$$[\gamma^\mu (i\hbar\partial_\mu + eA_\mu(x)) - mc] \psi_i(x) = 0, \quad (3.9.15)$$

where i is a labeling of the Dirac solutions. The Feynman propagator associated with this Dirac equation satisfies the following Green's equation:

$$\left[\gamma^\mu \left(i\hbar \frac{\partial}{\partial y^\mu} + eA_\mu(y) \right) - mc \right] S_A(y, x) = \delta(y - x). \quad (3.9.16)$$

Notice that we have replace the 0 subscript by A , to indicate that this propagator includes the external four-potential (not the free-propagator case). As mentioned by Itzykson and Zuber [43, Pages 93-94], there exists no compact expression of the propagator S_A , and it is usually written as a perturbation expansion in powers of external four-potential $A_\mu(x)$. The reason behind this limitation originates from the fact that the local potential $A_\mu(y)$ becomes a non-local one in Fourier-space, as seen in eq.(H.6.3), and will thus complicate the evaluation of the solution. The last equation can be written as:

$$\left[i\hbar\gamma^\mu \frac{\partial}{\partial y^\mu} - mc \right] S_A(y, x) = \delta(y - x) - e\gamma^\mu A_\mu(y) S_A(y, x). \quad (3.9.17)$$

Notice that last term is the function that makes the equation non-homogeneous, and thus, $S_A(y, x)$ can be written as (see [8, eq.(2.35)] and [40, eq.(6.51)]):

$$S_A(y, x) = S_0(y, x) - e \int dz S_0(y, z) \gamma^\mu A_\mu(z) S_A(z, x), \quad (3.9.18)$$

which can be verified by simply plugging it in the defining equation.(3.9.16) and using the free propagator equation.(3.9.1). A derivation is found in the book of Itzykson and Zuber, but we note that his corresponding result [43, eq.(2-118)] misses the second free propagator ($S_0(y, z)$ of our last equation). If one iteratively replaces S_A at the very right of the last equation by its value (the two terms on the right side of the equal sign), one obtains a perturbative expansion of the propagator:

$$\begin{aligned} S_A(y, x) &= S_0(y, x) - e \int dz S_0(y, z) \gamma^\mu A_\mu(z) S_0(z, x) \\ &+ e^2 \int dz \int dw S_0(y, z) \gamma^\mu A_\mu(z) S_0(z, w) \gamma^\mu A_\mu(w) S_0(w, x) + \mathcal{O}(eA_\mu)^3, \end{aligned} \quad (3.9.19)$$

in powers of eA_μ , and written in terms of the free Dirac propagators only. This expansion is sometimes known as the Lippmann-Schwinger integral equation. We shall now restrict ourselves to the time-independent external potential case, and see how we can simplify our last expression.

3.9.4 Propagator for time-independent external potential

The Dirac propagator gets simplified once the external potential is time-independent, i.e., once we have $A_\mu(y) = A_\mu(\mathbf{y})$. In this case, the Dirac propagator of eq.(3.9.16) becomes:

$$\left[\gamma^\mu \left(i\hbar \frac{\partial}{\partial y^\mu} + eA_\mu(\mathbf{y}) \right) - mc \right] S_A(y, x) = \delta(x - y). \quad (3.9.20)$$

In this case, the perturbative expansion of the propagator $S_A(y, x)$ of eq.(3.9.19) can be simplified to a Green's function expansion, as we shall see in two sections.

3.9.5 Feynman electron propagator as a time-ordered vacuum expectation value

The Feynman propagator of a Dirac particle in the presence of a time-independent external potential can be written as a vacuum expectation value of the time-ordered product of two electronic field operators:

$$[S_A^F(x, y)]_{\alpha\beta} = \frac{1}{i\hbar} \langle 0_e | T [\Psi_\alpha(x) \bar{\Psi}_\beta(y)] | 0_e \rangle, \quad (3.9.21)$$

where the subscript $\alpha\beta$ on the square brackets indicate that this term is the matrix element of the 4×4 propagator matrix. The superscript F in eq.(3.9.21) indicates that the zeroth component of the momentum integral (energy integral) should be evaluated along the Feynman contour. We shall next see how the time-ordered product in the right side of the last equation leads to the Feynman choice of contour integration. The time-ordered product of the two electron field operators expands as:

$$\begin{aligned} T [\Psi_\alpha(x) \bar{\Psi}_\beta(y)] &= \sum_{E_i > 0} \sum_{E_j > 0} \psi_{i,\alpha}(x) \bar{\psi}_{j,\beta}(y) [\Theta(x^0 - y^0) a_i a_j^\dagger - \Theta(y^0 - x^0) a_j^\dagger a_i] \\ &+ \sum_{E_i > 0} \sum_{E_j < 0} \psi_{i,\alpha}(x) \bar{\psi}_{j,\beta}(x) [\Theta(x^0 - y^0) a_i b_j - \Theta(y^0 - x^0) b_j a_i] \\ &+ \sum_{E_i < 0} \sum_{E_j > 0} \psi_{i,\alpha}(x) \bar{\psi}_{j,\beta}(y) [\Theta(x^0 - y^0) b_i^\dagger a_j^\dagger - \Theta(y^0 - x^0) a_j^\dagger b_i^\dagger] \\ &+ \sum_{E_i < 0} \sum_{E_j < 0} \psi_{i,\alpha}(x) \bar{\psi}_{j,\beta}(y) [\Theta(x^0 - y^0) b_i^\dagger b_j - \Theta(y^0 - x^0) b_j b_i^\dagger], \end{aligned} \quad (3.9.22)$$

where we have use the electron field operator expression of eq.(3.5.9). The vacuum expectation value of this time-ordered product gives two non-vanishing contributions, from the first and last terms of this last equation, and one gets the following vacuum expectation expression:

$$\begin{aligned} &\langle 0_e | T [\Psi_\alpha(x) \bar{\Psi}_\beta(x)] | 0_e \rangle \\ &= \sum_i e^{-\frac{i}{\hbar} E_i(t_x - t_y)} [\Theta(+E_i) \Theta(x^0 - y^0) - \Theta(-E_i) \Theta(y^0 - x^0)] \psi_{i,\alpha}(\mathbf{x}) \bar{\psi}_{i,\beta}(\mathbf{y}). \end{aligned} \quad (3.9.23)$$

One can now use Jordan's lemma of appendix F.4 (see also [106, eq.(15.6)]) to write:

$$e^{+\frac{i}{\hbar} E_i(t_y - t_x)} [\Theta(+E_i) \Theta(t_x - t_y) - \Theta(-E_i) \Theta(t_y - t_x)] = \frac{1}{2\pi i} \int_{C_F} dz \frac{e^{-\frac{i}{\hbar} z(t_x - t_y)}}{E_i - z}, \quad (3.9.24)$$

and the vacuum expectation value becomes:

$$\langle 0_e | T [\Psi_\alpha(x) \bar{\Psi}_\beta(x)] | 0_e \rangle = \frac{1}{2\pi i} \int_{C_F} dz \sum_i \frac{\psi_{i,\alpha}(\mathbf{x}) \psi_{i,\theta}^\dagger(\mathbf{y})}{E_i - z} [\gamma^0]_{\theta,\beta} e^{-\frac{i}{\hbar} z(t_x - t_y)}. \quad (3.9.25)$$

The fraction present in the last integral is the Dirac Green's function $G_{\alpha\theta}(\mathbf{x}, \mathbf{y}; z)$, in its spectral form. Notice that the time ordered product has lead to an expression where the energy contour integral is evaluated along the Feynman path, and this is the reason why this propagator obtained from a time ordered product of electron field operators is called a Feynman propagator. We should also note that different products of field operators will lead to the retarded and advanced propagators, as presented in figure 3.8.1 for the photon propagator case. We now make the assumption that the electron propagator can be written as [52, eq.(17)]:

$$\begin{aligned} & [S_A^F(x, y)]_{\alpha\beta} \\ &= \frac{1}{i\hbar} \sum_i e^{-\frac{i}{\hbar} E_i(t_x - t_y)} [\Theta(+E_i) \Theta(x^0 - y^0) - \Theta(-E_i) \Theta(y^0 - x^0)] \psi_{i,\alpha}(\mathbf{x}) \bar{\psi}_{i,\beta}(\mathbf{y}). \\ &= \frac{1}{i\hbar} \frac{1}{2\pi i} \int_{C_F} dz \frac{\psi_{i,\alpha}(\mathbf{x}) \psi_{i,\theta}^\dagger(\mathbf{y})}{E_i - z} [\gamma^0]_{\theta,\beta} e^{-\frac{i}{\hbar} z(t_x - t_y)}. \end{aligned} \quad (3.9.26)$$

To verify that this is indeed a propagator, we plug it in the Dirac equation. When the four-gradient operator ∂_μ acts on the (time) Heaviside functions, it gives a Kronecker delta that gives non-vanishing contribution for the time-derivative ($\mu = 0$), and a Dirac delta in time:

$$\frac{\partial}{\partial x^\mu} \Theta(x^0 - y^0) = +\delta_\mu^0 \delta(x^0 - y^0) \quad (3.9.27)$$

$$\frac{\partial}{\partial x^\mu} \Theta(y^0 - x^0) = -\delta_\mu^0 \delta(x^0 - y^0). \quad (3.9.28)$$

We now plug these relations in our Dirac equation that acts on the propagator and get:

$$\begin{aligned} & [\gamma^\mu (i\hbar\partial_\mu + eA_\mu(\mathbf{x})) - mc\delta]_{\theta\alpha} [S_A^F(x, y)]_{\alpha\beta} \\ &= \sum_{E_i > 0} \left[+\gamma^\mu \delta_\mu^0 \delta(x^0 - y^0) + \frac{1}{i\hbar} \Theta(x^0 - y^0) [\gamma^\mu (i\hbar\partial_\mu + eA_\mu(\mathbf{x})) - mc] \right]_{\theta\alpha} \psi_{i,\alpha}(x) \bar{\psi}_{i,\beta}(y) \\ &- \sum_{E_i < 0} \left[-\gamma^\mu \delta_\mu^0 \delta(x^0 - y^0) + \frac{1}{i\hbar} \Theta(y^0 - x^0) [\gamma^\mu (i\hbar\partial_\mu + eA_\mu(\mathbf{x})) - mc] \right]_{\theta\alpha} \psi_{i,\alpha}(x) \bar{\psi}_{i,\beta}(y), \end{aligned} \quad (3.9.29)$$

and since $\psi_{i,\alpha}(x)$ satisfies the α -component Dirac equation:

$$[\gamma^\mu (i\hbar\partial_\mu + eA_\mu(\mathbf{x})) - mc]_{\beta\alpha} \psi_{i,\alpha}(x) = 0, \quad (3.9.30)$$

the second and forth terms of the previous equation vanish. In addition, the Dirac delta in time does not allow $x^0 - y^0 \neq 0$, meaning that it is permitted to set $x^0 = y^0$ in the remaining terms of the expression, we can thus write:

$$\delta(x^0 - y^0) \psi_{i,\alpha}(\mathbf{x}) \bar{\psi}_{i,\beta}(\mathbf{y}) e^{-\frac{i}{\hbar} E_i(t_x - t_y)} = \delta(x^0 - y^0) \psi_{i,\alpha}(\mathbf{x}) \bar{\psi}_{i,\beta}(\mathbf{y}), \quad (3.9.31)$$

the expression simplifies to:

$$\begin{aligned} & [\gamma^\mu (i\hbar\partial_\mu + eA_\mu(\mathbf{x})) - mc\delta]_{\theta\alpha} [S_A^F(x, y)]_{\alpha\beta} \\ &= [\gamma^0]_{\theta\alpha} \delta(x^0 - y^0) \sum_i \psi_{i,\alpha}(\mathbf{x}) \psi_{i,\sigma}^\dagger(\mathbf{y}) [\gamma^0]_{\sigma\beta}. \end{aligned} \quad (3.9.32)$$

The final step is to notice that the sum over i reduces to a spatial Dirac delta function (completeness relation). The Hamiltonian is self-adjoint, and this means that its eigenvectors are orthogonal. We assume that they are normalized and get:

$$\int d^3\mathbf{x} \psi_i^\dagger(\mathbf{x}) \psi_j(\mathbf{x}) = \delta_{ij}. \quad (3.9.33)$$

We multiply the sum in question by $\psi_j^\dagger(\mathbf{x})$ from right, and integrate over the \mathbf{x} volume, so we can make use of the orthogonality relation, we therefore get:

$$\int d^3\mathbf{x} \psi_j^\dagger(\mathbf{x}) \sum_i \psi_i(\mathbf{x}) \psi_i^\dagger(\mathbf{y}) = \sum_i \delta_{ij} \psi_i^\dagger(\mathbf{y}) = \psi_j^\dagger(\mathbf{y}), \quad (3.9.34)$$

which shows that:

$$\sum_i \psi_i(\mathbf{x}) \psi_i^\dagger(\mathbf{y}) = \mathbb{1}_4 \delta(\mathbf{x} - \mathbf{y}), \quad (3.9.35)$$

and using $[\gamma^0]_{\theta\alpha} [\mathbb{1}_4]_{\alpha\sigma} [\gamma^0]_{\sigma\beta} = [\mathbb{1}_4]_{\theta\beta}$ as seen in the anticommutation relation of the gamma matrices, we finally get our wanted result:

$$\left[\gamma^\mu \left(i\hbar \frac{\partial}{\partial x^\mu} + eA_\mu(\mathbf{x}) \right) - mc\mathbb{1}_4 \right]_{\theta\alpha} [S_A^F(x, y)]_{\alpha\beta} = [\mathbb{1}_4]_{\theta\beta} \delta(x - y). \quad (3.9.36)$$

In addition, we should note that the retarded and advanced propagators also do satisfy the same (last) propagator/Green's function equation, and that they only differ by the contour integration or the different poles shiftings (boundary conditions).

3.9.6 Electron propagator and Green's function

The Feynman propagator which is written as a vacuum expectation value of the time-ordered product of two electron (Dirac) field operator given in eqs.(3.9.21,3.9.26) and can be written as [7, eq.(32)]:

$$[S_A^F(x, y)]_{\alpha\beta} = \frac{1}{i\hbar} \frac{1}{2\pi i} \int_{C_F} dz \sum_i \frac{\psi_{i,\alpha}(\mathbf{x}) \psi_{i,\beta}^\dagger(\mathbf{y})}{E_i - z} \gamma^0 e^{-\frac{i}{\hbar} z(t_x - t_y)}, \quad (3.9.37)$$

Eq.(3.9.37) contains the α, β matrix element of the 4×4 Dirac Green's function:

$$G_A(\mathbf{x}, \mathbf{y}; z) = \sum_i \frac{\psi_i(\mathbf{x}) \psi_i^\dagger(\mathbf{y})}{E_i - z}. \quad (3.9.38)$$

The reader must note that the sum runs over the outer products of the four-component Dirac spinors, and thus, this Green's function is a 4×4 matrix. As for the electron propagator formulas, coming from the electron field operator, these summations are very formal, and for unbound solutions these summations should be understood as integrals instead (continua of energy values). Using the fact that $\psi_i(\mathbf{x})$ satisfies the Dirac equation of time-independent potentials, and the closure relation eq.(3.9.35) associated with the time-independent wavefunction, this formula clearly satisfies the Green's function equation:

$$[c\boldsymbol{\alpha} \cdot (-i\hbar \nabla_{\mathbf{x}} + e\mathbf{A}(\mathbf{x})) - e\varphi(\mathbf{x}) + \beta mc^2 - z] G_A(\mathbf{x}, \mathbf{y}; z) = \mathbb{1}_4 \delta(\mathbf{x} - \mathbf{y}). \quad (3.9.39)$$

As for the propagator in the presence of an external potential: the S_A case, the Green's function can now be expanded in powers of the time-independent external potential. This can be done by plugging the electron propagator formula in which the Green's function appears (eq.(3.9.37)) in the propagator expansion expression of eq.(3.9.19). After integrating over all time-components, one obtains:

$$G_A(\mathbf{x}, \mathbf{y}; z) = G_0(\mathbf{x}, \mathbf{y}; z) + ec \int d\mathbf{w} G_0(\mathbf{x}, \mathbf{w}; z) \alpha^\mu A_\mu(\mathbf{w}) G_0(\mathbf{w}, \mathbf{y}; z) \\ + (ec)^2 \int d\mathbf{w} \int d\mathbf{v} G_0(\mathbf{x}, \mathbf{w}; z) \alpha^\mu A_\mu(\mathbf{w}) G_0(\mathbf{w}, \mathbf{v}; z) \alpha^\nu A_\nu(\mathbf{v}) G_0(\mathbf{v}, \mathbf{y}; z) + \mathcal{O}(eA_\mu)^3. \quad (3.9.40)$$

Another way to obtain this relation would be to play with the Dirac operators (the two ways are related). The two (bound and free) Green's functions we are planning to relate satisfy the following equations:

$$[c\boldsymbol{\alpha} \cdot (-i\hbar\nabla_x + e\mathbf{A}(\mathbf{x})) - e\varphi(\mathbf{x}) + \beta mc^2 - z] G_A(\mathbf{x}, \mathbf{y}; z) = \mathbb{1}_4 \delta(\mathbf{x} - \mathbf{y}) \quad (3.9.41)$$

$$[-i\hbar c\boldsymbol{\alpha} \cdot \nabla_x + \beta mc^2 - z] G_0(\mathbf{x}, \mathbf{y}; z) = \mathbb{1}_4 \delta(\mathbf{x} - \mathbf{y}), \quad (3.9.42)$$

respectively. Following the notation of Economou [107, Chapter 1] these equations are written in operator notation as:

$$[H - z] G_0(z) = \mathbb{1}_4 \quad (3.9.43)$$

$$[H - ce\alpha^\mu A_\mu - z] G_A(z) = \mathbb{1}_4, \quad (3.9.44)$$

where $G_{0,A}(z)$ are kernels, corresponding to the Green's functions $G_{0,A}(\mathbf{x}, \mathbf{y}; z)$ (see, for instance, [7, Section 5.2]). In the last two equations, $H = c\boldsymbol{\alpha} \cdot \hat{\mathbf{p}} + \beta mc^2$ is the free Dirac Hamiltonian. Both notations, real-space and operator are related by the following rules associated with the Dirac bracket notation (continuous position variable algebra) [107, eqs.(1.6-9)]:

$$\int d\mathbf{x} |\mathbf{x}\rangle \langle \mathbf{x}| = 1 \quad (3.9.45)$$

$$\langle \mathbf{x} | \mathbf{y} \rangle = \delta(\mathbf{x} - \mathbf{y}) \quad (3.9.46)$$

$$\langle \mathbf{x} | G_{0,A}(z) | \mathbf{y} \rangle = G_{0,A}(\mathbf{x}, \mathbf{y}; z) \quad (3.9.47)$$

$$\langle \mathbf{x} | H | \mathbf{y} \rangle = \delta(\mathbf{x} - \mathbf{y}) H(\mathbf{x}). \quad (3.9.48)$$

Using the well known operator identity:

$$\frac{1}{A - B} = \frac{1}{A} + \frac{1}{A} B \frac{1}{A} + \frac{1}{A} B \frac{1}{A} B \frac{1}{A} + \dots, \quad (3.9.49)$$

which can be verified by simply multiplying the last equation by $A - B$ (from any side), we can write $G_A(z)$ which is given in eq.(3.9.44), as [108, eq.(11)]:

$$G_A(z) = \frac{1}{H - z - ce\alpha^\mu A_\mu} \\ = \frac{1}{H - z} + \frac{1}{H - z} ce\alpha^\mu A_\mu \frac{1}{H - z} + \frac{1}{H - z} ce\alpha^\mu A_\mu \frac{1}{H - z} ce\alpha^\nu A_\nu \frac{1}{H - z} + \dots \\ = G_0(z) + (ce) G_0(z) \alpha^\mu A_\mu G_0(z) + (ce)^2 G_0(z) \alpha^\mu A_\mu G_0(z) \alpha^\nu A_\nu G_0(z) + \dots \quad (3.9.50)$$

One can then use rules just presented, by sandwiching the last equation between the bra $\langle \mathbf{x} |$ and the ket $|\mathbf{y}\rangle$, thus using eq.(3.9.47), and inserting the closure relation of eq.(3.9.45) in between every two operators, one directly obtains the wanted integral equation:

$$G_A(\mathbf{x}, \mathbf{y}; z) = G_0(\mathbf{x}, \mathbf{y}; z) + ce \int d\mathbf{w} G_0(\mathbf{x}, \mathbf{w}; z) \alpha^\mu A_\mu(\mathbf{w}) G_0(\mathbf{w}, \mathbf{y}; z) \\ + (ec)^2 \int d\mathbf{w} \int d\mathbf{v} G_0(\mathbf{x}, \mathbf{w}; z) \gamma^\mu A_\mu(\mathbf{w}) G_0(\mathbf{w}, \mathbf{v}; z) \gamma^\nu A_\nu(\mathbf{v}) G_0(\mathbf{v}, \mathbf{y}; z) + \mathcal{O}(eA_\mu)^3. \quad (3.9.51)$$

This expansion of the Green's function has probably originated from Feynman's work [52, eqs. 11-16]. In the case where the external four-potential contains only a scalar potential, $A_\mu(\mathbf{x}) = (\phi(\mathbf{x})/c, 0)$, the last expression reduces to:

$$G_\phi(\mathbf{x}, \mathbf{y}; z) = G_0(\mathbf{x}, \mathbf{y}; z) + e \int d\mathbf{w} G_0(\mathbf{x}, \mathbf{w}; z) \phi(\mathbf{w}) G_0(\mathbf{w}, \mathbf{y}; z) \\ + e^2 \int d\mathbf{w} \int d\mathbf{v} G_0(\mathbf{x}, \mathbf{w}; z) \phi(\mathbf{w}) G_0(\mathbf{w}, \mathbf{v}; z) \phi(\mathbf{v}) G_0(\mathbf{v}, \mathbf{y}; z) + \mathcal{O}(e\phi)^3. \quad (3.9.52)$$

Next goals

After our discussions on Wick's theorem, the electron and photon propagators, and their vacuum expectation value forms (contractions), we shall turn back to our problem:

1. Expand the \mathcal{S} -matrix in powers of the QED interaction Hamiltonian density.
2. Evaluate the time-ordered products involved in the $\hat{\mathcal{S}}$ -matrix expansion using Wick's theorem.
3. Calculate the energy-shift associated with each of the normal ordered terms which arise from Wick's theorem, and present its associated Feynman diagram.

3.10 \mathcal{S} -matrix expansion and Feynman diagrams

3.10.1 Wick's theorem for the \mathcal{S} -matrix in QED

The expansion of the \mathcal{S} -matrix in QED, leads to time-ordered products of the form of:

$$T \left[\hat{\mathcal{H}}_I(x_1, \epsilon) \dots \hat{\mathcal{H}}_I(x_n, \epsilon) \right], \quad (3.10.1)$$

where $\hat{\mathcal{H}}_I$ is given in eq.(3.5.21) by:

$$\hat{\mathcal{H}}_I(x; \epsilon) = -ec\bar{\Psi}(x) \gamma^\mu \Psi(x) A_\mu(x) e^{-\frac{\epsilon}{\hbar}|t|}. \quad (3.10.2)$$

We now take away the constants and the exponential term, and focus on:

$$T \left[\bar{\Psi}(x_1) \gamma^{\mu_1} A_{\mu_1}(x_1) \Psi(x_1) \dots \bar{\Psi}(x_n) \gamma^{\mu_n} A_{\mu_n}(x_n) \Psi(x_n) \right]. \quad (3.10.3)$$

Wick's theorem, discussed in section 3.7, tells us that this time-ordered product can be written as normal ordered products of: zero- one- two-contractions, and so on. The contraction of two operators was given in eq.(3.7.2):

$$\overline{A(x_1) B(x_2)} \equiv \langle 0 | T[A(x_1) B(x_2)] | 0 \rangle. \quad (3.10.4)$$

In evaluating the time-ordered product of eq.(3.10.3) two kinds of non-vanishing contractions will be encountered:

1. The contraction of two electron field operators:

$$\overline{\Psi_\alpha(x) \Psi_\beta(y)} = \langle 0_e | T[\Psi_\alpha(x) \bar{\Psi}_\beta(y)] | 0_e \rangle. \quad (3.10.5)$$

In section 3.9.5 we showed that this vacuum expectation value is related to the electron propagator by eq.(3.9.21), which means that the contraction of two electronic operators is now:

$$\overline{\Psi_\alpha(x) \Psi_\beta(y)} = i\hbar [S^F(x, y)]_{\alpha\beta}. \quad (3.10.6)$$

2. Similarly, the contraction of two photon field operators is given by:

$$\overline{A_\alpha(x) A_\beta(y)} \equiv \langle 0_p | T[A_\alpha(x) A_\beta(y)] | 0_p \rangle. \quad (3.10.7)$$

In section 3.8.3, we showed that this expectation value can be written in terms of the photon propagator using eq.(3.8.49). This relation leads to the following definition of the contraction:

$$\overline{A_\alpha(x) A_\beta(y)} = i\hbar D_{\alpha\beta}^F(x, y). \quad (3.10.8)$$

In addition, one can easily show that the following relations do hold:

$$\overline{\bar{\Psi}_\alpha(x) \Psi_\beta(y)} = -\overline{\Psi_\beta(y) \bar{\Psi}_\alpha(x)} \quad (3.10.9)$$

$$\overline{\Psi_\alpha(x) \Psi_\beta(y)} = 0_{\alpha,\beta} \quad (3.10.10)$$

$$\overline{\bar{\Psi}_\alpha(x) \bar{\Psi}_\beta(y)} = 0_{\alpha,\beta}. \quad (3.10.11)$$

As a conclusion, when contracting a normal ordered product through Wick's theorem, one should only evaluate the non-vanishing contractions of the form of: $\overline{\bar{\Psi}_\alpha(x) \Psi_\beta(y)}$ and $\overline{\Psi_\alpha(x) \bar{\Psi}_\beta(y)}$. In the appendix G, we derive the first few time-ordered products of electronic and photon field operators. We are now going to use the results we have got, in our expansion of the \mathcal{S} -matrix.

3.10.2 \mathcal{S} -matrix expansion for the no-photon BSQED

We shall now focus on the \mathcal{S} -matrix expression of eq.(3.4.16):

$$\begin{aligned} \hat{\mathcal{S}}(\epsilon, \lambda) = 1 + \frac{1}{1!} \frac{\lambda}{i\hbar c} \int d^4x_1 T[\hat{\mathcal{H}}_I(x_1, \epsilon)] \\ + \frac{1}{2!} \left(\frac{\lambda}{i\hbar c} \right)^2 \int d^4x_1 \int d^4x_2 T[\hat{\mathcal{H}}_I(x_1, \epsilon) \hat{\mathcal{H}}_I(x_2, \epsilon)] + \mathcal{O}(\lambda^3), \end{aligned} \quad (3.10.12)$$

and examine the following expectation value:

$$\langle \Phi_0^\alpha | \hat{\mathcal{S}}(\epsilon, \lambda) | \Phi_0^\alpha \rangle, \quad (3.10.13)$$

which enters in Sucher's energy expression.(3.4.19). In addition, we should be clear by stressing out that we are going to consider the no-photon case, and write our perturbed (corrected) state as:

$$|\Phi_0^\alpha\rangle = |N_e^\alpha, 0_p^\alpha\rangle. \quad (3.10.14)$$

This last notation indicates that we have N positive-energy real-electrons (first slot) and zero real-photons (second slot) in this state (as done by Indelicato in [16, page 151]). This state does not contain any occupied negative-energy solutions: the Dirac sea is empty. The reason why we say “real”, is that we are not considering physical (real) photons, we shall only deal with (virtual) photons that are generated by the photonic operator (in the \mathcal{S} -matrix expansion): emitted and absorbed by the creation and annihilation operators from the photonic vacuum state $|0_p^\alpha\rangle$. A discussion about the difference between real and virtual particles can be found in [109, section 5.2]. Our last assumption, means that all \mathcal{S} -matrices –popping up when expanding the main \mathcal{S} -matrix of eq.(3.10.12)– associated with an odd number of $\hat{\mathcal{H}}_I(x_1)$, will vanish under expectation value of eq.(3.10.13), because the \mathcal{S} -matrix is sandwiched between two photon vacuum states. To get a non-vanishing expectation value, all virtual photon creations need to be balanced by annihilations, and this is only possible when we have an even number of photonic operators, which after being contracted, will represent the propagation of a virtual photon between two spacetime points, as we shall soon see. By eliminating the odd terms of eq.(3.10.13) we get:

$$\begin{aligned} & \langle \Phi_0^\alpha | \hat{\mathcal{S}}(\epsilon, \lambda) | \Phi_0^\alpha \rangle \\ &= 1 + \frac{1}{2!} \left(\frac{\lambda}{i\hbar c} \right)^2 \int d^4x_1 \int d^4x_2 \langle \Phi_0^\alpha | T [\hat{\mathcal{H}}_I(x_1, \epsilon) \hat{\mathcal{H}}_I(x_2, \epsilon)] | \Phi_0^\alpha \rangle + \mathcal{O}(\lambda^4). \end{aligned} \quad (3.10.15)$$

The number 1 simply indicates that to the zeroth-order, no-interaction has occurred. We shall now analyze the second-order term:

$$\langle \Phi_0^\alpha | T [\hat{\mathcal{H}}_I(x_1, \epsilon) \hat{\mathcal{H}}_I(x_2, \epsilon)] | \Phi_0^\alpha \rangle. \quad (3.10.16)$$

Using Wick’s theorem, discussed in section 3.7 and the time-ordered products derived in the appendix chapter G we can write:

$$T [\hat{\mathcal{H}}_I(x_1, \epsilon) \hat{\mathcal{H}}_I(x_2, \epsilon)] = e^2 c^2 e^{-\frac{e}{\hbar}(|t_1|+|t_2|)} T [\bar{\Psi}(x_1) \gamma^{\mu_1} \Psi(x_1) \bar{\Psi}(x_2) \gamma^{\mu_2} \Psi(x_2)] T [A_{\mu_1}(x_1) A_{\mu_2}(x_2)] \quad , \quad (3.10.17)$$

where this step is justified by the fact that fermionic and photonic operators act on different spaces. We also note that we choose to label the gamma matrices indices with respect to the spacetime point of the associated current: μ_1 with x_1 , and so on. The above fermionic product is computed in the appendix eq.(G.1.11), and is found to be:

$$\begin{aligned} & T [\bar{\Psi}(x_1) \gamma^{\mu_1} \Psi(x_1) \bar{\Psi}(x_2) \gamma^{\mu_2} \Psi(x_2)] \\ &= : \bar{\Psi}(x_1) \gamma^{\mu_1} \Psi(x_1) \bar{\Psi}(x_2) \gamma^{\mu_2} \Psi(x_2) : \quad t_1 \\ &- i\hbar \text{Tr} [S^F(x_1, x_1) \gamma^{\mu_1}] : \bar{\Psi}(x_2) \gamma^{\mu_2} \Psi(x_2) : \quad t_2 \\ &- i\hbar \text{Tr} [S^F(x_2, x_2) \gamma^{\mu_2}] : \bar{\Psi}(x_1) \gamma^{\mu_1} \Psi(x_1) : \quad t_3 \\ &+ i\hbar : \bar{\Psi}(x_2) \gamma^{\mu_2} S^F(x_2, x_1) \gamma^{\mu_1} \Psi(x_1) : \quad t_4 \\ &+ i\hbar : \bar{\Psi}(x_1) \gamma^{\mu_1} S^F(x_1, x_2) \gamma^{\mu_2} \Psi(x_2) : \quad t_5 \\ &- \hbar^2 \text{Tr} [S^F(x_1, x_1) \gamma^{\mu_1}] \text{Tr} [S^F(x_2, x_2) \gamma^{\mu_2}] \quad t_6 \\ &+ \hbar^2 \text{Tr} [S^F(x_2, x_1) \gamma^{\mu_1} S^F(x_1, x_2) \gamma^{\mu_2}] \quad t_7 \end{aligned} \quad (3.10.18)$$

In addition, the photonic product is evaluated in the appendix eq.(G.2.3), where using Wick’s theorem, one obtains:

$$T [A_{\mu_1}(x_1) A_{\mu_2}(x_2)] = : A_{\mu_1}(x_1) A_{\mu_2}(x_2) : + i\hbar D_{\mu_1\mu_2}^F(x_1, x_2) \quad . \quad (3.10.19)$$

Recall that we are studying the no-(real)photon case, as seen in eq.(3.10.14). This means that the first term of the last equation (normal-ordered) will vanish under the photonic vacuum expectation value:

$$\langle 0_p^\alpha | : A_{\mu_1}(x_1) A_{\mu_2}(x_2) : | 0_p^\alpha \rangle = 0. \quad (3.10.20)$$

The second term contains no creation or annihilation operator, and will thus survive the vacuum expectation. This term represents the virtual photon propagation between x_2 and x_1 . Generally speaking, in the no-photon case, only fully contracted photon operator products can survive from the vacuum expectation value and contribute. This means that all the terms of eq.(3.10.18) will be multiplied by $i\hbar D_{\mu_1\mu_2}^F(x_1, x_2)$ in the vacuum expectation value of eq.(3.10.16). Terms t_2 and t_3 , as well as t_4 and t_5 , of eq.(3.10.18) lead to equal overall expressions each, and this can be seen by swapping the integration variables $x_1 \leftrightarrow x_2$ as well as the indices $\mu_1 \leftrightarrow \mu_2$, and using the following symmetry properties of the photon propagator:

$$D_F^{\mu\nu}(x-y) = D_F^{\nu\mu}(x-y) \quad (3.10.21)$$

$$D_F^{\mu\nu}(x-y) = D_F^{\mu\nu}(y-x), \quad (3.10.22)$$

where the first line comes from the fact the metric tensor is symmetric under indices swapping, while the second line can be obtained after performing a change of variables $q \rightarrow -q$ in the inverse Fourier transform integral of the momentum-space photon propagator given in eq.(3.8.24). These two relations allow us to reduce our time-ordered product to the following expressions:

$$\begin{aligned} & \frac{1}{e^2 c^2 e^{-\frac{\epsilon}{\hbar}(|t_1|+|t_2|)}} \langle \Phi_0^\alpha | T [\hat{\mathcal{H}}_I(x_1, \epsilon) \hat{\mathcal{H}}_I(x_2, \epsilon)] | \Phi_0^\alpha \rangle \\ &= i\hbar D_{\mu_1\mu_2}^F(x_1, x_2) \langle \Phi_0^\alpha | : \bar{\Psi}(x_1) \gamma^{\mu_1} \Psi(x_1) \bar{\Psi}(x_2) \gamma^{\mu_2} \Psi(x_2) : | \Phi_0^\alpha \rangle \quad \text{SP} \\ &+ 2\hbar^2 D_{\mu_1\mu_2}^F(x_1, x_2) \text{Tr} [S^F(x_1, x_1) \gamma^{\mu_1}] \langle \Phi_0^\alpha | : \bar{\Psi}(x_2) \gamma^{\mu_2} \Psi(x_2) : | \Phi_0^\alpha \rangle \quad \text{VP} \\ &- 2\hbar^2 D_{\mu_1\mu_2}^F(x_1, x_2) \langle \Phi_0^\alpha | : \bar{\Psi}(x_2) \gamma^{\mu_2} S^F(x_2, x_1) \gamma^{\mu_1} \Psi(x_1) : | \Phi_0^\alpha \rangle \quad \text{SE} \\ &- i\hbar^3 D_{\mu_1\mu_2}^F(x_1, x_2) \text{Tr} [S^F(x_1, x_1) \gamma^{\mu_1}] \text{Tr} [S^F(x_2, x_2) \gamma^{\mu_2}] \quad \text{V1} \\ &+ i\hbar^3 D_{\mu_1\mu_2}^F(x_1, x_2) \text{Tr} [S^F(x_2, x_1) \gamma^{\mu_1} S^F(x_1, x_2) \gamma^{\mu_2}] \quad \text{V2} \end{aligned} \quad (3.10.23)$$

The first three terms can be found in the work of Indelicato and Mohr [16, eqs.(181-183)] and correspond to the physical process, while the last two terms (fully contracted) correspond to vacuum process, and are not state dependent. These five contributions are presented in the following figs. 3.10.1a to 3.10.1e. We shall now give a few words on these diagrams:

1. Virtual photons (internal photon lines) are graphically represented by wiggly lines, that connect two vertices, at spacetime points x_1 and x_2 , in this case. Mathematically, these internal propagations represent a contraction of two photon field operators: $\overline{A_\mu(x_1)} A_\nu(x_2) = i\hbar D_{\mu\nu}^F(x_1, x_2)$.
2. External straight double electron lines represent bound-electrons, whose wavefunctions are solutions of the Dirac equation in the presence of an external potential.
3. Internal double electron lines, as in the bubbles of figs. 3.10.1b, 3.10.1d and 3.10.1e or the straight line of the self-energy diagram in fig. 3.10.1c, represent the propagation of virtual electrons (in the presence of external electromagnetic potential) between the spacetime points. Mathematically, this corresponds to a contraction of two fermion field operators: $\overline{\Psi_\mu(x_1)} \bar{\Psi}_\nu(x_2) = i\hbar [S^F(x_1, x_2)]_{\mu\nu}$.

Description of each of the presented diagrams:

1. The single-photon exchange (SP) of fig. 3.10.1a describes the retarded electron-electron interaction to its lowest-order, by the exchange of a virtual photon.
2. The vacuum polarization (VP) of fig. 3.10.1b describes the interaction between a bound electron and the vacuum polarization bubble at x_2 . This vacuum polarization bubble will be represented by a vacuum polarization current density which interacts with the electron through an instantaneous Coulombic interaction. In addition, the vacuum polarization density will be related to the trace in this VP term, of eq.(3.10.23).
3. The self-energy (SE) of fig. 3.10.1c represents the process of emission and absorption of a virtual photon by the bound electron. This diagram is very essential in QED. In 1947 Hans Bethe [110] removed the divergence of the energy-shift associated with this process in a fully non-relativistic framework and got an estimate for the Lamb-shift which agreed up to 96% with the experimental value. His contribution gave hope in the early troublesome (divergent) QED. A short interview with Bethe (on this subject) is found in [111].
4. Finally, the vacuum diagrams of figs. 3.10.1d and 3.10.1e. Notice that contrary to the first three diagrams, these two diagrams have no external legs (no bound-electron lines here), and this is mathematically identified by the absence of normal ordered products in their associated expressions in eq.(3.10.23), since they are full contracted. These two diagrams are sometimes called bubble, or disconnected diagrams, and can be understood to represent the interaction of the vacuum with itself.

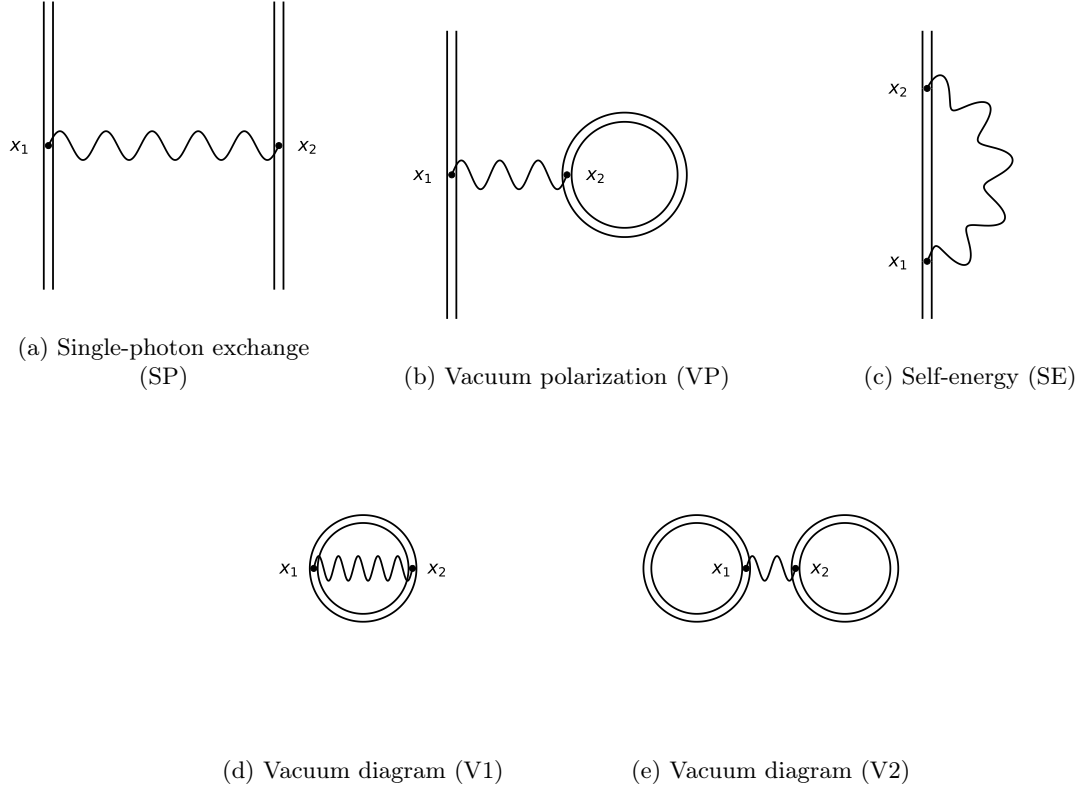


Figure 3.10.1: The lowest-order QED corrections: of order e^2 (two vertices).

We shall next discuss the distinction between the physical diagrams (first three), and the vacuum ones (last two), and see how the latter do not affect the level-shift of our studied bound-electron system. This distinction is defined by the following two points:

1. The physical diagrams: the ones having external electron lines, as the ones presented in figs. 3.10.1a to 3.10.1c: corresponding to terms which are not fully contracted.
2. The vacuum diagrams: diagrams having no external electron lines as the ones of figs. 3.10.1d and 3.10.1e: the full contracted terms.

In the next section, we shall see how the contributions from the latter terms can be discarded.

3.10.3 Physical and vacuum diagrams

We start by stating that the expectation value of the \mathcal{S} -matrix can be written as:

$$\langle \Phi_0^\alpha | \hat{\mathcal{S}}(\epsilon, \lambda) | \Phi_0^\alpha \rangle = \langle \Phi_0^\alpha | \hat{\mathcal{S}}(\epsilon, \lambda) | \Phi_0^\alpha \rangle_{\text{ph}} \langle 0_e, 0_p | \hat{\mathcal{S}}(\epsilon, \lambda) | 0_e, 0_p \rangle, \quad (3.10.24)$$

where $\langle \Phi_0^\alpha | \hat{\mathcal{S}}(\epsilon, \lambda) | \Phi_0^\alpha \rangle_{\text{ph}}$ contains all physical (ph) contributions of $\langle \Phi_0^\alpha | \hat{\mathcal{S}}(\epsilon, \lambda) | \Phi_0^\alpha \rangle$, i.e. it excludes the vacuum contributions of figs. 3.10.1d and 3.10.1e (with the higher-order ones). The

second term is $\langle 0_e, 0_p | \hat{\mathcal{S}}(\epsilon, \lambda) | 0_e, 0_p \rangle$, which is simply the vacuum expectation value of the \mathcal{S} -matrix (0 photons and 0 electrons). At first order the \mathcal{S} -matrix reduces to the unit operator, and our vacuum expectation value becomes:

$$\langle 0_e, 0_p | \hat{\mathcal{S}}(\epsilon, \lambda) | 0_e, 0_p \rangle = 1 + \mathcal{O}(e^2). \quad (3.10.25)$$

We write $\mathcal{O}(e^2)$, since the first order contribution will vanish under the vacuum expectation value, because it only contains one photon operator (as discussed previously). This is true for any odd number of photon field operators, or $\hat{\mathcal{H}}_I(x)$. We now turn to the second-order contribution, which is written as:

$$\frac{1}{2!} \left(\frac{\lambda}{i\hbar c} \right)^2 \int d^4x_1 \int d^4x_2 \langle 0_e, 0_p | T [\hat{\mathcal{H}}_I(x_1, \epsilon) \hat{\mathcal{H}}_I(x_2, \epsilon)] | 0_e, 0_p \rangle. \quad (3.10.26)$$

The reader should notice that any non-fully-contracted terms popping out of the Wick expansion will die under the vacuum expectation value, this means that only fully contracted terms will survive. Using the results of eq.(G.1.11) and eq.(G.2.3), we find:

$$\begin{aligned} & \langle 0_e, 0_p | T [\hat{\mathcal{H}}_I(x_1) \hat{\mathcal{H}}_I(x_2)] | 0_e, 0_p \rangle \\ &= i\hbar^3 e^2 c^2 e^{-\frac{\epsilon}{\hbar}(|t_1|+|t_2|)} \text{Tr} [S^F(x_2, x_1) \gamma^{\mu_1} S^F(x_1, x_2) \gamma^{\mu_2}] D_{\mu_1 \mu_2}^F(x_1, x_2) \\ & - i\hbar^3 e^2 c^2 e^{-\frac{\epsilon}{\hbar}(|t_1|+|t_2|)} \text{Tr} [S^F(x_1, x_1) \gamma^{\mu_1}] \text{Tr} [S^F(x_2, x_2) \gamma^{\mu_2}] D_{\mu_1 \mu_2}^F(x_1, x_2). \end{aligned} \quad (3.10.27)$$

These terms are obviously the V1 and V2 we had in eq.(3.10.23). One should notice that the vacuum expectation value of the \mathcal{S} -matrix collects all fully-contracted terms, while the $\langle \Phi_0^\alpha | \hat{\mathcal{S}}(\epsilon, \lambda) | \Phi_0^\alpha \rangle_{\text{ph}}$ expectation value collects the all the remaining partially-contracted terms. This analysis justifies our separation in eq.(3.10.24) between physical and vacuum contributions/diagrams, and which we graphically represent in fig. 3.10.2. The reader should finally note (for clarification purposes) that the diagrammatic product (SP \times V2), for instance, will be of e^4 -order, and will appear in the expansion of the forth-order $\mathcal{S}^{(4)}$ -matrix, which contains the following time-ordered product:

$$T [\hat{\mathcal{H}}_I(x_1, \epsilon) \hat{\mathcal{H}}_I(x_2, \epsilon) \hat{\mathcal{H}}_I(x_3, \epsilon) \hat{\mathcal{H}}_I(x_4, \epsilon)]. \quad (3.10.28)$$

See the fig. 3.10.2. Mathematically, this product of diagrams will be written as a product of two independent expressions, and it will be graphically represented by a diagram containing two disconnected sub-diagrams (SP and V2). This separation of contributions is the reason why the vacuum diagrams are called disconnected diagrams, while the physical-ones are called connected.

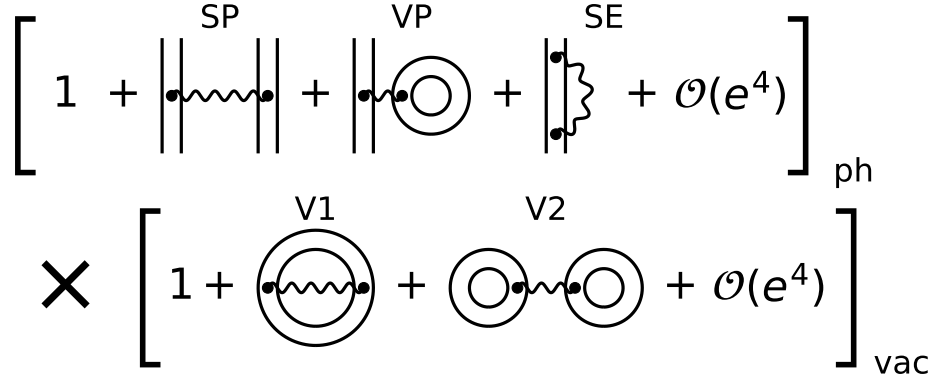


Figure 3.10.2: Distinction between physical and vacuum diagrams

This analysis is inspired by discussions made by Berestetskii *et al.* [105, section §103] and Fetter and Walecka [87, section 9] on the expansion of the exact (dressed) photon and electron propagator in terms of the free (bare) propagators. The form we are using in eq.(3.10.24) can be found, in the context of BSQED in the works of Mohr *et al.* [7, eq.(25)] and [104, eq.(19)], where the authors distinguish between connected and disconnected diagrams (in our language: physical and vacuum diagrams), as we have done. We shall now follow their analysis, by plugging eq.(3.10.24) in Sucher's energy formula of eq.(3.4.19), leading to [7, eq.(21)]:

$$\Delta E^\alpha = \lim_{\substack{\epsilon \rightarrow 0 \\ \lambda \rightarrow 1}} \frac{i\epsilon\lambda}{2} \left[\frac{\partial}{\partial \lambda} \ln \langle \Phi_0^\alpha | \hat{\mathcal{S}}(\epsilon, \lambda) | \Phi_0^\alpha \rangle_{\text{ph}} + \frac{\partial}{\partial \lambda} \ln \langle 0_e, 0_p | \hat{\mathcal{S}}(\epsilon, \lambda) | 0_e, 0_p \rangle \right]. \quad (3.10.29)$$

Notice that the last term contributes with the same energy-shift to all energy solutions E^α , since it does not depend on the state $|\Phi_0^\alpha\rangle$ in question. This means that the last term does not affect transition energies (what the experiment measures), as pointed out by Mohr [112, page 117], and thus it is discarded. The derivative of the logarithmic function in the last equation is given by:

$$\lambda \frac{\partial}{\partial \lambda} \ln \langle \Phi_0^\alpha | \hat{\mathcal{S}}(\epsilon, \lambda) | \Phi_0^\alpha \rangle_{\text{ph}} = \frac{\langle \Phi_0^\alpha | \lambda \frac{\partial}{\partial \lambda} \hat{\mathcal{S}}(\epsilon, \lambda) | \Phi_0^\alpha \rangle_{\text{ph}}}{\langle \Phi_0^\alpha | \hat{\mathcal{S}}(\epsilon, \lambda) | \Phi_0^\alpha \rangle_{\text{ph}}}, \quad (3.10.30)$$

where the derivative of the scattering matrix with respect to λ reads:

$$\lambda \frac{\partial}{\partial \lambda} \hat{\mathcal{S}}(\epsilon, \lambda) = \lambda T \left[\frac{1}{i\hbar c} \int d^4x e^{-\frac{\epsilon}{\hbar}|t|} \hat{\mathcal{H}}_I(x) e^{\frac{\lambda}{i\hbar c} \int d^4x_1 e^{-\frac{\epsilon}{\hbar}|t_1|} \hat{\mathcal{H}}_I(x_1)} \right], \quad (3.10.31)$$

which directly leads to the following expansion of the \mathcal{S} -matrix in powers of λ for both its numerator and denominator:

$$\lambda \frac{\partial}{\partial \lambda} \ln \langle \Phi_0^\alpha | \hat{\mathcal{S}}(\epsilon, \lambda) | \Phi_0^\alpha \rangle_{\text{ph}} = \frac{\langle \hat{\mathcal{S}}^{(1)} \rangle_{\text{ph}} + 2 \langle \hat{\mathcal{S}}^{(2)} \rangle_{\text{ph}} + 3 \langle \hat{\mathcal{S}}^{(3)} \rangle_{\text{ph}} + \dots}{1 + \langle \hat{\mathcal{S}}^{(1)} \rangle_{\text{ph}} + \langle \hat{\mathcal{S}}^{(2)} \rangle_{\text{ph}} + \langle \hat{\mathcal{S}}^{(3)} \rangle_{\text{ph}} + \dots}. \quad (3.10.32)$$

In the last expression we used $\langle \hat{\mathcal{S}}^{(i)} \rangle_{\text{ph}} = \langle \Phi_0^\alpha | \hat{\mathcal{S}}^{(i)}(\epsilon, \lambda) | \Phi_0^\alpha \rangle_{\text{ph}}$. Recall that $\hat{\mathcal{S}}^{(i)}(\epsilon, \lambda)$ is given in eq.(3.4.16). This fraction expansion can be expanded in powers of interaction Hamiltonian density,

and can be therefore written as:

$$\begin{aligned}
& \lambda \frac{\partial}{\partial \lambda} \ln \left\langle \Phi_0^\alpha \left| \hat{\mathcal{S}}(\epsilon, \lambda) \right| \Phi_0^\alpha \right\rangle_{\text{ph}} \\
&= \left\langle \hat{\mathcal{S}}^{(1)} \right\rangle_{\text{ph}} && \text{1st} \\
&+ 2 \left\langle \hat{\mathcal{S}}^{(2)} \right\rangle_{\text{ph}} - \left\langle \hat{\mathcal{S}}^{(1)} \right\rangle_{\text{ph}}^2 && \text{2nd} \\
&+ 3 \left\langle \hat{\mathcal{S}}^{(3)} \right\rangle_{\text{ph}} - 3 \left\langle \hat{\mathcal{S}}^{(1)} \right\rangle_{\text{ph}} \left\langle \hat{\mathcal{S}}^{(2)} \right\rangle_{\text{ph}} + \left\langle \hat{\mathcal{S}}^{(1)} \right\rangle_{\text{ph}}^3 && \text{3rd} \\
&+ 4 \left\langle \hat{\mathcal{S}}^{(4)} \right\rangle_{\text{ph}} - 4 \left\langle \hat{\mathcal{S}}^{(1)} \right\rangle_{\text{ph}} \left\langle \hat{\mathcal{S}}^{(3)} \right\rangle_{\text{ph}} - 2 \left\langle \hat{\mathcal{S}}^{(2)} \right\rangle_{\text{ph}}^2 + 4 \left\langle \hat{\mathcal{S}}^{(1)} \right\rangle_{\text{ph}}^2 \left\langle \hat{\mathcal{S}}^{(2)} \right\rangle_{\text{ph}} - \left\langle \hat{\mathcal{S}}^{(1)} \right\rangle_{\text{ph}}^4 && \text{4th} \\
&+ 5 \left\langle \hat{\mathcal{S}}^{(5)} \right\rangle_{\text{ph}} - 5 \left\langle \hat{\mathcal{S}}^{(1)} \right\rangle_{\text{ph}} \left\langle \hat{\mathcal{S}}^{(4)} \right\rangle_{\text{ph}} - 5 \left\langle \hat{\mathcal{S}}^{(2)} \right\rangle_{\text{ph}} \left\langle \hat{\mathcal{S}}^{(3)} \right\rangle_{\text{ph}} + 5 \left\langle \hat{\mathcal{S}}^{(1)} \right\rangle_{\text{ph}}^2 \left\langle \hat{\mathcal{S}}^{(3)} \right\rangle_{\text{ph}} && \text{5th} \\
&+ 5 \left\langle \hat{\mathcal{S}}^{(1)} \right\rangle_{\text{ph}} \left\langle \hat{\mathcal{S}}^{(2)} \right\rangle_{\text{ph}}^2 - 5 \left\langle \hat{\mathcal{S}}^{(1)} \right\rangle_{\text{ph}}^3 \left\langle \hat{\mathcal{S}}^{(2)} \right\rangle_{\text{ph}} + \left\langle \hat{\mathcal{S}}^{(5)} \right\rangle_{\text{ph}} && \text{5th} \\
&+ 6 \left\langle \hat{\mathcal{S}}^{(6)} \right\rangle_{\text{ph}} - 6 \left\langle \hat{\mathcal{S}}^{(1)} \right\rangle_{\text{ph}} \left\langle \hat{\mathcal{S}}^{(5)} \right\rangle_{\text{ph}} - 6 \left\langle \hat{\mathcal{S}}^{(2)} \right\rangle_{\text{ph}} \left\langle \hat{\mathcal{S}}^{(4)} \right\rangle_{\text{ph}} + 6 \left\langle \hat{\mathcal{S}}^{(1)} \right\rangle_{\text{ph}}^2 \left\langle \hat{\mathcal{S}}^{(4)} \right\rangle_{\text{ph}} - 3 \left\langle \hat{\mathcal{S}}^{(3)} \right\rangle_{\text{ph}}^2 && \text{6th} \\
&+ 12 \left\langle \hat{\mathcal{S}}^{(1)} \right\rangle_{\text{ph}} \left\langle \hat{\mathcal{S}}^{(2)} \right\rangle_{\text{ph}} \left\langle \hat{\mathcal{S}}^{(3)} \right\rangle_{\text{ph}} - 6 \left\langle \hat{\mathcal{S}}^{(1)} \right\rangle_{\text{ph}}^3 \left\langle \hat{\mathcal{S}}^{(3)} \right\rangle_{\text{ph}} + 2 \left\langle \hat{\mathcal{S}}^{(2)} \right\rangle_{\text{ph}}^3 - 9 \left\langle \hat{\mathcal{S}}^{(1)} \right\rangle_{\text{ph}}^2 \left\langle \hat{\mathcal{S}}^{(2)} \right\rangle_{\text{ph}}^2 && \text{6th} \\
&+ 6 \left\langle \hat{\mathcal{S}}^{(1)} \right\rangle_{\text{ph}}^4 \left\langle \hat{\mathcal{S}}^{(2)} \right\rangle_{\text{ph}} - \left\langle \hat{\mathcal{S}}^{(1)} \right\rangle_{\text{ph}}^6 && \text{6th} \\
&+ \dots
\end{aligned} \tag{3.10.33}$$

In the last equation, the i -th labelings on the right side indicates that the corresponding lines are of i -order in the interaction Hamiltonian density $\mathcal{H}_I(x_1)$. Expressions up to the fourth order are given in literature, see, for instance, [7, eq.(42)].

3.10.4 The BSQED corrections of the second-order e^2

Our focus is on the physical contributions of the second-order e^2 processes. Using the result of the last equation.(3.10.33) we can use Sucher's energy expression of eq.(3.10.29) to write our second-order energy-shift as:

$$\Delta E^\alpha = \lim_{\epsilon \rightarrow 0} i\epsilon \left\langle \Phi_0^\alpha \left| \hat{\mathcal{S}}^{(2)}(\epsilon, 1) \right| \Phi_0^\alpha \right\rangle_{\text{ph}}. \tag{3.10.34}$$

In the next subsections, we shall evaluate the energy-shifts associated with each of the three physical processes in eq.(3.10.29) which are presented in figs. 3.10.1a to 3.10.1c. We now write the second-order $\hat{\mathcal{S}}^{(2)}$ -matrix as a sum of the three physical processes sub matrices of eq.(3.10.23):

$$\hat{\mathcal{S}}^{(2)}(\epsilon, 1) = \hat{\mathcal{S}}_{\text{SP}}^{(2)}(\epsilon, 1) + \hat{\mathcal{S}}_{\text{VP}}^{(2)}(\epsilon, 1) + \hat{\mathcal{S}}_{\text{SE}}^{(2)}(\epsilon, 1). \tag{3.10.35}$$

The individual terms are thus given by:

$$\begin{aligned} \hat{\mathcal{S}}_{\text{SP}}^{(2)}(\epsilon, 1) &= +\frac{e^2}{2i\hbar} \int d^4x_1 \int d^4x_2 e^{-\frac{\epsilon}{\hbar}(|t_1|+|t_2|)} D_{\mu_1\mu_2}^F(x_1, x_2) \\ &\quad \times : \bar{\Psi}(x_1) \gamma^{\mu_1} \Psi(x_1) \bar{\Psi}(x_2) \gamma^{\mu_2} \Psi(x_2) : \end{aligned} \quad (3.10.36)$$

$$\begin{aligned} \hat{\mathcal{S}}_{\text{VP}}^{(2)}(\epsilon, 1) &= -e^2 \int d^4x_1 \int d^4x_2 \text{Tr}[\gamma^{\mu_2} S^F(x_2, x_2)] e^{-\frac{\epsilon}{\hbar}(|t_1|+|t_2|)} D_{\mu_1\mu_2}^F(x_1, x_2) \\ &\quad \times : \bar{\Psi}(x_1) \gamma^{\mu_1} \Psi(x_1) : \end{aligned} \quad (3.10.37)$$

$$\begin{aligned} \hat{\mathcal{S}}_{\text{SE}}^{(2)}(\epsilon, 1) &= +e^2 \int d^4x_1 \int d^4x_2 S_{\beta_2\alpha_1}^F(x_2, x_1) \gamma_{\alpha_1\beta_1}^{\mu_1} \gamma_{\alpha_2\beta_2}^{\mu_2} e^{-\frac{\epsilon}{\hbar}(|t_1|+|t_2|)} D_{\mu_1\mu_2}^F(x_1, x_2) \\ &\quad \times : \bar{\Psi}_{\alpha_2}(x_2) \Psi_{\beta_1}(x_1) : \end{aligned} \quad (3.10.38)$$

In the following sections, we shall evaluate the three energy-shifts:

$$\Delta E_X^\alpha = \lim_{\epsilon \rightarrow 0} i\epsilon \left\langle \Phi_0^\alpha \left| \hat{\mathcal{S}}_X^{(2)}(\epsilon, 1) \right| \Phi_0^\alpha \right\rangle_{\text{ph}}, \quad X = \text{SP, VP, SE} \quad (3.10.39)$$

which correct the total energy E^α of a system consisting of N non-interacting bound-electrons described by the multi-electronic state $|\Phi_0^\alpha\rangle$.

3.10.5 Single-photon exchange

The energy-shift associated with the single-photon exchange process is given by:

$$\begin{aligned} \Delta E_{\text{SP}}^\alpha &= \frac{e^2}{2\hbar} \lim_{\epsilon \rightarrow 0} \epsilon \int d^4x_1 \int d^4x_2 e^{-\frac{\epsilon}{\hbar}(|t_1|+|t_2|)} D_{\mu_1\mu_2}^F(x_1, x_2) \\ &\quad \times \left\langle \Phi_0^\alpha \left| : \bar{\Psi}(x_1) \gamma^{\mu_1} \Psi(x_1) \bar{\Psi}(x_2) \gamma^{\mu_2} \Psi(x_2) : \right| \Phi_0^\alpha \right\rangle. \end{aligned} \quad (3.10.40)$$

We now use the photon propagator expression of eq.(3.8.24) and expand the field operators as done in eq.(3.5.13) to obtain the following expression:

$$\begin{aligned} \Delta E_{\text{SP}}^\alpha &= -\frac{\hbar e^2 c}{2\epsilon_0} \lim_{\epsilon \rightarrow 0} \epsilon \int d^3x_1 \int d^3x_2 \lim_{\delta \rightarrow 0} \int \frac{d^4p}{(2\pi\hbar)^4} \frac{e^{+\frac{i}{\hbar}\mathbf{p} \cdot (\mathbf{x}_1 - \mathbf{x}_2)}}{p_0^2 - |\mathbf{p}|^2 + i\delta} \\ &\quad \times \left\langle \Phi_0^\alpha \left| : c_i^\dagger c_j c_k^\dagger c_l : \right| \Phi_0^\alpha \right\rangle \bar{\psi}_i(\mathbf{x}_1) \gamma^\mu \psi_j(\mathbf{x}_1) \bar{\psi}_k(\mathbf{x}_2) \gamma_\mu \psi_l(\mathbf{x}_2) \\ &\quad \times \int dt_1 \int dt_2 e^{-\frac{\epsilon}{\hbar}|t_1| - \frac{i}{\hbar}(E_j - E_i + cp_0)t_1} e^{-\frac{\epsilon}{\hbar}|t_2| - \frac{i}{\hbar}(E_l - E_k - cp_0)t_2}, \end{aligned} \quad (3.10.41)$$

where we isolate the time-integrals at the end line. This time-integral can be then written as:

$$\begin{aligned} &\int dt_1 \int dt_2 e^{-\frac{\epsilon}{\hbar}|t_1| - \frac{i}{\hbar}(E_j - E_i + cp_0)t_1} e^{-\frac{\epsilon}{\hbar}|t_2| - \frac{i}{\hbar}(E_l - E_k - cp_0)t_2} \\ &= (2\pi\hbar)^2 \Delta_\epsilon(E_i - E_j - cp_0) \Delta_\epsilon(E_l - E_k - cp_0), \end{aligned} \quad (3.10.42)$$

using the function $\Delta_\epsilon(a)$, given in eq.(I.1.9) of the appendix. We shall now evaluate the energy-component momentum integral, which acts on the photon propagator denominator and the delta functions Δ_ϵ , using eq.(I.1.14):

$$\begin{aligned} &c \int dp_0 \frac{1}{p_0^2 - |\mathbf{p}|^2 + i\delta} \Delta_\epsilon(E_i - E_j - cp_0) \Delta_\epsilon(E_l - E_k - cp_0) \\ &= \frac{\Delta_{2\epsilon}(E_i - E_j - E_l + E_k)}{\left(\frac{E_i - E_j}{c}\right)^2 - |\mathbf{p}|^2 + i\epsilon}, \end{aligned} \quad (3.10.43)$$

which holds in the limit $\epsilon \rightarrow 0$, the function $\Delta_\epsilon(x)$ behaves like a Dirac delta:

$$\lim_{\epsilon \rightarrow 0} \Delta_\epsilon(x) = \delta(x) \quad (3.10.44)$$

Next, we shall evaluate the action of the space-component momentum integral which will act on the last denominator. Using eq.(I.3.5), this radial integral is found to be:

$$\int \frac{d^3p}{(2\pi\hbar)^3} \frac{e^{+\frac{i}{\hbar}\mathbf{p} \cdot (\mathbf{x}_1 - \mathbf{x}_2)}}{p_0^2 - \mathbf{p}^2 + i\epsilon} = -\frac{e^{+\frac{i}{\hbar}\sqrt{p_0^2 + i\epsilon}|\mathbf{x}_1 - \mathbf{x}_2|}}{4\pi\hbar^2 |\mathbf{x}_1 - \mathbf{x}_2|}, \quad (3.10.45)$$

with $p_0 = (E_i - E_j)/c$. Finally, we have the expectation value of the creation and annihilation operators string in eq.(3.10.41), which reduces to the following product of Kronecker deltas:

$$\left\langle \Phi_0^\alpha \left| : c_i^\dagger c_j c_k^\dagger c_l : \right| \Phi_0^\alpha \right\rangle = - \left\langle \Phi_0^\alpha \left| c_i^\dagger c_k^\dagger c_j c_l \right| \Phi_0^\alpha \right\rangle = \delta_{ij}\delta_{kl} - \delta_{il}\delta_{jk}. \quad (3.10.46)$$

The reader should note that in the last expression, we assumed that the single-electron states j and l of the N -electron state $|\Phi_0^\alpha\rangle$ were already occupied. Finally, the limit of vanishing $\epsilon \rightarrow 0$ is evaluated with respect to eq.(I.1.13), which leads to a Kronecker delta term which manifests the energy conservation at the vertices. See, for instance, [15]. After collecting all the above results, our energy expression simplifies to the following one:

$$\begin{aligned} \Delta E_{\text{SP}}^\alpha &= \frac{e^2}{2} \int d^3x_1 \int d^3x_2 \bar{\psi}_i(\mathbf{x}_1) \gamma^\mu \psi_j(\mathbf{x}_1) \frac{e^{+\frac{i}{c\hbar}|E_i - E_j||\mathbf{x}_1 - \mathbf{x}_2|}}{4\pi\epsilon_0 |\mathbf{x}_1 - \mathbf{x}_2|} \bar{\psi}_k(\mathbf{x}_2) \gamma_\mu \psi_l(\mathbf{x}_2) \\ &\quad \times \delta_{E_i + E_k, E_j + E_l} \{ \delta_{ij}\delta_{kl} - \delta_{il}\delta_{jk} \}. \end{aligned} \quad (3.10.47)$$

The term in the curly brackets leads to the distinction between a direct and an exchange term:

$$\begin{aligned} \Delta E_{\text{SP}}^\alpha &= \frac{e^2}{2} \int d^3x_1 \int d^3x_2 \bar{\psi}_i(\mathbf{x}_1) \gamma^\mu \psi_i(\mathbf{x}_1) \frac{1}{4\pi\epsilon_0 |\mathbf{x}_1 - \mathbf{x}_2|} \bar{\psi}_j(\mathbf{x}_2) \gamma_\mu \psi_j(\mathbf{x}_2) \quad \text{Direct} \\ &\quad - \frac{e^2}{2} \int d^3x_1 \int d^3x_2 \bar{\psi}_i(\mathbf{x}_1) \gamma^\mu \psi_j(\mathbf{x}_1) \frac{e^{+\frac{i}{c\hbar}|E_i - E_j||\mathbf{x}_1 - \mathbf{x}_2|}}{4\pi\epsilon_0 |\mathbf{x}_1 - \mathbf{x}_2|} \bar{\psi}_j(\mathbf{x}_2) \gamma_\mu \psi_i(\mathbf{x}_2) \quad \text{Exchange} \end{aligned} \quad (3.10.48)$$

as found in the work of Mohr [19, eq.(54)]. We shall now discuss these two terms:

1. **The direct term** is equivalent to the Hartree one (in the Hartree-Fock theory), and describes the instantaneous interaction between two electron charge (four-)currents: $J^\mu(i, \mathbf{x}_1)$ and $J_\mu(j, \mathbf{x}_2)$, associated with the i -th and j -th electrons, with:

$$J^\mu(i, \mathbf{x}) = -ce\bar{\psi}_i(\mathbf{x}) \gamma^\mu \psi_i(\mathbf{x}). \quad (3.10.49)$$

In addition, we note that the effective interaction Hamiltonian associated with this direct contribution is given by:

$$H_{\text{Direct}} = \frac{e^2}{4\pi\epsilon_0 |\mathbf{x}_1 - \mathbf{x}_2|} [\alpha^\mu(1) \alpha_\mu(2)] = \frac{e^2}{4\pi\epsilon_0 |\mathbf{x}_1 - \mathbf{x}_2|} [1 + \boldsymbol{\alpha}(1) \cdot \boldsymbol{\alpha}(2)], \quad (3.10.50)$$

where the α^μ matrices are given in eq.(A.0.13). The numbers inside the round brackets: (1) and (2), are there to indicate that the associated matrices act on the current associated with \mathbf{x}_1 and \mathbf{x}_2 , respectively. Finally, we should note that this term accounts for the Coulomb (charge-charge) and Gaunt (current-current) interactions.

2. **The exchange term** is equivalent to the Fock term in the Hartree-Fock theory, and the associated exchange effective Hamiltonian is written as:

$$H_{\text{Exchange}} = \frac{e^2}{4\pi\epsilon_0 |\mathbf{x}_1 - \mathbf{x}_2|} [1 + \boldsymbol{\alpha}(1) \cdot \boldsymbol{\alpha}(2)] e^{+\frac{i}{c\hbar} |E_i - E_j| |\mathbf{x}_1 - \mathbf{x}_2|}. \quad (3.10.51)$$

See [7, eq.(461)] and [15, eq.(F.67)] and the corresponding discussions. In contrary to the previous term, this one describes the retarded exchange interaction between two currents, and the effect of retardation is captured in the exponential term. Notice that in the non-relativistic limit $c \rightarrow \infty$ (or zero-frequency limit), this exponential reduces to 1. In addition, while the direct energy-shift is a real quantity, the exchange energy-shift is a complex number, its real part corresponds to the physical energy-shift, and its imaginary component contains a QED corrections to the partial resonance width of excited-state that describes the inverse of its decay mean lifetime. See, for instance, [19, Page 1954].

It is thus more convenient to write the energy-shift associated with the single-photon exchange process as the real part of the last formula:

$$\begin{aligned} \Delta E_{\text{SP}}^\alpha = & \\ & + \frac{e^2}{2} \int d^3x_1 \int d^3x_2 \bar{\psi}_i(\mathbf{x}_1) \gamma^\mu \psi_i(\mathbf{x}_1) \frac{1}{4\pi\epsilon_0 |\mathbf{x}_1 - \mathbf{x}_2|} \bar{\psi}_j(\mathbf{x}_2) \gamma_\mu \psi_j(\mathbf{x}_2) \quad \text{Direct} \\ & - \frac{e^2}{2} \int d^3x_1 \int d^3x_2 \bar{\psi}_i(\mathbf{x}_1) \gamma^\mu \psi_j(\mathbf{x}_1) \frac{\cos\left(\frac{1}{c\hbar} |E_i - E_j| |\mathbf{x}_1 - \mathbf{x}_2|\right)}{4\pi\epsilon_0 |\mathbf{x}_1 - \mathbf{x}_2|} \bar{\psi}_j(\mathbf{x}_2) \gamma_\mu \psi_i(\mathbf{x}_2) \quad \text{Exchange} \end{aligned} \quad (3.10.52)$$

In the next section, we shall investigate the two remaining processes: the vacuum polarization and the self-energy, and we will see that the former contribution will be of direct instantaneous nature, as the direct term in this last expression, while the latter one will be of a retarded and exchange nature, as the exchange term we have just encountered.

3.10.6 Vacuum polarization

We shall now attack the vacuum polarization term, which will be of a central importance in this thesis. The corresponding energy-shift is given, with respect to eqs.(3.10.34 and 3.10.37) by:

$$\begin{aligned} \Delta E_{\text{VP}}^\alpha = & -e^2 i \lim_{\epsilon \rightarrow 0} \epsilon \int d^4x_1 \int d^4x_2 \text{Tr} [\gamma^{\mu_2} S^F(x_2, x_2)] e^{-\frac{\epsilon}{\hbar} (|t_1| + |t_2|)} D_{\mu_1 \mu_2}^F(x_1, x_2) \\ & \times \langle \Phi_0^\alpha | : \bar{\Psi}(x_1) \gamma^{\mu_2} \Psi(x_1) : | \Phi_0^\alpha \rangle. \end{aligned} \quad (3.10.53)$$

We first note that the trace $\text{Tr} [\gamma^{\mu_1} S^F(x_2, x_2)]$ is time-independent, as seen from eq.(3.9.37), at equal spacetime points. We now use the photon propagator expression.(3.8.24), expand the field operators, and isolate the time integrals to obtain the following expression:

$$\begin{aligned} \Delta E_{\text{VP}}^\alpha = & \frac{c\hbar^2 e^2 i}{\epsilon_0} \lim_{\epsilon \rightarrow 0} \epsilon \int d^3x_1 \int d^3x_2 \text{Tr} [\gamma^\mu S^F(x_2, x_2)] \lim_{\delta \rightarrow 0} \int \frac{d^4p}{(2\pi\hbar)^4} \frac{e^{+\frac{i}{\hbar} \mathbf{p} \cdot (\mathbf{x}_1 - \mathbf{x}_2)}}{p_0^2 - |\mathbf{p}|^2 + i\delta} \\ & \times \bar{\psi}_i(\mathbf{x}_1) \gamma_\mu \psi_j(\mathbf{x}_1) \langle \Phi_0^\alpha | : c_i^\dagger c_j : | \Phi_0^\alpha \rangle \int dt_1 \int dt_2 e^{-\frac{\epsilon}{\hbar} |t_1| + \frac{i}{\hbar} (E_i - E_j + c p_0) t_1} e^{-\frac{\epsilon}{\hbar} |t_2| - \frac{i}{\hbar} c p_0 t_2}. \end{aligned} \quad (3.10.54)$$

The time integral is evaluated using eq.(I.1.9):

$$\begin{aligned} & \int dt_1 \int dt_2 e^{-\frac{\epsilon}{\hbar}|t_1| + \frac{i}{\hbar}(E_i - E_j + cp_0)t_1} e^{-\frac{\epsilon}{\hbar}|t_2| - \frac{i}{\hbar}cp_0t_2} \\ &= (2\pi\hbar)^2 \Delta_\epsilon(E_i - E_j + cp_0) \Delta_\epsilon(cp_0). \end{aligned} \quad (3.10.55)$$

We now focus on the p_0 integral, and use the previous result of eq.(3.10.43) to write it as:

$$\begin{aligned} & c \int dp_0 \frac{1}{p_0^2 - |\mathbf{p}|^2 + i\delta} \Delta_\epsilon(E_i - E_j - cp_0) \Delta_\epsilon(cp_0) \\ &= \frac{\Delta_{2\epsilon}(E_i - E_j)}{\left(\frac{E_i - E_j}{c}\right)^2 - |\mathbf{p}|^2 + i\epsilon}. \end{aligned} \quad (3.10.56)$$

Using eq.(3.10.45) we can write our three-momentum integral as:

$$\int \frac{d^3p}{(2\pi\hbar)^3} \frac{e^{+\frac{i}{\hbar}\mathbf{p} \cdot (\mathbf{x}_1 - \mathbf{x}_2)}}{(E_i - E_j)^2 / c^2 - |\mathbf{p}|^2 + i\epsilon} = -\frac{e^{+\frac{i}{c\hbar}|E_i - E_j||\mathbf{x}_1 - \mathbf{x}_2|}}{4\pi\hbar^2 |\mathbf{x}_1 - \mathbf{x}_2|}. \quad (3.10.57)$$

We are left with the expectation value in eq.(3.10.54) that reduces to:

$$\langle \Phi_0^\alpha | : c_i^\dagger c_i : | \Phi_0^\alpha \rangle = \langle \Phi_0^\alpha | c_i^\dagger c_j | \Phi_0^\alpha \rangle = \delta_{ij}. \quad (3.10.58)$$

where, again, we assume that the single-electron state j , in the N -particle state $|\Phi_0^\alpha\rangle$, is already occupied. Finally, we use the result of eq.(I.1.13) which adds a Kronecker delta δ_{E_i, E_j} , showing energy conservation at the vertex, as expected. After collecting all the above findings, we can write:

$$\Delta E_{\text{VP}}^\alpha = -e^2 i\hbar \int d^3x_1 \int d^3x_2 \bar{\psi}_i(\mathbf{x}_1) \gamma^\mu \psi_j(\mathbf{x}_1) \frac{e^{+\frac{i}{c\hbar}|E_i - E_j||\mathbf{x}_1 - \mathbf{x}_2|}}{4\pi\epsilon_0 |\mathbf{x}_1 - \mathbf{x}_2|} \text{Tr} [\gamma_\mu S^F(x_2, x_2)] \delta_{ij} \delta_{E_i, E_j} \quad (3.10.59)$$

Notice that this point, that the last Kronecker delta will reduce the exponential to 1, and we thus find the energy-shift associated with the vacuum polarization to be:

$$\Delta E_{\text{VP}}^\alpha = -e^2 i\hbar \int d^3x_1 \int d^3x_2 \bar{\psi}_i(\mathbf{x}_1) \gamma^\mu \psi_i(\mathbf{x}_1) \frac{1}{4\pi\epsilon_0 |\mathbf{x}_1 - \mathbf{x}_2|} \text{Tr} [\gamma_\mu S^F(x_2, x_2)]. \quad (3.10.60)$$

This expression is found in the work of Schweber [4, eq.(205) 2nd line], Indelicato *et al.* [5, eq.(5)] as well as in the work of Mohr *et al.* [7, eq.(221)]. This energy-shift represents a process in which an electron current:

$$-ec\bar{\psi}_i(\mathbf{x}_1) \gamma^\mu \psi_i(\mathbf{x}_1), \quad (3.10.61)$$

associated with the i -th electron at \mathbf{x}_1 , instantaneously interacts with the vacuum polarization charge current, given by:

$$J_\mu^{\text{VP}}(\mathbf{x}_2) = ec i\hbar \text{Tr} [\gamma_\mu S^F(x_2, x_2)]. \quad (3.10.62)$$

This time-independent term is going to be discussed in detail in the next chapter, where we shall see that it can be written as:

$$J_\mu^{\text{VP}}(\mathbf{x}) = \frac{ec}{2} \left[\sum_{E_i > 0} \bar{\psi}_i(\mathbf{x}) \gamma_\mu \psi_i(\mathbf{x}) - \sum_{E_i < 0} \bar{\psi}_i(\mathbf{x}) \gamma_\mu \psi_i(\mathbf{x}) \right], \quad (3.10.63)$$

which is the average of the difference between positive and negative-energy Dirac currents. Furthermore, we shall see that if the time-independent external potential is purely scalar, then only the time-component of the last expression, known as the vacuum polarization density, will survive:

$$J_0^{\text{VP}}(\mathbf{x}) = \frac{ec}{2} \left[\sum_{E_i > 0} \psi_i^\dagger(\mathbf{x}) \psi_i(\mathbf{x}) - \sum_{E_i < 0} \psi_i^\dagger(\mathbf{x}) \psi_i(\mathbf{x}) \right] = c\rho^{\text{VP}}(\mathbf{x}), \quad (3.10.64)$$

and as a consequence, the vacuum polarization energy-shift will reduce to:

$$\Delta E_{\text{VP}}^\alpha = -e^2 i \hbar \int d^3 x_1 \int d^3 x_2 \psi_i^\dagger(\mathbf{x}_1) \psi_i(\mathbf{x}_1) \frac{1}{4\pi\epsilon_0 |\mathbf{x}_1 - \mathbf{x}_2|} \text{Tr} [\gamma_0 S^F(x_2, x_2)]. \quad (3.10.65)$$

This expression can be found in the work of Soff and Mohr [6, eqs.(6,8,9,10)]. We are now going to calculate the last energy-shift, associated with the (more) complicated non-local self-energy process.

3.10.7 Self-energy

Using Sucher's energy-shift formula of eq.(3.10.34), associated with second-order processes, and the self-energy \mathcal{S} -matrix expression from eq.(3.10.37), our energy-shift is written as:

$$\begin{aligned} \Delta E_{\text{SE}}^\alpha = & +ie^2 \lim_{\epsilon \rightarrow 0} \epsilon \int d^4 x_1 \int d^4 x_2 S_{\beta_2 \alpha_1}^F(x_2, x_1) \gamma_{\alpha_1 \beta_1}^{\mu_1} \gamma_{\alpha_2 \beta_2}^{\mu_2} \\ & \times e^{-\frac{\epsilon}{\hbar}(|t_1|+|t_2|)} D_{\mu_1 \mu_2}^F(x_1, x_2) \langle \Phi_0^\alpha | : \bar{\Psi}_{\alpha_2}(x_2) \Psi_{\beta_1}(x_1) : | \Phi_0^\alpha \rangle. \end{aligned} \quad (3.10.66)$$

The main complication associated with self-energy energy-shift comes from the time dependence of the electron propagator $S_{\beta_2 \alpha_1}^F(x_2, x_1)$. This was not the case for two previous processes, where:

- The single-photon exchange term in eq.(3.10.36) does not contain an electron propagator.
- The vacuum polarization term in eq.(3.10.37) contains $S^F(x_2, x_2)$, which is time-independent.

We first plug the photon and electron propagator expressions of eqs.(3.8.24 and 3.9.37) in our current expression of eq.(3.10.66), and follow the steps done in the previous processes, to obtain the following expression:

$$\begin{aligned} \Delta E_{\text{SE}}^\alpha = & \frac{e^2}{2\pi i} \int d^3 x_1 \int d^3 x_2 \int_{C_F} dz G_{\beta_2 \zeta_1}(\mathbf{x}_2, \mathbf{x}_1; z) \gamma_{\zeta_1 \alpha_1}^0 \\ & \times \gamma_{\alpha_1 \beta_1}^{\mu_1} \gamma_{\alpha_2 \beta_2}^{\mu_2} g_{\mu_1 \mu_2} \bar{\psi}_{i, \alpha_2}(\mathbf{x}_2) \psi_{j, \beta_1}(\mathbf{x}_1) \\ & \times \delta_{ij} \delta_{E_i, E_j} \frac{e^{+\frac{i}{\hbar} \sqrt{\frac{(z-E_i)^2}{c^2} + i\epsilon} |\mathbf{x}_1 - \mathbf{x}_2|}}{4\pi\epsilon_0 |\mathbf{x}_1 - \mathbf{x}_2|}. \end{aligned} \quad (3.10.67)$$

The Kronecker delta δ_{ij} coming from the expectation value forces both states to be identical, in addition, δ_{E_i, E_j} that comes from the limit of small ϵ indicates energy conservation. We shall now move our terms around to simplify our equation and obtain:

$$\begin{aligned} \Delta E_{\text{SE}}^\alpha = & \frac{e^2}{2\pi i} \int d^3 x_1 \int d^3 x_2 \int_{C_F} dz \psi_i^\dagger(\mathbf{x}_2) \alpha^\mu G(\mathbf{x}_2, \mathbf{x}_1; z) \alpha_\mu \psi_i(\mathbf{x}_1) \\ & \times \frac{e^{+\frac{i}{\hbar} \sqrt{\frac{(z-E_i)^2}{c^2} + i\epsilon} |\mathbf{x}_1 - \mathbf{x}_2|}}{4\pi\epsilon_0 |\mathbf{x}_1 - \mathbf{x}_2|}. \end{aligned} \quad (3.10.68)$$

This expression originates from the work of Baranger *et al.* [108, section II. first eq.], and can be found in Schweber [4, eq.(205)]. The identical form we are giving has first appeared in the work of Mohr [113, eq.(2.6)]. In this latter work, the author regularizes the self-energy expression (last equation) using the Pauli-Villars regularization, where the photon propagator term (the last fraction) is regularized by a counter-term designed to eliminate high momentum photon contributions (See propagator subtraction of [113, eq.(2.3)]). This regularized expression needs to be balanced with the relativistic self-energy mass-shift (first calculated by Feynman [114, eq.(9)]) that depends on the same momentum cutoff that was introduced for the photon propagator integral.

3.11 Furry's theorem

When evaluating the contribution of closed free-electron loops, one should note that loops with an odd number of vertices will yield a vanishing contribution. This theorem is known as the Furry's theorem, named after the work of Wendell H. Furry [115] where he showed that using the charge conjugation symmetry one can prove that the probability amplitude associated with a process containing a closed electron loop with an odd number of vertices, vanishes. Following [8, exercice 4.1], we define the matrix operator O , which is related to the charge conjugation matrix operation of eq.(2.8.7) by:

$$O = U_c \gamma^0 = \gamma^2 \gamma^0. \quad (3.11.1)$$

Once we apply this operator on the gamma matrices, one obtains [28, eq.(12.18)]:

$$O \gamma^\mu O^{-1} = -[\gamma^\mu]^t. \quad (3.11.2)$$

In addition, we need to know how the free electron propagator S associated with the Dirac equation:

$$S(x_2, x_1) = \int \frac{d^4 p}{(2\pi\hbar)^4} \frac{e^{-\frac{i}{\hbar} p \cdot (x_2 - x_1)}}{p^2 - mc} [\gamma^\mu p_\mu + mc \mathbb{1}_4], \quad (3.11.3)$$

behaves under this operation. Using eq.(3.11.2), we can write:

$$OS(x_2, x_1)O^{-1} = \int \frac{d^4 p}{(2\pi\hbar)^4} e^{-\frac{i}{\hbar} p \cdot (x_2 - x_1)} \frac{[\gamma^\mu]^t p_\mu + mc \mathbb{1}_4}{p^2 - mc}, \quad (3.11.4)$$

and after a change of variable $p \rightarrow -p$, which removes the negative sign in front of the transposed gamma matrices, the negative sign can be absorbed by the spacetime difference, and one obtains [4, Chapter 14 eq.(51)]:

$$OS(x_2, x_1)O^{-1} = \int \frac{d^4 p}{(2\pi\hbar)^4} e^{-\frac{i}{\hbar} p \cdot (x_1 - x_2)} \frac{[\gamma^\mu]^t p_\mu + mc \mathbb{1}_4}{p^2 - mc} = [S(x_1, x_2)]^t. \quad (3.11.5)$$

A free-electron loop with a single vertex contains the following term:

$$\text{Tr} [S^F(x_0, x_0) \gamma^\mu]. \quad (3.11.6)$$

This term is drawn in figure 3.11.1a. Following Furry's theorem, one can insert the unit matrix $O^{-1}O = \mathbb{1}_4$ in the trace:

$$\text{Tr} [S^F(x_0, x_0) \gamma^\mu] = \text{Tr} [OS^F(x_0, x_0)O^{-1}O\gamma^\mu O^{-1}],$$

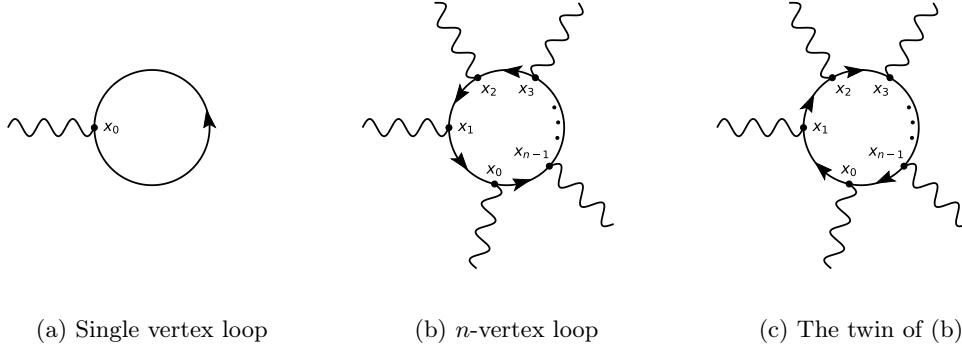


Figure 3.11.1: Free electron loops (free propagations).

and make use of eqs.(3.11.2 and 3.11.5) to get:

$$\text{Tr} [S^F(x_0, x_0) \gamma^\mu] = -\text{Tr} \left[[S^F(x_0, x_0)]^t [\gamma^\mu]^t \right] = -\text{Tr} [S^F(x_0, x_0) \gamma^\mu],$$

which allows us to write:

$$\text{Tr} [S^F(x_0, x_0) \gamma^\mu] = 0. \quad (3.11.7)$$

Alternatively, one can prove that this trace vanishes using a much simpler argument: We first write the trace as:

$$\text{Tr} [S^F(x_2, x_1) \gamma^\mu] = \int \frac{d^4 p}{(2\pi\hbar)^4} \frac{e^{-\frac{i}{\hbar} p \cdot (x_2 - x_1)}}{p^2 - mc} \text{Tr} [\gamma^\nu \gamma^\mu p_\nu + mc \gamma^\mu], \quad (3.11.8)$$

and using the results on gamma matrices traces eq.(B.1.17) and eq.(B.1.20), this expression simplifies to:

$$\text{Tr} [S^F(x_0, x_0) \gamma^\mu] = 4 \int \frac{d^4 p}{(2\pi\hbar)^4} \frac{e^{-\frac{i}{\hbar} p \cdot (x_2 - x_1)}}{p^2 - mc} \text{Tr} [p^\mu], \quad (3.11.9)$$

which clearly vanishes since the integrand is odd in the four-momentum p .

When dealing with more than a single vertex, the last argument cannot be used, and here is where Furry's theorem which generalizes the previous analysis to an arbitrary odd-number of vertices, applies. For a general n number of vertices of a free closed electron loop, one has the following term:

$$T_1 = \text{Tr} [S^F(x_0, x_1) \gamma^{\mu_1} S^F(x_1, x_2) \gamma^{\mu_2} S^F(x_2, x_3) \gamma^{\mu_3} \dots S^F(x_{n-2}, x_{n-1}) \gamma^{\mu_{n-1}} S^F(x_{n-1}, x_0) \gamma^{\mu_0}], \quad (3.11.10)$$

which we represent in figure 3.11.1b, where each vertex is mathematically represented by a gamma matrix, we choose γ^{μ_i} to represent the vertex at the x_i spacetime point. This diagram, as the associated equation, describes n free-electron propagations between the spacetime points:

$$x_0 \rightarrow x_{n-1} \rightarrow x_{n-2} \dots \rightarrow x_2 \rightarrow x_1 \rightarrow x_0. \quad (3.11.11)$$

When expanding the \mathcal{S} -matrix, one sees that with each term T_1 represented in figure 3.11.1b there exist a twin term, we shall call T_2 , that should be summed with T_1 . This second term is represented in figure 3.11.1c and corresponds to an opposite direction of electron propagations:

$$x_0 \rightarrow x_1 \rightarrow x_2 \dots \rightarrow x_{n-2} \rightarrow x_{n-1} \rightarrow x_0, \quad (3.11.12)$$

cf. eq.(3.11.11), given by:

$$T_2 = \text{Tr} [S^F(x_1, x_0) \gamma^{\mu_0} S^F(x_0, x_{n-1}) \gamma^{\mu_{n-1}} S^F(x_{n-1}, x_{n-2}) \dots S^F(x_3, x_2) \gamma^{\mu_2} S^F(x_2, x_1) \gamma^{\mu_1}]. \quad (3.11.13)$$

Using the same previous steps, we insert the unit operator $O^{-1}O = \mathbb{1}_4$, where O is given in eq. (3.11.1), in the expression of T_1 , and use the results of eqs.(3.11.2,3.11.5), to write this expression as:

$$T_1 = (-1)^n \text{Tr} [[S^F(x_1, x_0)]^t [\gamma^{\mu_1}]^t [S^F(x_2, x_1)]^t [\gamma^{\mu_2}]^t \times \dots [S^F(x_{n-1}, x_{n-2})]^t [\gamma^{\mu_{n-1}}]^t [S^F(x_0, x_{n-1})]^t [\gamma^{\mu_0}]^t], \quad (3.11.14)$$

which can be rewritten as:

$$T_1 = (-1)^n \text{Tr} [\gamma^{\mu_0} S^F(x_0, x_{n-1}) \gamma^{\mu_{n-1}} S^F(x_{n-1}, x_{n-2}) \gamma^{\mu_2} S^F(x_2, x_1) \gamma^{\mu_1} S^F(x_1, x_0)] = (-1)^n T_2. \quad (3.11.15)$$

This result leads to the final conclusion that free electron loops with odd number give vanishing contributions:

$$T = T_1 + T_2 = (1 + (-1)^n) T_1 = \begin{cases} 2T_1 & \text{for even } n \\ 0 & \text{for odd } n \end{cases}. \quad (3.11.16)$$

This result is used in two related contexts:

1. **In conventional QED**, where the electron field operator is expanded in the basis of the free Dirac-solutions: to study the scattering problem and its radiative corrections. In this case, the expansion of the \mathcal{S} -matrix will give some terms with closed free-electron loops.
2. **In BSQED**, where the electron field operator is expanded in the basis of the bound Dirac-solutions: to study the radiative corrections in the atomic/molecular problems. In this case, one expands the closed-loop of the bound electron propagator (the Furry picture) in powers of the external time-independent potential, as done for the vacuum polarization loop for instance.

3.12 Effective QED potentials

In this section we shall present the main effective potentials (to be added to the Dirac/Schrödinger Hamiltonian) used in numerical calculations to account for the lowest order vacuum polarization and self-energy QED corrections.

3.12.1 Vacuum polarization effective potentials

The existence of a charged particle (the polarizer), in space, polarizes the surrounding vacuum in which virtual electron-positron pairs are simultaneously generated (quantum electrodynamics). In turn, this cloud of electron-positron pairs affects back the polarizer, who initially created the cloud, in some sort of a self-interaction. This is known as the vacuum polarization effect. In order to include this effect in relativistic (and non-relativistic) calculations, one can use some already derived effective potentials, corresponding to some of the low-order vacuum polarization processes. This inclusion can be done by evaluating the following expectation value:

$$\Delta E^{\text{VP}} = -e \int d^3x \psi^\dagger(\mathbf{x}) V^{\text{VP}}(\mathbf{x}) \psi(\mathbf{x}), \quad (3.12.1)$$

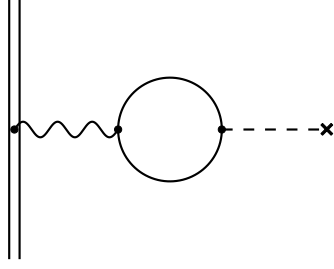


Figure 3.12.1: Uehling diagram:
Lowest-order VP process: $\alpha(\alpha Z)^1$

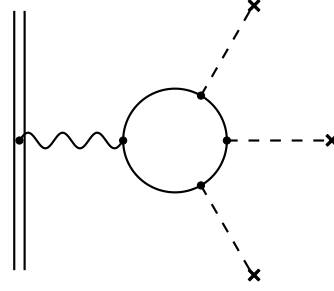


Figure 3.12.2: Wichmann-Kroll diagram:
Higher-order VP process: $\alpha(\alpha Z)^3$

of some vacuum polarization potential V^{VP} , with respect to the four-component Dirac spinors, which shifts the Dirac energy E by an amount ΔE^{VP} . The vacuum polarization effect, as presented in the last equation, is a local effect. We shall now list the main effective potentials which can be included in V^{VP} :

- $\alpha(\alpha Z)$ -order: The Uehling potential [116, eq.(25)], presented in figure 3.12.1. Uehling originally considered the point nuclear charge distribution model: $\rho^{\text{nuc}}(\mathbf{x}) = Ze\delta(\mathbf{x})$, in his derivation of this vacuum polarization potential. The corresponding expression for a general nuclear charge model $\rho^{\text{nuc}}(\mathbf{x})$ was provided by Wayne Fullerton and Rinker in [117, eqs.(3,4)].
- $\alpha(\alpha Z)^3$ -order: The Wichmann-Kroll [118] potential, presented in figure 3.12.2. In the cited work, Wichmann and Kroll calculated this potential associated with the $\alpha(\alpha Z)^3$ -order correction in Laplace-space, and have only evaluate the behavior of this potential, and its associated charge density at large distances (in real-space). Blomqvist [11, section 4], on the other hand, has evaluated the inverse Laplace transform, and obtained the real-space potential expression, for a point-charge nuclear model.
- $\alpha^2(\alpha Z)$ -order: The Källén-Sabry potential, whose processes are presented in figure 3.12.3. In their work, Källén and Sabry considered the problem in momentum-space, and computed the associated corrected polarization function [119], which can be related to the momentum-space potential. The real-space potential corresponding to this contribution was derived by Blomqvist [11, section 3], and the generalization to a general nuclear distribution was made by Wayne Fullerton and Rinker [117, eqs.(9-11)].

The expressions for the last two potentials are very complicated (see the cited references), and this does not only make the analytical evaluation impossible but also makes it very hard to employ these potentials in practical calculations. For this reason, Wayne Fullerton and Rinker [117] provided good approximating formulas for the first two potentials, which can be numerically evaluated in an efficient way. At the same time, Huang [10] proposed a fitting for the above potentials, but claimed that the approach of Wayne Fullerton and Rinker is more accurate. In addition, Fainshtein *et al.* provided an approximation for the Wichmann-Kroll potentials [120, section 4], and the higher-order $\alpha(\alpha Z)^{5,7}$ terms, and compared their results with the ones that are in principle, exact: Soff and Mohr [6], in addition to Gyulassy [121]. Finally, we note that Dzuba *et al.* have proposed an approximate form of the Wichmann-Kroll potential, which recovers the exact behavior at small and

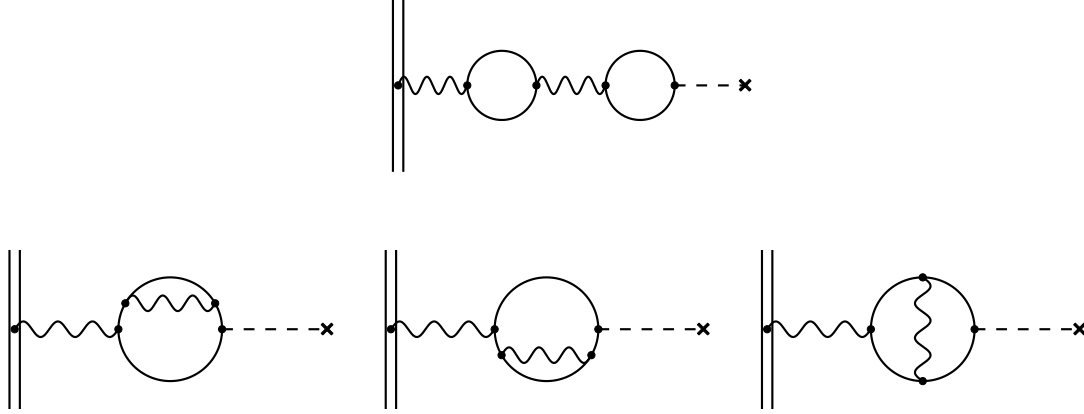


Figure 3.12.3: Källén-Sabry processes diagrams
Higher-order VP processes: $\alpha^2 (\alpha Z)$

large distances [122, eq.(34)]. For extra details and general discussions, the reader may consult the report prepared by Mohr *et al.* [7].

3.12.2 Self-energy effective potentials

The self-energy process describes an electron which emits and absorbs a virtual photon. Contrary to the vacuum polarization effect, the self-energy is non-local, which is the origin of its complexity. If we thus imagine a potential V^{SE} associated with the self-energy effect, acting on a Dirac electron with energy E and time-independent spinor ψ , the energy-shift this electron will feel is given by the following non-local integral:

$$\Delta E = -e \int d^3x \int d^3y \psi^\dagger(\mathbf{y}) V^{\text{SE}}(\mathbf{y}, \mathbf{x}) \psi(\mathbf{x}). \quad (3.12.2)$$

A detailed derivation of this “exact” energy-shift was first provided by Mohr [113], and later in a work of Indelicato and Mohr [123]. Due to the great complication that arise when attempting to obtain the effective potentials $V^{\text{SE}}(\mathbf{y}, \mathbf{x})$, several works proposed to use simple potentials forms that are parameterized to fit the exact energy-shifts that are obtained by expensive computations using complicated formulas. We shall now list these main effective potentials.

3.12.2.1 Pyykkö and Zhao potentials

In [124], Pyykkö and Zhao provide a review of the earlier attempts to construct effective potentials associated with the self-energy process, and propose a simple local effective-potential, of the following form:

$$V^{\text{SE}}(r) = B e^{-\beta r^2}, \quad (3.12.3)$$

for numerical practicality. The parameters B and β are functions of the nuclear charge Z , and are chosen to reproduce the “exact”:

- self-energy-shift for the 2s states of the hydrogen-like systems, taken from [125, 126].
- M1 hyperfine splitting for hydrogen-like [127] and lithium-like systems [128].

They then test their potential by calculating the two above quantities for some ns shell electrons with $n > 1$.

3.12.2.2 Flambaum and Ginges potentials

Flambaum and Ginges in [129] potentials. These authors consider the two potentials associated with the vertex correction process, of order $\alpha(\alpha Z)^1$, related to the (total) bound state self-energy of order $\alpha(\alpha Z)^{n \geq 1}$ by [130, eq.(9)]. This self-energy potential has two contributions:

- A magnetic term:

$$V_{\text{mag}}^{\text{SE}}(r) = \frac{\alpha \hbar}{4\pi m c} i \boldsymbol{\gamma} \cdot \boldsymbol{\nabla} \left[\phi^{\text{nuc}}(r) \left(\int_1^\infty dt \frac{e^{-\frac{2mc}{\hbar} tr}}{t^2 \sqrt{t^2 - 1}} - 1 \right) \right], \quad (3.12.4)$$

which gives the first order correction to the magnetic moment: the anomalous magnetic moment of the electron, first calculated by Schwinger. See, for instance, Mandl and Shaw [93, section 10.5]. $\phi^{\text{nuc}}(r)$ is the Coulombic nuclear potential.

- An electric term:

$$V_{\text{HF}}^{\text{SE}}(r) = -\frac{\alpha}{\pi} \phi^{\text{nuc}}(r) \int_1^\infty \frac{1}{\sqrt{t^2 - 1}} \left[\left(1 - \frac{1}{2t^2} \right) \left[\ln(t^2 - 1) + \ln \left(4 \frac{m^2 c^2}{\lambda^2} \right) \right] - \frac{3}{2} + \frac{1}{t^2} \right] e^{-\frac{2mc}{\hbar} tr}, \quad (3.12.5)$$

This term is called the high frequency term, because it contains a parameter λ which appears in the expression of Berestetskii *et al.* [105, eq.(117.10)]. See also Greiner and Reinhardt [8, eq.(5.91)], Itzykson and Zuber [43, eq.(7.45)], and Peskin and Schroeder [99, pages 195,196]. This parameter can be understood as a small fictitious photon mass, which needs to be plugged in the photon propagator denominator in order to make the divergent momentum-space integral (infrared divergence), associated with the vertex correction, convergent. Since Nature should be (is) independent of the man-made parameters, this photon mass should be ultimately taken to $\lambda \rightarrow 0$. Clearly, in this limit, the second logarithmic term of the last expression diverges, and we thus lose the low frequency contributions, from very small λ . To overcome this problem, Flambaum and Ginges introduced a low frequency fitting-potential:

$$V_{\text{LF}}^{\text{SE}}(r) = -\frac{B(Z)}{e_p} Z^4 \alpha^5 m c^2 e^{-Zr/a_B}, \quad (3.12.6)$$

where a_B is the Bohr radius, and e_p is the proton charge, and $B(Z)$ is a fitting function, optimized to reproduce the high p states self-energy-shifts (low frequencies = large distances = large quantum number, roughly speaking), which is missed by the HF term. In addition, for very small r , the integral of the HF term diverges (the exponential damper of the integral eq.(3.12.5) vanishes), and this motivated Flambaum and Ginges to modify the HF potential to:

$$V_{\text{HF}}^{\text{SE}}(r) = -A(Z, r) \frac{\alpha}{\pi} \phi^{\text{nuc}}(r) \int_1^\infty \frac{1}{\sqrt{t^2 - 1}} \left[\left(1 - \frac{1}{2t^2} \right) \left[\ln(t^2 - 1) + 4 \ln \left(\frac{1}{\alpha Z} + 0.5 \right) \right] - \frac{3}{2} + \frac{1}{t^2} \right] e^{-\frac{2mc}{\hbar} tr}, \quad (3.12.7)$$

where $A(Z, r)$ is a fitting function, introduced in order reproduce the radiative shifts associated with the high s states. Later, Thierfelder and Schwerdtfeger modified this function to $A_n(Z, r)$ [131, eq.(13)]: a principal quantum number n dependent fitting. These potentials with $A_n(Z, r)$ instead of $A(Z, r)$ were used by Pašteka *et al.* to calculate the self-energy corrections to the electron affinity and ionization potential of Gold [132]. We should finally note that this problematic infrared divergence disappears once the zero-potential self-energy contribution: of order $\alpha(\alpha Z)^0$ is added, as indicated by Snyderman [133, page 59].

3.12.2.3 Shabaev, Tupitsyn, and Yerokhin potentials

In [134], Shabaev *et al.* give the exact self-energy potential in their eq.(8):

$$V^{\text{SE}}(r, r', \hat{\mathbf{x}}, \hat{\mathbf{x}}'), \quad (3.12.8)$$

which is complicated to include in practical calculations. To overcome this difficulty, they split the self-energy potential into a local and a non-local part:

$$V^{\text{SE}}(r, r', \hat{\mathbf{x}}, \hat{\mathbf{x}}') = V_{\text{local}}^{\text{SE}}(r, r, \hat{\mathbf{x}}, \hat{\mathbf{x}}') + \{V^{\text{SE}} - V_{\text{local}}^{\text{SE}}\}_{\text{non-local}}. \quad (3.12.9)$$

- The local term $V_{\text{local}}^{\text{SE}}$ is simply chosen to be “local”, within a Compton wavelength λ_c :

$$V_{\text{local}}^{\text{SE}} = \sum_{\kappa} V_{\text{local}, \kappa}^{\text{SE}}(r) P_{\kappa}(\hat{\mathbf{x}}, \hat{\mathbf{x}}') \quad V_{\text{local}, \kappa}^{\text{SE}}(r) = A_{\kappa} e^{-\frac{r}{\lambda_c}}, \quad (3.12.10)$$

where P_{κ} is given by:

$$P_{\kappa} = \begin{bmatrix} G_{\kappa} & 0 \\ 0 & G_{-\kappa} \end{bmatrix}, \quad G_{\kappa} = \sum_{m_j} \Omega_{\kappa, m_j}(\hat{\mathbf{x}}) \Omega_{\kappa, m_j}^{\dagger}(\hat{\mathbf{x}}'). \quad (3.12.11)$$

The angular localization is to be compared with the relation [135, eq.(A.6)]. They then choose the coefficients A_{κ} associated with certain κ , such that the corresponding expectation value:

$$-e \int d^3x \int d^3x' \psi_{\kappa, \text{lowest}}^{\dagger}(\mathbf{x}) V_{\text{local}, \kappa}^{\text{SE}}(r, r, \hat{\mathbf{x}}, \hat{\mathbf{x}}') \psi_{\kappa, \text{lowest}}(\mathbf{x}') = \Delta E_{\kappa, \text{lowest}}^{\text{SE}}, \quad (3.12.12)$$

with respect to the lowest energy hydrogen-like state $\psi_{\kappa, \text{lowest}}$ of the radial Dirac κ -problem, reproduces the exact self-energy energy-shift $\Delta E_{\kappa, \text{lowest}}^{\text{SE}}$ associated with this state. They justify this step by the fact that in the non-relativistic self-energy is a local effect, as seen in the work of Bethe [110, eq.(9)].

- The remaining non-local $\{V^{\text{SE}} - V_{\text{local}}^{\text{SE}}\}_{\text{non-local}}$ term of eq.(3.12.9), is represented by the following finite-dimensional matrix operator:

$$\sum_{j, k}^n |\phi_j\rangle B_{jk} \langle \phi_k|, \quad (3.12.13)$$

where ϕ_j are hydrogen wavefunctions multiplied by a localization faction. Finally, the B_{jk} matrix elements should be related to the ones of the exact self-energy operator V^{SE} by:

$$\sum_{j, k}^n \langle \psi_i | |\phi_j\rangle B_{jk} \langle \phi_k | |\psi_l\rangle = \langle \psi_i | \{V^{\text{SE}} - V_{\text{local}}^{\text{SE}}\}_{\text{non-local}} | \psi_l\rangle, \quad (3.12.14)$$

which, under some restrictions, is more practical to evaluate (see the corresponding reference).

Our collaborator, Ayaki Sunaga has coded the Pyykkö and Zhao potential, the Flambaum and Ginges electric and magnetic potentials, in addition to the Uehling potential in the DIRAC code [136]. Implementation details and numerical computations associated with these self-energy effective potentials are presented in [137]. My contribution to this project was to provide the key steps in deriving of these effective potentials, starting from the \mathcal{S} -matrix formalism.

For a general view on the electron structure theory with quantum electrodynamic effects, in quantum chemistry, the reader may consult the work of Schwerdtfeger *et al.* [138], Pyykko [139], Kutzelnigg [140] Dyall *et al.* [141] and many chapters of the book edited by Liu [142].

3.13 Hartree-Fock with QED

At the end of this chapter, I would like to present the main ideas on a project I have worked on during this thesis. This project concerns the inclusion of the QED corrections in the 4-component relativistic Hartree-Fock theory. We shall first start with a brief description on the Hartree-Fock theory before turning to the real problem.

3.13.1 A Hartree-Fock warm-up

Hartree-Fock theory is the simplest approximation of the many-particle (electrons in our case) problem, where the total wavefunction is written as a Slater-determinant, which in turn is composed of single-particle wavefunctions:

$$\Phi_{\alpha_1, \dots, \alpha_n}(\mathbf{x}_1, \dots, \mathbf{x}_n) = \frac{1}{\sqrt{n!}} \begin{vmatrix} \psi_{\alpha_1}(\mathbf{x}_1) & \dots & \psi_{\alpha_1}(\mathbf{x}_n) \\ \vdots & \ddots & \vdots \\ \psi_{\alpha_n}(\mathbf{x}_1) & \dots & \psi_{\alpha_n}(\mathbf{x}_n) \end{vmatrix}. \quad (3.13.1)$$

This is the exact wavefunction for a system containing n non-interacting particles, and is here (in the Hartree-Fock theory) used as a trial function for the interacting problem. In addition, the exchange of any two coordinates $\mathbf{x}_i \leftrightarrow \mathbf{x}_j$ or state labels $\alpha_i \leftrightarrow \alpha_j$ leads to an overall minus sign (spin-statistics theorem), which indicates that this determinant is consistent with the Pauli exclusion principle (which follows from the spin-statistics theorem). The total Hamiltonian we are going to consider is given by the following expression:

$$H(\mathbf{x}_1, \dots, \mathbf{x}_n) = \sum_{i=1}^n h^D(\mathbf{x}_i) + \frac{1}{2} \sum_{i \neq j}^n g(\mathbf{x}_i, \mathbf{x}_j). \quad (3.13.2)$$

The first sum runs over the one-particle Dirac operators (each associated with one particle) given by:

$$h^D(\mathbf{x}) = [c\boldsymbol{\alpha} \cdot \hat{\mathbf{p}}_x + \beta mc^2 - e\varphi(\mathbf{x})], \quad (3.13.3)$$

and the second one contains the two-particle interaction Hamiltonians, given by:

$$g(\mathbf{x}_i, \mathbf{x}_j) = \frac{e^2}{4\pi\epsilon_0 r_{ij}} \alpha^\lambda(i) \alpha_\lambda(j) = \frac{e^2}{4\pi\epsilon_0 r_{ij}} - e^2 \frac{\boldsymbol{\alpha}(i) \cdot \boldsymbol{\alpha}(j)}{4\pi\epsilon_0 r_{ij}}, \quad \text{with } r_{ij} = |\mathbf{x}_i - \mathbf{x}_j|, \quad (3.13.4)$$

and accounts for the Coulomb (charge-charge) and Gaunt (current-current) interactions. The Hartree-Fock energy expression is the expectation value of the total Hamiltonian with respect to the Slater-determinant, and can be written as:

$$E^{\text{HF}} = h_{ii}^D + \frac{1}{2} [g_{ij,ij} - g_{ij,ji}]. \quad (3.13.5)$$

We should note that we are using i, j, k and l for indices that run over positive-energy occupied single-particle states. In the last expression, h_{ii} is the one-particle energy, given by the following integral:

$$h_{ij}^D = \int d\mathbf{x} \psi_i^\dagger(\mathbf{x}) h^D(\mathbf{x}) \psi_j(\mathbf{x}), \quad (3.13.6)$$

and the remaining two terms: $g_{ij,ij}$ and $g_{ij,ji}$ are the direct (Hartree) and exchange (Fock) two-electron integrals, respectively. This two-electron integral is given by:

$$\begin{aligned} g_{ij,kl} &= e^2 \int d\mathbf{x}_1 \int d\mathbf{x}_2 \psi_i^\dagger(\mathbf{x}_1) \psi_j^\dagger(\mathbf{x}_2) \frac{\alpha^\lambda(1) \alpha_\lambda(2)}{4\pi\epsilon_0 r_{12}} \psi_k(\mathbf{x}_1) \psi_l(\mathbf{x}_2) \\ &= e^2 \int d\mathbf{x}_1 \int d\mathbf{x}_2 \psi_i^\dagger(\mathbf{x}_1) \alpha^\lambda \psi_k(\mathbf{x}_1) \frac{1}{4\pi\epsilon_0 r_{12}} \psi_j^\dagger(\mathbf{x}_2) \alpha_\lambda \psi_l(\mathbf{x}_2). \end{aligned} \quad (3.13.7)$$

We now expand the Dirac solutions in a finite basis set:

$$\psi_i(\mathbf{x}) = c_{\mu,i} \chi_\mu(\mathbf{x}), \quad (3.13.8)$$

where $\{\chi_\mu\}_{\mu=1}^m$ is the full set of basis functions and $c_{\mu,i}$ are the corresponding coefficients. We note that Greek indices are used for basis set expansion. Using the last formula, the Hartree-Fock energy expression of eq.(3.13.5) becomes:

$$\begin{aligned} E^{\text{HF}} &= D_{\nu\mu}^{\text{HF}} h_{\mu\nu}^D && \text{HF1} \\ &+ \frac{1}{2} D_{\nu\mu}^{\text{HF}} D_{\theta\sigma}^{\text{HF}} g_{\mu\sigma,\nu\theta} && \text{HF2-Direct} \\ &- \frac{1}{2} D_{\nu\mu}^{\text{HF}} D_{\theta\sigma}^{\text{HF}} g_{\mu\sigma,\theta\nu} && \text{HF2-Exchange} \end{aligned} \quad (3.13.9)$$

where $D_{\nu\mu}^{\text{HF}}$ is the Hartree-Fock (atomic orbital) density-matrix matrix element:

$$D_{\nu\mu}^{\text{HF}} = c_{\nu,i} c_{\mu,i}^*, \quad (3.13.10)$$

which runs over all positive-energy occupied solutions.

3.13.2 Hartree-Fock with QED: The approach of Saue

The theory behind this problem is provided in a chapter written by Saue and Visscher in [143, section 2.2]. In his derivation, Saue arrives to a conclusion that in order to include QED effects in the Hartree-Fock theory one must perform the following replacement of the atomic-orbital (positive-energy occupied single-particle states) density matrix:

$$D_{\nu\mu}^{\text{HF}} \rightarrow D_{\nu\mu}^{\text{HF}} + D_{\nu\mu}^{\text{QED}}, \quad (3.13.11)$$

where $D_{\nu\mu}^{\text{QED}}$ can be written as:

$$D_{\nu\mu}^{\text{QED}} = \frac{1}{2} \left[\sum_{E_p > 0} c_{\nu,p} c_{\mu,p}^* - \sum_{E_p < 0} c_{\nu,p} c_{\mu,p}^* \right]. \quad (3.13.12)$$

The first sum runs over all positive-energy solutions, both occupied and non-occupied ones, while the second runs over the negative-energy ones. This density matrix modification leads to a modification of the Hartree-Fock energy:

$$E^{\text{HF}} \rightarrow E^{\text{HF}} + E^{\text{QED}}, \quad (3.13.13)$$

where the additional term E^{QED} was found to be:

$$\begin{aligned}
E^{\text{QED}} &= D_{\nu\mu}^{\text{QED}} h_{\mu\nu}^D && \text{1e} \\
&+ D_{\nu\mu}^{\text{HF}} D_{\theta\sigma}^{\text{QED}} g_{\mu\sigma,\nu\theta} && \text{VP} \\
&- D_{\nu\mu}^{\text{HF}} D_{\theta\sigma}^{\text{QED}} g_{\mu\sigma,\theta\nu} && \text{SE} \\
&+ \frac{1}{2} D_{\nu\mu}^{\text{QED}} D_{\theta\sigma}^{\text{QED}} g_{\mu\sigma,\nu\theta} && \text{V2} \\
&- \frac{1}{2} D_{\nu\mu}^{\text{QED}} D_{\theta\sigma}^{\text{QED}} g_{\mu\sigma,\theta\nu} && \text{V1}
\end{aligned} \tag{3.13.14}$$

The first term represents the one-particle energy of the vacuum electrons. The remaining four terms can be shown to be attributed to the four diagrams presented in figs. 3.10.1b to 3.10.1e, with a small difference we shall discuss. The reader should note that the second and third terms, with $D_{\nu\mu}^{\text{HF}} D_{\theta\sigma}^{\text{QED}}$, describe the interaction between the Hartree-Fock atomic electrons and the QED vacuum. Furthermore, the direct-term $D_{\nu\mu}^{\text{HF}} D_{\theta\sigma}^{\text{QED}} g_{\mu\sigma,\nu\theta}$ represents the vacuum polarization energy-shift of fig. 3.10.1b, while the exchange-term $-D_{\nu\mu}^{\text{HF}} D_{\theta\sigma}^{\text{QED}} g_{\mu\sigma,\theta\nu}$ is associated with the self-energy process, of fig. 3.10.1c. Finally, we have found last the last two-terms: $D_{\nu\mu}^{\text{QED}} D_{\theta\sigma}^{\text{QED}} [g_{\mu\sigma,\nu\theta} - g_{\mu\sigma,\theta\nu}]$ are the contributions attributed to the disconnected vacuum diagrams, presented in fig. 3.10.1d.

This machinery was coded by Saue in the relativistic DIRAC code [136]. We have performed multiple calculations using this code and observed that the QED energy given in the last expression does not converge with an increasing Gaussian basis set size. We have thus decided to address the problem from a different angle, through the following steps:

1. Deriving the $\mathcal{S}^{(2)}$ energy-shifts, as we have done in this thesis.
2. Combining all contributions in a single energy expression and compare the two approaches.

These two points are the topic of the next last section of this chapter.

3.13.3 Hartree-Fock with QED: The new approach

In this section, we are going to make use of the QED energy-shifts associated with the three physical processes of the second-order $\mathcal{S}^{(2)}$ -matrix, which we have derived in the current chapter section 3.10. These energy-shifts are given in eqs.(3.10.52,3.10.60 and 3.10.68). If we now combine these three-terms with the one-particle energy, we get the following expression:

	Terms
$E = \int d\mathbf{x} \psi_i^\dagger(\mathbf{x}) h^D(\mathbf{x}) \psi_i(\mathbf{x})$	a
$+ \frac{e^2}{2} \int d\mathbf{x}_1 \int d\mathbf{x}_2 \psi_i^\dagger(\mathbf{x}_1) \alpha^\lambda \psi_i(\mathbf{x}_1) \frac{1}{4\pi\epsilon_0 r_{12}} \psi_j^\dagger(\mathbf{x}_2) \alpha_\lambda \psi_j(\mathbf{x}_2)$	b
$- \frac{e^2}{2} \int d\mathbf{x}_1 \int d\mathbf{x}_2 \psi_i^\dagger(\mathbf{x}_1) \alpha^\lambda \psi_j(\mathbf{x}_1) \frac{1}{4\pi\epsilon_0 r_{12}} \cos\left(\frac{1}{c\hbar} E_i - E_j r_{12}\right) \psi_j^\dagger(\mathbf{x}_2) \alpha_\lambda \psi_i(\mathbf{x}_2)$	c
$- i\hbar e^2 \int d\mathbf{x}_1 \int d\mathbf{x}_2 \psi_i^\dagger(\mathbf{x}_1) \alpha^\lambda \psi_i(\mathbf{x}_1) \frac{1}{4\pi\epsilon_0 r_{12}} \text{Tr} [\gamma_0 S^F(x_2, x_2)]$	d
$+ e^2 \Re \left[\int d\mathbf{x}_1 \int d\mathbf{x}_2 \frac{1}{2\pi i} \int_{C_F} dz \psi_i^\dagger(\mathbf{x}_2) \alpha^\lambda G(\mathbf{x}_2, \mathbf{x}_1; z) \alpha_\lambda \psi_i(\mathbf{x}_1) \frac{e^{+\frac{i}{c\hbar} r_{12} \sqrt{(z-E_i)^2 + i\epsilon}}}{4\pi\epsilon_0 r_{12}} \right]$	e

(3.13.15)

The labeled terms are described in the following list, in addition to a comparison with the associated terms obtained by Saue:

- a The one-electron part: summed of all individual one-electron energies.
- b The direct Hartree term: found in the usual 4-component Hartree-Fock theory: the HF2-Direct term given in eq.(3.13.9).
- c The exchange Fock term: found in the usual 4-component Hartree-Fock theory. Notice that this term contains a retardation function: $\cos\left(\frac{1}{c\hbar}|E_i - E_j|r_{12}\right)$, which vanishes in the non-relativistic limit $c \rightarrow +\infty$. This cosine term is missing in the HF2-Exchange term of eq.(3.13.9), since in the referring derivation, the two-particle Hamiltonian does not contain the retardation exponent. This exponent comes from the Feynman gauge photon propagator, as noted in [7, eq.(461)], [15, eq.(F.67)], and seen in the current chapter.
- d The vacuum-polarization energy-shift: This is a real valued expression, and it coincides with the VP term obtained by Saue in eq.(3.13.14): $D_{\nu\mu}^{\text{HF}} D_{\theta\sigma}^{\text{QED}} g_{\mu\sigma,\nu\theta}$. This can be seen after writing the propagator in terms of the Dirac Green's function, and then writing the latter quantity in its spectral form, and evaluate the energy integral.
- e The self-energy energy-shift: This expression becomes the term $-D_{\nu\mu}^{\text{HF}} D_{\theta\sigma}^{\text{QED}} g_{\mu\sigma,\theta\nu}$ of eq.(3.13.14) once we:
 - 1) Eliminate the exponential function (non-relativistic limit).
 - 2) Use the spectral decomposition of the Green's function (eq.(3.9.38)).
 - 3) Evaluate the energy contour integration using the result of eq.(F.6.18).

Finally, we note that the only difference between our \mathcal{S} -matrix approach and the previous results of Saue is the absence of the retardation effect in all exchange terms: the exchange part of the electron-electron interaction term, the self-energy term, and the exchange vacuum diagram (that was already discarded from consideration).

A similar expression is found in the work of Greiner *et al.* [106, eq.(16.19)]. The self-consistent (Hartree-Fock) equation containing the single-photon exchange contribution can be found in the work of Plunien and Soff [144, eq.(18)], Rafelski *et al.* [145, eq.(26)] as well as Reinhardt [146, eqs.(4,6)] *et al.* in [147, eq.(4)]. An important reference to consider, in this context, is Gomboroff and Tolmachev [148], where different manipulations of different electron propagators are made, with connections to the Hartree-Fock theory. See, for instance, the self-consistent equation of [148, eq.(3.11)], which is contains both vacuum-polarization and self-energy effects.

Our discussion will end here, but this problem merits a detailed investigation. One must keep in mind that the vacuum polarization and the self-energy terms are both divergent, in the 1-potential term [7, 5], and 0-&1-potential terms [149, 133], respectively. In momentum-space, these divergences come from integrating over infinite momenta, while in the real-space, it comes from integration points where space-time integration points coincide. The expansion of the Bound Green's function in terms of the free ones adds more denominators to the integrand, and will as a result, reduce the superficial degree of divergence of the initially divergent integral. This is the reason why higher-order terms do not diverge.

The problem of divergences was solved a long time ago, using regularization and renormalization manipulations with pen and paper, and sometimes through some computational tricks. The real challenge now is to translate this machinery to our context, i.e., to be able to cure the QED divergences encountered in the finite basis set context. As far as we know, this problem has not yet been solved.

At the very last chapter of this thesis, we shall give few words on how we shall proceed. The next chapter is going to concern the vacuum polarization process only. We shall discuss it in great details and show how to numerically evaluate it in the finite basis context. Furthermore, we shall use our previous results on the discrete symmetries of the Dirac equation to simplify exact and numerical encountered expressions.

Chapter 4

Vacuum polarization

When you look at a vacuum in a quantum theory of fields, it isn't exactly nothing.

Peter Higgs

This chapter will discuss the vacuum polarization density in great detail. The first part will concern the mathematical quantities and manipulations associated with the different definitions of this density. Furthermore, the results on the discrete symmetries of the Dirac equation, which we have derived and discussed in chapter 2, are going to be used here to prove that:

1. The vacuum polarization density vanishes in the free particle problem (by \mathcal{C} -symmetry).
2. The vacuum polarization current (vector-components) vanishes in the purely scalar external potential case (by \mathcal{T} -symmetry).

In addition, we shall focus on the radial (atomic) problem and carefully present how one can construct this density in the framework of finite basis approximation (of the radial Dirac equation).

Next, we shall use the results of the first (theoretical) part of the chapter in attacking the numerical problem and present different numerical results with a detailed discussion. The most important result of this chapter will be to show how the consideration of the \mathcal{C} -symmetry (in the finite basis set) will significantly improve the quality of our numerical vacuum polarization densities. This consideration will eventually lead to physically accepted solutions: consistent with what we know from the exact theory. On the other hand, we shall see that ignoring this \mathcal{C} -symmetry, which unfortunately do happen in most of the conventional relativistic basis set calculations, will lead to problematic non-physical results that diverge from the physical problem.

4.1 Introduction

Hopefully, the vacuum polarization effect has (contrary to the self-energy), an intuitive physical picture that can be expressed as follows:

The presence of a charged particle in space polarizes (interacts through a photon with) the boiling vacuum soup, in which electron-positron pair bubbles are spontaneously generated from vacuum. This process gives rise to a vacuum charge density that eventually integrates to zero in the weak-field case [106, section 1.1]. Furthermore, the motion of

the polarizing charge will generate a corresponding vacuum polarization current density. This outside cloud will eventually affect its creator, by a self-interaction process, known as the vacuum polarization.

This process is sometimes referred to as the “photon self-energy” since a photon that describes the interaction between two charges creates the electron-positron bubble for a short time, then this pair will annihilate, and recreate a photon. Clearly, the absence of any inducer will not generate any polarization effects, since all individual polarizations will cancel each-others (on average), resulting in a zero vacuum polarization density everywhere.

Strictly speaking the vacuum polarization current J_μ^{VP} is given by the vacuum expectation value of the current operator \hat{j}_μ :

$$J_\mu^{\text{VP}}(x) = \frac{ec}{2} \left\langle 0_e \left| \hat{j}_\mu(x) \right| 0_e \right\rangle \quad (4.1.1)$$

$$\hat{j}_\mu(x) = \frac{ec}{2} [\Psi_\alpha(x), \bar{\Psi}_\beta(\text{SeeSchwinger})] (\gamma_\mu)_{\beta\alpha}. \quad (4.1.2)$$

See Schwinger [150, eq.(1.69)]. We first expand the field operators (in the context of hole theory) in the basis of Dirac’s solutions:

$$\Psi_\alpha(x) = \sum_i c_i \psi_{i,\alpha}(x), \quad (4.1.3)$$

where the annihilation operator c_i runs over all solutions. In the context of the Dirac hole theory, this summation can be split into two energy-signs sums:

$$\Psi_\alpha(x) = \sum_{E_i > 0} a_i \psi_{i,\alpha}(x) + \sum_{E_i < 0} b_i^\dagger \psi_{i,\alpha}(x), \quad (4.1.4)$$

where a_i annihilates positive-energy electrons, b_i creates a positive-energy positron (as done by Mohr *et al.* [7, eq.(3)]), and the quantity $\psi_{i,\alpha}$, stands for the α -th component of the i ’th Dirac solution. Note: the electron field operator was already introduced in section 3.5.2. Eight terms will appear in our current expression, where using eq.(3.5.12), one can see that only two of them will survive the vacuum expectation value:

$$+\frac{ec}{2} \sum_{E_i, E_j > 0} [\psi_i]_\alpha (\gamma_\mu)_{\beta\alpha} [\bar{\psi}_j]_\beta a_i a_j^\dagger \quad \text{and} \quad -\frac{ec}{2} \sum_{E_i, E_j < 0} [\bar{\psi}_i]_\beta (\gamma_\mu)_{\beta\alpha} [\psi_j]_\alpha b_i b_j^\dagger, \quad (4.1.5)$$

and lead to the following vacuum polarization current expression:

$$J_\mu^{\text{VP}}(x) = \frac{ec}{2} \left[\sum_{E_i > 0} \bar{\psi}_i(x) \gamma_\mu \psi_i(x) - \sum_{E_i < 0} \bar{\psi}_i(x) \gamma_\mu \psi_i(x) \right], \quad (4.1.6)$$

as a difference between positive- and negative-energy charge currents. This expression can be linked to the Feynman propagator by:

$$J_\mu^{\text{VP}}(x) = i\hbar ec \text{Tr} [\gamma_\mu S_A^F(x, y)]_{y \rightarrow x} \quad (4.1.7)$$

once the expansion expression of the propagator in eq.(3.9.26) is used, in addition to the fact that the Heaviside function has a value of one half for zero argument. We shall next show that in the case where our Dirac Hamiltonian is invariant under time-reversal symmetry, then this expression can be further simplified.

4.2 Vacuum polarization current in the time-reversible problem

When evaluating the energy-shift associated with the vacuum polarization process, Indelicato *et al.* [5, eq.(9) and appendix A] have claimed that the spatial components of the vacuum polarization four-current vanish for a spherically symmetric potential. Other references who noted the vanishing of these components are [118, Section II] and [6, Page 5067]. We shall show, with more straightforward arguments, that this is true for the more general case of a time-independent scalar potential. In the case where the external four-potential is time-independent, the vacuum polarization current also becomes time-independent, and reads:

$$J_{\mu}^{\text{VP}}(\mathbf{x}) = \frac{ec}{2} \left(\sum_{E_i > 0} \psi_i^{\dagger}(\mathbf{x}) \alpha_{\mu} \psi_i(\mathbf{x}) - \sum_{E_i < 0} \psi_i^{\dagger}(\mathbf{x}) \alpha_{\mu} \psi_i(\mathbf{x}) \right). \quad (4.2.1)$$

The reason behind this claim is the following: In the time-independent case, the Dirac solutions can be written as $\psi_i(x) = \psi_i(\mathbf{x}) e^{-\frac{iE_i}{\hbar}t}$ (see section 2.6.3), where the single-particle wavefunction $\psi_i(\mathbf{x})$ and the corresponding energy eigenvalue E_i form a solution of the time-independent Dirac equation:

$$[-i\hbar c \boldsymbol{\alpha} \cdot \boldsymbol{\nabla} + \beta mc^2 - e\varphi(\mathbf{x})] \psi_i(\mathbf{x}) = E_i \psi_i(\mathbf{x}). \quad (4.2.2)$$

As seen in section 2.8.2.1, for the case of the time-independent potential, the time-reversal symmetry gets violated if the vector potential $\mathbf{A}(\mathbf{x})$ does not vanish, which is why we have set it to zero (in the last equation). Furthermore, it can be easily shown that the time-reversed solution, i.e. $\mathcal{T}\psi_i$ satisfies the same equation:

$$[-i\hbar c \boldsymbol{\alpha} \cdot \boldsymbol{\nabla} + \beta mc^2 - e\varphi(\mathbf{x})] \mathcal{T}\psi_i(\mathbf{x}) = E_i \mathcal{T}\psi_i(\mathbf{x}), \quad (4.2.3)$$

with same energy E_i . $\mathcal{T} = UK_0$ was given in eq.(2.8.30). The conclusion is that for every solution $\psi_i(\mathbf{x})$ there exist a solution $\mathcal{T}\psi_i(\mathbf{x})$, and these solutions are time-reversal partners. For every four-current density $J_{\mu,i}$ associated with a solution $\psi_i(\mathbf{x})$:

$$J_{\mu,i}(\mathbf{x}) = -ec\psi_i^{\dagger}(\mathbf{x}) \alpha_{\mu} \psi_i(\mathbf{x}), \quad (4.2.4)$$

there exist another one associated with the time-reversed wavefunction $\mathcal{T}\psi_i$, describing a state with the same energy level E_i :

$$J_{\mu,i}^{\mathcal{T}}(\mathbf{x}) = -ec[\mathcal{T}\psi_i]^{\dagger}(\mathbf{x}) \alpha_{\mu} [\mathcal{T}\psi_i](\mathbf{x}) = -ec\psi_i^{\dagger}(\mathbf{x}) U^t \alpha_{\mu}^t U \psi_i(\mathbf{x}). \quad (4.2.5)$$

Using the following relation:

$$U^t \alpha_{\mu}^t U = \begin{cases} \alpha_{\mu} & \text{if } \mu = 0 \\ -\alpha_{\mu} & \text{if } \mu = 1, 2, 3 \end{cases}, \quad (4.2.6)$$

one comes to a conclusion that the sum of both currents (4.2.4 and 4.2.5), $J_{\mu,i} + J_{\mu,i}^{\mathcal{T}}$ vanishes for vector components $\mu = 1, 2, 3$, leading to a simplified expression of the vacuum polarization current:

$$\begin{aligned} J_0^{\text{VP}}(\mathbf{x}) &= \frac{ec}{2} \left(\sum_{E_i > 0} \psi_i^{\dagger}(\mathbf{x}) \psi_i(\mathbf{x}) - \sum_{E_i < 0} \psi_i^{\dagger}(\mathbf{x}) \psi_i(\mathbf{x}) \right) \\ J_{\mu}^{\text{VP}}(\mathbf{x}) &= 0 \quad \text{for } \mu = 1, 2, 3. \end{aligned} \quad (4.2.7)$$

where only the time component survives. The zeroth component current can be written as $J_0^{\text{VP}}(\mathbf{x}) = c\rho^{\text{VP}}(\mathbf{x})$ (first equation), where $\rho^{\text{VP}}(\mathbf{x})$ is the vacuum polarization charge density:

$$\rho^{\text{VP}}(\mathbf{x}) = \frac{e}{2} \left(\sum_{E_i > 0} \psi_i^\dagger(\mathbf{x}) \psi_i(\mathbf{x}) - \sum_{E_i < 0} \psi_i^\dagger(\mathbf{x}) \psi_i(\mathbf{x}) \right). \quad (4.2.8)$$

The roots of this expression of difference between opposite energy solutions dates back to the work of Dirac where he introduced the density matrix ρ_1 , whose trace gives the last difference. See Dirac [151, Page 152]. In addition, this definition of the vacuum polarization charge density seems to originate from the work of Wichmann and Kroll [118, eq.(2)], and is now be found everywhere.

4.3 Vacuum polarization density in the free-problem

In the absence of an external inducer, the vacuum polarization density must vanish:

$$\rho^{\text{VP}}(\mathbf{x}) = \frac{e}{2} \left[\sum_{E_i > 0} \psi_i^\dagger(\mathbf{x}) \psi_i(\mathbf{x}) - \sum_{E_j < 0} \psi_j^\dagger(\mathbf{x}) \psi_j(\mathbf{x}) \right] = 0. \quad (4.3.1)$$

This can be shown using the charge conjugation symmetry. In a previous section 2.8.1.1, we have studied the charge conjugation symmetry in the time-independent problem and came to a conclusion that in the free particle case (absence of an external potential) a spinor and its charge conjugation partner, are solutions of the same free Dirac equation with opposite energy signs, as seen in eqs.(2.8.12 and 2.8.13). Recall that $\psi_i(\mathbf{x})$ and E_i solve the free time-independent Dirac equation:

$$[c\boldsymbol{\alpha} \cdot \hat{\mathbf{p}} + \beta mc^2] \psi_i(\mathbf{x}) = E_i \psi_i(\mathbf{x}). \quad (4.3.2)$$

Using the equations we have just referred to, we can write the negative-energy product of solutions in the second sum of eq.(4.3.1) as charge conjugated positive-energy product of solutions:

$$\sum_{E_j < 0} \psi_j^\dagger(\mathbf{x}) \psi_j(\mathbf{x}) = \sum_{E_j > 0} [\mathcal{C}\psi_j(\mathbf{x})]^\dagger \mathcal{C}\psi_j(\mathbf{x}). \quad (4.3.3)$$

In addition, using the charge conjugation operation (given in eq.(2.8.8)), we can write the last product as:

$$[\mathcal{C}\psi_j(\mathbf{x})]^\dagger \mathcal{C}\psi_j(\mathbf{x}) = [\gamma^2 \psi_j^*(\mathbf{x})]^\dagger \gamma^2 \psi_j^*(\mathbf{x}) = \psi_j^t(\mathbf{x}) \psi_j^*(\mathbf{x}) = \psi_j^\dagger(\mathbf{x}) \psi_j(\mathbf{x}), \quad (4.3.4)$$

which shows that the the probability density of a free-particle solution is unchanged under charge conjugation (energy-sign flipping). Using this last result, our vacuum polarization density reduces to:

$$\rho^{\text{VP}}(\mathbf{x}) = \frac{e}{2} \left(\sum_{E_i > 0} \psi_i^\dagger(\mathbf{x}) \psi_i(\mathbf{x}) - \sum_{E_j > 0} \psi_j^\dagger(\mathbf{x}) \psi_j(\mathbf{x}) \right) = 0, \quad (4.3.5)$$

since every element of one sum, will be canceled by a same term coming from the second sum, but with a minus sign.

4.4 Vacuum polarization density in the atomic problem

We now restrict ourselves to the radial scalar potential, i.e. $\phi(\mathbf{x}) = \phi(r)$ (with $r = |\mathbf{x}|$). We have seen in section 2.7 that the Dirac solutions can, in this case, be written as:

$$\psi_{n,\kappa,m_j}(\mathbf{x}) = \begin{bmatrix} R_{n,\kappa}^L(r) \Omega_{\kappa,m_j}(\hat{\mathbf{x}}) \\ i R_{n,\kappa}^S(r) \Omega_{-\kappa,m_j}(\hat{\mathbf{x}}) \end{bmatrix}. \quad (4.4.1)$$

Since the Hamiltonian is now time-reversible, we are allowed to use the result of the previous section (eq.(4.2.7)), and write the vacuum polarization density as [118, eq.(2)]:

$$\rho^{\text{VP}}(\mathbf{x}) = \frac{e}{2} \sum_{n,\kappa,m_j} \text{sgn}(E_{n,\kappa}) \psi_{n,\kappa,m_j}^\dagger(\mathbf{x}) \psi_{n,\kappa,m_j}(\mathbf{x}); \quad \text{sgn}(E_{n,\kappa}) = \frac{E_{n,\kappa}}{|E_{n,\kappa}|}. \quad (4.4.2)$$

In this expression, the sum runs over quantum numbers instead of the previous “vague” index i . The reader should also note that this sum is justified when running over bound-state (discrete) solutions. For continuum states, energy is no longer quantized (the spectrum is no longer discrete), and thus, the sum over n is to be replaced by an integral (for each continuum) over the continuous energy variable. The individual terms of the previous summation read:

$$\psi_{n,\kappa,m_j}^\dagger(\mathbf{x}) \psi_{n,\kappa,m_j}(\mathbf{x}) = R_{n,\kappa}^L R_{n,\kappa}^L \Omega_{\kappa,m_j}^\dagger \Omega_{\kappa,m_j} + R_{n,\kappa}^S R_{n,\kappa}^S \Omega_{-\kappa,m_j}^\dagger \Omega_{-\kappa,m_j}. \quad (4.4.3)$$

The summation over outer-products of spherical spinors is given in eq.(D.4.88):

$$\sum_{m_j} \Omega_{\kappa,m_j}(\hat{\mathbf{x}}) \Omega_{\kappa,m_j}^\dagger(\hat{\mathbf{y}}) = \frac{|\kappa|}{4\pi} P_\ell(\hat{\mathbf{x}} \cdot \hat{\mathbf{y}}) \mathbb{1}_2 + \text{sgn}(\kappa) \frac{i}{4\pi} P'_\ell(\hat{\mathbf{x}} \cdot \hat{\mathbf{y}}) (\hat{\mathbf{x}} \times \hat{\mathbf{y}}) \cdot \boldsymbol{\sigma}, \quad (4.4.4)$$

where ℓ is the orbital (azimuthal) quantum number, related to κ by: $\ell = |\kappa + \frac{1}{2}| - \frac{1}{2}$. In the vacuum polarization density expression we have $\hat{\mathbf{y}} = \hat{\mathbf{x}}$, and the second term of the last expression will thus vanishes. In addition, using $P_\ell(1) = 1$, as seen in eq.(D.4.84). As a result, the last equation simplifies to:

$$\sum_{m_j} \Omega_{\kappa,m_j}(\hat{\mathbf{x}}) \Omega_{\kappa,m_j}^\dagger(\hat{\mathbf{x}}) = \frac{|\kappa|}{4\pi} \mathbb{1}_2, \quad (4.4.5)$$

which simplifies the radial vacuum polarization density of eq.(4.4.2) to:

$$\rho^{\text{VP}}(\mathbf{x}) = \frac{e}{4\pi} \sum_{n,\kappa} |\kappa| \text{sgn}(E_{n,\kappa}) \left[\left(R_{n,\kappa}^L(r) \right)^2 + \left(R_{n,\kappa}^S(r) \right)^2 \right]. \quad (4.4.6)$$

This formula can be found in the work of Wichmann and Kroll [118, eqs.(6-8)]. Other slightly different formulas are found in Soff and Mohr [6, eq.(20)], Gyulassy [152, eq.(19)] and Mohr *et al.* [7, eq.(232)], where one only needs to evaluate the integral along the Feynman path, which acts on the Green’s function denominator (see, for instance, eq.(3.9.38)):

$$\int_{C_F} \frac{dz}{E_i - z} = i\pi \text{sgn}(E_i). \quad (4.4.7)$$

The evaluation of this integral is presented in section F.6.1. Finally, this density can be written as a sum over κ -component vacuum polarization densities:

$$\rho^{\text{VP}}(\mathbf{x}) = \sum_{\kappa=\pm 1, \pm 2, \dots} \rho_\kappa^{\text{VP}}(\mathbf{x}), \quad (4.4.8)$$

where $\rho_\kappa^{\text{VP}}(\mathbf{x})$ is given by the following sum:

$$\rho_\kappa^{\text{VP}}(\mathbf{x}) = \frac{e|\kappa|}{4\pi} \sum_n \text{sgn}(E_{n,\kappa}) \left[(R_{n,\kappa}^L(r))^2 + (R_{n,\kappa}^S(r))^2 \right]. \quad (4.4.9)$$

This formula is going to be used in the numerical evaluation of the vacuum polarization density (in a finite basis), where the sum n will run over all the numerical solutions.

4.4.1 The free spherical vacuum polarization density

In a previous section 4.3, we used the charge conjugation symmetry to show that the vacuum polarization density should vanish in the free-particle problem (in the absence of an external potential). Furthermore, in section 2.8.1.2, we studied this symmetry in the spherical free problem. After combining these results, we shall show that in the free spherical problem, the vacuum polarization density vanishes due to the cancellation between opposite energy- and κ -sign contributions. We define the individual vacuum polarization density, associated with a solution of some specific κ and E_n as:

$$\rho_\kappa^{\text{VP}}(\mathbf{x}, E_n) = \frac{e|\kappa|}{4\pi} \text{sgn}(E_n) \left[(R_\kappa^L(r, E_n))^2 + (R_\kappa^S(r, E_n))^2 \right], \quad (4.4.10)$$

where $R_\kappa^L(r, E_n)$ and $R_\kappa^S(r, E_n)$ are the radial solutions of the free Dirac equation, given in eqs.(2.7.55 and 2.7.56). To this density we add the one associated with the opposite energy- and κ -sign:

$$\begin{aligned} & \rho_\kappa(\mathbf{x}, E_n) + \rho_{-\kappa}(\mathbf{x}, -E_n) \\ &= \frac{e|\kappa|}{4\pi} \text{sgn}(E_n) \left[(R_\kappa^L(r, E_n))^2 + (R_\kappa^S(r, E_n))^2 - (R_{-\kappa}^L(r, -E_n))^2 - (R_{-\kappa}^S(r, -E_n))^2 \right]. \end{aligned} \quad (4.4.11)$$

Using the relations of eq.(2.8.19), we find that the third and the fourth terms are equal to the first and second one, respectively, and thus:

$$\rho_\kappa(\mathbf{x}, E_n) + \rho_{-\kappa}(\mathbf{x}, -E_n) = 0. \quad (4.4.12)$$

This result leads to the conclusion that the total vacuum polarization density vanishes in the radial problem due to the cancellation between opposite energy and κ sign contributions. We shall come back to this result once we numerically evaluate the free particle problem.

4.4.2 Expansion of the vacuum polarization density

In this section, we shall only consider the case where the electron orbits in the field of a time-independent scalar potential $\phi(\mathbf{x})$. In this case the vacuum polarization density induced by this potential can be written as eq.(4.2.8):

$$\rho^{\text{VP}}(\mathbf{x}) = \frac{e}{2} \left(\sum_{E_i > 0} \psi_i^\dagger(\mathbf{x}) \psi_i(\mathbf{x}) - \sum_{E_i < 0} \psi_i^\dagger(\mathbf{x}) \psi_i(\mathbf{x}) \right). \quad (4.4.13)$$

This expression can be written in a slightly different way:

$$\rho^{\text{VP}}(\mathbf{x}) = \frac{e}{2\pi i} \int_{C_F} dz \sum_i \frac{\psi_i^\dagger(\mathbf{x}) \psi_i(\mathbf{x})}{E_i - z}, \quad (4.4.14)$$

where the contour integral is made along the Feynman path C_F , which goes below the negative-energy poles, and above the positive-energy ones. The reader may check section F.6.1 for this integral. The integrand of the last equation is simply the trace of the Green's function G_ϕ , given in eq.(3.9.38), which satisfies the following eq.(3.9.39):

$$[-i\hbar c\boldsymbol{\alpha} \cdot \nabla_x - e\phi(\mathbf{x}) + \beta mc^2 - z] G_\phi(\mathbf{x}, \mathbf{y}; z) = \mathbb{1}_4 \delta(\mathbf{x} - \mathbf{y}). \quad (4.4.15)$$

Using the expansion of eq.(3.9.52), this Green's function can be written as:

$$\begin{aligned} G_\phi(\mathbf{x}, \mathbf{y}; z) &= G_0(\mathbf{x}, \mathbf{y}; z) + e \int d\mathbf{w} G_0(\mathbf{x}, \mathbf{w}; z) \phi(\mathbf{w}) G_0(\mathbf{w}, \mathbf{y}; z) \\ &+ e^2 \int d\mathbf{w} \int d\mathbf{v} G_0(\mathbf{x}, \mathbf{w}; z) \phi(\mathbf{w}) G_0(\mathbf{w}, \mathbf{v}; z) \phi(\mathbf{v}) G_0(\mathbf{v}, \mathbf{y}; z) + \mathcal{O}(e\phi)^3. \end{aligned} \quad (4.4.16)$$

Our vacuum polarization density can be thus expanded in powers of the external scalar potential as:

$$\rho^{\text{VP}}(\mathbf{x}) = \rho^0(\mathbf{x}) + \rho^1(\mathbf{x}) + \rho^2(\mathbf{x}) + \mathcal{O}(e\phi)^3. \quad (4.4.17)$$

This last expression contains:

1. The zero-potential density:

$$\rho^0(\mathbf{x}) = \frac{e}{2\pi i} \int_{C_F} dz \text{Tr} [G_0(\mathbf{x}, \mathbf{x}, z)]. \quad (4.4.18)$$

2. The one-potential density:

$$\rho^1(\mathbf{x}) = \frac{e^2}{2\pi i} \int_{C_F} dz \int d\mathbf{w} G_0(\mathbf{x}, \mathbf{w}; z) \phi(\mathbf{w}) G_0(\mathbf{w}, \mathbf{x}; z). \quad (4.4.19)$$

This term can be called the Uehling density, but the reader should note that this term is divergent, and needs to be regularized and renormalized, so it can become well-defined. See, for instance, [5, section IV.B.].

3. The many-potential density:

$$\rho^{n \geq 2}(\mathbf{x}) = e^2 \int d\mathbf{w} \int d\mathbf{v} \text{Tr} [G_0(\mathbf{x}, \mathbf{w}; z) \phi(\mathbf{w}) G_\phi(\mathbf{w}, \mathbf{v}; z) \phi(\mathbf{v}) G_0(\mathbf{v}, \mathbf{x}; z)], \quad (4.4.20)$$

which accounts for all higher-order powers in the external potential

It should be noted that all terms of even powers of the external potential should vanish. This claim can be proved using charge conjugation symmetry: Furry's theorem, discussed in section 3.11. We shall now impose a further restriction, by consider the radial potential $\phi(\mathbf{x}) = \phi(|\mathbf{x}|)$, and we shall thus discuss the radial Green's function, in the next section, and then come back to the radial vacuum polarization density.

4.4.3 Radial Green's function

In the presence of a radial scalar potential the Dirac spinors can be written as:

$$\psi_{n,\kappa,m_j}(\mathbf{x}) = \begin{bmatrix} R_{n,\kappa}^L(r_x) \Omega_{\kappa,m_j}(\hat{\mathbf{x}}) \\ i R_{n,\kappa}^S(r_x) \Omega_{-\kappa,m_j}(\hat{\mathbf{x}}) \end{bmatrix}. \quad (4.4.21)$$

The Green's function of eq.(3.9.38) which is built out of the solutions of the Dirac equation, can be now written as:

$$G_\phi(\mathbf{x}, \mathbf{y}; z) = \sum_{n, \kappa, m_j} \frac{1}{E_{n, \kappa} - z} \times \begin{bmatrix} G_{n, \kappa}^{LL}(r_x, r_y) \Omega_{\kappa, m_j}(\hat{\mathbf{x}}) \Omega_{\kappa, m_j}^\dagger(\hat{\mathbf{y}}) & -i G_{n, \kappa}^{LS}(r_x, r_y) \Omega_{\kappa, m_j}(\hat{\mathbf{x}}) \Omega_{-\kappa, m_j}^\dagger(\hat{\mathbf{y}}) \\ i G_{n, \kappa}^{SL}(r_x, r_y) \Omega_{-\kappa, m_j}(\hat{\mathbf{x}}) \Omega_{\kappa, m_j}^\dagger(\hat{\mathbf{y}}) & G_{n, \kappa}^{SS}(r_x, r_y) \Omega_{-\kappa, m_j}(\hat{\mathbf{x}}) \Omega_{-\kappa, m_j}^\dagger(\hat{\mathbf{y}}) \end{bmatrix}, \quad (4.4.22)$$

where four radial elements of the form of $G_{n, \kappa}^{\alpha\beta}(r_x, r_y)$ are simply a product of two radial functions:

$$G_{n, \kappa}^{\alpha\beta}(r_x, r_y) = R_{n, \kappa}^\alpha(r_x) R_{n, \kappa}^\beta(r_y), \quad \alpha, \beta = L, S. \quad (4.4.23)$$

Using the result of eq.(2.7.21), in which the angular and radial parts of the $\boldsymbol{\alpha} \cdot \hat{\mathbf{p}}$ operator are decoupled, the Dirac operator that acts of the Green's function of equation.(3.9.39) (with $\mathbf{A}(\mathbf{x}) = 0$) becomes:

$$[c\boldsymbol{\alpha} \cdot \hat{\mathbf{p}}_x - e\varphi(r_x) - z] = \begin{bmatrix} +mc^2 - e\varphi(r_x) - z & -i\sigma_r \left[\hbar \frac{\partial}{\partial r} + \frac{1}{r} (\hbar + \hat{\kappa}_{\hat{\mathbf{x}}}) \right] \\ -i\sigma_r \left[\hbar \frac{\partial}{\partial r} + \frac{1}{r} (\hbar + \hat{\kappa}_{\hat{\mathbf{x}}}) \right] & -mc^2 - e\varphi(r_x) - z \end{bmatrix}. \quad (4.4.24)$$

The operator $\hat{\kappa}_{\hat{\mathbf{x}}}$ simply means that this operator will act on angular functions (spherical spinors) associated with the angular unit vector $\hat{\mathbf{x}}$, and not $\hat{\mathbf{y}}$ of eq.(4.4.22). The right hand side of eq.(3.9.39) is $\mathbb{1}_2 \delta(\mathbf{x} - \mathbf{y})$, which can be written in spherical coordinates, in terms of spherical spinors as we shall show. In spherical coordinates, the three-Dirac-delta can be written as [153, eq.(6.65)]:

$$\delta(\mathbf{x} - \mathbf{y}) = \frac{\delta(r_x - r_y)}{r_x r_y} \delta(\hat{\mathbf{x}} - \hat{\mathbf{y}}) \quad \text{with} \quad \delta(\hat{\mathbf{x}} - \hat{\mathbf{y}}) = \frac{\delta(\theta_x - \theta_y) \delta(\varphi_x - \varphi_y)}{\sin(\theta_x)}. \quad (4.4.25)$$

In addition, the two-component spherical spinors form a complete angular basis set [135, eq.(A.6)]:

$$\sum_{\kappa=\pm 1, \pm 2, \dots} \sum_{m_j=-|\kappa|+\frac{1}{2}}^{|\kappa|-\frac{1}{2}} \Omega_{\kappa, m_j}(\hat{\mathbf{x}}) \Omega_{\kappa, m_j}^\dagger(\hat{\mathbf{y}}) = \delta(\hat{\mathbf{x}} - \hat{\mathbf{y}}) \mathbb{1}_2. \quad (4.4.26)$$

These two equations lead to the following relation [154, eq.(3.6)]:

$$\mathbb{1}_2 \delta(\mathbf{x} - \mathbf{y}) = \frac{\delta(r_x - r_y)}{r_x r_y} \sum_{\kappa=\pm 1, \pm 2, \dots} \sum_{m_j=-|\kappa|+\frac{1}{2}}^{|\kappa|-\frac{1}{2}} \Omega_{\kappa, m_j}(\hat{\mathbf{x}}) \Omega_{\kappa, m_j}^\dagger(\hat{\mathbf{y}}). \quad (4.4.27)$$

Using this last result, the action of the operator of eq.(4.4.24) on the Green's function of eq.(4.4.22) in which radial and angular parts are separated, leads to four differential equations:

$$\begin{aligned} \sum_{n, \kappa} \frac{1}{E_{n, \kappa} - z} \left\{ [mc^2 - e\varphi(r_x) - z] G_{n, \kappa}^{LL}(r_x, r_y) - \hbar c \left[\frac{\partial}{\partial r_x} + \frac{1 - \kappa}{r_x} \right] G_{n, \kappa}^{SL}(r_x, r_y) \right\} &= \frac{\delta(r_x - r_y)}{r_x r_y} \\ \sum_{n, \kappa} \frac{1}{E_{n, \kappa} - z} \left\{ [mc^2 - e\varphi(r_x) - z] G_{n, \kappa}^{LS}(r_x, r_y) - \hbar c \left[\frac{\partial}{\partial r_x} + \frac{1 - \kappa}{r_x} \right] G_{n, \kappa}^{SS}(r_x, r_y) \right\} &= 0 \\ \sum_{n, \kappa} \frac{1}{E_{n, \kappa} - z} \left\{ \hbar c \left[\frac{\partial}{\partial r_x} + \frac{1 + \kappa}{r_x} \right] G_{n, \kappa}^{LL}(r_x, r_y) + [-mc^2 - e\varphi(r_x) - z] G_{n, \kappa}^{SL}(r_x, r_y) \right\} &= 0 \\ \sum_{n, \kappa} \frac{1}{E_{n, \kappa} - z} \left\{ \hbar c \left[\frac{\partial}{\partial r_x} + \frac{1 + \kappa}{r_x} \right] G_{n, \kappa}^{LS}(r_x, r_y) + [-mc^2 - e\varphi(r_x) - z] G_{n, \kappa}^{SS}(r_x, r_y) \right\} &= \frac{\delta(r_x - r_y)}{r_x r_y} \end{aligned} \quad (4.4.28)$$

that couple the four radial components of the Green's function. These equations can be combined into a single one (see [154, eq.(3.7)] and [7, eq.(98)]):

$$\sum_{\kappa} \begin{bmatrix} +mc^2 - e\varphi(r_x) - z & -\hbar c \left[\frac{\partial}{\partial r_x} + \frac{1-\kappa}{r_x} \right] \\ \hbar c \left[\frac{\partial}{\partial r_x} + \frac{1+\kappa}{r_x} \right] & -mc^2 - e\varphi(r_x) - z \end{bmatrix} G_{\kappa}(r_x, r_y; z) = \frac{\delta(r_x - r_y)}{r_x r_y} \mathbb{1}_2, \quad (4.4.29)$$

in which the radial Green's function associated with the κ -quantum number appears:

$$G_{\kappa}(r_x, r_y; z) = \sum_n \frac{1}{E_{n,\kappa} - z} \begin{bmatrix} G_{n,\kappa}^{LL}(r_x, r_y) & G_{n,\kappa}^{LS}(r_x, r_y) \\ G_{n,\kappa}^{SL}(r_x, r_y) & G_{n,\kappa}^{SS}(r_x, r_y) \end{bmatrix}, \quad (4.4.30)$$

and which includes a sum over all principal quantum numbers n while fixing κ . It should be finally noted that only bound-states have their energy quantized with respect to the principal quantum number n . This means that in all this section, when calculating the contributions of the continua, the sums over n should be replaced by two continuous sums (integrals) that scan the positive and negative-energy continua.

4.4.4 Radial vacuum polarization density and Green's function expansion

Following what we have done in section 4.4.2, and using the result of eq.(F.6.18):

$$\int_{C_F} \frac{dz}{E_{n,\kappa} - z} = i\pi \text{sgn}(E_{n,\kappa}), \quad (4.4.31)$$

the vacuum polarization density given in eq.(4.4.6) can be related to the radial Green's function, given in eq.(4.4.30) as [7, eq.(232)]:

$$\rho^{\text{VP}}(\mathbf{x}) = \frac{e}{4\pi^2 i} \sum_{\kappa} |\kappa| \int_{C_F} dz \text{Tr} [G_{\kappa}(r_x, r_x; z)] \quad , \quad (4.4.32)$$

and the density associated with an individual κ , given in eq.(4.4.9), can be thus written as:

$$\rho_{\kappa}^{\text{VP}}(\mathbf{x}) = \frac{e|\kappa|}{4\pi^2 i} \int_{C_F} dz \text{Tr} [G_{\kappa}(r_x, r_x; z)]. \quad (4.4.33)$$

Similarly to what we have done to the general Green's function (and electron propagator), this Green's function will be further expanded as:

$$G_{\kappa}(r_x, r_y; z) = G_{\kappa}^0(r_x, r_y; z) + e \int_0^{\infty} r_u^2 dr_u G_{\kappa}(r_x, r_u; z) \phi(r_u) G_{\kappa}^0(r_u, r_y; z), \quad (4.4.34)$$

in terms of the free Green's function. The validity of this equation can be checked by applying the Dirac operator $[h_x^D - e\phi(r_x) - z]$ on the left side of the last equation, and using eq.(4.4.29) with the fact that $G_{\kappa}^0(r_x, r_y; z)$ obeys the same equation, but with $\phi(r_x) = 0$. An expansion of the bound Green's function in terms of the free one, can be obtained by iteratively including the bound Green's function of the left side of the last equation, which ultimately leads to:

$$\begin{aligned} G_{\kappa}(r_x, r_y; z) &= G_{\kappa}^0(r_x, r_y; z) + e \int_0^{\infty} r_u^2 dr_u G_{\kappa}^0(r_x, r_u; z) \phi(r_u) G_{\kappa}^0(r_u, r_y; z) \\ &+ e^2 \int_0^{\infty} r_u^2 dr_u \int_0^{\infty} r_v^2 dr_v G_{\kappa}^0(r_x, r_v; z) \phi(r_v) G_{\kappa}^0(r_v, r_u; z) \phi(r_u) G_{\kappa}^0(r_u, r_y; z) + \mathcal{O}(e^3). \end{aligned} \quad (4.4.35)$$

This relation will allow us to write the vacuum polarization density of eq.(4.4.33) as:

$$\rho_{\kappa}^{\text{VP}}(\mathbf{x}) = \rho_{\kappa}^0(\mathbf{x}) + \rho_{\kappa}^1(\mathbf{x}) + \rho_{\kappa}^2(\mathbf{x}) + \mathcal{O}(e^4), \quad (4.4.36)$$

where the first three individual densities are given by:

$$\rho_{\kappa}^0(\mathbf{x}) = \frac{e|\kappa|}{4\pi^2 i} \int_{C_F} dz \text{Tr} [G_{\kappa}^0(r_x, r_x; z)] \quad (4.4.37)$$

$$\rho_{\kappa}^1(\mathbf{x}) = \frac{e^2|\kappa|}{4\pi^2 i} \int_0^{\infty} r_u^2 dr_u \phi(r_u) \int_{C_F} dz \text{Tr} [G_{\kappa}^0(r_x, r_u; z) G_{\kappa}^0(r_u, r_x; z)] \quad (4.4.38)$$

$$\begin{aligned} \rho_{\kappa}^2(\mathbf{x}) &= \frac{e^3|\kappa|}{4\pi^2 i} \int_0^{\infty} r_u^2 dr_u \int_0^{\infty} r_v^2 dr_v \phi(r_v) \phi(r_u) \\ &\times \int_{C_F} dz \text{Tr} [G_{\kappa}^0(r_x, r_v; z) G_{\kappa}^0(r_v, r_u; z) G_{\kappa}^0(r_u, r_x; z)] \end{aligned} \quad (4.4.39)$$

We shall come back to this result at the end of the chapter. Using Furry's theorem [115] (discussed in section 3.11), which is based on a charge conjugation symmetry argument, one can show that all even orders of vacuum polarization densities in the external scalar potential ϕ , vanish. In addition, we should note that $\rho_{\kappa}^1(\mathbf{x})$ contains the Uehling potential, and a divergent contribution. The numerical computation of this term is thus problematic, but, this problem can be overcome by simply calculating the difference between the total vacuum polarization density and the one-potential term:

$$\rho_{\kappa}^{\text{VP}}(\mathbf{x}) - \rho_{\kappa}^1(\mathbf{x}). \quad (4.4.40)$$

This expression is in principle finite, since the divergence in $\rho_{\kappa}^{\text{VP}}(\mathbf{x})$ is only present in its $\rho_{\kappa}^1(\mathbf{x})$. This trick was used by different authors:

1. By Rinker and Wilets [155, page 753]. These authors calculated the following difference:

$$\rho^{\text{VP}}(\mathbf{x}; Z) - \lim_{\delta \rightarrow 0} \frac{Z}{\delta} \rho^{\text{VP}}(\mathbf{x}; \delta), \quad (4.4.41)$$

which removes all contributions linear in Z (physical and unphysical/divergent). To see how this works, we expand the vacuum polarization density in powers of Z :

$$\rho^{\text{VP}}(\mathbf{x}; Z) = \frac{Z}{1!} \frac{\partial}{\partial Z} \rho^{\text{VP}}(\mathbf{x}; Z) \big|_{Z=0} + \frac{Z^3}{3!} \frac{\partial^3}{\partial Z^3} \rho^{\text{VP}}(\mathbf{x}; Z) \big|_{Z=0} + \mathcal{O}(Z^5). \quad (4.4.42)$$

The first-order derivative can be written as:

$$\frac{\partial}{\partial Z} \rho^{\text{VP}}(\mathbf{x}; Z) = \lim_{\delta \rightarrow 0} \frac{\rho^{\text{VP}}(\mathbf{x}, Z + \delta) - \rho^{\text{VP}}(\mathbf{x}, Z)}{\delta}, \quad (4.4.43)$$

which leads to the fact that the difference indeed removes the linear powers in Z :

$$\rho^{\text{VP}}(\mathbf{x}; Z) - \lim_{\delta \rightarrow 0} \frac{Z}{\delta} \rho^{\text{VP}}(\mathbf{x}, \delta) = + \frac{Z^3}{6} \frac{\partial^3}{\partial Z^3} \rho^{\text{VP}}(\mathbf{x}; Z) \big|_{Z=0} + \mathcal{O}(Z^5). \quad (4.4.44)$$

This means that one has to do a calculation with the real atomic charge Z , and another one with a very small atomic charge δ , and take the difference, as seen in the last expression.

2. Mohr *et al.* [7, pages 275-279]. These authors do a very similar trick, by taking the difference between the total and the one-potential vacuum polarization density of eqs.(4.4.36 and 4.4.38):

$$\begin{aligned} & \rho_{\kappa}^{\text{VP}}(\mathbf{x}) - \rho_{\kappa}^1(\mathbf{x}) \\ &= \frac{e|\kappa|}{4\pi^2 i} \int_{C_F} dz \left\{ \text{Tr} [G_{\kappa}(r_x, r_x; z)] - \int_0^{\infty} r_u^2 dr_u \phi(r_u) \text{Tr} [G_{\kappa}^0(r_x, r_u; z) G_{\kappa}^0(r_u, r_x; z)] \right\}. \end{aligned} \quad (4.4.45)$$

They then use the analytical expressions of these Green's functions to evaluate the corresponding difference.

One has to remember that by removing the divergence present in the term linear in Z , one also removes the physical contribution of this term: known as the Uehling contribution. This point should cause no problem since we know the exact form of the Uehling potential (See [117]), and it can easily be employed in the calculation to account for the missing physics, as done in the cited references. Next, we will see how one can calculate the total vacuum polarization density $\rho_{\kappa}^{\text{VP}}(\mathbf{x})$ in the framework of the finite basis approximation.

4.5 Vacuum polarization in a finite basis set

In this section, we shall discuss how the vacuum polarization density can be constructed in a finite basis set. In a spherical basis set, the radial functions are expanded as in eqs.(2.9.1 and 2.9.2) and the vacuum polarization density of eq.(4.4.9) becomes a sum that runs over all numerical solutions:

$$\rho_{\kappa}^{\text{VP}}(\mathbf{x}) = \frac{e|\kappa|}{4\pi r^2} \sum_{\alpha} \text{sgn}(E_{\alpha, \kappa}) \rho_{\kappa, \alpha}(r), \quad (4.5.1)$$

where $\rho_{\kappa, \alpha}(r) = [\mathcal{P}_{\alpha, \kappa}(r)]^2 + [\mathcal{Q}_{\alpha, \kappa}(r)]^2$ is the probability density associated with the numerical solution α . We should also note that in earlier calculations to numerically evaluate this vacuum polarization density, the integral of the vacuum polarization density:

$$\int d^3\mathbf{x} \rho_{\kappa}^{\text{VP}}(\mathbf{x}) = 0, \quad (4.5.2)$$

which should vanish, was calculated to present a precision indication of the done calculation. This was done by Rinker and Wilets [155, Pages 753,757] in addition to Soff and Mohr [6, Page 5074 eq.(70)]. In a finite basis calculation, this is not a problem of precision, since this integral will always vanish:

$$\int d^3\mathbf{x} \rho^{\text{VP}}(\mathbf{x}) = e \sum_{\kappa} |\kappa| \int_0^{\infty} dr \left(\sum_{\alpha_+=1}^n 1 - \sum_{\alpha_-=1}^n 1 \right) = 0. \quad (4.5.3)$$

In the last expression, α_{\pm} indicates that the index runs over the n positive and negative-energy solutions, respectively. The fact that both sums go from 1 to n (number of basis functions), is related to the fact that the numerical basis sets are (and should be) kinetically balanced. See, for instance, the work of Stanton and Havriliak [70].

4.5.1 VP density in restricted kinetic balance

In the RKB problem, the vacuum polarization density associated with the κ -Dirac problem of eq.(4.5.1) reduces to:

$$\begin{aligned} \rho_{\kappa}^{\text{VP}}(\mathbf{x}) = & \frac{e}{4\pi r^2} \sum_{\alpha=1}^{2n_{\kappa}} |\kappa| \operatorname{sgn}(E_{\alpha,\kappa}) \sum_{i,j}^{n_{\kappa}} \left\{ (c_{\alpha,\kappa,i}^L)^* c_{\alpha,\kappa,j}^L \pi_{\kappa,i}^L \pi_{\kappa,j}^L \right. \\ & \left. + \frac{\hbar^2}{4m^2 c^2} (c_{\alpha,\kappa,i}^S)^* c_{\alpha,\kappa,j}^S \left[\frac{d}{dr} \pi_{\kappa,i}^L + \frac{\kappa}{r} \pi_{\kappa,i}^L \right] \left[\frac{d}{dr} \pi_{\kappa,j}^L + \frac{\kappa}{r} \pi_{\kappa,j}^L \right] \right\}, \end{aligned} \quad (4.5.4)$$

where the sum runs over all solutions $\alpha = 1, \dots, 2n_{\kappa}$ of the numerical radial Dirac equation. The numerical density associated with a solution α is given in eq.(E.1.6).

We shall now present several calculations of this vacuum polarization density (in RKB) done on the Coulombic (point nucleus) hydrogen-like radon ($Z = 86$) atom: Rn^{85+} , using the last equation. We construct the four RKB matrix equations (see section E.1.1) corresponding to $\kappa = \pm 1, \pm 2$ quantum numbers, and use the 7z (largest available) basis exponents, given in section E.3. The results of the vacuum polarization density calculations are presents in figures (4.5.1, 4.5.2, 4.5.3 and 4.5.4), for $\kappa = -1, +1, -2$, and $+2$, respectively.

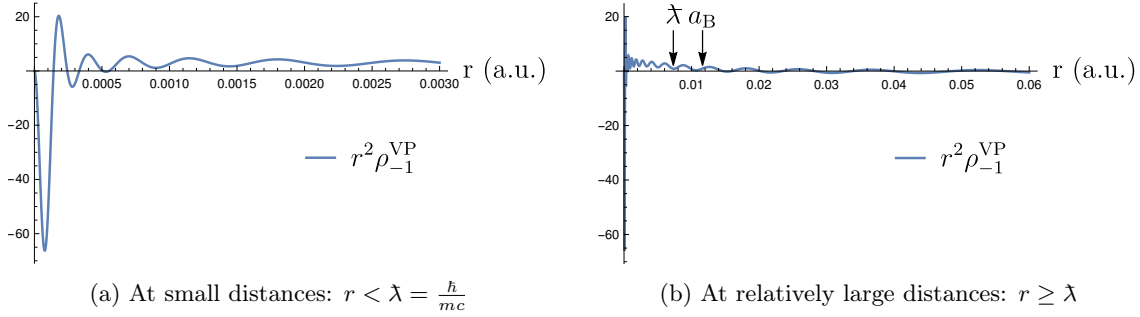


Figure 4.5.1: RKB VP density for Rn^{85+} and $\kappa = -1$.

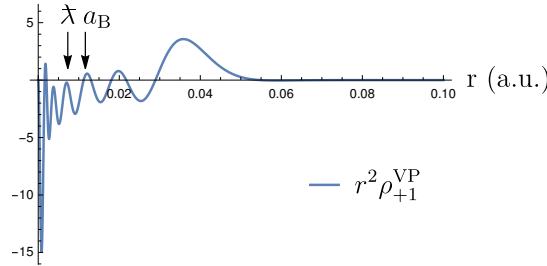


Figure 4.5.2: RKB VP density for Rn^{85+} and $\kappa = +1$.

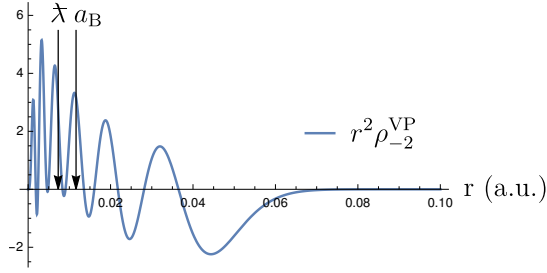


Figure 4.5.3: RKB VP density for Rn^{85+} and $\kappa = -2$.

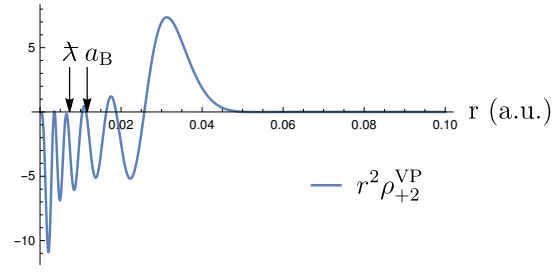


Figure 4.5.4: RKB VP density for Rn^{85+} and $\kappa = +2$.

We first analyze the first result of the $\kappa = -1$ calculation, which shows that the vacuum polarization density is a very local quantity, since its maximum magnitudes are reached within the Compton wavelength $\lambda \approx 0.0073$ a.u., as seen in figure 4.5.1a, but still have a wavy behavior which goes beyond the (radon atom) Bohr radius $a_B = 0.0116$ a.u. (where the ground-state electron is most probably found), as one notices in figure 4.5.1b. The second result is clearly unphysical, and shall be solved by the end of this chapter. The three remaining results, are less local, and the reason is because the set of s -exponents has higher exponent values (more localized), as one can see by comparing the first column of the three exponents tables E.3-E.5.

In order to see if the vacuum polarization density is well described by our basis sets, we perform three additional calculations on the $\kappa = -1$ problem ($s_{\frac{1}{2}}$), and present the obtained results in figure 4.5.5. In the first, second and third calculation, we simply augment the largest $7z$ s -basis (First column of table E.3) by one, two and three large tight exponents, and label the curves with $7z+i$ where $i = 1, 2, 3$, respectively. These additional exponents are generated using the even-tempering scheme, discussed in section E.3.1.

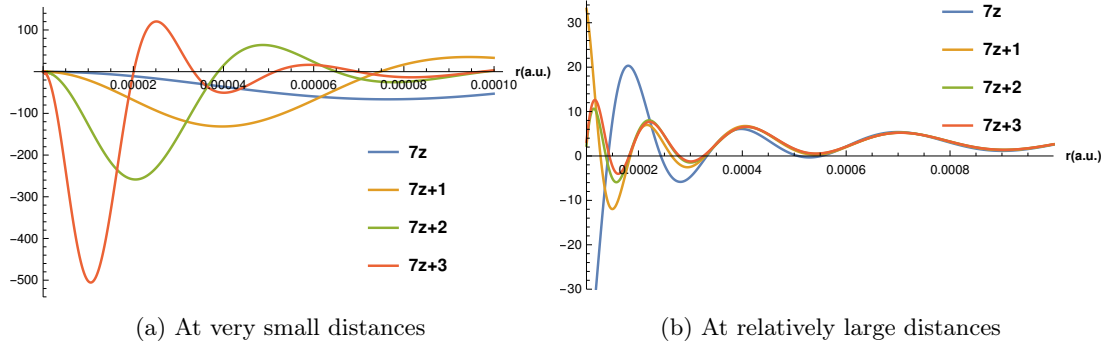


Figure 4.5.5: $s_{\frac{1}{2}}$ -problem vacuum polarization density in RKB using $7z$ Gaussian exponents. $7z+i$ indicates that the basis set is augmented with additional i tight Gaussian exponents.

As predicted, since we have introduced very tight Gaussians, the calculation can only differ in the vicinity of the nucleus, as seen in figure 4.5.5a, contrary to the relatively larger radii where the four curves rapidly overlap, as noticed in figure 4.5.5b.

What is problematic about the first figure is that it tells us that our density is very sensitive to the addition of tight exponents, and the vacuum polarization density does not converge in the vicinity of the nucleus. This density is always ready to absorb larger exponents, without converging.

This result clearly makes the physical validity of the results, questionable. The reader should note that divergent behavior is expected, since the calculated quantity is not regularized. We shall now focus on the qualitative improvement of our results. The solution to obtain quantitative vacuum densities will be suggested at the end of this thesis. In reality, we know that the dominant vacuum polarization effects (first-order: Uehling) should decay exponentially for $r > \lambda \approx 0.0073$ a.u. [8, page 283], and this is not the case here. The vacuum polarization density we are calculating is (in principle) complete, i.e. it contains the full expansion in powers of interaction with the external nuclear potential $(\alpha Z)^{n \geq 1}$. One can thus propose to calculate the dominant $(\alpha Z)^{n=1}$ density, what we call “the Uehling density” which generates the Uehling potential $U_{\text{uehling}}(\mathbf{x})$ (known analytically), using the Poisson equation from electrostatics:

$$\Delta U_{\text{uehling}} = -\frac{\rho_{\text{uehling}}(\mathbf{x})}{\varepsilon_0}, \quad (4.5.5)$$

and compare this density $\rho_{\text{uehling}}(\mathbf{x})$ with what we have found here. Unfortunately, this is not possible, since the vacuum polarization density coming from a point-nuclear charge is divergent. See, for instance, Greiner and Reinhardt [8, Pages 284-287]. In addition, Plunien *et al.* have considered the Uehling effect for a uniform sphere model, and showed that the associated density diverges logarithmically [156, eq.(28) and figure 5]. The calculation of $\rho_{\text{uehling}}(\mathbf{x})$ can be only done with a smooth nuclear charge model, as Gaussian- or Fermi-nuclei. This point is to be further investigated.

A part of the problem comes from the fact that RKB is designed for positive-energy solutions, and not the negative-energy ones (see section 2.10.1), and the vacuum polarization equation.(4.5.4) do need these negative-energy solutions. We will thus go to the evaluation of this density in the dual kinetic balance scheme, in the next section.

4.5.2 VP density in dual kinetic balance

In the dual kinetic balance scheme, the vacuum polarization density of eq.(4.5.1):

$$\rho_{\kappa}^{\text{VP}}(\mathbf{x}) = \frac{e|\kappa|}{4\pi r^2} \sum_{\alpha} \text{sgn}(E_{\alpha,\kappa}) \rho_{\kappa,\alpha}(r), \quad (4.5.6)$$

where the numerical density $\rho_{\kappa,\alpha}(r)$ associated with the α solution, is now given in eq.(E.2.12).

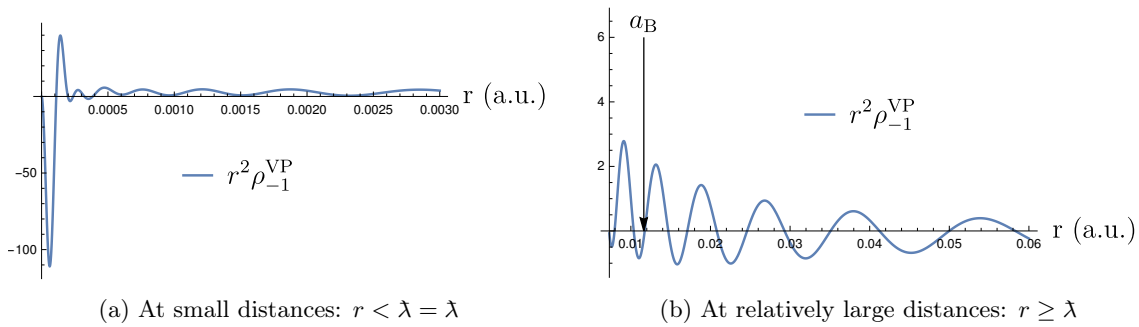
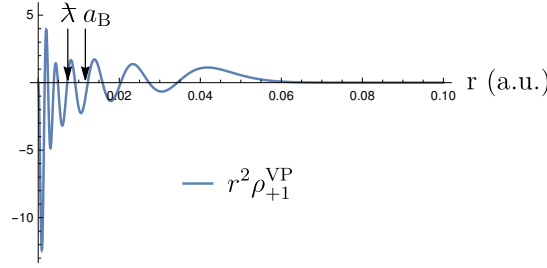
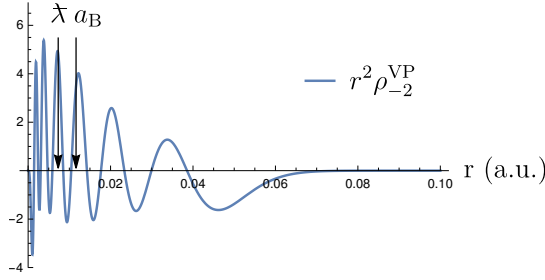
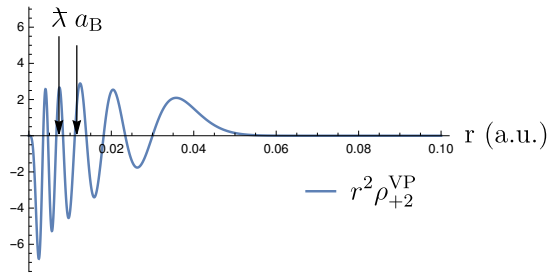


Figure 4.5.6: DKB VP density for Rn^{85+} and $\kappa = -1$.

Figure 4.5.7: DKB VP density for Rn^{85+} and $\kappa = +1$.Figure 4.5.8: DKB VP density: Rn^{85+} , $\kappa = -2$.Figure 4.5.9: DKB VP density: Rn^{85+} , $\kappa = +2$.

In this section, we repeat the same calculations we have done in the previous section, by building the four matrix equations with the four quantum numbers $\kappa = \pm 1, \pm 2$, but this time using the DKB prescription, whose elements are given in section E.2. The only difference we get is that the vacuum polarization density of ρ_{-1}^{VP} in figure 4.5.6a of DKB is more localized than the one previously obtained for RKB (using the same basis), which was presented in figure 4.5.1a. The second point to notice is that the two curves associated with $\kappa = \pm 2$, are very similar, and the reason behind this evidence is that the exponents used for these two problems are similar to each other (See tables E.4 and E.5). So a question that can come to mind is the following:

What could happen if we set the basis of the last two DKB matrix problems ($\kappa = \pm 2$) to be equal?

As seen in section 2.11.6, our basis will make the DKB method symmetric under charge conjugation. We shall thus perform a calculation in which we set the exponents associated with the opposite κ -sign problems to be equal.

4.5.3 \mathcal{C} -symmetric Dual Kinetic Balance

In this section, we shall perform a calculation in which we set exponents of the $\kappa = \pm 1$ and $\kappa = \pm 2$ problems to be separately equal. These bases are known as j -bases (see section E.3), and lead to a conservation of the \mathcal{C} -symmetry in the DKB problem as noted in our section 2.11.6 and by Dyall on [83, Page 38]. We therefore choose to set our exponents to be:

$$\begin{aligned} \zeta_{-1} &= \zeta_{+1} = \zeta_s \\ \zeta_{-2} &= \zeta_{+2} = \zeta_p \end{aligned} \quad (4.5.7)$$

where ζ_s and ζ_p are set to be the first column (7z-basis) exponents of tables E.3 and E.4.

We start with the densities associated with the $\kappa = \pm 1$ problems, presented in figure 4.5.10. The individual densities are very localized within the Compton wavelength $r \ll \lambda$. To have a closer look, we plot these densities at very small distances, within $r < \lambda/7$ (within the seventh of the Compton length) in figure 4.5.11. The upper figure 4.5.11a which contains individual density contributions, shows that the densities “interfere” constructively (match) at $r < 0.0002$ a.u., they then rapidly start to mismatch and a cancellation between the two contributions begins to take place. Furthermore, to observe how this cancellation evolves with larger distances, we plot these densities for distances starting from the Compton wavelength (the first plotted points on the left), and ending at approximately $18 \times a_B$, see figure 4.5.12. The two sub-figures show a very large cancellation between opposite κ -sign contributions at distances larger than the Compton wavelength.

The obtained results are quite promising, since our vacuum polarization density is now very much localized within the Compton wavelength, and vanishes outside it, as it should behave.

In addition, we present the same plots for the vacuum polarization density associated with the $\kappa = \pm 2$ problems in figs. 4.5.13 to 4.5.15. These figures show very similar results:

1. Fast decay of the vacuum polarization density at distances larger than the reduced Compton wavelength (and the Bohr radius).
2. Significant cancellation between different vacuum polarization density components.

The only difference between the two problems ($\kappa = \pm 1$ and $\kappa = \pm 2$) is that $\rho_{\pm 2}^{\text{VP}}$ is not as singular as $\rho_{\pm 1}^{\text{VP}}$ at the significantly small distances. That is justified because the basis functions used here are (very) small and not as localized as the ones used for $\kappa = \pm 1$. To prove our claim, we do an extra calculation where we set the same larger exponent used for $\kappa = \pm 1$, for the $\kappa = \pm 2$ problem, meaning that all exponents are now equal, and the corresponding results are finally shown in the extra calculations section 4.5.4 figs. 4.5.16 to 4.5.18.

The reader should constantly be reminded that most of these tests are qualitative rather than quantitative since we are not using the best basis sets but rather trying to discover how one can construct a more physical vacuum polarization density.

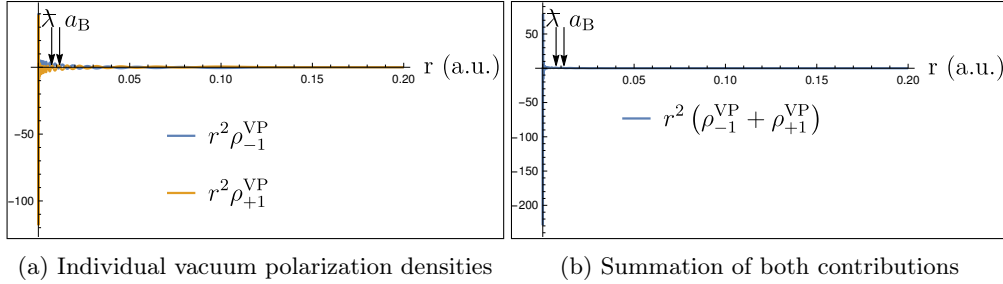
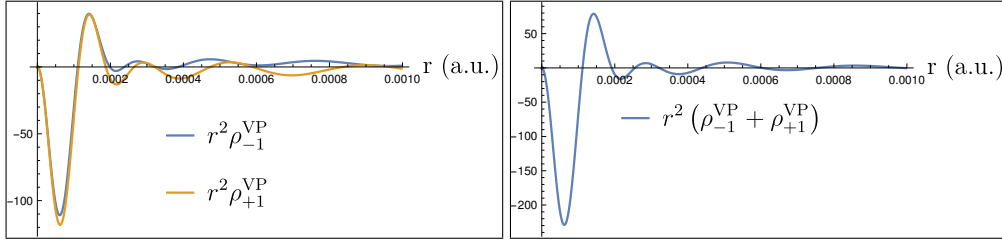
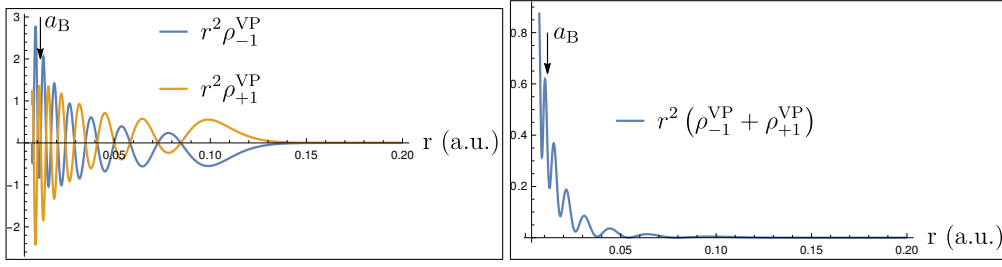


Figure 4.5.10: $r^2 \rho_{\pm 1}^{\text{VP}}$ for Rn^{85+} using \mathcal{C} -DKB : The whole view.



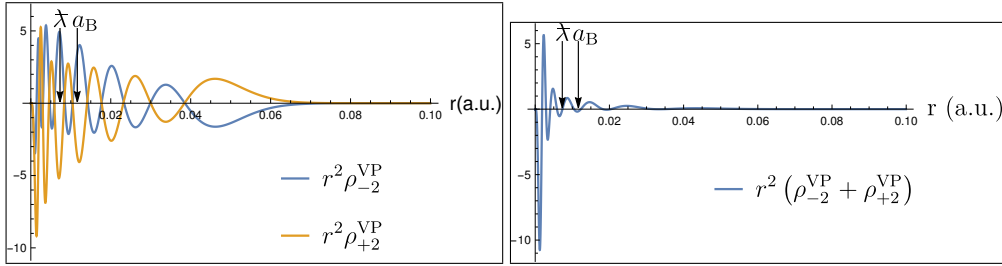
(a) Individual vacuum polarization densities

(b) Summation of both contributions

 Figure 4.5.11: $r^2 \rho_{\pm 1}^{VP}$ for Rn^{85+} using \mathcal{C} -DKB : At small distances: $r < \lambda/7$.


(a) Individual vacuum polarization densities

(b) Summation of both contributions

 Figure 4.5.12: $r^2 \rho_{\pm 1}^{VP}$ for Rn^{85+} using \mathcal{C} -DKB : At larger distances
 Note: curves are starting from $r = \lambda$.


(a) Individual vacuum polarization densities

(b) Summation of both contributions

 Figure 4.5.13: $r^2 \rho_{\pm 2}^{VP}$ for Rn^{85+} using \mathcal{C} -DKB : The whole view.

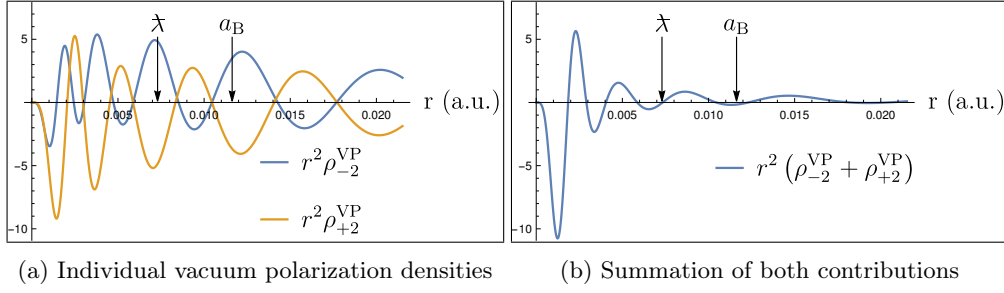


Figure 4.5.14: $r^2 \rho_{\pm 2}^{VP}$ for Rn^{85+} using \mathcal{C} -DKB : At small distances: $r < \lambda/7$.

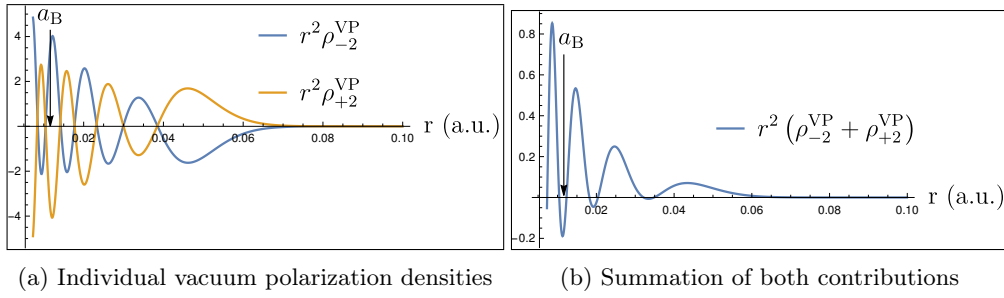
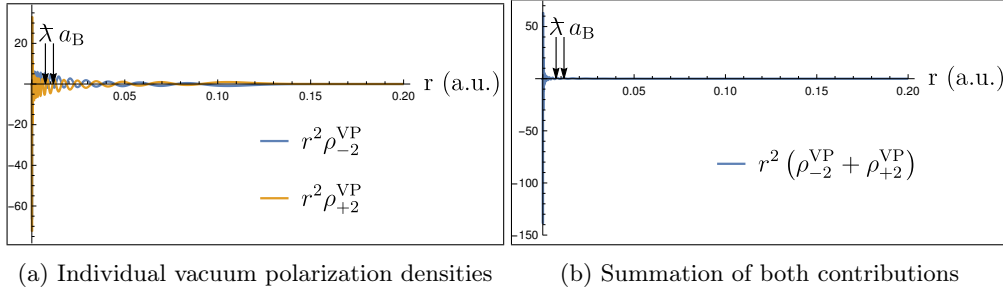
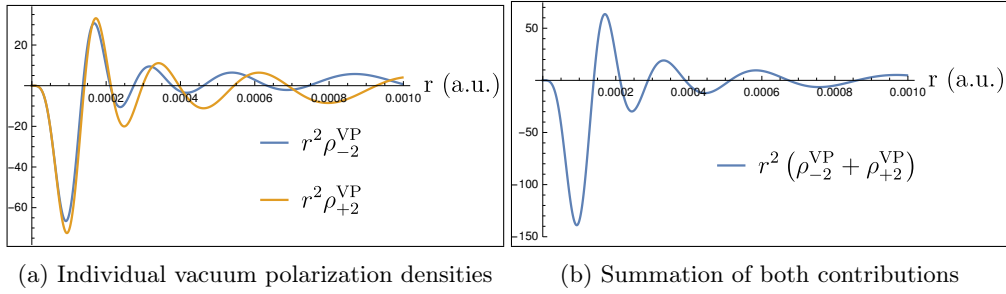
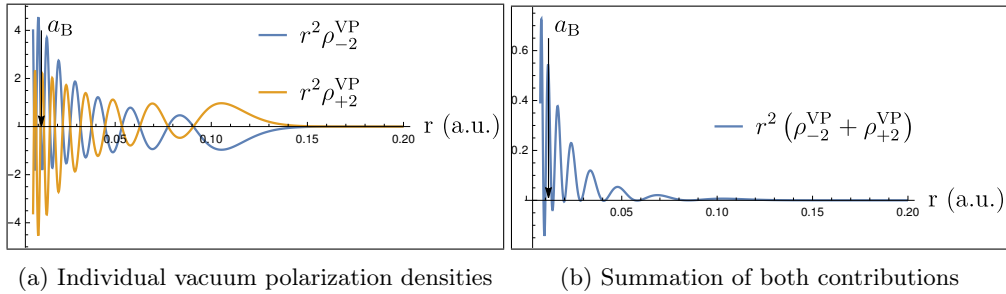


Figure 4.5.15: $r^2 \rho_{\pm 2}^{VP}$ for Rn^{85+} using \mathcal{C} -DKB : At larger distances
Note: curves are starting from $r = \lambda$.

4.5.4 Extra calculations: same exponents

Figure 4.5.16: $r^2 \rho_{\pm 2}^{VP}$ for Rn^{85+} using \mathcal{C} -DKB : The whole view.Figure 4.5.17: $r^2 \rho_{\pm 2}^{VP}$ for Rn^{85+} using \mathcal{C} -DKB : At small distances: $r < \lambda/7$.Figure 4.5.18: $r^2 \rho_{\pm 2}^{VP}$ for Rn^{85+} using \mathcal{C} -DKB : At larger distancesNote: curves are starting from $r = \lambda$.4.5.5 A closer look on numerical solutions of \mathcal{C} -DKB

In this section, we shall take a closer look at the individual numerical (probability) densities that contribute to the vacuum polarization density of the $\kappa = \pm 1$ problems, given in eq.(4.5.6). Recall that the basis used in these calculations contains 16 exponents (7z), given in table E.3, which means that the number of eigensolutions (dimensions of the Hamiltonian and overlap matrices) is 32. The reader should remember that this basis is symmetric under charge conjugation symmetry, and hence,

we shall call this problem: \mathcal{C} -DKB. The first and last five eigenvalues of both $\kappa = \pm 1$ problems are presented in the following table 4.1.

α	κ	
	-1	$+1$
1	+1.831E + 06	+1.830E + 06
2	+1.066E + 05	+1.067E + 06
3	+6.461E + 05	+6.470E + 05
4	+4.159E + 05	+4.171E + 05
5	+2.740E + 05	+2.752E + 05
\vdots	\vdots	\vdots
28	-4.493E + 05	-4.503E + 05
29	-6.943E + 05	-6.954E + 05
30	-1.117E + 06	-1.118E + 06
31	-1.895E + 06	-1.896E + 06
32	-3.780E + 06	-3.781E + 06

Table 4.1: First and last five eigenvalues of the $\kappa = \pm 1$ problems of Ru^{85+} using j -basis DKB.

These two columns show that solutions of the associated $\kappa = \pm 1$ problems, which are very high in energy ($|E| > 15 mc^2$) are very close. We have thus moved on to plot the energy signed probability densities:

$$\text{sgn}(E_{\alpha,\kappa}) r^2 \rho_{\alpha,\kappa}(r), \quad (4.5.8)$$

associated with the tabulated energy solutions and present them in fig. 4.5.19. In the total vacuum polarization density of eq.(4.5.1), all these probability densities are multiplied by the same factor $\frac{e|\pm 1|}{4\pi}$, which means that scales can be directly compared. We also note that for clarity purposes, we have presented the four figures in the same way the table is constructed, and multiply the negative-energy probability densities with a minus factor of 1 (as done in the last equation), to remind the reader that these lower plots will oppose the upper ones, due to the minus sign which is present for negative-energy solutions: see the last cited equation. By observation, one can see that:

1. The resemblance between eigenvalues, is accompanied by a clear resemblance between probability densities for both $\kappa = \pm 1$ problems.
2. After summing positive and negative contributions (figs. 4.5.19a and 4.5.19c and figs. 4.5.19b and 4.5.19d), a large cancellation between these opposite energy sign contributions will occur.
3. A numerical solution with large energy (absolute value) has a probability density closer to the nucleus compared to lower energy solutions.

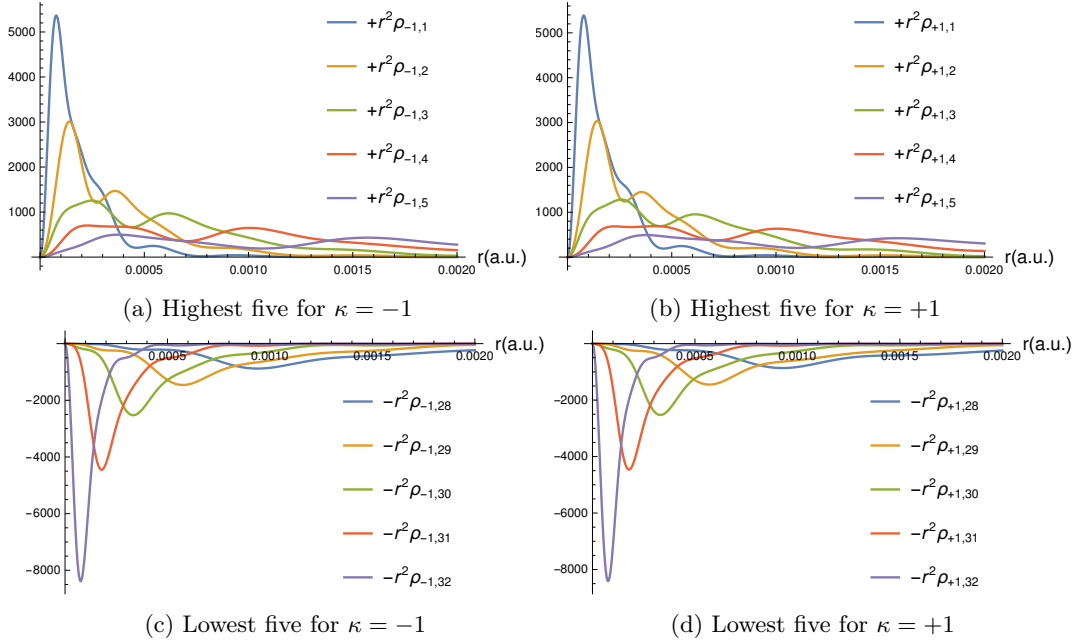
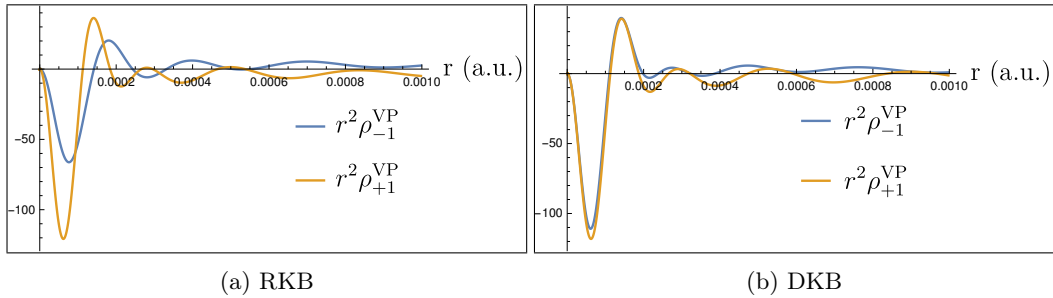


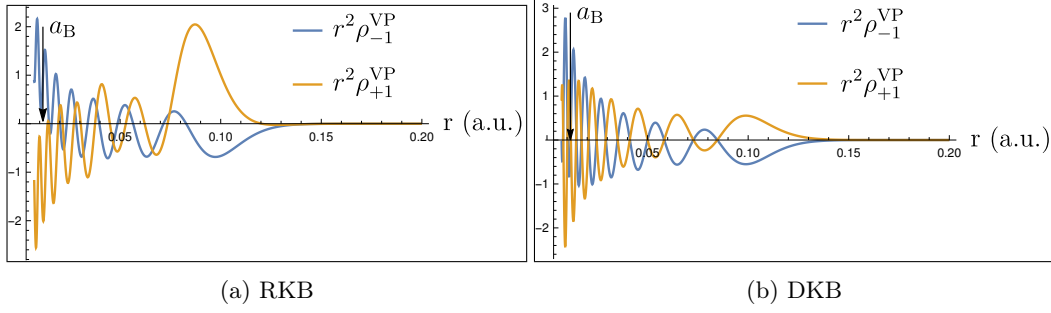
Figure 4.5.19: Probability densities associated with the highest- and lowest-five energy solutions.

4.5.6 Comparison between RKB and \mathcal{C} -DKB

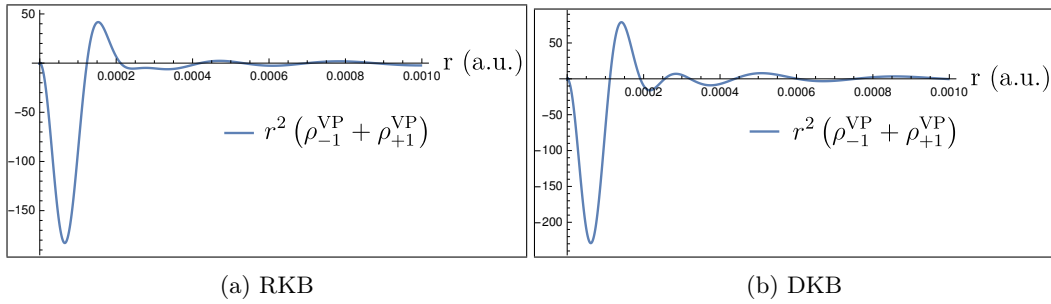
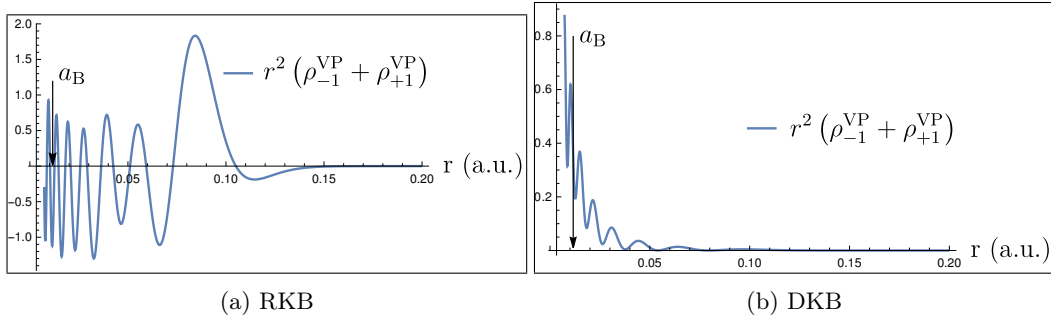
At this point, the reader might realize that it would be a good idea to compare the conventional RKB problem to the \mathcal{C} -symmetric DKB problem. To make these problems more comparable, we use the same basis set for both. We shall concentrate on the $\kappa = \pm 1$ problems and use the largest 7z j -basis, more precisely, this means that we shall use the s-exponents given in the first column of E.3. We present the results in which we compare both problems, in figs. 4.5.20 and 4.5.21. These figures show that:

1. At small distances, the DKB curves start with a nice matching between the components of the vacuum polarization density, while the RKB results show no such behavior.
2. More importantly, at relatively large distances, the DKB curves show a very nice destructive interference between both components, contrary to the RKB ones.

Figure 4.5.20: $\rho_{\pm 1}^{VP}$ for Rn^{85+} at very small distances: $r < \lambda/7$.

Figure 4.5.21: $\rho_{\pm 1}^{VP}$ for Rn^{85+} at relatively large distances: $r \geq \lambda$.

In the end, what matters, is the summation of the two vacuum polarization components, which will give the resultant effect, and take cancellations into account. We shall thus sum both density components for each of the last four figures, and present the results in figs. 4.5.22 and 4.5.23.

Figure 4.5.22: $r^2(\rho_{-1}^{VP} + \rho_{+1}^{VP})$ for Rn^{85+} at very small distances: $r < \lambda/7$.Figure 4.5.23: $r^2(\rho_{-1}^{VP} + \rho_{+1}^{VP})$ at relatively large distances: $r \geq \lambda$.

Clearly, the \mathcal{C} -DKB gets the credit. We shall next show that the RKB method gives rise to a non-vanishing vacuum polarization density in the free electron problem, which is a non-physical result, and is thus problematic.

4.5.7 Non-vanishing vacuum polarization density in RKB

As a consequence of the \mathcal{C} -symmetry violation in the RKB method, the free-particle vacuum polarization density (when we set $Z = 0$), does not vanish. We thus plot the vacuum polarization density components and their sum (using the 7z j -basis) in figs. 4.5.24a and 4.5.24b. This non-vanishing vacuum polarization density vanishes in DKB since j -basis obeys the vacuum polarization density, and this is shown in figs. 4.5.25a and 4.5.25b. We should note that the vacuum polarization density of fig. 4.5.25b, vanishes within our large numerical precision: up to 100 significant digits.

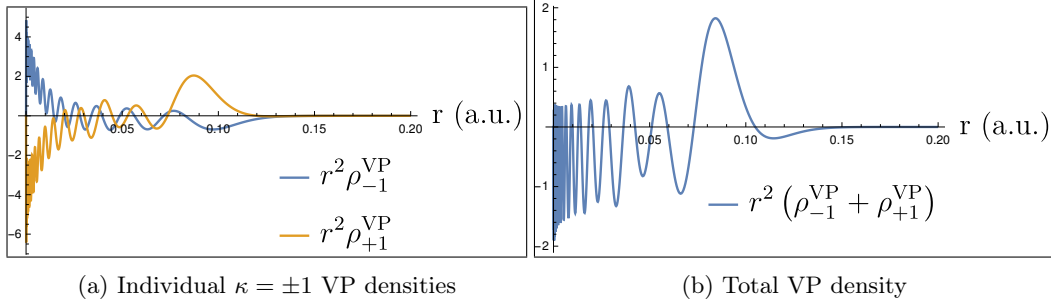


Figure 4.5.24: A non-vanishing free-particle VP density in RKB.
This is a non-physical result indicating \mathcal{C} -symmetry violation.

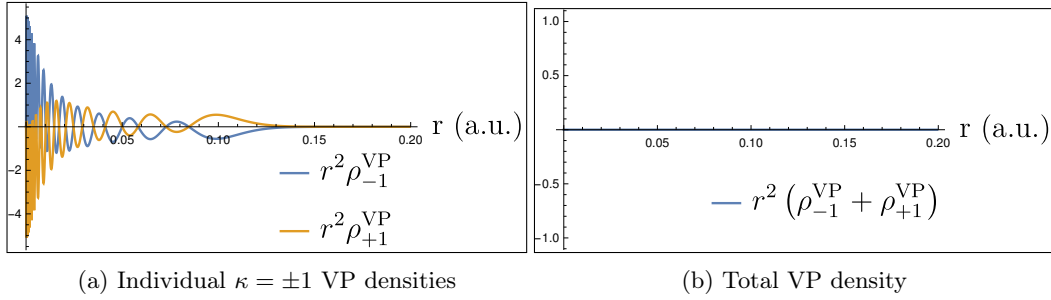


Figure 4.5.25: A vanishing free-particle VP density in \mathcal{C} -DKB.
This is a physical result indicating \mathcal{C} -symmetry obedience.

4.5.8 Conclusions

So far, the best results we got were the ones obtained when using the j -basis (discussed in E.3), which preserves the \mathcal{C} -symmetry in the framework of the DKB prescription. Furthermore, the conventional RKB (most popular) scheme, has the following weak points:

1. It fails in approximating the right coupling between large and small components of the negative-energy solutions.
2. It cannot preserve the \mathcal{C} -symmetry, (unless one uses the decoupled free basis: see section 2.11.2).
3. And most severely, it produces a non-vanishing vacuum polarization effect in the free-particle problem, as seen in the previous section.

We also note that the j -basis choice of exponents is a special case in which the \mathcal{C} -symmetry can be conserved, as discussed in section 2.11.6, where we mention that it should be better to work with exponents optimized for opposite κ , and opposite L/S problems. Nevertheless, we are going to use what we have in hands, the j -basis.

Finally, we would like to note that the non-vanishing vacuum polarization density which was found in the free-electron RKB method $Z = 0$ and shown in fig. 4.5.24b, looks very similar to the non-vanishing vacuum polarization density we have found for RKB where the nuclear charge was $Z = 86$ seen in fig. 4.5.23a at these large distances. This indication suggests that one can take the difference between these two results:

$$\rho_{\kappa}^{\text{VP}}(Z, r) - \rho_{\kappa}^{\text{VP}}(0, r), \quad (4.5.9)$$

in order to remove this spurious behavior, and obtain a better physical result. This point is to be further investigated.

4.6 Vacuum polarization expansion in the finite basis set

So far we have discussed how to evaluate the total vacuum polarization density associated with a certain κ , in a finite basis set, using the simple general expression of eq.(4.5.1). We have also learned how to expand the vacuum polarization density in powers of external scalar potential, and presented the results in eqs.(4.4.36, 4.4.37-4.4.39). We shall now see how one can build these individual terms of the expansion, in a finite basis set. The starting point is to realize that the exact Green's function of eq.(4.4.30):

$$G_{\kappa}(r_x, r_y; z) = \sum_n \frac{1}{E_{n,\kappa} - z} \begin{bmatrix} R_{n,\kappa}^L(r_x) R_{n,\kappa}^L(r_y) & R_{n,\kappa}^L(r_x) R_{n,\kappa}^S(r_y) \\ R_{n,\kappa}^S(r_x) R_{n,\kappa}^L(r_y) & R_{n,\kappa}^S(r_x) R_{n,\kappa}^S(r_y) \end{bmatrix}, \quad (4.6.1)$$

can be constructed in a basis set using numerical solutions, given in eq.(2.9.1). We shall call this numerical Green's function: \mathcal{G}_{κ} , and it is given (in analogy to the last equation) by:

$$\begin{aligned} \mathcal{G}_{\kappa}(r_x, r_y; z) &= \frac{1}{r_x r_y} \sum_{\alpha} \frac{\varphi_{\alpha,\kappa}(r_x) \varphi_{\alpha,\kappa}^{\dagger}(r_y)}{E_{\alpha,\kappa} - z} \\ &= \frac{1}{r_x r_y} \sum_{\alpha} \frac{1}{E_{\alpha,\kappa} - z} \begin{bmatrix} \mathcal{P}_{\alpha,\kappa}(r_x) \mathcal{P}_{\alpha,\kappa}(r_y) & \mathcal{P}_{\alpha,\kappa}(r_x) \mathcal{Q}_{\alpha,\kappa}(r_y) \\ \mathcal{Q}_{\alpha,\kappa}(r_x) \mathcal{P}_{\alpha,\kappa}(r_y) & \mathcal{Q}_{\alpha,\kappa}(r_x) \mathcal{Q}_{\alpha,\kappa}(r_y) \end{bmatrix}, \end{aligned} \quad (4.6.2)$$

where the sum runs over the numerical solutions α , of the radial κ Dirac problem. Similarly, we shall call the free (numerical) radial Dirac Green's function, \mathcal{G}_{κ}^0 , which can be obtained from \mathcal{G}_{κ} in the limit $Z \rightarrow 0$. In addition, we should note that the free numerical radial solutions, entering \mathcal{G}_{κ}^0 , are going to be called:

$$\varphi_{\alpha,\kappa}^0(r) = \begin{bmatrix} \mathcal{P}_{\alpha,\kappa}^0(r) \\ \mathcal{Q}_{\alpha,\kappa}^0(r) \end{bmatrix}, \quad (4.6.3)$$

and shall be associated with $E_{\alpha,\kappa}^0$ instead of $E_{\alpha,\kappa}$, which appears in the denominator of the Green's function. We shall now evaluate the first few terms of the vacuum polarization density expansion.

4.6.1 The zero-potential vacuum polarization density

Using the previous discussion, and definitions, the numerical zero-potential vacuum polarization density becomes:

$$\rho_{\kappa}^0(\mathbf{x}) = \frac{e|\kappa|}{4\pi^2 i} \int_{C_F} dz \operatorname{Tr} [\mathcal{G}_{\kappa}^0(r, r; z)] = \frac{e|\kappa|}{4\pi^2 i} \frac{1}{r^2} \sum_{\alpha} M_{\kappa}^{\alpha}(r) \int_{C_F} dz \frac{1}{E_{\alpha, \kappa}^0 - z}, \quad (4.6.4)$$

in the finite basis approximation. The function $M_{\kappa}^{\alpha}(r)$ is given by:

$$M_{\kappa}^{\alpha}(r) = [\varphi_{\alpha, \kappa}^0(r)]^{\dagger} \varphi_{\alpha, \kappa}^0(r) = \rho_{\alpha, \kappa}^{\text{Free}}(r), \quad (4.6.5)$$

is the probability density associated with the free solution α . The contour integral is evaluated in section F.6.18, and using the result of eq.(F.6.18), we can write:

$$\int_{C_F} dz \frac{1}{E_{\alpha, \kappa}^0 - z} = i\pi \operatorname{sgn}(E_{\alpha, \kappa}^0), \quad (4.6.6)$$

which reduces our density to:

$$\rho_{\kappa}^0(\mathbf{x}) = \frac{e|\kappa|}{4\pi} \frac{1}{r^2} \sum_{\alpha} \operatorname{sgn}(E_{\alpha, \kappa}^0) \rho_{\alpha, \kappa}^{\text{Free}}(r), \quad (4.6.7)$$

which is identical to the vacuum polarization we had in eq.(4.5.1), but this time containing the free probability densities instead.

4.6.2 The one-potential vacuum polarization density

The numerical one-potential vacuum polarization was found to be:

$$\rho_{\kappa}^1(\mathbf{x}) = \frac{e^2|\kappa|}{4\pi^2 i} \int_0^{\infty} r_y^2 dr_y \phi(r_y) \int_{C_F} dz \operatorname{Tr} [\mathcal{G}_{\kappa}^0(r_x, r_y; z) \mathcal{G}_{\kappa}^0(r_y, r_x; z)] \quad . \quad (4.6.8)$$

See eq.(4.4.38). This formula contains the trace of a product of two free Green's functions, which is found to be:

$$\begin{aligned} & \operatorname{Tr} [\mathcal{G}_{\kappa}^0(r_x, r_y; z) \mathcal{G}_{\kappa}^0(r_y, r_x; z)] \\ &= \frac{1}{r_x^2 r_y^2} \sum_{\alpha, \beta} \frac{1}{E_{\alpha, \kappa}^0 - z} \frac{1}{E_{\beta, \kappa}^0 - z} M_{\kappa}^{\alpha, \beta}(r_x, r_y). \end{aligned} \quad (4.6.9)$$

with the function $M_{\kappa}^{\alpha, \beta}(r_x, r_y)$, given by the following formula:

$$\begin{aligned} M_{\kappa}^{\alpha, \beta}(r_x, r_y) &= \operatorname{Tr} [\varphi_{\alpha, \kappa}^0(r_x) \varphi_{\alpha, \kappa}^{0\dagger}(r_y) \varphi_{\beta, \kappa}^0(r_y) \varphi_{\beta, \kappa}^{0\dagger}(r_x)] \\ &= [\varphi_{\beta, \kappa}^{\dagger}(r_x) \varphi_{\alpha, \kappa}(r_x) \varphi_{\alpha, \kappa}^{\dagger}(r_y) \varphi_{\beta, \kappa}(r_y)]_0. \end{aligned} \quad (4.6.10)$$

The subscript added to the last square brackets is a reminder that the inside solutions are free-ones. The complex integral whose terms come from denominators of the Green's functions is given by the following:

$$\int_{C_F} dz \frac{1}{E_{\alpha, \kappa}^0 - z} \frac{1}{E_{\beta, \kappa}^0 - z} = \pi i \frac{1 - \operatorname{sgn}(E_{\alpha, \kappa}^0 E_{\beta, \kappa}^0)}{|E_{\alpha, \kappa}^0| + |E_{\beta, \kappa}^0|}, \quad (4.6.11)$$

and was evaluated using the appendix result of eq.(F.6.30). Combining these findings, we can write the one-potential vacuum polarization density as:

$$\rho_\kappa^1(\mathbf{x}) = \frac{e^2 |\kappa|}{4\pi r_x^2} \sum_{\alpha, \beta} \frac{1 - \text{sgn}(E_{\alpha, \kappa}^0 E_{\beta, \kappa}^0)}{|E_{\alpha, \kappa}^0| + |E_{\beta, \kappa}^0|} [\varphi_{\beta, \kappa}^0(r_x)]^\dagger \varphi_{\alpha, \kappa}^0(r_x) \int_0^\infty dr_y \phi(r_y) [\varphi_{\alpha, \kappa}^0(r_y)]^\dagger \varphi_{\beta, \kappa}^0(r_y). \quad (4.6.12)$$

Finally, the integral we are left with is the α, β matrix-element of the potential (expectation-value) matrix:

$$V_{\alpha, \beta}^\kappa = \int_0^\infty dr_y \phi(r_y) [\varphi_{\alpha, \kappa}^0(r_y)]^\dagger \varphi_{\beta, \kappa}^0(r_y). \quad (4.6.13)$$

In addition, we shall call $s_{\beta, \alpha}^\kappa(r_x)$ the remaining r_x dependent terms:

$$s_{\beta, \alpha}^\kappa(r_x) = [\varphi_{\beta, \kappa}^0(r_x)]^\dagger \varphi_{\alpha, \kappa}^0(r_x). \quad (4.6.14)$$

We also note that the integral of this last quantity, gives the β, α element of the overlap matrix. Finally, using our new definitions, our one-potential vacuum polarization density becomes:

$$\rho_\kappa^1(\mathbf{x}) = \frac{e^2 |\kappa|}{4\pi r_x^2} \sum_{\alpha, \beta} \frac{1 - \text{sgn}(E_{\alpha, \kappa}^0 E_{\beta, \kappa}^0)}{|E_{\alpha, \kappa}^0| + |E_{\beta, \kappa}^0|} s_{\beta, \alpha}^\kappa(r_x) V_{\alpha, \beta}^\kappa. \quad (4.6.15)$$

We shall next generalize the steps we have followed in this section to derive the vacuum polarization density of an arbitrary order n . Afterwards, we shall show that once the used basis is \mathcal{C} -symmetric, then the numerical vacuum polarization density associated with an even order n should vanish.

4.6.3 The n -potential vacuum polarization density

In this final section, we would like to evaluate the general n -potential vacuum polarization density expression. This function is found to be:

$$\begin{aligned} \rho_\kappa^n(\mathbf{x}) &= \frac{e^{n+1} |\kappa|}{4\pi^2 i} \int_0^\infty r_1^2 dr_1 \dots \int_0^\infty r_n^2 dr_n \phi(r_1) \dots \phi(r_n) \\ &\times \int_{C_F} dz \text{Tr} [\mathcal{G}_\kappa^0(r, r_1; z) \mathcal{G}_\kappa^0(r_1, r_2; z) \dots \mathcal{G}_\kappa^0(r_{n-1}, r_n; z) \mathcal{G}_\kappa^0(r_n, r; z)]. \end{aligned} \quad (4.6.16)$$

Compare with eqs.(4.4.37, 4.4.38 and 4.4.39). The trace of the products of n Green's functions is given by:

$$\begin{aligned} &\text{Tr} [\mathcal{G}_\kappa^0(r, r_1; z) \mathcal{G}_\kappa^0(r_1, r_2; z) \dots \mathcal{G}_\kappa^0(r_{n-1}, r_n; z) \mathcal{G}_\kappa^0(r_n, r; z)] \\ &= \frac{1}{(r_1 \dots r_n)^2} \sum_{\alpha_1, \alpha_2, \dots, \alpha_n, \alpha_{n+1}} s_{\alpha_{n+1}, \alpha_1}^\kappa(r) \\ &\times [\varphi_{\alpha_1, \kappa}^\dagger(r_1) \varphi_{\alpha_2, \kappa}(r_1) \varphi_{\alpha_1, \kappa}^\dagger(r_2) \dots \varphi_{\alpha_n, \kappa}(r_{n-1}) \varphi_{\alpha_n, \kappa}^\dagger(r_n) \varphi_{\alpha_{n+1}, \kappa}(r_n)]_0 \\ &\times J(z, E_{\alpha_1, \kappa}^0, E_{\alpha_2, \kappa}^0, \dots, E_{\alpha_n, \kappa}^0, E_{\alpha_{n+1}, \kappa}^0), \end{aligned} \quad (4.6.17)$$

where we have used the function $s_{\alpha, \beta}^\kappa$ given in eq.(4.6.14), and J is the fraction given in eq.(F.6.33):

$$\begin{aligned} &J(z, E_{\alpha_1, \kappa}^0, E_{\alpha_2, \kappa}^0, \dots, E_{\alpha_n, \kappa}^0, E_{\alpha_{n+1}, \kappa}^0) \\ &= \frac{1}{(E_{\alpha_1, \kappa}^0 - z)(E_{\alpha_2, \kappa}^0 - z) \dots (E_{\alpha_n, \kappa}^0 - z)(E_{\alpha_{n+1}, \kappa}^0 - z)}. \end{aligned} \quad (4.6.18)$$

The contour integration of the last term along the Feynman path C_F gives $I(E_{\alpha_1, \kappa}^0, \dots, E_{\alpha_{n+1}, \kappa}^0)$. This integral is introduced in the appendix eq.(F.6.1), its final solution is provided at the end of the referred appendix in eq.(F.6.52). Using our previous definition of the potential matrix element in eq.(4.6.13), our vacuum density reduces to:

$$\rho_{\kappa}^n(\mathbf{x}) = \frac{e^{n+1} |\kappa|}{4\pi^2 r^2 i} \sum_{\alpha_1, \alpha_2, \dots, \alpha_n, \alpha_{n+1}} s_{\alpha_{n+1}, \alpha_1}^{\kappa}(r) \times V_{\alpha_1 \alpha_2}^{\kappa} V_{\alpha_2 \alpha_3}^{\kappa} \dots V_{\alpha_{n-1} \alpha_n}^{\kappa} V_{\alpha_n \alpha_{n+1}}^{\kappa} \times I(E_{\alpha_1, \kappa}^0, E_{\alpha_2, \kappa}^0, \dots, E_{\alpha_n, \kappa}^0, E_{\alpha_{n+1}, \kappa}^0), \quad (4.6.19)$$

in which sums run over all labels of the numerical free-particle solutions, with energy $E_{\alpha_i, \kappa}^0$ and wavefunction $\varphi_{\alpha_i, \kappa}^0$ of the κ -problem. Finally, we should note that in a practical numerical calculation, one might not need to go to very high orders of n , since, generally speaking, the larger n is, the smaller the density $\rho_{\kappa}^n(\mathbf{x})$ in, and thus the energy-shift will be negligible. This rule of thumb stays valid until one goes for large quantum numbers n and j , as indicated by Mohr *et al.* in [9] and [7, section 4.2. pages 270-274], where $\rho_{\kappa}^3(\mathbf{x})$ dominates $\rho_{\kappa}^1(\mathbf{x})$ at large distances. A method to deal with the divergent one-potential term $\rho_{\kappa}^1(\mathbf{x})$, is to totally remove it, as done in eq.(4.4.45). In our numerical expressions, this subtraction becomes:

$$\rho_{\kappa}^{\text{VP}}(\mathbf{x}) - \rho_{\kappa}^1(\mathbf{x}) = \frac{e |\kappa|}{4\pi r^2} \sum_{\alpha} \left\{ \text{sgn}(E_{\alpha, \kappa}) \rho_{\alpha, \kappa}(r) - e \sum_{\beta} \frac{1 - \text{sgn}(E_{\alpha, \kappa}^0 E_{\beta, \kappa}^0)}{|E_{\alpha, \kappa}^0| + |E_{\beta, \kappa}^0|} s_{\beta, \alpha}^{\kappa}(r) V_{\alpha, \beta}^{\kappa} \right\}. \quad (4.6.20)$$

We remind the reader that $\rho_{\alpha, \kappa}(r)$ is the probability density associated with the α numerical solution in the presence of an external scalar potential. While the second term contains free-solutions and energies only. This last expression removes the one-potential contributions (containing the divergence) from the total vacuum polarization density, which means that this difference only contains the remaining terms $\rho_{\kappa}^0(\mathbf{x}) + \rho_{\kappa}^2(\mathbf{x}) + \rho_{\kappa}^3(\mathbf{x}) + \dots$. This subtraction was done by Mohr *et al.* in [7, section 4.2, eq.(237)], Gyulassy [152, eq.(21)], Greiner *et al.* [106, section 15.2 eq.(15.34)], and finally, Rinker and Wilets [155, page 753] (see 4.4.4). One possible problem which may be faced when evaluating this formula is the fact that it contains free energies and density in the right term, and bound ones, in the left one. It would be thus necessary to use the same set of basis functions for both free and bound problems, in order to render the combination meaningful.

We have stated in multiple locations of the thesis that the vacuum polarization density $\rho_{\kappa}^n(\mathbf{x})$ with even n , vanishes. In the next section, we shall show that if the basis we are using obeys the charge conjugation symmetry, then all vacuum polarization densities with even orders n should vanish.

4.6.4 Furry's theorem in the finite basis set

We start by the opposite κ -sign vacuum polarization density, of order n (cf. eq.(4.6.19)):

$$\rho_{-\kappa}^n(\mathbf{x}) = \frac{e^{n+1} |-\kappa|}{4\pi^2 r^2 i} \sum_{\alpha_1, \alpha_2, \dots, \alpha_n, \alpha_{n+1}} s_{\alpha_{n+1}, \alpha_1}^{-\kappa}(r) \times V_{\alpha_1 \alpha_2}^{-\kappa} V_{\alpha_2 \alpha_3}^{-\kappa} \dots V_{\alpha_{n-1} \alpha_n}^{-\kappa} V_{\alpha_n \alpha_{n+1}}^{-\kappa} \times I(E_{\alpha_1, -\kappa}^0, E_{\alpha_2, -\kappa}^0, \dots, E_{\alpha_n, -\kappa}^0, E_{\alpha_{n+1}, -\kappa}^0). \quad (4.6.21)$$

If our basis is symmetric under charge conjugation, then it should satisfy the condition of eq.(2.11.1) discussed in section 2.11. Furthermore, since the numerical wavefunctions and energies entering in

eqs.(4.6.19 and 4.6.21) are solutions of the free-particle Dirac equation, then by charge conjugation symmetry we can relate between:

1. a solution $\varphi_{+\kappa,i}^0(r)$ associated with an energy level $E_{+\kappa,i}^0$ of the $+\kappa$ problem,
2. a solution $\varphi_{-\kappa,i}^0(r)$ associated with an energy level $E_{-\kappa,i}^0$ of the $-\kappa$ problem,

by the following equations (cf. eqs.(2.1 and 2.11.67)):

$$\varphi_{-\kappa,i}^0(r) = \sigma_1 \varphi_{+\kappa,i}^0(r) \quad (4.6.22)$$

$$E_{-\kappa,i}^0 = -E_{+\kappa,i}^0. \quad (4.6.23)$$

The first line directly allows us to write the following relations:

$$s_{\alpha,\beta}^\kappa(r) = s_{\alpha,\beta}^{-\kappa}(r) \quad (4.6.24)$$

$$V_{\alpha\beta}^{-\kappa} = V_{\alpha\beta}^{+\kappa}. \quad (4.6.25)$$

We are now left with the integral I in eq.(4.6.21), and we shall now show how one can relate it to the previous opposite sign κ density of eq.(4.6.19). This integral can be written as:

$$I(E_{\alpha_1,-\kappa}^0, E_{\alpha_2,-\kappa}^0, \dots, E_{\alpha_n,-\kappa}^0, E_{\alpha_{n+1},-\kappa}^0) \quad (4.6.26)$$

$$= I(-E_{\alpha_1,\kappa}^0, -E_{\alpha_2,\kappa}^0, \dots, -E_{\alpha_n,\kappa}^0, -E_{\alpha_{n+1},\kappa}^0) \quad (4.6.27)$$

$$= \int_{C_F} dz \frac{1}{(-\epsilon_{\alpha_1,\kappa}^0 - z) \dots (-\epsilon_{\alpha_{n+1},\kappa}^0 - z)}. \quad (4.6.28)$$

We now perform the usual trick of shifting the positive poles below the real axis and the negative ones above it, so we can take the integral along the real axis. This can be done by the following energy replacement:

$$E_i^0 \rightarrow \epsilon_i^0 = E_i^0 - i\delta \text{sgn}(E_i^0), \quad (4.6.29)$$

with δ a small positive real number. Our integral now becomes:

$$(-1)^{n+1} \int_{-\infty}^{+\infty} dx \frac{1}{(\epsilon_{\alpha_1,\kappa}^0 + x) \dots (\epsilon_{\alpha_{n+1},\kappa}^0 + x)}, \quad (4.6.30)$$

where in the last step we extract all minus signs from the denominator factors. Using the change of variables $x \rightarrow -x$, our integral can be finally written as:

$$\begin{aligned} & I(E_{\alpha_1,-\kappa}^0, E_{\alpha_2,-\kappa}^0, \dots, E_{\alpha_n,-\kappa}^0, E_{\alpha_{n+1},-\kappa}^0) \\ &= (-1)^{n+1} \int_{-\infty}^{+\infty} dx \left[(\epsilon_{\alpha_1,\kappa}^0 - x) \dots (\epsilon_{\alpha_{n+1},\kappa}^0 - x) \right]^{-1} \\ &= (-1)^{n+1} I(E_{\alpha_1,\kappa}^0, E_{\alpha_2,\kappa}^0, \dots, E_{\alpha_n,\kappa}^0, E_{\alpha_{n+1},\kappa}^0), \end{aligned} \quad (4.6.31)$$

which relates to the opposite κ -sign contour integrations, by a factor of $(-1)^{n+1}$. All this discussion guides us to the conclusion that:

$$\rho_{-\kappa}^n(\mathbf{x}) = (-1)^{n+1} \rho_{+\kappa}^n(\mathbf{x}). \quad (4.6.32)$$

From this equation, we can understand two points:

1. The vacuum polarization density which sums both κ -signs vacuum polarization components:

$$\rho_{|\kappa|}^n(\mathbf{x}) = \rho_{+\kappa}^n(\mathbf{x}) + \rho_{-\kappa}^n(\mathbf{x}) = \left[1 + (-1)^{n+1}\right] \rho_{+\kappa}^n(\mathbf{x}), \quad (4.6.33)$$

vanishes in the \mathcal{C} -symmetric basis set, for any even order of interactions (n) with the external potential: $\alpha(\alpha Z)^n$.

2. For odd n orders, one needs only to calculate the vacuum polarization density of one of the two $\pm\kappa$ problems.

These two cases are summarized in the following equation:

$$\rho_{|\kappa|}^n(\mathbf{x}) = \rho_{+\kappa}^n(\mathbf{x}) + \rho_{-\kappa}^n(\mathbf{x}) = \begin{cases} 2\rho_{+\kappa}^n(\mathbf{x}) = 2\rho_{-\kappa}^n(\mathbf{x}) & \text{for odd } n \\ 0 & \text{for even } n \end{cases}. \quad (4.6.34)$$

This result is to be compared with the result of Furry's theorem, previously given in eq.(3.11.16). This final result was found in the PhD thesis of Gyulassy [157, eq.(2.19)], and similar expressions were derived by Greiner *et al.* in [106, eq.(15.25) and section 15.3], in which the vacuum polarization density is given by a formula which is explicitly odd in the number of time-independent external potential in which the electron lives. These latter results need extra few manipulations to arrive at ours.

Chapter 5

Conclusions and perspectives

After these long discussions, we will let the dust settle down and present the main conclusions we have reached, in addition to our view on how we can proceed beyond the results obtained during the three years work on this thesis project.

5.1 Conclusions

5.1.1 Charge conjugation symmetry in a finite basis

Charge conjugation symmetry in RKB

We first note that the \mathcal{C} -symmetry is realizable within the finite basis approximation, using the conventional restricted kinetic balance scheme. This realization occurs after choosing the basis functions to be the decoupled large and small components of the free radial Dirac solutions, that are written in terms of the spherical Bessel functions (as discussed in sections 2.11.2, 2.11.4 and 2.11.5). In addition, we have found that one can select a particular scaling of these basis functions, related to the zeros of the spherical Bessel functions (of the first kind), and obtain an orthogonal set of functions (within a confinement sphere) that vanish at the walls of the confinement sphere (as seen in sections 2.11.3 and 2.11.5). This result can be employed in the simulation of the relativistic confinement problem, and is important to consider for the calculations of the vacuum polarization density. This density, which (analytically speaking), contains a sum over bound-solutions and integrals over the continuum ones, reduces to two sums in the confinement problem as noted by Schlemmer and Zahn in [158, page 33].

Charge conjugation symmetry in DKB

We also note that the \mathcal{C} -symmetry can be smoothly realized in the dual kinetic balance scheme, as we have seen in section 2.11.6. This goal can be attained by setting the large and small components of some κ -basis, equal to the small and large component basis functions of the opposite κ -sign basis, respectively (see eq.(2.11.61)). The reader should notice that if the chosen basis set is κ -independent then this means that to realize the charge conjugation symmetry, one must, for each set of basis functions associated with some κ , introduce the same basis for the opposite sign κ problem, as (for instance) done by Shabaev *et al.* in [81, eqs.(10,11)].

5.1.2 Vacuum polarization density derivations and calculations

Concerning the vacuum polarization density calculations, we have provided a closed expressions of the expanded density in powers of the external scalar potential. These expressions can be directly employed in numerical codes. We have in addition shown that if a chosen set of basis functions does not respect the charge conjugation symmetry, one will obtain unphysical results, such as non-vanishing vacuum polarization density in the free particle problem, as seen in section 4.5.7 when using the RKB method. Generally speaking, in this case, one will obtain non-vanishing vacuum polarization densities for even powers in the external potential:

$$\rho_{|\kappa|}^n(\mathbf{x}) = \rho_{\kappa}^n(\mathbf{x}) + \rho_{-\kappa}^n(\mathbf{x}) \neq 0, \quad \text{for even } n \quad (5.1.1)$$

which is certainly unphysical. We finally note that the best vacuum polarization density results were obtained once the \mathcal{C} -symmetric dual kinetic balance basis was used, where we have observed the following physical features of the numerically obtained vacuum polarization density:

1. All densities associated with even powers of interaction with the external potentials do vanish:

$$\rho_{|\kappa|}^n(\mathbf{x}) = \rho_{\kappa}^n(\mathbf{x}) + \rho_{-\kappa}^n(\mathbf{x}) = 0, \quad \text{for even } n \quad (5.1.2)$$

which is inline with Furry's theorem. The reader can check fig. 4.5.25 and eq.(4.6.34).

2. The total vacuum polarization densities cancel very nicely for distances exceeding the Compton wavelength, as seen in figs. 4.5.21b and 4.5.23b. This point is consistent with what we know about the behavior of the (exact) vacuum polarization density, at relatively large distances.
3. One must only calculate the vacuum polarization density associated with one κ -sign, since we have shown that opposite κ -sign densities of an odd n -order density are equal (eq.(4.6.34)):

$$\rho_{\kappa}^n = \rho_{-\kappa}^n, \quad (5.1.3)$$

in the \mathcal{C} -symmetric bases.

4. In a finite basis calculation, one can remove the divergent behavior of the vacuum polarization density by eliminating the one-potential term, as done in eq.(4.6.20):

$$\begin{aligned} \rho_{\kappa}^{n \geq 2}(\mathbf{x}) &= \rho_{\kappa}^{\text{VP}}(\mathbf{x}) - \rho_{\kappa}^1(\mathbf{x}) \\ &= \frac{e|\kappa|}{4\pi r^2} \sum_{\alpha} \left\{ \text{sgn}(E_{\alpha,\kappa}) \rho_{\alpha,\kappa}(r) - e \sum_{\beta} \frac{1 - \text{sgn}(E_{\alpha,\kappa}^0 E_{\beta,\kappa}^0)}{|E_{\alpha,\kappa}^0| + |E_{\beta,\kappa}^0|} s_{\beta,\alpha}^{\kappa}(r) V_{\alpha,\beta}^{\kappa} \right\} \end{aligned} \quad (5.1.4)$$

This subtraction also removes the physical (Uehling) part of $\rho_{\kappa}^1(\mathbf{x})$, which can be easily added afterwards, since the Uehling potential has relatively simple expression.

5.2 Perspectives

All animals are equal but some animals are more equal than others.

George Orwell

All infinities are infinite but some infinities are more infinite than others.

Maen Salman

The first problem we are currently working on concerns translating the regularization / renormalization machinery of the vacuum polarization density (which is usually done analytically) into the language of the finite basis approximation. In order to express our words clearly, we shall give few words on regularization and renormalization.

5.2.1 Regularization and renormalization

Regularization is a mathematical trick in which one modifies a divergent integral by introducing some fictitious (auxiliary) parameters, such that the modified integral becomes convergent (but parameter dependent). The main regularization techniques that are used in the QED context are:

1. **The Pauli-Villars regularization** [159], where one modifies the propagator that lives under the divergent integral. For the vacuum polarization problem, one modifies the electron propagator and adds to it some auxiliary mass propagators designed to cancel the existing divergence(s). This can be done in momentum-space as done by Greiner and Reinhardt in [8, eq.(5.20)], or in real-space, as done by Indelicato *et al.* in [5, section III]. On the other hand, for the self-energy integral, one can modify the photon propagator using a propagator associated with a fictitious photon mass (momentum cutoff Λ). See, for instance, Peskin and Schroeder [99, eq.(7.17) and below].
2. **The dimensional regularization** introduced by 't Hooft and Veltman in [160], where one replaces the spacetime dimensions: $d = 4$, of the divergent integral, by $d = 4 - \epsilon$, where ϵ is a small positive number. Fortunately, integrals that were divergent for $d = 4$ are convergent for $d = 4 - \epsilon$. For further details about this regularization scheme, the reader can consult Ohlsson [33, section 13.3], Peskin and Schroeder [99, pages 249-251], and Mandl and Shaw [93, section 10.3].

The reader should remember that for any regularization choice, the obtained expressions are parameters-dependent: on the auxiliary masses, the large momentum cutoff Λ , or the dimensional parameter ϵ . The next trick is to evaluate the parameters-dependent integrals first, (note that the integrals are now convergent) and then absorb the obtained parameter-dependent divergent terms in the bare charge and mass. This absorption of divergences by the bare physical quantities is known as the renormalization technique, and consists of a redefinition of these quantities. The main idea here, is that one must distinguish between:

- The bare electron mass and charge: The ones we can obtain from the experiment if Nature's QED button is switched off. This is surely impossible to achieve.
- The experimental electron mass and charge: The numbers we get from the experiment. These numbers already account for the QED corrections, since Nature's QED button is always switched on.

This renormalization technique is justified after realizing that our equations contain the bare electron mass and charge instead of the experimental ones. Afterward, when we add the QED corrections to these equations, we obtain diverging quantities. In addition, since:

1. We do not know what the bare quantities are.
2. We know that the QED corrections should be finite and infinity is just a concept that cannot be physically measured, as mentioned by Hilbert in [79, page 201].

This leads to a conclusion that one can absorb the parameter-dependent divergences by the bare quantities, such that the final (overall) mass and charge are fixed (chosen) to be the experimental ones. This fact tells us that the QED theory needs the experimental values of the electron mass and charge, as expressed by Feynman's words in [84]:

We know what kind of a dance to do experimentally to measure this number very accurately, but we don't know what kind of a dance to do on a computer to make this number come out without putting it in secretly!

For further detailed discussions about the regularization and renormalization techniques, the reader may consult Huang [161], Zeidler [162, section 2.2], Mandl and Shaw [93, chapter 10], Ohlsson [33, chapter 13], Bethe and Salpeter [163, section 19], and Lindgren [15, chapter 12].

5.2.2 Regularization and renormalization in a finite basis

Being inspired by the regularization and renormalization techniques (briefly discussed in the previous section) we attacked this problem in the finite basis context, from two independent angles that are represented by the following two projects:

1. The momentum cutoff project

This project concerns eliminating the large-momentum contributions from the vacuum polarization density calculations by introducing a numerical momentum cutoff. This is usually done analytically (in literature) using the Pauli-Villars regularization, and we have tried to adapt it to the numerical problem. We have recently finished writing the associated simulation code, and tests will be soon running.

2. The variation of physical constants project

This project concerns varying the physical constants numerically, which we can thus call a “numerical renormalization” project. We have already run several calculations where we vary (tweak) the mass and the charge of the electron, and study how the numerically calculated QED quantities evolve with respect to these variations. The results of this project have not been thoroughly analyzed and deserve further investigation.

5.2.3 Hartree-Fock with QED

This part of the conclusions section concerns section 3.13 of this thesis, where we have discussed the inclusion of the QED corrections in the Hartree-Fock theory. Although not presented in the thesis, several numerical tests were carried out using the theoretical results of Saue [143] (see section 3.13.2), which was coded by Saue in the DIRAC code [136]. These results showed that the QED energy correction to the Hartree-Fock energy (given in eq.(3.13.14)) does not converge with an increasing size of the basis set. The reason behind these diverging results can be traced to the following two problematic points:

1. The utilized code uses the RKB prescription, which does not properly describe the negative-energy solutions, whereas the QED quantities are constructed from both positive and negative-energy solutions. As a consequence, the charge conjugation symmetry is violated in these calculations, and this is problematic.
2. The divergent nature of the QED quantities, as we have numerically seen in fig. 4.5.5.

The first point can be solved by working with the DKB prescription, or \mathcal{C} -DKB (symmetric under charge conjugation), while the second point is the more problematic one, and calls for a radical solution. In addition, in section 3.13.3, we have provided the results of our QED energy correction derivation, which includes the corrections of the second-order $\mathcal{S}^{(2)}$ -matrix and compared our result with the one previously obtained by Saue in [143]. The conclusion was that the results of Saue contained all these corrections, but missed the retardation effects in the exchange terms. These results are to be further analyzed and massaged such that they can be employed in practical Hartree-Fock calculations.

Final words

The divergences faced when numerically calculating the QED quantities call for an urgent need for a numerical regularization/renormalization procedure, which should eventually lead to converging numerical QED quantities (with increasing size of the finite basis set). This is not a simple task since the numerical translation of such exceptional and delicate mathematical manipulations (regularization of divergent integrals) is an extremely tricky task. The reader should finally note that the error associated with the Hartree-Fock method is high, and is (generally speaking) beyond the corrections provided by the QED theory. However, what is important is the success of this machinery, which will open the road for more sophisticated methods that include higher-order electron correlation effects, such as coupled-cluster and configuration interaction methods, and will thus (at least in principle) provide extremely accurate numerical results that are exceptionally well matching with the experimental values.

Chapter 6

French résumé

L'objectif principal de cette thèse est de traduire les corrections de l'électrodynamique quantique (QED) au langage de la chimie quantique relativiste: dans le cadre de l'approximation de l'équation de Dirac en base finie. Inconsciemment, notre cerveau est habitué à associer de grandes vitesses à de grandes distances, ce qui fait qu'il nous est difficile de comprendre, à première vue, pourquoi la théorie atomique des électrons pourrait devoir tenir compte de la relativité restreinte. On peut cependant montrer que la vitesse moyenne d'un électron occupant l'état fondamental d'un atome hydrogénoïde est donnée par $v = (\alpha Z) c$, où $\alpha = e^2 / (4\pi\epsilon_0 \hbar c) \approx 1/137$ est la constante de structure fine fondamentale (adimensionnelle), Z est le numéro atomique, et c est la vitesse de la lumière. Cette expression simple indique que les effets relativistes peuvent être négligés pour les éléments légers, mais qu'ils doivent être généralement prises en compte, en particulier pour les éléments lourds. En 1928, Paul Dirac a proposé une théorie (équation) quantique relativiste qui, malgré sa forme simple (mathématiquement compacte), était capable de rendre compte d'une grande partie de la physique, qui manquait dans la théorie originale de Schrödinger. Malgré sa supériorité (généralité) par rapport à l'équation de Schrödinger, l'équation de Dirac n'a pas réussi à prédire des divers phénomènes quantiques, et notamment les deux suivants :

1. Le moment magnétique de spin de l'électron, dont on a constaté expérimentalement qu'il est d'environ $g_{\text{exp.}} \approx 2.0023193$ [1], et qui a été prédit par la théorie de Dirac comme étant $g_{\text{Dirac}} = 2$.
2. Le décalage de Lamb (Lamb shift) [2]: la séparation entre les niveaux d'énergie $2s_{\frac{1}{2}}$ and $2p_{\frac{1}{2}}$ de l'atome d'hydrogène, dont la dégénérescence est prévue par la théorie de Dirac.

Il s'est avéré qu'une grande partie de la raison de cet écart réside dans la théorie de l'électrodynamique quantique (QED), qui a donné des résultats numériques capables de combler merveilleusement un pourcentage énorme de l'écart entre la théorie Dirac et l'expérience. La QED est la théorie qui couple le champ électronique quantifié avec le champ photonique quantifié, par la densité hamiltonienne d'interaction: $\mathcal{H}^{\text{QED}}(x) = -ec\bar{\Psi}(x)\gamma^\mu\Psi(x)A_\mu(x)$, où Ψ (et $\bar{\Psi}$) et A_μ sont les opérateurs de champ de l'électron (et du positron) et du photon, respectivement. Dans ce contexte, l'Hamiltonien total contient l'Hamiltonien électronique libre (électrons sans interaction) en plus de l'Hamiltonien photonique libre (en l'absence de toute source électromagnétique). Dans le formalisme de la matrice \mathcal{S} , l'Hamiltonien (densité) de couplage ci-dessus entre les deux champs (électronique et photonique) est traité d'une manière perturbative (en puissances de cette interaction), comme nous le verrons dans le chapitre 3.

Pour donner une idée générale du problème, nous parlerons des corrections QED d'ordre le plus bas. Dans son ordre le plus bas e^2 , et sans photons réels, la matrice de diffusion (scattering matrix) donne lieu à trois corrections QED:

1. L'échange d'un seul photon (single-photon exchange) entre deux électrons.
2. La polarisation du vide (vacuum-polarization).
3. La auto-énergie (self-energy).

La première correction concerne l'interaction entre deux électrons, à son ordre le plus bas, où un électron ressent l'existence de l'autre électron par l'échange d'un photon virtuel. Cette correction n'existe que si le nombre d'électrons dans notre système est d'au moins 2, et nous montrerons qu'elle contient deux contributions, dont l'une est locale : comme le terme directe de Hartree, et l'autre est non-locale : comme le terme d'échange, dans la théorie de Hartree-Fock.

Les deuxième et troisième corrections ne contiennent qu'un seul électron réel, ces corrections doivent donc être prises en compte pour tous les systèmes, partant du simple atome d'hydrogène (1 électron) jusqu'aux molécules compliquées à plusieurs électrons.

Nous allons maintenant nous concentrer sur les atomes simples à 1 électron, où les deux dernières corrections peuvent être prises en compte. La deuxième correction représente l'effet de polarisation du vide, qui décrit l'interaction d'un électron avec une bulle de vide (qui représente la production d'une paire électron-positron). Cette bulle représente le courant de densité de polarisation du vide, générée dans l'espace lorsqu'un inducteur (tel qu'un atome) existe, voir [5] et [6].

De plus, en l'absence d'inducteur, cette correction s'annule, ce qui peut être démontré à l'aide du théorème de Furry qui est basé sur un argument de symétrie de conjugaison de charge. Ce théorème sera discuté dans la section 3.11. L'effet de polarisation du vide est très localisé, et vit à de très petites distances près du noyau, fortement à des distances plus petites que la longueur d'onde de Compton (réduite): $r < \frac{\hbar}{mc}$. Plus précisément, le potentiel associé à la polarisation du vide d'ordre le plus bas (la contribution la plus importante), c'est-à-dire le potentiel de Uehling : d'ordre α (αZ), décroît exponentiellement lorsque r (distance nucléaire) devient plus grand que la longueur d'onde de Compton, ce qui a été mentionné dans les travaux de Mohr *et al.* dans [7, Page 268] et Greiner et Reinhardt dans [8, Page 283]. Le potentiel associé à la polarisation du vide d'ordre supérieur (en puissance du potentiel externe) : Le terme de Wichmann-Kroll de α (αZ)³, décroît plus lentement que le potentiel de Uehling, et par conséquent, cette correction de Wichmann-Kroll domine celle de Uehling pour les états atomiques avec de grands nombres quantiques n et j (s'éloignant du noyau) comme le montrent les travaux de Soff et Mohr [9, Table I] et Huang [10, eqs.(23-25), eqs.(30,33)]. D'une manière générale, les états liés inférieurs seront plus affectés par les effets de polarisation du vide, que les plus élevés (en énergies). Il convient de noter qu'un processus associé à un ordre α^m (αZ) ^{n} est représenté par un diagramme de Feynman contenant m photons virtuels (lignes de photons internes), tandis que n dans (αZ) ^{n} représente le nombre d'interactions avec le potentiel nucléaire classique. Le potentiel effectif (de QED) associé à un tel processus est généralement (dans la littérature) écrit comme V_{mn} . Cette notation a été utilisée par Huang [10] and Blomqvist [11], et autres.

Contrairement à la polarisation du vide, l'auto-énergie est un effet non-local, et il est donc (généralement) plus compliqué à évaluer, dans les deux sens : mathématiquement (analytiquement), et numériquement. Cet effet décrit l'émission d'un photon et son absorption par un photon virtuel, et les deux ordres chronologiques de l'absorption et l'émission sont autorisés. Dans les atomes électroniques, l'auto-énergie est la correction QED dominante, et ce fait peut être observé dans le travail de Soff *et al.* [12, Figure. 10] où ils montrent différentes contributions au décalage de Lamb

(dans les atomes hydrogénoïde) : Le décalage de Lamb est la séparation entre les états $2s_{\frac{1}{2}}$ et $2p_{\frac{1}{2}}$ dans les atomes hydrogénoïde, que l'équation de Dirac ne parvient pas à prédire, et qui est largement décrit par ces deux corrections QED.

Ce fait de la dominance de la correction de l'auto-énergie dans les atomes électroniques est inversé dès que l'on considère l'atome muonique, au lieu de l'atome électronique. La raison de cette affirmation est due à la très grande masse du muon. Avec une masse d'environ $m_\mu \approx 200m_e$, le muon orbite donc deux cents fois plus près du noyau (par rapport à l'électron), ce qui se traduit par une modification du rayon de Bohr: $a_B^\mu \approx \frac{a_B^e}{200}$. À ces très petites distances, l'effet de polarisation du vide vit, et domine donc la self énergie, comme le mentionnent Mohr *et al.* [7, Page 266] Greiner et Reinhardt [8, Pages 288-290] (voir également les travaux de Dubler *et al.* [14]).

Une fois que le développement de perturbation (correction) de l'énergie (ou de la fonction d'onde) est effectuée, on obtient deux types de contributions :

- Les corrections radiatives : dans lesquelles les diagrammes de Feynman représentatifs contiennent des boucles électroniques ou des boucles électron-photon.
- Les corrections non radiatives : dans lesquelles les électrons n'échangent que des photons virtuels. Dans son ordre le plus bas, deux électrons peuvent échanger un photon unique, ce qui donne lieu à l'interaction électron-électron (y compris l'effet de retardement dans le terme d'échange). Les diagrammes d'ordre supérieur tiennent compte des échanges de photons d'ordre supérieur (corrections de corrélation).

Pour des discussions sur cette distinction, le lecteur peut consulter le livre de Lindgren [15], ainsi que le chapitre d'Indelicato et Mohr [16].

Jusqu'à présent, en chimie quantique, les effets de corrélation sont très bien étudiés et compris, alors que les corrections radiatives ne le sont pas. L'inclusion de ces corrections QED dans les calculs numériques est une tâche très difficile, en raison de l'énorme complication qui apparaît lorsqu'un système est constitué d'un nombre relativement important d'électrons en orbite autour d'un potentiel nucléaire moléculaire (généralement non radial). Les principales tentatives pour prendre en compte ces corrections radiatives ont été faites en incluant certaines des corrections d'ordre inférieur sous la forme de potentiels effectifs, décrivant la polarisation du vide et les processus d'auto-énergie. Ces potentiels seront discutés dans la section 3.12. Le lecteur doit noter que les deux principales limitations, associées à l'inclusion des corrections QED dans les calculs numériques sont:

1. Bien que les potentiels effectifs d'auto-énergie (discutés dans la section 3.12.2) aient démontré leur capacité à obtenir des corrections d'énergie précises -par rapport à des calculs plus sophistiqués- (rappelons que ces potentiels sont faits pour cela), leur validité pour d'autres quantités telles que la fonction d'onde ou les propriétés moléculaires (liées aux énergies corrigées par ces potentiels) est sans doute discutable. Cette faiblesse vient simplement du fait que ces potentiels sont ajustés/paramétrés pour reproduire les bons décalages d'énergie.
2. On peut, en principe, procéder de la manière rigoureuse, en utilisant des méthodes beaucoup plus précises, sans avoir besoin d'aucun type d'ajustement (fitting) énergétique (comme pour les potentiels d'auto-énergie effectifs), comme cela a été fait dans : [6, 7, 17, 18, 19, 20] et de nombreuses autres références connexes, pour obtenir de très bons résultats. Malheureusement, cette voie n'est pas très bien adaptée aux calculs pratiques et ne peut être empruntée que pour des systèmes "simples", comme les atomes à un ou quelques électrons, mais pas pour les molécules à plusieurs électrons, ce qui est la raison évidente pour laquelle nous utilisons plutôt les potentiels effectifs.

En raison de ces deux limitations, nous décidons de suivre une voie complètement différente : Calculer ces corrections à la manière de la chimie quantique : d'une manière numérique rapide. Dans cette procédure, les quantités QED sont construites à partir des solutions numériques (énergies et fonctions d'onde) de l'équation de Dirac. Les principaux avantages de ce choix de voie sont les suivants :

1. Les quantités résultantes sont (en principe) exemptes de paramétrage (ajustement) énergétique, et les quantités résultantes, telles que les fonctions d'onde et les propriétés moléculaires, sont donc plus valides, en principe du moins.
2. Les calculs numériques ne sont pas très coûteux (numériquement parlant), comme nous nous y attendions jusqu'à présent.

En raison de la complexité de la correction de l'auto-énergie non-locale, cette thèse se concentrera sur la correction de la polarisation du vide, car elle est relativement plus facile à manipuler, tant analytiquement que numériquement. Le lecteur doit noter que cette manipulation (massage) de la chimie quantique relativiste pour tester sa capacité à calculer la densité de polarisation du vide, conduit à une meilleure compréhension de la façon dont nous pouvons étendre nos compétences/manipulations acquises, pour résoudre le problème de la polarisation du vide, au:

1. Problème de self énergie (dans l'ensemble de base fini).
2. Le problème Hartree-Fock qui inclut les corrections QED.
3. L'inclusion des corrections de QED dans les méthodes de chimie quantique de haut niveau.

Malheureusement, la thèse est limitée dans le temps, et ces trois points seront au-delà de ce projet de doctorat. Néanmoins, nous allons donner notre vision sur la façon dont on peut s'attaquer à ces problèmes dans la section 3.13 et la section finale de cette thèse, qui concerne nos perspectives sur les futures étapes à suivre.

Chapitre 3 : L'équation de Dirac

Dans le chapitre 2, nous discuterons de l'équation de Dirac et de ses symétries discrètes associées, à la fois sous la forme mathématique abstraite et une fois que cette équation est approximée par un nombre fini de fonctions de base, typiquement par des fonctions gaussiennes. La symétrie de conjugaison de charge (symétrie \mathcal{C}) sera d'une importance centrale dans cette thèse, et l'étude qui lui est associée a donné naissance à notre article intitulé "Charge Conjugation Symmetry in the Finite Basis Approximation of the Dirac Equation" [21] où nous indiquons soigneusement les conditions qui rendent l'ensemble de base fini \mathcal{C} -symétrique. Dans l'approximation par ensemble de bases, un ensemble de fonctions de base doit être soigneusement conçu pour éviter les instabilités numériques et l'apparition de solutions non physiques (fallacieuses: spurious). Ce chapitre aborde les différents choix de schémas de base et présente leurs avantages et inconvénients. À la fin du chapitre, nous présenterons les résultats de quelques calculs effectués sur le problème de Dirac à un électron en présence d'un potentiel coulombien: $-\frac{Ze^2}{4\pi\epsilon_0 r}$, et nous discuterons la réalisation pratique de la symétrie de conjugaison de charge, dans l'approximation des bases finies. À la fin de ce chapitre, le lecteur devrait avoir une idée générale de la manière dont l'équation de Dirac est approximée dans une base finie.

Conjugaison de charge

La symétrie de conjugaison des charges, ou symétrie \mathcal{C} , relie une particule à son antiparticule correspondante : celle-ci possède les mêmes caractéristiques physiques que la particule, à l'exception d'une charge de signe opposé. Pour dériver l'opérateur de conjugaison de charge, nous commençons par l'équation de Dirac d'un électron dans un quadri-potential arbitraire $A_\mu(x)$:

$$[\gamma^\mu (i\hbar\partial_\mu + eA_\mu(x)) - mc] \psi(x) = 0. \quad (6.0.1)$$

Ce quadri-potential est une fonction des potentiels scalaire et vecteur: $A_\mu(x) = (\varphi(x)/c, \mathbf{A}(x))$. L'objectif est de déterminer quelles opérations doivent être effectuées sur la fonction d'onde pour que la fonction modifiée satisfasse à l'équation positronique:

$$[\gamma^\mu (i\hbar\partial_\mu - eA_\mu(x)) - mc] \mathcal{C}\psi(x) = 0, \quad (6.0.2)$$

qui décrit le comportement d'un positron: une particule ayant la même masse que l'électron, mais ayant un signe de charge opposé. Nous commençons par conjuguer (complexe) la première équation, de façon à ce que le nombre imaginaire ait un signe moins:

$$[(\gamma^\mu)^* (-i\hbar\partial_\mu + eA_\mu(x)) - mc] \psi^*(x) = 0. \quad (6.0.3)$$

On voit à ce point que pour obtenir l'équation de Dirac décrivant le positron (eq.(6.0.2)), il suffit d'appliquer une opération matricielle, que nous appellerons U_c , qui inverse le signe des matrices gamma complexes conjuguées dans la dernière équation, c'est-à-dire en respectant les conditions suivantes:

$$U_c (\gamma^\mu)^* U_c^{-1} = -\gamma^\mu, \quad (6.0.4)$$

et donc, conduisant à l'équation conjuguée de charge suivante:

$$[U_c (\gamma^\mu)^* U_c^{-1} (-i\hbar\partial_\mu + eA_\mu(x)) - mc] U_c \psi^*(x) = 0 \quad (6.0.5)$$

$$[\gamma^\mu (i\hbar\partial_\mu - eA_\mu(x)) - mc] \mathcal{C}\psi(x) = 0, \quad (6.0.6)$$

où l'opérateur de conjugaison de charge $\mathcal{C} = U_c \mathcal{K}_0$ contient les deux opérations: l'opérateur matriciel U_c et la conjugaison complexe \mathcal{K}_0 . Dans la représentation de Dirac des matrices gamma (eq.(2.4.10)), la matrice U_c respectant les quatre conditions de l'eq.(6.0.4) se trouve être (jusqu'à un facteur de phase):

$$U_c = \gamma^2. \quad (6.0.7)$$

En résumé, nous avons commencé par un électron, dont la fonction d'onde $\psi(x)$ satisfait l'équation de Dirac de l'électron.(6.0.1) et nous avons fini par un positron, dont la fonction d'onde $\mathcal{C}\psi(x)$ satisfait l'équation d'antiparticule correspondante: eq.(6.0.2). La forme finale de l'opération \mathcal{C} est donc:

$$\mathcal{C} = \gamma^2 \mathcal{K}_0; \quad \mathcal{K}_0: \text{Complex conjugation} \quad (6.0.8)$$

Le terme "conjugaison de charge" a été inventé (coined) par Kramers [62]. Cette symétrie a conduit Dirac à prédire l'existence de l'anti-électron, c'est-à-dire du positron. En présence d'un potentiel indépendant du temps $A_\mu(x) = A_\mu(\mathbf{x})$, l'équation de Dirac indépendante du temps peut être écrite comme:

$$[c\boldsymbol{\alpha} \cdot [-i\hbar\boldsymbol{\nabla} + e\mathbf{A}(\mathbf{x})] + \beta mc^2 - e\varphi(\mathbf{x})] \psi(\mathbf{x}) = +E\psi(\mathbf{x}), \quad (6.0.9)$$

où la précédente fonction d'onde dépendante du temps est liée à la dernière par: $\psi(x) = e^{-\frac{i}{\hbar}Et}\psi(\mathbf{x})$. La solution à charge conjuguée $\mathcal{C}\psi(\mathbf{x})$, obéit à la même équation mais avec une énergie et une charge élémentaire de signes opposés:

$$[c\boldsymbol{\alpha} \cdot [-i\hbar\nabla - e\mathbf{A}(\mathbf{x})] + \beta mc^2 + e\varphi(\mathbf{x})] \mathcal{C}\psi(\mathbf{x}) = -E\mathcal{C}\psi(\mathbf{x}). \quad (6.0.10)$$

Ce signe d'énergie négatif supplémentaire peut (en outre) être attribué au fait que l'opérateur \mathcal{C} contient un opérateur de conjugaison complexe, qui inverse le signe de l'exposant $e^{+\frac{iE}{\hbar}t}$ de la fonction d'onde de l'éq.(2.6.26):

$$\mathcal{C}\psi(x) = \mathcal{C}\psi(\mathbf{x}) e^{-\frac{iE}{\hbar}t} = \gamma^2 \psi^*(\mathbf{x}) e^{+\frac{iE}{\hbar}t}. \quad (6.0.11)$$

Dans le régime indépendant du temps, la symétrie de conjugaison des charges permet donc de relier les fonctions d'onde des particules d'énergie et de charge opposés, comme le prédisent les éqs.(6.0.9 et 6.0.10). En outre, le lecteur doit noter que dans le cas d'un electron libre, qui est un cas particulier du problème indépendant du temps, les éqs.(6.0.9 and 6.0.10) se réduisent à :

$$[c\boldsymbol{\alpha} \cdot [-i\hbar\nabla] + \beta mc^2] \psi(\mathbf{x}) = +E\psi(\mathbf{x}) \quad (6.0.12)$$

$$[c\boldsymbol{\alpha} \cdot [-i\hbar\nabla] + \beta mc^2] \mathcal{C}\psi(\mathbf{x}) = -E\mathcal{C}\psi(\mathbf{x}), \quad (6.0.13)$$

Ces équations montrent que les partenaires à charge conjuguée appartiennent au même problème: ils résolvent la même équation mais avec un signe d'énergie opposé, ce qui permet de conclure que la symétrie de conjugaison des charges lie les solutions libres à énergie opposée.

L'équation de Dirac radiale et son approximation en base finie

En présence d'un potentiel radial purement scalaire $\varphi(r)$, on peut montrer que l'opérateur de moment angulaire total $\mathbf{J} = \mathbf{L} + \mathbf{\Sigma}$, où $\mathbf{\Sigma}$ est la matrice de spin 4×4 , commute avec l'opérateur de Dirac:

$$[J_i, H_D] = 0, \quad \text{with } H_D = c\boldsymbol{\alpha} \cdot \hat{\mathbf{p}} + \beta mc^2 - e\varphi(r) \quad (6.0.14)$$

En conséquence, on peut, après une analyse plus poussée, montrer que le spinor de Dirac à quatre composantes peut être écrit comme:

$$\psi_{\kappa, m_j}(\mathbf{x}) = \frac{1}{r} \begin{bmatrix} P_{\kappa}(r) \Omega_{\kappa, m_j}(\theta, \varphi) \\ iQ_{\kappa}(r) \Omega_{-\kappa, m_j}(\theta, \varphi) \end{bmatrix}, \quad (6.0.15)$$

où $\Omega_{\kappa, m_j}(\theta, \varphi)$ sont les spinors sphériques à deux composantes. Les fonctions radiales P_{κ} et Q_{κ} résolvent l'équation de Dirac radiale :

$$\begin{bmatrix} mc^2 - e\varphi(r) - E & -c\hbar \left[\frac{d}{dr} - \frac{\kappa}{r} \right] \\ c\hbar \left[\frac{d}{dr} + \frac{\kappa}{r} \right] & -mc^2 - e\varphi(r) - E \end{bmatrix} \begin{bmatrix} P_{\kappa}(r) \\ Q_{\kappa}(r) \end{bmatrix} = 0 \quad (6.0.16)$$

L'objectif est maintenant d'effectuer des calculs numériques dans lesquels ces fonctions radiales sont approximées par un nombre fini de fonctions de base radiales. Pour effectuer ces calculs, on spécifie un ensemble des fonctions de base pour chaque composant de la solution de Dirac, associé à un nombre quantique κ , et ainsi on approche les fonctions radiales exactes $P_{\kappa}(r)$ et $Q_{\kappa}(r)$ par des développements sur les éléments des ensembles de base, comme suit:

$$\begin{aligned} P_{\kappa}(r) &\approx \mathcal{P}_{\kappa}(r) = \sum_{i=1}^{n_{\kappa}^L} c_{\kappa, i}^L \pi_{\kappa, i}^L(r) \\ Q_{\kappa}(r) &\approx \mathcal{Q}_{\kappa}(r) = \sum_{i=1}^{n_{\kappa}^S} c_{\kappa, i}^S \pi_{\kappa, i}^S(r) \end{aligned} \quad (6.0.17)$$

Les fonctions $\pi_{\kappa,i}^{L/S}(r)$ sont de grandes et petites fonctions de base radiales, associées aux coefficients d'expansion $c_{\kappa,i}^{L/S}$, et $n_{\kappa}^{L/S}$ est le nombre d'éléments de base pour chacun des ensembles. À proprement parler, la α -ième solution numérique (radiale) de l'équation de Dirac est approximée par:

$$\varphi_{\alpha,\kappa}(r) = \begin{bmatrix} \mathcal{P}_{\alpha,\kappa}(r) \\ \mathcal{Q}_{\alpha,\kappa}(r) \end{bmatrix} = \sum_{i=1}^{n_{\kappa}^L} c_{\alpha,\kappa,i}^L \begin{bmatrix} \pi_{\kappa,i}^L(r) \\ 0 \end{bmatrix} + \sum_{i=1}^{n_{\kappa}^S} c_{\alpha,\kappa,i}^S \begin{bmatrix} 0 \\ \pi_{\kappa,i}^S(r) \end{bmatrix}, \quad (6.0.18)$$

ce qui conduit à la représentation matricielle suivante du problème des valeurs propres de Dirac:

$$H_{\kappa} \mathbf{c}_{\alpha,\kappa} = \epsilon_{\alpha,\kappa} S_{\kappa} \mathbf{c}_{\alpha,\kappa}, \quad (6.0.19)$$

où les éléments de cette équation sont la matrice hamiltonienne H_{κ} de dimensions $(n_{\kappa}^L + n_{\kappa}^S) \times (n_{\kappa}^L + n_{\kappa}^S)$, la matrice de recouvrement S_{κ} (mêmes dimensions) et les solutions propres $\mathbf{c}_{\alpha,\kappa}$ de dimensions $(n_{\kappa}^L + n_{\kappa}^S) \times 1$ associées à la valeur propre d'énergie $\epsilon_{\alpha,\kappa}$ et à la solution numérique $\varphi_{\alpha,\kappa}(r)$. Ces termes sont respectivement donnés par:

$$H_{\kappa} = \begin{bmatrix} mc^2 S_{\kappa}^{LL} - e\varphi_{\kappa}^{LL} & c\hbar \Pi_{\kappa} \\ c\hbar \Pi_{\kappa}^t & -mc^2 S_{\kappa}^{SS} - e\varphi_{\kappa}^{SS} \end{bmatrix} \quad (6.0.20)$$

$$S_{\kappa} = \begin{bmatrix} S_{\kappa}^{LL} & 0 \\ 0 & S_{\kappa}^{SS} \end{bmatrix}; \quad \{\epsilon_{\alpha,\kappa}, \mathbf{c}_{\alpha,\kappa}\} = \left\{ \epsilon_{\alpha,\kappa}, \begin{bmatrix} \mathbf{c}_{\alpha,\kappa}^L \\ \mathbf{c}_{\alpha,\kappa}^S \end{bmatrix} \right\}. \quad (6.0.21)$$

Les éléments des matrices sont donnés par les intégrales radiales suivantes:

$$[S_{\kappa}^{XX}]_{ij} = \int_0^{\infty} \pi_{\kappa,i}^X \pi_{\kappa,j}^X dr \quad (6.0.22)$$

$$[\varphi_{\kappa}^{XX}]_{ij} = \int_0^{\infty} \pi_{\kappa,i}^X \varphi \pi_{\kappa,j}^X dr \quad (6.0.23)$$

$$[\Pi_{\kappa}]_{ij} = - \int_0^{\infty} \pi_{\kappa,i}^L \left[\frac{d}{dr} - \frac{\kappa}{r} \right] \pi_{\kappa,j}^S dr, \quad (6.0.24)$$

où X peut être l'une des deux lettres $X = L, S$ (grandes et petites composantes). Les premiers calculs numériques de l'équation de Dirac radiale à un électron dans le cadre des ensembles de base finis (ainsi que la méthode Hartree-Fock relativiste à quatre composantes pour plusieurs électrons), qui reposaient sur notre connaissance des calculs non relativistes, ont échoué. La raison principale de ces échecs est due au fait que les fonctions de base à grande et petite composantes π_{κ}^L et π_{κ}^S ne respectaient pas le bon couplage qui est vu dans l'équation de Dirac radiale dans eq.(6.0.16). Ce point va être discuté dans la prochaine section et la solution s'est avérée être d'utiliser ce que l'on appelle: l'équilibre cinétique (kinetic balance), que nous allons discuter dans la prochaine section.

Balances cinétiques

L'équation de Dirac radiale donnée dans eq.(6.0.16) peut être écrite sous une forme légèrement différente:

$$Q_{\kappa} = \frac{\hbar}{mc} \frac{1}{1 + \frac{e\varphi + E}{mc^2}} \left[\frac{d}{dr} + \frac{\kappa}{r} \right] P_{\kappa} \quad (6.0.25)$$

$$P_{\kappa} = \frac{\hbar}{mc} \frac{1}{1 - \frac{e\varphi + E}{mc^2}} \left[\frac{d}{dr} - \frac{\kappa}{r} \right] Q_{\kappa}. \quad (6.0.26)$$

Pour la partie positive du spectre, les solutions qui nous intéressent (les solutions liées) se situent autour de $E \approx mc^2$ (juste en dessous). Après avoir supposé que $e\varphi$ (le potentiel électrique) est négligeable devant mc^2 , et donc, devant E , le couplage entre la petite et la grande composante (première équation) peut être approximé par:

$$Q_\kappa \approx \frac{\hbar}{2mc} \left[\frac{d}{dr} + \frac{\kappa}{r} \right] P_\kappa, \quad (6.0.27)$$

qui est connue sous le nom de condition d'équilibre cinétique restreint (the restricted kinetic balance condition). Dans le langage des ensembles de bases finies (discuté dans la section précédente), cette approximation se traduit par le développement numérique suivant:

$$\begin{bmatrix} \mathcal{P}_{\alpha,\kappa}(r) \\ \mathcal{Q}_{\alpha,\kappa}(r) \end{bmatrix} = \sum_{i=1}^{n_\kappa} c_{\alpha,\kappa,i}^L \begin{bmatrix} \pi_{\kappa,i}^L(r) \\ 0 \end{bmatrix} + \sum_{i=1}^{n_\kappa} c_{\alpha,\kappa,i}^S \begin{bmatrix} 0 \\ \frac{\hbar}{2mc} \left[\frac{d}{dr} + \frac{\kappa}{r} \right] \pi_{\kappa,i}^L(r) \end{bmatrix}. \quad (6.0.28)$$

De même, on peut faire la même chose avec les solutions d'énergie négative qui sont proches de $-mc^2$, et obtenir une approximation de la fonction radiale de la grande composante en fonction de la petite:

$$P_\kappa \approx \frac{\hbar}{2mc} \left[\frac{d}{dr} - \frac{\kappa}{r} \right] Q_\kappa. \quad (6.0.29)$$

Cette condition est connue comme la condition d'équilibre cinétique inverse (the inverse kinetic balance condition) [80], et conduit au développement suivant des solutions numériques:

$$\varphi_{\alpha,\kappa}(r) = \begin{bmatrix} \mathcal{P}_{\alpha,\kappa}(r) \\ \mathcal{Q}_{\alpha,\kappa}(r) \end{bmatrix} = \sum_{i=1}^{n_\kappa} c_{\alpha,\kappa,i}^L \begin{bmatrix} \frac{\hbar}{2mc} \left[\frac{d}{dr} - \frac{\kappa}{r} \right] \pi_{\kappa,i}^S(r) \\ 0 \end{bmatrix} + \sum_{i=1}^{n_\kappa} c_{\alpha,\kappa,i}^S \begin{bmatrix} 0 \\ \pi_{\kappa,i}^S(r) \end{bmatrix}. \quad (6.0.30)$$

Une prescription plus intéressante (jusqu'à un certain point), est connue sous le nom de condition d'équilibre cinétique double (dual kinetic balance condition) [81], qui combine les deux prescriptions précédentes, où le développement numérique se fait de la manière suivante:

$$\varphi_{\alpha,\kappa}(r) = \begin{bmatrix} \mathcal{P}_{\alpha,\kappa}(r) \\ \mathcal{Q}_{\alpha,\kappa}(r) \end{bmatrix} = \sum_{i=1}^{n_\kappa^L} c_{\alpha,\kappa,i}^- \begin{bmatrix} \pi_{\kappa,i}^+(r) \\ \frac{\hbar}{2mc} \left[\frac{d}{dr} + \frac{\kappa}{r} \right] \pi_{\kappa,i}^+(r) \end{bmatrix} + \sum_{i=1}^{n_\kappa^S} c_{\alpha,\kappa,i}^- \begin{bmatrix} \frac{\hbar}{2mc} \left[\frac{d}{dr} - \frac{\kappa}{r} \right] \pi_{\kappa,i}^-(r) \\ \pi_{\kappa,i}^-(r) \end{bmatrix}, \quad (6.0.31)$$

Cette prescription est plus démocratique entre les solutions d'énergie positive et négative, et montrera des résultats importants pour le calcul de la densité de polarisation du vide.

La symétrie \mathcal{C} dans l'ensemble de base fini

Nous disons qu'un ensemble de base est symétrique sous la symétrie \mathcal{C} , si la conjugaison de charge de tout élément de l'ensemble de base est un élément de l'ensemble de base lui-même :

$$\mathcal{C}\varphi_i \in \{\varphi_i\}_{i=1}^n, \quad \forall i. \quad (6.0.32)$$

Nous allons ensuite voir comment cette condition peut être remplie dans un calcul relativiste pratique, plus spécifiquement, dans le contexte de l'équilibre cinétique restreint et double. Dans la première prescription, l'analyse nous guidera dans la découverte d'un nouveau choix de fonctions de base qui a une application très importante : simuler le problème de l'électron relativiste confiné.

La symétrie \mathcal{C} avec la condition d'équilibre cinétique

Après avoir forcé cette dernière condition à être remplie (satisfaite) dans le problème de l'équilibre cinétique (restricted kinetic balance), nous constatons que les fonctions de base doivent être limitées aux formes suivantes:

$$\begin{aligned}\pi_{\kappa,i}^L &= j_\ell(b_{\kappa,i}r) \\ \pi_{\kappa,i}^S &= \frac{\hbar b_{\kappa,i} \text{sgn}(\kappa)}{2mc} j_{\ell-\text{sgn}(\kappa)}(b_{\kappa,i}r),\end{aligned}\quad (6.0.33)$$

où $b_{\kappa,i}$ sont des nombres constants réels : des “scalings” des fonctions de Bessel sphériques. Dans la figure 6.0.1 nous traçons ces fonctions à grande et petite composantes pour $\kappa = -1, -2$: fonctions de type $s_{\frac{1}{2}}$ et $p_{\frac{3}{2}}$, avec un ensemble de constantes choisies au hasard:

$$b_{\kappa,i} = i, \quad \text{for } i = 1, \dots, 5. \quad (6.0.34)$$

Ces fonctions sont normalisées dans la boîte sphérique de rayon $r = 10$.

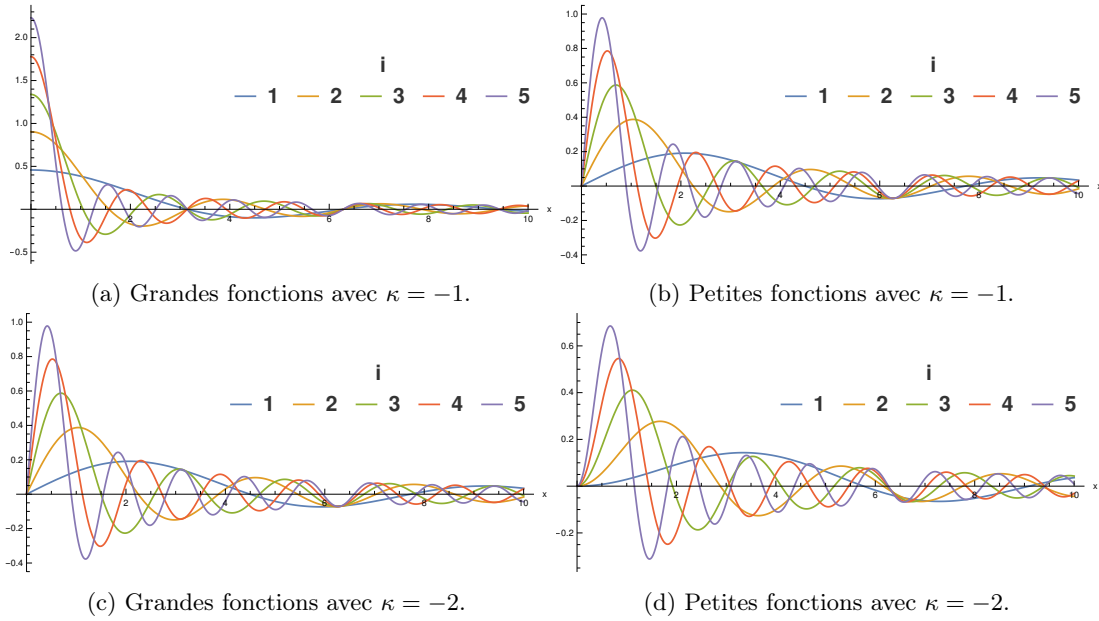


Figure 6.0.1: La base RKB symétrique sous \mathcal{C} , avec $b_{\kappa,i} = i \times 10$, for $i = 1, \dots, 5$.

Le problème de ces fonctions est qu'elles ne s'annulent pas aux parois de la boîte sphérique, et la solution de ce problème sera discutée dans la section suivante.

Une nouvelle base pour simuler les électrons relativistes confinés

On peut imaginer un système où l'électron est confiné sphériquement dans une sphère de grand rayon R et choisir les facteurs d'échelle $b_{\kappa,i}$ comme étant:

$$b_{\kappa,i} = \frac{\gamma_{\kappa,i}}{R}, \quad (6.0.35)$$

où $\gamma_{\kappa,i}$ est le i -ième zéro de la fonction de Bessel sphérique de première espèce (first-kind) d'ordre κ : $j_\kappa(r)$. Ce choix des coefficients $b_{\kappa,i}$ par rapport à cette dernière équation force les fonctions radiales à s'annuler à $r = R$, et assure l'orthogonalité de ces fonctions dans la sphère:

$$\int_0^R dr r^2 j_\kappa\left(\gamma_{\kappa,i} \frac{r}{R}\right) j_\kappa\left(\gamma_{\kappa,j} \frac{r}{R}\right) = \frac{R^3}{2} (j_{\kappa+1}(\gamma_{\kappa,i}))^2 \delta_{ij}. \quad (6.0.36)$$

On peut donc normaliser ces fonctions, et introduire:

$$\tilde{j}_\kappa\left(\gamma_{\kappa,i} \frac{r}{R}\right) = \frac{1}{|j_{\kappa+1}(\gamma_{\kappa,i})|} \sqrt{\frac{2}{R^3}} j_\kappa\left(\gamma_{\kappa,i} \frac{r}{R}\right). \quad (6.0.37)$$

Nous appellerons ces fonctions : les fonctions de base de Bessel confinées. Dans la figure 6.0.2, nous traçons les quatre éléments de base confinés correspondant aux quatre premiers zéros des fonctions de Bessel sphériques $b_{\kappa,i}$.

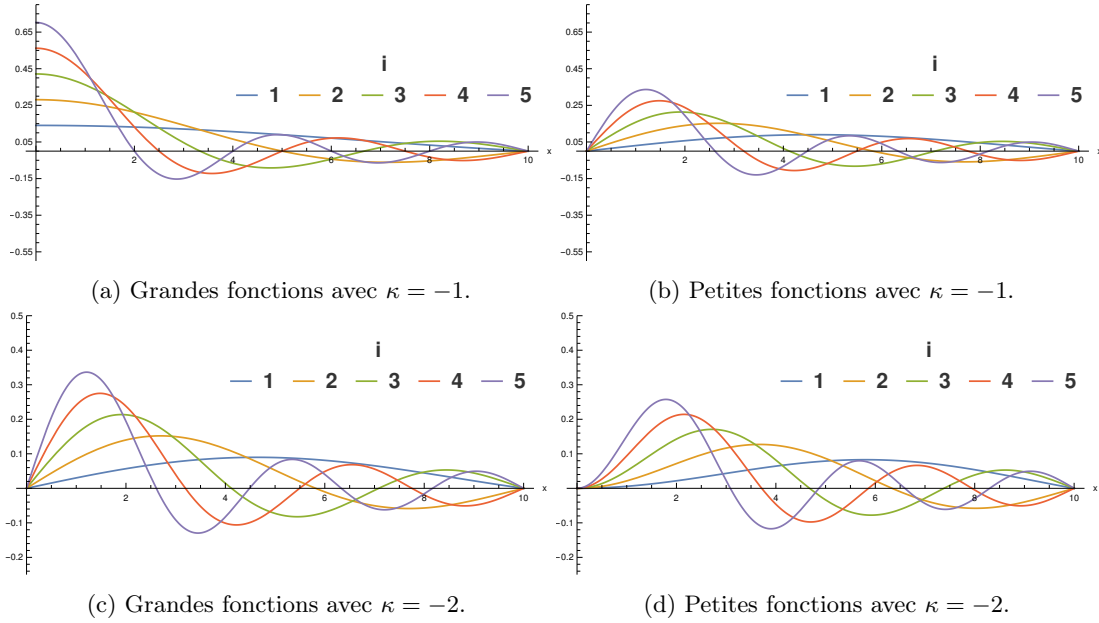


Figure 6.0.2: La base de Bessel confinée: avec $b_{\kappa,i} = \frac{\gamma_{\kappa,i}}{R}$.

La symétrie \mathcal{C} avec la condition d'équilibre cinétique double

En suivant les mêmes précédentes, nous avons trouvé que dans le problème d'équilibre cinétique dual, il suffit de poser les conditions suivantes :

$$\begin{aligned} \pi_{-\kappa,i}^-(r) &= \pi_{\kappa,i}^+(r) \\ \pi_{-\kappa,i}^+(r) &= \pi_{\kappa,i}^-(r) \end{aligned} \quad (6.0.38)$$

pour que la symétrie \mathcal{C} soit satisfaite (sans aucune restriction sur le type de fonctions de base). Ce choix spécial de fonctions de base conduira aux résultats les plus physiques de la densité de polarisation du vide, par rapport à toutes les autres bases considérées.

Chapitre 4 : Électrodynamique quantique

Dans ce chapitre 3, nous déduirons la matrice \mathcal{S} (matrice de diffusion) et présenterons la machinerie mathématique qui lui est associée. De plus, nous calculerons les matrices $\mathcal{S}^{(2)}$; du second ordre associées aux trois processus physiques de la QED discutés dans la section précédente. De plus, les trois décalages d'énergie correspondants vont être dérivés. Habituellement, ces dérivations sont présentées très brièvement dans la littérature, avec beaucoup d'étapes sautées. Nous avons donc décidé de fournir une dérivation détaillée qui convient (jusqu'à un certain point) à un nouvel approche de l'électrodynamique quantique de l'état lié (BSQED), dans le contexte de la théorie de la matrice \mathcal{S} . En outre, nous discuterons brièvement des potentiels effectifs de la QED dans la dernière partie de ce chapitre. Enfin, ce chapitre se terminera par une discussion générale sur les fondements de l'inclusion des corrections QED dans l'approximation multi-électronique la plus simple, c'est-à-dire la théorie de Hartree-Fock, sans avoir besoin d'utiliser les potentiels effectifs. Une fois que ce mécanisme sera opérationnel, cela ouvrira la voie à des méthodes de chimie quantique plus sophistiquées, telles que "Coupled-cluster" ou à interaction de configuration (configuration interaction). Il convient également de noter que l'inclusion de ces corrections de manière autoconsistante permettra d'inclure des corrections d'ordre supérieur. Le principal défi reste la gestion des divergences qui existent, non seulement sur le papier mais aussi dans les calculs numériques. Ces divergences peuvent être observées en inspectant les quantités QED numériques non convergentes lorsque la taille de l'ensemble de base (nombre de fonctions de base) est augmentée.

Corrections QED de second ordre

Dans ce chapitre, nous dérivons entièrement les décalages d'énergie électrodynamique quantique des électrons liés. Le premier est le déplacement de l'énergie d'échange d'un seul photon qui est donné par :

$$\begin{aligned} \Delta E_{\text{SP}}^{\alpha} &= \frac{e^2}{2} \int d^3x_1 \int d^3x_2 \bar{\psi}_i(\mathbf{x}_1) \gamma^{\mu} \psi_i(\mathbf{x}_1) \frac{1}{4\pi\epsilon_0 |\mathbf{x}_1 - \mathbf{x}_2|} \bar{\psi}_j(\mathbf{x}_2) \gamma_{\mu} \psi_j(\mathbf{x}_2) \quad \text{Direct} \\ &- \frac{e^2}{2} \int d^3x_1 \int d^3x_2 \bar{\psi}_i(\mathbf{x}_1) \gamma^{\mu} \psi_j(\mathbf{x}_1) \frac{e^{+\frac{i}{c\hbar}|E_i - E_j||\mathbf{x}_1 - \mathbf{x}_2|}}{4\pi\epsilon_0 |\mathbf{x}_1 - \mathbf{x}_2|} \bar{\psi}_j(\mathbf{x}_2) \gamma_{\mu} \psi_i(\mathbf{x}_2) \quad \text{Exchange} \end{aligned} \quad (6.0.39)$$

contenant un terme direct et un terme d'échange, similaires à ceux obtenus dans la théorie Hartree-Fock à 4 composantes. Cette correction tient également compte de l'effet de retardement (à son ordre le plus bas). La seconde est le décalage de l'énergie de polarisation du vide :

$$\Delta E_{\text{VP}}^{\alpha} = -e^2 i \hbar \int d^3x_1 \int d^3x_2 \psi_i^{\dagger}(\mathbf{x}_1) \psi_i(\mathbf{x}_1) \frac{1}{4\pi\epsilon_0 |\mathbf{x}_1 - \mathbf{x}_2|} \text{Tr} [\gamma_0 S^F(x_2, x_2)]. \quad (6.0.40)$$

Ce terme décrit l'interaction d'un électron lié avec la bulle de polarisation du vide représentée par la trace dans la dernière équation. Enfin, nous obtenons le décalage d'énergie propre (self-energy):

$$\begin{aligned} \Delta E_{\text{SE}}^{\alpha} &= \frac{e^2}{2\pi i} \int d^3x_1 \int d^3x_2 \int_{C_F} dz \psi_i^{\dagger}(\mathbf{x}_2) \alpha^{\mu} G(\mathbf{x}_2, \mathbf{x}_1; z) \alpha_{\mu} \psi_i(\mathbf{x}_1) \\ &\times \frac{e^{+\frac{i}{\hbar} \sqrt{\frac{(z - E_i)^2}{c^2} + i\epsilon} |\mathbf{x}_1 - \mathbf{x}_2|}}{4\pi\epsilon_0 |\mathbf{x}_1 - \mathbf{x}_2|}. \end{aligned} \quad (6.0.41)$$

Ce terme décrit un processus dans lequel un électron lié émet un photon (virtuel), puis le réabsorbe. Cela entraîne une modification de la masse de l'électron.

Hartree-Fock avec QED : L'approche de Saue

La théorie derrière ce problème est fournie dans un chapitre écrit par Saue et Visscher dans [143, section 2.2]. Dans sa dérivation, Saue arrive à la conclusion que pour inclure les effets QED dans la théorie Hartree-Fock, il faut effectuer le remplacement suivant de la matrice de densité atomique-orbitale (états de particules uniques occupées à énergie positive):

$$D_{\nu\mu}^{\text{HF}} \rightarrow D_{\nu\mu}^{\text{HF}} + D_{\nu\mu}^{\text{QED}}, \quad (6.0.42)$$

où $D_{\nu\mu}^{\text{QED}}$ peut être écrit comme:

$$D_{\nu\mu}^{\text{QED}} = \frac{1}{2} \left[\sum_{E_p > 0} c_{\nu,p} c_{\mu,p}^* - \sum_{E_p < 0} c_{\nu,p} c_{\mu,p}^* \right]. \quad (6.0.43)$$

La trace de cette dernière quantité donne la densité de polarisation du vide. La première somme porte sur toutes les solutions à énergie positive, qu'elles soient occupées ou non, tandis que la seconde porte sur les solutions à énergie négative. Cette modification de la matrice de densité entraîne une modification de l'énergie:

$$E^{\text{HF}} \rightarrow E^{\text{HF}} + E^{\text{QED}}, \quad (6.0.44)$$

où le terme additionnel E^{QED} est trouvé comme étant :

$$\begin{aligned} E^{\text{QED}} &= D_{\nu\mu}^{\text{QED}} h_{\mu\nu}^D \\ &+ D_{\nu\mu}^{\text{HF}} D_{\theta\sigma}^{\text{QED}} [g_{\mu\sigma,\nu\theta} - g_{\mu\sigma,\theta\nu}] \\ &+ \frac{1}{2} D_{\nu\mu}^{\text{QED}} D_{\theta\sigma}^{\text{QED}} [g_{\mu\sigma,\nu\theta} - g_{\mu\sigma,\theta\nu}]. \end{aligned} \quad (6.0.45)$$

Le premier terme représente l'énergie unipolaire des électrons du vide. Nous devons maintenant nous concentrer sur la deuxième ligne de la dernière équation. Le lecteur doit noter que ces termes avec $D_{\nu\mu}^{\text{HF}} D_{\theta\sigma}^{\text{QED}}$ décrivent l'interaction entre les solutions de Hartree-Fock et le vide de la QED. De plus, le terme direct $D_{\nu\mu}^{\text{HF}} D_{\theta\sigma}^{\text{QED}} g_{\mu\sigma,\nu\theta}$ représente le décalage d'énergie de polarisation du vide, tandis que le terme d'échange $-D_{\nu\mu}^{\text{HF}} D_{\theta\sigma}^{\text{QED}} g_{\mu\sigma,\theta\nu}$ est associé au processus d'auto-énergie. Enfin, nous avons trouvé les deux derniers termes : $D_{\nu\mu}^{\text{QED}} D_{\theta\sigma}^{\text{QED}} [g_{\mu\sigma,\nu\theta} - g_{\mu\sigma,\theta\nu}]$ sont les contributions attribuées aux diagrammes de vide non physiques.

Cette machinerie a été codée par Saue dans le code DIRAC relativiste [136]. Nous avons effectué de nombreux calculs à l'aide de ce code et avons observé que l'énergie QED donnée dans la dernière expression ne converge pas avec une taille croissante de l'ensemble de base gaussien. Nous avons donc décidé d'attaquer le problème sous un angle différent, en suivant les étapes suivantes :

1. Dérivation des décalages d'énergie de $\mathcal{S}^{(2)}$, comme nous l'avons fait dans ce chapitre.
2. Combinaison de toutes les contributions en une seule expression énergétique. Voir la section suivante.

Hartree-Fock avec QED : La nouvelle approche

Dans cette section, nous allons utiliser les décalages d'énergie associés aux trois processus physiques de la matrice d'ordre 2 : $\mathcal{S}^{(2)}$, que nous avons obtenue dans ce chapitre. Si nous combinons main-

tenant tous les trois termes, avec l'énergie d'une particule, on obtient l'expression suivante :

	Termes
$E = \int d\mathbf{x} \psi_i^\dagger(\mathbf{x}) \hat{h}^D(\mathbf{x}) \psi_i(\mathbf{x})$	a
$+ \frac{e^2}{2} \int d\mathbf{x}_1 \int d\mathbf{x}_2 \psi_i^\dagger(\mathbf{x}_1) \alpha^\lambda \psi_i(\mathbf{x}_1) \frac{1}{4\pi\epsilon_0 r_{12}} \psi_j^\dagger(\mathbf{x}_2) \alpha_\lambda \psi_j(\mathbf{x}_2)$	b
$- \frac{e^2}{2} \int d\mathbf{x}_1 \int d\mathbf{x}_2 \psi_i^\dagger(\mathbf{x}_1) \alpha^\lambda \psi_j(\mathbf{x}_1) \frac{1}{4\pi\epsilon_0 r_{12}} \cos\left(\frac{1}{c\hbar} E_i - E_j r_{12}\right) \psi_j^\dagger(\mathbf{x}_2) \alpha_\lambda \psi_i(\mathbf{x}_2)$	c
$- e^2 i\hbar \int d\mathbf{x}_1 \int d\mathbf{x}_2 \psi_i^\dagger(\mathbf{x}_1) \alpha^\lambda \psi_i(\mathbf{x}_1) \frac{1}{4\pi\epsilon_0 r_{12}} \text{Tr} [\gamma_0 S^F(x_2, x_2)]$	d
$+ e^2 \Re \left[\frac{1}{2\pi i} \int d\mathbf{x}_1 \int d\mathbf{x}_2 \int_{C_F} dz \psi_i^\dagger(\mathbf{x}_2) \alpha^\lambda G(\mathbf{x}_2, \mathbf{x}_1; z) \alpha_\lambda \psi_i(\mathbf{x}_1) \frac{e^{+\frac{i}{c\hbar} r_{12} \sqrt{(z-E_i)^2 + i\epsilon}}}{4\pi\epsilon_0 r_{12}} \right]$	e

(6.0.46)

Les termes étiquetés sont indiqués dans la liste suivante :

- a** L'énergie d'un électron : somme de toutes les énergies individuelles des particules uniques qui n'interagissent pas.
- b** Le terme Hartree direct, trouvé dans la théorie Hartree-Fock habituelle à 4 composants.
- c** Le terme d'échange de Fock, que l'on trouve dans la théorie Hartree-Fock habituelle à 4 composants. Remarquez que ce terme contient une fonction de retardement : $\cos\left(\frac{1}{c\hbar} |E_i - E_j| r_{12}\right)$, qui disparaît dans la limite non relativiste $c \rightarrow +\infty$. Ce terme cosinus est absent de l'approche précédente de Saue, puisque dans la dérivation de référence, l'hamiltonien à deux particules ne contient pas l'exposant de retardement. Cet exposant provient du propagateur de photons de la jauge de Feynman, comme indiqué dans [7, eq.(461)] et [15, eq.(F.67)].
- d** Le décalage énergétique de la polarisation du vide. Ce terme est le même que celui obtenu par Saue : $D_{\nu\mu}^{\text{HF}} D_{\theta\sigma}^{\text{QED}} g_{\mu\sigma,\nu\theta}$.
- e** Le décalage de l'énergie propre. Cette expression devient le terme $-D_{\nu\mu}^{\text{HF}} D_{\theta\sigma}^{\text{QED}} g_{\mu\sigma,\theta\nu}$ une fois que nous avons éliminé la fonction exponentielle, et évalué l'intégration du contour.

Une expression similaire se trouve dans les travaux de Greiner et al [106, eq.(16.19)]. L'équation autoconsistante (Hartree-Fock) contenant la contribution d'échange de photons uniques se trouve dans les travaux de Plunien et Soff [144, eq.(18)], Rafelski et al [145, eq.(26)] ainsi que Reinhard [146, eqs.(4,6)] et al dans [147, eq.(4)]. Une référence importante à considérer, dans ce contexte, est Gomberoff et Tolmachev [148], où différentes manipulations de différents propagateurs d'électrons sont effectuées, avec des connexions à la théorie Hartree-Fock. Voir par exemple l'équation autoconsistante de [148, eq.(3.11)], qui contient à la fois les effets de polarisation du vide et d'auto-énergie.

Notre discussion s'arrête ici, mais ce problème mérite une étude détaillée. Il faut garder à l'esprit que la polarisation du vide et les termes d'auto-énergie sont tous deux divergents, dans le terme de potentiel 1 [7, 5], et les termes de potentiel 0-1 [149, 133], respectivement. Le problème des divergences demande un effort exceptionnel, et il n'est pas évident de trouver comment remédier à ces divergences dans le contexte des ensembles finis. Pour autant que nous le sachions, ce problème n'a jamais été résolu.

Chapitre 5 : Polarisation du vide

Le chapitre 4 sera consacré au problème de la polarisation dans le vide, déjà rencontré dans le chapitre 3. Nous nous concentrerons d'abord sur la dérivation des quantités mathématiques, puis nous attaquerons au problème de l'évaluation numérique. Plusieurs calculs de densité de polarisation dans le vide associés à différents choix d'ensembles de base seront effectués, présentés et discutés en détail. De plus, nous utiliserons ce que nous avons appris dans le premier chapitre sur la symétrie \mathcal{C} pour concevoir de meilleures fonctions de base. De plus, la symétrie de renversement du temps (symétrie \mathcal{T}) sera utilisée pour simplifier l'expression de la densité de polarisation du vide dans les cas où les potentiels vectoriels externes disparaissent. La première partie concernera les quantités et manipulations mathématiques associées aux différentes définitions de cette densité. De plus, les résultats sur les symétries discrètes de l'équation de Dirac, que nous avons dérivés et discutés dans le chapitre 2, vont être utilisés pour simplifier certains des calculs de la densité de polarisation du vide.

En outre, nous nous concentrerons sur le problème radial (atomique) et présenterons soigneusement comment on peut construire cette densité dans le cadre de l'approximation en base finie (de l'équation de Dirac radiale).

Ensuite, nous utiliserons les résultats de la première partie (théorique) du chapitre pour attaquer le problème numérique et présenterons différents résultats numériques avec une discussion détaillée. Le résultat le plus important de ce chapitre sera de montrer comment la prise en compte de la symétrie \mathcal{C} (dans l'ensemble de base fini) améliorera significativement la qualité de nos densités numériques de polarisation dans le vide. Cette prise en compte conduira finalement à des solutions physiquement acceptées : cohérentes avec ce que nous savons de la théorie exacte. D'autre part, nous verrons que le non-respect de cette symétrie \mathcal{C} , qui se produit malheureusement dans les ensembles de base relativistes conventionnels, conduira à des résultats non physiques problématiques qui divergent du problème physique.

On peut montrer que le courant de polarisation du vide s'écrit comme suit :

$$J_{\mu}^{\text{VP}}(x) = \frac{ec}{2} \left[\sum_{E_i > 0} \bar{\psi}_i \gamma_{\mu} \psi_i - \sum_{E_i < 0} \bar{\psi}_i \gamma_{\mu} \psi_i \right]. \quad (6.0.47)$$

Dans le cas où le quadri-potentiel externe est indépendant du temps, le courant de polarisation du vide devient également indépendant du temps et se lit comme suit :

$$J_{\mu}^{\text{VP}}(\mathbf{x}) = \frac{ec}{2} \left(\sum_{E_i > 0} \psi_i^{\dagger}(\mathbf{x}) \alpha_{\mu} \psi_i(\mathbf{x}) - \sum_{E_i < 0} \psi_i^{\dagger}(\mathbf{x}) \alpha_{\mu} \psi_i(\mathbf{x}) \right). \quad (6.0.48)$$

En utilisant la symétrie de renversement du temps, le courant de polarisation du vide :

$$J_0^{\text{VP}}(\mathbf{x}) = \frac{ec}{2} \left(\sum_{E_i > 0} \psi_i^{\dagger}(\mathbf{x}) \psi_i(\mathbf{x}) - \sum_{E_i < 0} \psi_i^{\dagger}(\mathbf{x}) \psi_i(\mathbf{x}) \right) \quad (6.0.49)$$

$$J_{\mu}^{\text{VP}}(\mathbf{x}) = 0 \quad \text{for } \mu = 1, 2, 3.$$

où seule la composante temporelle survit. Le courant de composante nulle peut être écrit sous la forme $J_0^{\text{VP}}(\mathbf{x}) = c\rho^{\text{VP}}(\mathbf{x})$ (première équation), où $\rho^{\text{VP}}(\mathbf{x})$ est la densité de charge de polarisation du vide :

$$\rho^{\text{VP}}(\mathbf{x}) = \frac{e}{2} \left(\sum_{E_i > 0} \psi_i^{\dagger}(\mathbf{x}) \psi_i(\mathbf{x}) - \sum_{E_i < 0} \psi_i^{\dagger}(\mathbf{x}) \psi_i(\mathbf{x}) \right). \quad (6.0.50)$$

Les racines de cette différence entre les solutions d'énergie opposées remontent aux travaux de Dirac où il a introduit la matrice densité ρ_1 , dont la trace donne la dernière différence. Voir [151, Page 152]. De plus, cette définition de la densité de charge de polarisation du vide semble provenir des travaux de Wichmann et Kroll [118, eq.(2)].

Densité de polarisation du vide dans le problème libre

En l'absence d'un inducteur externe, la densité de polarisation du vide devrait (en principe) disparaître :

$$\rho^{\text{VP}}(\mathbf{x}) = \frac{e}{2} \left(\sum_{E_i > 0} \psi_i^\dagger(\mathbf{x}) \psi_i(\mathbf{x}) - \sum_{E_j < 0} \psi_j^\dagger(\mathbf{x}) \psi_j(\mathbf{x}) \right) = 0. \quad (6.0.51)$$

Ceci sera démontré en utilisant la symétrie de conjugaison des charges. Rappelons que $\psi_i(\mathbf{x})$ et E_i résolvent l'équation de Dirac libre indépendante du temps :

$$[c\boldsymbol{\alpha} \cdot \hat{\mathbf{p}} + \beta mc^2] \psi_i(\mathbf{x}) = E_i \psi_i(\mathbf{x}). \quad (6.0.52)$$

En utilisant les équations auxquelles nous venons de nous référer, nous pouvons écrire les solutions d'énergie négative de la deuxième somme de l'éq.(6.0.51) comme des solutions d'énergie positive conjuguées par la symétrie \mathcal{C} :

$$\sum_{E_j < 0} \psi_j^\dagger(\mathbf{x}) \psi_j(\mathbf{x}) = \sum_{E_j > 0} [\mathcal{C}\psi_j(\mathbf{x})]^\dagger \mathcal{C}\psi_j(\mathbf{x}). \quad (6.0.53)$$

De plus, en utilisant l'opération de conjugaison de charge, nous pouvons écrire le dernier produit comme :

$$[\mathcal{C}\psi_j(\mathbf{x})]^\dagger \mathcal{C}\psi_j(\mathbf{x}) = [\gamma^2 \psi_j^*(\mathbf{x})]^\dagger \gamma^2 \psi_j^*(\mathbf{x}) = \psi_j^\dagger(\mathbf{x}) \psi_j(\mathbf{x}), \quad (6.0.54)$$

ce qui montre que la densité de probabilité est inchangée sous conjugaison de charge. En utilisant ce dernier résultat, notre densité de polarisation du vide se réduit à :

$$\rho^{\text{VP}}(\mathbf{x}) = \frac{e}{2} \left(\sum_{E_i > 0} \psi_i^\dagger(\mathbf{x}) \psi_i(\mathbf{x}) - \sum_{E_j > 0} \psi_j^\dagger(\mathbf{x}) \psi_j(\mathbf{x}) \right) = 0, \quad (6.0.55)$$

qui disparaît clairement, puisque chaque élément d'une somme, sera annulé par un même terme provenant de la seconde somme, main ayant un signe moins.

Densité de polarisation du vide dans le problème atomique

Nous nous limitons maintenant au potentiel scalaire radial. Dans ce cas, les solutions de Dirac peuvent être écrites comme :

$$\psi_{n,\kappa,m_j}(\mathbf{x}) = \frac{1}{r} \begin{bmatrix} P_{n,\kappa}(r) \Omega_{\kappa,m_j}(\hat{\mathbf{x}}) \\ iQ_{n,\kappa}(r) \Omega_{-\kappa,m_j}(\hat{\mathbf{x}}) \end{bmatrix}. \quad (6.0.56)$$

En utilisant cette dernière forme de solution, et quelques propriétés des spinors sphériques, on peut écrire la densité de polarisation du vide comme :

$$\rho^{\text{VP}}(\mathbf{x}) = \frac{e}{4\pi r^2} \sum_{n,\kappa} |\kappa| \operatorname{sgn}(E_{n,\kappa}) [P_{n,\kappa}^2(r) + Q_{n,\kappa}^2(r)]. \quad (6.0.57)$$

Cette formule se trouve dans [118, eqs.(6-8)]. D'autres formules légèrement différentes se trouvent dans [6, eq.(20)], [152, eq.(19)] et [7, eq.(232)]. Enfin, cette densité peut être écrite comme une somme sur les densités de polarisation du vide à composante κ :

$$\rho^{\text{VP}}(\mathbf{x}) = \sum_{\kappa=\pm 1, \pm 2, \dots} \rho_{\kappa}^{\text{VP}}(\mathbf{x}), \quad (6.0.58)$$

où $\rho_{\kappa}^{\text{VP}}(\mathbf{x})$ est donné par la somme suivante:

$$\rho_{\kappa}^{\text{VP}}(\mathbf{x}) = \frac{e|\kappa|}{4\pi r^2} \sum_n \text{sgn}(E_{n,\kappa}) [P_{n,\kappa}^2(r) + Q_{n,\kappa}^2(r)]. \quad (6.0.59)$$

Cette formule sera utilisée dans l'évaluation numérique de la densité de polarisation du vide (dans une base finie), où la somme n sera calculée sur toutes les solutions numériques.

Polarisation du vide dans un ensemble de base fini

Une fois que nous nous limitons au problème de la base finie, où les fonctions radiales sont approximées par :

$$\begin{bmatrix} P_{\alpha,\kappa}(r) \\ Q_{\alpha,\kappa}(r) \end{bmatrix} \approx \begin{bmatrix} \mathcal{P}_{\alpha,\kappa}(r) \\ \mathcal{Q}_{\alpha,\kappa}(r) \end{bmatrix} = \sum_i c_{\alpha,\kappa,i}^L \begin{bmatrix} \pi_{i,\kappa}^L(r) \\ 0 \end{bmatrix} + \sum_i c_{\alpha,\kappa,i}^S \begin{bmatrix} 0 \\ \pi_{i,\kappa}^L(r) \end{bmatrix} \quad (6.0.60)$$

La densité de polarisation numérique du vide peut être écrite comme :

$$\rho_{\kappa}^{\text{VP}}(\mathbf{x}) = \frac{e|\kappa|}{4\pi r^2} \sum_{\alpha} \text{sgn}(E_{\alpha,\kappa}) \rho_{\kappa,\alpha}(r), \quad (6.0.61)$$

où $\rho_{\kappa,\alpha}(r) = [\mathcal{P}_{\alpha,\kappa}(r)]^2 + [\mathcal{Q}_{\alpha,\kappa}(r)]^2$ est la densité de probabilité associée à la solution numérique α . Nous devons également noter que dans les calculs précédents pour évaluer cette densité de polarisation du vide, (numériquement), l'intégrale de la densité de polarisation du vide :

$$\int d^3\mathbf{x} \rho_{\kappa}^{\text{VP}}(\mathbf{x}) = 0, \quad (6.0.62)$$

qui devrait disparaître, a été calculé pour présenter une indication précise du calcul effectué. Cela a été fait par Rinker et Wilets [155, Pages 753,757] ainsi que par Soff et Mohr [6, Page 5074 eq.(70)]. Dans un calcul en base finie, ce n'est pas un problème de précision, puisque cette intégrale s'évanouira toujours :

$$\int d^3\mathbf{x} \rho^{\text{VP}}(\mathbf{x}) = e \sum_{\kappa} |\kappa| \int_0^{\infty} dr \left(\sum_{\alpha_+=1}^n 1 - \sum_{\alpha_-=1}^n 1 \right) = 0. \quad (6.0.63)$$

Dans la dernière expression, α_{\pm} indique que l'indice passe sur les n solutions d'énergie positive et négative, respectivement.

Densité de polarisation du vide dans RKB et \mathcal{C} -DKB

Nous présentons les résultats dans lesquels nous comparons les deux problèmes, en figs. 6.0.3 and 6.0.4. Ces figures montrent que:

1. Aux petites distances, les courbes DKB commencent par une belle correspondance entre les composantes de la densité de polarisation du vide, alors que les résultats RKB ne montrent pas un tel comportement.
2. Plus important encore, à des distances relativement grandes, les courbes DKB montrent une très belle interférence destructive entre les deux composantes, contrairement aux courbes RKB.

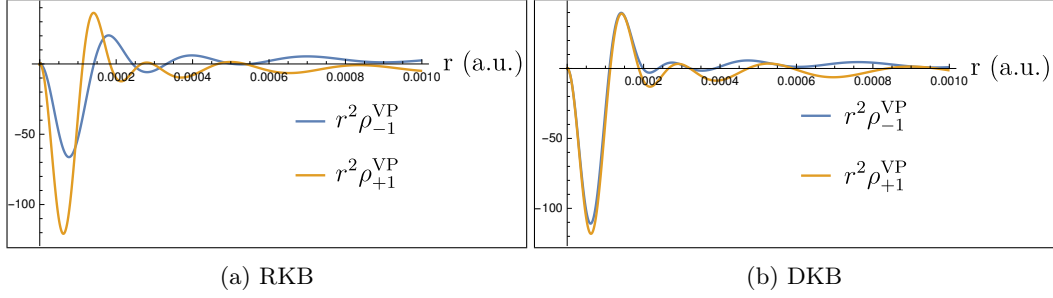


Figure 6.0.3: Densités de polarisation de vide de $\kappa = \pm 1$ à très petites distances : $r < \lambda/7$.

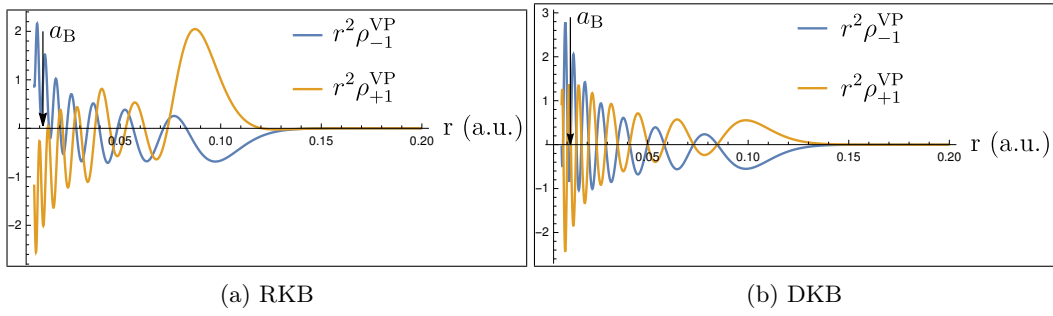


Figure 6.0.4: Densités de polarisation du vide de $\kappa = \pm 1$ à des distances relativement grandes.

Au final, ce qui compte, c'est la sommation des deux composantes de la polarisation du vide, qui donnera l'effet résultant, et tiendra compte des annulations. Nous présentons donc les résultats comparables des sommations de ces composantes pour chacune des quatre dernières figures, en figs. 6.0.5 and 6.0.6.

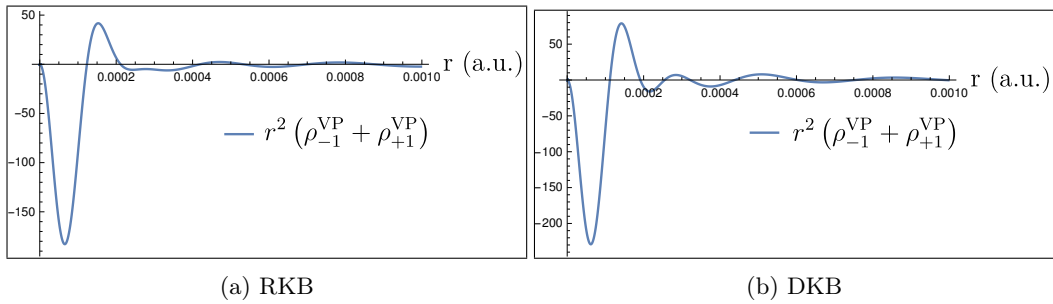


Figure 6.0.5: $r^2(\rho_{-1}^{VP} + \rho_{+1}^{VP})$ à de très petites distances : $r < \lambda/7$.

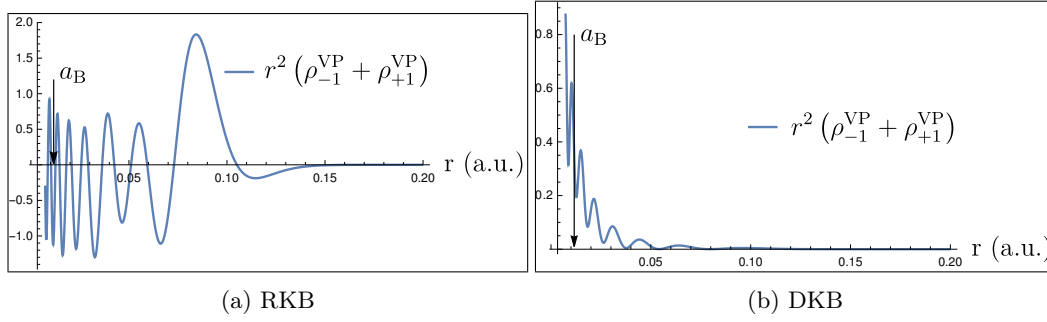


Figure 6.0.6: $r^2(\rho_{-1}^{VP} + \rho_{+1}^{VP})$ à des distances relativement grandes.

Il est clair que c'est la DKB- \mathcal{C} qui a le mérite. Nous montrerons ensuite que la méthode RKB donne lieu à une densité de polarisation du vide qui ne s'annule pas dans le problème de l'électron libre, ce qui est un résultat non-physique, et donc problématique.

Conclusions et perspectives

Après les longues discussions, nous laisserons retomber la poussière et présenterons les principales conclusions auxquelles nous sommes parvenus, ainsi que notre point de vue sur la façon dont nous pouvons aller au-delà des résultats obtenus dans ce projet de thèse.

Conclusions

Symétrie de conjugaison de charge dans une base finie

Symétrie de conjugaison de charge dans RKB

Nous notons d'abord que la symétrie \mathcal{C} est réalisable dans l'approximation de base finie, en utilisant le schéma conventionnel d'équilibre cinétique restreint. Cette réalisation se produit après avoir choisi les fonctions de base comme étant les composantes petites et grandes découplées des solutions radiales libres de Dirac, qui sont écrites en termes de fonctions de Bessel sphériques (comme discuté dans les sections 2.11.2, 2.11.4 et 2.11.5). De plus, nous avons découvert que l'on peut sélectionner une échelle particulière de ces fonctions de base, liée aux zéros des fonctions de Bessel sphériques (première espèce), et obtenir un ensemble orthogonal de fonctions (dans une sphère de confinement) qui disparaissent aux parois de la sphère de confinement (comme on le voit dans les sections 2.11.3 et 2.11.5). Ce résultat peut être utilisé dans la simulation du problème de confinement relativiste, et il est important de le prendre en compte pour les calculs de la densité de polarisation du vide. Cette densité, qui (analytiquement parlant), contient une somme sur les solutions limites et des intégrales sur les solutions continues, se réduit à deux sommes dans le problème de confinement comme l'ont noté Schlemmer et Zahn dans [158, page 33].

Symétrie de la conjugaison des charges dans DKB

Nous notons également que la symétrie \mathcal{C} peut être réalisée sans problème dans le schéma d'équilibre cinétique double, comme nous l'avons vu dans la section 2.11.6. Ce but peut être atteint en fixant les grandes et petites composantes d'une base κ , égales aux fonctions de base des petites et grandes

composantes de la base κ de signe opposé, respectivement (voir eq.(2.11.61)). Le lecteur doit remarquer que si l'ensemble de base choisi est indépendant du κ , cela signifie que pour réaliser la symétrie de conjugaison de charge, il faut, pour chaque ensemble de fonctions de base associé à un certain κ , introduire la même base pour le problème du κ de signe opposé, comme (par exemple) l'ont fait Shabaev *et al.* dans [81, eqs.(10,11)].

Calculs de la densité de polarisation dans le vide

En ce qui concerne les calculs de la densité de polarisation du vide, nous notons que si un ensemble choisi de fonctions de base ne respecte pas la symétrie de conjugaison de charge, on obtiendra des résultats non physiques, tels que la densité de polarisation du vide non nulle dans le problème des particules libres, comme on l'a vu dans la section 4.5.7 lorsqu'on utilise la méthode RKB. D'une manière générale, on obtiendra des densités de polarisation du vide non nulles pour des puissances paires en potentiel externe:

$$\rho_{|\kappa|}^n(\mathbf{x}) = \rho_{\kappa}^n(\mathbf{x}) + \rho_{-\kappa}^n(\mathbf{x}) \neq 0, \quad \text{for even } n \quad (6.0.64)$$

ce qui n'est certainement pas physique. Nous notons enfin que les meilleurs résultats de densité de polarisation dans le vide ont été obtenus une fois que la base d'équilibre cinétique double symétrique \mathcal{C} a été utilisée, où nous avons observé les caractéristiques physiques suivantes de la densité de polarisation dans le vide obtenue numériquement :

1. Toutes les densités associées aux puissances paires d'interaction avec le potentiel externe disparaissent:

$$\rho_{|\kappa|}^n(\mathbf{x}) = \rho_{\kappa}^n(\mathbf{x}) + \rho_{-\kappa}^n(\mathbf{x}) = 0, \quad \text{for even } n \quad (6.0.65)$$

ce qui est en accord avec le théorème de Furry. Le lecteur peut vérifier fig. 4.5.25 et eq.(4.6.34).

2. Les densités de polarisation totales du vide s'annulent très bien pour les distances dépassant la longueur d'onde de Compton, comme on peut le voir dans figs. 4.5.21b and 4.5.23b. Ce point est cohérent avec ce que nous savons du comportement de la densité de polarisation du vide (exacte), à des distances relativement grandes.
3. Il suffit de calculer la densité de polarisation du vide associée à un κ , puisque nous avons montré que les densités de signes κ opposés d'une densité d'ordre n impair sont égales (eq.(4.6.34)):

$$\rho_{\kappa}^n = \rho_{-\kappa}^n, \quad (6.0.66)$$

dans ces bases symétriques (sous symétrie \mathcal{C}).

4. Dans un calcul en base finie, on peut supprimer le comportement divergent de la densité de polarisation du vide en éliminant le terme de potentiel unique, comme cela est fait dans l'éq.(4.6.20):

$$\begin{aligned} \rho_{\kappa}^{n \geq 2}(\mathbf{x}) &= \rho_{\kappa}^{\text{VP}}(\mathbf{x}) - \rho_{\kappa}^1(\mathbf{x}) \\ &= \frac{e|\kappa|}{4\pi r^2} \sum_{\alpha} \left\{ \text{sgn}(E_{\alpha,\kappa}) \rho_{\alpha,\kappa}(r) - e \sum_{\beta} \frac{1 - \text{sgn}(E_{\alpha,\kappa}^0 E_{\beta,\kappa}^0)}{|E_{\alpha,\kappa}^0| + |E_{\beta,\kappa}^0|} s_{\beta,\alpha}^{\kappa}(r) V_{\alpha,\beta}^{\kappa} \right\}. \end{aligned} \quad (6.0.67)$$

Cette soustraction supprime également la partie physique (Uehling) de $\rho_{\kappa}^1(\mathbf{x})$, qui peut facilement être ajoutée par la suite.

Perspectives

Le premier problème sur lequel nous travaillons actuellement concerne la traduction de la machinerie de régularisation/renormalisation de la densité de polarisation du vide (qui se fait habituellement de manière analytique) dans le langage de l'approximation en base finie. Afin d'exprimer clairement nos propos, nous donnerons quelques mots sur la régularisation et la renormalisation.

Régularisation et renormalisation

La régularisation est une astuce mathématique qui permet de modifier une intégrale divergente en y introduisant des paramètres fictifs (auxiliaires), de sorte que l'intégrale modifiée devienne convergente (mais dépendante des paramètres). Les principales techniques de régularisation utilisées dans le contexte de la QED sont les suivantes :

1. **La régularisation de Pauli-Villars** [159], où l'on modifie le propagateur qui vit sous l'intégrale divergente. Pour le problème de la polarisation du vide, on modifie le propagateur de l'électron et on lui ajoute des propagateurs de masse auxiliaires destinés à annuler la ou les divergences existantes (voir par exemple Greiner et Reinhardt [8, eq.(5.20)]). D'autre part, pour l'intégrale d'auto-énergie, on peut modifier le propagateur du photon en utilisant un propagateur associé à une masse fictive du photon (coupure d'impulsion Λ). Voir par exemple, Peskin et Schroeder [99, eq.(7.17) et en dessous].
2. **La régularisation dimensionnelle** introduite par 't Hooft et Veltman [160], où l'on remplace les dimensions de l'espace-temps : 4, de l'intégrale divergente, par $4-\epsilon$, où ϵ est un petit nombre positif. Pour plus de détails sur ce schéma de régularisation, le lecteur peut consulter Ohlsson [33, section 13.3], Peskin et Schroeder [99, pages 249-251] et Mandl et Shaw [93, section 10.3].

Le lecteur doit se rappeler que pour tout choix de régularisation, les expressions obtenues dépendent des paramètres : des masses auxiliaires, de la coupure des grands impulsions Λ , ou du paramètre dimensionnel ϵ . L'astuce suivante consiste à évaluer d'abord les intégrales dépendantes des paramètres, puis à absorber les termes divergents dépendants des paramètres obtenus dans la charge et la masse nues. Cette absorption des divergences par les quantités physiques nues est connue sous le nom de technique de renormalisation, et consiste en une redéfinition de ces quantités. L'idée principale ici, est que l'on doit distinguer entre :

- La masse et la charge de l'électron nu : Celles que nous pouvons obtenir de l'expérience si le bouton QED de la nature est désactivé. C'est impossible à réaliser.
- La masse et la charge expérimentales de l'électron : Les chiffres que nous obtenons de l'expérience. Ces chiffres tiennent déjà compte des corrections QED, puisque le bouton QED de la nature est toujours activé.

Cette technique de renormalisation est justifiée après avoir réalisé que nos équations contiennent la masse et la charge de l'électron nu au lieu des valeurs expérimentales. Par la suite, lorsque nous ajoutons les corrections QED à ces équations, nous obtenons des quantités divergentes. De plus, puisque :

1. Nous ne savons pas quelles sont les quantités nues
2. et nous savons que les corrections de la QED devraient être finies (et l'infini n'est qu'un concept),

Ceci mène à la conclusion que l'on peut absorber les divergences dépendant des paramètres par les quantités nues, de sorte que la masse et la charge finales (globales) sont fixées (choisies) pour être les valeurs expérimentales. Ce fait nous indique que la théorie QED a besoin des valeurs expérimentales de la masse et de la charge de l'électron, comme exprimé par les mots de Feynman dans [84]:

We know what kind of a dance to do experimentally to measure this number very accurately, but we don't know what kind of a dance to do on a computer to make this number come out without putting it in secretly!

Pour des discussions plus détaillées sur les techniques de régularisation et de renormalisation, le lecteur peut consulter Huang [161], Zeidler [162, section 2.2], Mandl et Shaw [93, chapter 10], Ohlsson [33, chapter 13], Bethe et Salpeter [163, section 19], et Lindgren [15, chapter 12].

Régularisation et renormalisation dans une base finie

En nous inspirant des techniques de régularisation et de renormalisation (brièvement abordées dans la section précédente), nous avons attaqué ce problème dans le contexte des bases finies, sous deux angles indépendants qui sont présentés par les deux projets suivants :

1. Le projet de coupure d'impulsions

Ce projet vise à éliminer les contributions des grandes impulsions des calculs de densité de polarisation du vide en introduisant une sorte de coupure numérique de momentum. Ceci est généralement fait analytiquement (dans la littérature) en utilisant la régularisation de Pauli-Villars, et nous avons essayé de l'adapter au problème numérique. Nous avons récemment terminé l'écriture du code de simulation associé, et des tests seront bientôt effectués.

2. Le projet de variation des constantes physiques

Ce projet concerne la variation numérique des constantes physiques, que nous pouvons donc appeler une "renormalisation numérique". Nous avons déjà effectué plusieurs calculs où nous faisons varier (tweak) la masse et la charge de l'électron, et étudions comment les quantités QED calculées numériquement évoluent par rapport à ces variations. Ce projet n'a pas été achevé et mérite d'être approfondi.

Hartree-Fock avec QED

Cette partie des conclusions concerne la section 3.13 de cette thèse, où nous avons discuté de l'inclusion des corrections QED dans la théorie Hartree-Fock. Bien que non présentés dans la thèse, plusieurs tests numériques ont été effectués en utilisant les résultats théoriques de Saue [143] (voir section 3.13.2), qui ont été codés par Saue dans le logiciel DIRAC [136]. Ces résultats ont montré que la correction d'énergie QED ne converge pas avec l'augmentation de la taille de l'ensemble de base. La raison de ces résultats divergents peut être attribuée aux deux points problématiques suivants :

1. Le code utilisé utilise la prescription RKB, qui ne décrit pas correctement les solutions d'énergie négative, alors que les quantités QED sont construites à partir de solutions d'énergie positive et négative.
2. La nature divergente des quantités de la QED, comme nous l'avons vu par exemple en fig. 4.5.5.

Le premier point peut être résolu en travaillant avec la prescription DKB, ou \mathcal{C} -DKB (symétrique sous conjugaison de charges), tandis que le second point est plus problématique, et appelle une solution radicale.

De plus, dans la section 3.13.3, nous avons fourni les résultats de notre dérivation de la correction d'énergie QED, qui inclut les corrections de la matrice d'ordre 2: $\mathcal{S}^{(2)}$ et comparé notre résultat avec celui obtenu précédemment par Saue dans [143]. Ces résultats doivent être analysés plus avant et massés de manière à pouvoir être utilisés dans des calculs Hartree-Fock pratiques.

Dernières paroles

Les divergences rencontrées lors du calcul numérique des quantités de la QED nécessitent un besoin urgent d'une procédure de régularisation/renormalisation numérique dans le contexte numérique, qui devrait finalement conduire à la convergence des quantités numériques de la QED (avec une taille croissante de l'ensemble de base fini). Ce n'est pas une tâche simple car la traduction numérique de traitements mathématiques aussi exceptionnels (régularisation d'intégrales divergentes) peut être un objectif très délicat à atteindre. Le lecteur doit enfin noter que l'erreur associée à la méthode Hartree-Fock est élevée, et se situe généralement au-delà des corrections fournies par la théorie QED. Cependant, ce qui est important, c'est le succès de cette machinerie, qui ouvrira la voie à des méthodes plus sophistiquées incluant des effets de corrélation électronique d'ordre supérieur, telles que la méthode d'interaction de configuration (configuration interaction) et "coupled-cluster", et fournira ainsi (au moins en principe) des résultats numériques extrêmement précis qui correspondent exceptionnellement aux résultats expérimentaux.

Appendix A

Notations and definitions

The four-quantities are defined as:

$$x^\mu = (x^0, x^1, x^2, x^3) = (ct, \mathbf{x}) \quad \text{Position} \quad (\text{A.0.1})$$

$$\partial_\mu = \frac{\partial}{\partial x^\mu} = \left(\frac{1}{c} \frac{\partial}{\partial t}, \frac{\partial}{\partial x^1}, \frac{\partial}{\partial x^2}, \frac{\partial}{\partial x^3} \right) = \left(\frac{1}{c} \frac{\partial}{\partial t}, \boldsymbol{\nabla} \right) \quad \text{Gradient} \quad (\text{A.0.2})$$

$$\hat{p}^\mu = i\hbar \partial^\mu = \left(\frac{i\hbar}{c} \frac{\partial}{\partial t}, -i\hbar \boldsymbol{\nabla} \right) \quad \text{Momentum operator} \quad (\text{A.0.3})$$

$$p^\mu = \left(\frac{E}{c}, \mathbf{p} \right) \quad \text{Momentum variable} \quad (\text{A.0.4})$$

$$A^\mu = (A^0, A^1, A^2, A^3) = \left(\frac{\varphi}{c}, \mathbf{A} \right) \quad \text{Potential} \quad (\text{A.0.5})$$

$$j^\mu = -ce\bar{\psi}\gamma^\mu\psi = \begin{cases} c[-e\psi^\dagger\psi] = c\rho & \text{if } \mu = 0 \\ -e\psi^\dagger c\boldsymbol{\alpha}\psi = \mathbf{j} & \text{otherwise} \end{cases} \quad \text{Probability current} \quad (\text{A.0.6})$$

Notice that bold quantities are three-quantities (vectors), while unbold ones are four-quantities. We choose to work with the following Minkowski metric tensor:

$$g_{\mu\nu} = g^{\mu\nu} = \text{diag}(+1, -1, -1, -1). \quad (\text{A.0.7})$$

The gamma matrices, given by the following four-vector:

$$\gamma^\mu = (\gamma^0, \gamma^1, \gamma^2, \gamma^3) = (\gamma^0, \boldsymbol{\gamma}), \quad (\text{A.0.8})$$

are chosen to be the ones associated with the Dirac representation:

$$\gamma^\mu = \left(\begin{bmatrix} \mathbb{1}_2 & 0 \\ 0 & -\mathbb{1}_2 \end{bmatrix}, \begin{bmatrix} 0 & \boldsymbol{\sigma} \\ -\boldsymbol{\sigma} & 0 \end{bmatrix} \right), \quad (\text{A.0.9})$$

where one sees the Pauli spin matrices $\boldsymbol{\sigma}$. These gamma matrices obey specific anticommutation relations (generating a Clifford algebra):

$$\{\gamma^\mu, \gamma^\nu\} = \gamma^\mu\gamma^\nu + \gamma^\nu\gamma^\mu = 2g^{\mu\nu}\mathbb{1}_4. \quad (\text{A.0.10})$$

We are also going to use the fifth gamma matrix, defined as:

$$\gamma^5 := \frac{i\epsilon_{\mu\nu\sigma\theta}}{4!} \gamma^\mu \gamma^\nu \gamma^\sigma \gamma^\theta = i\gamma^0\gamma^1\gamma^2\gamma^3, \quad (\text{A.0.11})$$

and which satisfies the following relations:

$$\{\gamma^\mu, \gamma^5\} = 0, \quad \text{for } \mu = 1, \dots, 4. \quad (\text{A.0.12})$$

In the Dirac representation γ^5 is $\gamma^5 = \begin{bmatrix} 0 & \mathbb{1}_2 \\ \mathbb{1}_2 & 0 \end{bmatrix}$. In addition, we are going to use the α^μ matrix vector, given by:

$$\alpha^\mu = \gamma^0 \gamma^\mu = (I_4, \boldsymbol{\alpha}); \quad \rightarrow \quad \boldsymbol{\alpha} = \begin{bmatrix} 0 & \boldsymbol{\sigma} \\ \boldsymbol{\sigma} & 0 \end{bmatrix}. \quad (\text{A.0.13})$$

The Dirac spinor ψ , satisfies the Dirac equation:

$$[i\hbar\gamma^\mu\partial_\mu - mc]\psi = 0, \quad (\text{A.0.14})$$

while the associated Dirac adjoint $\bar{\psi}$, is given by:

$$\bar{\psi} = \psi^\dagger \gamma^0, \quad (\text{A.0.15})$$

and satisfies the adjoint Dirac equation:

$$\bar{\psi} \left[-i\hbar\gamma^\mu \overleftarrow{\partial}_\mu - mc \right] = 0, \quad (\text{A.0.16})$$

where the arrow pointing to the left indicates that the four-gradient acts to the left. Quantities with one upper index are called contravariant vectors, while others with lower index are covariant vectors. One can transform from contravariant to covariant four-vector by applying the metric tensor:

$$a^\mu = g^{\mu\nu} a_\nu \quad (\text{A.0.17})$$

$$a_\mu = g_{\mu\nu} a^\nu, \quad (\text{A.0.18})$$

which directly leads to the fact that:

$$g^{\mu\nu} g_{\sigma\nu} = \delta^\mu_\sigma. \quad (\text{A.0.19})$$

In addition, this can be generalized a rank- n tensor, where one needs to multiply the expression n metric tensors in order to change the n indices between covariant and contravariant. Finally, we note that we shall use (as done here), the Einstein summation convention, where the presence of an index twice in the same formula, indicates that a sum is implicitly taken.

Appendix B

Identities

B.1 Gamma matrices

B.1.1 Products

The gamma matrix products we shall encounter are the following ones:

$$\gamma^\mu \gamma_\mu = 4\mathbb{1}_4 \quad (\text{B.1.1})$$

$$\gamma^\mu \gamma^\nu \gamma_\mu = -2\gamma^\nu \quad (\text{B.1.2})$$

$$\gamma^\mu \gamma^\nu \gamma^\sigma \gamma_\mu = 4g^{\nu\sigma} \mathbb{1}_4 \quad (\text{B.1.3})$$

$$\gamma^\mu \gamma^\nu \gamma^\sigma \gamma^\theta \gamma_\mu = -2\gamma^\theta \gamma^\sigma \gamma^\nu \quad (\text{B.1.4})$$

Proof of B.1.1

We first write the anticommutation relations of eq.(A.0.10) as:

$$\gamma^\mu \gamma_\nu + \gamma_\nu \gamma^\mu = 2\delta_\nu^\mu \mathbb{1}_4. \quad (\text{B.1.5})$$

After setting $\mu = \nu$, we directly obtain:

$$\gamma_\mu \gamma^\mu = 4\mathbb{1}_4, \quad (\text{B.1.6})$$

where we used $\delta_\mu^\mu = 4$.

Proof of B.1.2

Using the anticommutation relations of eq.(A.0.10), the left hand side of our equation can be written as:

$$\gamma^\mu \gamma^\nu \gamma_\mu = 2\gamma^\mu g_\mu^\nu - \gamma^\mu \gamma_\mu \gamma^\nu. \quad (\text{B.1.7})$$

We now use the previous result to write:

$$\gamma^\mu \gamma^\nu \gamma_\mu = -2\gamma^\nu. \quad (\text{B.1.8})$$

Proof of B.1.3

In the associated equation, we need to pull γ^μ and γ_μ closer to each other, so we can make use of the previous results, we start by writing:

$$\gamma^\mu \gamma^\nu \gamma^\sigma \gamma_\mu = 2\gamma^\mu \gamma^\nu g_\mu^\sigma - \gamma^\mu \gamma^\nu \gamma_\mu \gamma^\sigma, \quad (\text{B.1.9})$$

using the previous result, we obtain:

$$\gamma^\mu \gamma^\nu \gamma^\sigma \gamma_\mu = 4g^{\sigma\nu} \mathbb{1}_4. \quad (\text{B.1.10})$$

Proof of B.1.4

Following the same previous steps, one can show that:

$$\gamma^\mu \gamma^\nu \gamma^\sigma \gamma^\theta \gamma_\mu = 2\gamma^\mu \gamma^\nu \gamma^\sigma g_\mu^\theta - \gamma^\mu \gamma^\nu \gamma^\sigma \gamma_\mu \gamma^\theta \quad (\text{B.1.11})$$

$$= 2\gamma^\theta \gamma^\nu \gamma^\sigma - 4g^{\sigma\nu} \gamma^\theta \quad (\text{B.1.12})$$

$$= -2\gamma^\theta \gamma^\sigma \gamma^\nu. \quad (\text{B.1.13})$$

B.1.2 Traces of gamma matrices**B.1.2.1 $\text{Tr} [\gamma^\mu] = 0$**

Since the square of the fifth gamma matrix of eq.(A.0.11) is the identity operator, we are allowed to write the trace of a single gamma matrix as:

$$\text{Tr} [\gamma^\mu] = \text{Tr} [\gamma^5 \gamma^5 \gamma^\mu], \quad (\text{B.1.14})$$

and since this matrix anticommutes with all the gamma matrices, we can move the middle matrix to the right and get a minus sign:

$$\text{Tr} [\gamma^\mu] = -\text{Tr} [\gamma^5 \gamma^\mu \gamma^5]. \quad (\text{B.1.15})$$

One can now use the cyclic property of the trace, and $\gamma^5 \gamma^5 = 1$ again, to show that:

$$\text{Tr} [\gamma^\mu] = -\text{Tr} [\gamma^\mu], \quad (\text{B.1.16})$$

which indicates that the gamma matrices are traceless:

$$\text{Tr} [\gamma^\mu] = 0. \quad (\text{B.1.17})$$

B.1.2.2 $\text{Tr} [\gamma^\mu \gamma^\nu] = 4g^{\mu\nu}$

The trace of the product of two gamma matrices is:

$$\text{Tr} [\gamma^\mu \gamma^\nu] = 4g^{\mu\nu}. \quad (\text{B.1.18})$$

Using the cyclic property of the trace operator, this trace can be written as the sum of two traces:

$$\text{Tr} [\gamma^\mu \gamma^\nu] = \frac{1}{2} (\text{Tr} [\gamma^\mu \gamma^\nu] + \text{Tr} [\gamma^\nu \gamma^\mu]), \quad (\text{B.1.19})$$

which can now be combined into one trace, using the anticommutation relation. One directly gets:

$$\text{Tr} [\gamma^\mu \gamma^\nu] = g^{\mu\nu} \text{Tr} [\mathbb{1}_4] = 4g^{\mu\nu}. \quad (\text{B.1.20})$$

B.1.2.3 $\text{Tr} [\gamma^{\mu_1} \dots \gamma^{\mu_n}] = 0$ for odd n

The vanishing trace of an odd number of gamma matrices was clearly satisfied for $n = 1$. For $n = 3$ we follow the same procedure, and write:

$$\text{Tr} [\gamma^\mu \gamma^\nu \gamma^\sigma] = \text{Tr} [\gamma^5 \gamma^5 \gamma^\mu \gamma^\nu \gamma^\sigma] \quad (\text{B.1.21})$$

$$= -\text{Tr} [\gamma^5 \gamma^\mu \gamma^5 \gamma^\nu \gamma^\sigma] \quad (\text{B.1.22})$$

$$= +\text{Tr} [\gamma^5 \gamma^\mu \gamma^\nu \gamma^5 \gamma^\sigma] \quad (\text{B.1.23})$$

$$= -\text{Tr} [\gamma^5 \gamma^\mu \gamma^\nu \gamma^\sigma \gamma^5] \quad (\text{B.1.24})$$

$$= -\text{Tr} [\gamma^\mu \gamma^\nu \gamma^\sigma], \quad (\text{B.1.25})$$

which shows that the trace of three gamma matrices vanishes. The reader should start to see the general pattern. The moving of the right fifth gamma matrix to the very right gives an overall minus sign for each exchange of matrices, and this allows us to write:

$$\begin{aligned} \text{Tr} [\gamma^{\mu_1} \dots \gamma^{\mu_n}] &= \text{Tr} [\gamma^5 \gamma^5 \gamma^{\mu_1} \dots \gamma^{\mu_n}] \\ &= (-1)^n \text{Tr} [\gamma^5 \gamma^{\mu_1} \dots \gamma^{\mu_n} \gamma^5] \\ &= (-1)^n \text{Tr} [\gamma^{\mu_1} \dots \gamma^{\mu_n}], \end{aligned} \quad (\text{B.1.26})$$

leading to the conclusion that the trace of any odd number of gamma matrices vanishes.

B.1.2.4 $\text{Tr} [\gamma^\mu \gamma^\nu \gamma^\rho \gamma^\sigma]$

Using the anticommutation relation of the gamma matrices of eq.(A.0.10), we can write this trace as:

$$\text{Tr} [\gamma^\mu \gamma^\nu \gamma^\rho \gamma^\sigma] = \text{Tr} [(2g^{\mu\nu} - \gamma^\nu \gamma^\mu) \gamma^\rho \gamma^\sigma] \quad (\text{B.1.27})$$

$$= 8g^{\mu\nu} g^{\rho\sigma} - \text{Tr} [\gamma^\nu \gamma^\mu \gamma^\rho \gamma^\sigma], \quad (\text{B.1.28})$$

where we obtained the first term using the previous result of eq.(B.1.20). We next focus on the remaining term that can be similarly written as:

$$\text{Tr} [\gamma^\nu \gamma^\mu \gamma^\rho \gamma^\sigma] = \text{Tr} [\gamma^\nu (2g^{\mu\rho} - \gamma^\rho \gamma^\mu) \gamma^\sigma] \quad (\text{B.1.29})$$

$$= 8g^{\mu\rho} g^{\nu\sigma} - \text{Tr} [\gamma^\nu \gamma^\rho \gamma^\mu \gamma^\sigma]. \quad (\text{B.1.30})$$

We are left with the last term that can be also written as:

$$\text{Tr} [\gamma^\nu \gamma^\rho \gamma^\mu \gamma^\sigma] = \text{Tr} [\gamma^\nu \gamma^\rho (2g^{\mu\sigma} - \gamma^\sigma \gamma^\mu)] \quad (\text{B.1.31})$$

$$= 8g^{\mu\sigma} g^{\nu\rho} - \text{Tr} [\gamma^\nu \gamma^\rho \gamma^\sigma \gamma^\mu]. \quad (\text{B.1.32})$$

Notice that the last trace (in the last line) is identical to the parent trace we started with. We can thus combine the three results and obtain our seeked trace:

$$\text{Tr} [\gamma^\mu \gamma^\nu \gamma^\rho \gamma^\sigma] = 4g^{\mu\nu} g^{\rho\sigma} - 4g^{\rho\mu} g^{\nu\sigma} + 4g^{\mu\sigma} g^{\nu\rho}. \quad (\text{B.1.33})$$

B.1.2.5 $\text{Tr} [\gamma^{\mu_1} \dots \gamma^{\mu_n}]$ for even n

Following the same arguments, and using previous results, one can generate the trace of any even number of gamma matrices, which becomes a tedious work for large number of gamma matrices. This kind of traces can be calculated using “DiracTrace” command (see second link) of the “Feyncalc” Mathematica package [164]. If one favors pen and paper, we have found a nice technique that can be used to facilitate this calculation. This technique was inspired by our study and manipulations done with Wick’s theorem. The trace is found, without providing its proof, to be equal to 4 multiplied by the sum of all possible fully contracted gamma matrix product:

$$\text{Tr} [\gamma^{\mu_1} \gamma^{\mu_2} \gamma^{\mu_3} \gamma^{\mu_4} \dots \gamma^{\mu_n}] = 4 \sum_{\text{full cont.}} (\gamma^{\mu_1} \gamma^{\mu_2} \gamma^{\mu_3} \gamma^{\mu_4} \dots \gamma^{\mu_n}). \quad (\text{B.1.34})$$

The contraction of two gamma matrices, lets say γ^{μ_1} and γ^{μ_2} is represented by a line that joins these two operators, and is defined to be the metric tensor $g^{\mu_1 \mu_2}$:

$$\overline{\gamma^{\mu_1} \gamma^{\mu_2}} = g^{\mu_1 \mu_2}. \quad (\text{B.1.35})$$

In addition, a minus sign should be added at each time two matrices are swapped in order to bring the contracted matrices next to each others. Here are two examples, where one needs to perform one and two swappings of gamma matrices respectively:

$$\overline{\gamma^{\mu} \gamma^{\nu} \gamma^{\rho} \gamma^{\sigma}} = -\overline{\gamma^{\mu} \gamma^{\rho} \gamma^{\nu} \gamma^{\sigma}} \quad (\text{B.1.36})$$

$$\overline{\gamma^{\mu} \gamma^{\nu} \gamma^{\rho} \gamma^{\sigma}} = \overline{\gamma^{\mu} \gamma^{\sigma} \gamma^{\nu} \gamma^{\rho}} \quad (\text{B.1.37})$$

in order to get contracted partners together. An easier way to get the right signs, is to realize that the minimum number of swappings one needs to perform, to get contracted terms together is equal to the number of intersections of the contraction lines (above). As a consequence, one gets an overall minus sign if the contraction lines intersect for odd times (as in the first equation), and a plus sign for even intersections (as in the second equation).

- For $n = 2$, we clearly have the right result of eq.(B.1.20):

$$\frac{1}{4} \text{Tr} [\gamma^{\mu} \gamma^{\nu}] = \overline{\gamma^{\mu} \gamma^{\nu}} = g^{\mu \nu}. \quad (\text{B.1.38})$$

- For $n = 4$, we obtain the result eq.(B.1.33) in a much faster way:

$$\frac{1}{4} \text{Tr} [\gamma^{\mu} \gamma^{\nu} \gamma^{\rho} \gamma^{\sigma}] = \overline{\gamma^{\mu} \gamma^{\nu} \gamma^{\rho} \gamma^{\sigma}} + \overline{\gamma^{\mu} \gamma^{\rho} \gamma^{\nu} \gamma^{\sigma}} + \overline{\gamma^{\mu} \gamma^{\sigma} \gamma^{\nu} \gamma^{\rho}} \quad (\text{B.1.39})$$

$$= g^{\mu \nu} g^{\rho \sigma} - g^{\mu \rho} g^{\nu \sigma} + g^{\mu \sigma} g^{\nu \rho}. \quad (\text{B.1.40})$$

- For $n = 6$, we get:

$$\begin{aligned}
\frac{1}{4} \text{Tr} [\gamma^\mu \gamma^\nu \gamma^\rho \gamma^\sigma \gamma^\tau \gamma^\theta] &= \overline{\gamma^\mu \gamma^\nu \gamma^\rho \gamma^\sigma \gamma^\tau} \gamma^\theta + \overline{\gamma^\mu \gamma^\nu \gamma^\rho \gamma^\sigma \gamma^\tau} \gamma^\theta + \overline{\gamma^\mu \gamma^\nu \gamma^\rho \gamma^\sigma \gamma^\tau} \gamma^\theta \\
&+ \overline{\gamma^\mu \gamma^\nu \gamma^\rho \gamma^\sigma \gamma^\tau} \gamma^\theta + \overline{\gamma^\mu \gamma^\nu \gamma^\rho \gamma^\sigma \gamma^\tau} \gamma^\theta + \overline{\gamma^\mu \gamma^\nu \gamma^\rho \gamma^\sigma \gamma^\tau} \gamma^\theta \\
&+ \overline{\gamma^\mu \gamma^\nu \gamma^\rho \gamma^\sigma \gamma^\tau} \gamma^\theta + \overline{\gamma^\mu \gamma^\nu \gamma^\rho \gamma^\sigma \gamma^\tau} \gamma^\theta + \overline{\gamma^\mu \gamma^\nu \gamma^\rho \gamma^\sigma \gamma^\tau} \gamma^\theta \\
&+ \overline{\gamma^\mu \gamma^\nu \gamma^\rho \gamma^\sigma \gamma^\tau} \gamma^\theta + \overline{\gamma^\mu \gamma^\nu \gamma^\rho \gamma^\sigma \gamma^\tau} \gamma^\theta + \overline{\gamma^\mu \gamma^\nu \gamma^\rho \gamma^\sigma \gamma^\tau} \gamma^\theta \\
&+ \overline{\gamma^\mu \gamma^\nu \gamma^\rho \gamma^\sigma \gamma^\tau} \gamma^\theta + \overline{\gamma^\mu \gamma^\nu \gamma^\rho \gamma^\sigma \gamma^\tau} \gamma^\theta + \overline{\gamma^\mu \gamma^\nu \gamma^\rho \gamma^\sigma \gamma^\tau} \gamma^\theta \quad (\text{B.1.41})
\end{aligned}$$

$$\begin{aligned}
&= g^{\mu\nu} (+g^{\rho\sigma} g^{\tau\theta} - g^{\rho\tau} g^{\sigma\theta} + g^{\rho\theta} g^{\sigma\tau}) \\
&+ g^{\mu\rho} (-g^{\nu\sigma} g^{\tau\theta} + g^{\nu\tau} g^{\sigma\theta} - g^{\nu\theta} g^{\sigma\tau}) \\
&+ g^{\mu\sigma} (+g^{\nu\rho} g^{\tau\theta} - g^{\nu\tau} g^{\rho\theta} + g^{\nu\theta} g^{\rho\tau}) \\
&+ g^{\mu\tau} (-g^{\nu\rho} g^{\sigma\theta} + g^{\nu\sigma} g^{\rho\theta} - g^{\nu\theta} g^{\rho\sigma}) \\
&+ g^{\mu\theta} (+g^{\nu\rho} g^{\sigma\tau} - g^{\nu\sigma} g^{\rho\tau} + g^{\nu\tau} g^{\rho\sigma}). \quad (\text{B.1.42})
\end{aligned}$$

Appendix C

Spherical Bessel functions

C.1 The Bessel equation and its solutions

The Bessel equation is of the following form:

$$z^2 \frac{d^2 \omega}{dz^2} + z \frac{d\omega}{dz} + (z^2 - \nu^2) \omega = 0, \quad (\text{C.1.1})$$

and its solution can be written as a linear combination of two linearly independent solutions:

$$\omega_\nu(z) = c_1 J_\nu(z) + c_2 Y_\nu(z), \quad (\text{C.1.2})$$

known as the Bessel functions of the first and second kind respectively. These functions can be written as [60, eqs.(9.1.2 and 9.1.10)]:

$$J_\nu(z) = \left(\frac{z}{2}\right)^\nu \sum_{k=0}^{\infty} (-1)^k \frac{(z^2/4)^k}{k! \Gamma(\nu + k + 1)} \quad (\text{C.1.3})$$

$$Y_\nu(z) = \frac{J_\nu(z) \cos(\nu\pi) - J_{-\nu}(z)}{\sin(\nu\pi)}, \quad (\text{C.1.4})$$

where these formulas are valid for integer values of ν , including zero. After calling $\alpha_{\nu i}$ the position of the i -th positive zero of the $J_\nu(z)$ Bessel function, the orthogonality of the Bessel function can be expressed as [165, eq.(10.22.37)] [166, eqs.(14.44 and 14.46)]:

$$\int_0^1 dt t J_\nu(\alpha_{\nu i} t) J_\nu(\alpha_{\nu j} t) = \frac{1}{2} (J_{\nu+1}(\alpha_{\nu i}))^2 \delta_{ij}, \quad (\text{C.1.5})$$

using the change of variables $t = \frac{r}{R}$, this integral becomes:

$$\int_0^R dr r J_\nu\left(\alpha_{\nu i} \frac{r}{R}\right) J_\nu\left(\alpha_{\nu j} \frac{r}{R}\right) = \frac{R^2}{2} (J_{\nu+1}(\alpha_{\nu i}))^2 \delta_{ij}. \quad (\text{C.1.6})$$

C.2 Spherical Bessel equation and solutions

The solution of following differential equation [60, section 10.1.1] [165, eq.(10.47.1)]:

$$z^2 \frac{d^2 u}{dz^2} + 2z \frac{du}{dz} + (z^2 - n(n+1)) u = 0; \quad n = 0, \pm 1, \pm 2, \dots \quad (\text{C.2.1})$$

can be written as a linear combination:

$$u(z) = c_1 j_n(z) + c_2 y_n(z), \quad (\text{C.2.2})$$

of two linearly independent functions $j_n(z)$ and $y_n(z)$ called the spherical Bessel functions of the first and second kind, respectively. Here $z = x + iy$ represents the complex variable. We then introduce a function $U = zu$, which thus satisfies the following equation:

$$\left[\frac{d^2}{dz^2} - \frac{n(1+n)}{z^2} + 1 \right] U = 0; \quad U = zu. \quad (\text{C.2.3})$$

The spherical Bessel functions are related to the ordinary Bessel functions (of the first and second kind) by the following formulas [165, eqs. 10.47.3-4]:

$$j_n(z) = \sqrt{\frac{\pi}{2z}} J_{n+\frac{1}{2}}(z) \quad (\text{C.2.4})$$

$$y_n(z) = \sqrt{\frac{\pi}{2z}} Y_{n+\frac{1}{2}}(z), \quad (\text{C.2.5})$$

and can be written using Rayleigh's formula in terms of derivatives of some trigonometric functions as [60, eqs.(10.1.25-26)]:

$$j_n(z) = +z^n \left(-\frac{1}{z} \frac{d}{dz} \right)^n \frac{\sin z}{z} \quad (\text{C.2.6})$$

$$y_n(z) = -z^n \left(-\frac{1}{z} \frac{d}{dz} \right)^n \frac{\cos z}{z}. \quad (\text{C.2.7})$$

In figures C.2.1a and C.2.1b we plot the seven spherical Bessel functions of the first and second kind, corresponding to integer orders: $n = 0, \pm 1, \pm 2, \pm 3$.

C.3 Limiting forms

For small z approaching zero, the spherical Bessel functions behave as [165, 10.52.1-2]:

$$j_n(z) \sim \frac{z^n}{(2n+1)!!} \quad (\text{C.3.1})$$

$$y_n(z) \sim -\frac{(2n-1)!!}{z^{n+1}}, \quad (\text{C.3.2})$$

where the double factorial $!!$ gives different outputs for different integer parities:

$$n!! = \begin{cases} n(n-2)(n-4)\dots 4 \cdot 2 & \text{for } n \text{ even} \\ n(n-1)(n-3)\dots 3 \cdot 1 & \text{for } n \text{ odd} \end{cases} \quad (\text{C.3.3})$$

For large z , these functions behave as [165, 10.52.3]:

$$j_n(z) \sim +z^{-1} \sin\left(z - \frac{n\pi}{2}\right) + e^{|\Im(z)|} \mathcal{O}(z^{-2}) \quad (\text{C.3.4})$$

$$y_n(z) \sim -z^{-1} \cos\left(z - \frac{n\pi}{2}\right) + e^{|\Im(z)|} \mathcal{O}(z^{-2}). \quad (\text{C.3.5})$$

These limiting forms indicate that for large and purely real z , these functions vanish, since the trigonometric functions are damped by the z^{-1} term, and lower orders vanish. If z has an imaginary component then these functions will diverge for large z , because of the exponential $e^{|\Im(z)|}$.

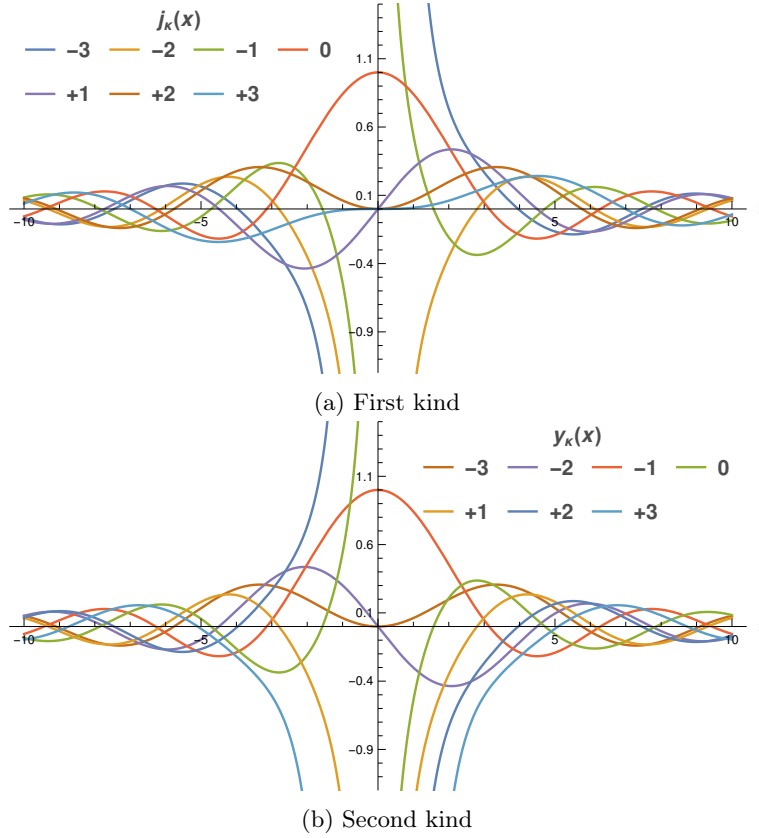


Figure C.2.1: Few spherical Bessel functions of integer order.

C.4 Normalization to Dirac-delta

The spherical Bessel functions of the first-kind respects the following normalization:

$$\int_0^\infty dr r^2 j_\ell(kr) j_\ell(k'r) = \frac{\pi}{2k^2} \delta(k - k'). \quad (\text{C.4.1})$$

This identity can be shown as follows: We start with the well-known integral:

$$\int d^3x e^{i(\mathbf{k}_1 - \mathbf{k}_2) \cdot \mathbf{x}} = (2\pi)^3 \delta(\mathbf{k}_1 - \mathbf{k}_2), \quad (\text{C.4.2})$$

and using the plane wave expansion [56, eq.(5.23)], the exponential can be expanded in the basis of the spherical Bessel functions and the spherical harmonics:

$$e^{i\mathbf{k} \cdot \mathbf{x}} = 4\pi \sum_{\ell=0}^{\infty} i^\ell j_\ell(kr) \sum_{m=-\ell}^{\ell} Y_{\ell,m}^*(\hat{\mathbf{k}}) Y_{\ell,m}(\hat{\mathbf{x}}). \quad (\text{C.4.3})$$

This relation allows us to write the previous one as:

$$\begin{aligned} \int d^3 \mathbf{x} e^{i(\mathbf{k}_1 - \mathbf{k}_2) \cdot \mathbf{x}} &= \sum_{\ell=0}^{\infty} \sum_{\ell'=0}^{\infty} \sum_{m=-\ell}^{\ell} \sum_{m'=-\ell'}^{\ell'} (4\pi)^2 i^{\ell+\ell'} Y_{\ell,m}^* (\hat{\mathbf{k}}_1) Y_{\ell',m'} (-\hat{\mathbf{k}}_2) \\ &\times \int_0^{\infty} r^2 dr j_{\ell}(k_1 r) j_{\ell'}(k_2 r) \int_0^{\pi} \sin \theta_x d\theta_x \int_0^{2\pi} d\varphi_x Y_{\ell,m}(\hat{\mathbf{x}}) Y_{\ell',m'}^*(\hat{\mathbf{x}}). \end{aligned} \quad (\text{C.4.4})$$

We now use the orthonormalization condition of eq.(D.3.8), and the parity identity of eq.(D.3.18) of the spherical harmonics, to simplify our previous equation to:

$$\begin{aligned} \int d^3 \mathbf{x} e^{i(\mathbf{k}_1 - \mathbf{k}_2) \cdot \mathbf{x}} &= (4\pi)^2 \sum_{\ell=0}^{\infty} \sum_{m=-\ell}^{\ell} Y_{\ell,m}^* (\hat{\mathbf{k}}_1) Y_{\ell,m} (\hat{\mathbf{k}}_2) \\ &\times \int_0^{\infty} r^2 dr j_{\ell}(k_1 r) j_{\ell}(k_2 r). \end{aligned} \quad (\text{C.4.5})$$

We then use the completeness relation of spherical harmonics [167, eq.(3.56)]:

$$\sum_{\ell=0}^{\infty} \sum_{m=-\ell}^{\ell} Y_{\ell,m}^* (\hat{\mathbf{k}}_1) Y_{\ell,m} (\hat{\mathbf{k}}_2) = \delta(\cos \theta_1 - \cos \theta_2) \delta(\varphi_1 - \varphi_2) = \frac{1}{\sin \theta_1} \delta(\theta_1 - \theta_2) \delta(\varphi_1 - \varphi_2), \quad (\text{C.4.6})$$

and write the three- Dirac-delta in spherical coordinates [107, eq.(A.8)]:

$$\delta(\mathbf{k}_1 - \mathbf{k}_2) = \frac{1}{k_1^2} \delta(k_1 - k_2) \delta(\cos \theta_1 - \cos \theta_2) \delta(\varphi_1 - \varphi_2), \quad (\text{C.4.7})$$

to obtain our wanted orthogonality relation [167, eq.(3.112)]:

$$\int_0^{\infty} r^2 dr j_{\ell}(k_1 r) j_{\ell}(k_2 r) = \frac{\pi}{2k_1^2} \delta(k_1 - k_2). \quad (\text{C.4.8})$$

C.5 Derivatives

Using [60, eq.(10.1.23)] that is valid for $f_{\kappa}(z) = j_{\kappa}(z)$, $y_{\kappa}(z)$:

$$\left(\frac{1}{z} \frac{d}{dz} \right)^m [z^{\kappa+1} f_{\kappa}(z)] = z^{\kappa-m+1} f_{\kappa-m}(z); \quad \begin{cases} \kappa &= 0, \pm 1, \pm 2, \dots \\ m &= 1, 2, 3, 4, \dots \end{cases} \quad (\text{C.5.1})$$

For $m = 1, 2, 3$, one obtains:

$$\frac{d}{dz} f_{\kappa}(z) + \frac{\kappa+1}{z} f_{\kappa}(z) = f_{\kappa-1}(z) \quad (\text{C.5.2})$$

$$\frac{d^2}{dz^2} f_{\kappa}(z) + \frac{2\kappa+1}{z} \frac{d}{dz} f_{\kappa}(z) + \frac{\kappa^2-1}{z^2} f_{\kappa}(z) = f_{\kappa-2}(z) \quad (\text{C.5.3})$$

$$\frac{d^3}{dz^3} f_{\kappa}(z) + \frac{3\kappa}{z} \frac{d^2}{dz^2} f_{\kappa}(z) + \frac{3((\kappa-1)\kappa-1)}{z^2} \frac{d}{dz} f_{\kappa}(z) + \frac{(\kappa-3)(\kappa-1)(\kappa+1)}{z^3} f_{\kappa}(z) = f_{\kappa-3}(z) \quad (\text{C.5.4})$$

then one can replace in the m -th order equation, the expressions of lower order derivatives from previous equations.

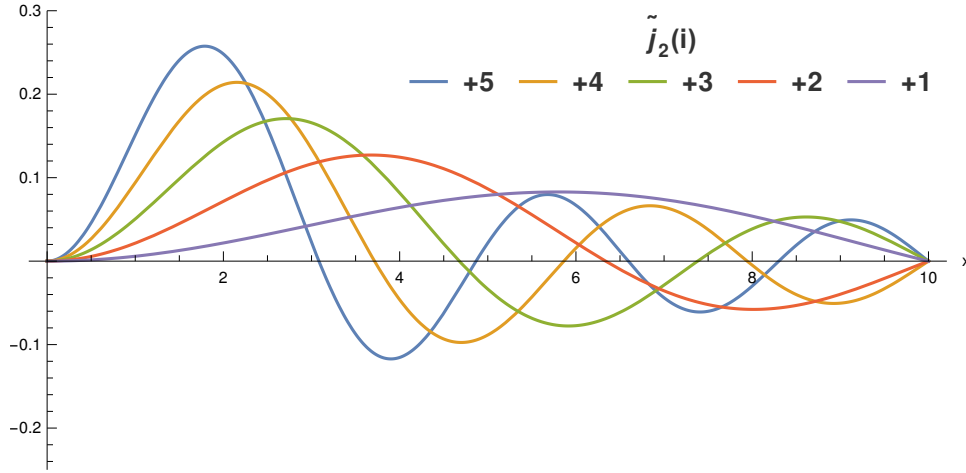


Figure C.6.1: First five second-order spherical Bessel basis elements with $\tilde{j}_2(i) = \tilde{j}_2(\gamma_{2i} \frac{r}{a})$

C.6 Orthogonality within a spherical box

Using the ordinary Bessel function orthogonality relation of eq.(C.1.6), and the fact that these can be written in terms of the spherical Bessel functions eq.(C.2.5), one obtains:

$$\int_0^R dr r^2 j_n \left(\gamma_{ni} \frac{r}{R} \right) j_n \left(\gamma_{nj} \frac{r}{R} \right) = \frac{R^3}{2} (j_{n+1}(\gamma_{ni}))^2 \delta_{ij}, \quad (\text{C.6.1})$$

where $\gamma_{ni} = \alpha_{n+\frac{1}{2},i}$, representing the i -th zero of the n -th order spherical Bessel functions, which coincides with the i -th zero of the $n + \frac{1}{2}$ -th order ordinary Bessel function (of the first kind), clearly seen in eq.(C.2.4). This means that in a spherical box of radius a , one is able to construct an orthonormal spherical Bessel basis set, whose elements are characterized by different positive integer numbers i of the $\alpha_{n+\frac{1}{2},i}$ number. Orthonormal functions clearly become:

$$\tilde{j}_n \left(\gamma_{ni} \frac{r}{R} \right) = \frac{1}{|j_{n+1}(\gamma_{ni})|} \sqrt{\frac{2}{R^3}} j_n \left(\gamma_{ni} \frac{r}{R} \right). \quad (\text{C.6.2})$$

In figure C.6.1 we plot the first five basis element of the (orthonormal) spherical Bessel basis associated with the second-order $n = 2$ function. The numerical values of the first ten factors (zeros locations) γ_{ni} are computed using Mathematica [22] for $n = \pm 1, \pm 2, \pm 3$ and ± 4 , and are tabulated in table C.1. Zeros of the positive orders can be found in [60, Table 10.6]

$i \backslash n$	-1	$+1$
1	1.5707963267948966192	4.4934094579090641753
2	4.7123889803846898577	7.7252518369377071642
3	7.8539816339744830962	10.904121659428899827
4	10.995574287564276335	14.066193912831473480
5	14.137166941154069573	17.220755271930768740
6	17.278759594743862812	20.371302959287562845
7	20.420352248333656050	23.519452498689006546
8	23.561944901923449288	26.666054258812673528
9	26.703537555513242527	29.811598790892958837
10	29.845130209103035765	32.956389039822476725
$i \backslash n$	-2	$+2$
1	2.7983860457838871367	5.7634591968945497914
2	6.1212504668980683013	9.0950113304763551561
3	9.3178664617910653789	12.322940970566582052
4	12.486454395223781428	15.514603010886748230
5	15.644128370333027630	18.689036355362822202
6	18.796404366210157169	21.853874222709765792
7	21.945612879981044573	25.012803202289612466
8	25.092910412112097360	28.167829707993623875
9	28.238936575260272929	31.320141707447174536
10	31.384074017889858488	34.470488331284988666
$i \backslash n$	-3	$+3$
1	3.9595279165010953532	6.9879320005005199591
2	7.4516100642145034005	10.417118547379364764
3	10.715647375791512567	13.698023153249248999
4	13.921686012308781694	16.923621285213839579
5	17.103359117208740899	20.121806174453818286
6	20.272369140216529383	23.304246988939651352
7	23.433926142067802430	26.476763664539128150
8	26.590716631086271085	29.642604540315809172
9	29.744270680556556397	32.803732385196107943
10	32.895525188224304150	35.961405804709033069
$i \backslash n$	-4	$+4$
1	5.0884980139408550205	8.1825614525712427017
2	8.7337103225929058514	11.704907154570390558
3	12.067543686098046067	15.039664707616520808
4	15.315389681151238085	18.301255959541990220
5	18.525210372145093296	21.525417733399945437
6	21.714547286348721223	24.727565547835033371
7	24.891502692735838467	27.915576199421360642
8	28.060374592908179463	31.093933214079307175
9	31.223666727770478198	34.265390086101585783
10	34.382940654644671865	37.431736768201494726

Table C.1: $\gamma_{n,i}$: First ten zeros of the spherical Bessel functions $j_n(x)$ of orders $n = \pm 1, \dots, \pm 4$.

Appendix D

Identities

D.1 Dirac relation

The Dirac relation that first appeared in [30, eq.(16)], is given by:

$$(\boldsymbol{\sigma} \cdot \mathbf{a})(\boldsymbol{\sigma} \cdot \mathbf{b}) = \mathbf{a} \cdot \mathbf{b} + i\boldsymbol{\sigma} \cdot (\mathbf{a} \times \mathbf{b}), \quad (\text{D.1.1})$$

which can be proved as follows:

$$(\boldsymbol{\sigma} \cdot \mathbf{a})(\boldsymbol{\sigma} \cdot \mathbf{b}) = \sigma_j \sigma_k a_j b_k. \quad (\text{D.1.2})$$

The product of Pauli matrices can be written as:

$$\sigma_j \sigma_k = \delta_{jk} \mathbb{1}_2 + i\varepsilon_{jkl} \sigma_l, \quad (\text{D.1.3})$$

where ε_{jkl} is the cyclic Levi-Civita symbol. When this relation is inserted in the previous equation, it leads to the wanted result:

$$(\boldsymbol{\sigma} \cdot \mathbf{a})(\boldsymbol{\sigma} \cdot \mathbf{b}) = [\delta_{jk} \mathbb{1}_2 + i\varepsilon_{jkl} \sigma_l] a_j b_k \quad (\text{D.1.4})$$

$$= a_j b_j + i\varepsilon_{jkl} \sigma_l a_j b_k \quad (\text{D.1.5})$$

$$= \mathbf{a} \cdot \mathbf{b} + i\boldsymbol{\sigma} \cdot (\mathbf{a} \times \mathbf{b}). \quad (\text{D.1.6})$$

D.2 Spin angular momentum

The spin angular momentum operator is given by:

$$\mathbf{S} = \frac{\hbar}{2} \boldsymbol{\sigma}, \quad (\text{D.2.1})$$

where $\boldsymbol{\sigma}$ are Pauli spin matrices. The spin states are defined as the eigenvectors of the $\mathbf{S}^2 = \frac{\hbar^2}{4} \boldsymbol{\sigma}^2$ operator:

$$\begin{bmatrix} 1 \\ 0 \end{bmatrix} \quad \text{and} \quad \begin{bmatrix} 0 \\ 1 \end{bmatrix}. \quad (\text{D.2.2})$$

The four-component spin angular momentum operator will be called $\boldsymbol{\Sigma}$, and is given by:

$$\boldsymbol{\Sigma} = \mathbb{1}_2 \otimes \mathbf{S} = \begin{bmatrix} \mathbf{S} & 0 \\ 0 & \mathbf{S} \end{bmatrix}. \quad (\text{D.2.3})$$

D.3 Spherical Harmonics

The spherical harmonics $Y_{\ell,m}(\hat{\mathbf{x}})$ are given by [61, eq.(B.93)]:

$$Y_{\ell,m}(\hat{\mathbf{x}}) = (-1)^m \sqrt{\frac{(2\ell+1)(\ell-m)!}{4\pi(\ell+m)!}} P_{\ell}^m(\cos\theta) e^{im\varphi}, \quad (\text{D.3.1})$$

where $\hat{\mathbf{x}} = (\theta, \varphi)$ represent the spherical angles associated with the unit vector $\frac{\mathbf{x}}{|\mathbf{x}|}$ that points in the position direction. The spherical harmonic satisfies both equations:

$$[\mathbf{L}^2 - \hbar^2 \ell(\ell+1)] Y_{\ell,m}(\theta, \varphi) = 0 \quad (\text{D.3.2})$$

$$[L_z^2 - \hbar m] Y_{\ell,m}(\theta, \varphi) = 0, \quad (\text{D.3.3})$$

where the orbital angular momentum (azimuthal) quantum number, and the associated magnetic quantum number are restricted to the following integer values:

$$\ell = 0, 1, 2, \dots \quad (\text{D.3.4})$$

$$m = -\ell, -\ell+1, \dots, \ell-1, \ell \quad (\text{D.3.5})$$

where the squared \mathbf{L} and L_z operators are given by:

$$\mathbf{L}^2 = L_x^2 + L_y^2 + L_z^2 = -\hbar^2 \left[\frac{1}{\sin\theta} \frac{\partial}{\partial\theta} \left(\sin\theta \frac{\partial}{\partial\theta} \right) + \frac{1}{\sin^2\theta} \frac{\partial^2}{\partial\varphi^2} \right] \quad (\text{D.3.6})$$

$$L_z^2 = -\hbar^2 \frac{\partial^2}{\partial\varphi^2}. \quad (\text{D.3.7})$$

The above expression is normalized, meaning that functions satisfy the following orthonormalization condition:

$$\int_0^\pi \sin\theta d\theta \int_0^{2\pi} d\varphi Y_{\ell,m}(\hat{\mathbf{x}}) Y_{\ell',m'}^*(\hat{\mathbf{x}}) = \delta_{\ell\ell'} \delta_{mm'}. \quad (\text{D.3.8})$$

$P_{\ell}^m(x)$ are the associated Legendre polynomials [61, eq.(B.72)], and are related to the Legendre polynomials $P_{\ell}(x)$ [61, eq.(B.71)] by the Rodrigues' formula:

$$\begin{aligned} P_{\ell}^m(x) &= (1-x^2)^{m/2} \frac{d^m}{dx^m} P_{\ell}(x) & \text{with } P_{\ell}(x) &= \frac{1}{2^{\ell}\ell!} \frac{d^{\ell}}{dx^{\ell}} (x^2-1)^{\ell}; \\ &= \frac{1}{2^{\ell}\ell!} (1-x^2)^{m/2} \frac{d^{\ell+m}}{dx^{\ell+m}} (x^2-1)^{\ell}. \end{aligned} \quad (\text{D.3.9})$$

For negative integer m , the first formula does not work, and the differential operator becomes an integral as seen in [165, section 14.6(ii)]. The last formula is not problematic, and is valid for $-1 \leq x \leq 1$, for a zero or positive integer ℓ , for integer values of m , with $|m| \leq \ell$. An associated Legendre polynomial with $-m$ can be related to the corresponding $+m$ polynomial by [166, eq.(15.81)]:

$$P_{\ell}^{-m}(x) = (-1)^m \frac{(\ell-m)!}{(\ell+m)!} P_{\ell}^m(x). \quad (\text{D.3.10})$$

D.3.1 Complex conjugation

The complex conjugation of the spherical harmonic function of eq.(D.3.1), flips the sign of the exponential phase factor. We start by complex conjugating the expression, and obtain:

$$Y_{\ell,m}^*(\hat{\mathbf{x}}) = (-1)^m \sqrt{\frac{(2\ell+1)(\ell-m)!}{4\pi(\ell+m)!}} P_{\ell}^m(\cos\theta) e^{-im\varphi}, \quad (\text{D.3.11})$$

using eq.(D.3.10) and the following equation:

$$\sqrt{\frac{(\ell-m)!}{(\ell+m)!}} = \sqrt{\frac{(\ell+m)!}{(\ell-m)!} \frac{(\ell-m)!}{(\ell+m)!}}, \quad (\text{D.3.12})$$

we obtain the complex conjugated spherical harmonic:

$$Y_{\ell,m}^*(\hat{\mathbf{x}}) = (-1)^m Y_{\ell,-m}(\hat{\mathbf{x}}). \quad (\text{D.3.13})$$

D.3.2 Parity

Under parity transformation (space inversion) $\hat{\mathbf{x}} \rightarrow -\hat{\mathbf{x}}$, the spherical coordinates angles transform as:

$$\theta \rightarrow \pi - \theta \quad (\text{D.3.14})$$

$$\varphi \rightarrow \pi + \varphi, \quad (\text{D.3.15})$$

leading to the following spherical harmonic function:

$$Y_{\ell,m}(-\hat{\mathbf{x}}) = (-1)^m \sqrt{\frac{(2\ell+1)(\ell-m)!}{4\pi(\ell+m)!}} P_{\ell}^m(-\cos\theta) e^{im\varphi} e^{im\pi}. \quad (\text{D.3.16})$$

Clearly, from eq.(D.3.9), one can conclude that the associated Legendre polynomial is of $(-1)^{\ell+m}$ parity:

$$P_{\ell}^m(-x) = (-1)^{m+\ell} P_{\ell}^m(x). \quad (\text{D.3.17})$$

This leads to $(-1)^{\ell}$ parity transformation for spherical harmonics:

$$Y_{\ell,m}(-\hat{\mathbf{x}}) = (-1)^{\ell} Y_{\ell,m}(\hat{\mathbf{x}}). \quad (\text{D.3.18})$$

D.4 Spherical spinors

D.4.1 Clebsch-Gordan coefficients: Angular momenta coupling

The Clebsch-Gordan coefficients arise from the expansion of the total angular momentum state that couples two single angular momenta states, in a basis formed out of the uncoupled state vectors. Assuming one has two angular momenta states $|j_1, m_1\rangle$ and $|j_2, m_2\rangle$, being the eigenvectors of some squared- and z -component angular momenta operators, meaning that these states satisfy the following equations:

$$\mathbf{J}_1^2 |j_1, m_1\rangle = \hbar j_1(j_1 + 1) |j_1, m_1\rangle \quad (\text{D.4.1})$$

$$J_{1z} |j_1, m_1\rangle = \hbar m_1 |j_1, m_1\rangle, \quad (\text{D.4.2})$$

for angular momentum 1, and:

$$\mathbf{J}_2^2 |j_2, m_2\rangle = \hbar j_2 (j_2 + 1) |j_2, m_2\rangle \quad (\text{D.4.3})$$

$$J_{2z} |j_2, m_2\rangle = \hbar m_2 |j_2, m_2\rangle, \quad (\text{D.4.4})$$

for angular momentum 2. Where the squared operators are given by $\mathbf{J}_{1,2}^2 = J_{1,2x}^2 + J_{1,2y}^2 + J_{1,2z}^2$, summing over individual squared operator vector components. The angular momentum operators act on vector spaces of dimensions $2j_1 + 1$ and $2j_2 + 1$ spanned by the basis vectors (eigenvectors):

$$|j_1, m_1\rangle; \quad \text{with } m_1 \in \{-j_1, -j_1 + 1, \dots, +j_1 - 1, +j_1\} \quad (\text{D.4.5})$$

$$|j_2, m_2\rangle; \quad \text{with } m_2 \in \{-j_2, -j_2 + 1, \dots, +j_2 - 1, +j_2\}. \quad (\text{D.4.6})$$

In addition, these operators obey the angular momentum algebra, i.e. satisfy the following commutation relations:

$$[J_i, J_j] = i\hbar \epsilon_{ijk} J_k; \quad i, k, j \in \{x, y, z\} \quad (\text{D.4.7})$$

$$[\mathbf{J}^2, J_j] = 0. \quad (\text{D.4.8})$$

The total angular momentum operator that couples both angular momenta operators, has the following form:

$$\mathbf{J} = \mathbf{J}_1 \otimes 1 + 1 \otimes \mathbf{J}_2, \quad (\text{D.4.9})$$

acts on a space of dimensions $(2j_1 + 1)(2j_2 + 1)$ whose basis elements (we shall call uncoupled) are formed by the tensor product of both basis elements:

$$|j_1, m_1, j_2, m_2\rangle = |j_1, m_1\rangle \otimes |j_2, m_2\rangle, \quad (\text{D.4.10})$$

in the following manner:

$$\mathbf{J} |j_1, m_1, j_2, m_2\rangle = \mathbf{J}_1 |j_1, m_1\rangle \otimes |j_2, m_2\rangle + |j_1, m_1\rangle \otimes \mathbf{J}_2 |j_2, m_2\rangle. \quad (\text{D.4.11})$$

In addition, it can be shown that the total angular momentum is an angular momentum itself, that satisfies its own commutation relations:

$$[J_i, J_j] = [J_{1i}, J_{1j}] \otimes 1 + 1 \otimes [J_{2i}, J_{2j}] = i\epsilon_{ijk} J_k \quad (\text{D.4.12})$$

$$[\mathbf{J}^2, J_i] = 0 \quad (\text{D.4.13})$$

with

$$\mathbf{J}^2 = \mathbf{J}_1^2 \otimes 1 + 2\mathbf{J}_1 \otimes \mathbf{J}_2 + 1 \otimes \mathbf{J}_2^2 \quad (\text{D.4.14})$$

$$J_i = \mathbf{J}_{1i} \otimes 1 + 1 \otimes \mathbf{J}_{2i}, \quad (\text{D.4.15})$$

using the following property of tensor products:

$$(a \otimes b)(c \otimes d) = ac \otimes bd; \quad \text{with } \begin{cases} u &= ac \\ v &= bd \end{cases} \quad (\text{D.4.16})$$

which indicates that the product of two tensor products is a tensor product itself. The coupled total angular momentum states are defined as the set of vector that satisfies the following total angular momentum commutation relations:

$$\mathbf{J}^2 |j, m_j\rangle = \hbar^2 j(j+1) |j, m_j\rangle \quad (\text{D.4.17})$$

$$J_z |j, m_j\rangle = \hbar m_j |j, m_j\rangle. \quad (\text{D.4.18})$$

After the insertion of the unity operator associated with the uncoupled basis (closure relation):

$$\sum_{m_1=-j_1}^{j_1} \sum_{m_2=-j_2}^{j_2} |j_1, m_1, j_2, m_2\rangle \langle j_1, m_1, j_2, m_2| = 1, \quad (\text{D.4.19})$$

the coupled vector can be written as:

$$|j, m_j\rangle = \sum_{m_1=-j_1}^{j_1} \sum_{m_2=-j_2}^{j_2} C(j_1, j_2, j; m_1, m_2, m_j) |j_1, m_1, j_2, m_2\rangle, \quad (\text{D.4.20})$$

where $C(j_1, j_2, j; m_1, m_2, m_j) = \langle j_1, m_1, j_2, m_2 | j, m_j \rangle$ are the Clebsch-Gordon coefficients which correspond to the expansion of the coupled angular momenta states in the basis of the uncoupled ones, and are constructed with the account for the coupled states to be orthonormalized:

$$\langle j', m_{j'} | j, m_j \rangle = \delta_{j,j'} \delta_{m_j, m_{j'}}, \quad (\text{D.4.21})$$

An exact expression of these coefficients was derived by Wigner in 1931 [168, pages 205-206]:

$$\begin{aligned} C(j_1, j_2, j; m_1, m_2, m_j) &= \delta_{m_j, m_1+m_2} \sqrt{(2j+1)} \frac{(j+j_1-j_2)!(j-j_1+j_2)!(j_1+j_2-j)!(j+m_j)!(j-m_j)!}{(j+j_1+j_2+1)!(j_1-m_1)!(j_1+m_1)!(j_2-m_2)!(j_2+m_2)!} \\ &\times \sum_{\nu} \frac{(-1)^{\nu+j_2+m_2}}{\nu!} \frac{(j_2+j+m_1-\nu)!(j_1-m_1+\nu)!}{(j-j_1+j_2-\nu)!(j+m_j-\nu)!(\nu+j_1-j_2-m_j)!}, \end{aligned} \quad (\text{D.4.22})$$

and later on by Racah in 1942 [169, eq.(15-16)], here the sum over ν runs over all integer values such that none of the factorials have negative arguments. After a lengthy derivation based on the angular momentum algebra, one arrives to a conclusion that these coefficients are non-zero only in the case of:

$$m_j = m_1 + m_2 \quad (\text{D.4.23})$$

$$|j_1 - j_2| \leq j \leq j_1 + j_2. \quad (\text{D.4.24})$$

The first condition, seen also in the Kronecker delta of eq.(D.4.22), indicates that the two sums over magnetic numbers in eq.(D.4.20) reduce to one sum (over one of the two quantum numbers). As a result, we write the total angular momentum state of eq.(D.4.20) as:

$$|j, m_j\rangle = \sum_{m_2=-j_2}^{j_2} C(j_1, j_2, j; m_j - m_2, m_2, m_j) |j_1, m_j - m_2, j_2, m_2\rangle. \quad (\text{D.4.25})$$

For a full derivation of the Clebsch-Gordan coefficients, the reader may consult [56, chapter III], [170, section 2.3] and [171, Complement BX].

D.4.1.1 Spin-orbit coupling

In the following we will restrict ourselves to the case where the first angular momentum is the orbital one, while the second is the spin one:

$$\mathbf{J}_1 = \mathbf{L} \quad (\text{D.4.26})$$

$$\mathbf{J}_2 = \mathbf{S}, \quad (\text{D.4.27})$$

$j \backslash m_2$	$+\frac{1}{2}$	$-\frac{1}{2}$
$\ell + \frac{1}{2}$	$+\sqrt{\frac{\ell+m_j+\frac{1}{2}}{2\ell+1}}$	$+\sqrt{\frac{\ell-m_j+\frac{1}{2}}{2\ell+1}}$
$\ell - \frac{1}{2}$	$-\sqrt{\frac{\ell-m_j+\frac{1}{2}}{2\ell+1}}$	$+\sqrt{\frac{\ell+m_j+\frac{1}{2}}{2\ell+1}}$

Table D.1: The four possible Clebsch-Gordan coefficients for $\mathbf{J} = \mathbf{L} \otimes 1 + 1 \otimes \mathbf{S}$.

and the total angular momentum is thus the one that combines both angular momenta:

$$\mathbf{J} = \mathbf{L} \otimes 1 + 1 \otimes \mathbf{S}. \quad (\text{D.4.28})$$

These angular momenta have the following quantum numbers with their associated magnetic numbers:

$$j_1 = \ell \quad m_1 = m_\ell = -\ell, \dots, +\ell \quad \text{Orbit} \quad (\text{D.4.29})$$

$$j_2 = s = \frac{1}{2} \quad m_2 = m_s = \pm \frac{1}{2} \quad \text{Spin} \quad (\text{D.4.30})$$

which gives four cases for the total angular momentum quantum number of eqs.(D.4.23 and D.4.24):

$$j = \ell \pm' \frac{1}{2} \quad (\text{D.4.31})$$

$$m_j = m_\ell \pm \frac{1}{2}, \quad (\text{D.4.32})$$

where the primed \pm' sign is set to distinguish between both quantum numbers once plugged into one expression. In this case, the Clebsch-Gordan coefficients of eq.(D.4.22) reduce to:

$$\begin{aligned} C\left(\ell, \frac{1}{2}, \ell \pm' \frac{1}{2}; M \mp \frac{1}{2}, \pm \frac{1}{2}, M\right) &= \mp \sqrt{(2\ell \pm' 1 + 1) \frac{(\ell \pm' \frac{1}{2} + M)! (\ell \pm' \frac{1}{2} - M)!}{(2\ell \pm' \frac{1}{2} + \frac{3}{2}) (2\ell \pm' \frac{1}{2} + \frac{1}{2}) (\ell - M \pm \frac{1}{2})! (\ell + M \mp \frac{1}{2})!}} \\ &\times \sum_{\nu} \frac{(-1)^{\nu}}{\nu!} \frac{(\ell \pm' \frac{1}{2} + M \mp \frac{1}{2} - \nu + \frac{1}{2})! (\ell - M \pm \frac{1}{2} + \nu)!}{(\frac{1}{2} \pm' \frac{1}{2} - \nu)! (\ell \pm' \frac{1}{2} + M - \nu)! (\nu + \ell - \frac{1}{2} - M)!}, \end{aligned} \quad (\text{D.4.33})$$

giving the four possible coefficients shown in table D.1, and the total angular momentum state becomes:

$$|j, m_j\rangle = \sum_{m_2 = -\frac{1}{2}}^{\frac{1}{2}} C\left(\ell, \frac{1}{2}, \ell \pm' \frac{1}{2}; m_j - m_2, m_2, m_j\right) \left|\ell, m_j - m_2, \frac{1}{2}, m_2\right\rangle. \quad (\text{D.4.34})$$

D.4.2 Spherical spinors

For the two possible j 's, we have the two following spin-orbit coupling states:

$$\left|\ell + \frac{1}{2}, m_j\right\rangle = +\sqrt{\frac{\ell - m_j + \frac{1}{2}}{2\ell + 1}} \left|\ell, m_j + \frac{1}{2}, \frac{1}{2}, -\frac{1}{2}\right\rangle + \sqrt{\frac{\ell + m_j + \frac{1}{2}}{2\ell + 1}} \left|\ell, m_j - \frac{1}{2}, \frac{1}{2}, +\frac{1}{2}\right\rangle \quad (\text{D.4.35})$$

$$\left|\ell - \frac{1}{2}, m_j\right\rangle = +\sqrt{\frac{\ell + m_j + \frac{1}{2}}{2\ell + 1}} \left|\ell, m_j + \frac{1}{2}, \frac{1}{2}, -\frac{1}{2}\right\rangle - \sqrt{\frac{\ell - m_j + \frac{1}{2}}{2\ell + 1}} \left|\ell, m_j - \frac{1}{2}, \frac{1}{2}, +\frac{1}{2}\right\rangle, \quad (\text{D.4.36})$$

which after projection on the spherical angles give the following spatial (continuous) eigenfunctions:

$$\langle \theta, \varphi \left| \ell + \frac{1}{2}, m_j \right\rangle = \sqrt{\frac{\ell - m_j + \frac{1}{2}}{2\ell + 1}} \langle \theta, \varphi \left| \ell, m_j + \frac{1}{2}, \frac{1}{2}, -\frac{1}{2} \right\rangle + \sqrt{\frac{\ell + m_j + \frac{1}{2}}{2\ell + 1}} \langle \theta, \varphi \left| \ell, m_j - \frac{1}{2}, \frac{1}{2}, +\frac{1}{2} \right\rangle \quad (\text{D.4.37})$$

$$\langle \theta, \varphi \left| \ell - \frac{1}{2}, m_j \right\rangle = +\sqrt{\frac{\ell + m_j + \frac{1}{2}}{2\ell + 1}} \langle \theta, \varphi \left| \ell, m_j + \frac{1}{2}, \frac{1}{2}, -\frac{1}{2} \right\rangle - \sqrt{\frac{\ell - m_j + \frac{1}{2}}{2\ell + 1}} \langle \theta, \varphi \left| \ell, m_j - \frac{1}{2}, \frac{1}{2}, +\frac{1}{2} \right\rangle. \quad (\text{D.4.38})$$

These eigenfunctions can be written as (see Johnson [172, eq.(1.115)] and Rose [56, page 152]):

$$\Omega_{\ell+\frac{1}{2}, m_j}(\theta, \varphi) = \begin{bmatrix} +\sqrt{\frac{\ell+m_j+\frac{1}{2}}{2\ell+1}} Y_{\ell, m_j-\frac{1}{2}} \\ \sqrt{\frac{\ell-m_j+\frac{1}{2}}{2\ell+1}} Y_{\ell, m_j+\frac{1}{2}} \end{bmatrix}; \quad \Omega_{\ell-\frac{1}{2}, m_j}(\theta, \varphi) = \begin{bmatrix} -\sqrt{\frac{\ell-m_j+\frac{1}{2}}{2\ell+1}} Y_{\ell, m_j-\frac{1}{2}} \\ \sqrt{\frac{\ell+m_j+\frac{1}{2}}{2\ell+1}} Y_{\ell, m_j+\frac{1}{2}} \end{bmatrix}, \quad (\text{D.4.39})$$

and are known as the spherical spinors (two component spherical harmonics), and are the coordinate-space representation of the total angular momentum state:

$$\Omega_{j, m_j}(\theta, \varphi) \equiv \langle \theta, \varphi | j, m_j \rangle, \quad (\text{D.4.40})$$

that couple spin and orbital angular momenta. In addition, by introducing a quantum number (we shall call) κ , that is defined as:

$$\kappa = \begin{cases} j + \frac{1}{2} = \ell & \text{for } j = \ell - \frac{1}{2} \\ -j - \frac{1}{2} = -(\ell + 1) & \text{for } j = \ell + \frac{1}{2} \end{cases}, \quad (\text{D.4.41})$$

our two spherical spinors can be written in a compact one function, as [173, eq.(2.1.7)]:

$$\Omega_{\kappa, m_j}(\hat{\mathbf{x}}) = \begin{bmatrix} \text{sgn}(-\kappa) \sqrt{\frac{\kappa+\frac{1}{2}-m_j}{2\kappa+1}} Y_{\ell, m_j-\frac{1}{2}}(\hat{\mathbf{x}}) \\ \sqrt{\frac{\kappa+\frac{1}{2}+m_j}{2\kappa+1}} Y_{\ell, m_j+\frac{1}{2}}(\hat{\mathbf{x}}) \end{bmatrix}. \quad (\text{D.4.42})$$

D.4.3 Orthonormalization

The completeness relation associated with the spherical-angles states (continuous variable) is given by:

$$\int \sin \theta d\theta d\varphi |\theta, \varphi\rangle \langle \theta, \varphi| = \mathbb{1}_1. \quad (\text{D.4.43})$$

The Clebsh-Gordan coefficients are constructed with the account of the orthonormalization of the coupled states as seen in eq.(D.4.21). After the insertion of the previous relation in the orthonormalization condition, one obtains:

$$\int \sin \theta d\theta d\varphi \langle j', m_{j'} | \theta, \varphi \rangle \langle \theta, \varphi | j, m_j \rangle = \delta_{j, j'} \delta_{m_j, m_{j'}}. \quad (\text{D.4.44})$$

The reader should notice that these scalar products are by definition, the spherical spinors of eq.(D.4.40), which directly tells us that the spherical spinors are orthonormalized, i.e. :

$$\int \sin \theta d\theta d\varphi \Omega_{j', m_{j'}}^\dagger(\theta, \varphi) \Omega_{j, m_j}(\theta, \varphi) = \delta_{j, j'} \delta_{m_j, m_{j'}}. \quad (\text{D.4.45})$$

To make sure that this is the case, evaluate this last equation. The scalar product of two spherical spinors, and obtain:

$$I_{\kappa, \kappa', m_j, m'_j} = \iint \sin \theta d\theta d\varphi \Omega_{\kappa, m_j}^\dagger(\hat{\mathbf{x}}) \Omega_{\kappa', m'_j}(\hat{\mathbf{x}}) \quad (\text{D.4.46})$$

$$= \left(\text{sgn}(\kappa' \kappa) \sqrt{\frac{\kappa + \frac{1}{2} - m_j}{2\kappa + 1} \frac{\kappa' + \frac{1}{2} - m_j}{2\kappa' + 1}} + \sqrt{\frac{\kappa + \frac{1}{2} + m_j}{2\kappa + 1} \frac{\kappa' + \frac{1}{2} + m_j}{2\kappa' + 1}} \right) \delta_{\ell, \ell'} \delta_{m_j, m'_j}, \quad (\text{D.4.47})$$

where ℓ and ℓ' are associated with κ and κ' respectively. The second Kronecker delta in the last equation simply forces m'_j to be equation to m_j , while the second one forces $\ell' = \ell$, i.e. for two cases of κ 's :

$$\begin{cases} \kappa' = \kappa & \text{for } \text{sgn}(\kappa' \kappa) = +1 \\ \kappa' = -\kappa - 1 & \text{for } \text{sgn}(\kappa' \kappa) = -1 \end{cases}. \quad (\text{D.4.48})$$

1. for $\kappa' = \kappa$, the integral simplifies to 1:

$$I_{\kappa, \kappa', m_j, m'_j} = \left(\frac{\kappa + \frac{1}{2} + m_j}{2\kappa + 1} + \frac{\kappa + \frac{1}{2} + m_j}{2\kappa + 1} \right) \delta_{m_j, m'_j} = \delta_{m_j, m'_j}. \quad (\text{D.4.49})$$

2. for $\kappa' = -\kappa - 1$, it simplifies to 0:

$$I_{\kappa, \kappa', m_j, m'_j} = \left(-\sqrt{\frac{\kappa + \frac{1}{2} - m_j}{2\kappa + 1} \frac{\kappa + \frac{1}{2} + m_j}{2\kappa + 1}} + \sqrt{\frac{\kappa + \frac{1}{2} + m_j}{2\kappa + 1} \frac{\kappa + \frac{1}{2} - m_j}{2\kappa + 1}} \right) \delta_{\ell, \ell'} \delta_{m_j, m'_j} = 0. \quad (\text{D.4.50})$$

As a conclusion, the two cases lead to the fact that the spherical spinors are normalized:

$$I_{\kappa, \kappa', m_j, m'_j} = \iint \sin \theta d\theta d\varphi \Omega_{\kappa, m_j}^\dagger(\hat{\mathbf{x}}) \Omega_{\kappa', m'_j}(\hat{\mathbf{x}}) \quad (\text{D.4.51})$$

$$= \delta_{\kappa, \kappa'} \delta_{m_j, m'_j}. \quad (\text{D.4.52})$$

D.4.4 Parity

Using eq.(D.3.18), one can obtain the parity transformed spherical spinor:

$$\Omega_{\kappa, m_j}(-\hat{\mathbf{x}}) = (-1)^\ell \Omega_{\kappa, m_j}(\hat{\mathbf{x}}). \quad (\text{D.4.53})$$

D.4.5 Complex conjugation

The complex conjugated spherical spinor is:

$$\Omega_{\kappa, m_j}^*(\hat{\mathbf{x}}) = \begin{bmatrix} \text{sgn}(-\kappa) \sqrt{\frac{\kappa + \frac{1}{2} - m_j}{2\kappa + 1}} Y_{\ell, m_j - \frac{1}{2}}^*(\hat{\mathbf{x}}) \\ \sqrt{\frac{\kappa + \frac{1}{2} + m_j}{2\kappa + 1}} Y_{\ell, m_j + \frac{1}{2}}^*(\hat{\mathbf{x}}) \end{bmatrix}, \quad (\text{D.4.54})$$

using eq.(D.3.13), the complex conjugated spinor can be written as:

$$\Omega_{\kappa, m_j}^*(\hat{\mathbf{x}}) = \begin{bmatrix} \operatorname{sgn}(-\kappa) \sqrt{\frac{\kappa + \frac{1}{2} - m_j}{2\kappa + 1}} (-1)^{m_j - \frac{1}{2}} Y_{\ell, -m_j + \frac{1}{2}}(\hat{\mathbf{x}}) \\ \sqrt{\frac{\kappa + \frac{1}{2} + m_j}{2\kappa + 1}} (-1)^{m_j + \frac{1}{2}} Y_{\ell, -m_j - \frac{1}{2}}(\hat{\mathbf{x}}) \end{bmatrix} \quad (\text{D.4.55})$$

$$= (-1)^{m_j - \frac{1}{2}} i \operatorname{sgn}(-\kappa) \sigma_2 \Omega_{\kappa, -m_j}, \quad (\text{D.4.56})$$

D.4.6 $\sigma_r \Omega_{\kappa, m_j}$

The radial Pauli matrix is given by the scalar product of the Pauli spin vector $\boldsymbol{\sigma} = \sigma_i \mathbf{e}_i$ with the radial unit vector $\mathbf{n}(\theta, \varphi) = \frac{\mathbf{x}}{|\mathbf{x}|}$, and it is thus a function of polar and azimuthal spherical coordinate angles:

$$\sigma_r = \boldsymbol{\sigma} \cdot \mathbf{e}_r = \sigma_r(\theta, \varphi) = \begin{bmatrix} \cos \theta & e^{-i\varphi} \sin \theta \\ e^{i\varphi} \sin \theta & -\cos \theta \end{bmatrix}. \quad (\text{D.4.57})$$

We would first like to show that the total angular momentum operator:

$$\mathbf{J} = \mathbf{L} + \mathbf{S}, \quad (\text{D.4.58})$$

that is a sum of the orbital and spin angular momentum operator, commutes with the radial Pauli matrix given in eq.(D.4.57) as mentioned in [32, section 3.2.2]:

$$[\mathbf{J}, \sigma_r] = 0, \quad (\text{D.4.59})$$

component-wise, this equation is equivalent to writing:

$$[J_i, \boldsymbol{\sigma} \cdot \mathbf{e}_r] = \frac{1}{r} [L_i + S_i, \boldsymbol{\sigma} \cdot \mathbf{x}]; \quad i = 1, 2, 3 \quad (\text{D.4.60})$$

we then use the expressions of the spin and orbital angular momentum operators:

$$S_i = \frac{\hbar}{2} \sigma_i \quad (\text{D.4.61})$$

$$L_i = -i\hbar \epsilon_{ijk} x_j \partial_k, \quad (\text{D.4.62})$$

where the position vector $\mathbf{x} = r\mathbf{n} = x_i \mathbf{e}_i$, with component x_i and Cartesian basis vector \mathbf{e}_i , and the gradient operator $\partial_i = \frac{\partial}{\partial x_i}$. The radial spin-matrix can be written as:

$$\sigma_r = \boldsymbol{\sigma} \cdot \mathbf{e}_r = \frac{1}{r} \boldsymbol{\sigma} \cdot \mathbf{x} = \frac{1}{r} \sigma_j x_j. \quad (\text{D.4.63})$$

The commutator of eq.(D.3.13) becomes:

$$[J_i, \sigma_r] = \frac{1}{r} \left(-i\hbar \epsilon_{ijk} x_j \sigma_l [\partial_k, x_l] + \frac{\hbar}{2} [\sigma_i, \sigma_j] x_j \right), \quad (\text{D.4.64})$$

we then use the anticommutation relation:

$$[\partial_i, x_j] = \partial_i(x_j) + x_j \partial_i - x_j \partial_i = \delta_{ij} \quad (\text{D.4.65})$$

$$[\sigma_i, \sigma_j] = 2i\epsilon_{ijk} \sigma_k, \quad (\text{D.4.66})$$

to finally get the desired result [39, eq.(6.4)]:

$$[J_i, \sigma_r] = \frac{1}{r} (-i\hbar \epsilon_{ijk} x_j \sigma_k + i\hbar \epsilon_{ijk} x_j \sigma_k) = 0, \quad (\text{D.4.67})$$

meaning that the total angular momentum operator commutes with σ_r , leading to:

$$\mathbf{J}^2 \sigma_r \Omega_{\kappa, m_j} = \mathbf{J} \cdot \sigma_r \mathbf{J} \Omega_{\kappa, m_j} = \sigma_r \mathbf{J}^2 \Omega_{\kappa, m_j} = \hbar^2 j(j+1) \sigma_r \Omega_{\kappa, m_j} \quad (\text{D.4.68})$$

$$J_z \sigma_r \Omega_{\kappa, m_j} = \sigma_r J_z \Omega_{\kappa, m_j} = \hbar m_j \sigma_r \Omega_{\kappa, m_j}, \quad (\text{D.4.69})$$

which means that $\sigma_r \Omega_{\kappa, m_j}$ is an eigenvector of \mathbf{J}^2 and J_z operators, with the eigenvalues $\hbar^2 j(j+1)$ and $\hbar m_j$ respectively. This shows that the $\sigma_r \Omega_{\kappa, m_j}$ vector is associated with (j, m_j) quantum numbers, which leaves us with two choices of κ (two parities) corresponding to the same total quantum number j :

$$\kappa = \pm \left(j + \frac{1}{2} \right). \quad (\text{D.4.70})$$

This leads us to the conclusion that this eigenvector can be written as a linear combination of these two spinors:

$$\sigma_r \Omega_{\kappa, m_j} = \alpha \Omega_{\kappa, m_j} + \beta \Omega_{-\kappa, m_j}, \quad (\text{D.4.71})$$

where α and β are pure constants. Being guided by the torch of parity operation, the guessed ansatz can be simplified, as done in [32, section 3.2.2], [56, section 31], [28, page 272] and [172, section 1.5.1]. Using spherical coordinate parity operation (space inversion) as done in $\hat{\mathbf{x}} \rightarrow -\hat{\mathbf{x}}$, manifested in eqs.(D.3.14 and D.3.15), that transforms the radial Pauli matrix as:

$$\sigma_r(\theta, \varphi) \rightarrow \sigma_r(\pi - \theta, \pi + \varphi) = -\sigma_r(\theta, \varphi), \quad (\text{D.4.72})$$

and the parity transformed spherical spinor of eq.(D.4.53):

$$\Omega_{\kappa, m_j}(-\hat{\mathbf{x}}) = (-1)^\ell \Omega_{\kappa, m_j}(\hat{\mathbf{x}}), \quad (\text{D.4.73})$$

we can simplify our ansatz:

$$\sigma_r \Omega_{\kappa, m_j} (-1)^{\ell+1} = \alpha (-1)^\ell \Omega_{\kappa, m_j} + \beta (-1)^{\ell'} \Omega_{-\kappa, m_j}; \quad \text{with } \begin{cases} \ell = \left| \kappa + \frac{1}{2} \right| - \frac{1}{2} \\ \ell' = \left| \kappa - \frac{1}{2} \right| - \frac{1}{2} \end{cases} \quad (\text{D.4.74})$$

which can be rewritten as:

$$\sigma_r \Omega_{\kappa, m_j} = \alpha (-1)^{\ell+\ell+1} \Omega_{\kappa, m_j} + \beta (-1)^{\ell'+\ell+1} \Omega_{-\kappa, m_j}, \quad (\text{D.4.75})$$

using the following expression:

$$\ell' + \ell + 1 = \left| \kappa + \frac{1}{2} \right| + \left| \kappa - \frac{1}{2} \right| = 2|\kappa|, \quad (\text{D.4.76})$$

our expression becomes:

$$\sigma_r \Omega_{\kappa, m_j} = -\alpha \Omega_{\kappa, m_j} + \beta \Omega_{-\kappa, m_j}, \quad (\text{D.4.77})$$

which (cf. eq.(D.4.71)) directly indicates that α should vanish, leading to the following expression:

$$\sigma_r \Omega_{\kappa, m_j} = \beta \Omega_{-\kappa, m_j}. \quad (\text{D.4.78})$$

The final task is to determine the value of the β constant, this is done by evaluating both sides of the last equation, the simplest choice would be to evaluate the expression at vanishing polar angle $\theta = 0$ (North pole). From eqs.(D.4.57 and D.4.42), we get:

$$\sigma_r(0, \varphi) = \begin{bmatrix} 1 & 0 \\ 0 & -1 \end{bmatrix} \quad (\text{D.4.79})$$

$$\Omega_{\kappa, m_j}(0, \varphi) = \begin{bmatrix} \text{sgn}(-\kappa) \sqrt{\frac{\kappa + \frac{1}{2} - m_j}{2\kappa + 1}} Y_{\ell, m_j - \frac{1}{2}}(0, \varphi) \\ \sqrt{\frac{\kappa + \frac{1}{2} + m_j}{2\kappa + 1}} Y_{\ell, m_j + \frac{1}{2}}(0, \varphi) \end{bmatrix}, \quad (\text{D.4.80})$$

where the spherical harmonic at the north pole becomes:

$$Y_{\ell, m}(0, \varphi) = (-1)^m \sqrt{\frac{(2\ell + 1)(\ell - m)!}{4\pi(\ell + m)!}} P_{\ell}^m(1) e^{im\varphi}, \quad (\text{D.4.81})$$

we still need to evaluate $P_{\ell}^m(1)$. Eq.(D.3.9) shows that the factor of $(1 - x^2)^{m/2}$ will cause the associated Legendre polynomial to vanish at $x = \pm 1$ in the case of $m \neq 0$, meaning that $P_{\ell}^m(1)$ can be written as:

$$P_{\ell}^m(1) = \delta_{m,0} P_{\ell}(1). \quad (\text{D.4.82})$$

The Legendre polynomial can be written as [174, eq.(1)]:

$$P_{\ell}(x) = \sum_{k=0}^{\ell} \binom{\ell}{k} \binom{-\ell-1}{k} \left(\frac{1-x}{2}\right)^k, \quad (\text{D.4.83})$$

showing that at $x = 1$, all the summation terms will vanish except the one associated with $k = 0$:

$$P_{\ell}(1) = \binom{\ell}{0} \binom{-\ell-1}{0} = 1, \quad (\text{D.4.84})$$

which leads to the following reduced expression for the spherical harmonic function [165, eq.(14.30.4)]:

$$Y_{\ell, m}(0, \varphi) = \sqrt{\frac{2\ell + 1}{4\pi}} \delta_{m,0}. \quad (\text{D.4.85})$$

Collecting all the findings, one reaches the conclusion that $\beta = 1$, i.e. :

$$\sigma_r \Omega_{\kappa, m_j} = -\Omega_{-\kappa, m_j}. \quad (\text{D.4.86})$$

D.4.7 $\sum_{m_j} \Omega_{\kappa, m_j}(\hat{\mathbf{x}}) \Omega_{\kappa, m_j}^{\dagger}(\hat{\mathbf{y}})$

The summation over outer product of spherical spinors with same quantum numbers gives [175, eqs.(9a,b)]:

$$\sum_{m_j} \Omega_{\kappa, m_j}(\hat{\mathbf{x}}) \Omega_{\kappa, m_j}^{\dagger}(\hat{\mathbf{y}}) = \begin{cases} \frac{\ell}{4\pi} P_{\ell}(\hat{\mathbf{x}} \cdot \hat{\mathbf{y}}) I_2 + \frac{i}{4\pi} P'_{\ell}(\hat{\mathbf{x}} \cdot \hat{\mathbf{y}}) (\hat{\mathbf{x}} \times \hat{\mathbf{y}}) \cdot \boldsymbol{\sigma} & \kappa > 0 \\ \frac{\ell+1}{4\pi} P_{\ell}(\hat{\mathbf{x}} \cdot \hat{\mathbf{y}}) I_2 - \frac{i}{4\pi} P'_{\ell}(\hat{\mathbf{x}} \cdot \hat{\mathbf{y}}) (\hat{\mathbf{x}} \times \hat{\mathbf{y}}) \cdot \boldsymbol{\sigma} & \kappa < 0 \end{cases}, \quad (\text{D.4.87})$$

where P'_{ℓ} is simply a derivative of the associated Legendre polynomial P_{ℓ} , and $\ell = |\kappa + \frac{1}{2}| - \frac{1}{2}$ is the famous azimuthal quantum number. The last two equations can be combined into a single general one (for both positive and negative κ values) [135, eq.(3.12)]:

$$\sum_{m_j} \Omega_{\kappa, m_j}(\hat{\mathbf{x}}) \Omega_{\kappa, m_j}^{\dagger}(\hat{\mathbf{y}}) = \frac{|\kappa|}{4\pi} P_{|\kappa + \frac{1}{2}| - \frac{1}{2}}(\hat{\mathbf{x}} \cdot \hat{\mathbf{y}}) I_2 + \text{sgn}(\kappa) \frac{i}{4\pi} P'_{|\kappa + \frac{1}{2}| - \frac{1}{2}}(\hat{\mathbf{x}} \cdot \hat{\mathbf{y}}) (\hat{\mathbf{x}} \times \hat{\mathbf{y}}) \cdot \boldsymbol{\sigma}. \quad (\text{D.4.88})$$

D.4.8 $\sum_{m_j} \Omega_{-\kappa, m_j}(\hat{\mathbf{x}}) \Omega_{\kappa, m_j}^\dagger(\hat{\mathbf{y}})$

For the summation over outer product of spherical spinors with opposite κ sign, we have [175, eqs.(10a,b)]:

$$\sum_{m_j} \Omega_{-\kappa, m_j}(\hat{\mathbf{x}}) \Omega_{\kappa, m_j}^\dagger(\hat{\mathbf{y}}) = \begin{cases} +\frac{1}{4\pi} P'_{\ell+1}(\hat{\mathbf{x}} \cdot \hat{\mathbf{y}}) \hat{\mathbf{x}} \cdot \boldsymbol{\sigma} - \frac{1}{4\pi} P'_\ell(\hat{\mathbf{x}} \cdot \hat{\mathbf{y}}) \hat{\mathbf{y}} \cdot \boldsymbol{\sigma} & \kappa > 0 \\ -\frac{1}{4\pi} P'_{\ell+1}(\hat{\mathbf{x}} \cdot \hat{\mathbf{y}}) \hat{\mathbf{x}} \cdot \boldsymbol{\sigma} + \frac{1}{4\pi} P'_\ell(\hat{\mathbf{x}} \cdot \hat{\mathbf{y}}) \hat{\mathbf{y}} \cdot \boldsymbol{\sigma} & \kappa < 0 \end{cases}. \quad (\text{D.4.89})$$

Again, these two formulas can be combined into one [135, eq.(3.14)]:

$$\sum_{m_j} \Omega_{-\kappa, m_j}(\hat{\mathbf{x}}) \Omega_{\kappa, m_j}^\dagger(\hat{\mathbf{y}}) = \frac{\text{sgn}(\kappa)}{4\pi} [P'_{\ell+1}(\hat{\mathbf{x}} \cdot \hat{\mathbf{y}}) \hat{\mathbf{x}} \cdot \boldsymbol{\sigma} - P'_\ell(\hat{\mathbf{x}} \cdot \hat{\mathbf{y}}) \hat{\mathbf{y}} \cdot \boldsymbol{\sigma}], \quad (\text{D.4.90})$$

which can be obtained from the previous sum by applying the $\boldsymbol{\sigma} \cdot \hat{\mathbf{x}}$ operator which flips the sign of κ and adds an overall minus sign once applied on a spherical spinor. (See, for instance, eq.(D.4.86) and [135, eq.(A.8)]).

Appendix E

Matrix equations and integrals for kinetic balances

The general eigenvalue equation associated with different considered schemes is of the following form:

$$H_\kappa \mathbf{c}_{\alpha,\kappa} = \epsilon_{\alpha,\kappa} S_\kappa \mathbf{c}_{\alpha,\kappa}, \quad (\text{E.0.1})$$

where H_κ and S_κ are the matrix representations of the Dirac Hamiltonian and the overlap matrix, respectively. The vector $\mathbf{c}_{\alpha,\kappa}$ and the corresponding scalar quantity $\epsilon_{\alpha,\kappa}$ are solutions of this numerical equation: eigenvector and the associated eigenvalue, respectively. Finally, the index α is added to differentiate between solutions of the same equation, and can thus run from 1 to n , which represents the dimensions of the Hamiltonian matrix, i.e., the number of basis functions. In the following sections, we are going to present the structure of the elements of this equation, as well as there matrix-elements which are radial integrals.

E.1 Restricted and Inverse Kinetic Balances (RKB and IKB)

For restricted and inverse kinetic balances, the numerical Dirac solutions are expanded in some large and small basis set as follows:

$$\varphi_{\alpha,\kappa}(r) = \sum_{i=1}^{n_\kappa^L} c_{\alpha,\kappa,i}^L \begin{bmatrix} \varphi_{\kappa,i}^L(r) \\ 0 \end{bmatrix} + \sum_{i=1}^{n_\kappa^S} c_{\alpha,\kappa,i}^S \begin{bmatrix} 0 \\ \varphi_{\kappa,i}^S(r) \end{bmatrix}, \quad (\text{E.1.1})$$

where $\varphi_{\kappa,i}^L(r)$ and $\varphi_{\kappa,i}^S(r)$ are large and small radial basis functions, and are specified for each scheme as the following:

1. In RKB, one sets:

$$\varphi_{\kappa,i}^L(r) = \pi_{\kappa,i}^L(r) \quad (\text{E.1.2})$$

$$\varphi_{\kappa,i}^S(r) = \frac{\hbar}{2mc} \left[\frac{d}{dr} + \frac{\kappa}{r} \right] \pi_{\kappa,i}^L(r). \quad (\text{E.1.3})$$

2. In IKB, one sets:

$$\varphi_{\kappa,i}^L(r) = \frac{\hbar}{2mc} \left[\frac{d}{dr} - \frac{\kappa}{r} \right] \pi_{\kappa,i}^S(r) \quad (\text{E.1.4})$$

$$\varphi_{\kappa,i}^S(r) = \pi_{\kappa,i}^S(r). \quad (\text{E.1.5})$$

The radial probability densities associated with a $\varphi_{\alpha,\kappa}$ solution are found to be:

1. For RKB:

$$\begin{aligned} \rho_{\alpha,\kappa}(r) &= \varphi_{\alpha,\kappa}^\dagger(r) \varphi_{\alpha,\kappa}(r) \\ &= \sum_{i=1}^{n_\kappa} \sum_{j=1}^{n_\kappa} \left[(c_{\alpha,\kappa,i}^L)^* c_{\alpha,\kappa,j}^L \pi_{\kappa,i}^L \pi_{\kappa,j}^L \right. \\ &\quad \left. + (c_{\alpha,\kappa,i}^S)^* c_{\alpha,\kappa,j}^S \frac{\hbar^2}{4m^2 c^2} \left[\frac{d}{dr} \pi_{\kappa,i}^L(r) + \frac{\kappa}{r} \pi_{\kappa,i}^L \right] \left[\frac{d}{dr} \pi_{\kappa,j}^L + \frac{\kappa}{r} \pi_{\kappa,j}^L \right] \right]. \end{aligned} \quad (\text{E.1.6})$$

2. For IKB:

$$\begin{aligned} \rho_{\alpha,\kappa}(r) &= \varphi_{\alpha,\kappa}^\dagger(r) \varphi_{\alpha,\kappa}(r) \\ &= \sum_{i=1}^{n_\kappa} \sum_{j=1}^{n_\kappa} \left[(c_{\alpha,\kappa,i}^S)^* c_{\alpha,\kappa,j}^S \pi_{\kappa,i}^S \pi_{\kappa,j}^S \right. \\ &\quad \left. + (c_{\alpha,\kappa,i}^S)^* c_{\alpha,\kappa,j}^S \frac{\hbar^2}{4m^2 c^2} \left[\frac{d}{dr} \pi_{\kappa,i}^S(r) - \frac{\kappa}{r} \pi_{\kappa,i}^S \right] \left[\frac{d}{dr} \pi_{\kappa,j}^S - \frac{\kappa}{r} \pi_{\kappa,j}^S \right] \right]. \end{aligned} \quad (\text{E.1.7})$$

In order to be consistent with a crucial property of the probability density that it should integrate to 1, the coefficients $c_{\alpha,\kappa}^L$ and $c_{\alpha,\kappa}^S$ are chosen such that this condition is fulfilled. Finally, we shall note that the Hamiltonian, the overlap matrix (associated with each of these two schemes), and the corresponding matrix elements, are given in the next sections.

E.1.1 RKB matrices

In the RKB scheme, the large component radial functions are first introduced, then the small component functions are generated with respect to the kinetic balance condition:

$$\pi_{\kappa,i}^S(r) = \frac{\hbar}{2mc} \left[\frac{d}{dr} + \frac{\kappa}{r} \right] \pi_{\kappa,i}^L(r); \quad i = 1, \dots, n_\kappa^L, \quad (\text{E.1.8})$$

meaning that the number basis functions for both components is equal $n_\kappa^S = n_\kappa^L$, and we shall call it n_κ . The elements of the matrix equation of eq.(E.0.1) in RKB are found to be:

$$H_\kappa = \begin{bmatrix} mc^2 S_\kappa^{L_\kappa L_\kappa} - e\phi^{L_\kappa L_\kappa} & T_\kappa^{L_\kappa L_\kappa} \\ T_\kappa^{L_\kappa L_\kappa} & -\frac{1}{2} T_\kappa^{L_\kappa L_\kappa} - \frac{e\hbar^2}{4m^2 c^2} W_\kappa^{L_\kappa L_\kappa} \end{bmatrix} \quad (\text{E.1.9})$$

$$S_\kappa = \begin{bmatrix} S_\kappa^{L_\kappa L_\kappa} & 0 \\ 0 & \frac{1}{2mc^2} T_\kappa^{L_\kappa L_\kappa} \end{bmatrix}, \quad c_{\alpha,\kappa} = \begin{bmatrix} c_{\alpha,\kappa}^L \\ c_{\alpha,\kappa}^S \end{bmatrix}_{\alpha,\kappa}. \quad (\text{E.1.10})$$

The matrices H_κ and S_κ have the dimensions of $(2n_\kappa \times 2n_\kappa)$, and the eigenvectors have the following structure:

$$c_{\alpha,\kappa} = [c^L \quad c^S]_{\alpha,\kappa}^t = [c_{\alpha,\kappa,1}^L \quad \dots \quad c_{\alpha,\kappa,n_\kappa}^L \quad c_{\alpha,\kappa,1}^S \quad \dots \quad c_{\alpha,\kappa,n_\kappa}^S]^t, \quad (\text{E.1.11})$$

where the superscript t stands for transpose, to simply indicate that this is a row vector. The matrix elements of the sub-matrices of H_κ and S_κ are given in eqs.(E.1.15-E.1.18) below.

E.1.2 IKB matrices

As we have seen before, the inverse kinetic balance scheme is the negative-energy version of the restricted kinetic balance, where -contrary to the latter- the small component radial functions are first introduced, then the large ones are generated using the IKB condition:

$$\pi_{\kappa,i}^L(r) = \frac{\hbar}{2mc} \left[\frac{d}{dr} - \frac{\kappa}{r} \right] \pi_{\kappa,i}^S(r); \quad i = 1, \dots, n_\kappa^S \quad (\text{E.1.12})$$

This choice of basis functions lead to the following expressions of the Hamiltonian and the overlap matrices:

$$H_\kappa = \begin{bmatrix} \frac{1}{2} T_{-\kappa}^{S_\kappa S_\kappa} - \frac{e\hbar^2}{4m^2 c^2} W_{-\kappa}^{S_\kappa S_\kappa} & -T_{-\kappa}^{S_\kappa S_\kappa} \\ -T_{-\kappa}^{S_\kappa S_\kappa} & -mc^2 S_{S_\kappa S_\kappa} - e\phi^{S_\kappa S_\kappa} \end{bmatrix} \quad (\text{E.1.13})$$

$$S_\kappa = \begin{bmatrix} \frac{1}{2mc^2} T_{-\kappa}^{S_\kappa S_\kappa} & 0 \\ 0 & S_{S_\kappa S_\kappa} \end{bmatrix}, \quad \mathbf{c}_{\alpha,\kappa} = \begin{bmatrix} \mathbf{c}^L \\ \mathbf{c}^S \end{bmatrix}_{\alpha,\kappa}. \quad (\text{E.1.14})$$

Again, the matrix elements of the sub-matrices of H_κ and S_κ are given in eqs.(E.1.15-E.1.18) below.

E.1.3 Integrals

The matrix elements of the sub-matrices for both (RKB and IKB) schemes are given by:

$$[S^{X_\kappa X_\kappa}]_{ij} = \int_0^\infty \pi_i^{X_\kappa} \pi_j^{X_\kappa} dr \quad (\text{E.1.15})$$

$$[\phi^{X_\kappa X_\kappa}]_{ij} = \int_0^\infty \pi_i^{X_\kappa} \phi(r) \pi_j^{X_\kappa} dr \quad (\text{E.1.16})$$

$$[T_{\kappa'}^{X_\kappa X_\kappa}]_{ij} = \frac{-\hbar^2}{2m} \int_0^\infty \pi_i^{X_\kappa} \left[\frac{d^2}{dr^2} \pi_j^{X_\kappa} - \frac{\kappa'(1+\kappa')}{r^2} \pi_j^{X_\kappa} \right] dr \quad (\text{E.1.17})$$

$$[W_{\kappa'}^{X_\kappa X_\kappa}]_{ij} = \int_0^\infty \left[\frac{d}{dr} \pi_i^{X_\kappa} + \frac{\kappa'}{r} \pi_i^{X_\kappa} \right] \phi(r) \left[\frac{d}{dr} \pi_j^{X_\kappa} + \frac{\kappa'}{r} \pi_j^{X_\kappa} \right] dr. \quad (\text{E.1.18})$$

To eliminate any possible suspicions that the reader might have, we note that κ' , which appears in the last two integrals, does not indicate that we have two different κ 's for the same problem. This additional κ was introduced for simplicity purposes, to be able to write a general form of the integrals for both schemes. Making this decision has facilitated the linking between the two schemes by the charge conjugation symmetry.

E.2 Dual Kinetic Balance (DKB)

The dual kinetic balance scheme “combines” the two previous schemes, and expands the radial Dirac solutions in the following basis:

$$\varphi_{\alpha,\kappa}(r) = \sum_{i=1}^{n_{\kappa}^{[+]}} c_{\alpha,\kappa,i}^{[+]} \varphi_{\kappa,i}^{[+]}(r) + \sum_{i=1}^{n_{\kappa}^{[-]}} c_{\alpha,\kappa,i}^{[-]} \varphi_{\kappa,i}^{[-]}(r); \quad (\text{E.2.1})$$

$$\varphi_{\kappa,i}^{[+]}(r) = \begin{bmatrix} \pi_{\kappa,i}^{[+]}(r) \\ \frac{i\hbar}{2mc} \left[\frac{d}{dr} + \frac{\kappa}{r} \right] \pi_{\kappa,i}^{[+]}(r) \end{bmatrix} \quad (\text{E.2.2})$$

$$\varphi_{\kappa,i}^{[-]}(r) = \begin{bmatrix} \frac{\hbar}{2mc} \left[\frac{d}{dr} - \frac{\kappa}{r} \right] \pi_{\kappa,i}^{[-]}(r) \\ i\pi_{\kappa,i}^{[-]}(r) \end{bmatrix}. \quad (\text{E.2.3})$$

The use of these basis functions will lead to the following matrices of H_{κ} and S_{κ} which enters in the eigenvalue equation of eq.(E.0.1):

$$H_{\kappa} = \begin{bmatrix} m_e c^2 S^{++} + \frac{3}{2} T^{++} - e\phi^{++} - \frac{e\hbar^2}{4m_e^2 c^2} W^{++} & \frac{\hbar}{2m_e c} [-eA^{+-} + B^{+-}] \\ \frac{\hbar}{2m_e c} [-eA^{-+} - B^{-+}] & -m_e c^2 S^{--} - \frac{3}{2} T^{--} - e\phi^{--} - \frac{e\hbar^2}{4m_e^2 c^2} W^{--} \end{bmatrix} \quad (\text{E.2.4})$$

$$S_{\kappa} = \begin{bmatrix} S^{++} + \frac{1}{2m_e c^2} T^{++} & 0 \\ 0 & S^{SS} + \frac{1}{2m_e c^2} T^{--} \end{bmatrix}, \quad c_{\alpha,\kappa} = \begin{bmatrix} \mathbf{c}^{[+]} \\ \mathbf{c}^{[-]} \end{bmatrix}_{\alpha,\kappa}. \quad (\text{E.2.5})$$

The matrix elements of the sub-matrices are given by the following radial integrals:

$$S_{ij}^{\pm\pm} = \int_0^{\infty} \pi_{\kappa,i}^{\pm} \pi_{\kappa,j}^{\pm} dr \quad (\text{E.2.6})$$

$$\phi_{ij}^{\pm\pm} = \int_0^{\infty} \pi_{\kappa,i}^{\pm} \phi(r) \pi_{\kappa,j}^{\pm} dr \quad (\text{E.2.7})$$

$$T_{ij}^{\pm\pm} = \frac{-\hbar^2}{2m_e} \int_0^{\infty} \pi_{\kappa,i}^{\pm} \left[\frac{d^2}{dr^2} \pi_{\kappa,j}^{\pm} \mp \frac{\kappa(1 \pm \kappa)}{r^2} \pi_{\kappa,j}^{\pm} \right] dr \quad (\text{E.2.8})$$

$$W_{ij}^{\pm\pm} = \int_0^{\infty} \left[\frac{d}{dr} \pi_{\kappa,i}^{\pm} \pm \frac{\kappa}{r} \pi_{\kappa,i}^{\pm} \right] \phi(r) \left[\frac{d}{dr} \pi_{\kappa,j}^{\pm} \pm \frac{\kappa}{r} \pi_{\kappa,j}^{\pm} \right] dr \quad (\text{E.2.9})$$

$$A_{ij}^{\pm\mp} = \int_0^{\infty} \pi_{\kappa,i}^{\pm} \phi(r) \left[\frac{d}{dr} \pi_{\kappa,j}^{\mp} \mp \frac{\kappa}{r} \pi_{\kappa,j}^{\mp} \right] dr + \int_0^{\infty} \left[\frac{d}{dr} \pi_{\kappa,i}^{\pm} \pm \frac{\kappa}{r} \pi_{\kappa,i}^{\pm} \right] \phi(r) \pi_{\kappa,j}^{\mp} dr \quad (\text{E.2.10})$$

$$B_{ij}^{\pm\mp} = \frac{\hbar^2}{2m} \int_0^{\infty} \left[\frac{d}{dr} \pi_{\kappa,i}^{\pm} \pm \frac{\kappa}{r} \pi_{\kappa,i}^{\pm} \right] \left[\frac{d^2}{dr^2} \pi_{\kappa,j}^{\mp} \pm \frac{\kappa'(1 \mp \kappa')}{r^2} \pi_{\kappa,j}^{\mp} \right] dr. \quad (\text{E.2.11})$$

Finally, for some solution α of the DKB problem, the radial probability density is found to be:

$$\begin{aligned}
 \rho_{\kappa,\alpha}(r) = & \sum_{i=1}^{n_{\kappa}^{[+]}} \sum_{j=1}^{n_{\kappa}^{[+]}} \left(c_{\alpha,\kappa,i}^{[+]} \right)^* c_{\alpha,\kappa,j}^{[+]} \left\{ \pi_{\kappa,i}^L \pi_{\kappa,j}^L + \frac{\hbar^2}{4m^2 c^2} \left[\frac{d}{dr} \pi_{\kappa,i}^L + \frac{\kappa}{r} \pi_{\kappa,i}^L \right] \left[\frac{d}{dr} \pi_{\kappa,j}^L + \frac{\kappa}{r} \pi_{\kappa,j}^L \right] \right\} \\
 & + \sum_{i=1}^{n_{\kappa}^{[-]}} \sum_{j=1}^{n_{\kappa}^{[-]}} \left(c_{\alpha,\kappa,i}^{[-]} \right)^* c_{\alpha,\kappa,j}^{[-]} \left\{ \pi_{\kappa,i}^S \pi_{\kappa,j}^S + \frac{\hbar^2}{4m^2 c^2} \left[\frac{d}{dr} \pi_{\kappa,i}^S - \frac{\kappa}{r} \pi_{\kappa,i}^S \right] \left[\frac{d}{dr} \pi_{\kappa,j}^S - \frac{\kappa}{r} \pi_{\kappa,j}^S \right] \right\} \\
 & + \frac{\hbar}{2mc} \sum_{i=1}^{n_{\kappa}^{[+]}} \sum_{j=1}^{n_{\kappa}^{[-]}} \left(c_{\alpha,\kappa,i}^{[+]} \right)^* c_{\alpha,\kappa,j}^{[-]} \left\{ \pi_{\kappa,i}^L \left[\frac{d}{dr} \pi_{\kappa,j}^S - \frac{\kappa}{r} \pi_{\kappa,j}^S \right] + \left[\frac{d}{dr} \pi_{\kappa,i}^L + \frac{\kappa}{r} \pi_{\kappa,i}^L \right] \pi_{\kappa,j}^S \right\} \\
 & + \frac{\hbar}{2mc} \sum_{i=1}^{n_{\kappa}^{[-]}} \sum_{j=1}^{n_{\kappa}^{[+]}} \left(c_{\alpha,\kappa,i}^{[-]} \right)^* c_{\alpha,\kappa,j}^{[+]} \left\{ \left[\frac{d}{dr} \pi_{\kappa,i}^S - \frac{\kappa}{r} \pi_{\kappa,i}^S \right] \pi_{\kappa,j}^L + \pi_{\kappa,i}^S \left[\frac{d}{dr} \pi_{\kappa,j}^L + \frac{\kappa}{r} \pi_{\kappa,j}^L \right] \right\}.
 \end{aligned} \tag{E.2.12}$$

where the vectors $\mathbf{c}_{\alpha,\kappa}$ associated with the α -solution are chosen such that this density should integrate to one, i.e. $\int_0^\infty dr \rho_{\kappa,\alpha} = 1$ for all $\alpha = 1, \dots, n_{\kappa}^{[+]} + n_{\kappa}^{[-]}$.

E.3 Exponents for Gaussian function

In this section we shall present the sets of exponents which we have used in our numerical calculations. These exponents were discussed in the work of Almoukhalalati *et al.* [24], recently published online [176], and are used in the DIRAC program [136]. A few points to note about these exponents:

1. They are associated with the following large component radial Gaussian-type functions:

$$\pi_{\kappa,i}^L = r^{|\kappa+\frac{1}{2}|+\frac{1}{2}} e^{-\zeta_{\kappa,i} r^2}, \tag{E.3.1}$$

(see section 2.9.2) and are optimized within the machinery of restricted kinetic balance (see section 2.10.1), such that they lead to the lowest possible numerical energy value for some two-electron atoms, in the presence of a Gaussian nuclear charge distribution.

2. Although they were optimized for two-electron noble gases (last column of the periodic table), we have tested them for one-electron systems (hydrogen-like atoms), and they gave a very good agreement with the exact hydrogen-like atom solutions, as seen in section 2.10.2.
3. They were optimized with respect to the quantum number ℓ , and not κ , and this means that basis functions with same ℓ , have the same set of exponents:
 - (a) For $\kappa = -1$ ($s_{\frac{1}{2}}$ -problem), one has to use the s -type functions given in table E.3.
 - (b) For $\kappa = +1, -2$ ($p_{\frac{1}{2}}$ - and $p_{\frac{3}{2}}$ -problems), one must use the p -type functions exponents, given in table E.4.
 - (c) For $\kappa = +2, -3$ ($d_{\frac{3}{2}}$ - and $d_{\frac{5}{2}}$ -problems), one must use the d -type functions exponents, given in table E.5, and so on.

This choice of exponents is presented in table E.1, where sets whose boxes have same dot color, have the same set of exponents. ζ_{κ} is the set of exponents associated with the κ -type functions.

state	κ	ℓ	j	ζ_κ
$s_{\frac{1}{2}}$	-1	0	$\frac{1}{2}$	•
$p_{\frac{1}{2}}$	+1	1	$\frac{1}{2}$	•
$p_{\frac{3}{2}}$	-2	1	$\frac{3}{2}$	•
$d_{\frac{3}{2}}$	+2	2	$\frac{3}{2}$	•
$d_{\frac{5}{2}}$	-3	2	$\frac{5}{2}$	•

 Table E.1: ℓ -basis exponents

Note: Same color dots indicates same exponents lists.

Another choice would be to use the j - instead of ℓ -basis, where the exponents are optimized for the same total angular-momentum number j basis functions, as seen in figure E.2. Finally, the reader should guess that the best would be to lift any restriction on these sets of exponents, and optimized every set independently, and this corresponds to κ -basis. These different choices of bases where discussed and carefully analyzed and compared by Dyllal and Fægri in [177].

state	κ	ℓ	j	ζ_κ
$s_{\frac{1}{2}}$	-1	0	$\frac{1}{2}$	•
$p_{\frac{1}{2}}$	+1	1	$\frac{1}{2}$	•
$p_{\frac{3}{2}}$	-2	1	$\frac{3}{2}$	•
$d_{\frac{3}{2}}$	+2	2	$\frac{3}{2}$	•
$d_{\frac{5}{2}}$	-3	2	$\frac{5}{2}$	•

 Table E.2: j -basis exponents

Note: Same color dots indicates same exponents lists.

For general discussions on the Gaussian basis sets, the reader may consult: Helgaker *et al.* [178, chapter 8] and Dyllal and Fægri in [179, section 11.9] and [177].

E.3.1 Even-tempered Gaussians

In addition, the sets of exponents we have just presented, we are going to use the even-tempering scheme to generate additional Gaussian exponents. This scheme was introduced by Feller and Klaus in [180] (See [181] and [178, Section 8.2.3]) to generate Gaussian exponents for non-relativistic calculations, where for each ℓ (a good quantum number in the radial Schrödinger equation) one specifies two parameters, $\zeta_{1,\ell}$ (the first exponent) and β_ℓ (the scaling constant) to generate the next exponents, with respect to the following formula:

$$\zeta_{\ell,i} = \zeta_{\ell,1} \beta_\ell^{i-1}, \quad \text{with } i = 1, 2, \dots \quad (\text{E.3.2})$$

Instead of optimized and one optimizes the two parameters $\zeta_{\ell,1}$ and β_ℓ instead of the whole set of exponents, which enormously reduces the computational cost. Helgaker *et al.* [178, Figure 8.4] pointed out that the fully optimized set of exponents, which minimizes the energy, followed (very closely) the prediction of the last formula. This is seen in the cited figure, where the authors have plotted $\log(\zeta_{\ell,i})$, and found that they almost line up.

The largest basis set we have in our hands is the 7z. In the vacuum polarization density calculation, we needed to introduce very localized Gaussians (higher exponents), following the even-

7z	6z	5z	4z	3z	2z
5.8413458E+07	5.6910312E+07	5.4043845E+07	4.8993564E+07	3.3526742E+07	3.4484684E+06
1.5531813E+07	1.4713079E+07	1.3275931E+07	1.1067847E+07	5.9306744E+06	3.6923025E+05
5.3033082E+06	4.7693949E+06	4.0265471E+06	3.0808231E+06	1.3524801E+06	6.1605336E+04
2.0092707E+06	1.6787224E+06	1.3234208E+06	9.3885611E+05	3.5289156E+05	1.3185882E+04
8.3035089E+05	6.3067462E+05	4.6528771E+05	3.0895847E+05	1.0250448E+05	3.3404023E+03
3.6124592E+05	2.4732853E+05	1.7202273E+05	1.0803130E+05	3.2447091E+04	9.3911904E+02
1.6395640E+05	1.0086548E+05	6.6577154E+04	3.9869685E+04	1.1044445E+04	
7.6632011E+04	4.2543096E+04	2.6826170E+04	1.5428093E+04	3.9952910E+03	
3.6732324E+04	1.8514164E+04	1.1213551E+04	6.2270005E+03	1.5167049E+03	
1.7978788E+04	8.2895199E+03	4.8439940E+03	2.6065438E+03	5.8681930E+02	
8.9693806E+03	3.8086902E+03	2.1532081E+03	1.1219542E+03		
4.5521983E+03	1.7894327E+03	9.7737077E+02	4.8350360E+02		
2.3464240E+03	8.5356835E+02	4.4132872E+02			
1.2249044E+03	4.0285078E+02				
6.4315186E+02					
3.3118848E+02					

Table E.3: Radon s -type Gaussian functions ($\ell = 0$) exponents.

7z	6z	5z	4z	3z	2z
3.3436172E+05	1.6092405E+05	7.7792547E+04	3.5857677E+04	1.5093991E+04	5.3548941E+03
7.3358674E+04	3.7874384E+04	1.8377697E+04	8.1101373E+03	3.0468887E+03	
2.5301044E+04	1.2582090E+04	5.6451169E+03	2.1888393E+03		
9.8395322E+03	4.4359439E+03	1.7585052E+03			
3.7497293E+03	1.5092686E+03				
1.3518228E+03					

Table E.4: Radon p -type Gaussian functions ($\ell = 1$) exponents.

7z	6z	5z	4z	3z	2z
1.1320821E+05	7.0005907E+04	3.9272318E+04	1.9426551E+04	7.9563465E+03	
3.8026495E+04	2.2122068E+04	1.1213149E+04	4.6751886E+03		
1.5750652E+04	8.0351979E+03	3.3892042E+03			
6.3759559E+03	2.7176536E+03				
2.3124403E+03					

Table E.5: Radon d -type Gaussian functions ($\ell = 2$) exponents.

tempering scheme, to question our ability to describe this density. The last formula tells us that if we have a basis set containing n exponents (ordered by increasing order), the additional tight exponent ζ_{n+1} is obtained, by recurrence, from the last two exponents by:

$$\zeta_{\ell,n+1} = \frac{\zeta_{\ell,n}^2}{\zeta_{\ell,n-1}}. \quad (\text{E.3.3})$$

Taking for example the 7z s -basis which contains 16-exponents, the additional exponent will be:

$$\zeta_{0,17} = \frac{\zeta_{0,16}^2}{\zeta_{0,15}} = 2.1968665\text{E} + 08. \quad (\text{E.3.4})$$

Appendix F

Complex integrations

F.1 Cauchy's integral theorem

Cauchy's integral theorem states that if $f(z)$ is an analytic function in a simply connected region of the complex plane, then the closed integral along any closed contour γ , within that region, vanishes:

$$\oint_{\gamma} f(z) dz = 0. \quad (\text{F.1.1})$$

A region is said to be simply connected if any closed loops within it, can be shrunk and eventually form a point.

Proof

Conventionally, this theorem is proved as follows: A complex function $f(z)$ can be written as:

$$f(z) = u(z) + iv(z), \quad (\text{F.1.2})$$

where $u(z)$ and $v(z)$ its real and imaginary components. In addition, an infinitesimal displacement in the complex plane, can also be decomposed into real and complex components:

$$dz = dx + idy. \quad (\text{F.1.3})$$

After substituting these formulas in the contour integral of eq.(F.1.1), we get:

$$\oint_{\gamma} f(z) dz = \oint_{\gamma} (udx - vdy) + i \oint_{\gamma} (udy + vdx). \quad (\text{F.1.4})$$

At this point, we are left with two real integrals. Using Stokes' theorem, a closed line integral of some vector field \mathbf{F} along some curve γ , can be written as an integral of the associated curl field $\nabla \times \mathbf{F}$, along a surface σ that is bounded by that closed curve γ :

$$\oint_{\gamma} \mathbf{F} \cdot d\mathbf{x} = \iint_{\sigma} (\nabla \times \mathbf{F}) \cdot d\boldsymbol{\sigma}. \quad (\text{F.1.5})$$

This last equation will allow us to write the previous equation as:

$$\oint_{\gamma} f(z) dz = \iint_{\sigma} \left(-\frac{\partial v}{\partial x} - \frac{\partial u}{\partial y} \right) dxdy + i \iint_{\sigma} \left(\frac{\partial u}{\partial x} - \frac{\partial v}{\partial y} \right) dxdy. \quad (\text{F.1.6})$$

Since $f(z)$ is assumed to be analytic, then u and v must satisfy the Cauchy-Riemann equations:

$$\begin{aligned}\frac{\partial u}{\partial x} &= +\frac{\partial v}{\partial y} \\ \frac{\partial u}{\partial y} &= -\frac{\partial v}{\partial x},\end{aligned}\tag{F.1.7}$$

and the last contour integral must thus vanish:

$$\oint_{\gamma} f(z) dz = 0.\tag{F.1.8}$$

F.2 Cauchy's integral formula

The Cauchy's integral formula states that if $f(z)$ satisfies the same requirements satisfied in the previous section, then the following integral enclosing the pole $z = a$ can be written as:

$$f(a) = \frac{1}{2\pi i} \oint_{\gamma} dz \frac{f(z)}{z-a}.\tag{F.2.1}$$

The proof of this theorem can be found in all elementary complex analysis textbooks, we cite [182, section 3.8] and [183, section 54].

F.3 Cauchy's differential formula

Cauchy's integral formula concerns closed integrals that surrounds simple poles. This formalism can be extended to any higher-order poles. Let, for instance $f(z)$ be an analytic function in the region enclosed by some closed contour γ , then one can write:

$$f^{(n-1)}(a) = \frac{(n-1)!}{2\pi i} \oint dz \frac{f(z)}{(z-a)^n}.\tag{F.3.1}$$

The proof of this theorem can be found in [183, section 55].

F.4 Jordan's lemma

In our derivations we are going to use an important result provided by Jordan's lemma. This lemma tells us that if we have a function $f(z)$, which satisfies the following condition:

$$\lim_{z \rightarrow \infty} \sup_{z \in \gamma^+(r)} |f(z)| = 0, \quad \text{for } \Im[z] > 0,\tag{F.4.1}$$

the following integral along the upper-half plane semi-circle contour $\gamma^+(r)$ of radius r :

$$\lim_{r \rightarrow +\infty} \int_{\gamma^+(r)} dz f(z) e^{ia+z} = 0,\tag{F.4.2}$$

vanishes, for a_+ a positive real constant. The corresponding contour is presented in figure F.4.1a. Similarly, if the following condition:

$$\lim_{z \rightarrow \infty} \sup_{z \in \gamma^-(r)} |f(z)| = 0, \quad \text{for } \Im[z] < 0,\tag{F.4.3}$$

holds, then the following integral along the lower semi-circle contour of radius r :

$$\lim_{r \rightarrow +\infty} \int_{\gamma^-(r)} dz f(z) e^{ia_- z} = 0, \quad (\text{F.4.4})$$

vanishes, for a negative real constant a_- . This contour, $\gamma^-(r)$ is presented in figure F.4.1b.

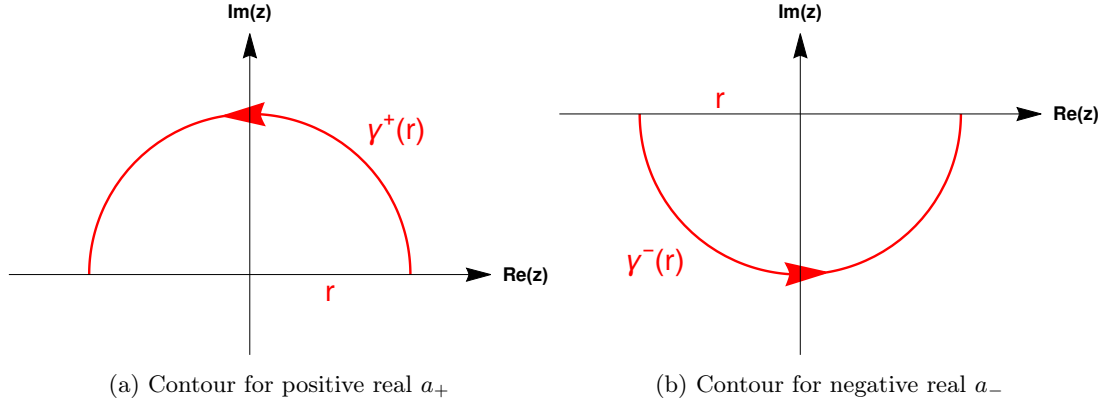


Figure F.4.1: Contours for Jordna's lemma.

In the following sections we are going to prove this lemma for both signs of the exponent factor a_{\pm} , and reach conclusions which will help us evaluate Fourier transform integrals. This section is inspired by [183, section 88], [182, Chapter 5] and [166, section 11.8].

F.4.1 Upper half-plane

Let $r_0 > 0$ and $r \geq r_0$, and $\gamma^+(r)$ be the semicircle contour of radius r , cantered at the origin, that scans the region of the $\theta = [0, \pi]$ in a counterclockwise direction, as seen in figure F.4.2. Supposing that $f(z)$ is analytic in the upper half plane outside the semi-circle of radius $|z| = r_0$, and that this function vanishes for large upper plane z points, i.e. :

$$\lim_{z \rightarrow \infty} \sup_{z \in \gamma^+(r)} |f(z)| = 0, \quad \text{for } \Im[z] > 0, \quad (\text{F.4.5})$$

where $\sup_{z \in \gamma^+(r)} |f(z)|$ represent the supremum of the $|f(z)|$ function for z being at the upper semicircle $\gamma^+(r)$. In the large radius limit, the integral along the upper semicircle contour γ^+ , vanishes:

$$\lim_{r \rightarrow \infty} \int_{\gamma^+(r)} f(z) e^{ia_+ z} dz = 0, \quad (\text{F.4.6})$$

for positive real constant a_+ .

Proof

For the upper plane, we would like to evaluate:

$$\lim_{r \rightarrow \infty} \int_{\gamma^+} f(z) e^{ia_+ z} dz. \quad (\text{F.4.7})$$

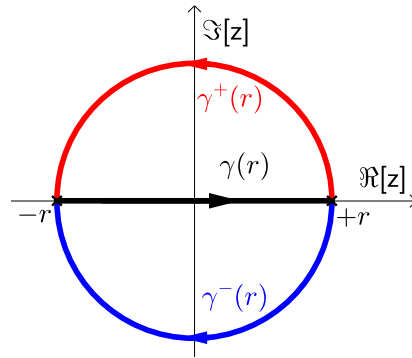


Figure F.4.2: Integration contours

Notice that we can take the absolute value of the integral [184, page 104]:

$$\left| \int_{\gamma^+} f(z) e^{ia_+z} dz \right| = \left| \int_0^\pi f(re^{i\theta}) e^{ia_+re^{i\theta}} re^{i\theta} i d\theta \right| \quad (\text{F.4.8})$$

$$\leq r \int_0^\pi |f(re^{i\theta})| e^{-a_+r \sin \theta} d\theta, \quad (\text{F.4.9})$$

this last quantity is smaller or equal to the supremum of $f(z)$, for z on the γ^+ contour:

$$\left| \int_{\gamma^+} f(z) e^{ia_+z} dz \right| \leq r \sup_{z \in \gamma^+} |f(z)| \int_0^\pi e^{-a_+r \sin \theta} d\theta \quad (\text{F.4.10})$$

$$= 2r \sup_{z \in \gamma^+} |f(z)| \int_0^{\frac{\pi}{2}} e^{-a_+r \sin \theta} d\theta, \quad (\text{F.4.11})$$

to simplify our expression, we would like to replace the exponential integrand by a simpler one (that can be solved analytically) which has higher value on the interval $\theta \in [0, \frac{\pi}{2}]$. One option is to replace $\sin(\theta)$ by $\frac{2\theta}{\pi}$, since as seen in figure F.4.3, we have:

$$\sin(\theta) \geq \frac{2\theta}{\pi}, \quad \text{for } 0 \leq \theta \leq \frac{\pi}{2}, \quad (\text{F.4.12})$$

and continue to write:

$$\left| \int_{\gamma^+} f(z) e^{ia_+z} dz \right| \leq 2r \sup_{z \in \gamma^+} |f(z)| \int_0^{\frac{\pi}{2}} e^{-\frac{a_+r^2}{\pi} \theta} d\theta \quad (\text{F.4.13})$$

$$= \frac{\pi}{a_+} [1 - e^{-a_+r}] \sup_{z \in \gamma^+} |f(z)| \quad (\text{F.4.14})$$

$$< \frac{\pi}{a_+} \sup_{z \in \gamma^+} |f(z)|. \quad (\text{F.4.15})$$

We clearly see that if $f(z)$ vanishes for large z with $\Im[z] > 0$ (upper half-plane), then the main integral will vanish:

$$\lim_{r \rightarrow \infty} \int_{\gamma^+} f(z) e^{ia_+z} dz = 0. \quad (\text{F.4.16})$$

F.4.2 Lower half-plane

For lower half-plane, we would expect the following limit of integral to vanish:

$$\lim_{r \rightarrow \infty} \int_{\gamma^-(r)} f(z) e^{ia_-z} dz = 0, \quad (\text{F.4.17})$$

in the case where $f(z)$ is an analytic function in the lower half-plane for $|z| = r$ larger of some radius r_0 (outside the semicircle), and a_- is some negative real constant. The contour γ^- is the lower half-plane semicircle, presented in figure F.4.2 in blue.

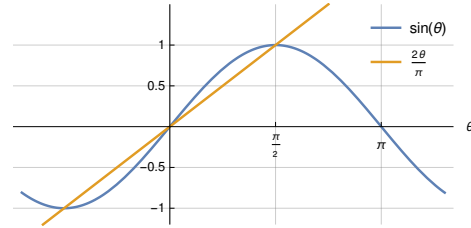


Figure F.4.3: A simple plot.

Proof

Following the previous derivation, we write:

$$\left| \int_{\gamma^-} f(z) e^{ia-z} dz \right| \leq r \int_{\pi}^{2\pi} |f(re^{i\theta})| e^{-a-r \sin \theta} d\theta \quad (\text{F.4.18})$$

$$\leq r \sup_{z \in \gamma^-} |f(z)| \int_{\pi}^{2\pi} e^{-a-r \sin \theta} d\theta, \quad (\text{F.4.19})$$

where $\sup_{z \in \gamma^-} |f(z)|$ is the supremum of the $|f(z)|$ for z being on γ^- . Notice that for the lower half-plane, $\sin \theta$ is negative, meaning that the overall exponential sign is negative. The last inequality can be written as:

$$\left| \int_{\gamma^-} f(z) e^{ia-z} dz \right| \leq 2r \sup_{z \in \gamma^-} |f(z)| \int_0^{\frac{\pi}{2}} e^{+a-r \sin \theta} d\theta, \quad (\text{F.4.20})$$

we then use the condition of eq.(F.4.12), to write:

$$\left| \int_{\gamma^-} f(z) e^{ia-z} dz \right| \leq \frac{\pi}{a_-} \sup_{z \in \gamma^-} |f(z)| \int_0^{a-r} e^u du \quad (\text{F.4.21})$$

$$= \frac{\pi}{a_-} [e^{a-r} - 1] \sup_{z \in \gamma^-} |f(z)| \quad (\text{F.4.22})$$

$$< -\frac{\pi}{a_-} \sup_{z \in \gamma^-} |f(z)|, \quad (\text{F.4.23})$$

which clearly vanishes in the limit $r \rightarrow \infty$, provided that:

$$\lim_{z \rightarrow \infty} \sup_{z \in \gamma^-(r)} |f(z)| = 0, \quad \text{with } \Im[z] < 0. \quad (\text{F.4.24})$$

F.5 Conclusion

- For positive real constant a_+ , we had:

$$\lim_{r \rightarrow \infty} \int_{\gamma^+(r)} f(z) e^{ia+z} dz = 0, \quad (\text{F.5.1})$$

provided that:

$$\lim_{z \rightarrow \infty} \sup_{z \in \gamma^+(r)} |f(z)| = 0, \quad \text{for } \Im[z] > 0, \quad (\text{F.5.2})$$

This result means that if we would like to evaluate the integral along the real axis, we can write:

$$\int_{-\infty}^{+\infty} f(x) e^{ia+x} dx = \lim_{r \rightarrow \infty} \oint_{(r)}^+ f(z) e^{ia+z} dz, \quad (\text{F.5.3})$$

where $\oint_{(r)}^+$ is the upper half-plane closed contour integral that combines $\gamma^+(r)$ and the integral along the real axis presented by the black contour $\gamma(r)$ of figure F.4.2.

- For negative real constant a_- , we had:

$$\lim_{r \rightarrow \infty} \int_{\gamma^-(r)} f(z) e^{ia-z} dz = 0, \quad (\text{F.5.4})$$

provided that:

$$\lim_{z \rightarrow \infty} \sup_{z \in \gamma^-(r)} |f(z)| = 0, \quad \text{for } \Im[z] < 0. \quad (\text{F.5.5})$$

This result means that if we would like to evaluate the integral along the real axis, we can write:

$$\int_{-\infty}^{+\infty} f(x) e^{ia-x} dx = \lim_{r \rightarrow \infty} \oint_{(r)}^- f(z) e^{ia-z} dz, \quad (\text{F.5.6})$$

where $\oint_{(r)}^-$ is the lower half-plane closed contour integral that combines $\gamma^-(r)$ and the integral along the real axis presented by the $\gamma(r)$ contour.

- The advantage of expressing these integrals in terms of closed contour integrations, is that it allows the use of the Cauchy integral formula, which can in many cases reduce the computation effort, or provide solution for integrals that seemed not to be resolvable.

F.6 $\alpha(Z\alpha)^n$: n -potential interactions complex integral

In the derivation of the vacuum polarization expansion, one encounters an integral of the following form:

$$I(E_{i_1}, \dots, E_{i_{n+1}}) = \int_{C_F} \frac{dz}{(E_{i_1} - z) \dots (E_{i_{n+1}} - z)}, \quad (\text{F.6.1})$$

associated with the n -potential interaction with the external potential, or what is known as $(\alpha Z)^n$ expansion. The integrand denominators come from the eigen-decomposion of the Green's functions (see eq.(3.9.38)), E_i . The C_F subscript indicates that this integral is to be evaluated along the Feynman contour: diving below negative-energy solutions, and flying above the positive-energy solutions and continuum as seen in figure F.6.1a. This integral can be slightly modified by introducing what is sometimes called “Feynman prescription”, where energy poles are shifted with respect to:

$$E_{i_\alpha} \rightarrow \epsilon_{i_\alpha} = E_{i_\alpha} - i\delta \text{sgn}(E_{i_\alpha}); \quad 0 < \delta \ll 1, \quad \text{and} \quad \alpha = 1, \dots, n, \quad (\text{F.6.2})$$

and the contour integral can now be evaluated along the real x -axis, as seen in figure F.6.1b. At the end of the calculation, the limit $\delta \rightarrow 0$ has to be evaluated. The integral becomes:

$$I(E_{i_1}, \dots, E_{i_{n+1}}) = \int_{-\infty}^{+\infty} \frac{dx}{(\epsilon_{i_1} - x) \dots (\epsilon_{i_{n+1}} - x)}, \quad (\text{F.6.3})$$

which we seek to solve and provide a compact analytical expression of it. The general attack strategy is going to be the following:

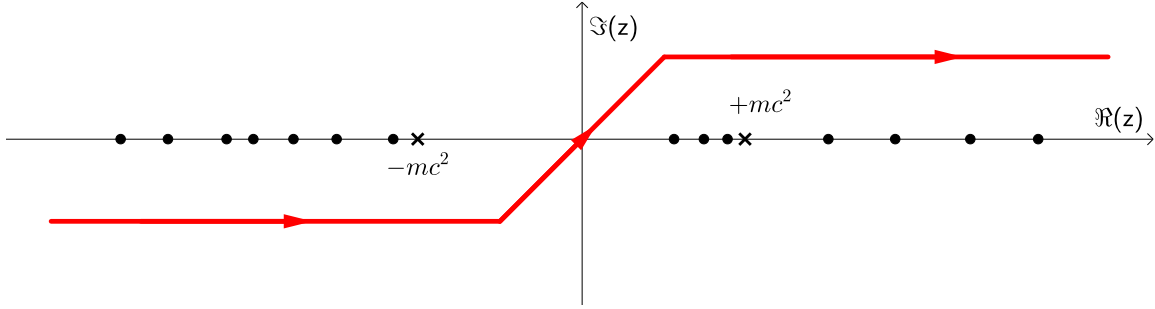
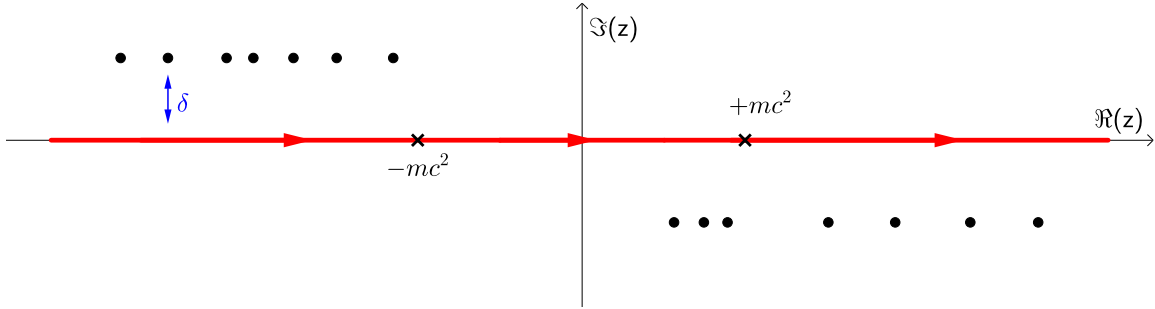
1. The previous integral can be written as:

$$I(E_{i_1}, \dots, E_{i_{n+1}}) = \lim_{r \rightarrow \infty} I_\gamma(r); \quad (\text{F.6.4})$$

$$\text{with } I_\gamma(r) = \int_{-r}^{+r} \frac{dx}{(\epsilon_{i_1} - x) \dots (\epsilon_{i_{n+1}} - x)}. \quad (\text{F.6.5})$$

2. Poles are going to be enclosed by closed contours, which we shall call $I_o(r)$:

$$I_o(r) = \oint \frac{dz}{(\epsilon_{i_1} - x) \dots (\epsilon_{i_{n+1}} - x)} = I_\gamma(r) + I_{\gamma^\pm}(r), \quad (\text{F.6.6})$$

(a) Contour integral of eq. F.6.1 along the Feynman path C_F .

(b) Modification of the Feynman contour and poles shifting with respect to eq. (F.6.2).

Figure F.6.1: The contour is modified such that the integral can be evaluated along the real axis. Black dots represent the bound Green's function poles: eigenvalues of the Dirac equation in the presence of the nuclear potential. Positive- and negative-energy poles are thus shifted below and above the real axis, respectively, and the integral is now evaluated along the real axis.

so we can take advantage of Cauchy's integral formula. This closed integral combines the previous contour integral (along the real axis) with $I_{\gamma^{\pm}}(r)$ that correspond to contours along upper- and lower-plane semi-circles (of radius r) γ^{\pm} respectively. These arc integrations vanish for large radii in most of the encountered cases.

3. Finally, our integral of eq.(F.6.3) can be written as a limit for large radius r of the contours difference:

$$I(E_{i_1}, \dots, E_{i_{n+1}}) = \lim_{r \rightarrow \infty} (I_o(r) - I_{\gamma^{\pm}}(r)). \quad (\text{F.6.7})$$

In the next subsections we shall evaluate this integral associated with zero- and one-potential interactions, known as $\alpha(\alpha Z)^{n=1,2}$ terms by hand, and write a general formula of the result for arbitrary n .

F.6.1 Zero-potential integral: One pole

What we call the zero potential term is the one associated with $n = 0$, meaning that the integral of eq.(F.6.3) reduces to:

$$I(E_i) = \int_{-\infty}^{+\infty} \frac{dx}{\epsilon_i - x} = \lim_{r \rightarrow \infty} I_{\gamma}(r), \quad (\text{F.6.8})$$

where I_{γ_r} corresponds to the integral along the real axis, that goes from $-r$ to $+r$:

$$I_{\gamma}(r) = \int_{-r}^{+r} \frac{dx}{\epsilon_i - x}. \quad (\text{F.6.9})$$

In order to take make use of the Cauchy integral formula, the pole is besieged by a closed loop. Two cases are to be taken into account:

negative-energy pole $E_i < 0$

In this case, ϵ_i lies in the upper complex half-plane, and one can write:

$$I_o(r) = I_{\gamma}(r) + I_{\gamma^-}(r). \quad (\text{F.6.10})$$

The first integral (on the l.h.s.) represents the closed integral of figure F.6.2a enclosing the pole, which can be written as a sum over the two contour integrals: The one along the real axis curve γ_r that is shown in red, and the arc integral along the γ^- curve shown in blue.

1. The arc integral can be evaluated as follows:

$$I_{\gamma^-}(r) = \int_{\gamma^-} \frac{dz}{\epsilon_i - z} = i \int_0^{\pi} \frac{re^{i\theta} d\theta}{\epsilon_i - re^{i\theta}}, \quad (\text{F.6.11})$$

for very large r this integral reduces to $-i\pi$.

2. The closed integral is then evaluated using Cauchy's integral formula (discussed in section F.2), and one obtains:

$$I_o(r) = \oint \frac{dz}{\epsilon_i - z} = -2i\pi. \quad (\text{F.6.12})$$

3. Finally, we obtain:

$$I(E_i) = \lim_{r \rightarrow \infty} (I_o(r) - I_{\gamma^-}(r)) = -i\pi. \quad (\text{F.6.13})$$

positive-energy pole $E_i > 0$

In this case, the energy pole lies in the lower complex half-plane, and we write:

$$I_o(r) = I_{\gamma}(r) + I_{\gamma^+}(r), \quad (\text{F.6.14})$$

where the closed contour integral is shown in figure F.6.2b as the combination of the integral along the real axis (red contour) and the integral along the semicircle that goes from polar angle $\theta = 2\pi$ to π (blue one).

1. The arc integral can be evaluated as follows:

$$I_{\gamma^+}(r) = \int_{\gamma^+} \frac{dz}{\epsilon_i - z} = i \int_{2\pi}^{\pi} \frac{re^{i\theta} d\theta}{\epsilon_i - re^{i\theta}}, \quad (\text{F.6.15})$$

which for large radius, reduces to $+i\pi$.

2. The closed integral is evaluated using Cauchy's integral formula (discussed in section F.2), and one obtains:

$$I_o(r) = +2i\pi. \quad (\text{F.6.16})$$

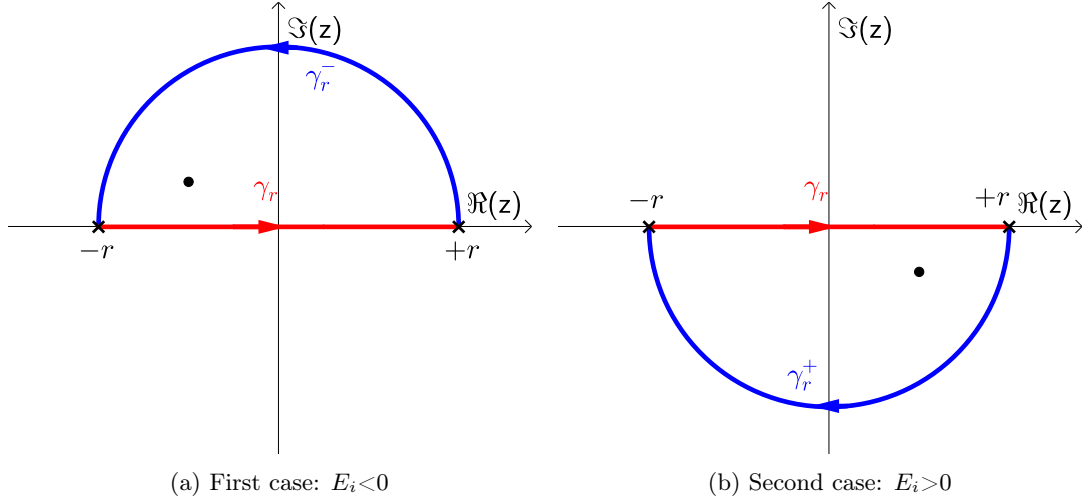


Figure F.6.2: The two possible pole scenarios for the zero-potential (one-pole) complex integration.

3. Finally, we obtain:

$$I(E_i) = \lim_{r \rightarrow \infty} (I_o(r) - I_{\gamma^+}(r)) = +i\pi. \quad (\text{F.6.17})$$

Combining the findings of eqs.(F.6.13 and F.6.17) that corresponds to the two possible scenarios (positive and negative-energy poles) we obtain the following result:

$$I(E_i) = \int_{-\infty}^{+\infty} \frac{dx}{\epsilon_i - x} = i\pi \text{sgn}(E_i). \quad (\text{F.6.18})$$

F.6.2 One-potential integral: Two poles

In the one-potential integral, two Green's functions are involved, meaning that two denominators will appear in eq.(F.6.3). We thus have:

$$I(E_i, E_j) = \int_{-\infty}^{+\infty} \frac{dx}{(\epsilon_i - x)(\epsilon_j - x)} = \lim_{r \rightarrow \infty} I_\gamma(r), \quad (\text{F.6.19})$$

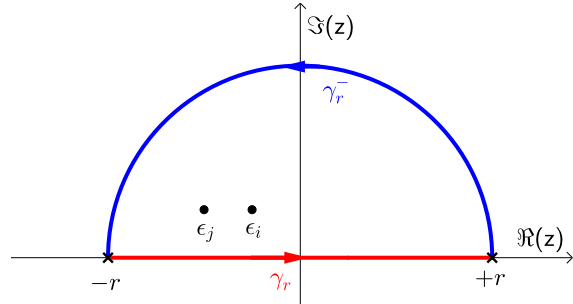
where $I_\gamma(r)$ is given by:

$$I_\gamma(r) = \int_{-r}^{+r} \frac{dx}{(\epsilon_i - x)(\epsilon_j - x)}. \quad (\text{F.6.20})$$

Again, this integral is going to be written as the following difference:

$$I_\gamma(r) = I_o(r) - I_{\gamma^\pm}(r). \quad (\text{F.6.21})$$

In this case, four possible scenarios can occur (different combinations of energies' signs):

Figure F.6.3: $\text{sgn}(E_i, E_j) = (-1, -1)$

First case $E_i, E_j > 0$

As presented in figure F.6.4, both poles correspond to positive-energy levels. The closed integral is found to vanish:

$$I_o(r) = \frac{1}{\epsilon_j - \epsilon_i} \oint \frac{dz}{z - \epsilon_j} + \frac{1}{\epsilon_i - \epsilon_j} \oint \frac{dz}{z - \epsilon_i} = 0. \quad (\text{F.6.22})$$

The contour integration along the γ^+ arc path reads:

$$I_{\gamma^+}(r) = \int_{2\pi}^{\pi} \frac{ire^{i\theta} d\theta}{(\epsilon_i - re^{i\theta})(\epsilon_j - re^{i\theta})}. \quad (\text{F.6.23})$$

Notice that for large radius this integral vanishes since there are more r powers in the denominator. We thus reach the conclusion that in the case where both poles are positive, our integral vanishes:

$$I(E_i, E_j) = 0. \quad (\text{F.6.24})$$

Second case $E_i, E_j < 0$

This case is presented in figure F.6.3, the closed contour integration as well as the integral along the γ^+ curve vanish as in the previous case:

$$I(E_i, E_j) = 0. \quad (\text{F.6.25})$$

So far, we conclude that in the case where both poles have same energy sign, the integral in question will vanish. Next we attack the opposite energy sign poles.

Third case $E_i > 0, E_j < 0$

In this case the lower half-plane closed integral only encloses the ϵ_j pole, as presented in figure F.6.6, meaning that the closed integral will give a non-vanishing contribution:

$$I_o(r) = \frac{1}{\epsilon_i - \epsilon_j} \oint \frac{dz}{z - \epsilon_i} = \frac{-2\pi i}{\epsilon_i - \epsilon_j}. \quad (\text{F.6.26})$$

The arc integral will clearly vanish in the limit of large r :

$$I_{\gamma^+}(r) = \int_{2\pi}^{\pi} \frac{ire^{i\theta} d\theta}{(\epsilon_i - re^{i\theta})(\epsilon_j - re^{i\theta})}, \quad (\text{F.6.27})$$

leading to the following integral result:

$$I(E_i, E_j) = \frac{2\pi i}{\epsilon_j - \epsilon_i} = \frac{2\pi i}{-|\epsilon_j| - |\epsilon_i|}. \quad (\text{F.6.28})$$

Fourth case $E_i < 0, E_j > 0$

This case is trivial, because it is the same as the previous case, with labels $i \rightleftharpoons j$ exchanged, the integral is thus:

$$I(E_i, E_j) = \frac{2\pi i}{\epsilon_i - \epsilon_j}. \quad (\text{F.6.29})$$

Final expression

As a conclusion, we combine the four results (of the four possible scenarios), and write:

$$I(E_i, E_j) = \int_{-\infty}^{+\infty} \frac{dx}{(\epsilon_i - x)(\epsilon_j - x)} = \pi i \frac{1 - \text{sgn}(E_i E_j)}{|E_i| + |E_j|}, \quad (\text{F.6.30})$$

which vanishes if both energy poles are of the same sign.

F.6.3 n -potential integral: $n + 1$ poles

At this point, the reader can start guessing that if all poles have the same sign, then the integral we are calculating will vanish (as seen in the case of $n = 1$). This can be easily seen by the following reasoning: Assuming that the poles are all positive-energy ones (laying in the lower complex half plane), then one can choose the closed loop to be along the upper half-plane. The closed integral will obviously vanish (no poles inside), in addition to the integral along the arc will have the following form:

$$I_{\gamma^+}(r) = \int_{2\pi}^{\pi} \frac{ire^{i\theta} d\theta}{(\epsilon_1 - re^{i\theta}) \dots (\epsilon_{n+1} - re^{i\theta})}, \quad (\text{F.6.31})$$

which obviously vanish for large r , for $n \geq 1$. This holds similarly in the other case where all poles negative-energy ones, and one can integrate along the lower complex plane closed contour.

The general n -potential integral includes the following integral:

$$I(E_1, \dots, E_{n+1}) = \int_{-\infty}^{+\infty} J(x, E_1, \dots, E_{n+1}) dx; \quad (\text{F.6.32})$$

$$J(x, E_1, \dots, E_{n+1}) = \frac{1}{(\epsilon_1 - x) \dots (\epsilon_{n+1} - x)}, \quad (\text{F.6.33})$$

this integrand can be written as:

$$J(z, E_1, \dots, E_{n+1}) = (-1)^{n+1} \frac{1}{(z - \epsilon_1) \dots (z - \epsilon_{n+1})}. \quad (\text{F.6.34})$$

- In the case where all poles are distinct $E_i \neq E_j$, $\forall i, j$, it can be shown that the integrand can be written as:

$$\frac{1}{(z - \epsilon_1) \dots (z - \epsilon_{n+1})} = \sum_{i=1}^{n+1} \frac{1}{\prod_{j \neq i} (\epsilon_i - \epsilon_j)} \frac{1}{(z - \epsilon_i)}, \quad (\text{F.6.35})$$

and the integral is evaluated using Cauchy's integral theorem.

- In general, poles may coincide and things become a bit more complicated.

We then reorder poles such that the first m are positive, stored in $g(z)$, and $f(z)$ collects the remaining $(n+1-m)$ negative-poles:

$$J(z, E_1, \dots, E_{n+1}) = (-1)^{n+1} g(z) f(z) \quad (\text{F.6.36})$$

$$g(z) = \frac{1}{(z - \epsilon_1) \dots (z - \epsilon_m)} \quad m \text{ positive poles} \quad (\text{F.6.37})$$

$$f(z) = \frac{1}{(z - \epsilon_{m+1}) \dots (z - \epsilon_{n+1})} \quad (n+1-m) \text{ negative poles} \quad (\text{F.6.38})$$

We then choose to integrate along the lower semi-circle, thus only $g(z)$ will contribute to the Cauchy's theorem. Coinciding poles of $g(z)$ are collected together, we write it as:

$$g(z) = \frac{1}{(z - \epsilon_1)^{\alpha_1} \dots (z - \epsilon_k)^{\alpha_k}}, \quad (\text{F.6.39})$$

saying that we have k distinct $(z - \epsilon_i)$ poles, each is associated with a multiplicity of α_i . k can only be smaller or equal to m (equal, in the case where all poles are distinct), and the sum of all exponents should be equal to m :

$$\sum_{i=1}^k \alpha_i = m \quad (\text{F.6.40})$$

and using partial fraction decomposition, $g(z)$ can be written as:

$$g(z) = \sum_{i=1}^k \sum_{j=1}^{\alpha_i} \frac{A_{i,j}}{(z - \epsilon_i)^j}, \quad (\text{F.6.41})$$

which can be seen as a Laurent series. The task now is to determine the coefficients $A_{i,j}$. One way to do so, is by introducing a function $g_a(z)$, given by:

$$g_a(z) = (z - \epsilon_a)^{\alpha_a} g(z), \quad (\text{F.6.42})$$

which expands as:

$$\begin{aligned} g_a(z) &= \frac{(z - \epsilon_a)^{\alpha_a} A_{1,1}}{(z - \epsilon_1)^1} + \dots + \frac{(z - \epsilon_a)^{\alpha_a} A_{1,\alpha_1}}{(z - \epsilon_1)^{\alpha_1}} \\ &+ \dots \\ &+ (z - \epsilon_a)^{\alpha_a-1} A_{a,1} + \dots + (z - \epsilon_a)^2 A_{a,\alpha_a-2} + (z - \epsilon_a) A_{a,\alpha_a-1} + A_{a,\alpha_a} \\ &+ \dots \\ &+ \dots + \frac{(z - \epsilon_a)^{\alpha_a} A_{k,\alpha_k}}{(z - \epsilon_k)^{\alpha_k}}. \end{aligned} \quad (\text{F.6.43})$$

From the third line of the last equation, one directly observes the following equations:

$$A_{a,\alpha_a} = g_a|_{z=\epsilon_a} \quad (\text{F.6.44})$$

$$A_{a,\alpha_a-1} = \frac{d}{dz} g_a|_{z=\epsilon_a} \quad (\text{F.6.45})$$

$$A_{a,\alpha_a-2} = \frac{1}{2!} \frac{d^2}{dz^2} g_a|_{z=\epsilon_a} \quad (\text{F.6.46})$$

⋮

These equation lead to the final expression of the coefficients $A_{i,j}$, that is:

$$A_{i,\alpha_i-k} = \frac{1}{k!} \frac{d^k}{dz^k} g_i \big|_{z=\epsilon_i}, \quad (\text{F.6.47})$$

which can be rewritten as:

$$A_{i,j} = \frac{1}{(\alpha_i - j)!} \frac{d^{\alpha_i-j}}{dz^{\alpha_i-j}} g_i \big|_{z=\epsilon_i}. \quad (\text{F.6.48})$$

We now collect the findings, and write the closed integral as:

$$I_o = (-1)^{n+1} \sum_{i=1}^k \sum_{j=1}^{\alpha_i} \frac{1}{(\alpha_i - j)!} \frac{d^{\alpha_i-j}}{dz^{\alpha_i-j}} g_i \big|_{z=\epsilon_i} \oint \frac{f(z)}{(z - \epsilon_i)^j} dz. \quad (\text{F.6.49})$$

Clearly, we can employ the Cauchy differential formula (see section F.3), and get:

$$I_o = 2\pi i (-1)^n \sum_{i=1}^k \sum_{j=1}^{\alpha_i} \frac{g_i^{(\alpha_i-j)}(\epsilon_i) f^{(j-1)}(\epsilon_i)}{(j-1)! (\alpha_i - j)!}. \quad (\text{F.6.50})$$

The integration along the lower semi-circle vanishes for $n \geq 1$, as discussed at the beginning of this section. Only for $n = 0$, we get a non-vanishing contribution, which in the limit of large radius reduces to:

$$\lim_{r \rightarrow \infty} I_{\gamma^+}(r) = i\pi, \quad (\text{F.6.51})$$

as seen in section F.6.1. We finally write the ultimate result of our derivation, to be:

$$\begin{aligned} I(E_{i_1}, \dots, E_{i_{n+1}}) &= \int_{C_F} \frac{dz}{(\epsilon_{i_1} - z) \dots (\epsilon_{i_{n+1}} - z)} \\ &= 2\pi i (-1)^n \sum_{i=1}^k \sum_{j=1}^{\alpha_i} \frac{g_i^{(\alpha_i-j)}(\epsilon_i) f^{(j-1)}(\epsilon_i)}{(j-1)! (\alpha_i - j)!} - i\pi \delta_{n,0}. \end{aligned} \quad (\text{F.6.52})$$

We built a MATHEMATICA program that computes this integral, using the above derivation results, and compared it with the slow numerical complex integration done by Mathematica. This code was uploaded to [185].

Appendix G

Time-ordered products

When expanding the $\hat{\mathcal{S}}$ -matrix in powers of interaction Hamiltonian density $\mathcal{H}(x) = j^\mu(x) A_\mu(x)$, one uses Wick's theorem, discussed in section 3.7 to write time-ordered products of electronic and photonic field operators in terms of normal ordered contractions. In this appendix, we present the first few orders of time-ordered products that appear in the \mathcal{S} -matrix expansion.

G.1 Electronic field currents

Using Wick's theorem of section 3.7, we expand the time-ordered product of the first few products of electron field operators. We then use the fact that the contraction of two electron operators gives an electron propagator:

$$\overline{\Psi}_\mu(x_1) \Psi_\nu(x_2) = \langle 0 | \Psi_\mu(x_1) \bar{\Psi}_\nu(x_2) | 0 \rangle = i\hbar S_{\mu\nu}^F(x_1, x_2). \quad (\text{G.1.1})$$

This relation is discussed in section 3.9.5. A single current: $\bar{\Psi}(x_1) \gamma^\mu \Psi(x_1)$ is a scalar function, and we shall write it as $\bar{\Psi}_{\alpha_1}(x_1) \gamma_{\alpha_1\beta_1}^\mu \Psi_{\beta_1}(x_1)$ (α and β are matrix element indices). This notation will allow us to clearly detect the existence of traces. An example is the second-order BSQED corrections, where we shall encounter the following traces:

$$\gamma_{\alpha_1\beta_1}^\mu S_{\beta_1\alpha_1}^F(x_1, x_1) = \text{Tr} [\gamma^\mu S^F(x_1, x_1)] \quad (\text{G.1.2})$$

$$\gamma_{\alpha_2\beta_2}^\nu S_{\beta_2\alpha_1}^F(x_2, x_1) \gamma_{\alpha_1\beta_1}^\mu S_{\beta_1\alpha_2}^F(x_1, x_2) = \text{Tr} [\gamma^\nu S^F(x_2, x_1) \gamma^\mu S^F(x_1, x_2)]. \quad (\text{G.1.3})$$

G.1.1 First-order

In matrix notation, the single current is written as:

$$\text{T} [\bar{\Psi}(x) \gamma^\mu \Psi(x)] = \gamma_{\alpha\beta}^\mu \text{T} [\bar{\Psi}_\alpha(x) \Psi_\beta(x)], \quad (\text{G.1.4})$$

where the time-ordered term can be written (using Wick's theorem) as:

$$\text{T} [\bar{\Psi}_\alpha(x) \Psi_\beta(x)] = : \bar{\Psi}_\alpha(x) \Psi_\beta(x) : + \overline{\bar{\Psi}_\alpha(x) \Psi_\beta(x)} \quad (\text{G.1.5})$$

$$= : \bar{\Psi}_\alpha(x) \Psi_\beta(x) : - i\hbar S_{\beta\alpha}^F(x, x), \quad (\text{G.1.6})$$

which finally leads to the following expression:

$$\text{T} [\bar{\Psi}(x) \gamma^\mu \Psi(x)] = : \bar{\Psi}(x) \gamma^\mu \Psi(x) : - i\hbar \text{Tr} [\gamma^\mu S^F(x, x)]. \quad (\text{G.1.7})$$

G.1.2 Second-order

In the second-order scattering matrix, appears a two-current product, which can be written in terms of matrix elements as:

$$T [\bar{\Psi}(x_1) \gamma^{\mu_1} \Psi(x_1) \bar{\Psi}(x_2) \gamma^{\mu_2} \Psi(x_2)] = \gamma_{\alpha_1 \beta_1}^{\mu_1} \gamma_{\alpha_2 \beta_2}^{\mu_2} T [\bar{\Psi}_{\alpha_1}(x_1) \Psi_{\beta_1}(x_1) \bar{\Psi}_{\alpha_2}(x_2) \Psi_{\beta_2}(x_2)]. \quad (\text{G.1.8})$$

Using Wick's theorem, the time-ordered product can be written as a normal ordering of all possible contractions (zero, ones, and twos):

$$\begin{aligned} & T [\bar{\Psi}_{\alpha_1}(x_1) \Psi_{\beta_1}(x_1) \bar{\Psi}_{\alpha_2}(x_2) \Psi_{\beta_2}(x_2)] \\ &= : \bar{\Psi}_{\alpha_1}(x_1) \Psi_{\beta_1}(x_1) \bar{\Psi}_{\alpha_2}(x_2) \Psi_{\beta_2}(x_2) : \\ &+ : \overbrace{\bar{\Psi}_{\alpha_1}(x_1) \Psi_{\beta_1}(x_1)} \bar{\Psi}_{\alpha_2}(x_2) \Psi_{\beta_2}(x_2) : \\ &+ : \bar{\Psi}_{\alpha_1}(x_1) \overbrace{\Psi_{\beta_1}(x_1) \bar{\Psi}_{\alpha_2}(x_2)} \Psi_{\beta_2}(x_2) : \\ &+ : \bar{\Psi}_{\alpha_1}(x_1) \Psi_{\beta_1}(x_1) \overbrace{\bar{\Psi}_{\alpha_2}(x_2) \Psi_{\beta_2}(x_2)} : \\ &+ : \bar{\Psi}_{\alpha_1}(x_1) \Psi_{\beta_1}(x_1) \bar{\Psi}_{\alpha_2}(x_2) \Psi_{\beta_2}(x_2) : \\ &+ : \bar{\Psi}_{\alpha_1}(x_1) \overbrace{\Psi_{\beta_1}(x_1) \bar{\Psi}_{\alpha_2}(x_2)} \Psi_{\beta_2}(x_2) : \\ &+ : \bar{\Psi}_{\alpha_1}(x_1) \Psi_{\beta_1}(x_1) \overbrace{\bar{\Psi}_{\alpha_2}(x_2) \Psi_{\beta_2}(x_2)} : \\ &+ : \bar{\Psi}_{\alpha_1}(x_1) \Psi_{\beta_1}(x_1) \bar{\Psi}_{\alpha_2}(x_2) \Psi_{\beta_2}(x_2) : \\ &+ : \overbrace{\bar{\Psi}_{\alpha_1}(x_1) \Psi_{\beta_1}(x_1)} \overbrace{\bar{\Psi}_{\alpha_2}(x_2) \Psi_{\beta_2}(x_2)} : \\ &+ : \bar{\Psi}_{\alpha_1}(x_1) \overbrace{\Psi_{\beta_1}(x_1) \bar{\Psi}_{\alpha_2}(x_2)} \Psi_{\beta_2}(x_2) : \\ &+ : \bar{\Psi}_{\alpha_1}(x_1) \Psi_{\beta_1}(x_1) \overbrace{\bar{\Psi}_{\alpha_2}(x_2) \Psi_{\beta_2}(x_2)} : \\ &+ : \bar{\Psi}_{\alpha_1}(x_1) \Psi_{\beta_1}(x_1) \bar{\Psi}_{\alpha_2}(x_2) \Psi_{\beta_2}(x_2) : \end{aligned} \quad (\text{G.1.9})$$

In the previous equation, we only included non-vanishing contractions which are of the form of $\overbrace{\bar{\Psi}_{\alpha}(x) \Psi_{\beta}(y)}$ and $\overbrace{\Psi_{\alpha}(x) \bar{\Psi}_{\beta}(y)}$. After evaluating contractions, the last expression simplifies to:

$$\begin{aligned} T [\bar{\Psi}_{\alpha_1}(x_1) \Psi_{\beta_1}(x_1) \bar{\Psi}_{\alpha_2}(x_2) \Psi_{\beta_2}(x_2)] &= : \bar{\Psi}_{\alpha_1}(x_1) \Psi_{\beta_1}(x_1) \bar{\Psi}_{\alpha_2}(x_2) \Psi_{\beta_2}(x_2) : \\ &+ i\hbar S_{\beta_1 \alpha_1}^F(x_1, x_1) : \Psi_{\beta_2}(x_2) \bar{\Psi}_{\alpha_2}(x_2) : \\ &- i\hbar S_{\beta_2 \alpha_1}^F(x_2, x_1) : \Psi_{\beta_1}(x_1) \bar{\Psi}_{\alpha_2}(x_2) : \\ &+ i\hbar S_{\beta_1 \alpha_2}^F(x_1, x_2) : \bar{\Psi}_{\alpha_1}(x_1) \Psi_{\beta_2}(x_2) : \\ &- i\hbar S_{\beta_2 \alpha_2}^F(x_2, x_2) : \bar{\Psi}_{\alpha_1}(x_1) \Psi_{\beta_1}(x_1) : \\ &- \hbar^2 S_{\beta_1 \alpha_1}^F(x_1, x_1) S_{\beta_2 \alpha_2}^F(x_2, x_2) \\ &+ \hbar^2 S_{\beta_2 \alpha_1}^F(x_2, x_1) S_{\beta_1 \alpha_2}^F(x_1, x_2). \end{aligned} \quad (\text{G.1.10})$$

After the plugging of the gamma matrices, $\gamma_{\alpha_1\beta_1}^{\mu_1}\gamma_{\alpha_2\beta_2}^{\mu_2}$ as seen in eq.(G.1.8), the time-ordered product becomes:

$$\begin{aligned}
& \text{T} [\bar{\Psi}(x_1) \gamma^\mu \Psi(x_1) \bar{\Psi}(x_2) \gamma^\nu \Psi(x_2)] \\
& = : \bar{\Psi}(x_1) \gamma^\mu \Psi(x_1) \bar{\Psi}(x_2) \gamma^\nu \Psi(x_2) : \\
& - i\hbar \text{Tr} [\gamma^\mu S^F(x_1, x_1)] : \bar{\Psi}(x_2) \gamma^\nu \Psi(x_2) : \\
& - i\hbar S_{\beta_2\alpha_1}^F(x_2, x_1) [\gamma^\mu]_{\alpha_1\beta_1} [\gamma^\nu]_{\alpha_2\beta_2} : \Psi_{\beta_1}(x_1) \bar{\Psi}_{\alpha_2}(x_2) : \\
& - i\hbar S_{\beta_1\alpha_2}^F(x_1, x_2) [\gamma^\nu]_{\alpha_2\beta_2} [\gamma^\mu]_{\alpha_1\beta_1} : \Psi_{\beta_2}(x_2) \bar{\Psi}_{\alpha_1}(x_1) : \\
& - i\hbar \text{Tr} [\gamma^\nu S^F(x_2, x_2)] : \bar{\Psi}(x_1) \gamma^\mu \Psi(x_1) : \\
& - \hbar^2 \text{Tr} [S^F(x_1, x_1) \gamma^\mu] \text{Tr} [S^F(x_2, x_2) \gamma^\nu] \\
& + \hbar^2 \text{Tr} [S^F(x_2, x_1) \gamma^\mu S^F(x_1, x_2) \gamma^\nu] .
\end{aligned} \tag{G.1.11}$$

G.1.3 Third-order

The time-ordered three currents term reads:

$$\begin{aligned}
& \text{T} [\bar{\Psi}(x_1) \gamma^{\mu_1} \Psi(x_1) \bar{\Psi}(x_2) \gamma^{\mu_2} \Psi(x_2) \bar{\Psi}(x_3) \gamma^{\mu_3} \Psi(x_3)] \\
& = \gamma_{\alpha_1\beta_1}^{\mu_1} \gamma_{\alpha_2\beta_2}^{\mu_2} \gamma_{\alpha_3\beta_3}^{\mu_3} \text{T} [\bar{\Psi}_{\alpha_1}(x_1) \Psi_{\beta_1}(x_1) \bar{\Psi}_{\alpha_2}(x_2) \Psi_{\beta_2}(x_2) \bar{\Psi}_{\alpha_3}(x_3) \Psi_{\beta_3}(x_3)] .
\end{aligned} \tag{G.1.12}$$

The possible contractions for the time-ordered term in the square brackets, are presented in table G.1, where same color dots represent a single contraction between the associated terms. Using

Wick's theorem, one can write:

$$\begin{aligned}
& T \left[\bar{\Psi}_{\alpha_1}(x_1) \Psi_{\beta_1}(x_1) \bar{\Psi}_{\alpha_2}(x_2) \Psi_{\beta_2}(x_2) \bar{\Psi}_{\alpha_3}(x_3) \Psi_{\beta_3}(x_3) \right] \\
& =: \bar{\Psi}_{\alpha_1}(x_1) \Psi_{\beta_1}(x_1) \bar{\Psi}_{\alpha_2}(x_2) \Psi_{\beta_2}(x_2) \bar{\Psi}_{\alpha_3}(x_3) \Psi_{\beta_3}(x_3) : \\
& - i\hbar S_{\beta_1\alpha_1}^F(x_1, x_1) : \bar{\Psi}_{\alpha_2}(x_2) \Psi_{\beta_2}(x_2) \bar{\Psi}_{\alpha_3}(x_3) \Psi_{\beta_3}(x_3) : - i\hbar S_{\beta_2\alpha_1}^F(x_2, x_1) : \Psi_{\beta_1}(x_1) \bar{\Psi}_{\alpha_2}(x_2) \bar{\Psi}_{\alpha_3}(x_3) \Psi_{\beta_3}(x_3) : \\
& - i\hbar S_{\beta_3\alpha_1}^F(x_3, x_1) : \Psi_{\beta_1}(x_1) \bar{\Psi}_{\alpha_2}(x_2) \Psi_{\beta_2}(x_2) \bar{\Psi}_{\alpha_3}(x_3) : + i\hbar S_{\beta_1\alpha_2}^F(x_1, x_2) : \bar{\Psi}_{\alpha_1}(x_1) \Psi_{\beta_2}(x_2) \bar{\Psi}_{\alpha_3}(x_3) \Psi_{\beta_3}(x_3) : \\
& + i\hbar S_{\beta_3\alpha_3}^F(x_1, x_3) : \bar{\Psi}_{\alpha_1}(x_1) \bar{\Psi}_{\alpha_2}(x_2) \Psi_{\beta_2}(x_2) \Psi_{\beta_3}(x_3) : - i\hbar S_{\beta_2\alpha_2}^F(x_2, x_2) : \bar{\Psi}_{\alpha_1}(x_1) \Psi_{\beta_1}(x_1) \bar{\Psi}_{\alpha_3}(x_3) \Psi_{\beta_3}(x_3) : \\
& - i\hbar S_{\beta_3\alpha_2}^F(x_3, x_2) : \bar{\Psi}_{\alpha_1}(x_1) \Psi_{\beta_1}(x_1) \Psi_{\beta_2}(x_2) \bar{\Psi}_{\alpha_3}(x_3) : + i\hbar S_{\beta_2\alpha_3}^F(x_2, x_3) : \bar{\Psi}_{\alpha_1}(x_1) \Psi_{\beta_1}(x_1) \bar{\Psi}_{\alpha_2}(x_2) \Psi_{\beta_3}(x_3) : \\
& - i\hbar S_{\beta_3\alpha_3}^F(x_3, x_3) : \bar{\Psi}_{\alpha_1}(x_1) \Psi_{\beta_1}(x_1) \bar{\Psi}_{\alpha_2}(x_2) \Psi_{\beta_2}(x_2) : \\
& - \hbar^2 S_{\beta_1\alpha_1}^F(x_1, x_1) S_{\beta_2\alpha_2}^F(x_2, x_2) : \bar{\Psi}_{\alpha_3}(x_3) \Psi_{\beta_3}(x_3) : - \hbar^2 S_{\beta_1\alpha_1}^F(x_1, x_1) S_{\beta_3\alpha_2}^F(x_3, x_2) : \Psi_{\beta_2}(x_2) \bar{\Psi}_{\alpha_3}(x_3) : \\
& + \hbar^2 S_{\beta_1\alpha_1}^F(x_1, x_1) S_{\beta_2\alpha_3}^F(x_2, x_3) : \bar{\Psi}_{\alpha_2}(x_2) \Psi_{\beta_3}(x_3) : - \hbar^2 S_{\beta_1\alpha_1}^F(x_1, x_1) S_{\beta_3\alpha_3}^F(x_3, x_3) : \bar{\Psi}_{\alpha_2}(x_2) \Psi_{\beta_2}(x_2) : \\
& + \hbar^2 S_{\beta_2\alpha_1}^F(x_2, x_1) S_{\beta_1\alpha_2}^F(x_1, x_2) : \bar{\Psi}_{\alpha_3}(x_3) \Psi_{\beta_3}(x_3) : - \hbar^2 S_{\beta_2\alpha_1}^F(x_2, x_1) S_{\beta_1\alpha_3}^F(x_1, x_3) : \bar{\Psi}_{\alpha_2}(x_2) \Psi_{\beta_3}(x_3) : \\
& + \hbar^2 S_{\beta_2\alpha_1}^F(x_2, x_1) S_{\beta_3\alpha_2}^F(x_3, x_2) : \Psi_{\beta_1}(x_1) \bar{\Psi}_{\alpha_3}(x_3) : - \hbar^2 S_{\beta_2\alpha_1}^F(x_2, x_1) S_{\beta_3\alpha_3}^F(x_3, x_3) : \Psi_{\beta_1}(x_1) \bar{\Psi}_{\alpha_2}(x_2) : \\
& + \hbar^2 S_{\beta_3\alpha_1}^F(x_3, x_1) S_{\beta_1\alpha_2}^F(x_1, x_2) : \Psi_{\beta_2}(x_2) \bar{\Psi}_{\alpha_3}(x_3) : + \hbar^2 S_{\beta_3\alpha_1}^F(x_3, x_1) S_{\beta_1\alpha_3}^F(x_1, x_3) : \bar{\Psi}_{\alpha_2}(x_2) \Psi_{\beta_2}(x_2) : \\
& - \hbar^2 S_{\beta_3\alpha_1}^F(x_3, x_1) S_{\beta_2\alpha_2}^F(x_2, x_2) : \Psi_{\beta_1}(x_1) \bar{\Psi}_{\alpha_3}(x_3) : + \hbar^2 S_{\beta_3\alpha_1}^F(x_3, x_1) S_{\beta_2\alpha_3}^F(x_2, x_3) : \Psi_{\beta_1}(x_1) \bar{\Psi}_{\alpha_2}(x_2) : \\
& - \hbar^2 S_{\beta_1\alpha_2}^F(x_1, x_2) S_{\beta_2\alpha_3}^F(x_2, x_3) : \bar{\Psi}_{\alpha_1}(x_1) \Psi_{\beta_3}(x_3) : + \hbar^2 S_{\beta_1\alpha_2}^F(x_1, x_2) S_{\beta_3\alpha_3}^F(x_3, x_3) : \bar{\Psi}_{\alpha_1}(x_1) \Psi_{\beta_2}(x_2) : \\
& + \hbar^2 S_{\beta_1\alpha_3}^F(x_1, x_3) S_{\beta_2\alpha_2}^F(x_2, x_2) : \bar{\Psi}_{\alpha_1}(x_1) \Psi_{\beta_3}(x_3) : - \hbar^2 S_{\beta_1\alpha_3}^F(x_1, x_3) S_{\beta_3\alpha_2}^F(x_3, x_2) : \bar{\Psi}_{\alpha_1}(x_1) \Psi_{\beta_2}(x_2) : \\
& - \hbar^2 S_{\beta_2\alpha_2}^F(x_2, x_2) S_{\beta_3\alpha_3}^F(x_3, x_3) : \bar{\Psi}_{\alpha_1}(x_1) \Psi_{\beta_1}(x_1) : + \hbar^2 S_{\beta_3\alpha_2}^F(x_3, x_2) S_{\beta_2\alpha_3}^F(x_2, x_3) : \bar{\Psi}_{\alpha_1}(x_1) \Psi_{\beta_1}(x_1) : \\
& + i\hbar^3 S_{\beta_1\alpha_1}^F(x_1, x_1) S_{\beta_2\alpha_2}^F(x_2, x_2) S_{\beta_3\alpha_3}^F(x_3, x_3) - i\hbar^3 S_{\beta_1\alpha_1}^F(x_1, x_1) S_{\beta_3\alpha_2}^F(x_3, x_2) S_{\beta_2\alpha_3}^F(x_2, x_3) \\
& - i\hbar^3 S_{\beta_2\alpha_1}^F(x_2, x_1) S_{\beta_1\alpha_2}^F(x_1, x_2) S_{\beta_3\alpha_3}^F(x_3, x_3) + i\hbar^3 S_{\beta_2\alpha_1}^F(x_2, x_1) S_{\beta_1\alpha_3}^F(x_1, x_3) S_{\beta_3\alpha_2}^F(x_3, x_2) \\
& + i\hbar^3 S_{\beta_3\alpha_1}^F(x_3, x_1) S_{\beta_1\alpha_2}^F(x_1, x_2) S_{\beta_2\alpha_3}^F(x_2, x_3) - i\hbar^3 S_{\beta_3\alpha_1}^F(x_3, x_1) S_{\beta_1\alpha_3}^F(x_1, x_3) S_{\beta_2\alpha_2}^F(x_2, x_2).
\end{aligned}
\tag{G.1.13}$$

G.2 Photon field products

Using Wick's theorem, we expand the time-ordered product of the first few products of photon field operators. We then use the fact that the contraction of two field operators gives a photon propagator:

$$\overline{A_\mu(x_1) A_\nu(x_2)} = \langle 0 | A_\mu(x_1) A_\nu(x_2) | 0 \rangle = i\hbar D_{\mu\nu}^F(x_1, x_2). \quad (\text{G.2.1})$$

This relation is discussed in section 3.8.3.

G.2.1 First-order

$$\text{T}[A_\mu(x)] = : A_\mu(x) : = A_\mu(x). \quad (\text{G.2.2})$$

G.2.2 Second-order

$$\begin{aligned} \text{T}[A_\mu(x_1) A_\nu(x_2)] &= : A_\mu(x_1) A_\nu(x_2) : + \overline{A_\mu(x_1) A_\nu(x_2)} \\ &= : A_\mu(x_1) A_\nu(x_2) : + i\hbar D_{\mu\nu}^F(x_1, x_2). \end{aligned} \quad (\text{G.2.3})$$

G.2.3 Third-order

$$\begin{aligned} \text{T}[A_\mu(x_1) A_\nu(x_2) A_\sigma(x_3)] &= : A_\mu(x_1) A_\nu(x_2) A_\sigma(x_3) : + \overline{A_\mu(x_1) A_\nu(x_2)} A_\sigma(x_3) : \\ &\quad : \overline{A_\mu(x_1) A_\sigma(x_3)} A_\nu(x_2) : + : A_\mu(x_1) \overline{A_\nu(x_2) A_\sigma(x_3)} : \end{aligned} \quad (\text{G.2.4})$$

$$\begin{aligned} &= : A_\mu(x_1) A_\nu(x_2) A_\sigma(x_3) : + i\hbar D_{\mu\nu}^F(x_1, x_2) : A_\sigma(x_3) : \\ &\quad + i\hbar D_{\mu\sigma}^F(x_1, x_3) : A_\nu(x_2) : + i\hbar D_{\nu\sigma}^F(x_2, x_3) : A_\mu(x_1) : \end{aligned} \quad (\text{G.2.5})$$

G.2.4 Fourth-order

$$\begin{aligned} \text{T}[A_\mu(x_1) A_\nu(x_2) A_\sigma(x_3) A_\theta(x_4)] &= : A_\mu(x_1) A_\nu(x_2) A_\sigma(x_3) A_\theta(x_4) : \\ &\quad + \overline{A_\mu(x_1) A_\nu(x_2)} A_\sigma(x_3) A_\theta(x_4) : \\ &\quad + \overline{A_\mu(x_1) A_\sigma(x_3)} A_\nu(x_2) A_\theta(x_4) : \\ &\quad + \overline{A_\mu(x_1) A_\theta(x_4)} A_\nu(x_2) A_\sigma(x_3) : \\ &\quad + : A_\mu(x_1) \overline{A_\nu(x_2) A_\sigma(x_3)} A_\theta(x_4) : \\ &\quad + : A_\mu(x_1) \overline{A_\nu(x_2) A_\theta(x_4)} A_\sigma(x_3) : \\ &\quad + : A_\mu(x_1) A_\nu(x_2) \overline{A_\sigma(x_3) A_\theta(x_4)} : \\ &\quad + \overline{A_\mu(x_1) A_\nu(x_2)} \overline{A_\sigma(x_3) A_\theta(x_4)} : \\ &\quad + \overline{A_\mu(x_1) A_\sigma(x_3)} \overline{A_\nu(x_2) A_\theta(x_4)} : \\ &\quad + \overline{A_\mu(x_1) A_\theta(x_4)} \overline{A_\nu(x_2) A_\sigma(x_3)} : \\ &\quad + : A_\mu(x_1) A_\nu(x_2) A_\sigma(x_3) \overline{A_\theta(x_4)} : \\ &\quad + : A_\mu(x_1) A_\nu(x_2) \overline{A_\sigma(x_3) A_\theta(x_4)} : \\ &\quad + : A_\mu(x_1) \overline{A_\nu(x_2) A_\sigma(x_3)} A_\theta(x_4) : \\ &\quad + : A_\mu(x_1) \overline{A_\nu(x_2) A_\theta(x_4)} A_\sigma(x_3) : \\ &\quad + : A_\mu(x_1) A_\nu(x_2) \overline{A_\sigma(x_3) A_\theta(x_4)} : \\ &\quad + : A_\mu(x_1) \overline{A_\nu(x_2) A_\sigma(x_3) A_\theta(x_4)} : \end{aligned} \quad (\text{G.2.6})$$

The final result is found to be:

$$\begin{aligned}
T[A_\mu(x_1) A_\nu(x_2) A_\sigma(x_3) A_\theta(x_4)] = & T[A_\mu(x_1) A_\nu(x_2) A_\sigma(x_3) A_\theta(x_4)] : \\
& + i\hbar D_{\mu\nu}^F(x_1, x_2) : A_\sigma(x_3) A_\theta(x_4) : \\
& + i\hbar D_{\mu\nu}^F(x_1, x_3) : A_\nu(x_2) A_\theta(x_4) : \\
& + i\hbar D_{\mu\theta}^F(x_1, x_4) : A_\nu(x_2) A_\sigma(x_3) : \\
& + i\hbar D_{\nu\sigma}^F(x_2, x_3) : A_\mu(x_1) A_\theta(x_4) : \\
& + i\hbar D_{\nu\theta}^F(x_2, x_4) : A_\mu(x_1) A_\sigma(x_3) : \\
& + i\hbar D_{\sigma\theta}^F(x_3, x_4) : A_\mu(x_1) A_\nu(x_2) : \\
& - \hbar^2 D_{\mu\nu}^F(x_1, x_2) D_{\sigma\theta}^F(x_3, x_4) \\
& - \hbar^2 D_{\mu\sigma}^F(x_1, x_3) D_{\nu\theta}^F(x_2, x_4) \\
& - \hbar^2 D_{\mu\theta}^F(x_1, x_4) D_{\nu\sigma}^F(x_2, x_3).
\end{aligned} \tag{G.2.7}$$

G.2.5 Fifth-order

In the case of five photon field operators, the possible contractions are presented in table G.2, and Wick's theorem allows us to write:

$$\begin{aligned}
T[A_\mu(x_1) A_\nu(x_2) A_\sigma(x_3) A_\theta(x_4) A_\gamma(x_5)] \\
= & A_\mu(x_1) A_\nu(x_2) A_\sigma(x_3) A_\theta(x_4) A_\gamma(x_5) : \\
& + i\hbar D_{\mu\nu}^F(x_1, x_2) : A_\sigma(x_3) A_\theta(x_4) A_\gamma(x_5) : + i\hbar D_{\mu\sigma}^F(x_1, x_3) : A_\nu(x_2) A_\theta(x_4) A_\gamma(x_5) : \\
& + i\hbar D_{\mu\theta}^F(x_1, x_4) : A_\nu(x_2) A_\sigma(x_3) A_\gamma(x_5) : + i\hbar D_{\mu\gamma}^F(x_1, x_5) : A_\nu(x_2) A_\sigma(x_3) A_\theta(x_4) : \\
& + i\hbar D_{\nu\sigma}^F(x_2, x_3) : A_\mu(x_1) A_\theta(x_4) A_\gamma(x_5) : + i\hbar D_{\nu\theta}^F(x_2, x_4) : A_\mu(x_1) A_\sigma(x_3) A_\gamma(x_5) : \\
& + i\hbar D_{\nu\gamma}^F(x_2, x_5) : A_\mu(x_1) A_\sigma(x_3) A_\theta(x_4) : + i\hbar D_{\sigma\theta}^F(x_3, x_4) : A_\mu(x_1) A_\nu(x_2) A_\gamma(x_5) : \\
& + i\hbar D_{\sigma\gamma}^F(x_3, x_5) : A_\mu(x_1) A_\nu(x_2) A_\theta(x_4) : + i\hbar D_{\theta\gamma}^F(x_4, x_5) : A_\mu(x_1) A_\nu(x_2) A_\sigma(x_3) : \tag{G.2.8} \\
& - \hbar^2 D_{\mu\nu}^F(x_1, x_2) D_{\sigma\theta}^F(x_3, x_4) : A_\gamma(x_5) : - \hbar^2 D_{\mu\nu}^F(x_1, x_2) D_{\sigma\gamma}^F(x_3, x_5) : A_\theta(x_4) : \\
& - \hbar^2 D_{\mu\nu}^F(x_1, x_2) D_{\theta\gamma}^F(x_4, x_5) : A_\sigma(x_3) : - \hbar^2 D_{\mu\sigma}^F(x_1, x_3) D_{\nu\theta}^F(x_2, x_4) : A_\gamma(x_5) : \\
& - \hbar^2 D_{\mu\sigma}^F(x_1, x_3) D_{\nu\gamma}^F(x_2, x_5) : A_\theta(x_4) : - \hbar^2 D_{\mu\sigma}^F(x_1, x_3) D_{\theta\gamma}^F(x_4, x_5) : A_\nu(x_2) : \\
& - \hbar^2 D_{\mu\theta}^F(x_1, x_4) D_{\nu\sigma}^F(x_2, x_3) : A_\gamma(x_5) : - \hbar^2 D_{\mu\theta}^F(x_1, x_4) D_{\nu\gamma}^F(x_2, x_5) : A_\sigma(x_3) : \\
& - \hbar^2 D_{\mu\theta}^F(x_1, x_4) D_{\sigma\gamma}^F(x_3, x_5) : A_\nu(x_2) : - \hbar^2 D_{\mu\gamma}^F(x_1, x_5) D_{\nu\sigma}^F(x_2, x_3) : A_\theta(x_4) : \\
& - \hbar^2 D_{\mu\gamma}^F(x_1, x_5) D_{\nu\theta}^F(x_2, x_4) : A_\sigma(x_3) : - \hbar^2 D_{\mu\gamma}^F(x_1, x_5) D_{\sigma\theta}^F(x_3, x_4) : A_\nu(x_2) :
\end{aligned}$$

Appendix H

Fourier transforms

H.1 Definitions

The four-dimensional Fourier-transform of a function $F(x)$ and its inverse are given by:

$$F(p) = \int d^4x e^{+\frac{i}{\hbar} p \cdot x} F(x) \quad (\text{H.1.1})$$

$$F(x) = \int \frac{d^4p}{(2\pi\hbar)^4} e^{-\frac{i}{\hbar} p \cdot x} F(p). \quad (\text{H.1.2})$$

One can easily check whether the constant factors are right or not by simply going in and out the Fourier space, i.e. by writing:

$$F(p) = \int d^4x e^{+\frac{i}{\hbar} p \cdot x} F(x) = \int \frac{d^4q}{(2\pi\hbar)^4} F(q) \int d^4x e^{+\frac{i}{\hbar} (p-q) \cdot x} \quad (\text{H.1.3})$$

$$= \int d^4q F(q) \delta(p-q) = F(p). \quad (\text{H.1.4})$$

When the functions that need to be manipulated with these transforms are three-dimensional, i.e. dependent on the bold \mathbf{x} instead of x , one has:

$$F(\mathbf{p}) = \int d^3x e^{-\frac{i}{\hbar} \mathbf{p} \cdot \mathbf{x}} F(\mathbf{x}) \quad (\text{H.1.5})$$

$$F(\mathbf{x}) = \int \frac{d^3p}{(2\pi\hbar)^3} e^{+\frac{i}{\hbar} \mathbf{p} \cdot \mathbf{x}} F(\mathbf{p}). \quad (\text{H.1.6})$$

We shall see that for a time-independent function $F(x) = F(\mathbf{x})$, a Dirac function appears for the time-component momentum (in momentum space). Equation (H.1.1) becomes in this case:

$$F(p) = \int d^4x e^{+\frac{i}{\hbar} p \cdot x} F(x) = \int d^3x e^{+\frac{i}{\hbar} \mathbf{p} \cdot \mathbf{x}} F(\mathbf{x}) \int dx_0 e^{+\frac{i}{\hbar} p_0 x_0}, \quad (\text{H.1.7})$$

using the result of eq. (H.2.2) and eq. (H.1.5):

$$F(p) = 2\pi\hbar \delta(p_0) F(\mathbf{p}). \quad (\text{H.1.8})$$

H.2 Dirac δ distribution

The inverse Fourier transform of the Dirac δ function is given by:

$$\int d^4x e^{+\frac{i}{\hbar}p \cdot x} \delta(x) = e^0 = 1, \quad (\text{H.2.1})$$

and thus one can write the Dirac function as given by the inverse Fourier of eq.(H.1.2):

$$\delta(x) = \int \frac{d^4p}{(2\pi\hbar)^4} e^{-\frac{i}{\hbar}p \cdot x} 1. \quad (\text{H.2.2})$$

H.3 Derivative transformation

The inverse Fourier transform of the four-gradient function, is given by:

$$\int d^4x e^{+\frac{i}{\hbar}p \cdot x} \left\{ \frac{\partial}{\partial x^\mu} \psi_n(x) \right\} = -\frac{i}{\hbar} p_\mu \psi_n(p). \quad (\text{H.3.1})$$

This can be seen by writing $\psi_n(x)$ as an inverse Fourier-transform eq.(H.1.2), and letting the gradient act on the Fourier exponent:

$$\int d^4x e^{+\frac{i}{\hbar}p \cdot x} \frac{\partial}{\partial x^\mu} \psi_n(x) = \int d^4x e^{+\frac{i}{\hbar}p \cdot x} \frac{\partial}{\partial x^\mu} \left\{ \int \frac{d^4q}{(2\pi\hbar)^4} e^{-\frac{i}{\hbar}q \cdot x} \psi_n(q) \right\} \quad (\text{H.3.2})$$

$$= -\frac{i}{\hbar} \int \frac{d^4q}{(2\pi\hbar)^4} q_\mu \psi_n(q) \int d^4x e^{+\frac{i}{\hbar}(p-q) \cdot x}. \quad (\text{H.3.3})$$

The x integral is first evaluated using eq.(H.2.2):

$$\int d^4x e^{+\frac{i}{\hbar}p \cdot x} \frac{\partial}{\partial x^\mu} \psi_n(x) = -\frac{i}{\hbar} \int d^4q q_\mu \psi_n(q) \delta(p-q) \quad (\text{H.3.4})$$

$$= -\frac{i}{\hbar} p_\mu \psi_n(p). \quad (\text{H.3.5})$$

Alternatively, one can chose to work in momentum space, and then get:

$$\int \frac{d^4p}{(2\pi\hbar)^4} e^{-\frac{i}{\hbar}p \cdot x} \left\{ \frac{\partial}{\partial p^\mu} \psi_n(p) \right\} = +\frac{i}{\hbar} x_\mu \psi_n(x). \quad (\text{H.3.6})$$

H.4 Product transformation

Having a product of functions $\psi_n(x)$ and $\psi_m(x)$, it transforms as:

$$\int d^4x e^{+\frac{i}{\hbar}p \cdot x} \{\psi_n(x) \psi_m(x)\} = \int \frac{d^4q}{(2\pi\hbar)^4} \psi_n(q) \psi_m(p-q), \quad (\text{H.4.1})$$

known as the convolution theorem, stating that a product in real space, is a convolution of the transformed functions in momentum space. Alternatively, in momentum-space, we have:

$$\int \frac{d^4p}{(2\pi\hbar)^4} e^{-\frac{i}{\hbar}p \cdot x} \{\psi_n(p) \psi_m(p)\} = \int d^4y \psi_m(y) \psi_n(x-y), \quad (\text{H.4.2})$$

where the product of functions in momentum space, is a convolution of the real-space functions.

H.5 Locality in real- and momentum-space

A local operator \hat{H} in real-space, becomes a non-local operator in momentum-space, and vice versa. This can be clearly seen by evaluating the Fourier transforms of the terms inside the expectation values of a:

1. Local potential:

$$\int d^3x \varphi_n^\dagger(\mathbf{x}) \hat{H}(\mathbf{x}) \varphi_n(\mathbf{x}) = \int \frac{d^3q}{(2\pi\hbar)^3} \int \frac{d^3p}{(2\pi\hbar)^3} \varphi_n^\dagger(\mathbf{q}) \hat{H}(\mathbf{q} - \mathbf{p}) \varphi_n(\mathbf{p}). \quad (\text{H.5.1})$$

2. Non-local potential:

$$\int d^3x \int d^3y \varphi_n^\dagger(\mathbf{y}) \hat{H}(\mathbf{y} - \mathbf{x}) \varphi_n(\mathbf{x}) = \int \frac{d^3p}{(2\pi\hbar)^3} \varphi_n^\dagger(\mathbf{p}) \hat{H}(\mathbf{p}) \varphi_n(\mathbf{p}). \quad (\text{H.5.2})$$

H.6 Dirac equation in Fourier-space

In the presence of an external electromagnetic potential, the Dirac equation reads eq.(2.6.24):

$$[\gamma^\mu (i\hbar\partial_\mu + eA_\mu(x)) - mc] \psi_n(x) = 0. \quad (\text{H.6.1})$$

After Fourier-transforming it, one obtains:

$$\int d^4x e^{+\frac{i}{\hbar}p \cdot x} [\gamma^\mu (i\hbar\partial_\mu + eA_\mu(x)) - mc] \psi_n(x) = 0, \quad (\text{H.6.2})$$

We now use the derivative transformation of eq.(H.3.1) with the convolution eq.(H.4.1) to obtain:

$$\gamma^\mu [p_\mu \psi_n(p) + e \int \frac{d^4q}{(2\pi\hbar)^4} A_\mu(p - q) \psi_n(q)] - mc \psi_n(p) = 0. \quad (\text{H.6.3})$$

Notice that the local external potential $A_\mu(x)$, becomes (in Fourier-space) non-local, as seen in section H.5. In the absence of this potential, the equation simplifies to:

$$(\gamma^\mu p_\mu - mc) \psi_n(p) = 0. \quad (\text{H.6.4})$$

Appendix I

Integrals

I.1 Time-integral and $\Delta_\epsilon(a)$

The goal of this section is to evaluate the integral:

$$I(\epsilon, a) = \int_{-\infty}^{+\infty} dx e^{-\epsilon|x|+iax}, \quad (\text{I.1.1})$$

where ϵ is a positive real number, while a is simply a real number. First we split the integral into two parts:

$$I(\epsilon, a) = \int_{-\infty}^0 dx e^{+\epsilon x+iax} + \int_0^{+\infty} dx e^{-\epsilon x+iax}. \quad (\text{I.1.2})$$

After performing the change of variables $x \rightarrow -x$ for the first integral, and swapping the integration direction, the two integrals can be combined into a single one:

$$I(\epsilon, a) = 2 \int_0^{+\infty} dx e^{-\epsilon x} \cos ax. \quad (\text{I.1.3})$$

We then use integration by parts:

$$I(\epsilon, a) = 2e^{-\epsilon x} \frac{\sin(ax)}{a} \Big|_0^{+\infty} + 2\frac{\epsilon}{a} \int_0^{+\infty} dx e^{-\epsilon x} \sin(ax) \quad (\text{I.1.4})$$

$$= \frac{2\epsilon}{a} \int_0^{+\infty} dx e^{-\epsilon x} \sin(ax). \quad (\text{I.1.5})$$

Again, we perform a second integration by parts:

$$I(\epsilon, a) = -\frac{2\epsilon}{a^2} \cos(ax) e^{-\epsilon x} \Big|_0^{+\infty} - 2\frac{\epsilon^2}{a^2} \int_0^{+\infty} dx \cos(ax) e^{-\epsilon x} \quad (\text{I.1.6})$$

$$= -\frac{2\epsilon}{a^2} - \frac{2\epsilon^2}{a^2} \int_0^{+\infty} dx \cos(ax) e^{-\epsilon x}. \quad (\text{I.1.7})$$

Notice that the last integral is the one we already started with. This allows us to write:

$$I(\epsilon, a) = \frac{2\epsilon}{a^2 + \epsilon^2}. \quad (\text{I.1.8})$$

Following [15, section A.3], we define the function $\Delta_\epsilon(a)$ as:

$$\Delta_\epsilon(a) = \frac{I(\epsilon, a)}{2\pi} = \frac{1}{\pi} \frac{\epsilon}{a^2 + \epsilon^2}. \quad (\text{I.1.9})$$

In the limit $\epsilon \rightarrow 0$, this function becomes a Dirac delta function. To see how this is true, we observe that in this limit, we have:

$$\lim_{\epsilon \rightarrow 0} \Delta_\epsilon(a) = \begin{cases} 0 & \text{for } a \neq 0 \\ \text{diverges} & \text{for } a = 0 \end{cases} \quad (\text{I.1.10})$$

In addition, this function integrates to one:

$$\int_{-\infty}^{+\infty} dx \Delta_\epsilon(x) = \frac{1}{\pi} \int_{-\infty}^{+\infty} du \frac{1}{u^2 + 1} = \frac{1}{\pi} \arctan(u) \Big|_{-\infty}^{+\infty} = 1, \quad (\text{I.1.11})$$

where we used the change of variables $u = \frac{x}{\epsilon}$. This allows us to write:

$$\lim_{\epsilon \rightarrow 0} \Delta_\epsilon(a) = \delta(a). \quad (\text{I.1.12})$$

This delta function can also be related to the Kronecker delta function:

$$\lim_{\epsilon \rightarrow 0} \pi \epsilon \Delta_\epsilon(a) = \lim_{\epsilon \rightarrow 0} \frac{\epsilon^2}{a^2 + \epsilon^2} = \begin{cases} 1 & \text{if } a = 0 \\ 0 & \text{if } a \neq 0 \end{cases} = \delta_{a,0}, \quad (\text{I.1.13})$$

which is going to be used while evaluating the QED energy-shifts using Sucher's formula. In addition, we are going to use the following relation:

$$\int dx \frac{1}{x^2 - c^2 + i\eta} \Delta_\epsilon(a - x) \Delta_\epsilon(b - x) \approx \frac{1}{a^2 - c^2 + i\epsilon} \Delta_{2\epsilon}(a - b), \quad (\text{I.1.14})$$

given by Lindgren [15, eq.(A.32)], when evaluating the timelike component momentum integral of the photon propagator. In this expression, η and ϵ are small positive numbers, and the approximation symbol is there to indicate that this relation holds for small ϵ . This should cause no problem, since at the end we shall evaluate energy-shifts which includes a limit $\epsilon \rightarrow 0$.

I.2 Angular Fourier integral

When evaluating the inverse Fourier transform of a radial function (in momentum space), an angular integral appears after separation of variables:

$$\int \frac{d^3q}{(2\pi)^3} e^{i\mathbf{q} \cdot \mathbf{x}} f(|\mathbf{q}|) = \int_0^\infty \frac{r_q^2 dr_q}{(2\pi)^3} f(r_q) \int d\Omega e^{+ir_q r_x \cos \theta}, \quad (\text{I.2.1})$$

where we use spherical coordinates by writing the Jacobian (determinant) as:

$$d^3q = r_q^2 dr_q \sin \theta d\theta d\varphi, \quad (\text{I.2.2})$$

where we use $r_z = |\mathbf{z}|$ as a radial distance associated with some three-vector \mathbf{z} , and assume (without any loss of generality) that the “z-axis” of this spherical coordinate system points in the direction

of the position vector \mathbf{x} in order to simplify our exponent. Our focus is going to be on the angular integral, we shall call $I(r_q, r_x)$:

$$I(r_x, r_q) = \int d\Omega e^{+ir_q r_x \cos \theta} = 2\pi \int_0^\pi \sin \theta d\theta e^{+ir_q r_x \cos \theta}. \quad (\text{I.2.3})$$

Using the change of variables $u = ir_q r_x \cos \theta$, we can write it as:

$$I(r_x, r_q) = \frac{2\pi i}{r_q r_x} \int_{+ir_q r_x}^{-ir_q r_x} du e^u = \frac{4\pi}{r_q r_x} \sin(r_q r_x). \quad (\text{I.2.4})$$

This finally allows us to write the inverse Fourier transform of a radial function (Fourier space) as a radial function (real space):

$$\int \frac{d^3 q}{(2\pi)^3} e^{+i\mathbf{q} \cdot \mathbf{x}} f(r_q) = \frac{1}{2\pi^2 r_x} \int_0^\infty r_q dr_q f(r_q) \sin(r_q r_x). \quad (\text{I.2.5})$$

I.3 Radial photon function

When evaluating the The inverse Fourier transform of the photon propagator, the spatial integral we shall call $I(q_0, \mathbf{x})$, reads:

$$I(q_0, \mathbf{x}) = \int \frac{d^3 q}{(2\pi)^3} \frac{e^{+i\mathbf{q} \cdot \mathbf{x}}}{q_0^2 - \mathbf{q}^2 + i\epsilon}. \quad (\text{I.3.1})$$

Using the result of the previous section, we can write this integral as:

$$I(q_0, \mathbf{x}) = \frac{1}{4\pi^2 i r_x} \int_0^\infty r_q dr_q \frac{e^{+ir_q r_x} - e^{-ir_q r_x}}{q_0^2 - r_q^2 + i\epsilon}. \quad (\text{I.3.2})$$

We now extend the integration limits to span the whole real line (as done in [105, page 303].), so we can use Jordan's lemma result. In order to do so, we perform a change of variables in the second integral: $r_q \rightarrow -r_q$ which allows us to write:

$$I(q_0, \mathbf{x}) = \frac{1}{4\pi^2 i r_x} \int_{-\infty}^{+\infty} r_q dr_q \frac{e^{+ir_q r_x}}{q_0^2 - r_q^2 + i\epsilon}, \quad (\text{I.3.3})$$

since r_x is always positive, we can use Jordan's lemma, for positive exponential factor, given in F.5.3, and write:

$$I(q_0, \mathbf{x}) = \frac{1}{4\pi^2 i r_x} \oint^+ r_q dr_q \frac{e^{+ir_q r_x}}{q_0^2 - r_q^2 + i\epsilon}, \quad (\text{I.3.4})$$

where \oint^+ indicates that the contour integral encloses poles in the upper half-plane, which in this case, is the single pole at $r_q = \sqrt{q_0^2 + i\epsilon}$, using Cauchy's integral formula, we directly obtain the following result:

$$\int \frac{d^3 q}{(2\pi)^3} \frac{e^{+i\mathbf{q} \cdot \mathbf{x}}}{q_0^2 - \mathbf{q}^2 + i\epsilon} = -\frac{e^{+i\sqrt{q_0^2 + i\epsilon}|\mathbf{x}|}}{4\pi |\mathbf{x}|}. \quad (\text{I.3.5})$$

Note that for real q_0 , this result reduces to:

$$\int \frac{d^3 q}{(2\pi)^3} \frac{e^{+i\mathbf{q} \cdot \mathbf{x}}}{q_0^2 - \mathbf{q}^2 + i\epsilon} = -\frac{e^{+i|q_0||\mathbf{x}|}}{4\pi |\mathbf{x}|}. \quad (\text{I.3.6})$$

For general complex number q_0 , the square root gives:

$$\sqrt{q_0^2} = \pm q_0, \quad (\text{I.3.7})$$

which comes from the fact that for fractional powers, complex numbers become multi-valued, and a full circular rotation about the associated branch point ($q_0 = 0$ in this case) leads to different complex number, which shows the presence of a discontinuity.

Appendix J

Quantum mechanical equations and currents

J.1 Free and interacting equations

In their free forms, the quantum mechanical equations are given by:

$$\begin{aligned} i\hbar \frac{\partial}{\partial t} \psi &= -\frac{\hbar^2}{2m} \nabla^2 \psi && \text{Schrödinger (1925)} \\ i\hbar \frac{\partial}{\partial t} \psi &= -\frac{\hbar^2}{2m} (\boldsymbol{\sigma} \cdot \nabla) (\boldsymbol{\sigma} \cdot \nabla) \psi && \text{Pauli (1927)} \\ 0 &= \left[\partial^\mu \partial_\mu + \frac{m^2 c^2}{\hbar^2} \right] \psi && \text{Klein-Gordon (1925 – 1926)} \\ 0 &= [i\hbar \gamma^\mu \partial_\mu - mc] \psi && \text{Dirac-equation (1928)} \end{aligned} \tag{J.1.1}$$

Using the Dirac relation of eq.(D.1.1) for Pauli matrices, one can clearly see that the free Pauli equation coincides with the free Schrödinger one, once some external electromagnetic potentials are turned on, this will no longer be the case. To obtain the interacting equations, we use the minimal coupling condition eq.(2.6.23):

$$i\hbar \partial_\mu \rightarrow i\hbar \partial_\mu + eA_\mu(x), \tag{J.1.2}$$

which splits into the following two substitutions (using eq.(A.0.5)):

$$i\hbar \frac{\partial}{\partial t} \rightarrow i\hbar \frac{\partial}{\partial t} + e\varphi(x) \tag{J.1.3}$$

$$-i\hbar \nabla \rightarrow -i\hbar \nabla + e\mathbf{A}(x), \tag{J.1.4}$$

which, in turn, leads to the following interacting equations:

$$\begin{aligned}
 i\hbar \frac{\partial}{\partial t} \psi &= \left[\frac{(-i\hbar \nabla + e\mathbf{A})^2}{2m} - e\varphi \right] \psi && \text{SE} \\
 i\hbar \frac{\partial}{\partial t} \psi &= \left[\frac{(-i\hbar \nabla + e\mathbf{A})^2}{2m} - e\varphi + \frac{e\hbar}{2m} \boldsymbol{\sigma} \cdot \mathbf{B} \right] \psi && \text{PE} \\
 0 &= \left[\left(\partial^\mu + \frac{e}{i\hbar} A^\mu(x) \right) \left(\partial_\mu + \frac{e}{i\hbar} A_\mu(x) \right) + \frac{m^2 c^2}{\hbar^2} \right] \psi && \text{KGE} \\
 0 &= [\gamma^\mu [i\hbar \partial_\mu + eA_\mu] - mc] \psi && \text{DE}
 \end{aligned} \tag{J.1.5}$$

where we use SE, PE, KGE, and DE for Schrödinger, Pauli, Klein-Gordon and Dirac equation. Few points to note about these equations:

1. An important thing to keep in mind is that the DE is a 4×4 equation, the Pauli one is a 2×2 equation, while SE and KGE are scalar equations, the corresponding solutions are therefore of four, two and one component functions, respectively.
2. The PE can be obtained from the SE by simply replacing the momentum operator [42, page 37 eqs.(9-4)]:

$$p^2 = -\hbar^2 \nabla^2 \rightarrow (i\hbar \nabla \cdot \boldsymbol{\sigma}) (i\hbar \nabla \cdot \boldsymbol{\sigma}), \tag{J.1.6}$$

and as mentioned before, this replacement makes a difference only in the case where EM potentials enters the equation, since in the absence of these potentials, the PE reduces to the SE, using the Dirac relation of eq.(D.1.1).

3. The difference between the Pauli and the Schrödinger equations is the presence of the term:

$$\frac{e\hbar}{2m} \boldsymbol{\sigma} \cdot \mathbf{B} = g\mu_B \mathbf{s} \cdot \mathbf{B}, \tag{J.1.7}$$

in the former equation. The corresponding elements of his last term are:

$$\begin{aligned}
 \mathbf{B} &= \nabla \times \mathbf{A} && \text{magnetic field} \\
 \mathbf{s} &= \frac{\boldsymbol{\sigma}}{2} && \text{spin operator} \\
 \mu_B &= \frac{e\hbar}{2m} && \text{Bohr magneton} \\
 g &= 2 && \text{electron g-factor}
 \end{aligned} \tag{J.1.8}$$

This extra term represents the interaction between the electron spin and the external magnetic field, and thus accounts for spin, which was missing in Schrödinger's theory. The motivation of Pauli in inventing his equation was to account for spin in the quantum theory by inventing the necessary algebra that can describe the electron's spin, or what he calls: "two-valuedness not describable classically" in his prominent Nobel prize lecture [45].

4. The DE is the most compact equation which accounts (naturally) for spin, and the fact that it is a matrix equation comes from the need for the gamma matrices to be matrices, so they can obey the anticommutation relations associated with their Clifford algebra, in order for the equation to be consistent with the relativistic KG equation, and thus obey the energy momentum relation.

5. In the non-relativistic limit:
 - (a) PE reduces to the SE since without relativity the magnetic field vanishes.
 - (b) The KGE reduces to the SE.
 - (c) The large component (two-component) DE spinor reduces to the PE solution.
6. Concerning the Dirac equation properties, the reader can consult chapters 1 and 2.

J.2 Probability currents

The probability currents associated with these quantum mechanical equations, i.e. that satisfy the continuity equation:

$$\partial_\mu j^\mu = 0; \quad \text{or} \quad \frac{\partial}{\partial t} \rho + \nabla \cdot \mathbf{j} = 0, \quad (\text{J.2.1})$$

are presented by the following equations:

$$\begin{aligned}
 \rho &= \psi^* \psi \\
 \mathbf{j} &= \frac{-i\hbar}{2m} (\psi^* \nabla \psi - \psi \nabla \psi^*) + \frac{e}{m} \mathbf{A} \psi^* \psi && \text{Schrödinger} \\
 \rho &= \psi^\dagger \psi \\
 \mathbf{j} &= \frac{-i\hbar}{2m} (\psi^\dagger \nabla \psi - \nabla (\psi^\dagger) \psi) + \frac{e}{m} \mathbf{A} \psi^\dagger \psi && \text{Pauli} \\
 j^\mu &= \frac{i\hbar}{2m} (\psi^* \partial^\mu \psi - \psi \partial^\mu \psi^*) + \frac{e}{m} A^\mu \psi^* \psi && \text{Klein-Gordon} \\
 j^\mu &= \frac{i\hbar}{2m} [\bar{\psi} \partial^\mu (\psi) - \partial^\mu (\bar{\psi}) \psi] + \frac{e}{m} A^\mu \bar{\psi} \psi + \frac{\hbar}{2m} \partial_\nu [\bar{\psi} \sigma^{\mu\nu} \psi] && \text{Dirac}
 \end{aligned} \quad (\text{J.2.2})$$

For interesting discussions about these quantum currents (mainly Pauli and Dirac ones), and how they relate to electron spin and thus its magnetic moment, the reader may consult [186] and [187] and their corresponding cited references.

Bibliography

- [1] D. Hanneke, S. Fogwell Hoogerheide, and G. Gabrielse. Cavity control of a single-electron quantum cyclotron: Measuring the electron magnetic moment. *Phys. Rev. A*, 83:052122, May 2011. doi:[10.1103/PhysRevA.83.052122](https://doi.org/10.1103/PhysRevA.83.052122).
- [2] Willis E. Lamb and Robert C. Retherford. Fine structure of the hydrogen atom by a microwave method. *Phys. Rev.*, 72:241–243, Aug 1947. URL: <https://link.aps.org/doi/10.1103/PhysRev.72.241>, doi:[10.1103/PhysRev.72.241](https://doi.org/10.1103/PhysRev.72.241).
- [3] W. H. Furry. On bound states and scattering in positron theory. *Phys. Rev.*, 81:115–124, Jan 1951. URL: <https://link.aps.org/doi/10.1103/PhysRev.81.115>, doi:[10.1103/PhysRev.81.115](https://doi.org/10.1103/PhysRev.81.115).
- [4] Silvan Samuel Schweber. *An Introduction to Relativistic Quantum Field Theory*. Dover Publications, 2011.
- [5] Paul Indelicato, Peter J. Mohr, and J. Sapirstein. Coordinate-space approach to vacuum polarization. *Phys. Rev. A*, 89:042121, Apr 2014. doi:[10.1103/PhysRevA.89.042121](https://doi.org/10.1103/PhysRevA.89.042121).
- [6] Gerhard Soff and Peter J. Mohr. Vacuum polarization in a strong external field. *Phys. Rev. A*, 38:5066–5075, Nov 1988. doi:[10.1103/PhysRevA.38.5066](https://doi.org/10.1103/PhysRevA.38.5066).
- [7] Peter J Mohr, Günter Plunien, and Gerhard Soff. QED corrections in heavy atoms. *Physics Reports*, 293(5-6):227–369, 1998. doi:[10.1016/S0370-1573\(97\)00046-X](https://doi.org/10.1016/S0370-1573(97)00046-X).
- [8] Walter Greiner and Joachim Reinhardt. *Quantum Electrodynamics*. Springer-Verlag Berlin Heidelberg, 4th edition, 2009. doi:[10.1007/978-3-540-87561-1](https://doi.org/10.1007/978-3-540-87561-1).
- [9] Gerhard Soff and Peter J. Mohr. Influence of vacuum-polarization corrections of order $\alpha(Z\alpha)$ and $\alpha(Z\alpha)^3$ in hydrogenlike uranium. *Phys. Rev. A*, 40:2174–2175, Aug 1989. doi:[10.1103/PhysRevA.40.2174](https://doi.org/10.1103/PhysRevA.40.2174).
- [10] K.-N. Huang. Calculation of the vacuum-polarization potential. *Phys. Rev. A*, 14:1311–1318, Oct 1976. doi:[10.1103/PhysRevA.14.1311](https://doi.org/10.1103/PhysRevA.14.1311).
- [11] J. Blomqvist. Vacuum polarization in exotic atoms. *Nuclear Physics*, 48:95–103, 1972. doi:[10.1016/0550-3213\(72\)90051-X](https://doi.org/10.1016/0550-3213(72)90051-X).
- [12] G. Soff, C. R. Hofmann, G. Plunien, and S. M. Schneider. *Quantum Electrodynamical Corrections in Highly Charged Ions*, pages 19–35. Springer US, Boston, MA, 1997. doi:[10.1007/978-1-4899-0081-4_2](https://doi.org/10.1007/978-1-4899-0081-4_2).

- [13] E. Borie and G. A. Rinker. The energy levels of muonic atoms. *Rev. Mod. Phys.*, 54:67–118, Jan 1982. doi:10.1103/RevModPhys.54.67.
- [14] T. Dubler, K. Kaeser, B. Robert-Tissot, L.A. Schaller, L. Schellenberg, and H. Schneuwly. Precision test of vacuum polarization in heavy muonic atoms. *Nuclear Physics A*, 294(3):397–416, 1978. doi:10.1016/0375-9474(78)90227-0.
- [15] Ingvar Lindgren. *Relativistic many-body theory: a new field-theoretical approach*, volume 63. Springer, 2nd edition, 2016. doi:10.1007/978-3-319-15386-5.
- [16] Paul Indelicato and Peter J. Mohr. *Introduction to Bound-State Quantum Electrodynamics*, pages 1–110. Springer, Berlin, Heidelberg, 2016. doi:10.1007/978-3-642-41611-8_36-1.
- [17] Peter J Mohr. Quantum electrodynamics calculations in few-electron systems. *Physica Scripta*, T46:44–51, jan 1993. doi:10.1088/0031-8949/1993/t46/005.
- [18] S. A. Blundell. Accurate screened QED calculations in high-Z many-electron ions. *Phys. Rev. A*, 46:3762–3775, Oct 1992. doi:10.1103/PhysRevA.46.3762.
- [19] Peter J. Mohr. Quantum electrodynamics of high-Z few-electron atoms. *Phys. Rev. A*, 32:1949–1957, Oct 1985. doi:10.1103/PhysRevA.32.1949.
- [20] Peter J. Mohr. *Status of Precision QED in Light and Heavy Atoms*, pages 17–41. Springer US, Boston, MA, 1987. doi:10.1007/978-1-4613-1889-7_2.
- [21] Maen Salman and Trond Saue. Charge Conjugation Symmetry in the Finite Basis Approximation of the Dirac Equation. *Symmetry*, 12, 2020. doi:10.3390/sym12071121.
- [22] Wolfram Research, Inc. Mathematica, Version 12.2. Champaign, IL, 2020.
- [23] Eite Tiesinga, Peter J Mohr, David B Newell, and Barry N Taylor. CODATA recommended values of the fundamental physical constants: 2018. *Journal of Physical and Chemical Reference Data*, 50(3):033105, 2021. doi:10.1063/5.0064853.
- [24] Adel Almoukhalalati, Stefan Knecht, Hans Jørgen Aa Jensen, Kenneth G Dyall, and Trond Saue. Electron correlation within the relativistic no-pair approximation. *The Journal of chemical physics*, 145(7):074104, 2016. doi:10.1063/1.4959452.
- [25] P. A. M. Dirac. The Evolution of the Physicist’s Picture of Nature. *Scientific American*, 208(5):45–53, 1963. URL: <http://www.jstor.org/stable/24936146>.
- [26] Walter Gordon. Der Comptoneffekt nach der Schrödingerschen theorie. *Zeitschrift für Physik*, 40(1-2):117–133, 1926. doi:10.1007/BF01390840.
- [27] Helge Kragh. Equation with the many fathers. The Klein–Gordon equation in 1926. *American Journal of Physics*, 52(11):1024–1033, 1984. doi:10.1119/1.13782.
- [28] Walter Greiner. *Relativistic quantum mechanics*. Springer, Berlin, Heidelberg, 3rd edition, 2000. doi:10.1007/978-3-662-04275-5.
- [29] Jagdish Mehra. *The golden age of theoretical physics*, volume 2. World Scientific, 2001.
- [30] Paul Adrien Maurice Dirac. The quantum theory of the electron. *Proceedings of the Royal Society of London. Series A*, 117(778):610–624, 1928. doi:10.1098/rspa.1928.0023.

- [31] O. Klein. Elektrodynamik und Wellenmechanik vom Standpunkt des Korrespondenzprinzips. *Zeitschrift für Physik A Hadrons and nuclei*, 41(6):407–442, Oct 1927. doi:10.1007/BF01400205.
- [32] Ian P. Grant. *Relativistic Quantum Theory of Atoms and Molecules*. Springer-Verlag New York, New York, 2007. doi:10.1007/978-0-387-35069-1.
- [33] Tommy Ohlsson. *Relativistic Quantum Physics: From Advanced Quantum Mechanics to Introductory Quantum Field Theory*. Cambridge University Press, 2011. doi:10.1017/CB09781139032681.
- [34] Paul Adrien Maurice Dirac. The physical interpretation of the quantum dynamics. *Proceedings of the Royal Society of London. Series A*, 113(765):621–641, 1927. doi:10.1098/rspa.1927.0012.
- [35] J. Mehra and H. Rechenberg. *The Historical Development of Quantum Theory*, volume 6. Springer-Verlag New York Berlin Heidelberg, 2000. URL: <https://link.springer.com/book/9780387952628>.
- [36] Silvan S Schweber. *QED and the men who made it: Dyson, Feynman, Schwinger, and Tomonaga*. Princeton University Press, 1994. URL: <https://press.princeton.edu/books/paperback/9780691033273/qed-and-the-men-who-made-it>.
- [37] Paul Adrien Maurice Dirac. *The principles of quantum mechanics*. Oxford university press, 4th edition, 1958. URL: <https://global.oup.com/academic/product/the-principles-of-quantum-mechanics-9780198520115?cc=fr&lang=en&>.
- [38] W. Greiner. *Quantum Mechanics: An Introduction*. Physics and Astronomy. Springer-Verlag Berlin Heidelberg, 4th edition, 2001. doi:10.1007/978-3-642-56826-8.
- [39] Franz Gross. *Relativistic quantum mechanics and field theory*. John Wiley & Sons, 2004. doi:10.1002/9783527617333.
- [40] James D. Bjorken and Sidney D. Drell. *Relativistic quantum mechanics*. Mcgraw-Hill, 1964.
- [41] W. Pauli. Contributions mathématiques à la théorie des matrices de Dirac. *Annales de l'institut Henri Poincaré*, 6(2):109–136, 1936. URL: <http://eudml.org/doc/78999>.
- [42] Richard P Feynman. *Quantum electrodynamics*. CRC Press, 1st edition, 1998. URL: <https://www.routledge.com/Quantum-Electrodynamics/Feynman/p/book/9780201360752>.
- [43] C. Itzykson and J.B. Zuber. *Quantum Field Theory*. Dover Books on Physics. Dover Publications, 1980. URL: <https://store.doverpublications.com/0486445682.html>.
- [44] Abraham Pais, Maurice Jacob, David I Olive, and Michael F Atiyah. *Paul Dirac: the man and his work*. Cambridge University Press, 2005/2003. URL: <https://www.cambridge.org/fr/academic/subjects/physics/history-philosophy-and-foundations-physics/paul-dirac-man-and-his-work?format=HB&isbn=9780521583824>.
- [45] Wolfgang Pauli. Exclusion Principle and Quantum Mechanics, 1946. URL: <https://www.nobelprize.org/prizes/physics/1945/pauli/lecture/>.
- [46] Franz Schwabl. *Advanced quantum mechanics*. Springer-Verlag Berlin Heidelberg, 4th edition, 2008. doi:10.1007/978-3-540-85062-5.

- [47] Paul Adrien Maurice Dirac. A theory of electrons and protons. *Proceedings of the Royal Society of London. Series A*, 126(801):360–365, 1930. doi:[10.1098/rspa.1930.0013](https://doi.org/10.1098/rspa.1930.0013).
- [48] Paul Adrien Maurice Dirac. Quantised singularities in the electromagnetic field. *Proceedings of the Royal Society of London. Series A*, 133(821):60–72, 1931. doi:[10.1098/rspa.1931.0130](https://doi.org/10.1098/rspa.1931.0130).
- [49] H. Weyl. *The Theory of Groups and Quantum Mechanics*. Dover Books on Mathematics. Dover Publications, 1950. Translated from the second (revised) German edition of 1931 by H. P. Robertson. URL: <https://store.doverpublications.com/0486602699.html>.
- [50] Carl D. Anderson. The Positive Electron. *Phys. Rev.*, 43:491–494, Mar 1933. doi:[10.1103/PhysRev.43.491](https://doi.org/10.1103/PhysRev.43.491).
- [51] Carl Anderson. *The Production and Properties of Positrons*. PA Norstedt & söner, 1936. Nobel lecture. URL: <https://www.nobelprize.org/prizes/physics/1936/anderson/lecture>.
- [52] R. P. Feynman. The Theory of Positrons. *Phys. Rev.*, 76:749–759, Sep 1949. doi:[10.1103/PhysRev.76.749](https://doi.org/10.1103/PhysRev.76.749).
- [53] Anthony Zee. *Quantum field theory in a nutshell*. Princeton university press, 2 edition, 2010.
- [54] S. Weinberg. *The Quantum Theory of Fields*, volume 2 of *The Quantum Theory of Fields 3 Volume Hardback Set*. Cambridge University Press, 1995. URL: <https://www.cambridge.org/core/books/quantum-theory-of-fields/22986119910BF6A2EFE42684801A3BDF>.
- [55] Murray Gell-Mann. The interpretation of the new particles as displaced charge multiplets. *Il Nuovo Cimento (1955-1965)*, 4(2):848–866, 1956. doi:[10.1007/BF02748000](https://doi.org/10.1007/BF02748000).
- [56] M.E. Rose. *Elementary Theory of Angular Momentum*. Dover books on physics and chemistry. Dover, 1995. URL: <https://books.google.fr/books?id=Fvf2KgcuzTkC>.
- [57] Paul Strange. *Relativistic Quantum Mechanics: With Applications in Condensed Matter and Atomic Physics*. Cambridge University Press, 1998. doi:[10.1017/CB09780511622755](https://doi.org/10.1017/CB09780511622755).
- [58] R A Swainson and G W F Drake. A unified treatment of the non-relativistic and relativistic hydrogen atom I: The wavefunctions. *Journal of Physics A: Mathematical and General*, 24(1):79–94, jan 1991. doi:[10.1088/0305-4470/24/1/019](https://doi.org/10.1088/0305-4470/24/1/019).
- [59] M.E. Rose. *Relativistic Electron Theory*. Wiley, 1961. URL: <https://books.google.fr/books?id=gh5RAAAAMAAJ>.
- [60] Milton Abramowitz and Irene A. Stegun, editors. *Handbook of Mathematical Functions with Formulas, Graphs, and Mathematical Tables*. National Bureau of Standards (became: National Institute of Standards and Technology), 10th printing edition, 1972.
- [61] Albert Messiah. *Quantum Mechanics: Two Volumes Bound as One*. Dover books on physics. Dover Publications, 1999.
- [62] Hendrik A. Kramers. The use of charge-conjugated wave-functions in the hole-theory of the electron. In *Proceedings of the Royal Academy of Amsterdam*, volume 40, pages 814–823, 1937. Available at <https://www.dwc.knaw.nl/DL/publications/PU00017118.pdf>.
- [63] Richard P Feynman. The reason for antiparticles. *Elementary particles and the laws of physics*, pages 1–59, 1986.

- [64] J. J. Sakurai and Jim Napolitano. *Modern Quantum Mechanics*. Cambridge University Press, 2nd edition, 2017. doi:10.1017/9781108499996.
- [65] S. P. Goldman. Variational representation of the Dirac-Coulomb Hamiltonian with no spurious roots. *Phys. Rev. A*, 31:3541–3549, Jun 1985. doi:10.1103/PhysRevA.31.3541.
- [66] II Tupitsyn and VM Shabaev. Spurious states of the Dirac equation in a finite basis set. *Optics and Spectroscopy*, 105(2):183–188, 2008. doi:10.1134/S0030400X08080043.
- [67] W.H.E. Schwarz and H. Wallmeier. Basis set expansions of relativistic molecular wave equations. *Molecular Physics*, 46(5):1045–1061, 1982. doi:10.1080/00268978200101771.
- [68] Ian P. Grant. Conditions for convergence of variational solutions of Dirac’s equation in a finite basis. *Phys. Rev. A*, 25:1230–1232, Feb 1982. doi:10.1103/PhysRevA.25.1230.
- [69] Werner Kutzelnigg. Completeness of a kinetically balanced Gaussian basis. *The Journal of chemical physics*, 126(20):201103, 2007. doi:10.1063/1.2744018.
- [70] Richard E Stanton and Stephen Havriliak. Kinetic balance: A partial solution to the problem of variational safety in Dirac calculations. *The Journal of chemical physics*, 81(4):1910–1918, 1984. doi:10.1063/1.447865.
- [71] Werner Kutzelnigg. Basis set expansion of the Dirac operator without variational collapse. *International Journal of Quantum Chemistry*, 25(1):107–129, 1984. doi:10.1002/QUA.560250112.
- [72] K G Dyall, I P Grant, and S Wilson. Matrix representation of operator products. *Journal of Physics B: Atomic and Molecular Physics*, 17(4):493–503, feb 1984. doi:10.1088/0022-3700/17/4/006.
- [73] Hasan Almannasreh. *The Dirac Equation: Numerical and Asymptotic Analysis*. PhD thesis, University of Gothenburg, 2012.
- [74] Pekka Pyykkö. Relativistic effects in structural chemistry. *Chemical Reviews*, 88(3):563–594, May 1988. doi:10.1021/cr00085a006.
- [75] L Visscher, PJC Aerts, O Visser, and WC Nieuwpoort. Kinetic balance in contracted basis sets for relativistic calculations. *International Journal of Quantum Chemistry*, 40(S25):131–139, 1991. doi:10.1002/qua.560400816.
- [76] Mathieu Lewin and Éric Séré. Spurious modes in Dirac calculations and how to avoid them. In *Many-electron approaches in physics, chemistry and mathematics*, pages 31–52. Springer, 2014. doi:10.1007/978-3-319-06379-9_2.
- [77] Mathieu Lewin and Éric Séré. Spectral pollution and how to avoid it. *Proceedings of the London Mathematical Society*, 100(3):864–900, 12 2009. doi:10.1112/plms/pdp046.
- [78] Maen Salman. Radial Dirac wavefunctions in the Coulombic hydrogen atom. <https://gitlab.com/maen.salman/radial-dirac-wavefunctions-in-the-coulombic-hydrogen-atom>, 2021.
- [79] David Hilbert. *On the infinite*, pages 183–201. Cambridge University Press, 2 edition, 1984. doi:10.1017/CB09781139171519.010.

- [80] Qiming Sun, Wenjian Liu, and Werner Kutzelnigg. Comparison of restricted, unrestricted, inverse, and dual kinetic balances for four-component relativistic calculations. *Theoretical Chemistry Accounts*, 129(3):423–436, 2011. doi:10.1007/s00214-010-0876-6.
- [81] Vladimir M. Shabaev, Ilya I. Tupitsyn, Vladimir A. Yerokhin, Günter Plunien, and G. Soff. Dual Kinetic Balance Approach to Basis-Set Expansions for the Dirac Equation. *Phys. Rev. Lett.*, 93:130405, Sep 2004. doi:10.1103/PhysRevLett.93.130405.
- [82] H.M. Quiney. The Dirac Equation in the Algebraic Approximation. In Stephen Wilson, editor, *Handbook of Molecular Physics and Quantum Chemistry*, chapter 22, pages 423–443. John Wiley & Sons, 2003.
- [83] Kenneth G. Dyall. A question of balance: Kinetic balance for electrons and positrons. *Chemical Physics*, 395:35–43, 2012. Recent Advances and Applications of Relativistic Quantum Chemistry. doi:10.1016/j.chemphys.2011.07.009.
- [84] R.P. Feynman. *QED: The Strange Theory of Light and Matter*. Princeton University Press, 2014. URL: <https://press.princeton.edu/books/paperback/9780691164090/qed>.
- [85] L.I. Schiff. *Quantum Mechanics*. McGraw-Hill Education, 3th edition, 1968.
- [86] Claude Cohen-Tannoudji, Bernard Diu, and Franck Laloe. *Quantum Mechanics: Volume I: Basic Concepts, Tools, and Applications*, volume 1. Wiley-VCH, 2nd edition, 2020. Translated from French by Susan Reid Hemley, Nicole Ostrowsky, and Dan Ostrowsky. URL: <https://www.wiley.com/en-us/Quantum+Mechanics%2C+Volume+1%3A+Basic+Concepts%2C+Tools%2C+and+Applications%2C+2nd+Edition-p-9783527822713>.
- [87] A.L. Fetter and J.D. Walecka. *Quantum Theory of Many-Particle Systems*. Dover Books on Physics. Dover Publications, 2012. URL: <https://store.doverpublications.com/0486428273.html>.
- [88] F. J. Dyson. The Radiation Theories of Tomonaga, Schwinger, and Feynman. *Phys. Rev.*, 75:486–502, Feb 1949. doi:10.1103/PhysRev.75.486.
- [89] Walter Greiner and Joachim Reinhardt. *Field Quantization*. Springer-Verlag Berlin Heidelberg, 1996. doi:10.1007/978-3-642-61485-9.
- [90] Claude Cohen-Tannoudji, Bernard Diu, and Franck Laloë. *Quantum Mechanics, Volume III: Fermions, Bosons, Photons, Correlations, and Entanglement*, volume 3. Wiley-VCH, 2nd edition, 2020. URL: <https://www.wiley.com/en-aw/Quantum+Mechanics%2C+Volume+3%3A+Fermions%2C+Bosons%2C+Photons%2C+Correlations%2C+and+Entanglement-p-9783527822751>.
- [91] Leonti N. Labzowsky, Galina L. Klimchitskaya, and Yu. Yu. Dmitriev. *Relativistic effects in the spectra of atomic systems*. IOP Publishing Press, 1993.
- [92] Steven Weinberg. *The Quantum Theory of Fields*, volume 1. Cambridge University Press, 1995. doi:10.1017/CB09781139644167.
- [93] Franz Mandl and Graham Shaw. *Quantum field theory*. John Wiley & Sons, 2010.
- [94] B. A. Lippmann and Julian Schwinger. Variational Principles for Scattering Processes. I. *Phys. Rev.*, 79:469–480, Aug 1950. doi:10.1103/PhysRev.79.469.

- [95] G. C. Wick. The evaluation of the collision matrix. *Phys. Rev.*, 80:268–272, Oct 1950. doi:[10.1103/PhysRev.80.268](https://doi.org/10.1103/PhysRev.80.268).
- [96] Murray Gell-Mann and Francis Low. Bound States in Quantum Field Theory. *Phys. Rev.*, 84:350–354, Oct 1951. doi:[10.1103/PhysRev.84.350](https://doi.org/10.1103/PhysRev.84.350).
- [97] Bryce S DeWitt. The operator formalism in quantum perturbation theory. 1955. URL: <https://escholarship.org/uc/item/39n7g9tp>.
- [98] J. Sucher. S-Matrix Formalism for Level-Shift Calculations. *Phys. Rev.*, 107:1448–1449, Sep 1957. doi:[10.1103/PhysRev.107.1448](https://doi.org/10.1103/PhysRev.107.1448).
- [99] M.E. Peskin and D.V. Schroeder. *An Introduction To Quantum Field Theory*. Frontiers in Physics. Avalon Publishing, 1995.
- [100] Gordon WF Drake. *Springer handbook of atomic, molecular, and optical physics*. Springer Science & Business Media, 2006. doi:[/10.1007/978-0-387-26308-3](https://doi.org/10.1007/978-0-387-26308-3).
- [101] M.D. Schwartz. *Quantum Field Theory and the Standard Model*. Cambridge University Press, 2013. URL: <https://books.google.fr/books?id=2RgXEAAQBAJ>.
- [102] N.N. Bogoliubov and D.V. Shirkov. *Quantum Fields*. Advanced book program. Benjamin/Cummings Publishing Company, 1982. Tranlated by Kvantovye polia. URL: <https://books.google.fr/books?id=wczvAAAAMAAJ>.
- [103] Lewis H. Ryder. *Quantum Field Theory*. Cambridge University Press, 2 edition, 1996. doi:[10.1017/CB09780511813900](https://doi.org/10.1017/CB09780511813900).
- [104] Peter J. Mohr. Quantum electrodynamics perturbation theory. *AIP Conference Proceedings*, 189(1):47–62, 1989. doi:[10.1063/1.38441](https://doi.org/10.1063/1.38441).
- [105] V.B. Berestetskii, E.M. Lifshitz, and L.P. Pitaevskii. *Quantum Electrodynamics: Volume 4*. Course of theoretical physics. Elsevier Science, 1982.
- [106] Walter Greiner, Berndt Müller, and Johann Rafelski. *Quantum Electrodynamics of Strong Fields*. Springer Berlin Heidelberg, 1985. doi:[10.1007/978-3-642-82272-8](https://doi.org/10.1007/978-3-642-82272-8).
- [107] Eleftherios N Economou. *Green’s functions in quantum physics*. Springer Series in Solid-State Sciences. Springer, Berlin, Heidelberg, 3rd edition, 2006. doi:[10.1007/3-540-28841-4](https://doi.org/10.1007/3-540-28841-4).
- [108] M. Baranger, H. A. Bethe, and R. P. Feynman. Relativistic Correction to the Lamb Shift. *Phys. Rev.*, 92:482–501, Oct 1953. doi:[10.1103/PhysRev.92.482](https://doi.org/10.1103/PhysRev.92.482).
- [109] Mark Thomson. *Modern Particle Physics*. Cambridge University Press, 2013. doi:[10.1017/CB09781139525367](https://doi.org/10.1017/CB09781139525367).
- [110] H. A. Bethe. The Electromagnetic Shift of Energy Levels. *Phys. Rev.*, 72:339–341, Aug 1947. doi:[10.1103/PhysRev.72.339](https://doi.org/10.1103/PhysRev.72.339).
- [111] Hans Bethe. Calculating the Lamb shift. <https://www.webofstories.com/play/hans.bethe/104>. Accessed: 2021-11-30.
- [112] Peter J. Mohr. *QUANTUM ELECTRODYNAMICS OF HIGH-Z FEW-ELECTRON ATOMS*, pages 111–141. Springer, Boston, MA, 1989. doi:[0.1007/978-1-4613-0833-1_3](https://doi.org/10.1007/978-1-4613-0833-1_3).

- [113] Peter J. Mohr. Self-energy radiative corrections in hydrogen-like systems. *Annals of Physics*, 88:26–51, Nov 1974. doi:10.1016/0003-4916(74)90398-4.
- [114] Richard P. Feynman. Relativistic Cut-Off for Quantum Electrodynamics. *Phys. Rev.*, 74:1430–1438, Nov 1948. doi:10.1103/PhysRev.74.1430.
- [115] Wendell H. Furry. A Symmetry Theorem in the Positron Theory. *Phys. Rev.*, 51:125–129, Jan 1937. doi:10.1103/PhysRev.51.125.
- [116] E. A. Uehling. Polarization Effects in the Positron Theory. *Phys. Rev.*, 48:55–63, Jul 1935. doi:10.1103/PhysRev.48.55.
- [117] L. Wayne Fullerton and G. A. Rinker. Accurate and efficient methods for the evaluation of vacuum-polarization potentials of order $Z\alpha$ and $Z\alpha^2$. *Phys. Rev. A*, 13:1283–1287, Mar 1976. doi:10.1103/PhysRevA.13.1283.
- [118] Eyvind H. Wichmann and Norman M. Kroll. Vacuum Polarization in a Strong Coulomb Field. *Phys. Rev.*, 101:843–859, Jan 1956. doi:10.1103/PhysRev.101.843.
- [119] G Källén and A Sabry. Fourth Order Vacuum Polarization. *Selsk. Mat. Fys. Medd*, 29(17), 1955. URL: <https://cds.cern.ch/record/212315?ln=bg>.
- [120] A G Fainshtein, N L Manakov, and A A Nekipelov. Vacuum polarization by a Coulomb field. Analytical approximation of the polarization potential. *Journal of Physics B: Atomic, Molecular and Optical Physics*, 24(3):559–569, feb 1991. doi:10.1088/0953-4075/24/3/012.
- [121] Miklos Gyulassy. Higher order vacuum polarization for finite radius nuclei. *Nuclear Physics A*, 244:497–525, June 1975. doi:10.1016/0375-9474(75)90554-0.
- [122] V. A. Dzuba, V. V. Flambaum, and J. S. M. Ginges. High-precision calculation of parity nonconservation in cesium and test of the standard model. *Phys. Rev. D*, 66:076013, Oct 2002. doi:10.1103/PhysRevD.66.076013.
- [123] Paul Indelicato and Peter J Mohr. Coordinate-space approach to the bound-electron self-energy. *Physical Review A*, 46(1):172, 1992.
- [124] Pekka Pyykkö and Li-Bo Zhao. Search for effective local model potentials for simulation of quantum electrodynamic effects in relativistic calculations. *Journal of Physics B: Atomic, Molecular and Optical Physics*, 36:1469, 03 2003. doi:10.1088/0953-4075/36/8/302.
- [125] T. Beier, P. J. Mohr, H. Persson, and G. Soff. Influence of nuclear size on QED corrections in hydrogenlike heavy ions. *Phys. Rev. A*, 58:954–963, Aug 1998. doi:10.1103/PhysRevA.58.954.
- [126] P. Indelicato and Peter J. Mohr. Coordinate-space approach to the bound-electron self-energy: Coulomb field calculation. *Phys. Rev. A*, 58:165–179, Jul 1998. doi:10.1103/PhysRevA.58.165.
- [127] V. A. Yerokhin and V. M. Shabaev. One-loop self-energy correction to the 1s and 2s hyperfine splitting in H-like systems. *Phys. Rev. A*, 64:012506, Jun 2001. doi:10.1103/PhysRevA.64.012506.

- [128] P. Boucard, S. Indelicato. Relativistic many-body and QED effects on the hyperfine structure of lithium-like ions. *The European Physical Journal D*, 8(1):59–73, Jan 2000. doi:[10.1007/s100530050009](https://doi.org/10.1007/s100530050009).
- [129] V. V. Flambaum and J. S. M. Ginges. Radiative potential and calculations of QED radiative corrections to energy levels and electromagnetic amplitudes in many-electron atoms. *Phys. Rev. A*, 72:052115, Nov 2005. doi:[10.1103/PhysRevA.72.052115](https://doi.org/10.1103/PhysRevA.72.052115).
- [130] Vladimir A. Yerokhin, Krzysztof Pachucki, and Vladimir M. Shabaev. One-loop self-energy correction in a strong binding field. *Phys. Rev. A*, 72:042502, Oct 2005. doi:[10.1103/PhysRevA.72.042502](https://doi.org/10.1103/PhysRevA.72.042502).
- [131] C. Thierfelder and P. Schwerdtfeger. Quantum electrodynamic corrections for the valence shell in heavy many-electron atoms. *Phys. Rev. A*, 82:062503, Dec 2010. doi:[10.1103/PhysRevA.82.062503](https://doi.org/10.1103/PhysRevA.82.062503).
- [132] LF Pašteka, E Eliav, A Borschevsky, U Kaldor, and P Schwerdtfeger. Relativistic coupled cluster calculations with variational quantum electrodynamics resolve the discrepancy between experiment and theory concerning the electron affinity and ionization potential of gold. *Physical review letters*, 118(2):023002, 2017. doi:[10.1103/PhysRevLett.118.023002](https://doi.org/10.1103/PhysRevLett.118.023002).
- [133] Neal J Snyderman. Electron radiative self-energy of highly stripped heavy atoms. *Annals of Physics*, 211(1):43–86, 1991. doi:[10.1016/0003-4916\(91\)90192-B](https://doi.org/10.1016/0003-4916(91)90192-B).
- [134] V. M. Shabaev, I. I. Tupitsyn, and V. A. Yerokhin. Model operator approach to the Lamb shift calculations in relativistic many-electron atoms. *Phys. Rev. A*, 88:012513, Jul 2013. doi:[10.1103/PhysRevA.88.012513](https://doi.org/10.1103/PhysRevA.88.012513).
- [135] Radosław Szmytkowski. Some summation formulae for spherical spinors. *Journal of Physics A: Mathematical and General*, 38(41):8993–9005, sep 2005. doi:[10.1088/0305-4470/38/41/011](https://doi.org/10.1088/0305-4470/38/41/011).
- [136] DIRAC, a relativistic ab initio electronic structure program, Release DIRAC21 (2021), written by R. Bast, A. S. P. Gomes, T. Saue, L. Visscher, and H. J. Aa. Jensen, with contributions from I. A. Aucar, V. Bakken, K. G. Dyall, S. Dubillard, U. Ekström, E. Eliav, T. Enevoldsen, E. Faßhauer, T. Fleig, O. Fossgaard, L. Halbert, E. D. Hedegård, T. Helgaker, B. Helmich-Paris, J. Henriksson, M. Iliaš, Ch. R. Jacob, S. Knecht, S. Komorovský, O. Kullie, J. K. Lærdahl, C. V. Larsen, Y. S. Lee, N. H. List, H. S. Nataraj, M. K. Nayak, P. Norman, G. Olejniczak, J. Olsen, J. M. H. Olsen, A. Papadopoulos, Y. C. Park, J. K. Pedersen, M. Pernpointner, J. V. Pototschnig, R. di Remigio, M. Repisky, K. Ruud, P. Sałek, B. Schimmelpfennig, B. Senjean, A. Shee, J. Sikkema, A. Sunaga, A. J. Thorvaldsen, J. Thyssen, J. van Stralen, M. L. Vidal, S. Villaume, O. Visser, T. Winther, and S. Yamamoto (available at <http://dx.doi.org/10.5281/zenodo.4836496>, see also <http://www.diracprogram.org>).
- [137] Ayaki Sunaga, Maen Salman, and Trond Saue. 4-component relativistic Hamiltonian with effective QED Potentials for molecular calculations. To be submitted.
- [138] Peter Schwerdtfeger, Lukáš F Pašteka, Andrew Punnett, and Patrick O Bowman. Relativistic and quantum electrodynamic effects in superheavy elements. *Nuclear Physics A*, 944:551–577, 2015. Special Issue on Superheavy Elements. doi:<https://doi.org/10.1016/j.nuclphysa.2015.02.005>.

- [139] Pekka Pyykkö. The Physics behind Chemistry and the Periodic Table. *Chemical Reviews*, 112(1):371–384, 2012. PMID: 21774555. doi:[10.1021/cr200042e](https://doi.org/10.1021/cr200042e).
- [140] Werner Kutzelnigg. Solved and unsolved problems in relativistic quantum chemistry. *Chemical Physics*, 395:16–34, 2012. Recent Advances and Applications of Relativistic Quantum Chemistry. doi:<https://doi.org/10.1016/j.chemphys.2011.06.001>.
- [141] Kenneth G Dyall, Charles W Bauschlicher Jr, David W Schwenke, and Pekka Pyykkö. Is the Lamb shift chemically significant? *Chemical Physics Letters*, 348(5):497–500, 2001. doi:[https://doi.org/10.1016/S0009-2614\(01\)01162-9](https://doi.org/10.1016/S0009-2614(01)01162-9).
- [142] Wenjian Liu. *Handbook of relativistic quantum chemistry*. Springer Berlin Heidelberg Berlin, Heidelberg, 2017. doi:[10.1007/978-3-642-40766-6](https://doi.org/10.1007/978-3-642-40766-6).
- [143] Trond Saue and Lucas Visscher. Four-component electronic structure methods for molecules. In Uzi Kaldor and Stephen Wilson, editors, *Theoretical chemistry and physics of heavy and superheavy elements*, pages 211–267. Springer Netherlands, Dordrecht, 2003. doi:[10.1007/978-94-017-0105-1_6](https://doi.org/10.1007/978-94-017-0105-1_6).
- [144] Günter Plunien and Gerhard Soff. *Quantum Electrodynamics of Highly Charged Ions*, pages 63–91. Springer Berlin Heidelberg, Berlin, Heidelberg, 1999. doi:[10.1007/978-3-642-58580-7_3](https://doi.org/10.1007/978-3-642-58580-7_3).
- [145] J. Rafelski, B. Müller, and W. Greiner. The charged vacuum in over-critical fields. *Nuclear Physics B*, 68(2):585–604, 1974. doi:[10.1016/0550-3213\(74\)90333-2](https://doi.org/10.1016/0550-3213(74)90333-2).
- [146] P. G. Reinhard. Quantum electrodynamics for strong fields and superheavy nuclei. *Lettere al Nuovo Cimento (1969-1970)*, 3(10):313–318, Mar 1970. doi:[10.1007/BF02755762](https://doi.org/10.1007/BF02755762).
- [147] P-G Reinhard, W Greiner, and H Arenhövel. Electrons in strong external fields. *Nuclear Physics A*, 166(2):173–197, 1971. doi:[10.1016/0375-9474\(71\)90421-0](https://doi.org/10.1016/0375-9474(71)90421-0).
- [148] L. Gomboroff and V. Tolmachev. Hartree-Fock Approximation in Quantum Electrodynamics. *Phys. Rev. D*, 3:1796–1804, Apr 1971. URL: <https://link.aps.org/doi/10.1103/PhysRevD.3.1796>, doi:[10.1103/PhysRevD.3.1796](https://doi.org/10.1103/PhysRevD.3.1796).
- [149] VA Yerokhin and VM Shabaev. First-order self-energy correction in hydrogenlike systems. *Physical Review A*, 60(2):800, 1999. doi:[10.1103/PhysRevA.60.800](https://doi.org/10.1103/PhysRevA.60.800).
- [150] Julian Schwinger. Quantum Electrodynamics. II. Vacuum Polarization and Self-Energy. *Phys. Rev.*, 75:651–679, Feb 1949. doi:[10.1103/PhysRev.75.651](https://doi.org/10.1103/PhysRev.75.651).
- [151] P. A. M. Dirac. Discussion of the infinite distribution of electrons in the theory of the positron. *Mathematical Proceedings of the Cambridge Philosophical Society*, 30:150–163, 1934. doi:[10.1017/S030500410001656X](https://doi.org/10.1017/S030500410001656X).
- [152] M Gyulassy. Non-linear vacuum polarization in strong fields. In *Quantum Electrodynamics of Strong Fields*, pages 685–700. Springer, 1983.
- [153] F.E. Harris. *Mathematics for Physical Science and Engineering: Symbolic Computing Applications in Maple and Mathematica*. Elsevier Science, 2014. doi:[10.1016/C2013-0-18495-4](https://doi.org/10.1016/C2013-0-18495-4).

- [154] Robin A Swainson and Gordon WF Drake. A unified treatment of the non-relativistic and relativistic hydrogen atom II: the Green functions. *Journal of Physics A: Mathematical and General*, 24(1):95, 1991. doi:[10.1088/0305-4470/24/1/020](https://doi.org/10.1088/0305-4470/24/1/020).
- [155] G. A. Rinker and L. Wilets. Vacuum polarization in strong, realistic electric fields. *Phys. Rev. A*, 12:748–762, Sep 1975. doi:[10.1103/PhysRevA.12.748](https://doi.org/10.1103/PhysRevA.12.748).
- [156] G. Plunien, T. Beier, Gerhard Soff, and H. Persson. Exact two-loop vacuum polarization correction to the Lamb shift in hydrogenlike ions. *The European Physical Journal D - Atomic, Molecular, Optical and Plasma Physics*, 1(2):177–185, Feb 1998. doi:[10.1007/s100530050078](https://doi.org/10.1007/s100530050078).
- [157] Miklos Gyulassy. *Higher Order Vacuum Polarization for Finite Radius Nuclei: Application to Muonic Lead and Heavy Ion Collisions*. PhD thesis, University of California, Berkeley., jan 1974.
- [158] Jan Schlemmer and Jochen Zahn. The current density in quantum electrodynamics in external potentials. *Annals of Physics*, 359:31–45, 2015. doi:[10.1016/j.aop.2015.04.006](https://doi.org/10.1016/j.aop.2015.04.006).
- [159] W. Pauli and F. Villars. On the Invariant Regularization in Relativistic Quantum Theory. *Rev. Mod. Phys.*, 21:434–444, Jul 1949. doi:[10.1103/RevModPhys.21.434](https://doi.org/10.1103/RevModPhys.21.434).
- [160] G. 't Hooft and M. Veltman. Regularization and renormalization of gauge fields. *Nuclear Physics B*, 44(1):189–213, 1972. doi:[https://doi.org/10.1016/0550-3213\(72\)90279-9](https://doi.org/10.1016/0550-3213(72)90279-9).
- [161] Kerson Huang. A critical history of renormalization. *International Journal of Modern Physics A*, 28(29):1330050, 2013. doi:[10.1142/S0217751X13300500](https://doi.org/10.1142/S0217751X13300500).
- [162] Eberhard Zeidler. *Quantum field theory II: Quantum electrodynamics: A bridge between mathematicians and physicists*, volume 2. Springer, 2009. doi:[10.1007/978-3-540-85377-0](https://doi.org/10.1007/978-3-540-85377-0).
- [163] Hans A. Bethe and Edwin E. Salpeter. *Quantum Mechanics of One- and Two-Electron Atoms*. Springer Berlin Heidelberg, 1957. doi:[10.1007/978-3-662-12869-5](https://doi.org/10.1007/978-3-662-12869-5).
- [164] Rolf Mertig, Manfred Böhm, and Ansgar Denner. Feyn Calc-Computer-algebraic calculation of Feynman amplitudes. *Computer Physics Communications*, 64(3):345–359, 1991. <https://feyncalc.github.io/> and <https://feyncalc.github.io/FeynCalcBook/ref/DiracTrace.html>. doi:[10.1016/0010-4655\(91\)90130-D](https://doi.org/10.1016/0010-4655(91)90130-D).
- [165] Frank WJ Olver, Daniel W Lozier, Ronald F Boisvert, and Charles W Clark. *NIST handbook of mathematical functions*. National Institute of Standards and Technology and Cambridge university press, 2010. URL: <https://www.nist.gov/publications/nist-handbook-mathematical-functions>.
- [166] George Arfken, Hans J Weber, and F Harris. *Mathematical Methods for Physicists. A Comprehensive Guide*, 2013. doi:[10.1016/C2009-0-30629-7](https://doi.org/10.1016/C2009-0-30629-7).
- [167] John David Jackson. *Classical electrodynamics*. John Wiley & Sons, 3rd edition, 1999.
- [168] Eugene Paul Wigner. *Gruppentheorie und ihre Anwendung auf die Quantenmechanik der Atomspektren*. Springer Fachmedien Wiesbaden GmbH, 1931. doi:[10.1007/978-3-663-02555-9](https://doi.org/10.1007/978-3-663-02555-9).

- [169] Giulio Racah. Theory of Complex Spectra. II. *Phys. Rev.*, 62:438–462, Nov 1942. doi: [10.1103/PhysRev.62.438](https://doi.org/10.1103/PhysRev.62.438).
- [170] Walter Greiner and Berndt Müller. *Quantum mechanics: symmetries*. Springer Science & Business Media, 2nd edition, 2012. doi: [10.1007/978-3-642-57976-9](https://doi.org/10.1007/978-3-642-57976-9).
- [171] Claude Cohen-Tannoudji, Bernard Diu, and Frank Laloe. Quantum mechanics, volume ii: Angular momentum, spin, and approximation methods. *Quantum Mechanics*, 2, 2020. Translated from French by Susan Reid Hemley, Nicole Ostrowsky, and Dan Ostrowsky. URL: <https://www.wiley.com/en-us/Quantum+Mechanics%2C+Volume+2%3A+Angular+Momentum%2C+Spin%2C+and+Approximation+Methods%2C+2nd+Edition-p-9783527345540>.
- [172] Walter R Johnson. *Atomic structure theory*. Springer-Verlag Berlin Heidelberg, 2007. doi: [10.1007/978-3-540-68013-0](https://doi.org/10.1007/978-3-540-68013-0).
- [173] Radosław Szmytkowski. Recurrence and differential relations for spherical spinors. *Journal of mathematical chemistry*, 42(3):397–413, 2007. doi: [10.1007/2Fs10910-006-9110-0](https://doi.org/10.1007/2Fs10910-006-9110-0).
- [174] Wolfram Koepf. *Hypergeometric Summation*. Springer-Verlag London, 2nd edition, 2014. doi: [10.1007/978-1-4471-6464-7](https://doi.org/10.1007/978-1-4471-6464-7).
- [175] A Bechler. Summation formulae for spherical spinors. *Journal of Physics A: Mathematical and General*, 26(21):6039–6042, nov 1993. doi: [10.1088/0305-4470/26/21/041](https://doi.org/10.1088/0305-4470/26/21/041).
- [176] Kenneth G Dyall. Basis sets for the 1s2 ground states of two- electron rare gas ions, December 2015. doi: [10.5281/zenodo.5773023](https://doi.org/10.5281/zenodo.5773023).
- [177] Kenneth G. Dyall and Knut Fægri. Optimization of Gaussian basis sets for Dirac-Hartree-Fock calculations. *Theoretica chimica acta*, 94(1):39–51, 1996. doi: [10.1007/BF00190154](https://doi.org/10.1007/BF00190154).
- [178] Trygve Helgaker, Poul Jorgensen, and Jeppe Olsen. *Molecular electronic-structure theory*. John Wiley & Sons, 2000. doi: [10.1002/9781119019572](https://doi.org/10.1002/9781119019572).
- [179] Kenneth G. Dyall and Knut Fægri. *Introduction to Relativistic Quantum Chemistry*. Oxford University Press, July 2007. doi: [10.1093/oso/9780195140866.001.0001](https://doi.org/10.1093/oso/9780195140866.001.0001).
- [180] David F. Feller and Klaus Ruedenberg. Systematic approach to extended even-tempered orbital bases for atomic and molecular calculations. *Theoretica chimica acta*, 52(3):231–251, Sep 1979. doi: [10.1007/BF00547681](https://doi.org/10.1007/BF00547681).
- [181] Ernest R. Davidson and David Feller. Basis set selection for molecular calculations. *Chemical Reviews*, 86(4):681–696, Aug 1986. doi: [10.1021/cr00074a002](https://doi.org/10.1021/cr00074a002).
- [182] Nakhle H. Asmar and Loukas Grafakos. *Complex Analysis with Applications*. Springer International Publishing, 2018. doi: [10.1007/978-3-319-94063-2](https://doi.org/10.1007/978-3-319-94063-2).
- [183] James Ward Brown and Ruel V Churchill. *Complex variables and applications*. McGraw-Hill Education, 9th edition, 2009. URL: <https://www.mheducation.com/highered/product/complex-variables-applications-brown-churchill/M9780073383170.html>.
- [184] L.V. Ahlfors. *Complex Analysis*. International series in pure and applied mathematics. McGraw-Hill Education, 3rd edition, 1979. URL: <https://books.google.fr/books?id=2MRuus-5GGoC>.

- [185] Maen Salman. Vacuum polarization integral program.
<https://gitlab.com/maen.salman/vacuum-polarization-integral.git>, 2021.
- [186] Marek Nowakowski. The quantum mechanical current of the Pauli equation. *American Journal of Physics*, 67(10):916–919, 1999. doi:10.1119/1.19149.
- [187] James M Wilkes. The Pauli and Lévy-Leblond equations, and the spin current density. *Eur. J. Phys.*, 41(3):035402, apr 2020. doi:10.1088/1361-6404/ab7495.